

Federal University of Rio Grande do Sul  
Engineering School  
Civil Engineering Post Graduation Program

**Stabilization of a Dispersive Clayey Sand**

**Ricardo José Wink de Menezes**

Porto Alegre  
2020

RICARDO JOSÉ WINK DE MENEZES

## **STABILIZATION OF A DISPERSIVE CLAYEY SAND**

Dissertation Submitted to the Board of Examiners from Post Graduation Civil Program of the Federal University of Rio Grande do Sul, as part of The Requirements for the Degree of Master of Engineering.

Porto Alegre  
2020

**RICARDO JOSÉ WINK DE MENEZES**

**STABILIZATION OF A DISPERSIVE CLAYEY SAND**

This master's thesis was judged suitable for the obtainment of the MASTER IN ENGINEERING, in the field of Geotechnical Engineering, and approved in its final version by the supervisor professor and by the Post Graduation Civil Engineering Program from the Federal University of Rio Grande do Sul.

Porto Alegre, November 16<sup>th</sup>, 2020

Prof. Lucas Festugato  
D. Sc., UFRGS, Brazil  
Supervisor

Prof. Nilo Cesar Consoli  
PPGEC/UFRGS Coordinator

**BOARD OF EXAMINERS**

**Prof. Cezar Augusto Burkert Bastos (FURG)**  
D. Sc. UFRGS, Brazil

**Prof. Nilo Cesar Consoli (UFRGS)**  
phD Concordia University, Canada

**Prof. Cesar Alberto Ruver (UFRGS)**  
D. Sc. UFRGS, Brazil

**Prof. Rodrigo Beck Saldanha (UFRGS)**  
D. Sc. UFRGS, Brazil

This work is dedicated to all geotechnical community  
aware of the development of scientific knowledge.

## ACKNOWLEDGEMENTS

First of all, I am very grateful to Lucas Festugato for all the years of friendship, teaching and advising in LEGG, classes, in my graduation conclusion work and, finally, in the present work. Combining patience and serenity with knowledge you know the best way to find a way.

I would like to express my gratitude to my wife, Aline, who supported me uninterruptedly during this great part of my dream, giving her time to help me in whatever I needed: in the lab and at home. I can't thank you enough for the help during this research and for, kindly, filling my heart with joy.

I would like to acknowledge Eduardo, my brother, for fraternity love and for helping me out during many of my scientific issues, so as my sister in law, Andrea. I would like to thank my parents for all the support along the way in becoming a Civil Engineer and, as a consequence, starting a new challenge to become a Master of Science in Engineering. I may not forget to express my gratitude to all my family too, which I could not be so close as I would like during the development of this research.

I must not forget to express my gratitude to FGS Geotecnia, as well as all the friends I made in the company, colleagues, and ex-colleagues, for making it possible for me to face this challenge. A special thanks go to Alisson, Anderson, and Bruno for the friendship and help since the beginning.

I thank my graduation colleagues and friends for partnership over all those years: Führ, Gonça, Grassioli, Hernando, Olindo, Palm, and Turra.

I would like to thank the L.A. group: Boris, Leonel and Abreu, and also to the Geovanis fraternity for making the nights more pleasant.

I would like to thank my old friends Dalpi, Eckert, Jiam, Herberts and Rapha for the partnership, even if distant sometimes.

I must express my sincere gratitude to Camila and Mateus, for helping me out with my first steps of this master's degree. Luckily, friends were more abundant than time.

Also, I would like to thank my colleagues from LEGG for the discussions and for sharing knowledge and experiences about their academic work, especially Alejandro, Gustavo Miguel, and Hugo.

Thanks to Guilherme Martins for helping me out with the characterization tests of the materials and to Hugo for helping me with the characterization tests and for bringing knowledge and new ideas for the development of this research.

I would like to show my appreciation to Pedro, Karina, Thales, Guilherme Martins, and Guilherme Rochedo, who helped me to collect the soil from Pelotas; Thales (again), Paulo, Rosanne, and Bruna for helping me out with the lab experiments, and Lucas Lerner for helping me out with a laboratory experiment.

I want to thank Cezar Bastos too, for the helpfulness during soil sampling and characterization of the soil.

I would like to express my gratitude to all my professors during this Master's degree, especially to Sérgio Marques, Cesar Ruver and Nilo Consoli for the great dedication. I would like to thank the dedicated professors I had during my graduation too.

I apologize if, due to an unexcusable memory lapse, I forgot someone.

Kick at the rock, Sam Johnson, break your bones:  
But cloudy, cloudy is the stuff of stones.

*Richard Wilbur*

## ABSTRACT

A few decades ago, Geotechnical Engineers had to face challenges dealing with soils with practically immutable properties, so they had to adapt the infrastructure to the as-is condition of the soil/rock mass. With the development of many ground improvement techniques, soils with undesirable properties could be replaced by one with more adequate properties. Those techniques were boosted into a conjuncture where there is a growing need for the occupation of peripheral zones of cities, where the behaviour of geotechnical materials is usually not as suitable as one of the occupied areas. However, conventional techniques to build in those zones tend to be expensive, turning many projects unfeasible. Thus, many researches have been carried out to understand the behaviour of soil improvement focusing on strength, stiffness, liquefiability, expansibility, collapsibility, and dispersibility properties. Thereby, this research aims to study the improvement effect in a clayey dispersive sand with the addition of lime and fly ash, comparing a commercial (dolomitic) and a byproduct lime (calcitic). Different admixtures were analyzed varying specific weight, lime, and fly ash content, for a curing period of 28 days. The applied methodology consists of Unconfined Compressive Strength (UCS) tests, Small Strain stiffness tests, and durability tests, all of them conducted at every dosage. The experimental program was developed from full factorial design methods and intended to evaluate the response variables related to many factors and the damage caused by the durability cycles. Results have indicated that a small amount of binder was enough to control the dispersive behaviour of the soil, though, in most cases not to grant durability, and it was found that the lime that leads to higher strength admixtures is not necessarily the one which promotes higher durability. Still, the response variables like strength, small strain stiffness, and loss of mass may be related. Besides that, a dosage methodology was proposed based on the porosity/volumetric binder (and lime) content ratio, and this key dosing parameter could be used in the behaviour prediction of cemented soils even when they undergo rough climate conditions.

**Keywords:** *Soil improvement; Soil Stabilization; Dispersive Soil; Unconfined Compressive Strength (UCS); Ultrasonic Waves; Porosity/Volumetric Binder Ratio; Porosity/Volumetric Lime Ratio; Soils Durability.*



## RESUMO

Há algumas décadas, Engenheiros Geotécnicos tinham que enfrentar desafios lidando com solos de propriedades praticamente imutáveis, tendo que adaptar a infraestrutura à condição natural da massa de solo/rocha. Com o desenvolvimento de diversas técnicas de melhoramento do terreno, as características indesejáveis do solo puderam ser substituídas por outras de melhores propriedades. Essas técnicas ganharam força em uma conjuntura em que há uma necessidade crescente de ocupação das zonas periféricas das cidades, onde materiais geotécnicos são usualmente não tão desejáveis quanto em áreas já ocupadas. No entanto, técnicas convencionais para construir nessas zonas tendem a ser dispendiosas, tornando muitos empreendimentos inviáveis. Portanto, diversas pesquisas tem sido feitas para compreender o comportamento de solos melhorados, principalmente quanto às propriedades de resistência, rigidez, liquefação, expansividade, colapsividade e dispersibilidade. Com isso, esta pesquisa visa ao estudo do efeito de uma areia argilosa dispersiva por meio da adição de cal e cinza volante, comparando-se cal comercial (dolomítica) e de resíduo (calcítica). Foram analisadas diferentes misturas, variando-se o peso específico e o teor de cal e de cinza, para um período de cura de 28 dias. A metodologia aplicada consiste em ensaios de Resistência a Compressão Simples (RCS), rigidez inicial, e ensaios de durabilidade, todos para cada uma das dosagens. O plano experimental foi desenvolvido a partir de um projeto fatorial completo, buscando-se avaliar as variáveis resposta em relação a diferentes fatores e ao dano causado por ciclos de durabilidade. Os resultados indicaram que uma pequena quantidade de reagente foi suficiente para controlar a dispersibilidade do solo, embora não necessariamente para conferir durabilidade a ele, e que a cal que gera misturas mais resistentes nem sempre é a que promove maior ganho de durabilidade. Ainda, variáveis resposta como resistência, rigidez inicial e perda de massa acumulada podem ser relacionadas. Além disso, uma metodologia de dosagem foi proposta baseada na razão porosidade/teor volumétrico de agente cimentante (e cal). Por fim, foi observado que o parâmetro-chave de dosagem poderia ser utilizado inclusive para a previsão do comportamento de solos cimentados quando submetidos a condições climáticas adversas.

**Palavras-chave:** *Melhoramento de solos; Estabilização de solos; Solos dispersivos; Resistência a Compressão Simples (RCS); Pulso Ultrassônico; Porosidade-Teor Volumétrico de Agente Cimentante; Porosidade-Teor Volumétrico de Cal; Durabilidade de Solos.*

## TABLE OF CONTENTS

<b>1 INTRODUCTION</b> .....	<b>11</b>
<b>1.1 SOILS IN ENGINEERING</b> .....	<b>11</b>
<b>1.2 SOIL IMPROVEMENT</b> .....	<b>12</b>
<b>1.3 SCOPE</b> .....	<b>12</b>
<b>1.4 OBJECTIVES</b> .....	<b>13</b>
<b>1.5 DELIMITATION</b> .....	<b>13</b>
<b>1.6 LIMITATION</b> .....	<b>13</b>
<b>1.7 RELEVANCE</b> .....	<b>14</b>
<b>1.8 STRUCTURE</b> .....	<b>14</b>
<b>2 LITERATURE REVIEW</b> .....	<b>16</b>
<b>2.1 MATERIALS</b> .....	<b>16</b>
2.1.1 Wear and Damage .....	16
2.1.2 Geomaterials.....	17
2.1.2.1 Granular media .....	17
2.1.2.2 Clay minerals.....	17
<b>2.2 WATER EROSION AND DISPERSIVE SOILS</b> .....	<b>20</b>
2.2.1 Erosion Issue .....	20
2.2.2 Dispersion phenomenon .....	26
2.2.3 Dispersion and chemical stability.....	28
2.2.4 Dispersibility in Southern Brazil .....	33
<b>2.3 STABILIZED SOILS</b> .....	<b>34</b>
2.3.1 Pozzolanic Reaction .....	34
2.3.2 Lime.....	35
2.3.3 Fly Ash .....	37
2.3.4 Mechanical behavior of stabilized soils .....	38
2.3.5 Durability of structured soils .....	40
2.3.6 Porosity and Cementitious Agent Content Ratio.....	42
<b>2.4 UNCONFINED COMPRESSIVE STRENGTH</b> .....	<b>44</b>
2.4.1 Cracks propagation and failure modes .....	44
2.4.2 Unconfined Compressive Stiffness .....	46
2.4.4 Unconfined Compressive Strength and Cemented Materials.....	51

2.4.5 Unconfined Compressive Strength and Durability.....	53
<b>2.5 SMALL STRAIN STIFFNESS .....</b>	<b>54</b>
2.5.1 Small Strain Behaviour.....	54
2.5.2 Shear waves .....	57
2.5.3 Compression waves .....	58
2.5.4 Poisson's ratio .....	59
2.5.5 Waves and cemented materials.....	60
2.5.6 Waves and degree of saturation.....	61
2.5.7 Ultrasonic Pulse Velocity .....	64
<b>2.6 EXPERIMENTAL AND FACTORIAL DESIGN .....</b>	<b>65</b>
2.6.1 Experimental planning.....	65
2.6.2 Factorial Experiments.....	66
<b>3 LABORATORY EXPERIMENTS DESIGN, REVIEW, AND PROCEDURES .....</b>	<b>68</b>
<b>3.1 PRELIMINARY TESTS.....</b>	<b>69</b>
3.1.1 Particle size.....	69
3.1.1.1 Sieve analysis .....	71
3.1.1.2 Light scattering.....	72
3.1.1.3 Sedimentation analysis .....	72
3.1.2 Atterberg Limits .....	73
3.1.3 Specific gravity.....	76
3.1.4 Compaction.....	77
3.1.5 Specific Surface Area .....	78
3.1.6 Initial Consumption of Lime .....	79
3.1.7 X-Ray Diffractometry.....	80
3.1.8 X-Ray Fluorescence .....	81
3.1.9 Apparent field-specific gravity.....	81
3.1.10 Water content.....	83
<b>3.2 DISPERSIBILITY EXPERIMENTS .....</b>	<b>83</b>
3.2.1 Salts concentration.....	84
3.2.2 Crumb test .....	84
3.2.3 Double Hydrometer test .....	85
3.2.4 Pinhole test .....	86
<b>3.3 DURABILITY, MECHANICAL AND GEOPHYSICAL TESTING .....</b>	<b>91</b>
3.3.1 Moulding and curing .....	91

3.3.2 Durability test .....	92
3.3.2.1 Wetting, drying, and brushing .....	92
3.3.2.2 Wetting and drying .....	94
3.3.3 Unconfined compressive strength test.....	95
3.3.3.1 Strength test after the curing period .....	96
3.3.3.2 Strength tests after durability cycles.....	97
3.3.4 Ultrasonic pulse velocity testing .....	97
3.3.4.1 UPV equipment .....	97
<b>4 MATERIALS CHARACTERIZATION AND EXPERIMENTAL DESIGN .....</b>	<b>99</b>
<b>4.1 SOIL CHARACTERIZATION .....</b>	<b>99</b>
4.1.1 Soil site characterization and geology .....	99
4.1.2 Soil grain size distribution and double hydrometer test .....	101
4.1.3 Soil Atterberg limits .....	103
4.1.4 Soil compaction .....	103
4.1.5 Soil X-ray diffraction .....	104
4.1.6 Soil solids specific gravity.....	105
4.1.7 Soil specific surface area .....	105
4.1.8 Soil apparent specific gravity .....	105
4.1.9 Soil crumb tests .....	105
4.1.10 Soil cation analysis .....	106
4.1.11 Soil pinhole tests.....	107
4.1.12 Soil dispersibility classification.....	107
<b>4.2 FLY ASH CHARACTERIZATION.....</b>	<b>108</b>
4.2.1 Fly ash grain size distribution.....	108
4.2.2 Fly ash solids specific gravity .....	109
4.2.3 Fly ash X-ray diffraction analysis .....	109
4.2.5 Fly ash specific surface area.....	110
<b>4.3 CALCITIC LIME CHARACTERIZATION .....</b>	<b>111</b>
4.3.1 Calcitic lime grain size distribution.....	111
4.3.2 Calcitic lime solids specific gravity.....	111
4.3.3 Calcitic lime X-ray diffraction analysis.....	111
4.3.4 Calcitic lime specific surface area .....	112
4.3.5 Calcitic lime x-ray fluorescence .....	112
<b>4.4 DOLOMITIC LIME CHARACTERIZATION .....</b>	<b>113</b>

4.4.1 Dolomitic lime grain size distribution.....	113
4.4.2 Dolomitic lime solids specific gravity.....	114
4.4.3 Dolomitic lime X-ray diffraction analysis.....	114
4.4.4 Dolomitic lime specific surface area .....	115
<b>4.5 ADMIXTURE CHARACTERIZATION .....</b>	<b>115</b>
4.5.1 Initial consumption of lime (ICL) .....	116
4.5.2 Compaction tests .....	116
4.5.3 Crumb test .....	117
4.5.4 Pinhole tests.....	117
<b>4.6 CHARACTERIZATION SUMMARY.....</b>	<b>118</b>
<b>4.7 EXPERIMENTAL DESIGN .....</b>	<b>119</b>
4.7.1 Durability tests design .....	120
4.7.2 Unconfined compressive strength tests design.....	121
4.7.3 UPV experimental design.....	122
<b>5 RESULTS.....</b>	<b>123</b>
<b>5.1 FACTORIAL RESULTS .....</b>	<b>123</b>
5.1.1 Effect of dry unit weight, fly ash, and lime content .....	124
5.1.1.1 Unconfined compressive strength .....	124
5.1.1.2 Small strain constraint modulus .....	133
5.1.1.3 Small strain shear modulus.....	141
5.1.1.4 Loss of mass .....	147
5.1.2 Addition of lime type effect .....	153
5.1.2.1 Unconfined compressive strength and lime type aid.....	153
5.1.2.2 Small strain constraint modulus and lime type aid.....	158
5.1.2.3 Small strain shear modulus and lime type aid.....	161
5.1.2.4 Loss of mass and lime type aid.....	164
5.1.3 Sample size effect addition.....	167
5.1.3.1 Unconfined compressive strength and slenderness ratio.....	167
5.1.3.2 Small strain constraint modulus and slenderness ratio.....	168
5.1.3.3 Small strain shear modulus and slenderness ratio .....	170
5.1.4 Factorial results evaluation.....	171
<b>5.2 RESPONSE VARIABLES INFLUENCED BY CURING AND DURABILITY CYCLES.....</b>	<b>172</b>
5.2.1 Curing effect on small strain stiffness .....	173

5.2.2 Unconfined compressive strength after cycles .....	176
5.2.3 Unconfined compressive secant modulus after cycles .....	178
5.2.4 Small strain constraint modulus throughout durability cycles .....	179
5.2.5 Small strain shear modulus throughout cycles .....	182
5.2.6 Loss of mass throughout cycles.....	185
5.2.7 Unconfined compressive strength durability ratio after durability cycles.....	188
<b>5.3 RELATION BETWEEN VARIABLES RESPONSE .....</b>	<b>190</b>
5.3.1 Unconfined compressive strength x unconfined compressive secant modulus.....	190
5.3.2 Unconfined compressive strength x small strain constraint modulus .....	192
5.3.3 Unconfined compressive strength x small strain shear modulus.....	195
5.3.4 Unconfined compressive strength x accumulated loss of mass.....	198
5.3.5 Unconfined compressive secant modulus x Accumulated loss of mass.....	199
5.3.6 Unconfined compressive secant modulus x small strain constraint modulus .....	199
5.3.7 Unconfined compressive secant modulus x small strain shear modulus.....	202
5.3.8 Small strain shear modulus x small strain constraint modulus.....	204
5.3.9 Accumulated loss of mass x small strain constraint modulus .....	207
5.3.10 Accumulated loss of mass x small strain shear modulus.....	209
<b>5.4 BINDER KEY PARAMETER RESULTS .....</b>	<b>211</b>
5.4.1 Unconfined Compressive strength x binder key parameter.....	211
5.4.2 Unconfined Compressive secant modulus x binder key parameter.....	214
5.4.3 Small strain constraint modulus x binder key parameter .....	217
5.4.4 Small strain shear modulus x binder key parameter.....	220
5.4.5 Small strain Poisson's ratio x binder key parameter .....	224
5.4.6 Accumulated loss of mass x binder key parameter .....	227
5.4.7 Binder key parameter evaluation.....	229
<b>5.5 LIME KEY PARAMETER RESULTS.....</b>	<b>230</b>
5.5.1 Unconfined Compressive strength x lime key parameter.....	230
5.5.2 Unconfined Compressive secant modulus x lime key parameter.....	234
5.5.3 Small strain constraint modulus x lime key parameter.....	238
5.5.4 Small strain shear modulus x lime key parameter.....	243
5.5.5 Small strain Poisson's ratio x lime key parameter .....	249
5.5.6 Accumulated loss of mass x lime key parameter .....	254
5.5.7 Lime key parameter evaluation .....	256
<b>5.6 SLENDERNESS RATIO RESULTS .....</b>	<b>258</b>

5.6.1 Unconfined compressive strength x slenderness ratio.....	258
5.6.2 Unconfined compressive secant modulus x slenderness ratio.....	260
5.6.3 Small strain constraint modulus x slenderness ratio.....	262
5.6.4 Small strain shear modulus x slenderness ratio .....	265
5.6.5 Slenderness ratio effect.....	269
<b>6 CONCLUSIONS AND REMARKS.....</b>	<b>271</b>
<b>6.1 SUMMARY OF CONCLUSIONS.....</b>	<b>271</b>
<b>6.2 SUGGESTIONS FOR FORTHCOMING RESEARCHES .....</b>	<b>272</b>
<b>REFERENCES .....</b>	<b>274</b>
<b>APPENDICES.....</b>	<b>302</b>
<b>APPENDIX I – SAMPLES THROUGHOUT DURABILITY CYCLES.....</b>	<b>303</b>
<b>APPENDIX II – SAMPLES FAILURE MODES.....</b>	<b>322</b>
<b>APPENDIX III – ANOVA TABLES .....</b>	<b>341</b>
APPENDIX III.1 – Effect of dry unit weight, fly ash, and lime content .....	342
APPENDIX III.2 – Addition of lime type effect.....	376
APPENDIX III.3 – Addition of sample size effect .....	392
<b>APPENDIX IV – COMPOSITION AND STRENGTH OF STUDIED SPECIMENS..</b>	<b>396</b>
APPENDIX IV.1 – Carbide lime (Calcitic) treatment .....	397
APPENDIX IV.2 – Primor lime (Dolomitic) treatment.....	400

## LIST OF FIGURES

Figure 1.1: Research structure.....	15
Figure 2.1: Diagram showing (A) a clay mineral layer; (B) a particle, made up of stacked layers; layer translation and deformation can give rise to a lenticular pore; (C) an aggregate, showing an interlayer space and an interparticle space; and (D) an assembly of aggregates, enclosing an interaggregate space (pore) (BERGAYA et al., 2006).....	19
Figure 2.2: Critical shear stress based on mean grain size (BRIAUD, 2008).....	21
Figure 2.3: Types of erosion: a) pipe or crack internal erosion; b) backward internal erosion (generalized or local, i.e., at the bottom of the pipe; c) internal contact erosion (between gravel and silt; d) suffusion, or the internal instability of a soil, or volume erosion (after from FELL & FRY, 2007). .....	23
Figure 2.4: Conditions for internal erosion triggering (after ZHANG et al., 2016).....	25
Figure 2.5: Diffuse electric double-layer (ISRAELACHVILI, 2011).....	29
Figure 2.6: Cationic exchange capacity (after VELDE & MEUNIER, 2008). .....	29
Figure 2.7 - Effect of CEC and ESP on clay dispersion (HARMSE & GERBER, 1988). .....	30
Figure 2.8 – SAR isocurves in dispersive soils chart (Sherard et al., 1976a).....	32
Figure 2.9 – Chart for the classification of dispersive soils (Sherard et al., 1976a).....	32
Figure 2.10: Illustration of different failure modes for rocks under unconfined compressive tests. (Basu et al., 2013).....	45
Figure 2.11: Diagram for classification of rocks on the basis of uniaxial mechanical properties. (HAWKES & MELLOR, 1970).....	47
Figure 2.12: Profile of lateral displacement in an unconfined compressive strength test. A. Perfect radial freedom at the specimen ends. B. Complete radial restraint at the specimen ends. C. Extrusion of an interfacial material at the platen/specimen contact (HAWKES & MELLOR, 1970).....	48
Figure 2.13: Stresses developed during unconfined compressive tests (KOTSOVOS, 1983). .....	49
Figure 2.14: UCS x H/D Ratio for clay specimens (after GUNELY & RUSEN, 2015).....	50
Figure 2.15: Relation between cohesion and UCS (MA & WANG, 2011). .....	51
Figure 2.16: Mohr-Coulomb envelope for idealized splitting tensile and unconfined compressive strength. ....	52
Figure 2.17: Stiffness degradation curve and equipments/structures strain range (MAIR, 1993) .....	55



Figure 2.18: Body waves – particle motion in a continuum during wave propagation. The perturbation propagates to the right. The dots can be considered as the centers of particles interconnected with springs, which represent contact stiffness. (a) Center positions before propagation. (b) Displaced positions during the propagation of a P-wave. (c) Displaced positions during the propagation of an S-wave (SANTAMARINA et al., 2001) .....	56
Figure 2.19: Effect of cementation in S-wave velocity (FERNANDEZ & SANTAMARINA, 2001).....	61
Figure 2.20: Contact between two grains where the menisci turn the contact radius from $b$ into $b'$ for the dry to the unsaturated state (PALMER & TRAVIOLIA, 1980). .....	62
Figure 2.21: Small strain shear modulus versus degree of saturation (WU et al., 1984). .....	63
Figure 3.1: Flow Chart for Classifying Coarse-Grained Soils (More Than 50 % Retained on No. 200 Sieve) – ASTM D 2487 (ASTM, 2018). .....	71
Figure 3.2: Sieves from left to right: 2.000 (#10), 1.180 (#16), 0.600 (#30), 0.425 (#40), 0.250 (#60), 0.150 (#100) and 0.075 mm (#200). .....	72
Figure 3.3: Hydrometer inside the glass cylinder.....	73
Figure 3.4: Consistency of cohesive soils (after from DAS, 2008).....	73
Figure 3.5: Soil liquid limit test with Casagrande’s device.....	74
Figure 3.6: Relation between Plasticity Index and Clay Fraction (after Skempton, 1953).....	75
Figure 3.7: Vacuum pump for the pycnometer analysis.....	76
Figure 3.8: ICL test apparatus. ....	79
Figure 3.9: XRD test (SURYANARAYANA & NORTON, 1998).....	80
Figure 3.10: (a) intact soil sample; (b) soil covered by wax. ....	82
Figure 3.11: Pure wax specimen. ....	82
Figure 3.12: hydrostatic balance.....	83
Figure 3.13: Crumb test dispersibility degree [ASTM D6572 (ASTM, 2020)].....	85
Figure 3.14: Criteria for dispersibility classification with the pinhole test [ASTMM D4647 (ASTM, 2020)]. .....	87
Figure 3.15: Comparison of cloudy colloidal appearance with perfectly clear water [ASTMM D4647 (ASTM, 2020)]. .....	87
Figure 3.16: Pinhole test equipment [ASTMM D4647 (ASTM, 2020)]. .....	88
Figure 3.17: Pinhole test flowchart [after NBR 14114 (ABNT, 1998)]. .....	89
Figure 3.18: Hole in the center of the sample.....	90
Figure 3.19: Pinhole test equipment. ....	90
Figure 3.20: Pinhole adopted turbidity pattern (a) slightly clear (b) slightly cloudy/dark.....	91

Figure 3.21: Soil, fly ash, and calcitic lime (yellow-brown, dark gray and white color, respectively) prepared for molding.....	91
Figure 3.22: Water curing tank with controlled temperature. ....	92
Figure 3.23: Typical behaviour of stabilized soil with a high mass loss after 12 cycles of wetting, drying and brushing durability tests. ....	93
Figure 3.24: Typical behaviour stabilized soils with a high mass loss after wetting and drying durability tests. ....	94
Figure 3.25: Unconfined compression equipment with 10 kN load cell. ....	95
Figure 3.26: Typical shear surface for medium-high cemented soils in unconfined compressive tests. ....	96
Figure 3.27: Soil portion taken for the samples moisture determination after failure.....	96
Figure 3.28: UPV equipment used. ....	97
Figure 3.29: Transducers arrangements (after PROCEQ S.A.©, 2017).....	98
Figure 3.30: Shear waves arrival time in PUNDIT tests (after PROCEQ S.A.©, 2017). ....	98
Figure 4.1: Map location of the soil target area (GOOGLE, 2020). ....	99
Figure 4.2: View of the soil sampling site.....	100
Figure 4.3: Regional lithological map (adapted from CPRM, 2004).....	101
Figure 4.4: Soil particle size distribution. ....	102
Figure 4.5: Compaction curve plotted (modified energy). ....	103
Figure 4.6: Compaction curve plotted (modified energy). ....	104
Figure 4.7: Soil XRD results. ....	104
Figure 4.8: In situ crumb test.....	105
Figure 4.9: Laboratory crumb test. ....	106
Figure 4.10: Fly ash grain size distribution. ....	109
Figure 4.11: Fly Ash XRD results. ....	110
Figure 4.12: Calcitic lime grain size distribution. ....	111
Figure 4.13: Calcitic lime XRD results. ....	112
Figure 4.14: Dolomitic lime grain size distribution. ....	114
Figure 4.15: Dolomitic lime XRD results. ....	115
Figure 4.16: ICL test with carbide lime.....	116
Figure 4.17: Admixtures compaction curves (modified energy).....	117
Figure 5.1: Pareto and main effects on response to unconfined compressive strength for calcitic lime treated samples after 0 cycles (samples H/D $\approx$ 2.0). ....	124

Figure 5.2: Pareto and main effects on response to unconfined compressive strength for dolomitic lime treated samples after 0 cycles (samples H/D $\approx$ 2.0).....	125
Figure 5.3: Pareto and main effects on response to unconfined compressive strength for calcitic lime treated samples after 1 cycle (samples H/D $\approx$ 2.0).....	126
Figure 5.4: Pareto and main effects on response to unconfined compressive strength for dolomitic lime treated samples after 1 cycle (samples H/D $\approx$ 2.0).....	127
Figure 5.5: Pareto and main effects on the response of unconfined compressive strength for calcitic lime treated samples after 4 cycles (samples H/D $\approx$ 2.0).....	128
Figure 5.6: Pareto and main effects on response to unconfined compressive strength for dolomitic lime treated samples after 4 cycles (samples H/D $\approx$ 2.0).....	129
Figure 5.7: Pareto and main effects on response to unconfined compressive strength for calcitic lime treated samples after 12 cycles (samples H/D $\approx$ 2.0). ....	130
Figure 5.8: Pareto and main effects on response to unconfined compressive strength for dolomitic lime treated samples after 12 cycles (samples H/D $\approx$ 2.0).....	131
Figure 5.9: Pareto and main effects on response to unconfined compressive strength for calcitic lime treated samples after 12 cycles (samples H/D $\approx$ 1.2). ....	131
Figure 5.10: Pareto and main effects on response to unconfined compressive strength for dolomitic lime treated samples after 12 cycles (samples H/D $\approx$ 1.2).....	132
Figure 5.11: Pareto and main effects on response to small strain constraint modulus for calcitic lime treated samples after 0 cycles (samples H/D $\approx$ 2.0). ....	133
Figure 5.12: Pareto and main effects on response to small strain constraint modulus for dolomitic lime treated samples after 0 cycles (samples H/D $\approx$ 2.0).....	134
Figure 5.13: Pareto and main effects on response to small strain constraint modulus for calcitic lime treated samples after 1 cycle (samples H/D $\approx$ 2.0).....	135
Figure 5.14: Pareto and main effects on response to small strain constraint modulus for dolomitic lime treated samples after 1 cycle (samples H/D $\approx$ 2.0).....	136
Figure 5.15: Pareto and main effects on response to small strain constraint modulus for calcitic lime treated samples after 28 days curing period (samples H/D $\approx$ 1.2).....	137
Figure 5.16: Pareto and main effects on response to small strain constraint modulus for dolomitic lime treated samples after 28 days curing period (samples H/D $\approx$ 1.2) .....	138
Figure 5.17: Pareto and main effects on response to small strain constraint modulus for calcitic lime treated samples after 1 cycle (samples H/D $\approx$ 1.2).....	138
Figure 5.18: Pareto and main effects on response to small strain constraint modulus for dolomitic lime treated samples after 1 cycle (samples H/D $\approx$ 1.2).....	139

Figure 5.19: Pareto and main effects on response to small strain constraint modulus for calcitic lime treated samples after 4 cycles (samples H/D $\approx$ 1.2). .....	140
Figure 5.20: Pareto and main effects on response to small strain shear modulus for calcitic lime treated samples after 0 cycles (samples H/D $\approx$ 2.0). .....	141
Figure 5.21: Pareto and main effects on response to small strain shear modulus for dolomitic lime treated samples after 0 cycles (samples H/D $\approx$ 2.0). .....	142
Figure 5.22: Pareto and main effects on response to small strain shear modulus for calcitic lime treated samples after 1 cycle (samples H/D $\approx$ 2.0). .....	143
Figure 5.23: Pareto and main effects on response to small strain shear modulus for dolomitic lime treated samples after 1 cycle (samples H/D $\approx$ 2.0). .....	144
Figure 5.24: Pareto and main effects on response to small strain shear modulus for calcitic lime treated samples after 0 cycles (samples H/D $\approx$ 1.2). .....	145
Figure 5.25: Pareto and main effects on response to small strain shear modulus for dolomitic lime treated samples after 0 cycles (samples H/D $\approx$ 1.2). .....	146
Figure 5.26: Pareto and main effects on response to small strain shear modulus for calcitic lime treated samples after 1 cycle (samples H/D $\approx$ 1.2). .....	146
Figure 5.27: Pareto and main effects on response to small strain shear modulus for calcitic lime treated samples after 4 cycles (samples H/D $\approx$ 1.2). .....	147
Figure 5.28: Pareto and main effects on response to the accumulated loss of mass for calcitic lime treated samples after 1 cycle (samples H/D $\approx$ 1.2). .....	148
Figure 5.29: Pareto and main effects on response to the accumulated loss of mass for dolomitic lime treated samples after 1 cycle (samples H/D $\approx$ 1.2). .....	149
Figure 5.30: Pareto and main effects on response to the accumulated loss of mass for calcitic lime treated samples after 4 cycles (samples H/D $\approx$ 1.2). .....	150
Figure 5.31: Pareto and main effects on response to the accumulated loss of mass for dolomitic lime treated samples after 1 cycle (samples H/D $\approx$ 1.2). .....	151
Figure 5.32: Pareto and main effects on response to the accumulated loss of mass for calcitic lime treated samples after 12 cycles (samples H/D $\approx$ 1.2). .....	152
Figure 5.33: Pareto and main effects on response to the accumulated loss of mass for dolomitic lime treated samples after 12 cycles (samples H/D $\approx$ 1.2). .....	153
Figure 5.34: Pareto and main effects on response to unconfined compressive strength for samples after 0 cycle (samples H/D $\approx$ 2.0). .....	154
Figure 5.35: Pareto and main effects on response to unconfined compressive strength for samples after 1 cycle (samples H/D $\approx$ 2.0). .....	155

Figure 5.36: Pareto and main effects on response to unconfined compressive strength for samples after 4 cycles (samples $H/D \approx 2.0$ ). .....	156
Figure 5.37: Pareto and main effects on response to unconfined compressive strength for samples after 12 cycles (samples $H/D \approx 2.0$ ). .....	157
Figure 5.38: Pareto and main effects on response to unconfined compressive strength for samples after 12 cycles (samples $H/D \approx 1.2$ ). .....	158
Figure 5.39: Pareto and main effects on response to small strain constraint modulus for samples after 0 cycle (samples $H/D \approx 2.0$ ). .....	159
Figure 5.40: Pareto and main effects on response to small strain constraint modulus for samples after 1 cycle (samples $H/D \approx 2.0$ ). .....	159
Figure 5.41: Pareto and main effects on response to small strain constraint modulus for samples after 0 cycle (samples $H/D \approx 1.2$ ). .....	160
Figure 5.42: Pareto and main effects on response to small strain constraint modulus for samples after 1 cycle (samples $H/D \approx 1.2$ ). .....	161
Figure 5.43: Pareto and main effects on response to small strain shear modulus for samples after 0 cycle (samples $H/D \approx 2.0$ ). .....	162
Figure 5.44: Pareto and main effects on response to small strain shear modulus for samples after 1 cycle (samples $H/D \approx 2.0$ ). .....	163
Figure 5.45: Pareto and main effects on response to small strain shear modulus for samples after 0 cycle (samples $H/D \approx 1.2$ ). .....	164
Figure 5.46: Pareto and main effects on response to the accumulated loss of mass for samples after 1 cycle (samples $H/D \approx 1.2$ ). .....	165
Figure 5.47: Pareto and main effects on response to the accumulated loss of mass for samples after 4 cycles (samples $H/D \approx 1.2$ ). .....	166
Figure 5.48: Pareto and main effects on response to the accumulated loss of mass for samples after 12 cycles (samples $H/D \approx 1.2$ ). .....	167
Figure 5.49: Pareto and main effects on response to unconfined compressive strength for samples after 12 cycles. ....	168
Figure 5.50: Pareto and main effects on response to small strain constraint modulus for samples after 0 cycle. ....	169
Figure 5.51: Pareto and main effects on response to small strain constraint modulus for samples after 1 cycle. ....	170
Figure 5.52: Pareto and main effects on response to small strain shear modulus for samples after 0 cycle. ....	171

Figure 5.53: Small strain constraint modulus for calcitic lime treated samples before and after curing.....	173
Figure 5.54: Small strain constraint modulus for dolomitic lime treated samples before and after curing.....	174
Figure 5.55: Small strain shear modulus for calcitic lime treated samples before and after curing. ....	175
Figure 5.56: Small strain shear modulus for dolomitic lime treated samples before and after curing.....	176
Figure 5.57: Unconfined compressive strength for calcitic lime treated samples after wetting-drying cycles.....	177
Figure 5.58: Unconfined compressive strength for dolomitic lime treated samples after wetting-drying cycles.....	177
Figure 5.59: Unconfined compressive secant modulus at failure for calcitic lime treated samples after wetting-drying cycles. ....	178
Figure 5.60: Unconfined compressive secant modulus at failure for dolomitic lime treated samples after wetting-drying cycles. ....	179
Figure 5.61: Small strain constraint modulus for calcitic lime treated samples throughout wetting-drying cycles. ....	180
Figure 5.62: Small strain constraint modulus for dolomitic lime treated samples throughout wetting-drying cycles. ....	180
Figure 5.63: Small strain constraint modulus for calcitic lime treated samples throughout wetting-drying-brushing cycles. ....	181
Figure 5.64: Small strain constraint modulus for dolomitic lime treated samples throughout wetting-drying-brushing cycles. ....	182
Figure 5.65: Small strain shear modulus for calcitic lime treated samples throughout wetting-drying cycles.....	183
Figure 5.66: Small strain shear modulus for dolomitic lime treated samples throughout wetting-drying cycles.....	183
Figure 5.67: Small strain shear modulus for calcitic lime treated samples throughout wetting-drying-brushing cycles. ....	184
Figure 5.68: Small strain shear modulus for dolomitic lime treated samples throughout wetting-drying-brushing cycles. ....	185
Figure 5.69: Accumulated loss of mass for calcitic lime treated samples throughout wetting-drying-brushing cycles. ....	186

Figure 5.70: Accumulated loss of mass for dolomitic lime treated samples throughout wetting-drying-brushing cycles. ....	186
Figure 5.71: Accumulated loss of mass for calcitic lime treated samples throughout wetting-drying cycles.....	187
Figure 5.72: Accumulated loss of mass for dolomitic lime treated samples throughout wetting-drying cycles.....	188
Figure 5.73: UDR for calcitic lime treated samples throughout wetting-drying cycles.....	189
Figure 5.74: UDR for dolomitic lime treated samples throughout wetting-drying cycles.....	189
Figure 5.75: Relation between $q_u$ and $E_{sec}$ after (a) 0 cycle (b) 1 cycle (c) 4 cycles (d) 12 cycles H/D $\approx$ 2.0 (e) 12 cycles H/D $\approx$ 1.2.....	191
Figure 5.76: Relation between $q_u$ and $M_0$ after (a) 0 cycle (b) 1 cycle (c) 4 cycles (d) 12 cycles H/D $\approx$ 2.0 (e) 12 cycles H/D $\approx$ 1.2.....	193
Figure 5.77: Relation between $q_u$ and $G_0$ after (a) 0 cycle (b) 1 cycle (c) 4 cycles (d) 12 cycles H/D $\approx$ 2.0 (e) 12 cycles H/D $\approx$ 1.2.....	196
Figure 5.78: Relation between $q_u$ and ALM for specimens with H/D $\approx$ 1.2 after 12 cycles..	198
Figure 5.79: Relation between $E_{sec}$ and ALM for specimens with H/D $\approx$ 1.2 after 12 cycles. ....	199
Figure 5.80: Relation between $E_{sec}$ and $M_0$ after (a) 0 cycle (b) 1 cycle (c) 4 cycles (d) 12 cycles (e) 12 cycles H/D $\approx$ 1.2.....	200
Figure 5.81: Relation between $E_{sec}$ and $G_0$ after (a) 0 cycle (b) 1 cycle (c) 4 cycles (d) 12 cycles H/D $\approx$ 2.0 (e) 12 cycles H/D $\approx$ 1.2.....	203
Figure 5.82: Relation between $G_0$ and $M_0$ for samples with H/D $\approx$ 2.0 after (a) 0 cycle (b) 1 cycle (c) 4 cycles (d) 12 cycles.....	204
Figure 5.83: Relation between $G_0$ and $M_0$ for samples with H/D $\approx$ 1.2 after (a) 0 cycle (b) 1 cycle (c) 4 cycles (d) 12 cycles.....	206
Figure 5.84: Relation between ALM and $M_0$ for samples with H/D $\approx$ 1.2 after (a) 1 cycle (b) 4 cycles (c) 12 cycles.....	208
Figure 5.85: Relation between ALM and $G_0$ for samples with H/D $\approx$ 1.2 after (a) 1 cycle (b) 4 cycles (c) 12 cycles.....	210
Figure 5.86: Relation between $q_u$ and $\eta/(B_{iv})^{0.13}$ after (a) 0 cycle (b) 1 cycle (c) 4 cycles (d) 12 cycles H/D $\approx$ 2.0 (e) 12 cycles H/D $\approx$ 1.2.....	212
Figure 5.87: Relation between $E_{sec}$ and $\eta/(B_{iv})^{0.13}$ after (a) 0 cycle (b) 1 cycle (c) 4 cycles (d) 12 cycles H/D $\approx$ 2.0 (e) 12 cycles H/D $\approx$ 1.2.....	215

Figure 5.88: Relation between $M_0$ and $\eta/(B_{iv})^{0.13}$ for samples with $H/D \approx 2.0$ after (a) 0 cycle (b) 1 cycle (c) 4 cycles (d) 12 cycles.....	217
Figure 5.89: Relation between $M_0$ and $\eta/(B_{iv})^{0.13}$ for samples with $H/D \approx 1.2$ after (a) 0 cycle (b) 1 cycle (c) 4 cycles (d) 12 cycles.....	219
Figure 5.90: Relation between $G_0$ and $\eta/(B_{iv})^{0.13}$ for samples with $H/D \approx 2.0$ after (a) 0 cycle (b) 1 cycle (c) 4 cycles (d) 12 cycles.....	221
Figure 5.91: Relation between $G_0$ and $\eta/(B_{iv})^{0.13}$ for samples with $H/D \approx 1.2$ after (a) 0 cycle (b) 1 cycle (c) 4 cycles (d) 12 cycles.....	223
Figure 5.92: Relation between $v_0$ and $\eta/(B_{iv})^{0.13}$ for samples with $H/D \approx 2.0$ after (a) 0 cycle (b) 1 cycle (c) 4 cycles (d) 12 cycles.....	225
Figure 5.93: Relation between $v_0$ and $\eta/(B_{iv})^{0.13}$ for samples with $H/D \approx 1.2$ after (a) 0 cycle (b) 1 cycle (c) 4 cycles (d) 12 cycles.....	226
Figure 5.94: Relation between ALM and $\eta/(B_{iv})^{0.13}$ for samples with $H/D \approx 1.2$ after (a) 1 cycle (b) 4 cycles (c) 12 cycles.....	228
Figure 5.95: Relation between $q_u$ and $\eta/(L_{iv})^e$ for calcitic lime treated soils after (a) 0 cycle (b) 1 cycle (c) 4 cycles (d) 12 cycles $H/D \approx 2.0$ (e) 12 cycles $H/D \approx 1.2$ .....	231
Figure 5.96: Relation between $q_u$ and $\eta/(L_{iv})^e$ for dolomitic lime treated soils after (a) 0 cycle (b) 1 cycle (c) 4 cycles (d) 12 cycles $H/D \approx 2.0$ (e) 12 cycles $H/D \approx 1.2$ .....	233
Figure 5.97: Relation between $E_{sec}$ and $\eta/(L_{iv})^e$ for calcitic lime treated soils after (a) 1 cycle (b) 4 cycles (c) 12 cycles $H/D \approx 2.0$ (d) 12 cycles $H/D \approx 1.2$ .....	235
Figure 5.98: Relation between $E_{sec}$ and $\eta/(L_{iv})^e$ for dolomitic lime treated soils after (a) 0 cycle (b) 1 cycle (c) 4 cycles (d) 12 cycles $H/D \approx 2.0$ (e) 12 cycles $H/D \approx 1.2$ .....	237
Figure 5.99: Relation between $M_0$ and $\eta/(L_{iv})^e$ for samples with $H/D \approx 2.0$ treated with calcitic lime after (a) 0 cycle (b) 1 cycle (c) 4 cycles (d) 12 cycles.....	238
Figure 5.100: Relation between $M_0$ and $\eta/(L_{iv})^e$ for samples with $H/D \approx 1.2$ treated with calcitic lime after (a) 0 cycle (b) 1 cycle (c) 4 cycles (d) 12 cycles.....	240
Figure 5.101: Relation between $M_0$ and $\eta/(L_{iv})^e$ for samples with $H/D \approx 2.0$ treated with calcitic lime after (a) 0 cycle (b) 1 cycle (c) 4 cycles (d) 12 cycles.....	241
Figure 5.102: Relation between $M_0$ and $\eta/(L_{iv})^e$ for samples with $H/D \approx 1.2$ treated with the dolomitic lime after (a) 0 cycle (b) 1 cycle (c) 4 cycles (d) 12 cycles.....	243
Figure 5.103: Relation between $G_0$ and $\eta/(L_{iv})^e$ for samples with $H/D \approx 2.0$ treated with calcitic lime after (a) 0 cycle (b) 1 cycle (c) 4 cycles (d) 12 cycles.....	244
Figure 5.104: Relation between $G_0$ and $\eta/(L_{iv})^e$ for samples with $H/D \approx 1.2$ treated with calcitic lime after (a) 0 cycle (b) 1 cycle (c) 4 cycles (d) 12 cycles.....	246



Figure 5.105: Relation between $G_0$ and $\eta/(L_{iv})^e$ for samples with $H/D \approx 2.0$ treated with dolomitic lime after (a) 0 cycle (b) 1 cycle (c) 4 cycles.....	247
Figure 5.106: Relation between $G_0$ and $\eta/(L_{iv})^e$ for samples with $H/D \approx 1.2$ treated with calcitic lime after (a) 0 cycle (b) 1 cycle (c) 4 cycles (d) 12 cycles.....	249
Figure 5.107: Relation between $v_0$ and $\eta/(L_{iv})^e$ for samples with $H/D \approx 2.0$ treated with calcitic lime after (a) 0 cycle (b) 1 cycle (c) 4 cycles (d) 12 cycles.....	250
Figure 5.108: Relation between $v_0$ and $\eta/(L_{iv})^e$ for samples with $H/D \approx 1.2$ treated with calcitic lime after (a) 0 cycle (b) 1 cycle (c) 4 cycles (d) 12 cycles.....	251
Figure 5.109: Relation between $v_0$ and $\eta/(L_{iv})^e$ for samples with $H/D \approx 2.0$ treated with dolomitic lime after (a) 0 cycle (b) 1 cycle (c) 4 cycles (d) 12 cycles. ....	252
Figure 5.110: Relation between $v_0$ and $\eta/(L_{iv})^e$ for samples with $H/D \approx 1.2$ treated with dolomitic lime after (a) 0 cycle (b) 1 cycle (c) 4 cycles (d) 12 cycles. ....	253
Figure 5.111: Relation between ALM and $\eta/(L_{iv})^e$ for samples with $H/D \approx 1.2$ treated with calcitic lime after (a) 1 cycle (b) 4 cycles (c) 12 cycles. ....	254
Figure 5.112: Relation between ALM and $\eta/(L_{iv})^e$ for samples with $H/D \approx 1.2$ treated with dolomitic lime after (a) 1 cycle (b) 4 cycles (c) 12 cycles. ....	255
Figure 5.113: Exponent $e$ determined for best-fit values after durability cycles. ....	257
Figure 5.114: Unconfined compressive strength for calcitic lime treated soils related to $\eta/L_{iv}$ and slenderness ratio.....	258
Figure 5.115: Unconfined compressive strength for dolomitic lime treated soils related to $\eta/L_{iv}$ and slenderness ratio.....	259
Figure 5.116: Unconfined compressive secant modulus for calcitic lime treated soils related to $\eta/L_{iv}$ and slenderness ratio.....	260
Figure 5.117: Unconfined compressive secant modulus for dolomitic lime treated soils related to $\eta/L_{iv}$ and slenderness ratio.....	261
Figure 5.118: Small strain constraint modulus for calcitic lime treated soils related to $\eta/L_{iv}$ and slenderness ratio. ....	262
Figure 5.119: Small strain constraint modulus for dolomitic lime treated soils related to $\eta/L_{iv}$ and slenderness ratio.....	264
Figure 5.120: Small strain shear modulus for calcitic lime treated soils related to $\eta/L_{iv}$ and slenderness ratio. ....	266
Figure 5.121: Small strain shear modulus for dolomitic lime treated soils related to $\eta/L_{iv}$ and slenderness ratio. ....	268

## LIST OF TABLES

Table 2.1: Chemical Requirements of Fly Ashes for use in Concrete (after ASTM C618, 2019)	37
Table 2.2: Durability Requirements (after USACE, 1984).	41
Table 2.3: Typical Poisson's ratio (POULOS, 2017).	60
Table 3.1: Experimental program tests.	68
Table 3.2: Classification based on the grain size distribution and LL – ASTM D2487 (ASTM, 2018).	70
Table 3.3: Activity index for some minerals (after Skempton, 1953).	75
Table 3.4: Proposed rating system for identification of dispersive soils (after BELL & WALKER, 1999).	84
Table 4.1: Soil grain size distribution parameters.	102
Table 4.2: Soil XRD Semi-quantitative analysis.	105
Table 4.3: Soil cations.	106
Table 4.4: Salts concentration-related parameters.	106
Table 4.5: pinhole test results with Pelotas soil.	107
Table 4.6: Pelotas soil dispersibility rating.	108
Table 4.7: Fly ash semi-quantitative analysis from XRD analysis.	110
Table 4.8: Calcitic lime semi-quantitative results from XRD analysis.	112
Table 4.9: X-Ray Fluorescence Spectrometry tests results on carbide lime.	113
Table 4.10: Primor dolomitic lime semi-quantitative composition from XRD analysis.	115
Table 4.11: Pinhole test results from dolomitic lime stabilized samples.	118
Table 4.12: Summarized materials' physical properties.	118
Table 4.13: Research factorial design.	119
Table 4.14: Wetting-drying-brushing Durability tests design.	120
Table 4.15: Wetting-drying durability tests design.	120
Table 4.16: Unconfined Compressive Strength Tests design.	121
Table 5.1: Exponent values in lime key parameter relations.	230
Table 5.2: Comparison between results for samples with different slenderness ratios.	270

## LIST OF SYMBOLS

ALM – Accumulated loss of mass

ALM<sub>n</sub> – Accumulated loss of mass after  $n$  durability cycles

B<sub>iv</sub> – Volumetric binder content

CL – Calcitic lime content

C<sub>c</sub> – Coefficient of curvature

C<sub>u</sub> – Coefficient of uniformity

C<sub>iv</sub> – Volumetric cement content

C<sub>c</sub> – Compression index

C<sub>v</sub> – Coefficient of consolidation

c' – Cohesion intercept

DL – Dolomitic lime content

D<sub>10</sub> – effective grain size

D<sub>30</sub> – effective grain size

D<sub>50</sub> – effective gran size (particle mean size)

D<sub>60</sub> – effective grain size

E – Longitudinal elastic modulus

E<sub>sec</sub> – Secant modulus

E<sub>sec,n</sub> – Secant modulus after  $n$  durability cycles

FA – Fly ash content

G<sub>0</sub> – Small strain shear modulus

$G_{0,n}$  – Small strain shear modulus after  $n$  durability cycles

$k_h$  – Hydraulic conductivity

LC – Lime content

LL – Liquid limit

LT – Lime type

$L_{iv}$  – Volumetric lime content

$M_0$  – Small strain constraint modulus

$M_{0,n}$  – Small strain constraint modulus after  $n$  durability cycles

$M_R$  – Modulus/strength ratio

PL – Plasticity limit

PI – Plasticity index

$q_u$  – Unconfined compressive strength

$q_{u,n}$  – Unconfined compressive strength after  $n$  durability cycles

SC – Clayey sand soil

SW – Soil/mixture dry unit weight

$S_r$  – degree of saturation

$S_s$  – Specific surface area

$t_p$  – P-wave travel time

$t_s$  – S-wave travel time

$t$  – time (or number of cycles) imposed on the specimens

$u_x$  – Particle motion in the x-direction

$u_y$  – Particle motion in the y-direction

$V_p$  – P-wave velocity

$V_s$  – S-wave velocity

$v_v$  – Specimen voids volume

$v_c$  – Specimen cement volume

$v_t$  – Specimen total volume

$w$  – moisture content

$\alpha$  – error rate in factorial analysis

$\gamma_d$  – Soil specific dry unit weight

$\gamma_s$  – Solids specific weight

$\epsilon_a$  – Axial strain

$\epsilon_{a \text{ máx.}}$  – Maximum axial strain

$\eta$  – Porosity

$\lambda$  – Wavelength

$\nu$  – Poisson's ratio

$\nu_0$  – Small strain Poisson's ratio

$\nu_{0,n}$  – Small strain Poisson's ratio after  $n$  durability cycles

$\rho$  – Bulk density

$\sigma'_0$  – Effective confinement stress

$\phi'$  – Effective friction angle

$\phi'_{cs}$  – Critical state effective friction angle

$\Phi_h$  – Pinhole test final hole diameter

$\Phi_n$  – Pinhole test needle diameter

$\psi$  – weathering-erosive susceptibility

$\omega$  – degree of the imposed weathering-erosive condition

## **LIST OF ABBREVIATIONS**

ABNT – Associação Brasileira de Normas Técnicas (Brazilian Association for Technical Standards)

ASTM – American Society for Testing Materials

BET – Brenauer-Emmet-Teller specific surface area testing method

CEC – Cation exchange capacity

CROSS – Cation ratio of soil structural stability

DOE – Design of experiments

EFA – Erosion function apparatus

ESP – Exchangeable sodium percentage

ICL – Initial consumption of lime

IE – Internal erosion

MCAR – Monovalent cations adsorption ratio

NCL – Normal compression line

NLA – National Lime Association

NBR – Norma Brasileira (Brazilian Standard)

SAR – Sodium adsorption ratio

SR – Slenderness ratio

TDS – Total dissolved salts

UFRGS – Universidade Federal do Rio Grande do Sul (Federal University of Rio Grande do Sul)

UCS – Unconfined compressive strength test

UDR – Unconfined compressive strength durability ratio

UPV – Ultrasonic pulse velocity

USCS – Unified soil classification system

XRD – X-Ray Diffraction

XRF – X-Ray Fluorescence



## 1 INTRODUCTION

When dealing with heterogeneous materials such as geomaterials, it is always a challenge for engineers to know what are the real intervenient conditions of concerning, whether it is imposed by the man (loads of a structure, vehicles, trains, machines) or by the environment (rainfall, earthquakes, UV radiation, animals, roots, seepage), and especially how these materials would behave under these particular conditions. As a consequence, engineers must deal with high uncertainties in the behavior of those materials.

### 1.1 SOILS IN ENGINEERING

Along with civilization development, to optimize their limited resources and production, when searching for a place to settle, mankind had three main concerns: water, fertile soil, and an appropriate place to raise buildings. Since nowadays, with the rise of the global population, it is understandable that most fertile and irrigated places have already been occupied, so as the best places to raise buildings, infrastructure, and earthworks. Thereby, recent civilization has to deal with these issues, which became a challenge for contemporary science. That is why Geotechnical Engineers will face increasingly poor soil conditions at tunnels, slopes, roads, excavations, dams, landfills, and foundation designs.

Poor condition soil may refer to many undesirable issues like soft clays, organic soils, liquefiable soils, expansive soils, high creep susceptibility, erodible soil, low particle strength, unfavourable anisotropy direction, collapsible or dispersive behavior, among others, depending on the conditions imposed to the soil mass. Those conditions are usually not easily evaluated and may lead to severe damages when not considered in the design, and when considered, in many cases, the development became impracticable.

Hence, there is a growing need not only for water treatment for purification and soil treatment for agriculture but also for improving their geotechnical quality for building. That is why in many cases it is not only important to know the soil behavior as it is, but mostly as it could be in case of a soil improvement application.

## 1.2 SOIL IMPROVEMENT

Soil Improvement is the alteration of any property of a soil to improve its engineering performance. Examples of soil improvement are increased strength (e.g. pavement subgrade), reduced compressibility (e.g. foundation of a structure), and reduced permeability (e.g. foundation of a dam). Soil improvement may be a temporary measure to permit the construction of a facility, or it may be a permanent measure to improve the performance of the completed facility. Soil improvement techniques can be classified in various ways: according to the nature of the process involved, the material added, the desired result, etc. (LAMBE & WHITMAN, 1979)

As above mentioned, one of the obstacles for geotechnical engineers is the dispersivity of some soils. This phenomenon is caused by the deflocculation in presence of pure or relatively pure water, forming colloidal suspensions and making the soil mass susceptible to erosion and piping. There are basically two ways to prevent the erosion of this kind of soil. One is through a full drainage system (superficial and subsuperficial) and maybe prevention from water to fall on the exposed soil in a slope, for example. That solution generally requires a huge and constant investment (MUKHLISIN & AZIZ, 2016), and drainage systems also need monitoring and cleanups to avoid clogging (PINKY, 2008). A second alternative is the soil improvement technique, through chemical stabilization and the creation of bonds between soil particles. In many cases, the costs associated with the second alternative may be a less costly and more viable alternative.

## 1.3 SCOPE

This study proposes to address the problem related to a natural dispersible soil with the soil improvement technique through the addition of fly ash and two different types of lime: calcitic and dolomite, analyzing durability, strength, stiffness, and key parameters for a more rational dosage method of admixture stabilization.

The materials involved were all characterized, especially the soil. The main tests of the experimental program consist of unconfined compressive strength test (UCS); Ultrasonic Pulse Velocity (UPV), related to small strain stiffness; and durability tests through wetting-drying-brushing or wetting-drying cycles.

## 1.4 OBJECTIVES

The primary objective of this research is to study the behaviour of mixtures of a natural dispersive soil, fly ash, and two types of lime (a calcitic and a dolomitic lime) in terms of strength, stiffness and, mostly, durability.

The secondary objectives are:

- a) The evaluation of soil dispersibility behaviour in treated samples.
- b) Determining the stiffness of the cemented admixtures through a small strain approach.
- c) To compare the durability, strength, and stiffness of treatments with a calcitic and dolomitic lime.
- d) To understand the effect of durability cycles on the mechanical response.
- e) To quantify the effect of dry unit weight, fly ash, and lime content on durability, strength, and stiffness through a full factorial experiment.
- f) To evaluate an applicable dosage methodology based on soil weight, binder, and lime content in the admixture.
- g) To analyze the slenderness ratio effect on mixture response to unconfined compressive strength tests.

## 1.5 DELIMITATION

The research is delimited to the study of a dispersive soil found in a southern region in Brazil, improving the soil with the addition of fly ash, which was obtained from a nearby coal mine, and two types of lime: calcitic and dolomitic.

## 1.6 LIMITATION

This work is limited to:

- a) 28 days of curing period.
- b) Unconfined test response.

## 1.7 RELEVANCE

The region of Pelotas (southern Brazil) faces problems with dispersive soils at different locations, as they are still difficult to overcome through conventional techniques. An alternative to improve the durability of those soils at the field is to improve with lime and pozzolans like fly ash.

This work is innovative since the behavior of dispersive improved soils are yet poorly understood, and the chemical addition could provide a costly alternative to more dispendious solutions that are frequently employed to prevent or to remediate intensive erosive processes or gullies.

The soil studied comes from an area with lateritic concretions, but only partially, insufficient to develop a resistance to the dispersion of particles in the whole site. Besides, its grain size distribution is not commonly presented by dispersive soils, and the low clay content may reduce the effect of the soil on cementation since the low amorphous particle content turns the pozzolanic reactions almost independent of the soil-lime reactions.

The comparison between a calcitic and a dolomitic lime is important too to assess the effect on durability response, which behaves differently than the strength response in chemical soil bond.

Beyond that, the soil strength is tested too upon strength throughout wetting and drying cycles, and a comparison is made between the standardized durability tests and a test without scratching and smaller samples for those soils.

## 1.8 STRUCTURE

The present work is outlined as structured as follows.

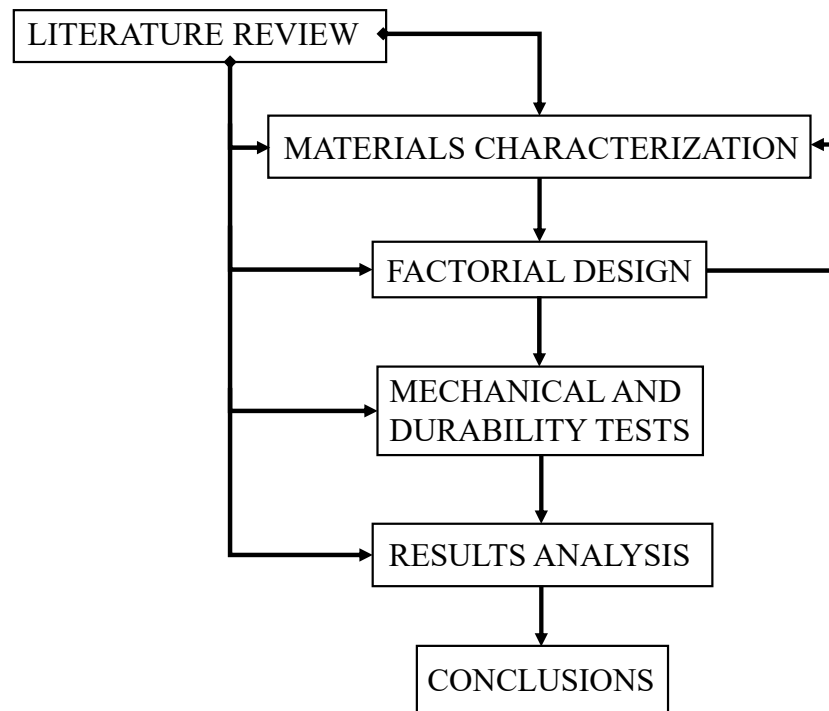


Figure 1.1: Research structure.

This research is structured as explained:

Chapter 1 presents the motivation, scope, objectives, limitation, and relevance of this work; Chapter 2 addresses the literature review; Chapter 3 brings an experimental review and characteristics of the experimental methodology employed. Chapter 4 contains the materials involved in this research, so as their specific characteristics and their relevant aspects. Chapter 5 regards the results of the tests developed in the research, which chapter 6 makes considerations about, remarks and suggestions for forthcoming studies. Next, the references consulted for the development of this work are presented. At last, the appendixes are stated.

## 2 LITERATURE REVIEW

This chapter focuses on the literature review that contributed to the realization of this research.

### 2.1 MATERIALS

There are different types of structures built by man – buildings, bridges, culverts, water tanks, storage bins, roads, transmission towers, machines, etc. Such structures are built up of several structural elements joined together suitably. Structures are designed to withstand loads, i. e., forces, and moments due to different causes. While some structures, like aircraft structures, machine foundations, etc. necessarily have to be designed for forces due to motion, many are designed considering them to be in equilibrium, or at rest. (SUBRAMANIAN, 2010)

Friction is the mechanical force which resists movement (dynamic or kinetic friction) or hinders movement (static friction) between two sliding or rolling surfaces in contact. [...] Friction occurs essentially in two different modes: sliding and rolling friction. The relationship between the frictional force and the load or weight of the sliding object differs for dry, or unlubricated, surfaces and lubricated surfaces. The coefficient of sliding friction is constant but depends on the type of material. (BART et al., 2013)

Strictly speaking, materials science involves investigating the relationship that exists between the structures and properties of materials. In contrast, materials engineering involves, on the basis of these structure-property correlations, designing or engineering the structure of a material to produce a predetermined set of properties. (CALLISTER, 2015)

#### 2.1.1 Wear and Damage

Wear is defined as progressive damage resulting in material loss due to contact between adjacent working parts. [...] The effects of wear are commonly detected by visual inspection of surfaces. (BART et al., 2013)

Wear by abrasion and erosion are forms of wear caused by contact between a particle and solid material. Abrasive wear is the loss of material by the passage of hard particles over a surface. Erosive wear is caused by the impact of particles against a solid surface. Cavitation is caused

by the localized impact of fluid against a surface during the collapse of bubbles. (STACHOWIAK & BATCHELOR, 2014)

### 2.1.2 Geomaterials

Generally, geomaterials are distinguished from common materials for their particularities, being often defined as porous/particulate materials derived from Earth Crust. Fookes (1991), more precisely, defined them as processed or unprocessed soils, rocks, or minerals used in the construction of buildings or structures, including man-made construction materials manufactured from soils, rocks, or minerals. The definition deliberately includes man-made materials such as bricks or cement but excludes allied engineering materials whose manufacturing is more extensive, such as steel and synthetic paints. (INGHAM, 2013). Most geotechnical engineering is at the top of a few 10s of meters of the ground. The materials are soils and rocks and the works are usually within the influence of groundwater (ATKINSON, 2014).

#### 2.1.2.1 Granular media

Granular materials are random assemblies of small grains in very large numbers. The property which differentiates granular materials from other solids, like, e.g., metals, is their pronounced pressure sensitivity, which is attributed to the existence of internal friction and which is developing at grain contacts. Granular materials are porous media. From a continuum mechanics point of view, their porous or granular structure is described by macroscopic properties of the granular assembly such as porosity and bulk density ( $\rho$ ). Since grains are practically incompressible and mass convection is in most cases negligible, mass balance yields that volume changes are simply due to changes in porosity. In the case of a granular medium that is fully saturated with a pore fluid of low viscosity (e. g. water), ‘effective’ stress is defined as a measure of the intergranular forces. (VARDOULAKIS, 2001)

The uncertainties regarding interior stresses in samples of sand have led to the development of models of granular media that are geometrically simpler than sand and for which the stresses and displacements can either be calculated or measured. (CUNDALL & STRACK, 1979).

#### 2.1.2.2 Clay minerals

Most naturally occurring deposits of clay are formed in water. In the presence of positively charged cations, as in marine environments, the fabric of the deposit will be flocculated. These

edge-to-face structures are characterized by initially random particle orientation and relatively open voids. With consolidation due to further accumulation of overburden soil, the clay particles tend toward more horizontal orientations. (ROWE, 2001).

It is important to note that some agencies classify clay as particles smaller than 0.005 mm in size, and others classify it as particles smaller than 0.002 mm in size. However, it needs to be realized that particles defined as clay on the basis of their size are not necessarily clay minerals (DAS, 2008). In scientific terminology clay is a natural earthy material with plastic properties when moist, of very fine grain-size and composed largely of hydrous aluminum and magnesium silicates. (GILLOT, 1987).

Accordingly, phyllosilicates of any size, such as macroscopic mica, vermiculite, and chlorite may be regarded as clay minerals (BERGAYA et al., 2006). As the name indicates, phyllosilicate minerals are layer structures. That is, the atomic arrangement is such that there are easily recognizable quasi-two-dimensional fragments, strongly bonded internally, which are stacked one on top of the other with a much weaker bonding between the layers. (GIESE, 2002). For simplicity sake, we refer to an assembly of layers as a ‘particle’ – often referred to as ‘crystallite’–, and an assembly of particles as an ‘aggregate’. Accordingly, we may distinguish between interlayer, interparticle, and interaggregate pores (figure 2.1). The arrangement of the particles or aggregates leads to different morphologies, such as plates, tubes, laths, and fibres. All phyllosilicates are therefore porous, containing pores of varied size and shape (BERGAYA et al., 2006) They have in common the same two types of structural element. These are  $\text{SiO}_4$  silica tetrahedron polymerized into sheets and the  $\text{Mg}(\text{OH})_2$  brucite-like, or  $\text{Al}(\text{OH})_3$  gibbsite-like, octahedral element both of which form sheet or layer structures (GILLOT, 1987).



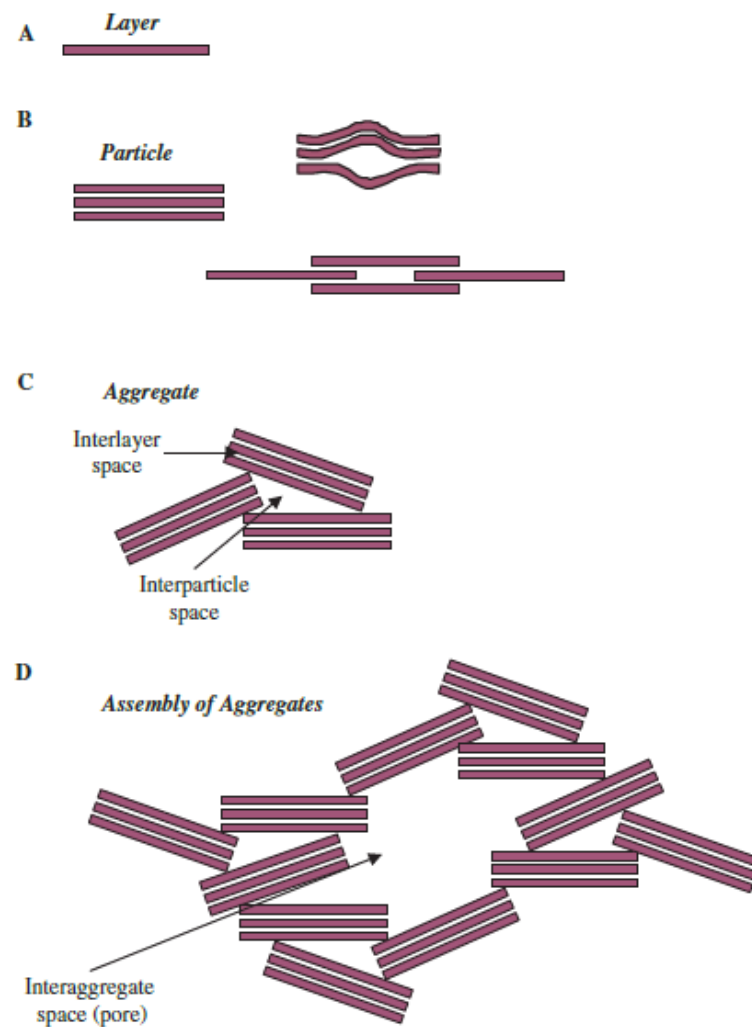


Figure 2.1: Diagram showing (A) a clay mineral layer; (B) a particle, made up of stacked layers; layer translation and deformation can give rise to a lenticular pore; (C) an aggregate, showing an interlayer space and an interparticle space; and (D) an assembly of aggregates, enclosing an interaggregate space (pore) (BERGAYA et al., 2006).

A clay particle is a colloid because of its small and irregular shape. The smaller a particle size the larger its specific surface (LAMBE & WHITMAN, 1979). The colloidal state of subdivision comprises particles with a size sufficiently small ( $\leq 1 \mu\text{m}$ ) not to be affected by gravitational forces but sufficiently large ( $\geq 1 \text{ nm}$ ) to show marked deviations from the properties of true solutions. In this particle size range, 1 nm (10 Å) to 1  $\mu\text{m}$  (1000 nm), the interactions are dominated by short-range forces, such as van der Waals attraction and surface forces (BERGNA, 1994) Mechanically, the layers are more strongly bonded than the interlayers so

that cleavage will always occur along the interlayer regions. [...] The stronger and more specific the interlayer bond is, generally, the more regular and perfect will be the stacking. [...] Conversely, the weaker and more diffuse the interlayer bonding, the less regular the stacking, the greater the number of stacking faults, and ultimately, one has a near-random stacking which is termed ‘turbostratic’ (GIESE, 2002).

Some materials may be crystalline (the material’s atoms are arranged in a periodic fashion) or they may be amorphous (the arrangement of the material’s atoms does not have long-range order). [...] The characteristics of crystals or grains (size, shape, etc.) and that of the regions between them, known as the grain boundaries, also affect the properties of materials. (ASKELAND & WRIGHT, 2016). In weathering conditions, the rocks are affected by interaction with slightly acidic rainwater which triggers either a congruent dissolution of the unstable minerals or the formation of clay minerals. [...] The amorphous layer (gel) is a by-product of incongruent dissolution. (VELDE & MEUNIER, 2008). The nearest neighbours of a particular atom may be essentially the same as in a crystal of the same chemical composition but there is no regularly repeated periodic pattern in the disposition of next nearest and more distant neighbours. Such solids are sometimes described as amorphous [...] The crystalline components are inorganic minerals and the amorphous constituents may be either inorganic or organic (GILLOT, 1987). The high strength and durability of Roman cement 2000 years ago is now known to be due to the use of a special volcanic ash that is an almost pure form of amorphous colloidal silica (BERGNA, 1994)

## 2.2 WATER EROSION AND DISPERSIVE SOILS

Erosion is damage caused to geomaterials by the action of wind, water, ice, and even by anthropic agents. This work focuses on erosion by water, where dispersion and soil erosion phenomena are strictly related since the second is a consequence of the first one, though the water erosion process can occur isolated from the dispersion occurrence. Paige-Green (2008) emphasizes that both dispersive and erodible soils increase the cost of construction, but dispersive ones may lead to far more serious problems.

### 2.2.1 Erosion Issue

Soil erosion, displacement of soil from the place of its formation by causative agents (e.g., raindrop, runoff, wind, gravity, etc), and its deposition at a depressional and/or protected site,

is a natural geologic phenomenon (LAL, 2003), but soil erosion has caused damages to a great variety of structures and economic activities. Damages associated with soil erosion and stream sedimentation have been reported on roads (XU et al., 2009), construction sites (KAUFMAN, 2000), ecological sites (CHEN et al., 2019), Bridge scour, migration of river meanders, the retreat of cliffs (BRIAUD, 2008), Levee overtopping (HUGHES, 2008), sequential failure of gully headwalls (BRADFORD et al., 1978), dams pipes (BONELLI, 2013), agroecosystems (MARTÍNEZ-MENA et al., 2020), among many others land and structures grievance.

Erosion involves the soil or rock through its erodibility, the water through its velocity, and the geometry of the obstacles through its size and shape. Knowledge of these three components is needed for any erosion problem to be studied and solved. (BRIAUD, 2008) Erodibility could be expressed as critical velocity or critical shear stress, values below which no erosion occurs. Values of critical shear stress based on mean grain size obtained from erosion function apparatus (EFA) tests, for non-dispersive soils, are presented in figure 2.2.

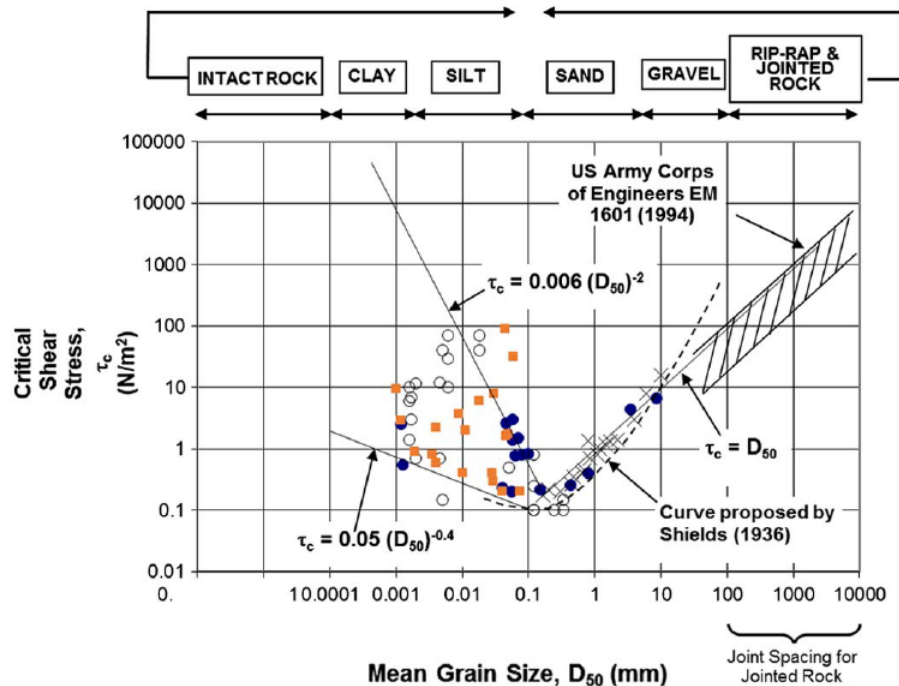


Figure 2.2: Critical shear stress based on mean grain size (BRIAUD, 2008)

Internal erosion (IE) refers to any process by which soil particles are eroded from within or beneath a water-retaining structure. IE is a particularly dangerous process as it gradually

degrades the integrity of a structure in a manner that is often completely undetectable (ROBBINS & GRIFFITHS, 2018). Internal erosion, also known as piping, is one of the major causes of earth dam failures (SALIBA et al., 2019). Piping refers to erosive action where sediments are removed by seepage forces, hence forming subsurface cavities and tunnels. For erosion tunnels to form, the soil must have some cohesion; the greater the cohesion, the wider the tunnel. In fact, fine sands and silts, especially those with dispersive characteristics, are most susceptible to piping failures. Obviously, the danger of piping occurs when the hydraulic gradient is high, that is, when there is a rapid loss of head over a short distance. (BELL, 2007)

Bonelli (2012) mentions there are four types of boundary conditions that cause internal soil erosion (figure 2.3):

- a) Erosion in concentrated leak: the water flows through a crack, a hole, or a hollow, thus eroding the walls;
- b) Backward erosion: the water flow erodes the surface of the soil from where it comes, thus causing a backward erosion of this exit surface;
- c) Contact erosion: the water flows through a very permeable soil, thus eroding a fine soil at the interface;
- d) Suffusion: the outflow erodes the smaller grains through the pores of the coarser grains.

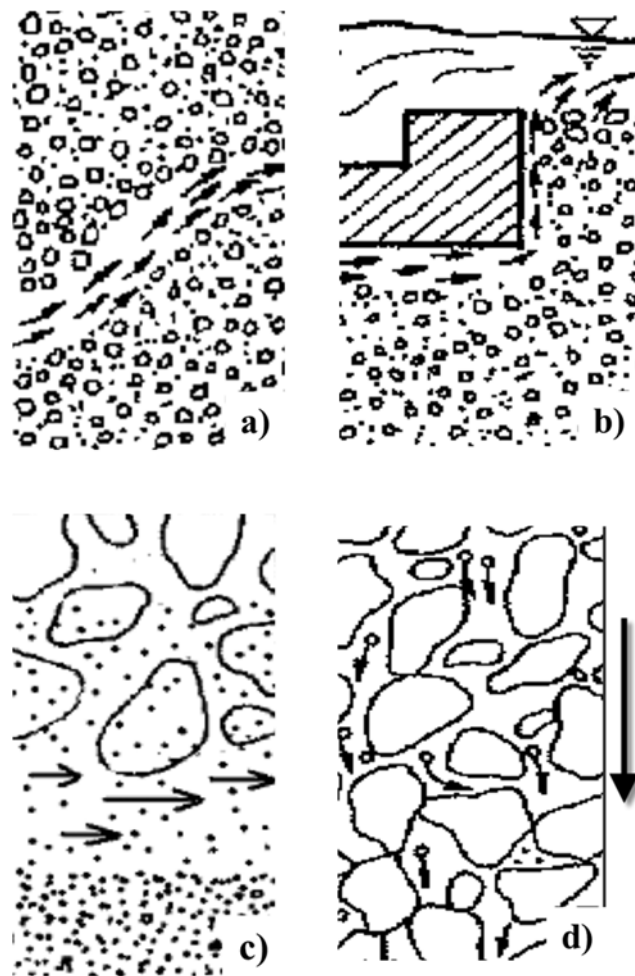


Figure 2.3: Types of erosion: a) pipe or crack internal erosion; b) backward internal erosion (generalized or local, i.e., at the bottom of the pipe; c) internal contact erosion (between gravel and silt; d) suffusion, or the internal instability of a soil, or volume erosion (after from FELL & FRY, 2007).

Zhang et al. (2016) outstand, based on laboratory, on-field internal erosion tests, and analysis of past failure/incident cases of embankments triggered by internal erosion, that this process can be divided into four phases: initiation, continuation, progression to form a pipe, and formation of a breach.

Besides the occurrence of internal erosion, more related to dams and embankments, Osman (2014) addressed four types of water erosion that are generally recognized:

- a) Splash or Rainsplash erosion: as a result of raindrops striking a bare soil surface, soil particles may be thrown through the air over distances of several centimeters. Continuous exposure to intense rainstorms considerably weakens the soil. The soil is also broken up by the weathering processes, both mechanical, by alternative wetting and drying, freezing and thawing and frost action, and biochemical (MORGAN, 2005);
- b) Sheet erosion: when a thin layer of soil is removed by raindrop impact and shallow surface flow from the whole slope, it is called sheet erosion. It removes the finest fertile topsoil with plenty of nutrients and organic matter. [...] Detached particles are transported by runoff water as overland flow. [...] Sheet erosion removes a deeper layer of soil gradually if allowed to proceed unhindered and the subsoil is exposed over a large area. [...] However, slopes are not so uniform over the whole area, and water accumulates in tiny channels so that the surface is crisscrossed by discontinuous rilllets. It is then known as the interrill erosion. (OSMAN, 2014);
- c) Rill erosion: when runoff water concentrates and flows through fingerlike channels (rills) from upland areas carrying soil particles, the erosion is called rill erosion, and the soil eroded from between the rills is called ‘inter-rill erosion’. Rill erosion is caused primarily by runoff, whereas inter-rill erosion results primarily from raindrop impact. Rills usually develop because of tillage marks, surface roughness or topographic variations and later by flow patterns of runoff. Once rill erosion begins, it typically progresses upslope by a series of intensely erodible head cuts. Place, where concentrated runoff from a slope is sufficient in volume and velocity to cut deep trenches or where concentrated water continues cutting in the same groove (such as rill) making a deep soil incision, is called gully (DAGAR & SINGH, 2018);
- d) Gully erosion: defined as the erosion process by which runoff water cuts new unstable channels into erodible soil and weathered rock (DAGAR & SINGH, 2018). Gully erosion begins when runoff concentrates into channels and rills develop which may later enlarge into deep trenches in the land surface over time. (LUFFMAN et al., 2015). According to Osman (2014), gullies are large channels deeper than 30 cm in steep slopes, and can be of two types: ephemeral

(shallow) or permanent (larger). It is defined as the erosion process whereby runoff water accumulates and often recurs in narrow channels and, over short periods, removes the soil from this narrow area to considerable depths. (POESEN et al., 2003) Gully erosion is a potentially lethal geomorphological process and thus constitutes a major threat to life and property (IONITA, 2015). Vendrusculo (2014) highlights the occurrence of this geomorphic process when rainfall, flow accumulation and slope are pronounced, besides the influence of wetting-drying (POEL et al., 1986) and freezing-thawing cycles (THOMAS et al., 2008). Gullies not only occur in marly badland and mountainous or hilly regions but also more globally in soils subjected to soil crusting such as loess and sandy soils or in soils prone to piping and tunneling such as dispersive soils (VALENTIN & POESEN, 2005).

According to Bastos (1999), erodibility is one of the main factors conditioning erosion in soils, is defined as the soil property associated with a higher or lower susceptibility of particles to detach from the soil mass, being transported by the action of an erosive agent. The triggering conditions for internal erosion are schematically shown in figure 2.4, where beyond erodibility (material conditions), the hydraulic and mechanical conditions are also accounted for:

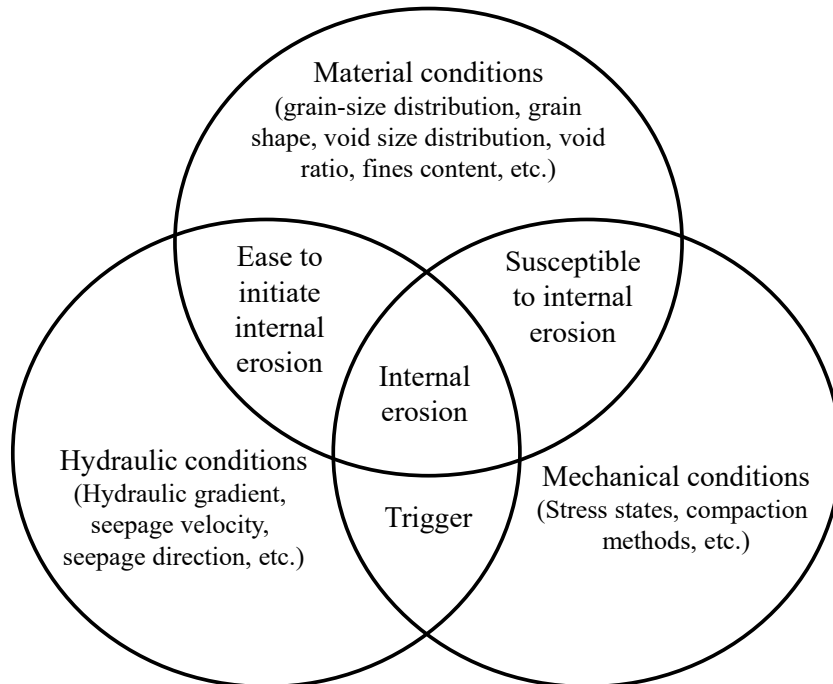


Figure 2.4: Conditions for internal erosion triggering (after ZHANG et al., 2016).

### 2.2.2 Dispersion phenomenon

Some fine-grained soils are structurally unstable, easily dispersed, and therefore, easily eroded. Soils in which the clay particles will detach spontaneously from each other and the soil structure and go into suspension in quiet water are termed dispersive clays (MITCHELL & SOGA, 2005). Dispersion occurs in cohesive soils when the repulsive forces between clay particles exceed the attractive forces, thus bringing about deflocculation so that, in the presence of relatively pure water, the particles repel each other to form colloidal suspensions. In non-dispersive soil, there is a definite threshold velocity below which flowing water causes no erosion. The individual particles cling to each other and are removed by water flowing with a certain erosive energy. By contrast, there is no threshold velocity for dispersive soil, the colloidal clay particles go into suspension even in quiet water and, therefore, these soils are highly susceptible to erosion and piping. Dispersive soils contain a moderate to a high content of clay material but there are no significant differences in the clay fractions of dispersive and non-dispersive soils, except that soils with less than 10% clay particles may not have enough colloids to support dispersive piping. Dispersive soils contain a higher content of dissolved sodium (up to 12%) in their pore water than do ordinary soils. The clay particles in soils with high salt contents exist as aggregates and coatings around silt and sand particles, and the soil, if flocculated. Dispersive soils generally occur in semi-arid regions where the annual rainfall is less than 860 mm (BELL & WALKER, 1999).

The dispersive soil behaviour has caused many damages, especially to embankments and dams and, according to Sherard (1974), the existence of highly dispersive clays family was not recognized until 1972, when the phenomena like eroded cavern ('bear caves') associated with failures could be explained.

The stability of soil aggregates, and hence that of pore systems, depends to a large extent upon the attractive and repulsive forces arising from intermolecular and electrostatic interactions between the soil solution and soil particles. When a dry soil aggregate is placed in contact with water, the interactive forces lower the potential energy of the water molecules; the resulting release of energy is used partly for the structural transformation of the clay surfaces in the aggregates, the rest being released as heat. Slaking, swelling, and clay dispersion are the major mechanisms by which the aggregates, and hence soil structure, are damaged during these transformations. (RENGASAMY & OLSSON, 1991).



The stages are given as below, from Rengasamy & Olsson (1991) research:

- a) Stage I to II – Initial Wetting of Air-Dry Aggregates:
  - The clay particles in air-dry aggregates in stage I are linked by strong attractive pressures of magnitude  $MN.m^{-2}$ . At this stage, the clay surfaces may have at least one layer of adsorbed water molecules and the distance between any two adjacent clay particles is generally less than 1 nm. On wetting, repulsive forces are generated (stage II).
- b) Stage II to III – Slaking
  - At stage III the net pressure is attractive. If the clay particles are calcium saturated, further wetting does not increase the interparticle distance beyond 2-3 nm. For example, while slow wetting may control slaking in calcic aggregates, it will not prevent a dispersive breakdown in sodic aggregates.
- c) Stage II to IV – Spontaneous Dispersion
  - When sodium is the principal adsorbed cation, the interparticle distance continuously increases with continued wetting to beyond 7 nm and the clay particles become completely independent of each other, resulting in clay dispersion (stage IV). The proportion of clay particles thus separated depends on the SAR. At unsaturated water contents, insufficient water leads to interparticle separation of 2 to 7 nm but not to the extent of complete separation; this swelling is in addition to the crystalline swelling occurring under non-sodic conditions. It appears that similar mechanisms are involved in interlayer separations in smectitic clays and interparticle separations induced by sodium in clays such as kaolinite and illite.
- d) Stage III to IV – Mechanical Dispersion
  - The application of mechanical pressure in the range of  $N m^{-2}$  to  $kN m^{-2}$  to the calcic clay aggregates in stage III is sufficient to separate the clay particles beyond 2 nm. At separating distances greater than  $2/k$ , where  $k$  defines double layer thickness in nm, electrical repulsive forces predominate. With continued wetting, the particles become progressively separated, finally reaching stage IV. Thus, a calcic clay aggregate disperses when

uniformly remoulded at or above a critical water content known as the water content for dispersion. At lower water contents, the attractive structural forces resist particle separation.

Physically, Aitchinson et al. (1963) explain piping occurs when, on deflocculation started by wetting, clay aggregates break into finer particles, and those clay particles in suspension are carried by the seepage flow through the inter-aggregate pores, causing the material loss through internal erosion. When the flow rate increases, macro failures take place, and the potential damages are higher.

### 2.2.3 Dispersion and chemical stability

The literature is rich in studies about dispersive soils, but most of the soils studied consist of clays. As explained, many soils may present erodibility without dispersive behaviour. Chemically, the dispersion phenomenon appears to be related to the ions concentration in clays. For Bell and Walker (1999), dispersion is dependant both on soil mineralogy and chemistry, but also on dissolved salts and pore eroding water.

Surface charge on a particle results in an unequal distribution of ions in the polar medium in the vicinity of the surface. Ions of opposite charge (counterions) are attracted to the surface, and ions of like charges (co-ions) are repelled away from the surface. This unequal distribution gives rise to a potential across the interface. The exact distribution of the counterions in the solution surrounding the charged surface. Electrostatic attraction, thermal motion, and forces other than electrostatic (specific adsorption) influence the counterions in the vicinity of the surface. A single charged surface and its dissolved counterions are collectively known as the *electrostatic diffuse double-layer* (Figure 2.5). Since the range of the electrostatic interaction is for many practical cases relatively short compared to the size of the charged particles, an approximation can reasonably be made whereby (model) spherical particles are replaced by (model) parallel infinite planes. (KRISTER, 2002).

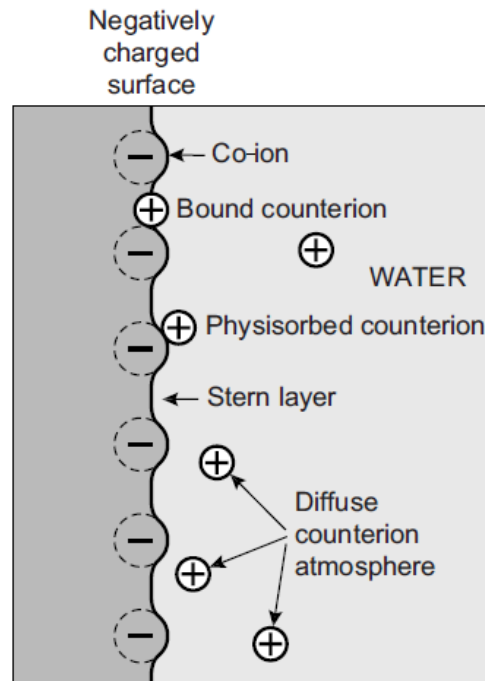


Figure 2.5: Diffuse electric double-layer (ISRAELACHVILI, 2011).

Some clay minerals can reversibly adjust the composition of their interlayer zone as a function of that of the solution. This property is known as the cation exchange capacity (CEC). It is measured by the number of positive charges held by exchanged cations expressed as milliequivalents per 100 g (meq) or more recently in centimols per kg ( $\text{cmol kg}^{-1}$ ). Cations can only be exchanged if they are weakly bonded to the external or internal surfaces (interlayer spaces) of crystals. (VELDE & MEUNIER, 2008). Nabil et al. (2020) also remarked that when CEC is too high, the strength of lime-treated soil tends to be lower because of the overconsumption of  $\text{Ca}^{++}$  ions needed in pozzolanic reactions. Figure 2.6 presents values of CEC for the most common minerals in clayey soils.

Mineral	CEC ( $\text{cmol.kg}^{-1}$ )
Kaolinite	5 – 15
Illite	25 – 40
Vermiculite	100 – 150
Montmorillonite	80 – 120
Chlorite	5 – 15

Figure 2.6: Cationic exchange capacity (after VELDE & MEUNIER, 2008).

The presence of exchangeable sodium is the main chemical factor contributing to dispersive clay behaviour. This is expressed in terms of the exchangeable sodium percentage, ESP (BELL & WALKER, 1999) by the equation (2.1). Sodic soils exhibit poor soil-water and soil-air relations; these properties adversely affect root growth restricting plant production and making the soils difficult to work when wet or dry. In Australian soils, when the adsorption of sodium on the surface of clays exceeds 6% of the total cation exchange capacity (exchangeable sodium percentage, ESP=6), the soil is sodic and is subject to serious structural degradation. The lower ESP for sodicity in Australian soils is attributed to the very low contents of soluble minerals, especially calcium, necessary to maintain the electrolyte concentration during leaching (RENGASAMY & OLSSON, 1991). Degrees of dispersibility are shown in figure 2.7 as a function of ESP and CEC.

$$\text{ESP} = \frac{\text{Exchangeable sodium}}{\text{CEC}} \quad \text{equation (2.1)}$$

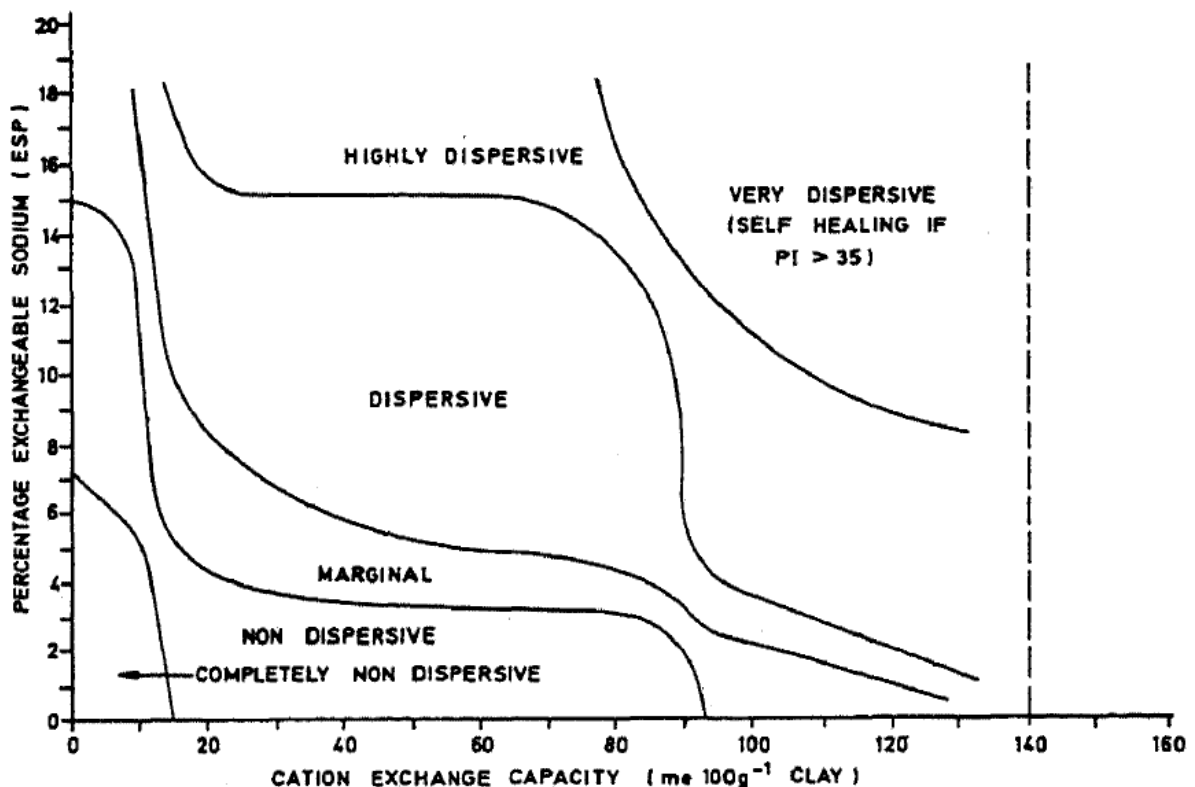


Figure 2.7 - Effect of CEC and ESP on clay dispersion (HARMSE & GERBER, 1988).

Measurement of ESP is time-consuming and costly; therefore, SAR measured in soil solution, which is highly correlated with soil ESP, is conveniently used as a measure of soil sodicity, and, in part, the effects of sodium on soil structure (RENGASAMY & MARCHUK, 2011). The sodium adsorption ratio, SAR, is used to quantify the role of sodium where free salts are present in the pore water (BELL, 2007) and are defined by equation (2.2)

$$\text{SAR} = \frac{\text{Na}}{\sqrt{\frac{(\text{Ca} + \text{Mg})}{2}}} \quad (2.2)$$

When investigating the high rate of dam failures due to piping, Aitchinson and Wood (1965) made laboratory and field studies of dams in different locations. They found dispersive characteristics of soils with SAR equal to or exceeding 2. In many cases, the problems faced were fixed up using more superficial soils with more calcium and less sodium for the compaction of the dam body.

Another simple method consists in the analysis of total dissolved salts (TDS) and the Sodium percentage (SP), proposed by Sherard (1972). The TDS and SP values are given by equation (2.3) and equation (2.4), respectively.

$$\text{TDS} = \text{Na} + \text{K} + \text{Ca} + \text{Mg} \quad (2.3)$$

$$\% \text{Na} = \frac{\text{Na}}{\text{Na} + \text{K} + \text{Ca} + \text{Mg}} \quad (2.4)$$

Those expressions are related to dispersibility as shown in figures 2.8 and 2.9.

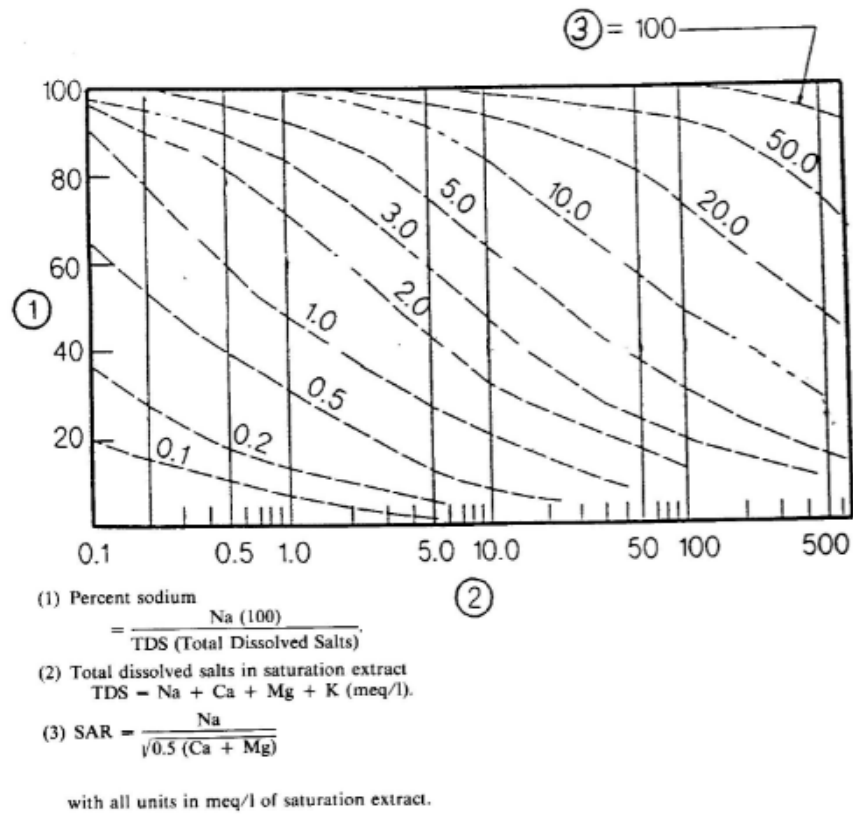


Figure 2.8 – SAR isocurves in dispersive soils chart (Sherard et al., 1976a).

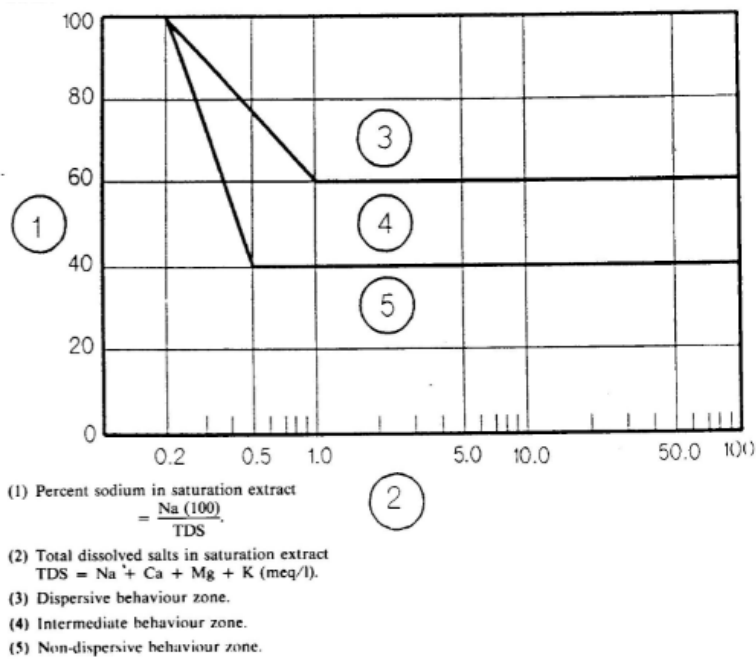


Figure 2.9 – Chart for the classification of dispersive soils (Sherard et al., 1976a).

To account for the effect of  $K^+$  and  $NH_4^+$  on adsorption ratio, Smiles and Smith (2004) proposed the monovalent cations adsorption ratio (MCAR) defined by equation (2.5). In their study, in spite of the high concentrations of  $NH_4^+$  in the effluents, the soil sampled presented no evidence of this exchangeable component. It was assumed that the ammonium was rapidly taken up by plants or oxidized.

$$MCAR = \frac{Na+K+NH_4}{\sqrt{\frac{(Ca + Mg)}{2}}} \quad (2.5)$$

The prevalent cations in soils have different flocculating power, that is, each one of them has a different effect on the deflocculation process. Rengasamy & Marchuk (2011) proposed a new ratio in substitution to SAR, based on the differential dispersive effects of Na and K and the flocculation power of Ca and Mg. Thereby, and the concept of ‘cation ratio of soil structural stability’ (CROSS) arose. From the derived flocculating power (Na = 1; K = 1.8; Ca = 45; Mg = 27), the CROSS value can be calculated by Equation (2.6).

$$CROSS = \frac{(Na + 0.56K)}{\sqrt{\frac{(Ca + 0.6Mg)}{2}}} \quad (2.6)$$

#### 2.2.4 Dispersibility in Southern Brazil

According to Barboza et al. (2009), Rio Grande do Sul Coastal Plain, the widest coastal plain in Brazil, preserves the geologic and geomorphologic registers of Cenozoic and Quaternary periods, developing many alluvial fans at the last one, and point out the sedimentary deposits at the Pelotas Basin.

Welter and Bastos (2003) studied dispersive soils from southern Brazil, nearby Pelotas, a county from the Rio Grande do Sul state. Those soils were found at the coastal plain, in seven sites where advanced erosive processes took place. Laboratory tests were carried, indicating all, except one, strong dispersive behaviour by the crumb test, and all dispersive percent above 57,5%. Based on the classification shown in Figure 2.8 and Figure 2.9, almost every sample was at the nondispersive zone, despite the dispersion verified. The author concluded that values of SAR of 1,5 correspond to a dispersive behaviour for those soils, classified also as non-lateritic soils (WELTER & BASTOS, 2003).

## 2.3 STABILIZED SOILS

The general objectives of mixing chemical additives with soil are to improve or control volume stability, strength and stress-strain properties, permeability, and durability. The development and maintenance of high strength and stiffness are achieved by the elimination of large pores, by bonding particles and aggregates together, by the maintenance of flocculent particle arrangements, and by prevention of swelling. (MITCHELL & SOGA, 2005) Soil-Cement mixtures are artificially structured materials with stable fabric due to the presence of artificial bonds. Those type of materials is used in several geotechnical applications such as in pavement base layers in transport infrastructures, embankment, dike, foundations (RIBEIRO et al., 2016, TRAN et al. 2014, BOARDMAN et al., 2001).

The term fabric refers to the arrangement of particles, particle groups, and pore spaces in soil. The term structure is sometimes used interchangeably with fabric. It is preferable, however, to use structure to refer to the combined effects of fabric, composition, and interparticle forces. It is necessary to consider the size, the form, and the function of different fabric units and to keep in mind the scale at which the fabric is of interest. (MITCHELL & SOGA, 2005)

### 2.3.1 Pozzolanic Reaction

Pozzolanic reactions consist of a large group of cementing reactions involving lime with silica or lime with silica and alumina (HUNTER, 1988). Natural and artificial pozzolans have been used to obtain hydraulic binders for over a thousand years. Hardening of pozzolanic cement pastes can result from the reaction between pozzolana and the lime that is added to the mix as hydrated lime or is produced following hydration of Portland cement silicates. The pozzolanic reaction does not alter cement clinker hydration; it complements and integrates the hydration process because it results in a lower portlandite content and an increase in calcium silicate hydrates (MASSAZZA, 1993).

Lime stabilization is achieved through cations exchange, flocculation agglomeration, lime carbonation, and pozzolanic reaction. Cations exchange and flocculation agglomerations reactions take place rapidly bringing immediate changes in soil properties, whereas pozzolanic reactions are time-dependent. These pozzolanic reactions involve interactions between soil silica and/or alumina and lime to form various types of cementation products thus enhancing the strength. (HARICHANE et al., 2011).



Henehara et al. (2001) studied the effect of pozzolan ratio and temperature on fly ash reactions with cement. They proved that not only the pozzolanic reaction rate increases with temperature but also the reaction initiation point. Also, when the fly ash content is lower, the reaction tends to take more time to deplete. Temperature acts as a catalyst in pozzolanic reactions, just accelerating its occurrence that would in any case, but not at the same time (RAO & SHIVANANDA, 2005; ZHANG et al., 2020).

### 2.3.2 Lime

Sometimes the term ‘lime’ is used to describe agricultural lime which is generally finely ground limestone, a useful soil amendment but not chemically active enough to lead to soil stabilization. Lime in the form of quicklime (calcium oxide – CaO), hydrated lime (calcium hydroxide – Ca[OH]<sub>2</sub>), or lime slurry can be used to treat soils. Quicklime is manufactured by chemically transforming calcium carbonate (limestone – CaCO<sub>3</sub>) into calcium oxide. Hydrated lime is created when quicklime chemically reacts with water. It is hydrated lime that reacts with clay particles and permanently transforms them into a strong cementitious matrix. (NATIONAL LIME ASSOCIATION, 2004). Stabilization by lime, which is frequently carried out to improve the mechanical properties of soils, results from the formation and development of cementitious calcium silicate aluminate hydrate gel. The gel produces interlocking and bonding of the soil particles, hence increasing the strength and abrasion resistance. (ARABI et al., 1988)

It is not necessary to have pure limestone to produce hydrated lime; a common impurity is magnesium carbonate in dolomitic rocks which yield dolomitic lime, i.e. lime with some magnesium oxide content. There is conflicting evidence of the effect of magnesium compounds and some caution should be exercised in the use of dolomitic limes. Other impurities may be ignored provided that any quantity estimates are based on the ‘free lime’ content of the lime (i.e. on the actual amount of CaO or Ca(OH)<sub>2</sub> present) (INGLES & METCALF, 1972). About lime impurities, National Lime Association (2004) states that most limes used for soil treatment are ‘high calcium’ limes, containing no more than 5 percent magnesium oxide or hydroxide, nevertheless, sometimes dolomitic lime should perform well in soil stabilization, but the magnesium fraction tends to react slower than the calcium fraction.

Two main mechanisms take place when wet soil is put in contact with lime: the first one is called modification, and the second is called solidification.

The initial, immediate, modification reaction occurs as a result of the cation exchange of calcium ( $\text{Ca}^{2+}$ ) ions for the existing cations at negative charge sites on the clay mineral lattice. The number of these charge sites is further enhanced in some clay minerals by the increase in pH caused by the presence of the  $\text{OH}^-$  ions. The result of cation exchange is increased flocculation of mineral particles and changes in the plasticity properties of the soil. In physical terms, the result is an apparently drier, more friable material (BOARDMAN et al., 2001). Short term reactions with cement and lime include replacement of monovalent adsorbed cations by  $\text{Ca}^{++}$ , adsorption of  $\text{Ca}(\text{OH})_2$  by particles, cementation at interparticle contacts, and establishment of a high pH (12.4) environment. (MITCHELL & SOGA, 2005).

The solidification process is the process when the carbonation and pozzolanic reaction adds beneficial effects to the mixture. It is a slower process than the modification stage, and is highly dependent on temperature, soil mineralogy and chemistry. [...] End products are a series of calcium silicate hydrates (CSH). Lime acquires silica from clays or other pozzolans in the soil to form CSH gel. Cement contains silica initially. In the long term the pH causes a breakdown of cementitious products. These reactions can continue for years. (MITCHELL & SOGA, 2005).

Those reactions are expressed by equations (2.7), (2.8) and (2.9). Borges (1979) states that these reactions still occur until there is no available reagent.



Where

C = CaO

S =  $\text{SiO}_2$

A =  $\text{Al}_2\text{O}_3$

H = H<sub>2</sub>O

It is not unusual that those reactions do originate other components. Components like ettringite were found in lime-treated soils. Ettringite is a calcium aluminum sulfate hydrate (CASH) mineral, and may cause damage to soils due to its expansive feature. (ALDAOOD et al., 2014; LITTLE et al., 2005).

### 2.3.3 Fly Ash

Fly ash is the ash resulting from the burning of pulverized bituminous, hard coals in power station furnaces. The furnaces are used to generate steam for the production of electricity. The furnace temperature is typically > 1400°C. (SEAR, 2001) The resulting material is a siliceous ash consisting of the oxides of silica, alumina and iron, and containing <10% calcium oxide. ASTM C618 (ASTM, 2019), a Standard on fly ash for use in concrete classifies fly ashes into two classes: class F covers the fly ashes with pozzolanic properties, and class C includes fly ashes having pozzolanic and also cementitious properties. Table 2.1 shows these ashes properties. ASTM D5239 (ASTM, 2018) discourses on fly ash specifically for soil stabilization, classifying fly ashes in non-self-cementing fly ash, and self-cementing fly ash, the last one containing free (uncombined) lime (0 to 7% by weight).

Table 2.1: Chemical Requirements of Fly Ashes for use in Concrete  
(after ASTM C618, 2019)

	Class		
	N	F	C
Silicon dioxide (SiO <sub>2</sub> ) plus aluminum oxide (Al <sub>2</sub> O <sub>3</sub> ) plus iron oxide (Fe <sub>2</sub> O <sub>3</sub> ), min, %	70	50	50
Calcium oxide (CaO), %	report only	18 max.	>18
Sulfur trioxide (SO <sub>3</sub> ), max, %	4	5	5
Moisture content, max, %	3	3	3
Loss on ignition, max, %	10	6 <sup>A</sup>	6

<sup>A</sup>The use of Class F pozzolan containing up to 12.0 % loss on ignition may be approved by the user if either acceptable performance records or laboratory test results

Both classes are pozzolans, defined as siliceous or siliceous and aluminous materials, and can provide an adequate array of divalent and trivalent cations ( $\text{Ca}^{2+}$ ,  $\text{Al}^{3+}$ ,  $\text{Fe}^{3+}$ , etc.) under ionized conditions that can promote flocculation of dispersed clay particles (ÇOKÇA, 2001).

When fly ashes are mixed with lime, C-S-H,  $\text{C}_4\text{AH}_{13}$  and  $\text{C}_2\text{SAH}_8$  are formed. If silicoaluminate fly ashes contain sulphates, besides C-S-H and  $\text{C}_4\text{AH}_{13}$ , ettringite is also formed.  $\text{C}_4\text{AH}_{13}$  decreases with time whereas the  $\text{C}_4\text{AcH}_{12}$  content increases. High-lime fly ashes can harden without further addition of lime since they contain variables amounts of free lime which, upon mixing, are transformed into  $\text{Ca}(\text{OH})_2$ . From a practical viewpoint, these fly ashes correspond to the artificial hydraulic limes obtained by mixing hydrated lime with pozzolana. (MASSAZZA, 1993)

Pozzolans contribute to the hardening properties of mortar or concrete in two ways; namely, by the filler effect and pozzolanic reaction. The physical or filler effect is defined as the proper arrangement of smaller particles in concrete or mortar specimen that increases the density as well as the compressive strength without any chemical reaction. These smaller particles fill the inter particular voids in mortar and concrete. As a result, it produces concrete with higher compressive strength compared to larger pozzolana particles. On the other hand, the pozzolanic effect is governed by the chemical reaction between pozzolans and cement or hydration products of cement. (KHAN et al., 2016)

Hardening is therefore the outcome of the pozzolanic reaction and of the occurrence of specific hydraulic compounds which, as in the case of  $\text{C}_2\text{S}$ , are formed during coal combustion. When high lime contents occur, also  $\text{C}_2\text{ASH}_8$  is eventually formed. If, however, lime is entirely or mainly combined with  $\text{Al}_2\text{O}_3$  and  $\text{SiO}_2$  in the glass, it becomes unreactive. As a consequence, no prominent pozzolanic reactions are evidenced and, at least for three months, no C-S-H is formed. (MASSAZZA, 1993)

#### 2.3.4 Mechanical behavior of stabilized soils

The introduction of a cementing agent into sand produces a material with two components of strength – that due to the cement itself and that due to friction. The friction angle of a cemented sand is similar to that of uncemented sands. A weakly-cemented sand shows a brittle failure mode at low confining pressures with a transition to ductile failure at higher confining

pressures. Density, grain size distribution, grain shapes, and grain arrangements all have a significant effect on the behavior of a cemented sand. (CLOUGH et al., 1981).

The cemented soil skeleton initially compresses under a load as would be expected, but with further straining, the cemented soil skeleton tends to dilate (as would a dense material) as demonstrated by the pore pressure response and the stress path plots. At low axial strains (below 1%), the cohesion caused by the calcite cement bonding between particles is the major component of strength. Up to yielding, the presence of bonding prevents the intact soil from dilating (SAXENA & LASTRICO, 1978) After yielding, the gradual degradation of the bonds and the disruption of the fabric inhibit the dilation of the soil, which is later recovered by a more rapid increase of the dilatancy until a maximum is reached, which both corresponds to and cause the higher peak strength. (CUCCOVILLO & COOP, 1999)

At normal engineering rates of loading, the structure is destroyed irreversibly by post-yield strain, but it may be recovered with further time, at least to some extent. It is thus convenient to define two void ratio-stress spaces, the space bounded by the line that defines the loosest possible packing for the destructured soil, and space outside this line in which the soil can only exist due to structure. Yield then may be followed by contraction and large strains. (LEROUEIL & VAUGHAN, 1990) The cohesive shear strength is destroyed around 1% strain and at the same time, the frictional strength becomes predominant. The cohesive shear strength is variable since the natural deposits have variable degrees of calcite cement solution. It was also observed that a very high hydrostatic confining stress can destroy the cementation (SAXENA & LASTRICO, 1978). Indraratna et al. (1995) related an increase in effective yield stress and a decrease in compression index ( $C_c$ ) for a soft clay treated with cement and for a fly ash mixed with cement. Rotta et al. (2003), from triaxial compression tests using an artificially cemented sand cured under stress, found that the same material may have a different position of the NCL (Normal Compression Line) due to the curing stress during consolidation, but after the primary yielding point, there is a convergence to the same NCL of the uncemented sand. Cemented soils have similarities with plain concrete/mortar and even soft rock (LEROUEIL & VAUGHAN, 1990), which, according to Kanji (2014), have intermediate behaviour between soils and hard rocks. Soft rock is a term that usually refers to a rock material with a uniaxial compressive strength (UCS) less than 20 MPa (AGUSTAWIJAYA, 2007). Martin and Chandler (1994) found out even hard rocks like granite have a similar behaviour when compressed, being characterized by a cohesion loss as friction is mobilized and the damage (i.e. cracks) is

manifested. Stress-strain curves for brittle rocks show three characteristic stress levels: crack initiation, long-term strength, and peak strength. [...] Once failure initiates, brittle rocks such as Lac du Bonnet granite, show significant strain softening in the post-peak region (MARTIN, 1997).

Coop and Atkinson (1993) studied the separate effect of cementing and grading testing a carbonate sand artificially cemented using gypsum casting plaster and gypsum powder. They found out that increasing gypsum and calcium carbonate fines do not change the critical state friction angle when the admixture is not cemented ( $\varphi'_{cs} = 40^\circ$ ). But when the cementation occurs, the friction angle falls ( $\varphi'_{cs} = 37^\circ$ ). It is explained by the adhesion of cement to the sand particles after yielding.

### 2.3.5 Durability of structured soils

Durability, which can be defined as the ability of a material to retain stability and integrity over the years of exposure to the destructive forces of weathering, is one of the most important properties (DEMPSEY & THOMPSON, 1968).

Cemented materials like concrete, mortar, and structured soils, when subject to aggressive weathering conditions, may have their durability evaluated. Failure of concrete after a period less than the lifetime for which it was designed may be caused by the environment or by a variety of internal causes. External causes may be physical or chemical: weathering, extremes of temperature, abrasion, or chemical action in the cement, aggregate, or reinforcement components. Internal causes may lie in the choice of materials or inappropriate combinations of materials and may be seen as alkali-aggregate expansion or other forms of failure. Of all the causes of lack of durability in concrete, the most widespread is excessive permeability. Permeable concrete is vulnerable to attack by almost all classes of aggressive agents (RAMEZANIANPOUR, 2014).

Volume and water content changes in soils are the consequences of environmental factors, such as drying-wetting cycles. Also, changes in the groundwater level generate the shrinkage and the swelling of the soil surface (BENCHOUK et al., 2012). When absorbing water, cracks occur in soil, causing a loss of strength and then an acceleration of soil degradation. Thus, the durability of cement-treated or stabilized soils is another concern for the mix design of cement stabilization under wetting-drying or/and freezing-thawing cycles (ZHANG et al., 2008).

Nabil et al. (2020) explain that the proportion of micropores (<0.3  $\mu\text{m}$ ) of stabilized soils is greater than non-stabilized, but unstabilized soils have more macropores (artificial inter-aggregate pores) than stabilized soils and, according to Aldaood et al. (2014), wetting-drying cycles lead to pores widening, resulting in microcracking, swelling and eventual failure of the matrix, especially when ettringite is formed. Utomo (1980) explains that alternate wetting and drying causes swelling and shrinkage of soil, but also affect the formation and changes of soil aggregates.

The durability test for Soil-Cement Mixtures is standardized by ASTM D559 (ASTM, 2015). This standard is based on the resistance of compacted soil-cement to repeated cycles of wetting (20°C), followed by drying (71°C) and brushing (26 to 28 strokes of approximately 13 N). This procedure is repeated 12 times. The mass loss is calculated from equation (2.10).

$$\text{Soil-cement loss} = \frac{C}{D} \quad (2.10)$$

Where

C = original calculated oven-dry mass minus the final corrected oven-dry mass

D = original calculated oven-dry mass

The USACE (1984) stated accumulated loss of mass base values for soils stabilized using Portland cement after durability cycles. According to this study, fine-grained soils admit lower mass loss values than coarse-grained ones. The durability requirements of ALM are presented in Table 0.2.

Table 2.2: Durability Requirements (after USACE, 1984).

Type of soil stabilized	Maximum allowable weight loss after 12 wet-dry or 6 freeze-thaw cycles (percent of initial specimen weight)
Granular, PI less than 10	11
Granular, PI greater than 10	8
Silt	8
Clays	6

### 2.3.6 Porosity and Cementitious Agent Content Ratio

Minimizing the cement content while attaining a satisfactory level of performance is the main objective of mixture proportioning; however, the absence of performance-predicting models precludes optimization (WILLIAMSON, CORTES, 2014). It is a long-known fact that decreasing the water-cement ratio decreases the porosity of the cement paste, which in turn increases the compressive and the tensile strengths and decreases the volume changes of the paste (YUDENFREUND et al., 1972). Thereby, many relations have been suggested to assess this effect, correlating strength with porosity and porosity related state parameters like ‘strength at zero porosity’ or ‘porosity at zero strength’ (RYSHKEWTICH, 1953; HASSELMAN, 1969; SCHILLER, 1971). Watson (1981) applied those correlations in order to assess the impact of porosity in cement paste and found a high degree of correlation. Chen et al. (2013) tested cement mortars strength for many water-cement ratios and a constant sand-cement ratio by applying a formulation for porous materials, where strength is not only a function of porosity and porosity related parameters but also of elastic stiffness parameters and stress state (ZHENG et al., 1992). Since those studies did not account for the dissociated effect of porosity and cement content, each sand/soil cement ratio must be tested with distinct water-cement ratios, and when there is more than a single component in the binder, demanding much time and cost into dosage determination.

The evolution of porosity with time in lime-pozzolan mortars was found by Papayianni and Stefanidou (2006): “It seems that the porosity is reduced with time. This is understandable because of the slow process of pozzolanic reaction and carbonation.” LI et al. (2015) found that the porosity of hardened concrete decreases with increasing curing ages.

Consoli et al. (2007), aiming for an efficient and low-cost dosage methodology, developed a parameter to predict the behaviour of compacted soil-cement mixtures under low confining pressures based on unconfined compressive tests. The method is based on the adimensional porosity and volumetric cement content ratio ( $\eta/c_{iv}$ ). This parameter is given by equation (2.11)

$$\frac{\eta}{c_{iv}} = \frac{v_v / v_t}{v_c / v_t} = \frac{v_v}{v_c} \quad (2.11)$$

Where



$\eta$  = specimen porosity

$c_{iv}$  = volumetric cement content

$v_v$  = specimen voids volume

$v_c$  = specimen cement volume

$v_t$  = specimen total volume – voids plus solids

They found out that when the denominator of this relation is raised to the 0.28 power, the coefficient of determination reaches values close to the unity, and the strength is defined by equation (2.12).

$$q_u = B \left( \frac{\eta}{c_{iv}^c} \right)^{-a} \quad (2.12)$$

Where

$B$  = multiplier empirical scalar

$c$  = adjusted exponent – thought to be a function of material (soil and cement) in the mixture

$a$  = best fit for exponential regression

Diambra et al. (2017) analyzed the equation (2.12) from a constitutive model perspective, by separating soil and cemented matrix, defining strength based on the Drucker-Prager criterion through the critical state theory approach (SCHOFIELD & WROTH, 1968; BEEN & JEFFERIES, 1985). The authors demonstrated that  $c$  and  $a$  values are dependent on soil and cementitious material used and that the multiplying factor  $B$  is dependent on soil frictional property and of cemented phase strength, being directly proportional to the exponent  $a$ . Also, it seems that  $a = 1/c$  for three different evaluated soils.

The relation was also extended for lime-treated soils, with an adaptation of the *volumetric lime content* ( $L_{iv}$ ) instead of cement (CONSOLI et al., 2009, 2011a, 2011b, 2012, 2014). Recently, a new parameter called  $\eta/B_{iv}$ , defined similarly to the previous one, but considering the Binder volumetric content as a sum of lime and pozzolana content, have shown strong correlations

with unconfined compressive strength for soil-pozzolana mixtures. (CONSOLI et al., 2018, 2019a, 2020a))

Since the first work regarding this key parameter with strength, this ratio, and its variables were correlated not only with unconfined compressive strength but also with splitting tensile strength, cohesion, friction angle, small strain stiffness, and durability (CONSOLI et al., 2010, 2012, 2013, 2016a, 2020b).

The intent is to find a single power function quantifying the influence of the binder's amount, porosity, and curing time (CONSOLI et al., 2016b), obtaining design parameters with no need for complex, time, and cost demanding tests.

## 2.4 UNCONFINED COMPRESSIVE STRENGTH

There are many ways to determine material strength. One of the most common and simple is the Unconfined/Uniaxial Compressive Strength (UCS). Li (2015) points out the importance of unconfined compressive strength tests to predict the mechanical behaviour of geomaterials, since it doesn't demand confining pressure like triaxial tests, being easy to conduct. Taylor et al. (2019b) highlighted the importance of unconfined compressive tests to assess the strength behaviour of near-surface soils, concluding, from unconfined compressive tests on compacted sands, that the effective stress principle is not representative of the unconfined or near-surface soil's shear strength.

### 2.4.1 Cracks propagation and failure modes

Usually, a material is considered brittle when it breaks at low elongation, not exceeding a few percentage points. The problem to be considered is to understand and determine the relations between the global mechanical behaviour of the material, often determined by a uniaxial test, and the fracture toughness, that is to say, the resistance to crack propagation. This requires considerations about fracture mechanism which take place near the crack tip since a crude model of crack propagation consists of visualizing a tiny fictitious tensile specimen ahead of the crack tip whose fracture starts the propagation of the crack. The stress needed to break atomic bonds, the theoretical fracture stress, is very large, of the order of  $E/10$ ,  $E$  being Young's modulus. The reason that actual fracture stresses are orders of magnitude lower is the heterogeneous distribution of the stresses in the material. (FRANÇOIS, 2001)

Bobet & Einstein (1998) investigated the behaviour of cracks and coalescence with specimens of gypsum, aiming the behavior of brittle materials: Two types of cracks occur: wing cracks, which are tensile cracks, and secondary cracks which initiate as shear cracks in a plane roughly co-planar with the flaw. The secondary cracks usually propagate as shear cracks in the same plane, but depending on the geometry, they also propagate out of the plane as either tensile or shear cracks.

Basu et al. (2013) observed different failure modes from the uniaxial compressive test on granite, schist, and sandstone rock samples, as indicated by figure 2.10:

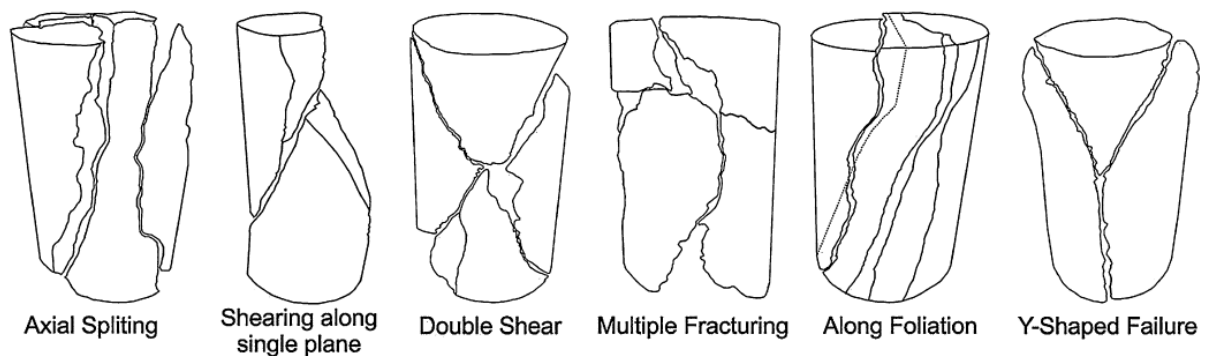


Figure 2.10: Illustration of different failure modes for rocks under unconfined compressive tests. (Basu et al., 2013).

When wing crack propagation along the maximum principal stress is constrained because of the existing microstructure, coalescence of adjacent wing cracks or wing cracks in close proximity generated from the tips of the suitably oriented microcracks takes place in order to release the strain energy in the form of shear fracture resulting in higher UCS than that generally portrayed by axial splitting. Multiple fracturing is essentially an irregular breakage or crumbling of the specimens which is likely to take place in order to release the strain energy in any feasible way when systematic coalescence of adjacent wing cracks even becomes restricted. (BASU et al., 2013) Fracture coalescence means the connection or merging of two or more fractures (or cracks) due to fracture propagation. Therefore, the study of the mechanism of fracture coalescence is of crucial importance in the study of the strength of fractured and jointed material such as rock masses and in particular the stability analysis of underground excavations and other rock engineering (SHEN, 1995).

Recently, evidence has been presented showing that the distribution of hydration products and porosity over the interface is quite non-uniform, and the view of a continuum interfacial transition zone must be doubted. Through the growth of isolated cracks, the global tangent stiffness of the concrete will gradually decrease. The decrease in stiffness is larger when the number of microcracks increases, or when the individual cracks increase in size (MIER, 1996)

#### 2.4.2 Unconfined Compressive Stiffness

Kuhinek et al. (2011) mentioned errors associated with the lack of flatness of uniaxial compressive strength samples and the stiffness of test equipment during axial displacement measures. The stiffness of the load cells is seen as an error source because the ideal load cell should have small stiffness to achieve good quality measurements, lowering the stiffness of the equipment on the tests. Bressani (1995) approached problems related to axial measurements on triaxial test samples, which carry some similarities with unconfined compressive strength samples. The main proposition is to ensure to get external displacement transducers (Linear Variable Differential Transformer) in association with local displacement measurements to avoid errors caused by the bedding effect on top of the samples during the early stage of the test. Factors like slenderness ratio and soil-structure friction can alter the stress-strain behaviour too.

Palchik (2011) carried unconfined compressive tests on carbonate rocks (dolomites, limestones, and chalks) with strength ranging from 14 to 273.9 MPa and elastic modulus from 6.10 to 82.30 GPa. Elastic modulus was found to be dependent on unconfined compressive strength ( $q_u$ ) and bulk density ( $\rho$ ). Also, the ratio between elastic modulus and compressive strength ( $M_R = E/q_u$ ) was calculated. Values obtained ranged between 60.9 and 1011.4 and were inversely related to the maximum axial strain ( $\epsilon_{a \max}$ ). Hawkes and Mellor (1970) evaluated unconfined tests on extensive rock samples and defined three categories of modulus/strength ratio ( $M_R$ ): high modulus, where the ratio is up to 500; mean modulus ratio, where the ratio is in a range from 200 to 500, and low modulus ratio when its value is below 1:200. Those relations are represented by the figure 2.11. Arslan et al. (2008), established for gypsum samples, besides  $M_R$ , an accurate linear relation between  $q_u$  and Poisson's ratio ( $\nu$ ) where  $\nu$  ranged between 0.15 and 0.40.

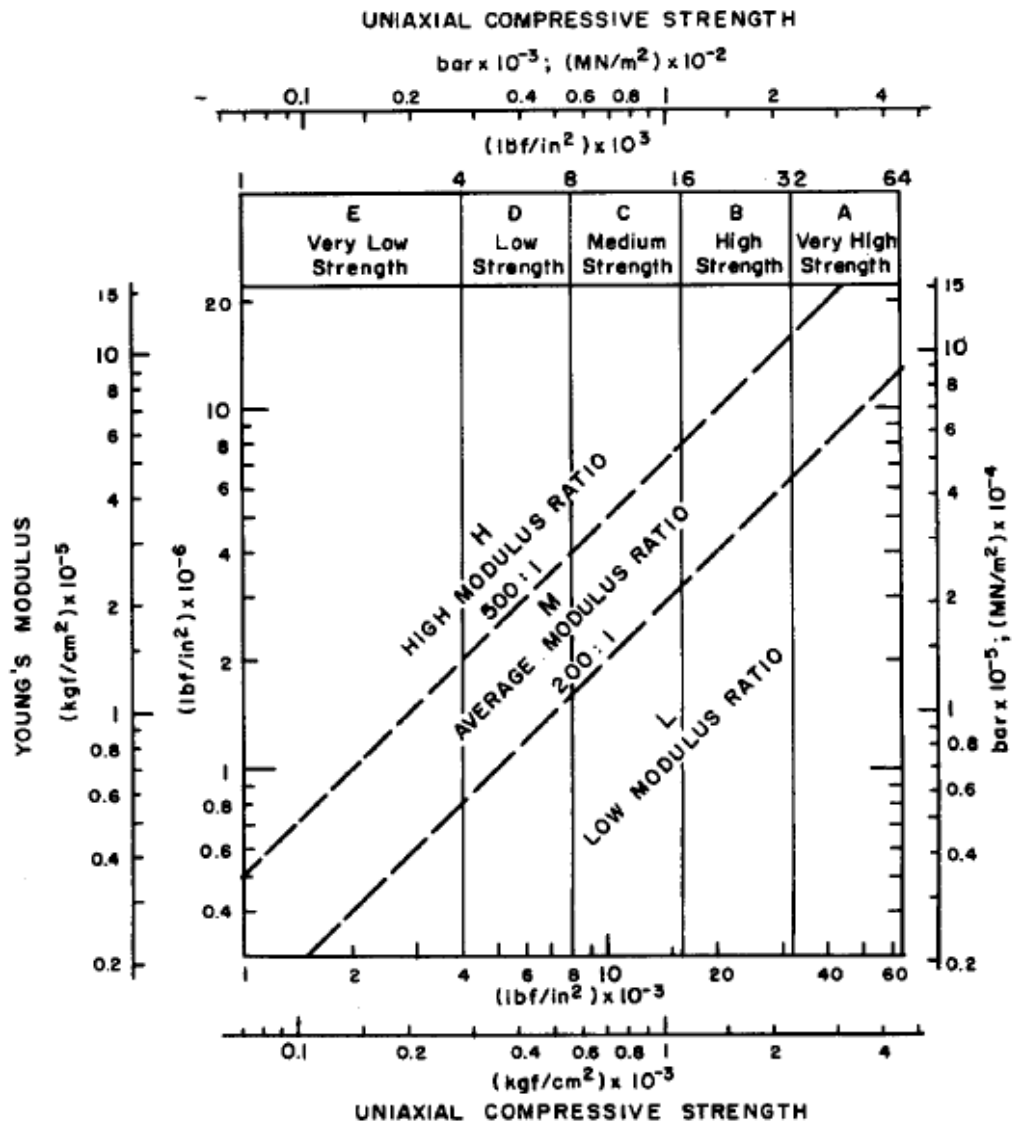


Figure 2.11: Diagram for classification of rocks on the basis of uniaxial mechanical properties. (HAWKES & MELLOR, 1970).

Pauw (1960) has shown the influence of concrete weight and test method on elastic modulus. His empirical formula was innovative for accounting for the effect of weight in stiffness, as expressed by equation (2.13):

$$E_c = 33 \times w^{3/2} \times \sqrt{f_c'} \quad (2.13)$$

Where

$E_c$  = static modulus of elasticity of the concrete

$w$  = air-dry weight of the concrete at the time of the test

$f_c'$  = compressive strength of the concrete at the time of the test

Rios (2009) run unconfined compressive tests on a granitic residual soil improved with cement (2, 4, 5, and 7%). Displacement was measured with LDTs (Local Deformation Transducers) and plotted initial tangent modulus against  $\eta/civ$ . Good trends emerged from this correlation.

### 2.4.3 Effect of sample height and base friction

When a specimen is pressed between a pair of rough and rigid platens, so that its ends are completely restrained radially, it tends to take on a barrel shape under load. With a short specimen ( $H/D = 1.0$ ) the profile of lateral deformation may show a true barrel shape, with a continuous smooth increase of deformation from the ends to the mid-section. With a longer specimen ( $H/D = 2.5$ ) the profile of lateral deformation is more likely to show approximately uniform deformation along the mid-portion of the specimen (HAWKES & MELLOR, 1970). Different profiles are shown in figure 2.12 according to deformation behaviour.

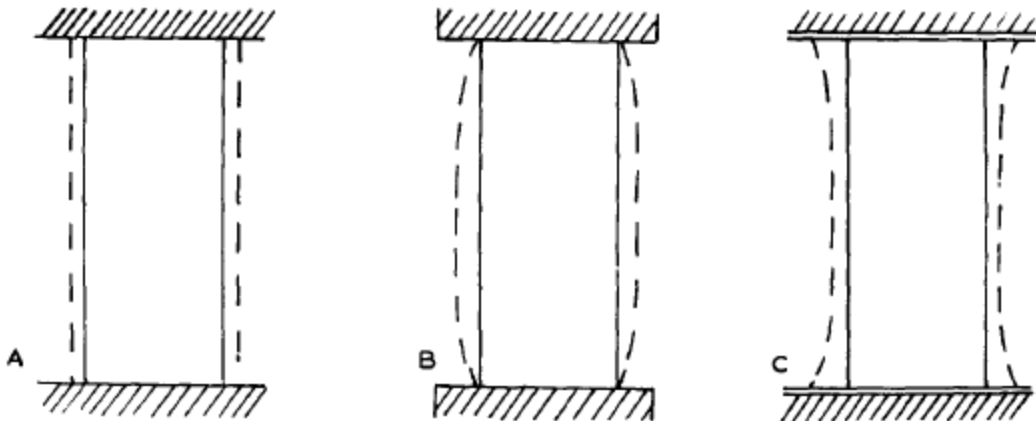


Figure 2.12: Profile of lateral displacement in an unconfined compressive strength test. A. Perfect radial freedom at the specimen ends. B. Complete radial restraint at the specimen ends. C. Extrusion of an interfacial material at the platen/specimen contact (HAWKES & MELLOR, 1970).

Loading devices such as brush and flexible platens are considered to induce a negligible frictional restraint at the specimen-platen interfaces when designed to allow displacements in

the direction orthogonal to loading compatible with tensile strains in concrete calculated on the basis of Poisson's ratio values up to 0.5 which is the maximum value for a continuous nonlinear-elastic material. Such relationships essentially describe the response of the central zone of the cylinders which is generally accepted to be subjected to a near-uniform uniaxial compressive stress in contrast to the complex and indefinable compressive state of stress imposed on the end zones by frictional restraints due to the interaction between specimen and loading device (KOTSOVOS, 1983).

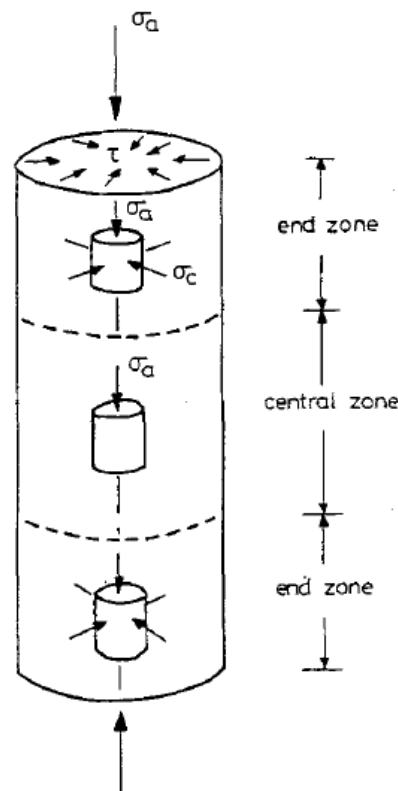


Figure 2.13: Stresses developed during unconfined compressive tests (KOTSOVOS, 1983).

Studies have been conducted on concrete specimens under uniaxial compression, using different interface materials on the platen interface, each one corresponding to distinct friction degrees. It has been shown that the pre-peak stress-strain behavior is apparently not influenced by the friction interface, but the post-peak is significantly influenced by this frictional change. (KOTSOVOS, 1983; KUMAR et al., 2016).

However, in concrete specimens, different from soil-lime admixtures, there is a great influence of the interfacial transition zone in strength, especially for high binder/aggregate ratio. (OLLIVIER et al., 1995)

So, those observations could be not valid for cemented soil, since its binder content and aggregate size are different from concrete and, consequently, its cracks, stress-strain behaviour and Poisson's ratio are much distinct. Studies may be done to confirm that behaviour for soil-cement specimens.

The Slenderness Ratio (Height/Diameter) is also a considerable variable in uniaxial compression strength. Tuncay and Hasancebi (2009) tested rock samples, which results suggest that there is a more pronounced steep curve of UCS x H/D ratios when the H/D values are between 1,50 to 2,50, becoming more stable after these values. Guneyli & Rusen (2015) tested cohesive clays and found more steep curves for H/D ratios below 2,0 (Figure 2.14). Both studies find an increase in UCS when decreasing H/D ratios.

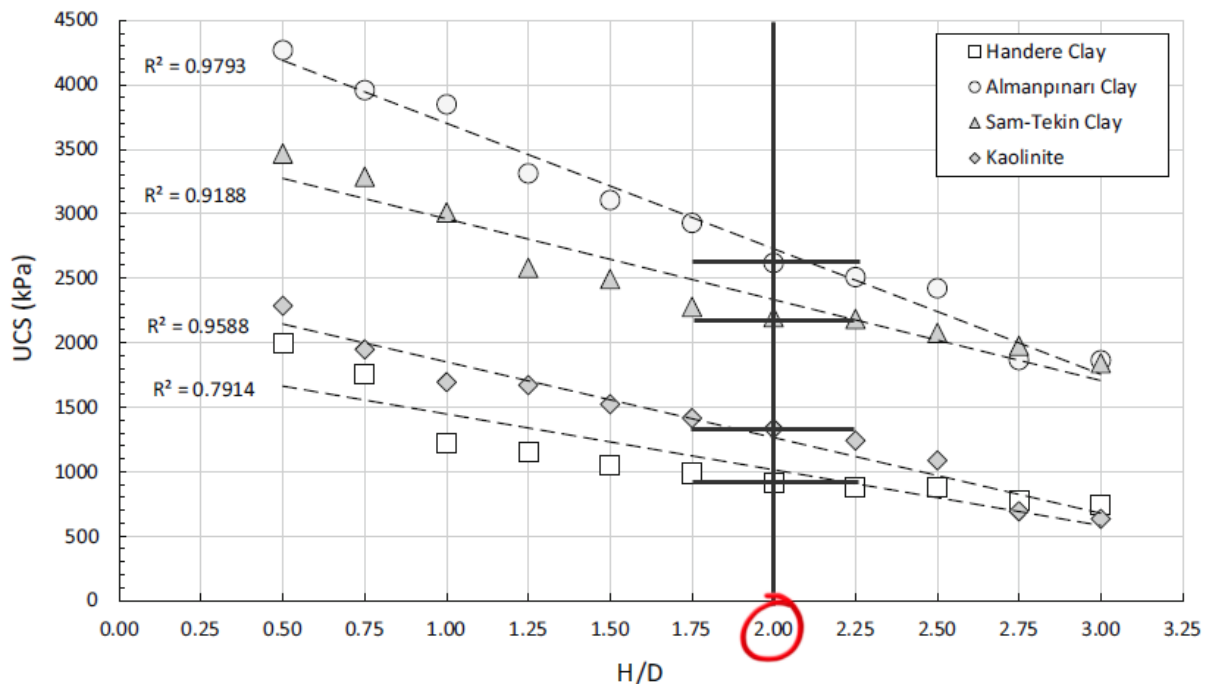


Figure 2.14: UCS x H/D Ratio for clay specimens (after GUNELY & RUSEN, 2015)



Dhir and Sangha (1973) investigated the behaviour of slenderness ratio ( $H/D$ ) on sandstone and concrete samples during uniaxial compressive strength tests. The authors conducted experiments with ratios of 1, 1.5, 2.0, 2.5, and 3.0. Overall and central zone deformation were evaluated, being that central zone deformation increases as slenderness ratio increases and the overall deformation decreases as  $H/D$  increases. The results also demonstrate a significant variation of maximum strains and modulus from ratios between 1 and 2, but for ratios above 2, the behaviour is approximately constant, with a slight change from 2 to 3.

#### 2.4.4 Unconfined Compressive Strength and Cemented Materials

As a need to find relations between constitutive parameters and UCS from soils, Ma & Wang (2011) presented a compilation of UCS results for stabilized soils varying from mud to sand (actual friction angle between  $20,8$  to  $38,7^\circ$ ), plotted in Figure 2.15 where a relation of cohesion ( $c$ ) and UCS was given by  $c = 3,2 \text{ UCS}^{0,6}$ .

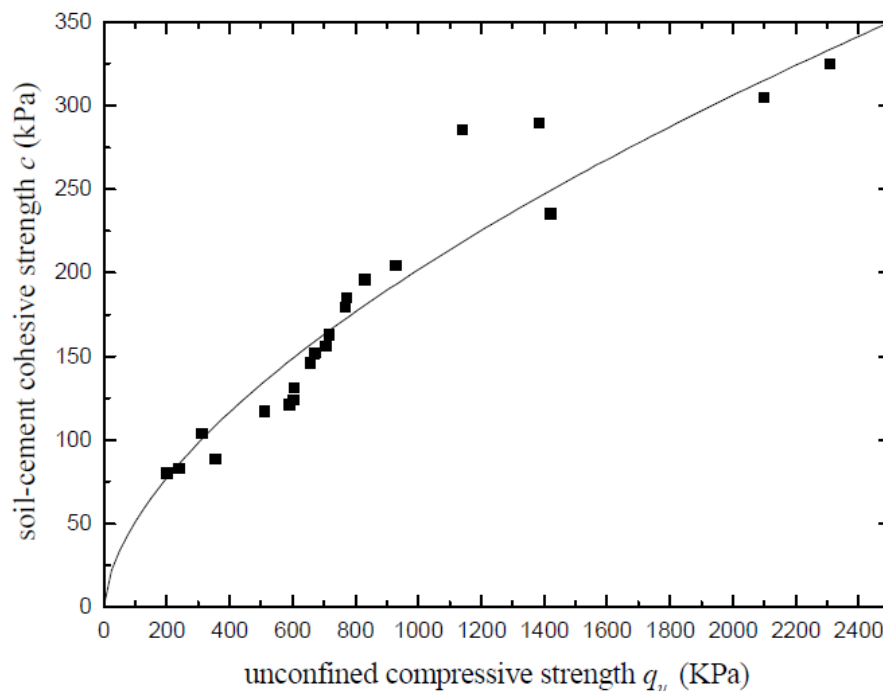


Figure 2.15: Relation between cohesion and UCS (MA & WANG, 2011).

For cohesive soils, Mohr-Coulomb strength parameters like cohesion intercept ( $c'$ ) and friction angle ( $\phi'$ ) can be obtained from the combination of unconfined compressive strength and splitting tensile strength as illustrates in the idealized model in figure 2.16.

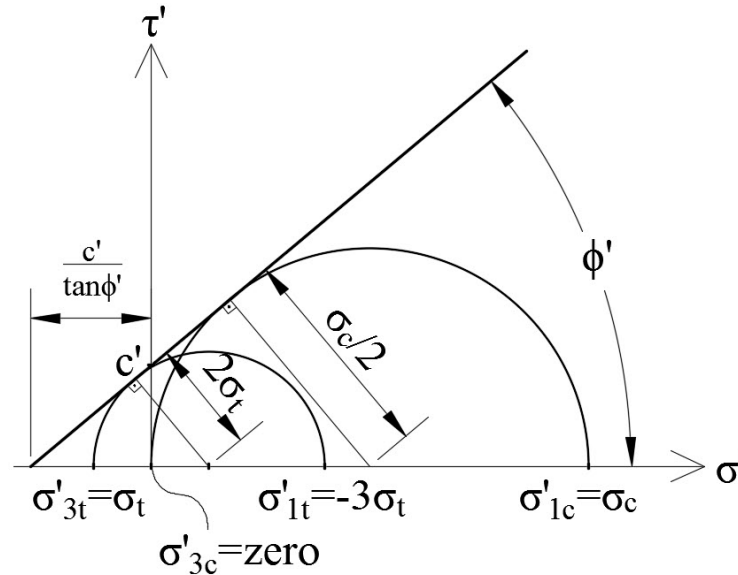


Figure 2.16: Mohr-Coulomb envelope for idealized splitting tensile and unconfined compressive strength.

This relation, however, demands many tests to assess the required cementitious agent dosage. From several compressions and splitting tensile tests on cemented soils, the ratio ( $\zeta$ ) between the strength obtained from those two tests have shown to be a scalar, independent of porosity and cement content. From that, compared with triaxial compression tests at low confining stresses, friction angle showed up to be dependent only on that ratio, and that cohesion is dependent on  $\zeta$  but also on  $q_u$  (CONSOLI et al., 2013; CONSOLI, 2013).

Since 2007, many researchers have shown the reliability of unconfined strength tests analysis using the key parameter  $\eta/c_{iv}$  and its variants. Fatthapour et al. (2014) analyzed the grain effect on artificial cemented sandstones through the parameter  $(\eta/c_{iv})^{-1}$ , yielding a linear relationship when plotted against compressive strength. Increasing soil grading in samples for the same cement content means strength increasing, but using the parameter  $(\eta/c_{iv})^{-1}$  proved to be effective in covering from well to poorly graded grains, expressed by the coefficient of uniformity ( $C_u$ ), though, a different grain size, expressed by mean grain size ( $D_{50}$ ) could not be normalized by this parameter, as well as angularity. It was only demonstrated that the fine-

grained soils and the angular ones reached higher unconfined compressive strength for the same  $(\eta/c_{iv})^{-1}$ .

Gunaydin et al. (2010) demonstrated, with linear regressions and artificial neural network analysis of cemented soils, that unconfined compressive strength, in many cases, is also dependent on water content, specific gravity and permeability.

#### 2.4.5 Unconfined Compressive Strength and Durability

Nabil et al. (2020) run unconfined compressive strength tests on lime stabilized soils subjected to wetting-drying-brushing cycles. The lower lime content mixtures lost their strength after cycles, but the higher lime content mixtures have shown strong improvement due to reaction acceleration. A relation arose from those tests between unconfined compressive strength after and before durability tests, as presented by equation (2.14)

$$\text{UDR} = \frac{q_{u,12}}{q_u} \quad (2.14)$$

Where

UDR = Unconfined Compressive Strength Durability Ratio

$q_{u,12}$  = Unconfined Compressive Strength after 12 cycles

$q_u$  = Unconfined Compressive Strength

Park (2010) tested cemented sands under unconfined compressive strength tests for three different conditions: after 28 days; after 28 days (wetted on the 13<sup>th</sup> day), after 28 days (wetted on the 27<sup>th</sup> day). The strength of the specimen air-cured for 27 days followed by wetting decreased by up to 65% compared to a 28 days cured specimen, while the specimen wetted after 13 days presented a strength increase due to cement hydration. Similar behaviour has been observed in soil modulus, wherefore, the author highlights the importance of accounting for the strength reduction caused by wetting when designing geotechnical structures.

## 2.5 SMALL STRAIN STIFFNESS

Soil is supposed to be the most complex material regarding the various civil engineering projects. For the determination of its index and engineering properties, particularly in the field, we commonly use direct methods which are destructive tests as well. [...] However, these methods are time-consuming and frequently halt the construction. So, for quicker assessment, non-destructive methods are used (PRITIRADHESHYAMNANDAGAWALI, 2018).

There is enormous scope for the development of improved instruments and techniques and for the experimental study of stiffness properties of soils and weak rocks at small strains (BURLAND, 1989).

### 2.5.1 Small Strain Behaviour

In most Engineering problems, the design methods usually focus on the strength approach, relegating the stress-strain behaviour to a less important field. Nevertheless, for many problems in Engineering, particularly in Geotechnical, the use, and even safety, are commanded by strains like foundations settlements. Besides this incoming concern about strains and displacements, small strains tend to get much more consideration in engineering problems.

If soil were Isotropic and linearly elastic it would be possible to determine the elastic constants  $E$  (Young's modulus) and  $\nu$  (Poisson's ratio) from a single simple test and then to use these constants to compute the relationship between stress and strain for other types of tests. With soils, such a simple approach is generally not possible. Hence several different tests have come into common use, each designed to study stress-strain behavior during a specific type of loading (LAMBE & WHITMAN, 1979)

Even though a linear range of stress-strain behaviour does not exist, for practical purposes it is convenient to determine stiffness parameters at very small strains (say  $<0.001\%$ ) and use these as a reference. Very-small-strain stiffness can be used to establish the stiffness profile, which has a profound influence on displacement patterns around new and existing infrastructure. And for those projects where strains will remain low, the operational stiffness will not be greatly different from the very-small-strain value (CLAYTON, 2011). As pointed by Mair (1993), different kinds of structures also affect soil strain due to stiffness degradation, as shown in figure 2.17.

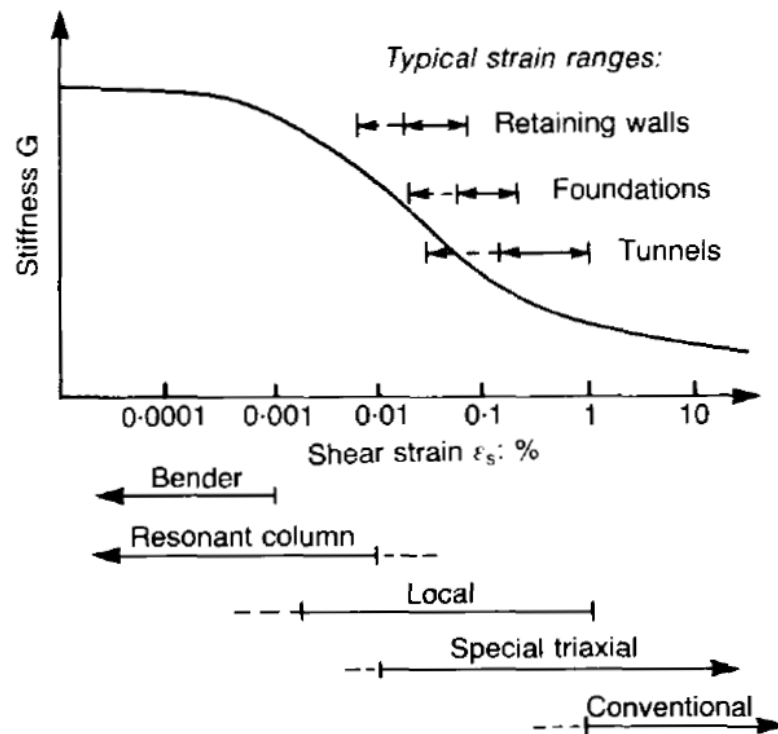


Figure 2.17: Stiffness degradation curve and equipments/structures strain range (MAIR, 1993)

According to Santamarina et al. (2001), some basic differences can be pointed out between small and large strains behaviour:

- a) while small-strain behavior takes place at constant fabric and is controlled by contact behavior, causing a minimal and reversible volume change, with no pore pressure build-up, large-strain behaviour is controlled by fabric changes, and can cause either contraction or dilation under drained loading conditions. Alternatively, it can cause positive or negative pore pressure changes under undrained loading conditions. Energy dissipation can be significant during shear because of frictional and viscous losses.
- b) particle characteristics may affect small- and large-strain behaviour differently too. As angularity and surface roughness increase the interlocking between particles and consequently the large-strain shear strength of the medium for low confinement, the formation of asperities (sharp particles) results in decreasing velocity across the medium.

The seismic field geophysical techniques used in geotechnical engineering make use of two types of seismic waves: surface waves, which in general propagate along with the interfaces between materials with different densities and/or stiffness, or along the ground surface, and body waves, which travel through the body of a solid, unaffected by its surface, with a velocity and ray path controlled only by the density and stiffness, and their vibration (CLAYTON, 2011). Body waves are regularly used in laboratory tests, and the two most frequent modes of body waves propagation, P-waves, and S-waves, are shown in figure 2.18:

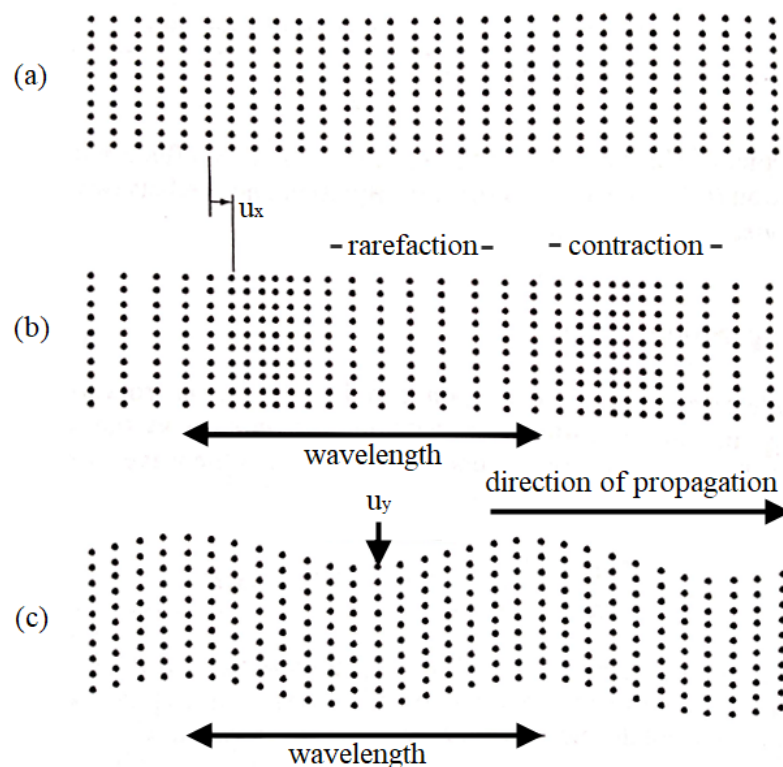


Figure 2.18: Body waves – particle motion in a continuum during wave propagation. The perturbation propagates to the right. The dots can be considered as the centers of particles interconnected with springs, which represent contact stiffness. (a) Center positions before propagation. (b) Displaced positions during the propagation of a P-wave. (c) Displaced positions during the propagation of an S-wave (SANTAMARINA et al., 2001)

It is widely recognized that soils behave nonlinearly from the very early stages of loading. (LEE et al., 2004). Burland (1989) emphasizes that in the past, dynamic measurements of Young's

modulus, or shear modulus, have tended to result in much higher values than static methods in the laboratory, but in recent cases, more accurate methods have shown good correlations, like a comparison of modulus obtained from shear waves to plate tests, and laboratory modulus at 0.01 % strain to in situ dynamic tests.

### 2.5.2 Shear waves

This mode of propagation corresponds to a wave traveling in the x-direction, but with particle motion in the y-direction ( $u_y \neq 0$ ), being the particle motion in perpendicular directions ( $u_x = u_z = 0$ ) (SANTAMARINA et al., 2001).

S-wave velocity ( $V_s$ ) leads to initial shear modulus ( $G_0$ ), which, based on continuous, isotropic, and homogeneous assumption, is given by the Equation (2.15):

$$G_0 = V_s^2 \rho \quad (2.15)$$

Where

$G_0$  = Small-strain shear modulus (kPa)

$V_s$  = Shear wave velocity (m/s)

$\rho$  = Bulk density

Shear waves provide a direct way of determining the dynamic shear modulus of the ground that is independent of Poisson's ratio. [...] The measurement of shear wave velocity provides a simple and quick way of obtaining the dynamic elastic properties of the ground. (ABBIS, 1981).

Yang and Gu (2013) run Bender Elements (BE) and Resonant Columns (RC) tests with three specimens, each corresponding to a different but uniform glass bead particle size (0.195, 0.920, and 1.750 mm). The results indicated differences below 10% between the two test results, and despite the small strain stiffness shear modulus ( $G_0$ ), results indicated a slight decrease when increasing the particle mean size ( $D_{50}$ ). In fact, it was assumed that there was no variation given the uncertainties in a laboratory test.

Shear wave velocity has been used by Ahmed et al. (2018) to determine effective mean stress ( $p'$ ), soil void ratio ( $e_0$ ), Overconsolidation Ratio (OCR), stiffness, and correlate them with

undrained shear strength ( $S_u$ ). A good correlation was found between parameters from many clays around the world.

Rocks may be considered similarly to coarse-grained soils. However, the volumetric component of deformation in rocks may be often small, and accordingly, it appears reasonable to assume that the behaviour of rocks can be represented by a non-linear elastic model based on the shear deformations. Assuming that a relation between shear modulus and small strain shear modulus accounting for stress level can be expressed by equation (2.16) (POULOS, 2018).

$$G = G_0 \left[ 1 - f \times \left( \frac{\tau}{\tau_u} \right)^g \right] \quad (2.16)$$

Where

$G$  = Shear modulus

$\tau$  = Shear stress

$\tau_u$  = Ultimate shear stress

$f, g$  = Empirical parameters, with typical values for many soils of  $f = 1,0$  and  $g = 0,3$

### 2.5.3 Compression waves

Santamarina et al. (2001) explain compression waves propagation mode cause dilation without rotation, and this mode of propagation occurs in parallel traveling x-direction to the motion ( $u_x \neq 0; u_y = u_z = 0$ ). The propagation velocity increases with the stiffness of a material, so P-wave velocity ( $V_p$ ) and bulk density of the media ( $\rho$ ), similarly for shear waves, leads to the constraint modulus ( $M_0$ ) as shown in equation (2.17):

$$M_0 = V_p^2 \rho \quad (2.17)$$

Where

$M_0$  = Small-strain constraint modulus (kPa)

$V_p$  = Compression wave velocity (m/s)



Two of the reasons for the low usage of P-wave piezoceramic elements in laboratory soil test are (i) the shear modulus is more applicable to describe deformation behavior of soil as the soil is loaded mostly in shear mode and (ii) this is an ineffective method for measuring p-wave velocity in saturated soils as the P-wave travels through the water phase faster than through the soil skeleton (LEONG et al., 2009). The principal difference is that in the porosity range 0.0-0.2, compressional waves travel somewhat more slowly in unsaturated rocks than in water-saturated rocks, and much more slowly, in the porosity range 0.2-0.8. The function,  $\eta = -0.175 \ln (V_p) + 1.56$  was obtained.

Besides providing information about the dynamic characteristics of soil, measurements of  $V_p$ , and  $V_s$  with piezoelectric transducers in the triaxial test or other laboratory tests also provide complementary information for data analysis and interpretation. For instance, measurements of  $V_p$  can be considered as an alternative method for verifying soil saturation (BRIGNOLI et al., 1996).

The effect of fracturing on the mechanical properties of rock can be investigated by recording the change of P- and S-wave velocities due to the presence of microcracks (SAROGLU & KALLIMOGIANNIS, 2017). P-waves are especially affected by cracks perpendicular to the propagation direction, whereas S waves are mostly influenced by cracks parallel to the propagation direction (PELLET & FABRE, 2007).

#### 2.5.4 Poisson's ratio

Poisson's ratio expresses how compression in the direction of loading is counteracted by lateral expansion in the perpendicular direction. Incompressible materials have a Poisson's ratio of 0.5. Such materials may compress in the direction of loading, but the volume is unchanged (FELLENIOUS, 2017).

When P- and S-waves are available, for isotropic materials, small strain Poisson's ratio ( $\nu_0$ ) may be calculated by equation (2.18):

$$\nu_0 = \frac{\frac{1}{2} \left( \frac{V_p}{V_s} \right)^2 - 1}{\left( \frac{V_p}{V_s} \right)^2 - 1} \quad (2.18)$$

Where

$\nu_0$  = Small-strain Poisson's ratio

Typical values of Poisson's ratio for different geomaterials are shown in table 2.3

Table 2.3: Typical Poisson's ratio (POULOS, 2017).

Material	Poisson's ratio $\nu$
Saturated soils under undrained conditions	0.5
Soft clays under drained conditions	0.3-0.4
Stiff clays under drained conditions	0.2-0.35
Loose sands and silts under drained conditions	0.3-0.4
Dense sands and silts under drained conditions	0.2-0.4
Rocks	0.10-0.35 (depends on rock type)

### 2.5.5 Waves and cemented materials

The stiffness of the skeleton in cemented materials increases with increasing cement content. The evolution of S-wave velocity and damping with cementation is demonstrated using a sand-cement mixture tested in a resonant column. Two specimens are isotropically confined to different stresses and allowed to harden at constant confinement: specimen A at  $\sigma'_0 = 70$  kPa and specimen B at  $\sigma'_0 = 415$  kPa. The S-wave velocity increases with time, and both specimens asymptotically approach the same stiffness (Figure 2.19); therefore, cementation prevails over effective stress. However, under high confinement, the behaviour of cemented and unsaturated materials becomes stress controlled, as in uncemented and saturated media. (SANTAMARINA et al., 2001)

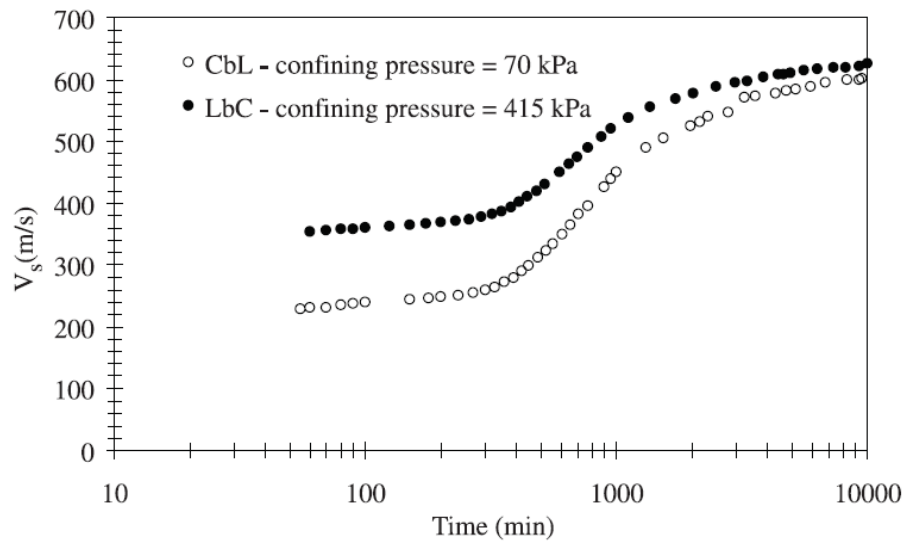


Figure 2.19: Effect of cementation in S-wave velocity (FERNANDEZ & SANTAMARINA, 2001)

Yesiller et al. (2001) measured unconfined compressive strength, secant modulus (1, 2, and 4% strain), and P-waves through ultrasonic pulse testing of a high-plasticity clay stabilized with cement, lime, and lime-fly ash.  $V_p$  has increased with curing time, strength, and secant modulus, which presented a high degree of correlation, especially for 2 and 4% strain.

In a study of artificially cemented clays, Trhlíková et al. (2012) carried tests on a kaolinite-cemented mixture and on pure kaolinite, using Bender Elements to assess shear modulus ( $G_0$ ) during consolidation, finding a nearly constant shear modulus of the cemented mixture, independently of the mean stress, until yielding. After that, both the cemented and the uncemented material increase in  $G_0$  with increasing in the mean stress.

Consoli et al. (2020b) stabilized a residual sandstone soil with fly ash and lime, and high coefficients of determination emerged when  $G_0$ , obtained from ultrasonic pulse velocity tests, was correlated with  $\eta/Biv$ ,  $q_u$ , and  $ALM$  (after 12 cycles). In addition,  $ALM$  and  $G_0$  from more stabilized soils were evaluated, and a reliable correlation comprising all of them was reached.

### 2.5.6 Waves and degree of saturation

The effect of the degree of saturation on P-waves velocity is a well-known fact. In saturated soil, the P-wave velocity is primarily controlled by the bulk modulus of the fluid, but it is also affected by the porosity and the bulk modulus of the material that makes the grains. [...] For

soils with lower degrees of saturation, the bulk modulus of the fluid approaches zero and the P-wave velocity reflects the stiffness of the skeleton including the effect of capillary forces, similar to S-waves (SANTAMARINA et al., 2001). A relation between P-wave velocity increasing and an increase in the degree of saturation in soils and rocks has been extensively related by many researchers (ISHIHARA et al., 2001; KAHRAMAN, 2007; HATANAKA & MASUDA, 2008; ABDI, 2018).

Shear waves cannot travel through water, but water and capillary forces may affect soil skeleton. Cho and Santamarina (2001) point out that the shear modulus in particulate materials depends on the effective interparticle contact forces and the ensuing contact stiffness, so the presence of water in unsaturated particulate materials increases the contact forces, but it also increases the density of the medium. Capillary forces add to skeletal contact forces increasing the stiffness of contacts and the skeleton [...]. The relative movement of menisci surrounding grain contacts causes viscous attenuation. (SANTAMARINA et al., 2001) – figure 2.20.

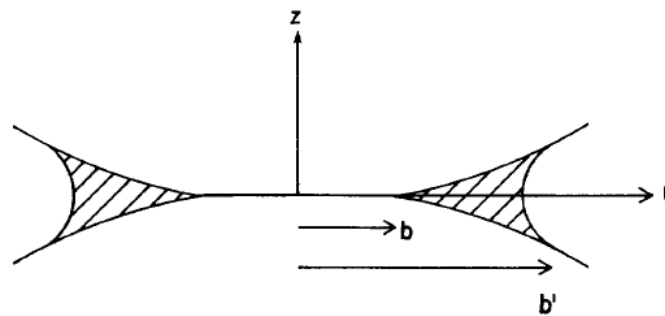


Figure 2.20: Contact between two grains where the menisci turn the contact radius from  $b$  into  $b'$  for the dry to the unsaturated state (PALMER & TRAVIOLIA, 1980).

Dong & Lu (2016) analyzed, with the Bender Element technique, shear waves in many soils under wetting and drying conditions, observing an increase in shear modulus ( $G_0$ ) for the drying conditions, and a steep curve close to the full saturating condition, corresponding to the lowest modulus. Clayey soils presented meaningful higher increments than sandy soils, but the tendency is similar.

At a frequency of 1 MHz, the shear-wave velocities do not always decrease when liquid pore saturants are added to rocks as theorized by Biot: agreement with theory is dependent upon pressure, porosity, fluid-mineral chemical interactions, and the presence of microcracks in the

cementing material (GREGORY et al., 1976). Wu et al. (1984) studied the effect of saturation in shear waves and small strain shear modulus response with resonant columns, which typical ranges are between 10 Hz and 1 kHz (ASTM D4015, 2015), testing fine-grained cohesionless soils. They concluded that capillary effects are most important for lower confining pressures, and their effect decrease as the confining pressure increases. From the relation between the degree of saturation and  $G_0$ , the equation (2.19) emerged, relating the peak, as presented in figure 2.21, with soils grain size.

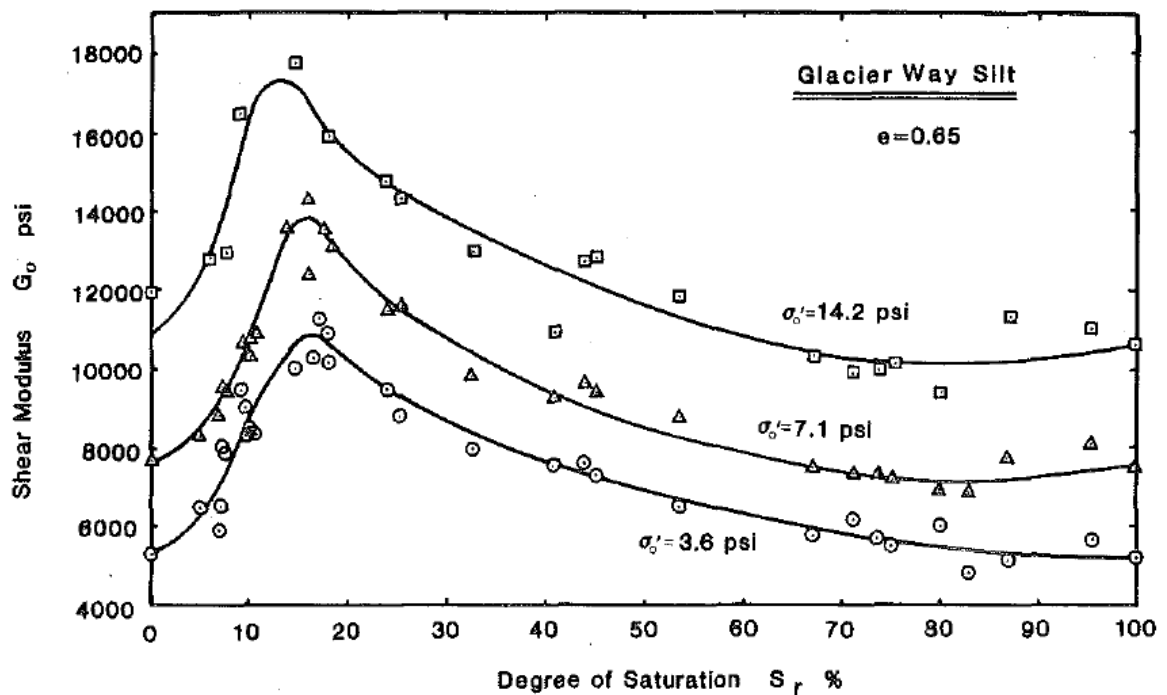


Figure 2.21: Small strain shear modulus versus degree of saturation (WU et al., 1984).

$$(S_r)_{opt.} = -6.5 \log_{10}(D_{10}) + 1.5 \quad (2.19)$$

Where

$(S_r)_{opt.}$  = Optimum degree of saturation

$D_{10}$  = Effective grain size (mm)

But some results are not in agreement with the exposed above between saturation and S-wave velocity. Some studies have not found a peak for S-wave velocity when plotted against the degree of saturation, since the maximum  $V_s$  found was very close to the dry condition (CHO & SANTAMARINA, 2001; DONG & LU, 2016; TAYLOR et al., 2019), some showing a relation between  $V_s$  and matric suction (WHALLEY et al., 2012), and there are studies even showing no influence of saturation on  $V_s$  (CHENG & LEONG, 2013). Dong and Lu (2016) underlined that the dependence of  $V_s$  and  $G_0$  on saturation degree, especially in the high suction range, are still not well understood.

### 2.5.7 Ultrasonic Pulse Velocity

Ultrasonic waves are elastic waves (stress) that propagate at frequencies higher than 20 kHz. This specific frequency separates spectra in two different ranges based on human hearing ability: audible, between 20 Hz and 20 kHz, and inaudible, frequencies higher than 20 kHz (ultrasound) (BORTOLOTTI, 2018).

Ultrasonic pulse velocity is non-destructive and relatively simple to carry out at both in-situ and laboratory conditions. The sonic velocity (SV) test has been used to determine the dynamic properties of rocks in different applications of rock and geotechnical engineering (ARMAN et al., 2017). The ultrasonic pulse velocity (UPV) is widely used because it can investigate the states of one material for a long time and repeatedly (KIM & KIM, 2015).

The most commonly used transducers have a natural frequency of 54 kHz. [...] Difficulties arise with small members as the medium under test cannot be considered as effectively infinite. This will occur when the path width is less than the wavelength ( $\lambda$ ), where  $\lambda =$  pulse velocity/frequency of vibration (BUNGEY, 2006).

Arman et al. (2017) prepared 49 limestones samples with different heights, diameters, and slenderness ratios (H/D). Diameters used were limited by the available bit, being 25.4, 38.1, and 50.8 mm. A 250 kHz frequency was adopted for both compression and shear wave measurement, and, as the slenderness ratio increases,  $V_p$ ,  $E_0$ ,  $V_s$ ,  $G_0$ , and  $\nu_0$  increase too.

Senthilmurugan & Ilamparuthi (2005) performed ultrasonic pulse velocity tests to assess the behaviour with respect to compaction of three clayey soils from Chennai, India.  $V_p$  was compared to dry density, unconfined compressive strength (UCS), and secant modulus at the unconfined compressive test. The velocities were a good indication of compaction degree, could

be correlated with UCS, and even with secant modulus for 50% ( $E_{50}$ ) and 100% ( $E_{max}$ ) of total strength.

Granja et al. (2014) attained a good agreement between Ultrasonic Pulse Velocity and Bender Elements when analyzing stiffness evolution of a cement paste cure, although the UPV method did not allow the waves monitoring in the initial stage of the curing process, probably due to the presence of air bubbles, as explained in the study.

## 2.6 EXPERIMENTAL AND FACTORIAL DESIGN

Design of Experiments (DOE) is a statistical tool deployed in various types of systems, process and product design, development, and optimization. It is a multipurpose tool that can be used in various situations such as design for comparisons, variable screening, transfer function identification, optimization, and robust design. It is a branch of applied statistics that are used for conducting scientific studies of a system, process of product in which input variables (Xs) were manipulated to investigate its effects on a measured response variable (Y) (DURAKOVIC, 2017).

### 2.6.1 Experimental planning

A well-conducted analysis of experiments depends on the first order of a carefully planned experimental design. Oehlert (2010) points out the importance of randomizing to avoid misinterpreting data, for example, doing analyses in random order, or randomizing any physical (e.g., to shuffle a deck of cards) or numerical (e.g., generate a random list of numbers for sequential data) act when is believed to produce random results with known properties.

The objective of statistical inference is to draw conclusions about a population using a sample from the population. [...] A random sample is a sample that has been selected from the population in such a way that every possible sample has an equal probability of being selected. In practice, it is sometimes difficult to obtain random samples, and random numbers generated by a computer program may be helpful. (MONTGOMERY, 2017).

An experiment is just a test or series of tests. [...] The validity of the conclusions that are drawn from an experiment depends to a large extent on how the experiment was conducted. Therefore, the design of the experiment plays a major role in the eventual solution to the problem that initially motivated the experiment. (MONTGOMERY & RUNGER, 2018)

## 2.6.2 Factorial Experiments

The strategy of experimentation that is extensively used in practice is the one-factor-at-a-time approach. This method consists of selecting a baseline level for each factor, then successively varying each factor over its range with other factors held constant at the baseline level. Though it is very useful in understanding the influence of anyone the factor on response of interest, its use is limited to analyzing the joint effect of factors on the response of interest. Factorial experimental design concept is very important in experiments involving several factors where it is necessary to study the joint effect of the factors on a response of interest (RAO & SUBBARAO, 2012).

We obtain a complete factorial design in  $k$  factors by choosing  $n_1$  levels of factor 1,  $n_2$  levels of factor 2, ..., and  $n_k$  levels of factor  $k$  and then selecting the  $n = n_1 \times n_2 \times \dots \times n_k$  runs obtained by taking all possible combinations of the levels selected (BOX & DRAPER, 2007).

When several factors are of interest in an experiment, a factorial experiment should be used. Generally, in a factorial experimental design, experimental trials (or runs) are performed at all combinations of factor levels. In a characterization experiment, we are interested in determining which factors affect the response. The effect of a factor is defined as the change in response produced by a change in the level of the factor. It is called a main effect because it refers to the primary factors in the study. In some experiments, the difference in response between the levels of one factor is not the same at all levels of the other factor. When this occurs, there is an interaction between the factors. Factorial experiments are the only way to discover interactions between variables. (MONTGOMERY & RUNGER, 2018)

The  $2^k$  design is particularly useful in the early stages of experimental work when many factors are likely to be investigated. It provides the smallest number of runs for which  $k$  factor can be studied in a complete factorial design. Because each factor has only two levels, we must assume that the response is approximately linear over the range of the factor levels chosen. The simplest type of  $2^k$  design is the  $2^2$  – that is, two factors A and B, each at two levels. We usually think of these levels as the factor's low and high levels. [...] Note that there must be at least two replicates ( $n \geq 2$ ) to compute an error sum of squares (MONTGOMERY & RUNGER, 2018).

Therefore, when the number of factors is moderately large, say,  $k \geq 4$  or 5, a common practice is to run only a single replicate of the  $2^k$  design and then pool or combine the higher-order



interactions as an estimate of error. Sometimes a single replicate of a  $2^k$  design is called an unreplicated  $2^k$  factorial design. When analyzing data from unreplicated factorial designs, occasionally real high-order interactions occur. The use of an error mean square obtained by pooling high-order interactions is inappropriate in these cases. A simple method of analysis can be used to overcome this problem. Construct a plot of the estimates of the effects on a normal probability scale. The effects that are negligible are normally distributed with mean zero and variance  $\sigma^2$  and tend to fall along a straight line on this plot, whereas significant effects have nonzero means and will not lie along the straight line. (MONTGOMERY & RUNGER, 2018).

A potential concern in the use of two-level factorial designs is the assumption of linearity in the factor effects. Of course, perfectly linearity is unnecessary, and the  $2^k$  system works quite well even then the linearity assumption holds only approximately. However, a method of replicating certain points in the  $2^k$  factorial provides protection against curvature and allows an independent estimate of error to be obtained. The method consists of adding center points to the  $2^k$  design. These consist of  $n_c$  replicated run at the point  $x_i = 0$  ( $i = 1, 2, \dots, k$ ). One important reason for adding the replicate runs at the design center is that center points do not affect the usual effects estimates in a  $2^k$  design. We assume that the  $k$  factors are quantitative (MONTGOMERY & RUNGER, 2018).

Regression also calculates colinearity diagnostics, predicted values, residuals, measures of fit and influence, and several statistics based on these measures. The basic specification is dependent, which initiates the equation(s) and defines at least one dependent variable, followed by the method, which specifies the method for selecting independent variables (GUNAYDIN et al., 2010).

### 3 LABORATORY EXPERIMENTS DESIGN, REVIEW, AND PROCEDURES

This chapter presents a brief description, standards, and procedures adopted for the laboratory tests and material characterization. The following table 3.1 summarizes the experiments run in this research: preliminary, dispersibility, durability, mechanical and geophysical tests.

Table 3.1: Experimental program tests.

Tests		Materials	
Preliminary	Grain size distribution	Light scattering	A; B; C; D
		Hydrometer sedimentation	A; B
	Atterberg limits	Liquid limit	A
		Plastic limit	A
	Field unit weight	Intact specimen density	A
	Specific gravity	Water pycnometer	A; B
	Compaction	Modified Proctor compaction	A; AB; ABC
	Mineralogy	XRD	A; B; C; D
	Chemical analysis	XRF	C
	Specific surface area	BET	A; B; C; D
Lime stabilization content	ICL	ABC	
Geophysical	Small strain stiffness	UPV - P-waves	ABC; ABD
		UPV - S-waves	ABC; ABD
Dispersibility	Visual deflocculation	Crumb test	A
	Chemical deflocculation power	Salts concentration	A
	Internal erosion	Pinhole	A; ABD
	Dispersibility ratio	Double hydrometer	A
Durability	Mass and properties loss	Wetting and drying	ABC; ABD
		Wetting, drying and brushing	ABC; ABD
Mechanical	Strength and stiffness	Unconfined compression	ABC; ABD

A = Soil    B = Fly ash    C = Carbide lime (calcitic)    D = Primor lime (dolomitic)

### 3.1 PRELIMINARY TESTS

When initiating a geotechnical design, or an experiment related to soil mechanics, it is essential to know some basic characteristics of the soil in order to assess some basic properties of those materials. These preliminary characteristics may be assessed through field description and, more accurately, by running laboratory tests, granting knowledge about probable soil behaviour, and how to improve it.

#### 3.1.1 Particle size

Particle size is one of the most discussed and informative characteristics of soils. However, there is still no unanimity in how grain size and grain size distribution have to be considered to classify a soil.

Besides the grain size, it is important to know how those particles are distributed in the soil mass. Gradation can be quantified through the coefficient of uniformity and coefficient of curvature. The coefficient of uniformity ( $C_u$ ) is calculated by equation (3.1). Low values of the coefficient of uniformity value mean that the soil gradation is uniform. High  $C_u$  values mean that the larger grains present in soil are much larger than the lower grains. The coefficient of curvature ( $C_c$ ) can be calculated by equation (3.2). Well graded soils are soils with  $C_c$  between 1 and 3.

$$C_u = \frac{D_{60}}{D_{10}} \quad (3.1)$$

$$C_c = \frac{(D_{30})^2}{D_{60} \times D_{10}} \quad (3.2)$$

Where

$C_u$  = Coefficient of uniformity

$C_c$  = Coefficient of curvature

$D_{60}$  = Grain diameter below which there are 60% of particles present in the soil

$D_{10}$  = Grain diameter below which there are 10% of particles present in the soil

$D_{30}$  = Grain diameter below which there are 30% of particles present in the soil

The first attempt to classify soils based on plasticity and grain size was done by Casagrande in 1942. Later, in 1950, a based Casagrande's system was incorporated by a Code Practice in Britain, which, in 1981, give rise to the form of the classification in the revised Code, published at the British Standard BS 5930. The American system, known as the Unified Soil Classification System (USCS), developed from Casagrande's system, was first published in 1953 and later redraft and published by ASTM in 1966 as the Standard Test Method for Classification of Soils for Engineering Purposes (DUMBLETON, 1981). Table 3.2 shows the classification according to USCS and is based on grain size, liquid, and plasticity limits.

Table 3.2: Classification based on the grain size distribution and LL – ASTM D2487 (ASTM, 2018).

Criteria for Assigning Group Symbols and Group Names Using Laboratory Tests <sup>A</sup>				Soil Classification		
				Group Symbol	Group Name <sup>B</sup>	
COARSE-GRAINED SOILS	Gravels (More than 50 % of coarse fraction retained on No. 4 sieve)	Clean Gravels (Less than 5 % fines <sup>C</sup> )	$C_u \geq 4.0$ and $1 \leq C_c \leq 3.0^D$	GW	Well-graded gravel <sup>E</sup>	
		Gravels with Fines (More than 12 % fines <sup>C</sup> )	$C_u < 4.0$ and/or $[C_c < 1 \text{ or } C_c > 3.0]^D$	GP	Poorly graded gravel <sup>E</sup>	
			Fines classify as ML or MH	GM	Silty gravel <sup>E,F,G</sup>	
	More than 50 % retained on No. 200 sieve	Sands (50 % or more of coarse fraction passes No. 4 sieve)	Clean Sands (Less than 5 % fines <sup>H</sup> )	$C_u \geq 6.0$ and $1.0 \leq C_c \leq 3.0^D$	SW	Well-graded sand <sup>I</sup>
			Sands with Fines (More than 12 % fines <sup>H</sup> )	$C_u < 6.0$ and/or $[C_c < 1.0 \text{ or } C_c > 3.0]^D$	SP	Poorly graded sand <sup>I</sup>
				Fines classify as ML or MH	SM	Silty sand <sup>F,G,I</sup>
FINE-GRAINED SOILS	Silts and Clays	inorganic	$PI > 7$ and plots on or above "A" line <sup>J</sup>	CL	Lean clay <sup>K,L,M</sup>	
		organic	$PI < 4$ or plots below "A" line <sup>J</sup>	ML	Silt <sup>K,L,M</sup>	
			$\frac{\text{Liquid limit} - \text{oven dried}}{\text{Liquid limit} - \text{not dried}} < 0.75$	OL	Organic clay <sup>K,L,M,N</sup> Organic silt <sup>K,L,M,O</sup>	
	50 % or more passes the No. 200 sieve	Silts and Clays	inorganic	$PI$ plots on or above "A" line	CH	Fat clay <sup>K,L,M</sup>
			organic	$PI$ plots below "A" line	MH	Elastic silt <sup>K,L,M</sup>
				$\frac{\text{Liquid limit} - \text{oven dried}}{\text{Liquid limit} - \text{not dried}} < 0.75$	OH	Organic clay <sup>K,L,M,P</sup> Organic silt <sup>K,L,M,O</sup>
HIGHLY ORGANIC SOILS	Primarily organic matter, dark in color, and organic odor		PT	Peat		

The classification for coarse-grained soils can be done according to the flow chart classification presented in figure 3.1.

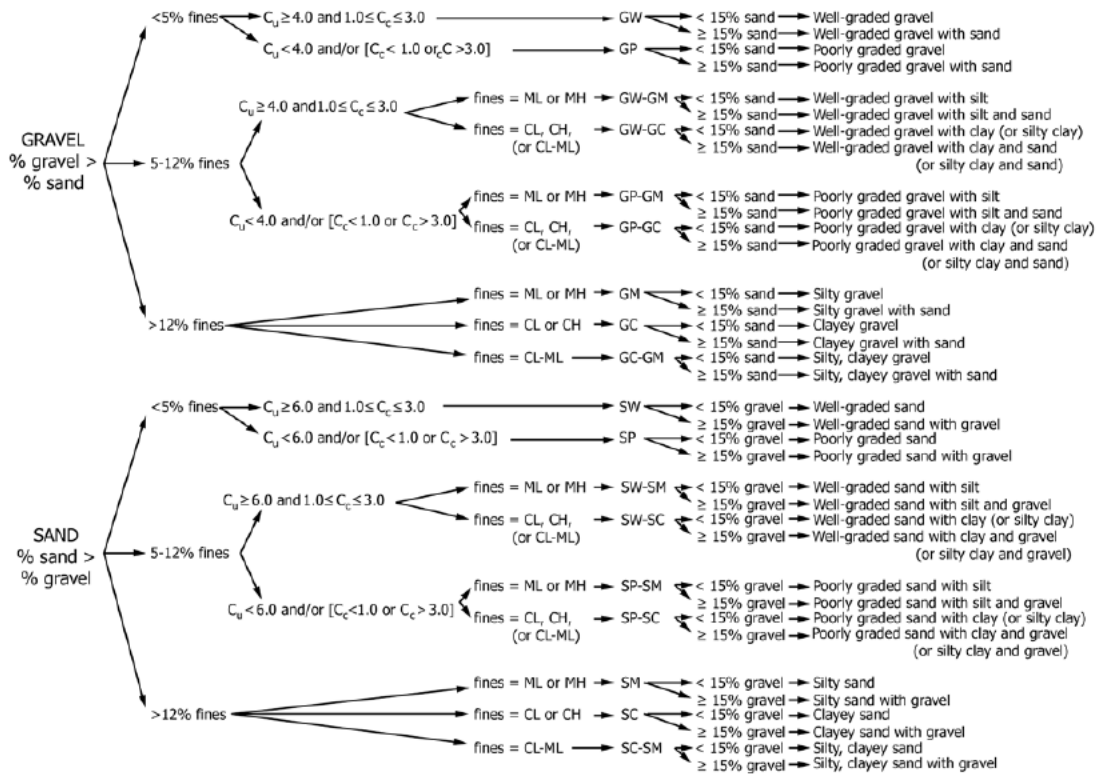


Figure 3.1: Flow Chart for Classifying Coarse-Grained Soils (More Than 50 % Retained on No. 200 Sieve) – ASTM D 2487 (ASTM, 2018).

The following tests are commonly used to assess the grain size of particulate media.

### 3.1.1.1 Sieve analysis

Sieve analysis is used to graduate soil particles with a diameter larger than 75 μm (No. 200 sieve). This test is done by passing soil through successive square opening sieves, registering the retained dry mass of particles for every sieve, starting from the wider opening sieve. For soils ranging between 75 μm and 75 mm (3” sieve), sieving analysis is standardized by ASTM D 6913 (ASTM, 2017). Sieve analysis for larger particle diameter is standardized by ASTM D 5519 (ASTM, 2015) that covers natural and man-made riprap materials and related materials like filter stone or coarse bedding materials. Results are presented in a plot of percent by mass against particle diameter. The sieve analysis was carried only to evaluate the grain size distribution between 2.000 and 0.075 mm (#10 and #200, respectively), as illustrated by figure 3.2.



Figure 3.2: Sieves from left to right: 2.000 (#10), 1.180 (#16), 0.600 (#30), 0.425 (#40), 0.250 (#60), 0.150 (#100) and 0.075 mm (#200).

### 3.1.1.2 Light scattering

This test is used to determine particle size distribution by light scattering. It is applied to the measurement of particulate materials of diameter up to  $0.4\ \mu\text{m}$ , but it may not be convenient for the analysis of flocculated particles.

### 3.1.1.3 Sedimentation analysis

Schramm and Scripture Jr. (1925) explained that when a clay suspension is falling in a fluid, the rate of material falling is independent of suspension strength and, based on Stokes' law, assuming spherical particles, grain size can be calculated because larger particles will fall faster than the smaller ones. According to this sedimentation theory, the settling ratio is related to particle diameter and density, fluid density and viscosity.

The sedimentation or hydrometer method is used to determine particle-size distribution using Stokes' concept for materials in the range of  $0.2$  to  $2,000\ \mu\text{m}$ . This test method is standardized by ASTM D 7928 (ASTM, 2017), which prescribes the soil to be put in distilled water in a glass cylinder with a capacity of  $1,000\ \text{mL}$ , where sedimentation is measured with a hydrometer along time (figure 3.3). To prevent fine particles from flocculating, a dispersion agent (deflocculant) composed of sodium hexametaphosphate ( $\text{NaPO}_3$ )<sub>6</sub> is used.



Figure 3.3: Hydrometer inside the glass cylinder.

The grain size distribution is obtained from the combination of sedimentation and sieve analysis and may be compared to light scattering grain size analysis.

Sedimentation analysis without deflocculant is similar to the analysis within a deflocculant solution, but the clay particles remain aggregated unless they are weakly bounded or the adsorbed salts result in dispersive behaviour in presence of water. Sedimentation without the aid of a deflocculating agent gives valuable information as to the condition of the clay (SCHRAMM & SCRIPTURE JR., 1925).

### 3.1.2 Atterberg Limits

In soil mechanics, the Atterberg limits are the most distinctive and easiest property of fine-grained soils to measure. (DOLINAR & SKRABL, 2013). Atterberg limits gather the limits associated with soil states: liquid limit, plastic limit, and shrinkage limit. These states are associated with water content, as outlined in figure 3.4.

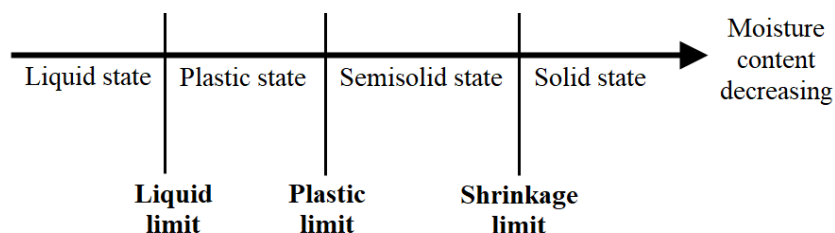


Figure 3.4: Consistency of cohesive soils (after from DAS, 2008).

ASTM D4318 (ASTM, 2017) covers liquid limit (LL) and plasticity limit (PL) tests for particles with a diameter smaller than  $425\ \mu\text{m}$  (sieve no. 40), and the plasticity index determination, calculated by subtracting PL from LL. The standard Casagrande's device is used for the liquid limit determination and, for plasticity limit, a small portion of soil mass is rolled until its shape comes to an approximately cylindrical form with 3.2 mm diameter, being the plasticity index the water content where this cylinder crumbles. Those tests were employed only for soil characterization. The liquid limit test is shown in figure 3.5.



Figure 3.5: Soil liquid limit test with Casagrande's device.

Odell et al. (1960) have shown that liquid limit, plastic limit, and plasticity index are strictly related to the amount of clay and organic carbon. Dolinar and Skrabl (2013) found out that, for non-swelling soils, the water content at the Atterberg limits depends mostly on size and portion of clay minerals, while for swelling soils the limits are also dependent on interlayer water quantity, which is dependent on the type of clay minerals, exchangeable cations and chemical composition of the pore water. In conclusion, a uniform criterion for determining the interdependence of the liquid and plastic limit values and different soil properties becomes tricky.

Skempton (1953) have shown that the plasticity index of soils is linearly related to the clay (soil particles smaller than  $2\ \mu\text{m}$ ) content. It was observed that the same clay content when comparing different clay minerals resulted in distinct plasticity indexes. That is, when plotting the clay content and plasticity index (figure 3.6), the linear slope depends on the clay minerals.



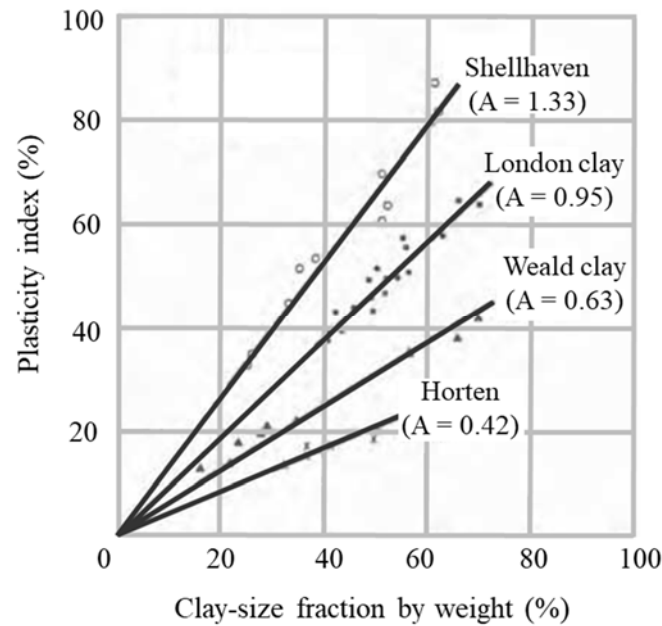


Figure 3.6: Relation between Plasticity Index and Clay Fraction (after Skempton, 1953).

This slope is called soil activity and can be expressed by the equation (3.3). The activity values of some minerals are presented in Table 3.3.

$$Activity = \frac{PI}{\text{percentage of clay size-fraction, by weight}} \quad (3.3)$$

Table 3.3: Activity index for some minerals (after Skempton, 1953).

Mineral	Activity
Quartz	0.00
Calcite	0.18
Mica (muscovite)	0.23
Kaolinite	0.33
	0.46
Illite	0.90
Ca-montmorillonite	1.50
Na-montmorillonite	7.20

Clays with an activity index below 0.75 were labeled as inactive clays, between 0.75 and 1.25 were classified as normal clays, and above 1.25 as active clays. According to Skempton (1953), activity values lower than 0.75 mean that the soil may possess at least one of the following characteristics: predomination of kaolinite among the clay fraction or little true clay minerals;

deposition in fresh water; in salt water with subsequently leaching by the percolation of fresh water. The author also states that clays combining those three characteristics are part of the least active group I, where the Activity is less than 0.5, and that the typical members of that group are late-glacial clays derives largely by mechanical erosion of non-argillaceous rocks by ice-sheets, and deposited in ice-dammed lakes.

### 3.1.3 Specific gravity

The specific gravity of soil solids plays an important role in soil mechanics, being used to determine many soil physical properties. The standard adopted was ASTM D 854 (ASTM, 2014), which specifies the determination of soils specific gravity by water pycnometer. A small amount of soil is put in a calibrated pycnometer with water, and by connecting the pycnometer to a vacuum pump (figure 3.7) and/or placed in a warm water bath. The specific solid gravity is determined by relating a pycnometer full of water with a pycnometer with soil inside. The test was executed by combining the vacuum system with the warm water bath.



Figure 3.7: Vacuum pump for the pycnometer analysis.

Typical values of specific soil gravity ( $\rho_s$ ) for most soils range from 2,500 to 2,800 kg/m<sup>3</sup>, depending on the predominant mineral in the soil (HOLTZ et al., 2011).

### 3.1.4 Compaction

Proctor (1933) noted that the principle of lubrication could be beneficially applied to the compaction of soils because, due to the viscous nature of the pore fluid, the ratio of water changes the compaction energy necessary for the compaction of the same soil. However, the suction effect probably plays an important role in compaction energy, since there is a peak in specific weight for given moisture content, decreasing with addition of water.

Mitchell (1969) reviewed works about the effect of temperature on the shear strength of soils and suggested that for constant structure and water content, lower strengths are associated with higher temperatures. Despite these results, tests have also shown that the influence of temperature during compaction/consolidation is more significant than during shear since the samples compacted in temperatures equal or higher than shear temperatures presented increasing in shear strength as the compaction/consolidation temperature increase. As the compaction tests were executed at about 30°C, a different temperature may affect compaction results.

There is a test used to determine the relationship between water content and dry unit weight of soils. The most widespread test is called the Proctor test and is based on successive blows applied on the soil by a rammer. This test is repeated for many water contents, allowing a compaction curve to be drawn, where dry unit weight is plotted against water content, and the peak of the curve is the maximum unit weight. There are basically two distinct energy compaction efforts: the original Proctor test, where a 600 kN.m/m<sup>3</sup> is applied to the soil, described in ASTM D698 (ASTM, 2012), and the modified effort test, when 2.700 kN.m/m<sup>3</sup> is applied on the sample, that can be done following ASTM D1557 (ASTM, 2015) guidelines. The Brazilian standard (NBR 7182) (ABNT, 2016) also includes the intermediate effort, where the applied energy is about 1.270 kN.m/m<sup>3</sup>. To assess the maximum reachable dry unit weight, a modified effort was applied in compaction tests with two different fly ash contents. Only the calcitic lime (carbide lime) was tested in compaction tests since the required energy for the compaction of this lime tends to be higher than for the dolomitic lime (Primor extra lime). As the lime reacts in the presence of water, only one compaction test was conducted.

Consoli et al. (2001) performed compaction tests on a silty sand treated with fly ash and carbide lime (a specific calcitic lime). Results show that when 25% (mass ratio) of fly ash is added to the soil, the peak dry unit weight decreases throughout a slight decrease in peak moisture

content. But when the carbide lime is added to that mixture, the optimum dry unit weight decreases, and the corresponding moisture content increases.

Modified energy tests were used particularly in the determination of the maximum moulding dry unit weight.

### 3.1.5 Specific Surface Area

The specific area of soils and soil constituents can range from less than  $0.1 \text{ m}^2/\text{g}$  to more than  $800 \text{ m}^2/\text{g}$ . Soils consisting primarily of sands (i. e. particles diameters of  $0.05 \text{ m}$ - $2.0 \text{ mm}$ ) typically possess relatively small specific surface areas, usually less than  $0.5 \text{ m}^2/\text{g}$ . In contrast, soils containing appreciable amounts of clay minerals and organic matter tend to exhibit much larger specific surface areas (PENNEL, 2016).

The magnitude of the surface area per mass, specific surface, is, therefore, a good indication of the relative influence of electrical forces on the behavior of the particle. The term colloid is used to describe a particle whose behavior is controlled by surface-derived forces rather than mass-derived forces. A clay particle is a colloid because of its small size and irregular shape. The smaller a particle size the larger its specific surface (LAMBE & WHITMAN, 1979). As the specific surface of a soil increase: the liquid limit  $LL$ , plastic limit,  $PL$ , plasticity index  $PI$ , and soil activity increase; the hydraulic conductivity  $k_h$  decreases; the electrical conductivity increases (surface conduction); the compression index  $C_c$  increases; the coefficient of consolidation  $c_v$  decreases; and the peak, constant volume, and residual friction angles decrease (SANTAMARINA et al., 2001).

In general, the specific surface area  $S_s = 1 \text{ m}^2/\text{g}$  boundary suggests a drastic change in the physical-chemical phenomena that take place within the soil. When the specific surface of the soil exceeds  $S_s = 1 \text{ m}^2/\text{g}$ , surface-related forces may control the soil response, alter fabric formation, cause shrinkage in unsaturated conditions, change the small strain stiffness, modify the threshold strain, affect strength, alter internal conduction and diffusion processes, and promote rich energy coupling mechanisms (SANTAMARINA et al., 2002).

According to Feng et al. (2018), the fly ash used in currently practical engineering is usually between  $0.3$  and  $0.4 \text{ m}^2/\text{g}$ , but higher values can be obtained from grinding. Although, higher specific surface values are not so unlikely in the Engineering literature, reaching values from

0.55 to even 7.2 m<sup>2</sup>/g (REDDY & GOURAV, 2011; CRISTELO et al., 2016; DONATELLO et al., 2010).

Oates (1998) points out that an increase in specific surface area of hydrated limes affects the absorption efficiency, and that most commercial hydrated limes present BET specific surface areas ranging from 10 to 20 m<sup>2</sup>/g.

The B.E.T. method, proposed by Brunauer et al. (1938), is widely used in the determination of soil specific surface area. The adsorption of nitrogen (N<sub>2</sub>) gas, in conjunction with the Brunauer-Emmett-Teller (BET) equation, is the most common method of surface area determination. However, it is widely recognized that N<sub>2</sub> does not access the interlayer surfaces of expandable clay minerals after sample drying. To overcome this limitation, the retention of polar compounds, such as ethylene glycol monoethyl ether (EMGE) or water, has been utilized to measure the total specific surface area (i.e., internal + external) of soils and expandable clay minerals (PENNEL, 2016).

### 3.1.6 Initial Consumption of Lime

The laboratory test method used to ensure the lowest percentage of lime that results in a stabilized soil-lime pH is standardized by ASTM D6276 (ASTM, 2019), and is based on pH measurements for mixtures with different lime concentration until the measured pH reaches 12.4 or a value close to that. The methodology is popularly known as the ICL (Initial Consumption of Lime) test and was conducted for the determination of the stabilization of the mixture composed of soil, fly ash, and carbide lime (figure 3.8).



Figure 3.8: ICL test apparatus.

### 3.1.7 X-Ray Diffractometry

Crystals, in general, are able to diffract x-rays, and the diffraction response depends on minerals composition.

The three basic components of an x-ray diffractometry are the X-ray source, specimen, X-ray detector, and they all lie on the circumference of a circle, which is known as the focusing circle. The angle between the plane of the specimen and the x-ray source is  $\theta$ , the Bragg angle. The angle between the projection of the x-ray source and the detector is  $2\theta$  (SURYANARAYANA & NORTON, 1998). The test is schematically illustrated in figure 3.9.

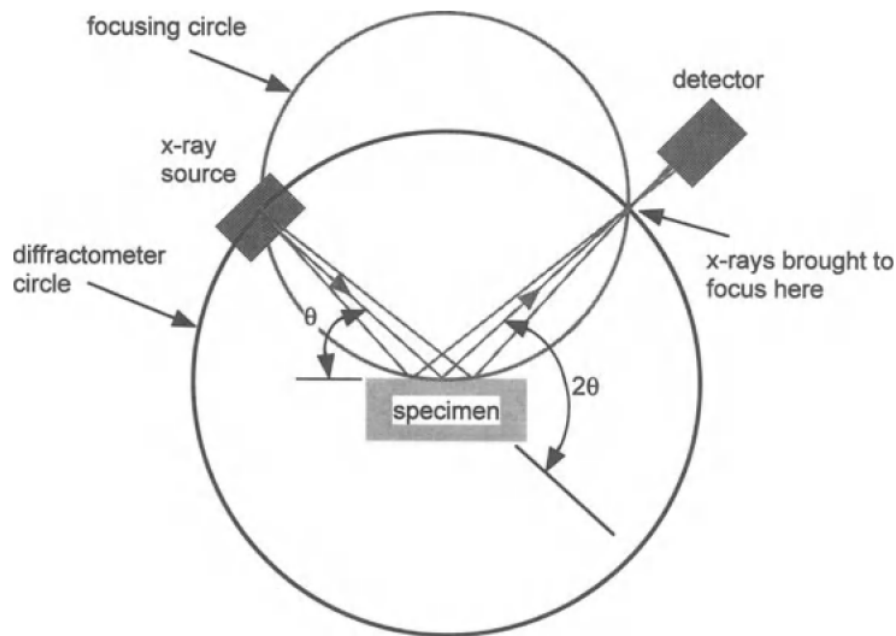


Figure 3.9: XRD test (SURYANARAYANA & NORTON, 1998).

Crystallographic planes in minerals refract X-rays at an intensity that depends on the amount of mineral in the volume of soil irradiated and the proportion of the mineral grains that are properly oriented (MITCHELL & SOGA, 2005). X-ray diffraction methods are used to determine the relative proportions of clay and other minerals present (BELL, 2004). One of the quantification methods of minerals proportion was proposed by Chung (1974), where the proportion of the mineral in a sample is calculated based on a Reference Intensity Ratio (RIR). Those references may be found in the literature for most minerals, however, results could be influenced by some sources of errors, and, for that, the analysis may be defined as a semi-quantitative analysis.

Beyond clay minerals identification, XRD has become one of the most prominent analytical techniques in the characterization of Portland cement-based systems (SNELLINGS et al., 2014), and is also the key to elucidating the lime stabilization reactions in soil (NABIL et al., 2020).

In the present study, basic XRD analysis developed an important role in the determination of soil, pozzolana, and limes mineralogy as well as an estimation of minerals amount.

According to Singh and Subramaniam (2016), the XRD may be used to assess the total amorphous content of a given material as expressed by the equation (3.4):

$$w_{amorphous} = 1 - \sum_{\alpha=1}^n w_{\alpha} \quad (3.4)$$

Where

$w_{amorphous}$  = total amorphous content

$w_{\alpha}$  = weight fraction of the  $\alpha$ th crystalline phase

$n$  = total number of crystalline phases

### 3.1.8 X-Ray Fluorescence

According to Waseda et al. (2011), when there are uncertainties about a sample composition, the type of elements and the composition ratio of the elements contained can be more accurately assessed through fluorescent X-ray analysis.

X-ray fluorescence (XRF) spectroscopy analysis is based on a material excitation by emitting high energy x-rays and measuring elements intensity. This method does not provide minerals crystallography identification, but the presence of some chemical elements.

### 3.1.9 Apparent field-specific gravity

In order to determine the field-specific gravity of the soil mass, intact specimens can be sampled from the field.

The water displacement method is widely applied for specific gravity, equivalent to bulk density, and is standardized by ASTM D7263 (ASTM, 2018). The methodology consists of

indirect volume measurements: a sample of soil is covered with wax and put in water to have its weight determined. The volume is then indirectly determined by the buoyant force applied by the water at the bottom of the sample.

In the case of Pelotas soil, intact samples were prepared (figure 3.10) to assess their apparent specific gravity. Also, before those tests, a pure wax, approximately spherical specimen, were prepared (figure 3.11) for the wax specific gravity determination.



Figure 3.10: (a) intact soil sample; (b) soil covered by wax.



Figure 3.11: Pure wax specimen.

In the test, the specimen was tied to a string which is suspended by a hook placed on an ordinary scale, as shown in figure 3.12.





Figure 3.12: hydrostatic balance.

### 3.1.10 Water content

Water content is usually determined by oven-drying soil specimen at 105°C to constant weight as determined by most standards, including ASTM D2216 (ASTM, 2019). However, according to Frydman et al. (2008), for saline soils, this procedure tends to underestimate water content, because when the soil is dried, the salts that were solubilized in water may account as the solid component, and their part in fluid weight is ignored. Soil properties like dry density, specific gravity, void ratio, Atterberg limits, compressibility, among others, are influenced by water content measurement, and the difference between their determination when conventional water content test is conducted and when the real water content is determined increases as the salinity of pore water increases (MESSAD & MOUSSAI, 2015).

## 3.2 DISPERSIBILITY EXPERIMENTS

To assess the dispersion phenomenon more tangibly, specific tests can be carried on the experimental program. The main dispersibility tests are chemical tests for the water-soluble salts in the soil, crumb, double hydrometer, and pinhole tests. There are many methodologies and tests to assess the dispersibility of soils, including the Pinhole test, CEC vs. ESP, Crumb Test, double hydrometer test, SAR, TDS vs. % Na. Based on the statistical reliability of dispersibility tests, Bell and Walker (1999) proposed ratings for the evaluation of dispersibility, given in Table 3.4.

Table 3.4: Proposed rating system for identification of dispersive soils (after BELL & WALKER, 1999)

Dispersibility test					
Pinhole test	Class	Dispersive	Moderate	Slightly	Nondispersive
	Rating	5	3	1	0
CEC vs. ESP	Class	Highly dispersive	Dispersive	Marginal	Nondispersive
	Rating	4	3	1	0
Crumb Test	Class	Strong reaction	Moderate	Slight	No reaction
	Rating	3	2	1	0
SAR	Class	Over 2	1.5-2		Less than 1.5
	Rating	2	1		0
TDS vs. %Na	Class	Dispersive	Intermediate		Nondispersive
	Rating	2	1		0
	Overall	Highly dispersive 12 or above	Moderately dispersive 8–11	Slightly dispersive 5–7	Nondispersive 4 or less

### 3.2.1 Salts concentration

The Brazilian standard NBR 13603 (ABNT, 1996) covers the US Soil Conservation procedures for the determination of dissolved salts in clay interstitial water. Flame photometry may be used for sodium and potassium concentration, and spectrophotometry for the determination of calcium and magnesium concentration.

Salts concentration is evaluated and compared to the dispersive behaviour presented in the literature.

### 3.2.2 Crumb test

The crumb test, developed by Australian scientists, consists of a qualitative test where the behaviour of an aggregate is evaluated at natural moisture condition when submerged in distilled water. It is considered a useful dispersion indicator, however, in only one direction. In other words, if the crumb test indicates dispersion, the soil is probably dispersive, but many dispersive clays do not react to the test. (BASTOS, 1999)

The test procedure consists of putting a soil clod in a glass container with distilled water. The soil response, when put into water, will be visually defined and classified according to a

dispersion gradation from 1 (non-dispersive) to 4 (highly dispersive) as shown in figure 3.13. ASTM D6572 (ASTM, 2020) provides instructions and recommendations for this test, indicating the Crumb test to be run in conjunction with a pinhole test and a double hydrometer test.

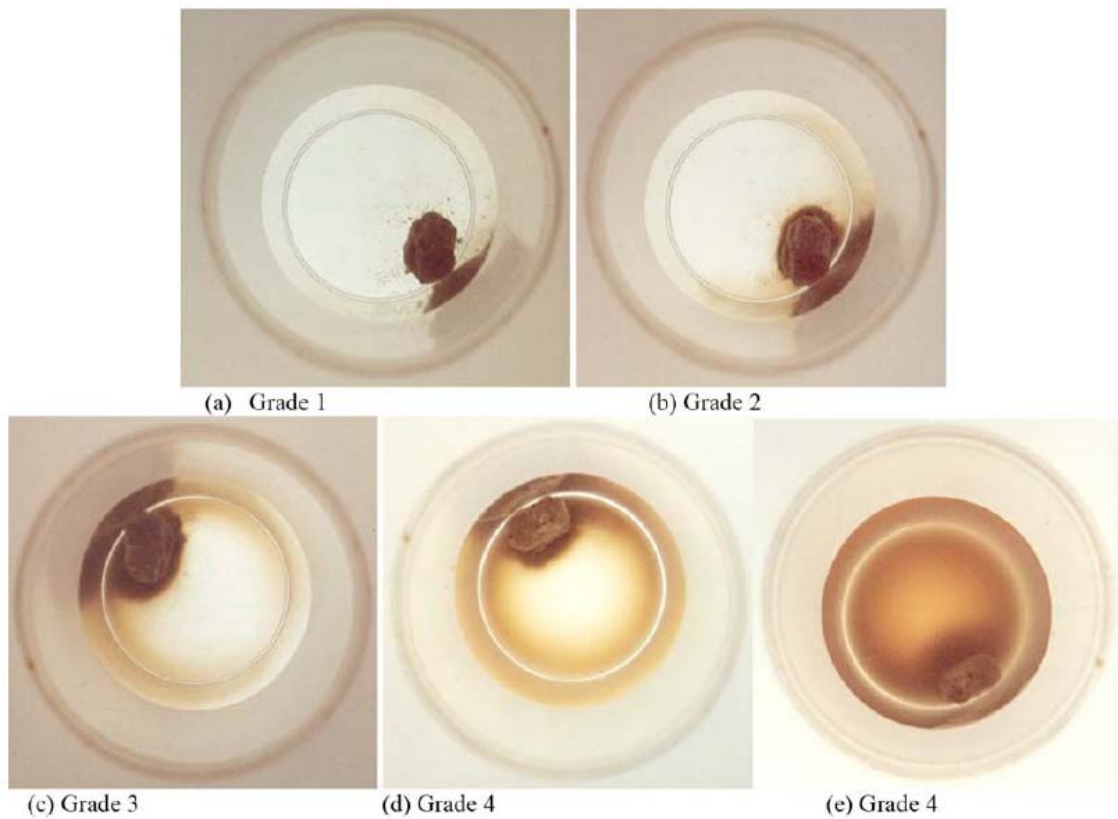


Figure 3.13: Crumb test dispersibility degree [ASTM D6572 (ASTM, 2020)]

Crumb tests were carried out on intact specimens in-field moisture conditions and also in the laboratory.

### 3.2.3 Double Hydrometer test

This test method is based on results obtained from hydrometer sedimentation tests with the aid of a deflocculant solution compared to the same test without a dispersion agent. The double hydrometer test is standardized by ASTM D4221 (ASTM, 2018), where the results are presented as a percent dispersion, calculated by equation (3.5). Obtained % Dispersion below

30 ranks the soil as nondispersive; from 30 to 50% the soil is classified as intermediate dispersive, and above 50% a soil is classified as dispersive.

$$ASTM\%Dispersion = \left( \frac{N_{m,2\mu m,nd}}{N_{m,2\mu m,d}} \right) \times 100 \quad (3.5)$$

Where

$N_{m,2\mu,nd}$  = mass percent finer than 2  $\mu\text{m}$  obtained from hydrometer test without deflocculant

$N_{m,2\mu,d}$  = mass percent finer than 2  $\mu\text{m}$  obtained from hydrometer test within deflocculant

The double hydrometer test is standardized by NBR 13602 (ABNT, 1996) in Brazil, where it is known as the Sedimentometric Comparative test, or SCS test, in recognition of the Soil Conservation Service contribution. In that standard, the compared particle diameter is 5  $\mu\text{m}$  instead of 2  $\mu\text{m}$ .

Middleton (1930) has proposed a similar relation to assess dispersibility, accounting also for larger particles flocculant behaviour, naming this relation as dispersion ratio (DR), expressed by the equation (3.6). Higher values of DR have been related to more rapidly erosive behaviour.

$$DR = \frac{N_{m,50\mu m,nd}}{N_{m,50\mu m,d}} \quad (3.6)$$

Where

$N_{m,50\mu,nd}$  = mass percent finer than 50  $\mu\text{m}$  obtained from hydrometer test without deflocculant

$N_{m,50\mu,d}$  = mass percent finer than 50  $\mu\text{m}$  obtained from hydrometer test within deflocculant

### 3.2.4 Pinhole test

Pinhole test was proposed by Sherard et al. (1976b) after studying problems related to dispersive soils. This test is based on the soil internal erosion assessment when it is subjected to a water flow, induced by many hydraulic gradients, through a 1 mm hole in the middle of the soil sample. ASTM D4647 (ASTM, 2020) covers a pinhole method where the water flow rate, final hole diameter, and collected water turbidity are evaluated. The soil is then classified as dispersive (D), moderately to slightly dispersive (ND4, ND3), and non-dispersive (ND2, ND1)

as schematically shown in figure 3.14. Figure 3.15 illustrates results for clear and dark water after the test. The test equipment is illustrated in figure 3.16.

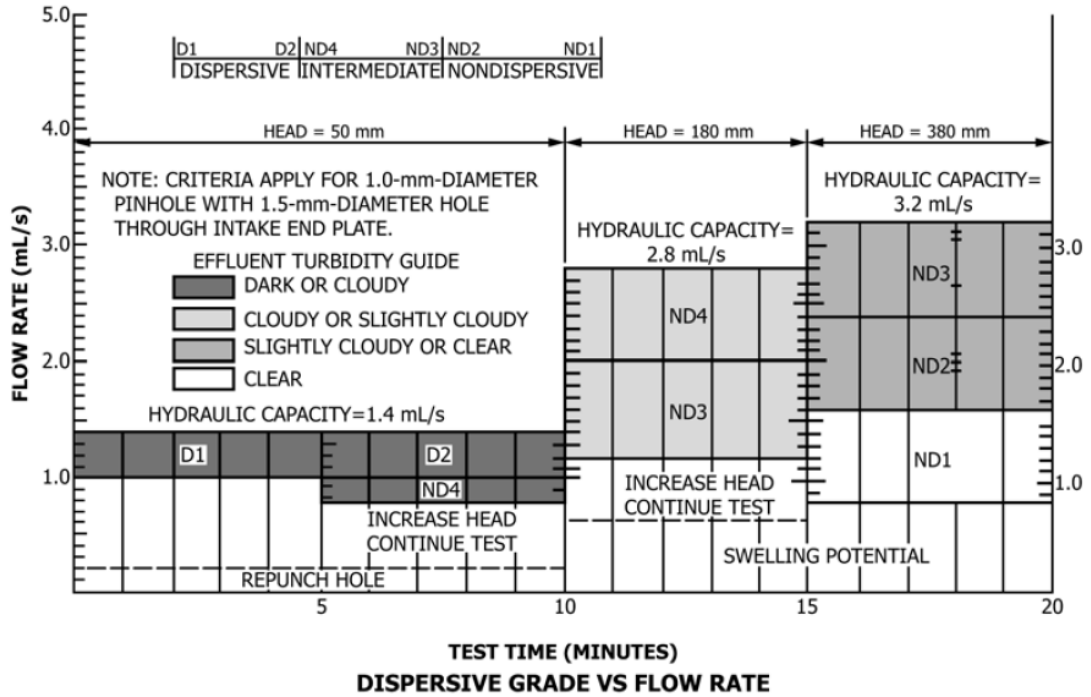


Figure 3.14: Criteria for dispersibility classification with the pinhole test [ASTMM D4647 (ASTM, 2020)].

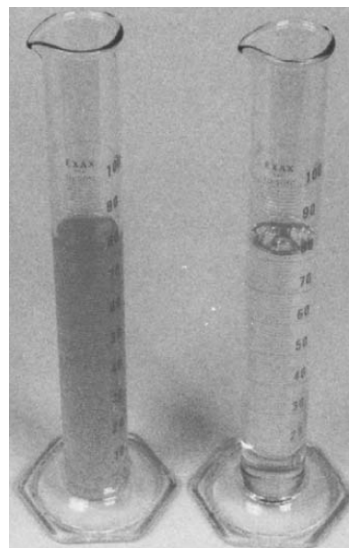


Figure 3.15: Comparison of cloudy colloidal appearance with perfectly clear water [ASTMM D4647 (ASTM, 2020)].

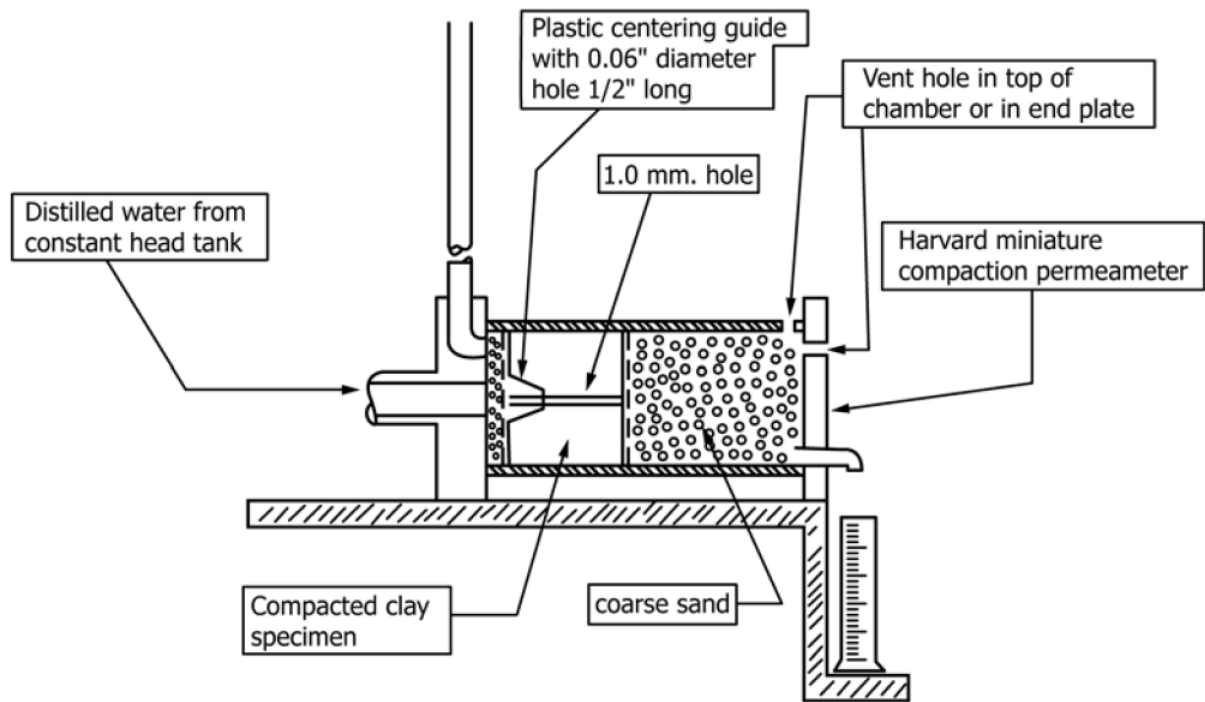
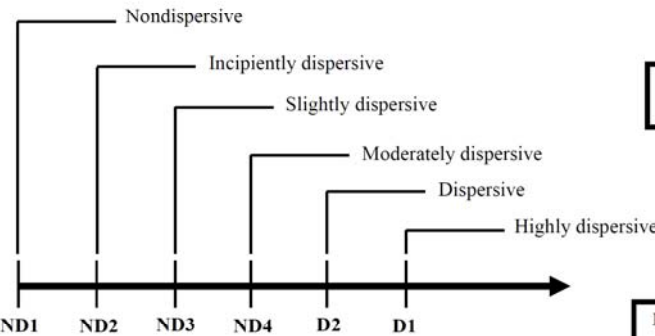
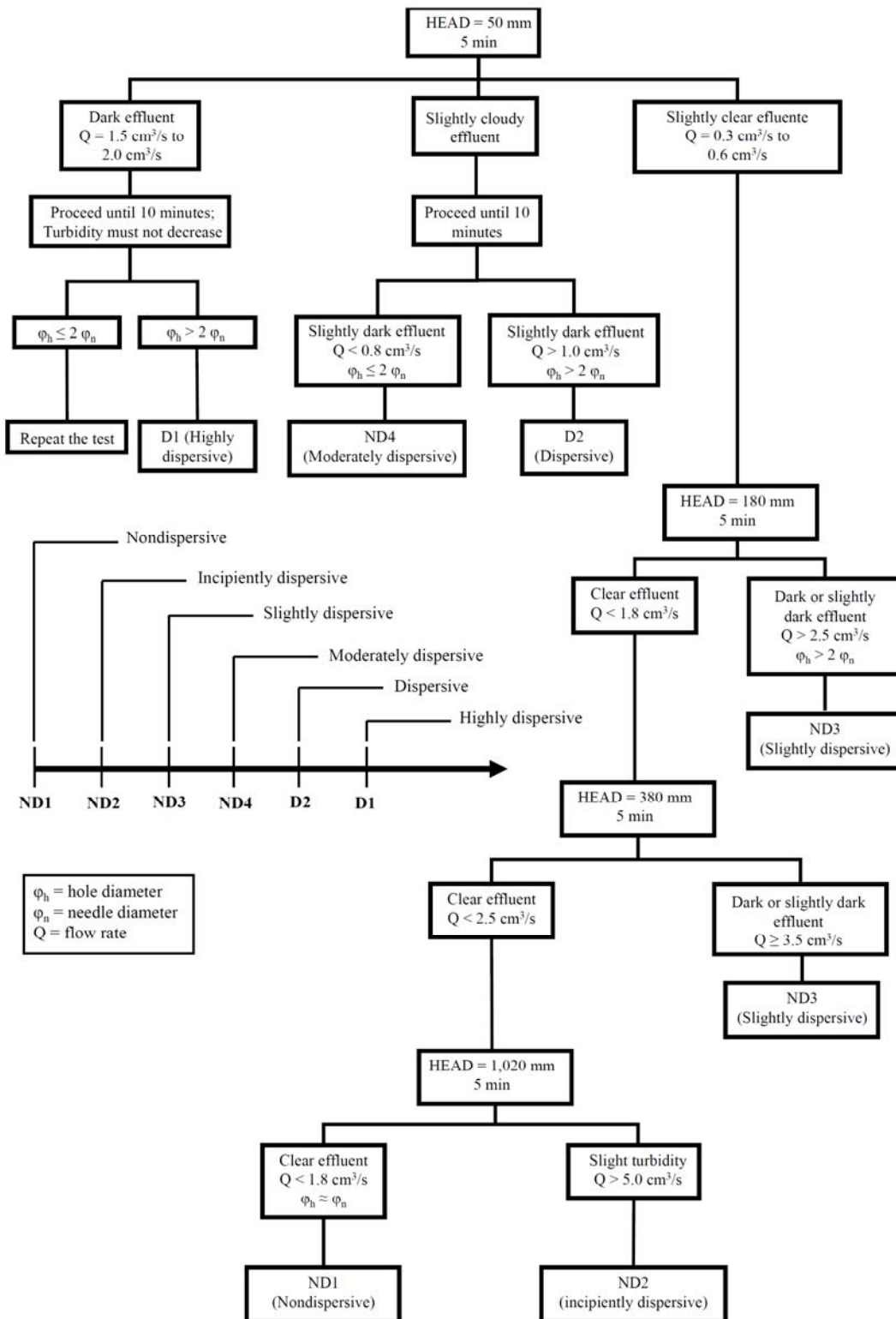


Figure 3.16: Pinhole test equipment [ASTMM D4647 (ASTM, 2020)].

The Brazilian standard NBR 14114 (ABNT, 1998) proposed a similar but distinct method for the dispersibility assessment with the pinhole test and, as the soil has, according to Welter and Bastos (2003), some peculiarities, the Brazilian standard was adopted. The flowchart presented in figure 3.17 indicates the procedure for the test procedure and classification, where the hole diameter (figure 3.18) is indicated as  $\Phi_h$  and the needle diameter as  $\Phi_n$ .



$\phi_h$  = hole diameter  
 $\phi_n$  = needle diameter  
 $Q$  = flow rate

Figure 3.17: Pinhole test flowchart [after NBR 14114 (ABNT, 1998)].



Figure 3.18: Hole in the center of the sample.

Despite being a commonly used test to assess dispersibility, Sherard (1987) relates a highly dispersive result from the pinhole test apparatus when analyzing a specific non-dispersive soil, known for a very erodible behaviour because of its high content of silt-sized particles. Those tests were carried on compacted soil specimens for different dry unit weights. Also, stabilized soils 28 days after mixing were tested but, inasmuch as the needle stiffness was very low, only loose soil mixtures were tested. The pinhole test apparatus is shown in figure 3.19.



Figure 3.19: Pinhole test equipment.

As there is no intermediate color pattern indicating the intermediate corresponding turbidity between dark cloudy colloidal appearance and clear water, the graduation presented in figure 3.20 was adopted in test interpretation. In slightly clear to slightly cloudy samples, it is possible to see the bricks through water, whereas in slightly cloudy to cloudy, it is not possible.



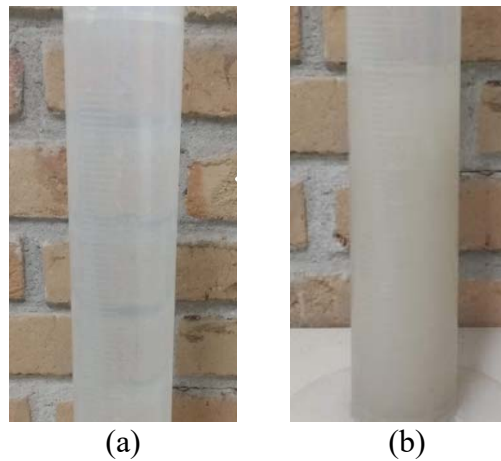


Figure 3.20: Pinhole adopted turbidity pattern (a) slightly clear (b) slightly cloudy/dark.

### 3.3 DURABILITY, MECHANICAL AND GEOPHYSICAL TESTING

After evaluating basic materials properties and dispersibility behaviour, an objective evaluation of more tangible engineering properties like durability, strength, and stiffness will be conducted. Herein, a lot of laboratory tests must be run.

#### 3.3.1 Moulding and curing

Before moulding, the soil was passed through the No. 10 sieve (2 mm opening), calcitic and dolomitic lime were passed through No. 100 sieve (150  $\mu\text{m}$  opening), and fly ash was not sieved. Sample moulding was done by mixing the soil with fly ash and lime in a dry state (figure 3.21) before adding water to the mixture.



Figure 3.21: Soil, fly ash, and calcitic lime (yellow-brown, dark gray and white color, respectively) prepared for molding.

Samples were statically compacted in three layers with the same thickness. After the third layer compaction, the mass was determined, and also height and diameter with three measurements each. Measurements were immediately followed by samples packing in plastic bags and putting into a water tank with a controlled temperature of  $23 \pm 2^\circ \text{C}$  (figure 3.22), according to ASTM D1632 (ASTM, 2017). The lower temperature limit was controlled by an electrical aquarium heater, and the upper temperature was controlled by the room air conditioner. The moisture determination was done by separating small amounts of the wet mixed materials and putting them into a  $100^\circ \text{C}$  oven for at least 24 h. A curing period of 28 days (4 weeks) was chosen as it was a feasible period for the research experiment and it is easier compared to similar studies and practical engineering problems.



Figure 3.22: Water curing tank with controlled temperature.

### 3.3.2 Durability test

Durability tests try to simulate, in controlled conditions, erosion, weathering, cracking, and/or abrasion, among other deleterious effects on materials.

#### 3.3.2.1 Wetting, drying, and brushing

Wetting, drying, and brushing tests are used to determine mass loss, water content, and volume changes when a cemented specimen is subjected to water submersion followed by heating and mechanical abrasion cycles.

The molding standard used for cemented soil durability tests is ASTM D 698 (ASTM, 2012), which prescribes a sample diameter of about 10.16 cm and a height of about 11.64 cm, indicating two cemented soil replicas to be molded. As the available mold used in this study

has an internal diameter of approximately 10.03 cm, the specimens were molded to achieve the same standard sample volume ( $943.69 \text{ cm}^3$ ), incurring an 11.94 cm height (Height/Diameter ratio =  $1.19 \approx 1.20$ ).

The durability test is usually covered by ASTM D 559 (ASTM, 2015), whereafter the stipulated curing period, a specimen is put into a potable water container for 5 h. After the wetting period, the specimen is removed from the water and put into an oven at  $71 \pm 3^\circ$  for 42 h, and then, a wire scratch brush is used to give 26 to 28 strokes on the specimen (18 to 20 on the sides and 4 on each end – base and top –) applying about a 13 N force. This procedure accounts for one cycle of 2 days (48 h). After each cycle, the mass is determined and the sample is measured. This process is repeated for 12 cycles. One of the specimen's replicas may not be scratched to allow for dry weight measuring after 12 cycles, comparing the brushed and the non-scratched specimen. In the present study, because of the small amount of soil, this test was conducted without molding replicates. Typical behaviour expected from soils subjected to this test is presented in figure 3.23. The more modification (quantified as the mass loss) a material undergoes, the less durable the material is.

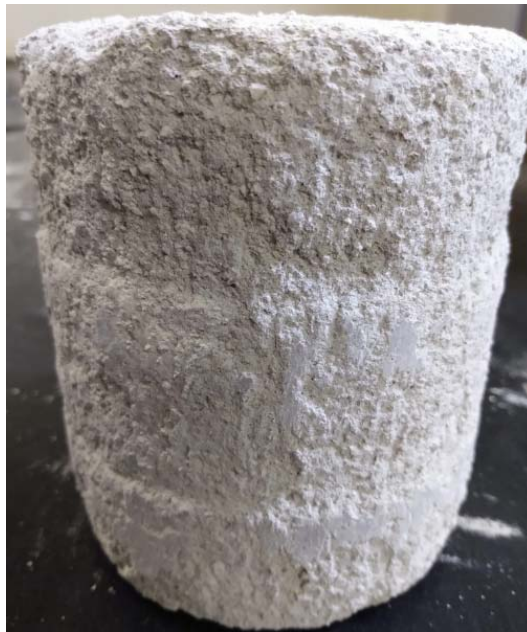


Figure 3.23: Typical behaviour of stabilized soil with a high mass loss after 12 cycles of wetting, drying and brushing durability tests.

### 3.3.2.2 Wetting and drying

Wetting and drying tests run in this study are based on the common durability test standardized by ASTM D 1557 (ASTM, 2012), but the samples are molded with lower volume, with a diameter of about 5.02 cm and a height of approximately 10.04 cm. Due to the low weight and volume, the specimen is not brushed, and mass loss is determined only after the 12<sup>th</sup> cycle by oven drying from 100° to 110°C. This test method was applied because the moulded samples demand less material and space in the water tank, and may also be compared to the soil-cement unconfined compressive tests because those specimens have the same size. Besides that, a mass loss can be observed without the need for brushing, isolating the abrasion and surface factors from the weathering and erosive durability. Packard and Chapman (1963) underline that the surface effects in concrete durability tests are not considered as necessarily reflecting the overall condition of the specimen.

As this procedure for the determination of mass loss lacks precision, only accumulated loss of mass values higher than 0.5% were considered. A typical behaviour expected from soils subjected to this durability test is presented in figure 3.24.



Figure 3.24: Typical behaviour stabilized soils with a high mass loss after wetting and drying durability tests.

### 3.3.3 Unconfined compressive strength test

This test was run for the determination of cemented soil cylinder specimens, based on ASTM D1633 (ASTM, 2017) methodology. At least 24 h before the test, the specimens were put in immersion inside the water curing tank, at  $23 \pm 2^\circ \text{C}$ . A constant strain rate of 1.14 mm/min was applied, and the displacement at failure was determined with a common mobile chronometer. To minimize errors caused by sample bedding during initial compression, only secant modulus at maximum strain was evaluated. Beyond that, for very cemented specimens, thereafter presenting brittleness failure, the installation of displacement measurements could be tricky and costly because of the potential damage on the equipment caused by the blow-up effect. When the rate of strain is constant, there could be at least a rough estimate of the axial displacement.

In the absence of radial displacement measurements, Poisson's ratio could not be evaluated. The applied force was determined using load cells and dynamometric rings. The test equipment used in this research can be seen in figure 3.25. Load cells with a capacity of 10, 20, and 50 kN were used. For higher loads, a dynamometric ring with 100 kN capacity was used.



Figure 3.25: Unconfined compression equipment with 10 kN load cell.

A typical brittle failure, common in most medium to high cemented soils, is shown in figure 3.26, where a near  $60^\circ$  shear plane is created.



Figure 3.26: Typical shear surface for medium-high cemented soils in unconfined compressive tests.

After failure, a portion corresponding to at least 20% of soil by mass was put dried in an oven for the determination of moisture content and failure soil dry unit weight (figure 3.27).



Figure 3.27: Soil portion taken for the samples moisture determination after failure.

### 3.3.3.1 Strength test after the curing period

This test covers the determination of strength after the stipulated curing period. The tested specimens were molded following ASTM D 698 procedures, except for the molding size. The samples were molded with a diameter of approximately 5.02 cm and a height of about 10.04 cm (slenderness ratio approximately 2).

### 3.3.3.2 Strength tests after durability cycles

In order to assess the strength degradation of stabilized admixtures under durability cycles, the study aims to test also samples' strength under uniaxial unconfined compression. The cycle influence will be analyzed too since the strength tests will be conducted for a distinct number of cycles (1, 4, and 12).

### 3.3.4 Ultrasonic pulse velocity testing

Ultrasonic pulse velocity tests (UPV) were conducted by using the Pundit Lab<sup>®</sup> equipment developed by Proceq S.A. (PROCEQ S.A. ©, 2017).

#### 3.3.4.1 UPV equipment

The Pundit Lab<sup>®</sup> equipment shown in figure 3.28 is widespread test equipment commonly used in concrete specimens but has proven to be reliable to assess cemented soils' small strain stiffness at unconfined stress conditions (BORTOLOTTI, 2017).



Figure 3.28: UPV equipment used.

Compression waves were measured using the direct arrangement presented in figure 3.29, where the path length is simply the distance between the transducers. The transducers were coupled using a common medical ultrasound gel and the emitted frequency was 54 kHz. The compression time-travel is automatically located by the equipment, and the velocity is calculated from the obtained time when waves travel through specimen length, considered as the wave path.

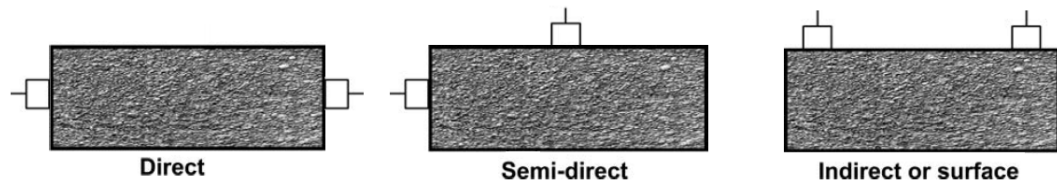


Figure 3.29: Transducers arrangements (after PROCEQ S.A.©, 2017).

For shear wave measurement, the same cables are used, but with different transducers. The interface gel is also different, being described as a shear gel, water-soluble organic substance with very high viscosity. The frequency used was 250 kHz, and the waveform was manually located as exemplified in figure 3.30. Every time the cables were connected to the equipment or changed, the Pundit Lab® was zeroed using a calibration rod.

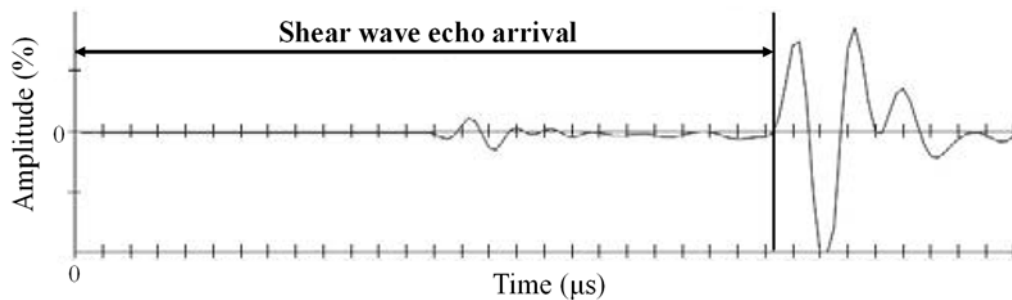


Figure 3.30: Shear waves arrival time in PUNDIT tests (after PROCEQ S.A.©, 2017).

UPV measurements were conducted in samples after 28 curing days (0 cycles), where the sample moisture is nearly equal to the moulding moisture, and for the samples subjected to durability cycles after 1, 4, and 12 cycles, when the moisture content is very low. Beyond those tests, some samples were tested immediately after moulding, in moulding moisture condition. Both P- and S-waves were measured for the determination of elastic stiffness and elastic relations.

The ultrasonic pulse velocity test in concrete is standardized by ASTM C597 (ASTM, 2016). ASTM D2845 (ASTM, 2008), a standard used for rock samples, was withdrawn in 2017. Soil-cement or soil-lime materials has no specific standard for UPV tests.



## 4 MATERIALS CHARACTERIZATION AND EXPERIMENTAL DESIGN

This chapter examines the materials used in this research and also the tests for the characterization of those materials, as well as the mixtures created from them. Next, the experimental design is presented.

### 4.1 SOIL CHARACTERIZATION

The soil studied was collected with manual work tools, with no need for careful on sample disturbance, since the intention was to remold the soil in the laboratory. Only for the determination of the field specific gravity, the soil was sampled at not disturbed state.

#### 4.1.1 Soil site characterization and geology

The soil was collected nearby Pelotas (figure 4.1), in the Rio Grande do Sul state, the southern province of Brazil. The area where the soil was collected is located close to a highway, and the site is characterized by a deep erosive process, with many gullies and ravines, forming even small valleys, with a poor ecosystem and vegetation coverage (Figure 4.2)

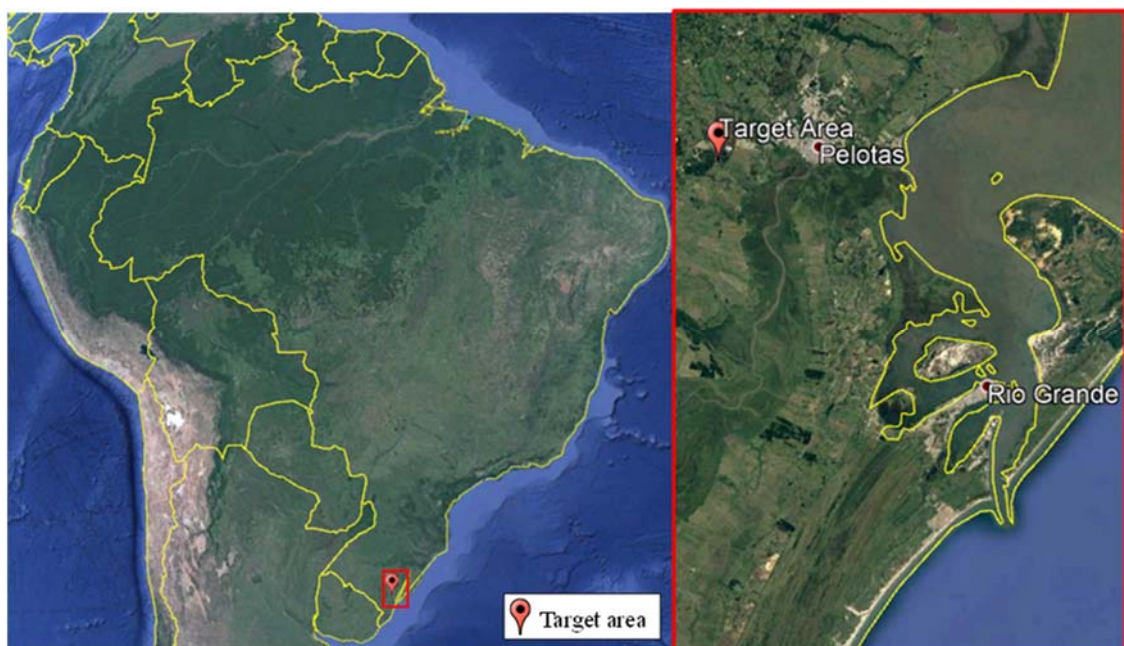


Figure 4.1: Map location of the soil target area (GOOGLE, 2020).



Figure 4.2: View of the soil sampling site.

This area is situated in the sedimentary basin of Pelotas. Its lithostratigraphic unit (Figure 4.3) is alluvial deposits, whose lithotypes are sands, clays, pebbles, polymictic conglomerates, and silts. It is characterized by the presence of sandy-clayey alluvial non-consolidated sediments, fine to medium-grained, with variegated colors, organic deposits, gravels, fine to coarse-grained sands, with some interposition of silty-clayey layers and organic deposits related to the inundation plains and fluvial canals (CPRM, 2004).

The regional geology is mainly associated with Pleistocene sedimentary deposits from an alluvial origin and those linked to the barrier II formation. Deposits of the lagoon plain associated with barrier II are composed of poorly selected silty-clay sands of light colors and incipient parallel flat lamination, with rework by the wind and concretions. The peat deposits unit presents heterogeneous peat interleaved or mixed with sand, silt, and clay, locally with diatomite. Nearby, the presence of Capão do Leão granite is also noted, being petrographically an equigranular medium to large granite. This granite presents centimetric injections of veins or late albite pockets, and its mineral assembly consists of quartz, alkali feldspar, and albite-rich plagioclase.

The deposits from the target area were formed by the marine transgression during the Pleistocene. The rising of relative sea-level during repeated glaciations has brought sands to those deposits.

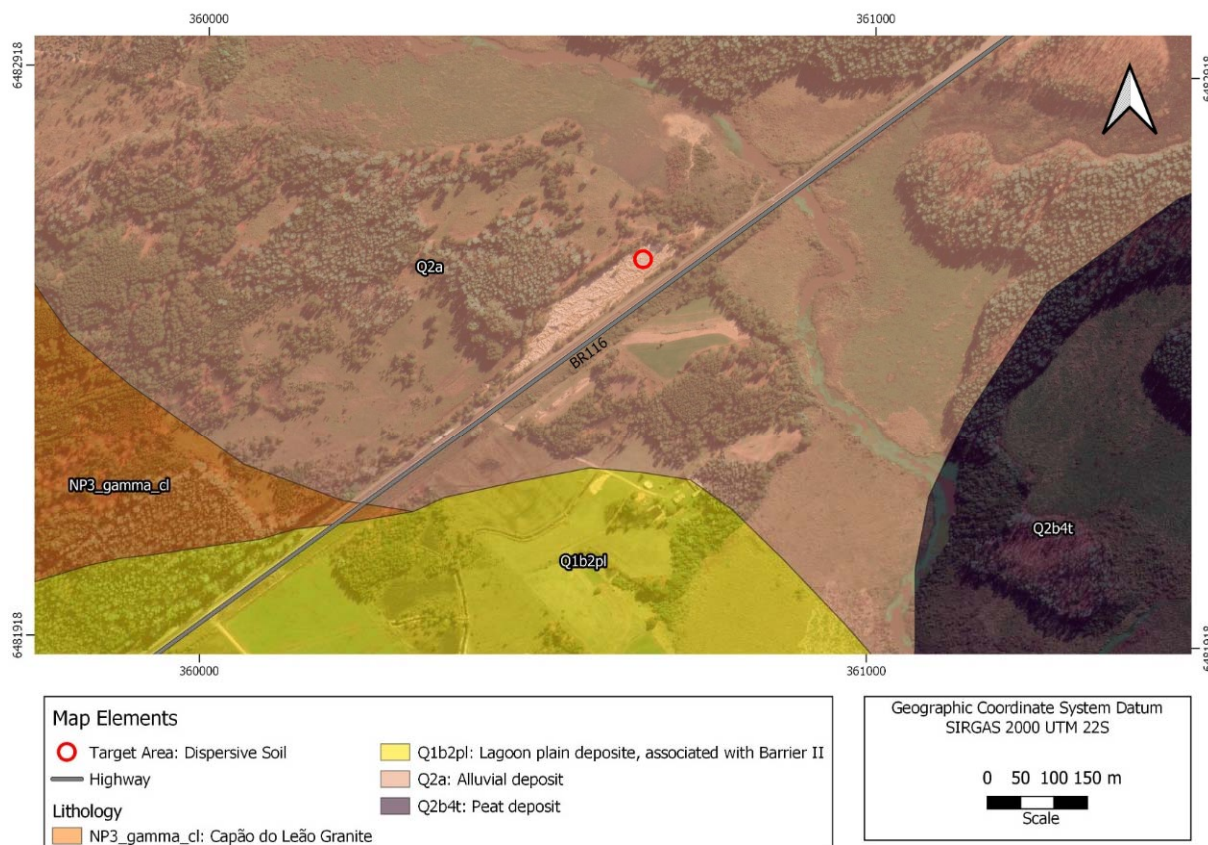


Figure 4.3: Regional lithological map (adapted from CPRM, 2004).

The characterization of the Pelotas soil depends on a large number of tests. To recognize the physical and chemical characteristics of this soil, the following tests were conducted.

#### 4.1.2 Soil grain size distribution and double hydrometer test

The granulometric study was done by sedimentation analysis. The sedimentation analysis was conducted with and without adding a deflocculant solution. The grain size distribution results are presented in figure 4.4. From the double hydrometer test, as the percent of dispersion is 55%, the soil is classified as dispersive. The dispersion ratio is 73.16%.

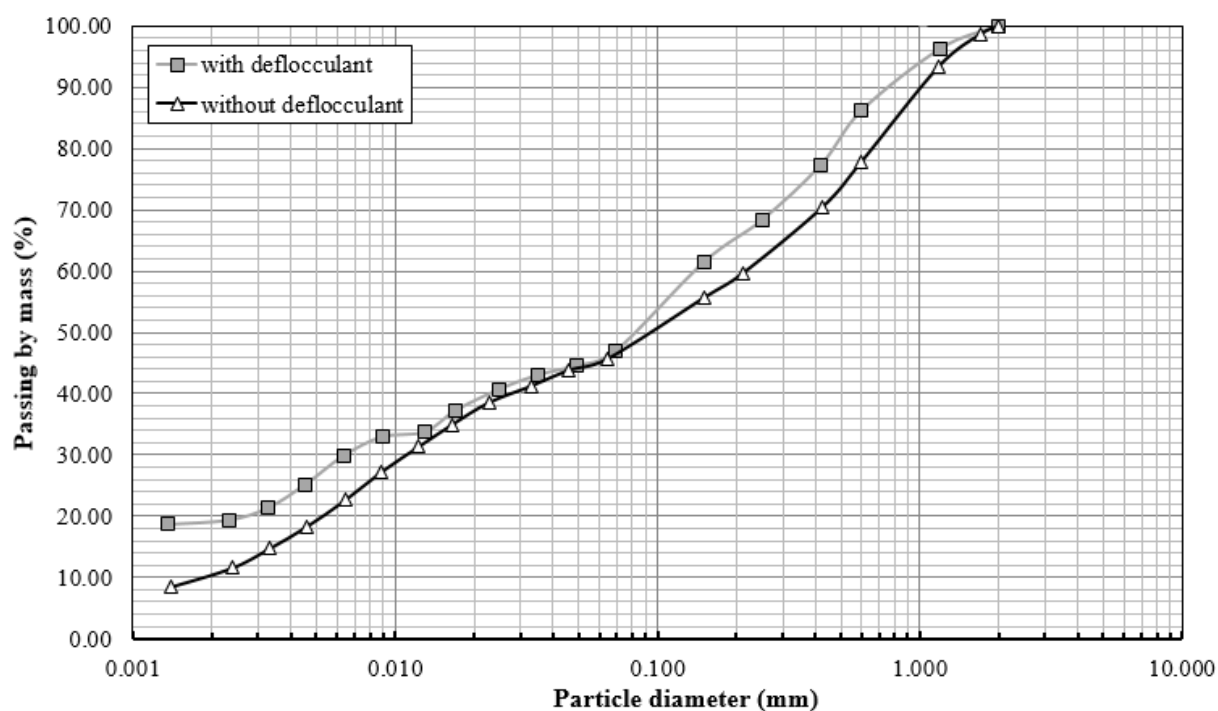


Figure 4.4: Soil particle size distribution.

The average grain size ( $D_{50}$ ) was found to be 0.085 mm, and the smallest particle diameter is 0.0014 mm and, despite 18.69% of soil particles are smaller than that and, resulting from that,  $D_{10}$  cannot be higher than 0.0014 mm. So, the coefficient of uniformity ( $C_u$ ) may be higher than 99 and the coefficient of curvature ( $C_c$ ) may not be lower than 0.21. The clay fraction ( $D < 0.002$  mm) was found to be 19.07% The grain size distribution coefficients are shown in table 4.1. Those parameters indicate the soil is nonuniform and well-graded.

Table 4.1: Soil grain size distribution parameters.

Soil parameter	
$D_{60}$ (mm)	0.139
$D_{50}$ (mm)	0.085
$D_{30}$ (mm)	0.0064
$D_{10}$ (mm)	<0.0014
$C_u$	>99.29
$C_c$	>0.21

### 4.1.3 Soil Atterberg limits

The Liquid Limit found was 20%, the Plasticity Limit 11% and, consequently, the Plasticity Index was 9%. These results, associated with the obtained grain size distribution data, according to the Soil Unified Classification System, classify the soil as a *clayey sand (SC)*. The activity, consequently, is 0.47. That result put the fine content of the studied soil in the least active group of clays. Figure 4.5 presents the soil results in the plasticity chart, where the Pelotas soil is approximately on the “U line”. This line is the upper limit of natural soils and may be used to check erroneous data (natural soils may not result in a plot above or from the left of this line).

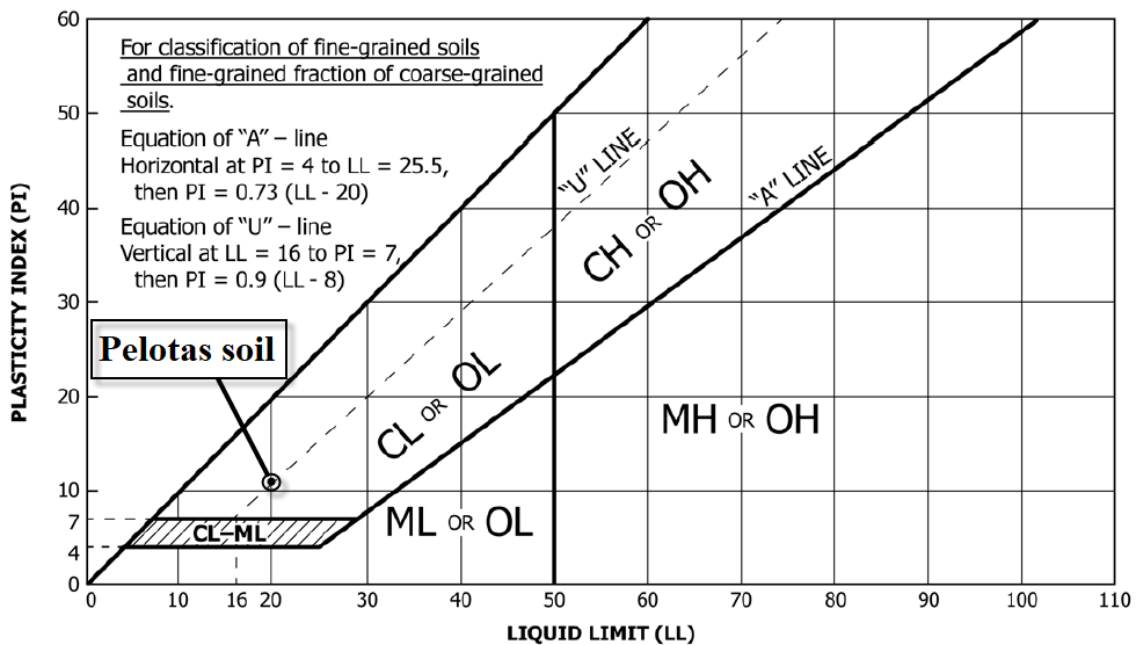


Figure 4.5: Compaction curve plotted (modified energy).

### 4.1.4 Soil compaction

The compaction soil test was conducted using the Proctor modified energy in order to define the highest feasible dry unit weight of the soil. The soil compaction tests resulted in the curve presented in Figure 4.6, where the maximum dry unit weight observed was 20,35 kN/m<sup>3</sup> and optimum water content was about 10 %.

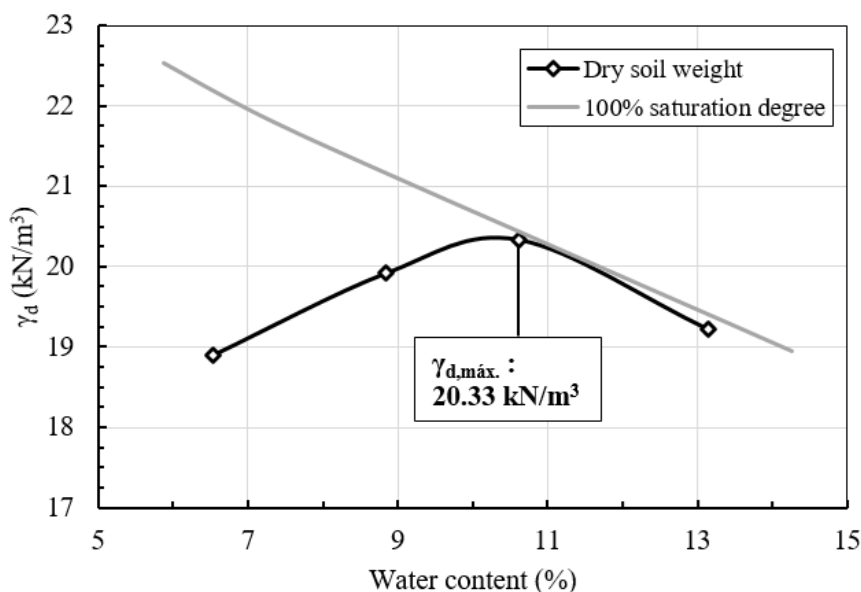


Figure 4.6: Compaction curve plotted (modified energy).

#### 4.1.5 Soil X-ray diffraction

X-Ray Diffractometry (XRD) analysis resulted in a composition of the following probable minerals: quartz, K-Feldspars, Muscovite, Montmorillonite, Illite, and Labradorite. The XRD diagram is presented in figure 4.7, and the semi-quantitative analysis is presented in table 4.2. The used database did not present data about the montmorillonite found to assess its amount. Oriented X-ray diffraction analysis could not be executed, so there are more uncertainties about the soil clay minerals.

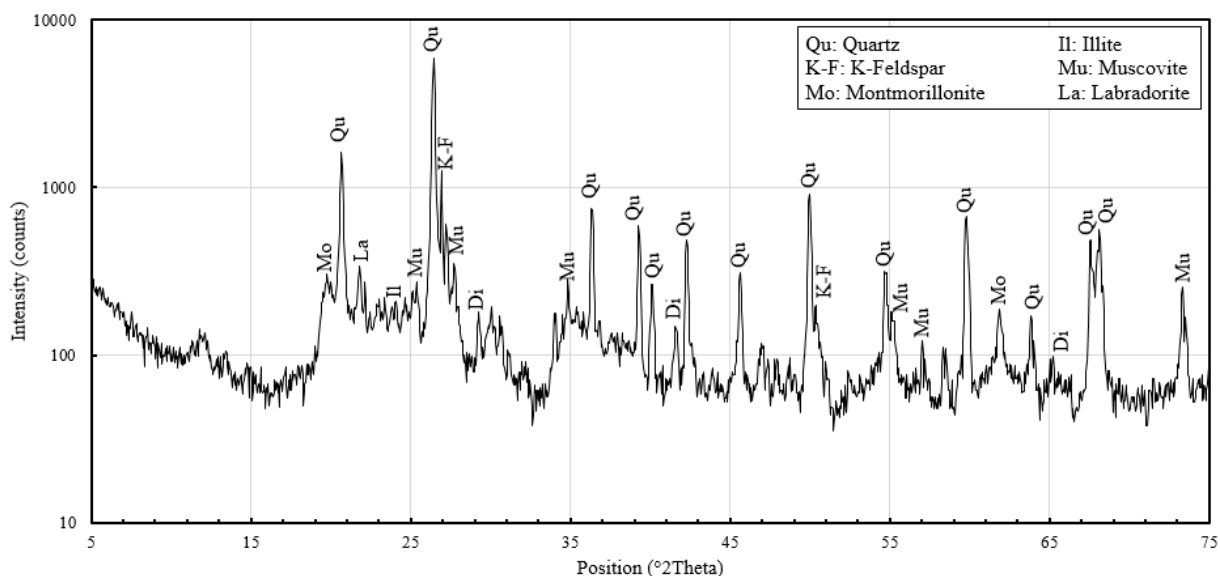


Figure 4.7: Soil XRD results.

Table 4.2: Soil XRD Semi-quantitative analysis.

Mineral phase	Semi-quantitative amount (%)
Quartz	41
Muscovite	26
Labradorite	14
K-Feldspar	12
Illite	7
Montmorillonite	-

#### 4.1.6 Soil solids specific gravity

The specific gravity determined from the Pelotas soil solids was  $25.97 \text{ kN/m}^3$ , based on the pycnometer test. This value is found to be in the expected soil range as it is a quartzitic soil.

#### 4.1.7 Soil specific surface area

The BET tests indicated a specific surface area of  $19.942 \text{ m}^2/\text{g}$  on the soil particles, a high value for sands, which indicates also the presence of surface electrical forces between particles.

#### 4.1.8 Soil apparent specific gravity

The soil apparent field specific gravity found by tests using a hydrostatic scale is  $17.50 \text{ kN/m}^3$ .

#### 4.1.9 Soil crumb tests

The crumb test was first conducted at the soil site to assess the deflocculation characteristics of the dispersive soil for a field water content condition. The results are shown in Figure 4.8. As samples were taken to the lab, a new test was executed, shown in figure 4.9. Distilled water was used in both field and laboratory tests.

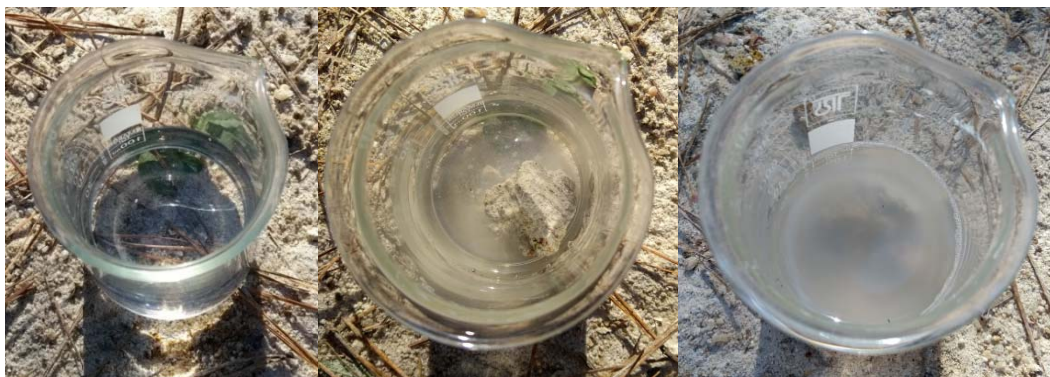


Figure 4.8: In situ crumb test.



Figure 4.9: Laboratory crumb test.

As can be seen, the occurrence of a “colloidal cloud”, very likely caused by deflocculation, indicates a dispersive behaviour. For both tests the soil reached the 4<sup>th</sup> grade of dispersion, classifying this soil as highly dispersive.

#### 4.1.10 Soil cation analysis

Chemical test results are shown in table 4.3.

Table 4.3: Soil cations.

Cation	Amount (meq/l)
Sodium - Na <sup>+</sup>	4.8
Potassium - K <sup>+</sup>	0.6
Calcium - Ca <sup>2+</sup>	7.3
Magnesium - Mg <sup>2+</sup>	4.8

The calculated TDS, SAR, and CROSS are shown in table 4.4.

Table 4.4: Salts concentration-related parameters.

Soil parameter	
TDS (meq/l)	17.50
% Na	0.27
SAR	1.95
CROSS	2.28



TDS x Na and the CROSS method suggested a nondispersive behaviour. The Sodium Adsorption Ratio (SAR) indicated a low to moderate dispersibility behaviour, but the Sodium Percentage indicated a more dispersive trend.

#### 4.1.11 Soil pinhole tests

The pinhole tests were conducted for three distinct soil dry unit weights: 14.0, 15.5, and 17.0 kN/m<sup>3</sup>.

The pinhole test results are shown in table 4.5 for different molded dry unit weights. As shown by the results, dispersibility results in pinhole are influenced by dry unit weight, but it is not the predominant variable in the dispersibility response since the flow rate is similar. Despite that the sample with the lower weight has presented more turbidity, all the samples were classified as moderate dispersive (ND4).

Table 4.5: pinhole test results with Pelotas soil.

Dry unit weight (kN/m <sup>3</sup> )	Aspect	Q (cm <sup>3</sup> /s)	
		0-5 min	5-10 min
14	Slightly dark	0.90	0.88
15.5	Slightly clear	0.78	0.75
17	Slightly clear	0.66	0.83

#### 4.1.12 Soil dispersibility classification

Based on the dispersibility rating proposed by Bell and Walker (2000), the soil dispersibility rate is shown in table 4.6. With an overall rating of 7, the soil is can be classified as slightly dispersive, but it must be emphasized that CEC tests have not been executed, so a slightly dispersive result in those tests would change the soil rating to 8 (moderately dispersive). The double hydrometer test classified the soil as highly dispersive, but this test is not accounted for in the presented rating classification.

Table 4.6: Pelotas soil dispersibility rating.

Dispersibility test rating	
Pinhole test	Moderate 3
CEC vs. ESP	N.A. 0-4
Crumb Test	Strong reaction 3
SAR	1.5-2 1
TDS vs. %Na	Nondispersive 0
Overall rating	Slightly dispersive 5-7

N.A. = not assessed

## 4.2 FLY ASH CHARACTERIZATION

Coal fly ashes are a byproduct of power stations. Fly ash behaviour may present high variability, depending on the coal formation and the burning process, and material deposition. The fly ash used in this study was obtained from Candiota power station, less than 150 km distant from the soil collected site.

### 4.2.1 Fly ash grain size distribution

The granulometric curve was done only by laser scattering and sedimentation tests with the aid of a deflocculant agent. The grain size distribution is presented in Figure 4.10. The sedimentation test is usually more trustworthy for soils with fine particles, since the laser scattering analysis may detect a set of flocculated grains as a unique particle, but based on the results presented, there are not deflocculant effects when this fly ash is put into water, since both curves are approximately equal.

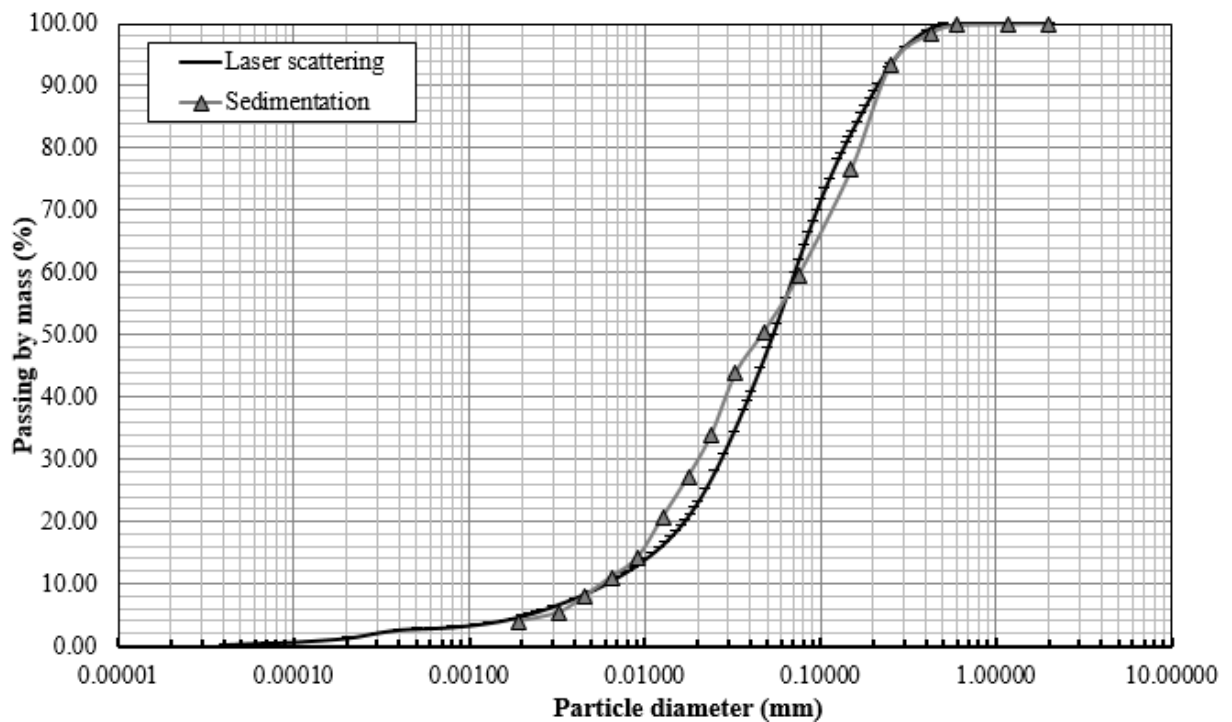


Figure 4.10: Fly ash grain size distribution.

#### 4.2.2 Fly ash solids specific gravity

The specific gravity found for fly ash is  $17.69 \text{ kN/m}^3$ , determined from water pycnometer tests.

#### 4.2.3 Fly ash X-ray diffraction analysis

XRD results are presented in figure 4.11. Results indicated the presence of Gibbsite [ $\text{Al}(\text{OH})_3$ ]; Calcium iron sulfate hydrate ( $\text{Ca}_4\text{Fe}_2\text{S}_2\text{O}_9 \cdot 12\text{H}_2\text{O}$ ); Aluminum oxide ( $\text{Al}_2\text{O}_3$ ); Calcite ( $\text{CaCO}_3$ ); Gypsum ( $\text{CaSO}_4 \cdot 2\text{H}_2\text{O}$ ) and quartz ( $\text{SiO}_2$ ).

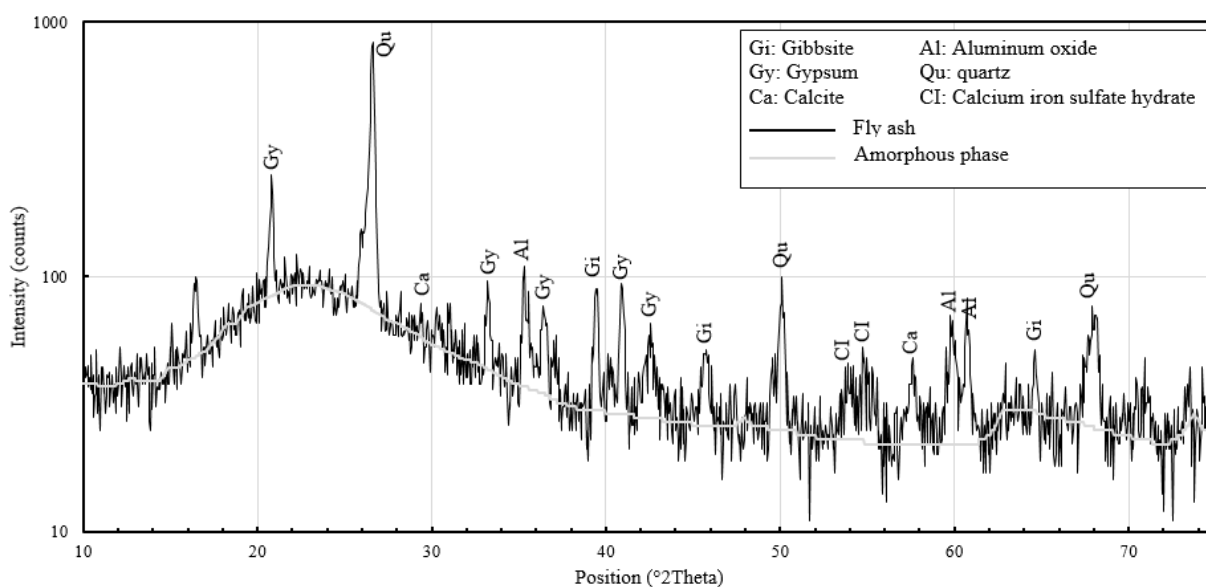


Figure 4.11: Fly Ash XRD results.

The semi-quantitative analysis is presented in table 4.7.

Table 4.7: Fly ash semi-quantitative analysis from XRD analysis.

Component	Semi-quantitative amount (%)
Gibbsite [Al(OH) <sub>3</sub> ]	57
Calcium iron sulfate hydrate [Ca <sub>4</sub> Fe <sub>2</sub> S <sub>2</sub> O <sub>9</sub> •12H <sub>2</sub> O]	15
Aluminum oxide [Al <sub>2</sub> O <sub>3</sub> ]	8
Calcite [CaCO <sub>3</sub> ]	8
Gypsum [CaSO <sub>4</sub> •2H <sub>2</sub> O]	8
Quartz [SiO <sub>2</sub> ]	5

The amorphous phase content was estimated as the relation between the integrated area of the amorphous phase and the integrated area from the peaks, calculated as equation (3.4), which resulted in an amorphous content of 59.73% in the fly ash.

#### 4.2.5 Fly ash specific surface area

The results indicated that the fly ash specific surface area is 2.934 m<sup>2</sup>/g, which is in the range of expected values considering common fly ashes used in civil engineering.

### 4.3 CALCITIC LIME CHARACTERIZATION

Carbide lime, the calcitic lime used, is a residue from acetylene gas production, obtained from a plant in southern Brazil. Some characterization results were obtained from Saldanha et al. (2018), which characterized this lime for geotechnical soil improvement purposes.

#### 4.3.1 Calcitic lime grain size distribution

The carbide lime granulometric curve, obtained from laser scattering, is shown in figure 4.12.

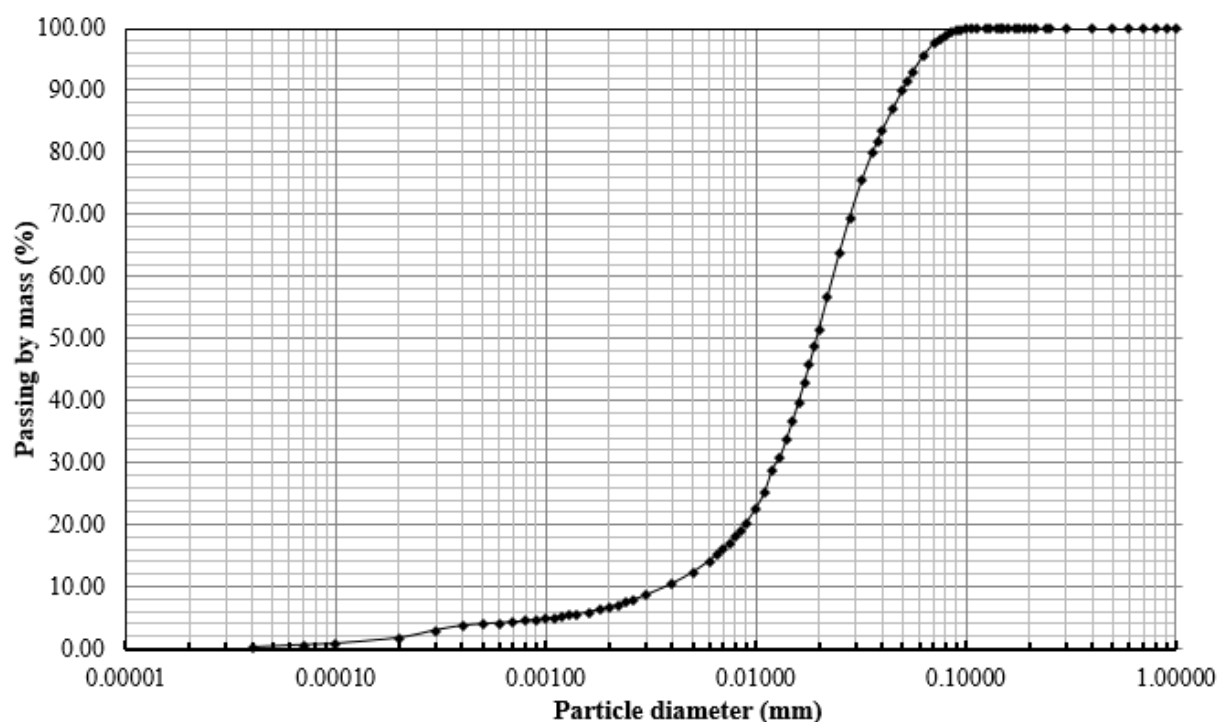


Figure 4.12: Calcitic lime grain size distribution.

#### 4.3.2 Calcitic lime solids specific gravity

The specific gravity found used carbide lime is 21.90 kN/m<sup>3</sup>, presented in Saldanha et al. (2018) characterization test results.

#### 4.3.3 Calcitic lime X-ray diffraction analysis

XRD results are presented in figure 4.13. The identified components were: portlandite [Ca(OH)<sub>2</sub>], calcite (CaCO<sub>3</sub>), and wollastonite (CaSiO<sub>3</sub>). A semi-quantitative analysis regarding portlandite and calcite are presented in table 4.8.

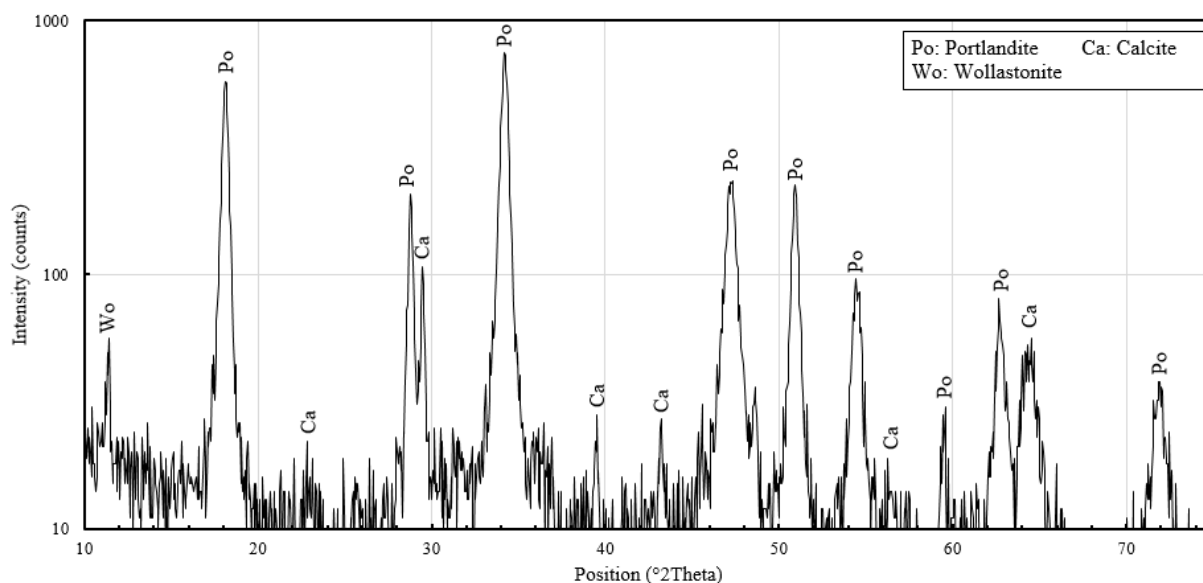


Figure 4.13: Calcitic lime XRD results.

A semi-quantitative analysis was obtained from the X-Ray diffraction tests as shown in table 4.8.

Table 4.8: Calcitic lime semi-quantitative results from XRD analysis.

Component	Semi-quantitative amount (%)
Portlandite [Ca(OH) <sub>2</sub> ]	84
Calcite [CaCO <sub>3</sub> ]	16
Wollastonite [CaSiO <sub>3</sub> ]	-

#### 4.3.4 Calcitic lime specific surface area

The specific surface found for calcitic lime in the present research is 13.63 m<sup>2</sup>/g, a medium to low specific surface area. Saldanha et al. (2018) found higher values (22.6 m<sup>2</sup>/g) for the carbide lime obtained from the same source. Higher specific surface values tend to improve the velocity of reactions.

#### 4.3.5 Calcitic lime x-ray fluorescence

The X-ray fluorescence was conducted by Saldanha et al. (2018), and the oxides content are shown in table 4.9.

Table 4.9: X-Ray Fluorescence Spectrometry tests results on carbide lime.

Chemical	Results from Saldanha et al. (2018)
CaO	74.00
SiO <sub>2</sub>	3.10
Al <sub>2</sub> O <sub>3</sub>	0.46
Fe <sub>2</sub> O <sub>3</sub>	0.26
MgO	0.72
SO <sub>3</sub>	0.54
Na <sub>2</sub> O	Not detected
K <sub>2</sub> O	Not detected

#### 4.4 DOLOMITIC LIME CHARACTERIZATION

The dolomitic lime is a commercially available material, called “Primor extra”. The characterization results will be shown next. Dalla Rosa (2009) presented, for the same lime, a specific gravity of 2.49 g/cm<sup>3</sup>, a calcium oxide (CaO) content of 44.8%, and 27.9 % of Magnesium oxide (MgO). The calcium oxide concentration is much lower than the carbide lime studied by Saldanha et al. (2018) but, as the carbide lime is a byproduct, it may present higher variability.

##### 4.4.1 Dolomitic lime grain size distribution

The Primor lime grain size distribution was obtained using the laser scattering method and is given by the granulometric curve presented in figure 4.14.

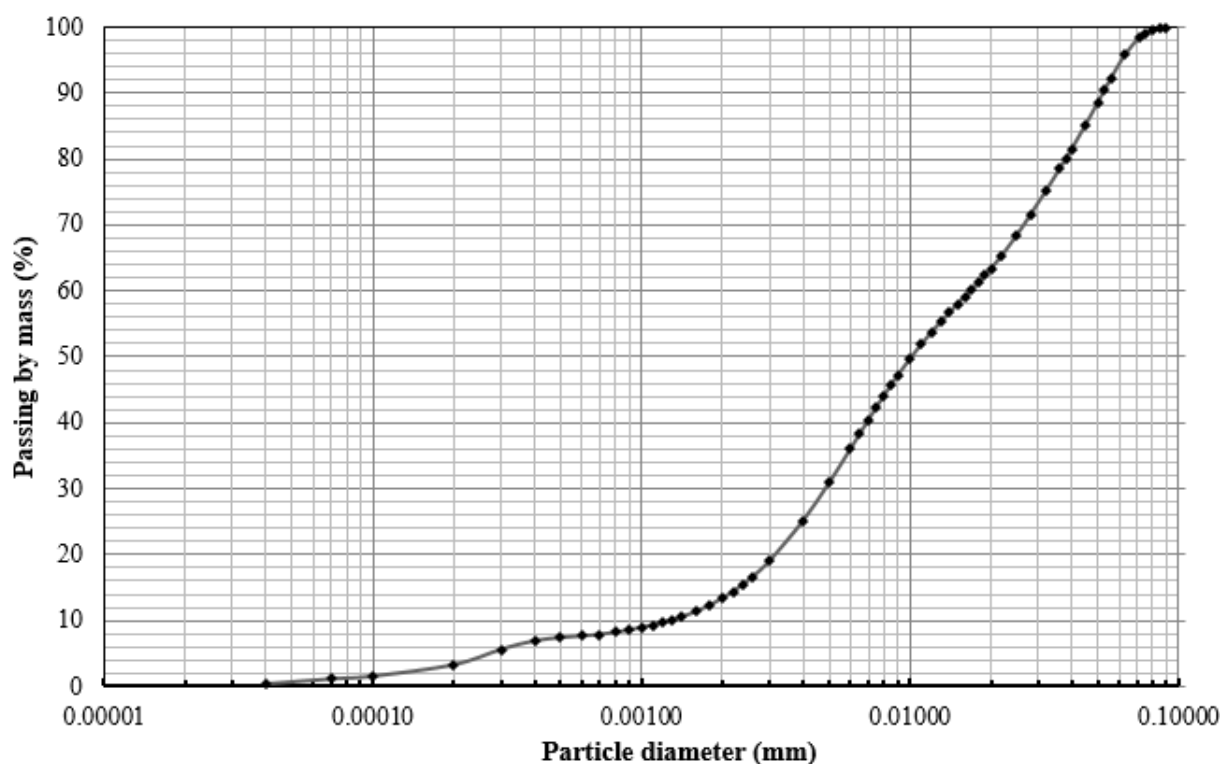


Figure 4.14: Dolomitic lime grain size distribution.

#### 4.4.2 Dolomitic lime solids specific gravity

Dalla Rosa (2009) has studied the same lime, which, according to the author, corresponds to a specific gravity of 2.49 kN/m<sup>3</sup>.

#### 4.4.3 Dolomitic lime X-ray diffraction analysis

XRD results are presented in figure 4.15. The identified components were: portlandite [Ca(OH)<sub>2</sub>], calcite (CaCO<sub>3</sub>), periclase (MgO), brucite [Mg(OH)<sub>2</sub>] and dolomite [CaMg(CO<sub>3</sub>)<sub>2</sub>]. A semi-quantitative analysis of the components is presented in table 4.10.



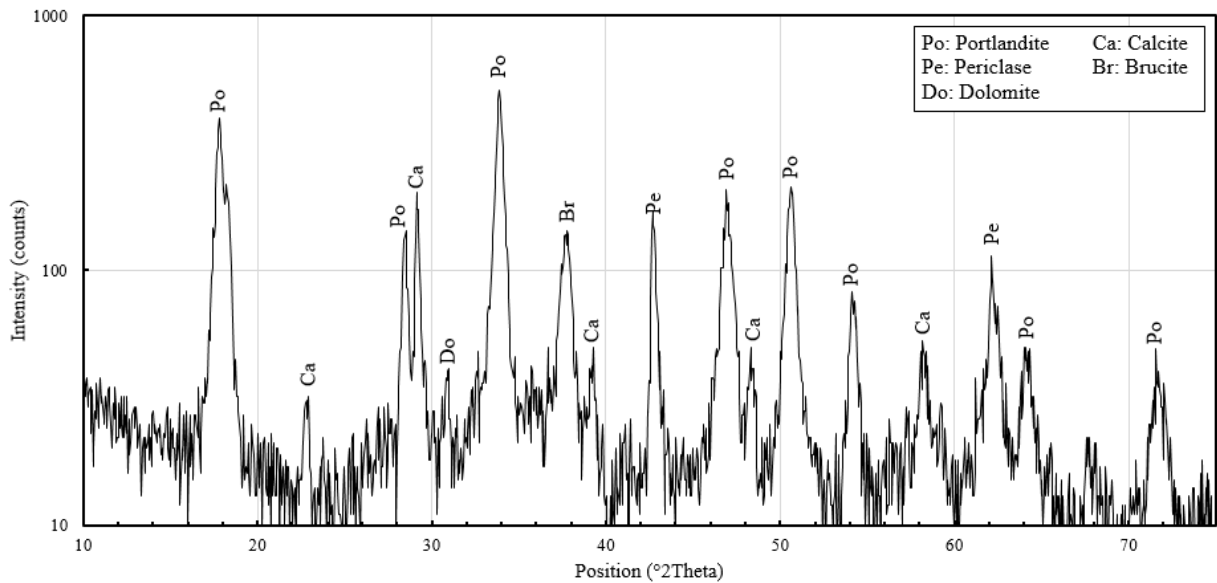


Figure 4.15: Dolomitic lime XRD results.

Table 4.10: Primor dolomitic lime semi-quantitative composition from XRD analysis.

Component	Semi-quantitative amount (%)
Portlandite [Ca(OH) <sub>2</sub> ]	61
Periclase [MgO]	17
Brucite [Mg(OH) <sub>2</sub> ]	13
Calcite [CaCO <sub>3</sub> ]	9
Dolomite [CaMg(CO <sub>3</sub> ) <sub>2</sub> ]	-

#### 4.4.4 Dolomitic lime specific surface area

The dolomitic lime specific surface found from BET is 10.110 m<sup>2</sup>/g, slightly lower than the calcitic lime, but inside the range for commercial typically hydrated limes (OATES, 1998).

## 4.5 ADMIXTURE CHARACTERIZATION

It is expected that some chemical and physical properties of the materials change when mixed, especially when strong reactions occur. So, those mixtures may be characterized separately from the primary material. Some characterization tests conducted with the mixed materials are presented below.

#### 4.5.1 Initial consumption of lime (ICL)

In order to design the lime content needed to stabilize the mixture, Initial consumption of lime (ICL) test was conducted. The test was conducted with carbide lime, and the plot results can be seen in figure 4.16. Results indicated a stabilization at 3% lime content but, as there is a need to stabilize the mixture and also improve their strength, a greater lime content is needed. So, a lime content of 5% was used and tested on both calcitic and dolomitic lime. Both presented increase in strength after 28 days, so the lime content of 5% was accepted.

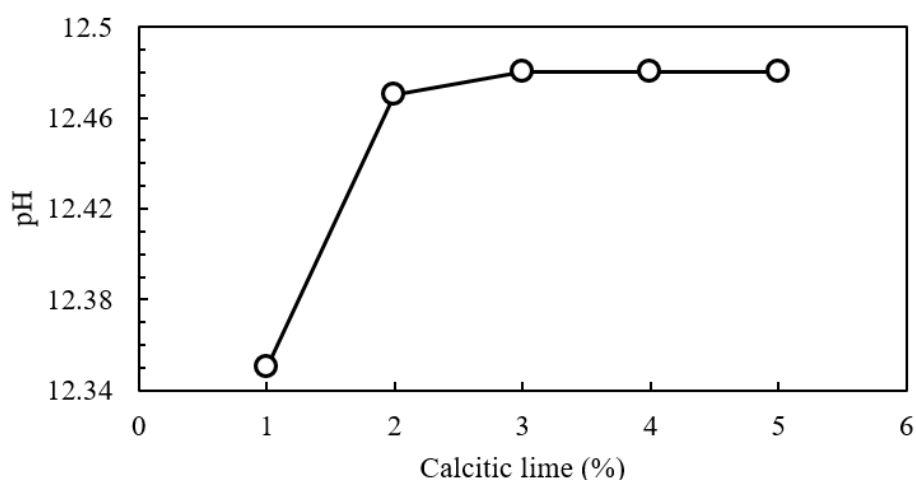


Figure 4.16: ICL test with carbide lime.

#### 4.5.2 Compaction tests

First, a pure soil material was used, resulting in a soil plot curve. Later, an amount of fly ash equivalent to 25% of the dry soil mass was added and a new compaction curve took shape.

The compaction tests to assess fly ash influence was conducted with a mixture of soil and 25% fly ash mass content (as it was set as the maximum fly ash in the experimental design) regarding the soil mass.

Next, an amount of carbide lime corresponding to 12% (defined as the maximum lime content) of the total dry soil and fly ash mass was added to the mixture. Due to the material limitation, only one point of this admixture was determined, and the maximum dry unit weight could not be assessed (judging by the saturation curve, the maximum dry unit weight of this material seems to correspond to the higher water content). The obtained compaction results (modified effort) are shown in Figure 4.17.

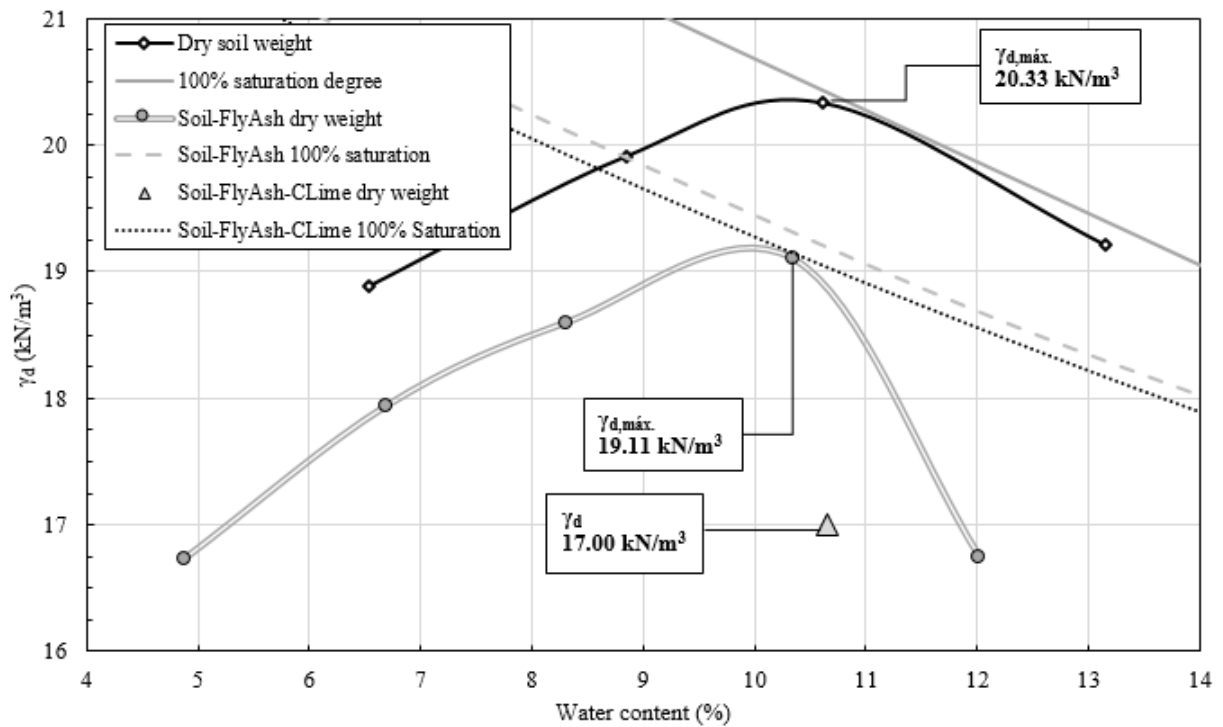


Figure 4.17: Admixtures compaction curves (modified energy).

As a consequence of those tests, the maximum dry unit weight chosen for the experimental design of the present research was  $17 \text{ kN/m}^3$ , and the moulding moisture content was adopted as 10.25%, regardless of the lime and fly ash content.

#### 4.5.3 Crumb test

To evaluate the colloidal cloud formation in stabilized mixtures, the crumb test was also conducted after 28 days curing period. Two specimens were moulded using 12.50 % of fly ash, a dry unit weight of  $14 \text{ kN/m}^3$ , and lime content of 5%. Each specimen was moulded with a different type of lime, calcitic and dolomitic. Both specimens have induced no colloidal cloud in the presence of distilled water, indicating a non-dispersive behaviour (grade 1).

#### 4.5.4 Pinhole tests

Pinhole tests were also conducted to evaluate the dispersibility of the stabilized soil. Four samples were moulded with mixed soil, fly ash and dolomitic lime, and tested after 28 days. The results are summarized in table 4.11. All the samples presented an effluent clear to slightly clear and, as the flow rate was less than  $4.0 \text{ cm}^3/\text{s}$ , all the tests resulted in a non-dispersive

behaviour, indicating that when chemically stabilized with fly ash and lime, low compaction energy is enough to suppress the dispersibility behaviour of this soil.

Table 4.11: Pinhole test results from dolomitic lime stabilized samples.

Dry unit weight (kN/m <sup>3</sup> )	Fly ash content (%)	Dolomitic lime content (%)	Flow rate (cm <sup>3</sup> /s)			
			Head (50 mm)	Head (180 mm)	Head (380 mm)	Head (1,020 mm)
14.0	12.5	5.0	0.38	0.66	0.95	1.36
14.0	12.5	12.5	0.39	0.59	0.90	1.30
14.0	25.0	5.0	0.14	0.51	0.85	1.19
14.0	25.0	12.5	0.33	0.46	0.82	1.06

#### 4.6 CHARACTERIZATION SUMMARY

Comparative characterization of physical properties from this research working materials is presented in Table 4.12.

Table 4.12: Summarized materials' physical properties.

Property	Material			
	Soil	Fly Ash	Calcitic lime	Dolomitic lime
Field dry unit weight (kN/m <sup>3</sup> )	17.50	-	-	-
Solids specific gravity (kN/m <sup>3</sup> )	25.97	17.69	21.90*	24.90**
Specific surface area (m <sup>2</sup> /g)	19.94	2.93	13.63	10.11
D > 0.06 mm (%)	54.32	45.45	5.58	5.72
0.002 < D < 0.06 mm (%)	26.99	50.60	87.77	80.91
D < 0.002 mm (%)	18.69	3.95	6.65	13.37
LL (%)	20	-	-	-
PL (%)	11	-	-	-
PI (%)	9	-	-	-

\*Saldanha et al. (2018)

\*\*Dalla Rosa (2009)

## 4.7 EXPERIMENTAL DESIGN

The experimental design was elaborated through the  $2^k$  factorial design, where three main factors were designed: dry unit weight, fly ash content, and lime content. Besides the corner points in the factorial design, a center point was used for these three factors, making it possible to evaluate the linearity of results. The secondary factor is the lime type (Carbide calcitic lime or Primor dolomitic lime). All the dosages were designed for both calcitic and dolomitic lime, but there is no intermediate lime type, so, this factor cannot present a center point. The last factor in the design is represented by the slenderness ratio, despite there are more differences regarding this factor that are not that simple as slenderness. The factorial can be explained by table 4.13. The maximum dry unit weight was determined based on compaction tests, and the minimum based on moulding experiments with these materials, as lower dry unit weights could lead to sudden undesigned failures. The lowest chosen lime content was based on the ICL test and a few tests on samples with 4% carbide lime content that presented very weak bounds after 28 days. The fly ash content and maximum lime content were based on several studies with cemented soils that adopted similar materials and contents (MOH et al., 1955, INDRARATNA et al., 1995, DAHALE et al., 2016, CONSOLI et al., 2011c, 2019c, SCHEUERMANN FILHO, 2019).

As an acceptance criterion, control limits of  $\pm 5\%$  to height, diameter, and dry unit weight were applied. The moisture content of  $10.25 \pm 10\%$  was defined for all the specimens tested. The samples beyond those limits were discarded.

Table 4.13: Research factorial design.

Factor	Lower corner point	Upper corner point	Center point
Dry Unit Weight (kN/m <sup>3</sup> )	14.00	17.00	15.50
Fly Ash Content (%)	12.50	25.00	18.75
Lime Content (%)	5.00	12.00	8.50
Lime Type	-1*	+1**	-
Slenderness Ratio	1.19	2.00	-

\*Calcitic lime

\*\*Dolomitic lime

#### 4.7.1 Durability tests design

As this study intends to analyze the influence of factors like soil weight, fly ash, and lime content, and also to compare two different limes in stabilized soil mixtures, all variables were tested (18 dosages) in durability tests. First, common durability tests were conducted, where after wetting and drying, the samples are brushed. The experimental durability tests are summarized in Table 4.14. After those tests, more durability tests were designed, where smaller but more slender samples are used, and brushing is not applied during the cycles. The design of those tests is presented in table 4.15.

In wetting-drying-brushing tests, no replicas were moulded. In wetting-drying tests, replicas were moulded only for calcitic lime treated specimens.

Table 4.14:Wetting-drying-brushing Durability tests design.

Dry Unit Weight (kN/m <sup>3</sup> )	Fly Ash Content (%)	Lime Content (%)	Lime Type	Slenderness Ratio	Durability Cycles (unity)
14.0	12.50	5.0	Calcitic & Dolomitic	1.2	12
		12.0			
15.5	18.75	5.0			
		12.0			
17.0	25.00	8.5			
		5.0			
		12.0			

Table 4.15: Wetting-drying durability tests design.

Dry Unit Weight (kN/m <sup>3</sup> )	Fly Ash Content (%)	Lime Content (%)	Lime Type	Slenderness Ratio	Durability Cycles (unity)
14.0	12.50	5.0	Calcitic & Dolomitic	2.0	1, 4, 12
		12.0			
15.5	25.00	5.0			
		12.0			
17.0	18.75	8.5			
		5.0			
		12.0			
17.0	25.00	5.0			
		12.0			

#### 4.7.2 Unconfined compressive strength tests design

Unconfined compressive strength tests were designed for each different dosage after a curing period of 28 days. Besides that, as a necessity to assess the effect of damage caused by cycles on soil strength, unconfined compressive strength tests were designed after 1, 4, and 12 durability cycles. Table 4.16 presents the unconfined compressive strength design summarized. The “cycle 0” corresponds to the samples that did not undergo durability cycles (tested after 28 days of curing).

All the specimens that were tested without the application of durability cycles (0 cycles) were moulded using a triplicate design (3 samples per dosage). The slender specimens moulded using calcitic lime, which have undergone only wetting-drying durability cycles, were replicated using 2 samples for a single dosage. All the rest of the samples were moulded with no replicas.

Table 4.16: Unconfined Compressive Strength Tests design.

Dry Unit Weight (kN/m <sup>3</sup> )	Fly Ash Content (%)	Lime Content (%)	Lime Type	Slenderness Ratio	Durability cycles before testing (unity)
14.0	12.50	5.0	Calcitic & Dolomitic	2.0	0, 1, 4, 12
		12.0			
15.5	25.00	5.0			
		12.0			
17.0	18.75	8.5			
		12.50			
17.0	25.00	5.0			
		12.0			
14.0	12.50	5.0	Calcitic & Dolomitic	1.2	12
		12.0			
15.5	25.00	5.0			
		12.0			
17.0	18.75	8.5			
		12.50			
17.0	25.00	5.0			
		12.0			

### 4.7.3 UPV experimental design

The ultrasonic pulse velocity tests were conducted at most of the strength/durability-tested samples. Small strain stiffness could be calculated after moulding, after 28 days curing period, and after the cycles, a few minutes after removing samples from the oven. However, some samples, after durability cycles, presented too much noise during measurements, so travel time could not be measured and so the samples' stiffness. Also, some samples could not be tested as a consequence of a delay issue in the interface gel supply.



## 5 RESULTS

This chapter presents the results from the factorial analysis, how the controllable dosing factors affect the response, the influence of durability cycles on variables response, how different response variables can be related, and even if those response variables can be predicted by key parameters. Thereby, durability, unconfined compressive strength, and ultrasonic pulse velocity test results are presented.

A qualitative comparison between brushed and non-brushed durability tests can be observed in Appendix I, where pictures taken along the cycles are shown. The failure modes of the soil specimens are presented in Appendix II showing a change in the failure mode trend from brittle to ductile when samples are damaged by durability cycles. The ANOVA tables are presented in Appendix III, and the composition and strength results of the samples are presented in Appendix IV.

### 5.1 FACTORIAL RESULTS

The results of the full factorial design presented herein are, firstly, the evaluation of response values of unconfined compressive strength, small strain stiffness, and accumulated loss of mass to the factors dry unit weight, fly ash content, and lime content ( $2^3$  full factorial design with central points).

Secondly, the response will be evaluated comparing factors like the lime aid ( $2^4$  full factorial), and the slenderness ratio ( $2^5$  full factorial), without center points.

Besides that, only the second-order interactions were considered in the factorial analysis. Higher interaction orders were considered to be difficult to evaluate as a physical relation and, for that, disregarded.

For all the specimens subjected to wetting-drying-brushing cycles, and also for a part of the specimens subjected to wetting-drying cycles, because of the lack of material, it was unfeasible to mold test replicates, and the results are less reliable.

Results are presented as Pareto effects on the response variable, as the plot of the main effects, and as regression equations. For the regression factorial equations, when there is a center point in the analysis, if all the variables are at their midpoints, the  $CtPt$  variable is 1, otherwise, it is

0. The error rate ( $\alpha$ ) was chosen to be 0.05, corresponding to a risk of 5% of concluding that a term is statistically significant when it is not.

The factorial analysis has a limitation since if one of the specimens corresponding to a factor is lost, the analysis cannot be made. So, if after a given number of cycles, a specimen is too damaged that its strength or small strain stiffness cannot be tested, and there are equivalent specimen to test, the factorial analysis may not be executed.

### 5.1.1 Effect of dry unit weight, fly ash, and lime content

The analysis of dry unit weight, fly ash, and lime (calcitic and dolomitic) contemplates unconfined compressive strength, small strain constraint, and shear modulus, and accumulated loss of mass.

#### 5.1.1.1 Unconfined compressive strength

Samples undergoing no durability cycles (0 cycles), samples after 1, 4, and 12 cycles, with slenderness ratio approximately 2.0, and samples after 12 durability cycles with a slenderness ratio of about 1.2 were evaluated.

The results for samples tested after 28 days curing period when stabilized with calcitic lime are presented in figure 5.1.

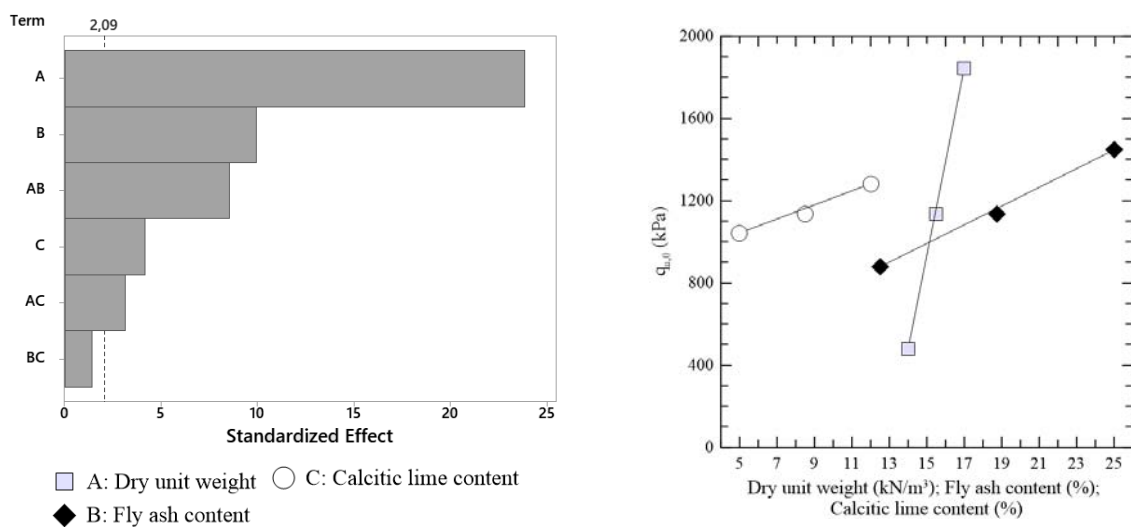


Figure 5.1: Pareto and main effects on response to unconfined compressive strength for calcitic lime treated samples after 0 cycles (samples H/D  $\approx$  2.0).

It can be observed that the dry unit weight effect is much more expressive than the others. The second more effective factor is fly ash, and only the interaction of fly ash and calcitic lime content seems to be negligible in response values. There is a linear tendency in unconfined compressive strength response, indicated by the main effects plot and by the low value of the center point variable presented in equation (5.1), where  $q_u$  is expressed in kPa.

$$q_{u,0 (H/D=2.0)} = 3,091 - 179.1DW - 374.7FA - 265.8CL + 26.09DW \times FA + 17.09DW \times CL + 1.86FA \times CL - 28.4CtPt \quad R^2 = 0.97 \quad (5.1)$$

Where

DW = Dry unit weight (kN/m<sup>3</sup>)

FA = Fly ash content (%)

CL = calcitic lime content (%)

The factorial results of unconfined compressive strength for dolomitic lime treated soils after 0 cycles are presented in figure 5.2.

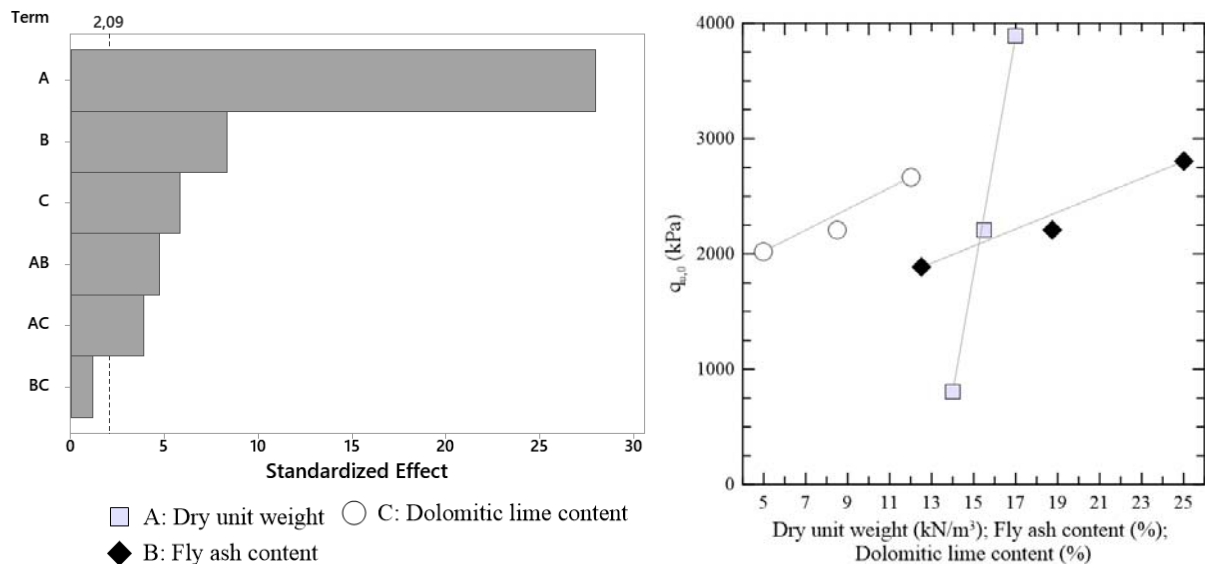


Figure 5.2: Pareto and main effects on response to unconfined compressive strength for dolomitic lime treated samples after 0 cycles (samples H/D  $\approx$  2.0).

As well as the calcitic lime treated samples, the effect of dry unit weight is high, and the interaction between fly ash and lime is negligible, but here the effect of the interaction between dry unit weight and fly ash is lower than the lime effect. There is also a linear tendency observed in response to the analyzed factors. The regression equation is expressed by equation (5.2).

$$q_{u,0 (H/D=2.0)} = 1,815 - 159DW - 383.1FA - 595DL + 27.85DW \times FA + 40.7DW \times DL + 2.94FA \times DL - 135CtPt \quad R^2 = 0.97 \quad (5.2)$$

Where

DL = dolomitic lime content (%)

The results for unconfined compressive strength of soils treated with fly ash and calcitic lime, after 1 wetting and drying cycle, are presented in figure 5.3. The effects are similar to the response after 28 days (0 cycles). The mathematical expression of this behaviour is presented by equation (5.3).

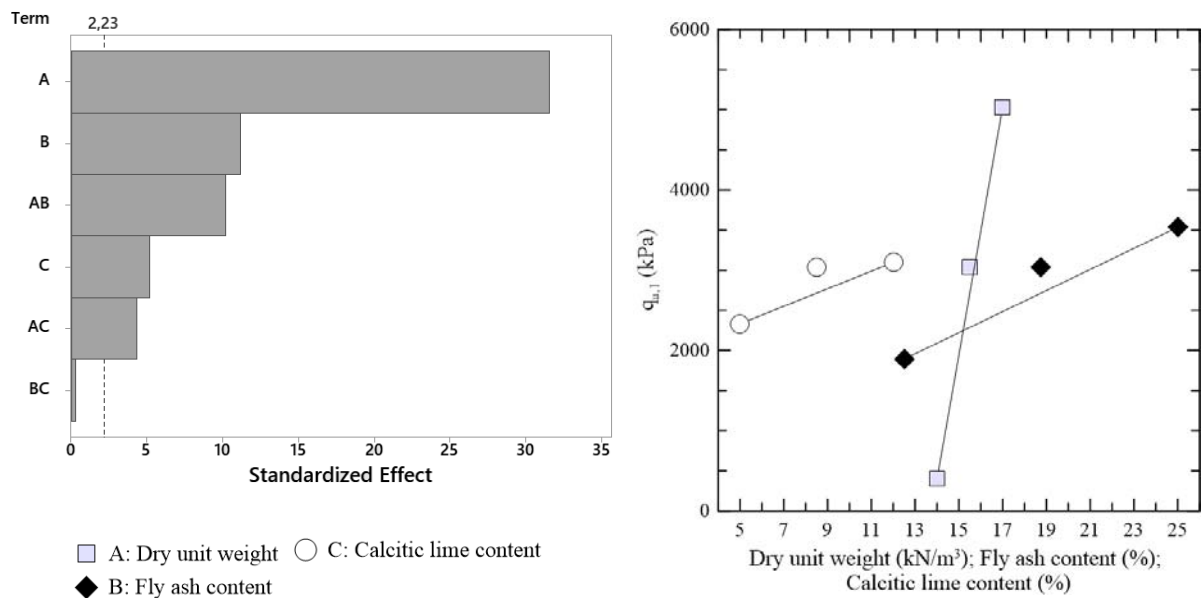


Figure 5.3: Pareto and main effects on response to unconfined compressive strength for calcitic lime treated samples after 1 cycle (samples H/D  $\approx$  2.0).

$$\begin{aligned}
 q_{u,1 (H/D=2.0)} = & 6,421 - 469DW - 1100FA - 807CL \\
 & + 80.04DW \times FA + 60.04DW \times CL - 1.06FA \times CL \\
 & + 320CtPt
 \end{aligned}
 \quad R^2 = 0.99 \quad (5.3)$$

Figure 5.4 presents the results for the factorial analysis of dolomitic lime treated soils after 1 wetting-drying cycle. It can be observed that, when compared to the results after 0 cycles, there is an increase in the dolomitic lime content effect and a relative decrease in the effect of fly ash. As there were no replicates in this analysis, the significance of the lower limit rises.

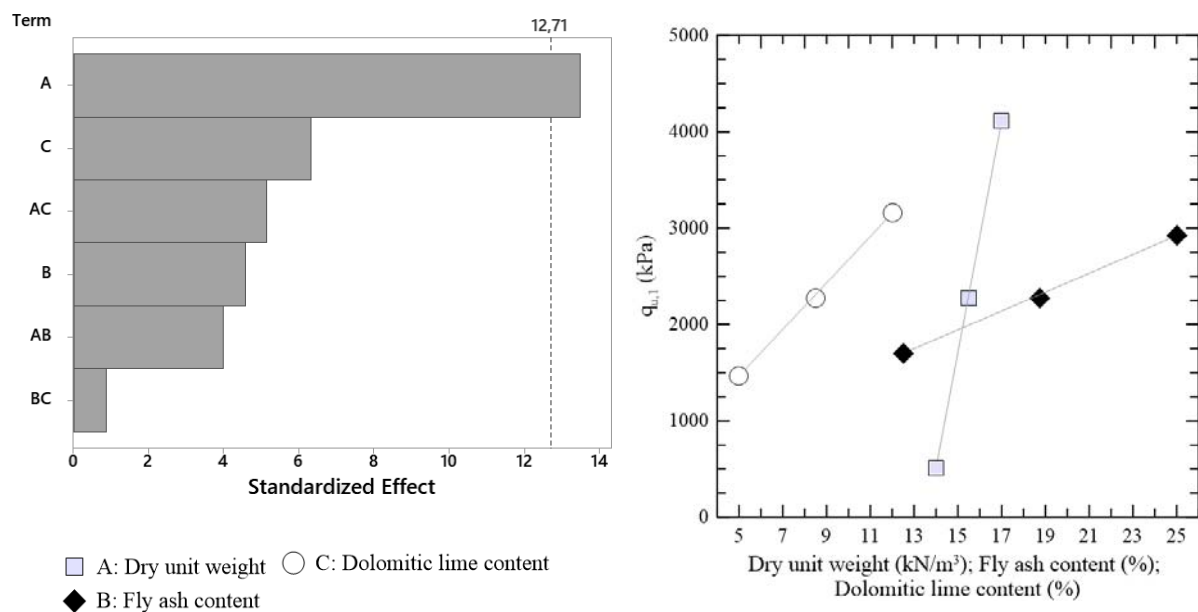


Figure 5.4: Pareto and main effects on response to unconfined compressive strength for dolomitic lime treated samples after 1 cycle (samples  $H/D \approx 2.0$ ).

The regression equation of the factorial analysis is shown below.

$$\begin{aligned}
 q_{u,1 (H/D=2.0)} = & 14,450 - 980DW - 829FA - 1,888DL \\
 & + 56.9DW \times FA + 131DW \times DL + 5.25FA \times DL \\
 & - 36CtPt
 \end{aligned}
 \quad R^2 = 0.97 \quad (5.4)$$

After 4 durability wetting-drying cycles, the analysis of unconfined strength resulted in the plots presented in figure 5.5. The effect of lime prevails over the fly ash, and the response of strength cannot be expressed by a linear relation anymore, as can be seen in the mean values of the maximum and minimum factors and by the regression equation – equation (5.5) –.

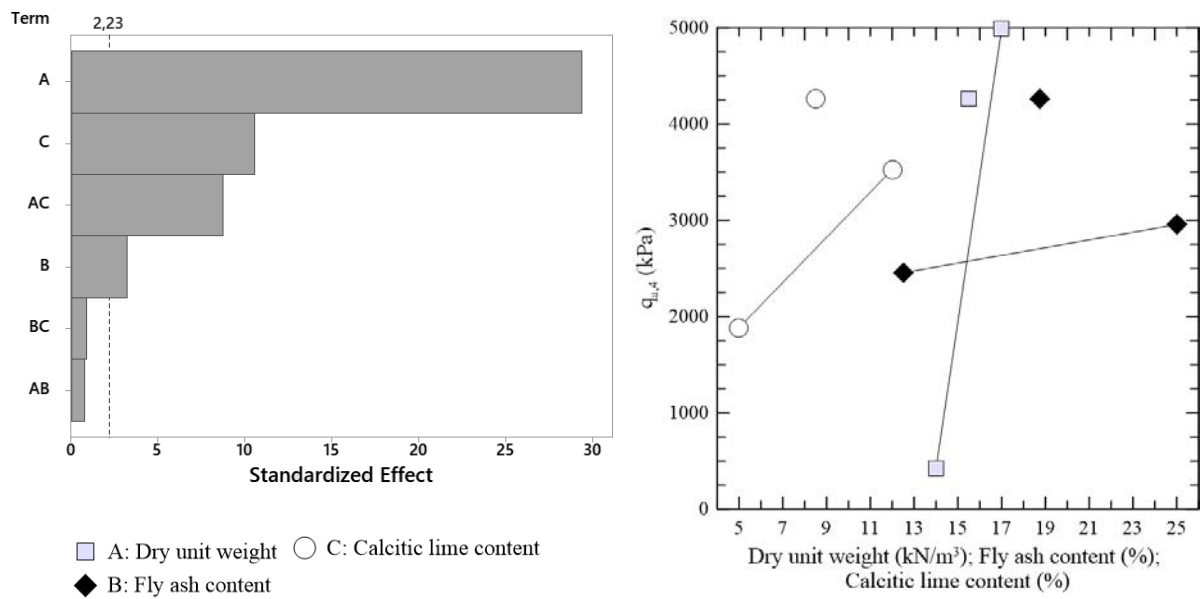


Figure 5.5: Pareto and main effects on the response of unconfined compressive strength for calcitic lime treated samples after 4 cycles (samples  $H/D \approx 2.0$ ).

$$\begin{aligned}
 q_{u,4 (H/D=2.0)} = & 5.174 + 298DW - 34FA - 1,713CL \\
 & + 6.55DW \times FA + 129.6DW \times CL - 3.23FA \times CL \\
 & + 1,557CtPt
 \end{aligned}
 \quad R^2 = 0.98 \quad (5.5)$$

Dolomitic lime treated soils results are presented in figure 5.6. A more pronounced effect of lime can be observed, so as a lower effect of fly ash in strength. A curvilinear response can be noticed too by the observation of the central points and regression equation expressed by equation (5.6).

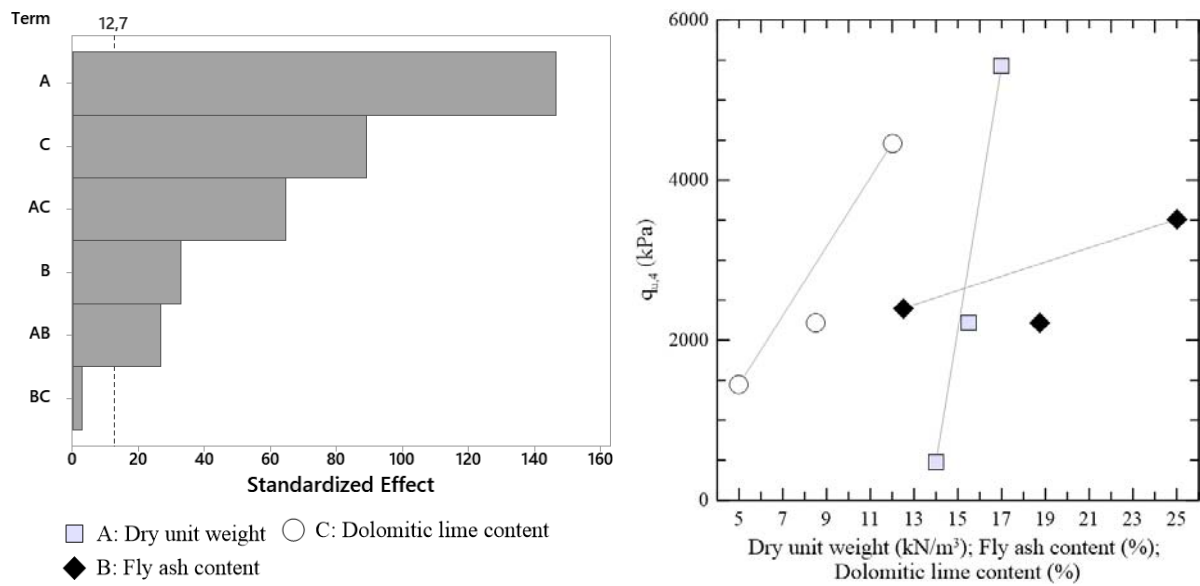


Figure 5.6: Pareto and main effects on response to unconfined compressive strength for dolomitic lime treated samples after 4 cycles (samples H/D  $\approx$  2.0).

$$\begin{aligned}
 q_{u,4 (H/D=2.0)} = & 13,975 - 1,031.4DW - 682.2FA - 2,845.6DL \\
 & + 48.49DW \times FA + 208.6DW \times DL + 2.298FA \times DL \\
 & - 735.2CtPt
 \end{aligned}
 \quad R^2 = 1.00 \quad (5.6)$$

After the 12<sup>th</sup> cycle, the tendency observed in the 1<sup>st</sup> and 4<sup>th</sup> cycle turns out to be more pronounced, as shown in figure 5.7. The lime is more effective in strength concerning dry unit weight, and the response may be no more expressed by a linear relationship when there is a need for accuracy on the determination of intermediate dosages response, as can be depicted by equation (5.7).

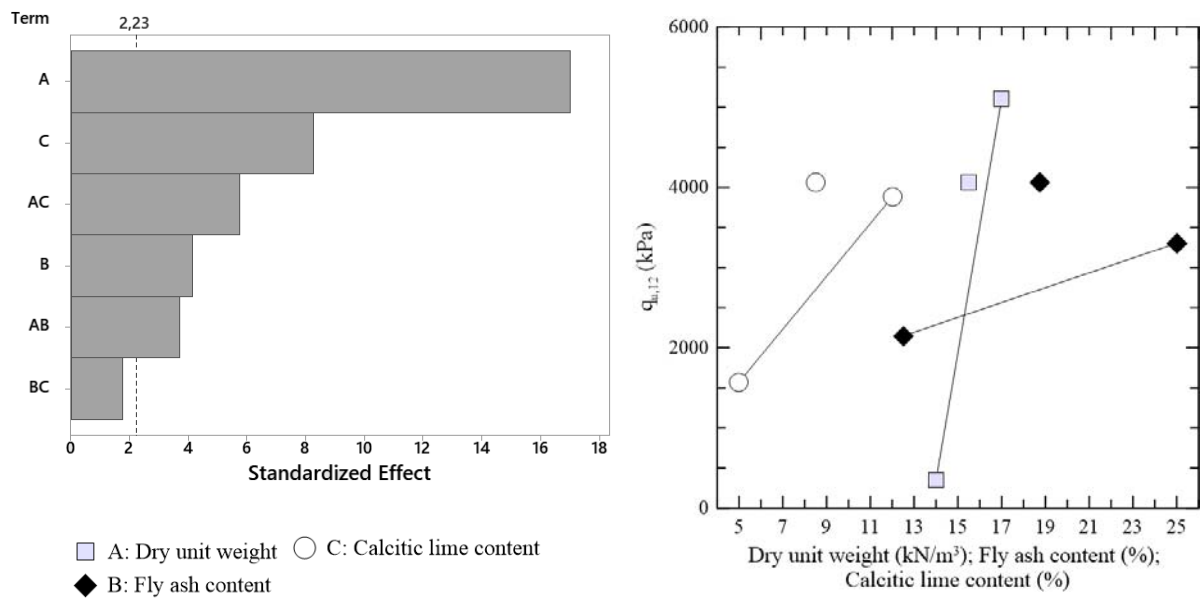


Figure 5.7: Pareto and main effects on response to unconfined compressive strength for calcitic lime treated samples after 12 cycles (samples  $H/D \approx 2.0$ ).

$$\begin{aligned}
 q_{u,12 (H/D=2.0)} = & 11,610 - 751DW - 858FA - 2,250CL \\
 & + 55.2DW \times FA + 152.9DW \times CL + 11.17FA \times CL \\
 & + 1,337CL \times Pt
 \end{aligned}
 \quad R^2 = 0.96 \quad (5.7)$$

When the response is evaluated after the 12<sup>th</sup> cycle undergoing dolomitic lime treated specimens, the results are shown in figure 5.8 arise. Surprisingly, the unconfined compressive strength presented a linear response. Besides that, the effect of lime was almost the same as dry unit weight, so as the interaction of dolomitic lime and dry unit weight. The regression equation is presented by equation (5.8).



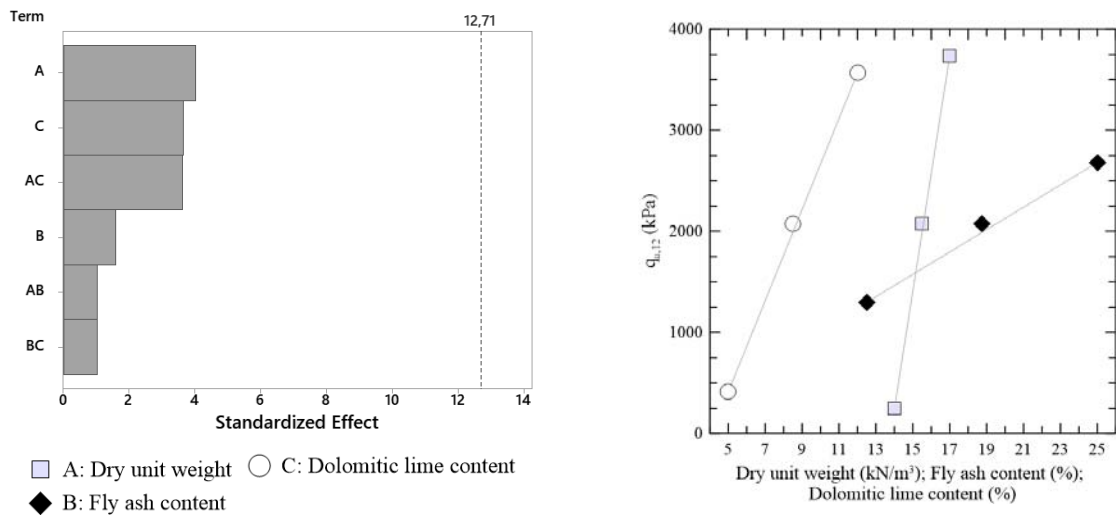


Figure 5.8: Pareto and main effects on response to unconfined compressive strength for dolomitic lime treated samples after 12 cycles (samples H/D ≈ 2.0).

$$\begin{aligned}
 q_{u,12} (H/D=2.0) = & 34,493 - 2,269DW - 803FA - 4,556DL \\
 & + 47.8DW \times FA + 298.4DW \times DL + 20.4FA \times DL \\
 & + 88CtPt
 \end{aligned}
 \quad R^2 = 0.98 \quad (5.8)$$

Results for samples subjected to wetting-drying-brushing cycles are presented in figure 5.9.

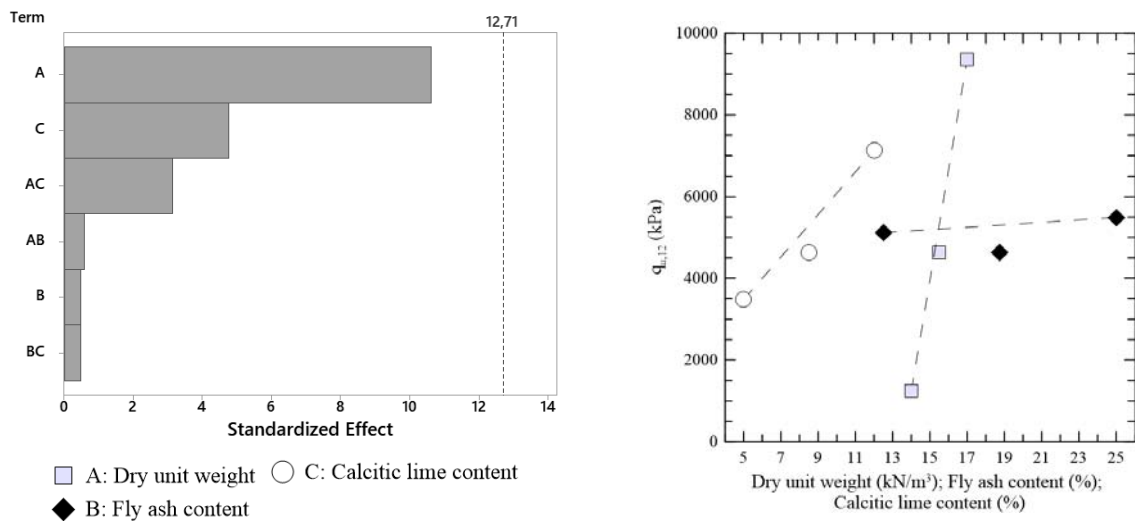


Figure 5.9: Pareto and main effects on response to unconfined compressive strength for calcitic lime treated samples after 12 cycles (samples H/D ≈ 1.2).

Those results present a similar response to the smaller samples, that were not brushed, except that the strength values are higher. The regression equation is presented next.

$$q_{u,12 (H/D=1.2)} = -19,951 + 1,221DW + 474FA - 2,854CL - 24.0DW \times FA + 227.9DW \times CL - 8.4FA \times CL + 678CtPt \quad R^2 = 0.95 \quad (5.9)$$

The following results, indicating the strong response of dolomitic lime treated soils has presented a similar behaviour when compared to the smaller and slender ( $H/D \approx 2.0$ ) specimens, which did not undergo brushing during cycles. The response may be expressed by the equation (5.10). It seems that there is an effect of lime content and dry unit weight, though it could not be confirmed as significant due to the lack of replicates.

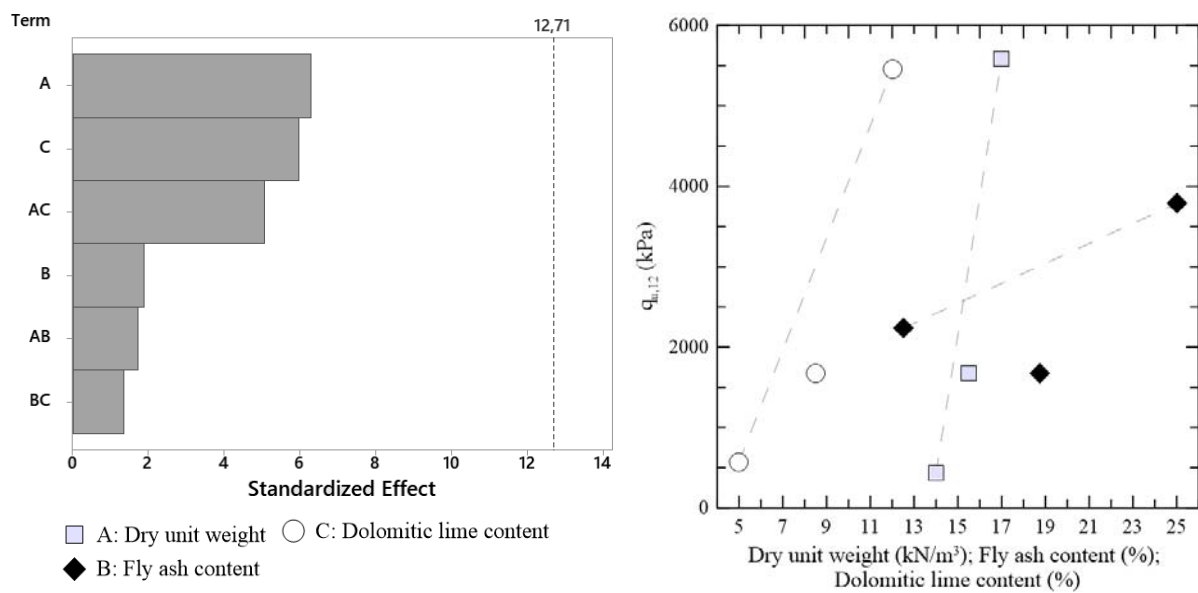


Figure 5.10: Pareto and main effects on response to unconfined compressive strength for dolomitic lime treated samples after 12 cycles (samples  $H/D \approx 1.2$ )

$$q_{u,12 (H/D=1.2)} = 46,224 - 3,063DW - 1,258FA - 5,911DL + 75.4DW \times FA + 396.0DW \times DL + 25.1FA \times DL - 1.333CtPt \quad R^2 = 0.93 \quad (5.10)$$

### 5.1.1.2 Small strain constraint modulus

Small strain constraint modulus determination can be highly affected by water content since a saturated sample indicates higher values than the same sample in a dry state. As in the condition after curing (28 days period) the moisture content is approximately 10%, it can distort real stiffness results so, it must be told that the constraint modulus of samples “after 0 cycles” can be overestimated by this test.

The factorial results after 0 cycles for constraint modulus of samples treated with calcitic lime are presented in figure 5.11. As observed, the effect of lime is very low, being possibly no effect at all. The more effective main factor is the dry unit weight, and the regression equation can be expressed by equation (5.11).

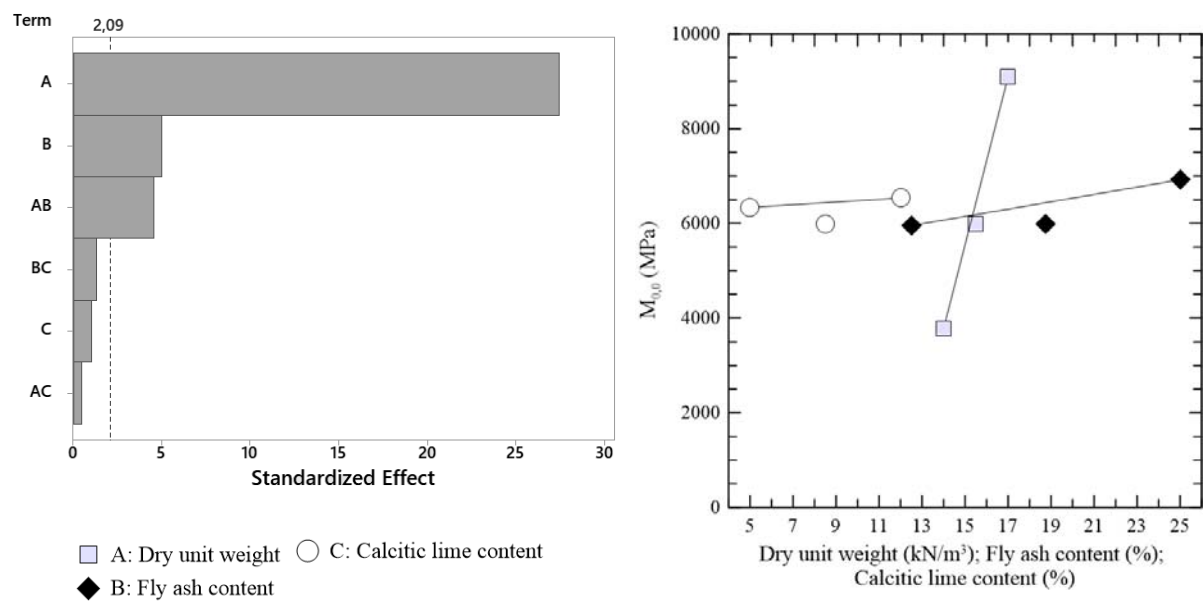


Figure 5.11: Pareto and main effects on response to small strain constraint modulus for calcitic lime treated samples after 0 cycles (samples  $H/D \approx 2.0$ ).

$$\begin{aligned}
 M_{0,0 (H/D=2.0)} = & -11,262 + 972DW - 600FA + 282CL \\
 & + 46.9DW \times FA - 9.3DW \times CL - 5.9FA \times CL \\
 & - 442CL^2
 \end{aligned}
 \quad R^2 = 0.98 \quad (5.11)$$

Results for  $M_{0,0}$  determined from specimens treated with dolomitic lime are presented in figure 5.12. There is a clear predominance of dry unit weight over the other factors, and the response is approximately linear. The regression equation is presented below.

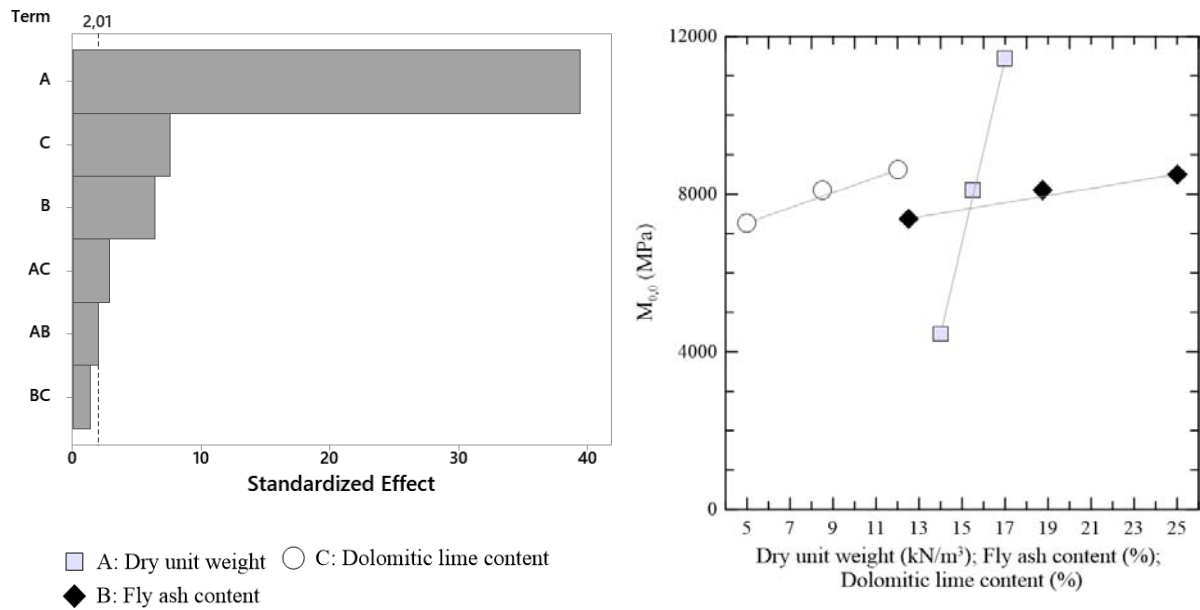


Figure 5.12: Pareto and main effects on response to small strain constraint modulus for dolomitic lime treated samples after 0 cycles (samples  $H/D \approx 2.0$ ).

$$\begin{aligned}
 M_{0,0 (H/D=2.0)} = & 18,685 + 1,561DW - 250FA - 657DL \\
 & + 18.91DW \times FA + 48.0DW \times DL + 5.57FA \times DL \\
 & + 169CtPt
 \end{aligned}
 \quad R^2 = 0.97 \quad (5.12)$$

Factorial results for calcitic lime treated specimens after 1 cycle are shown in figure 5.13.

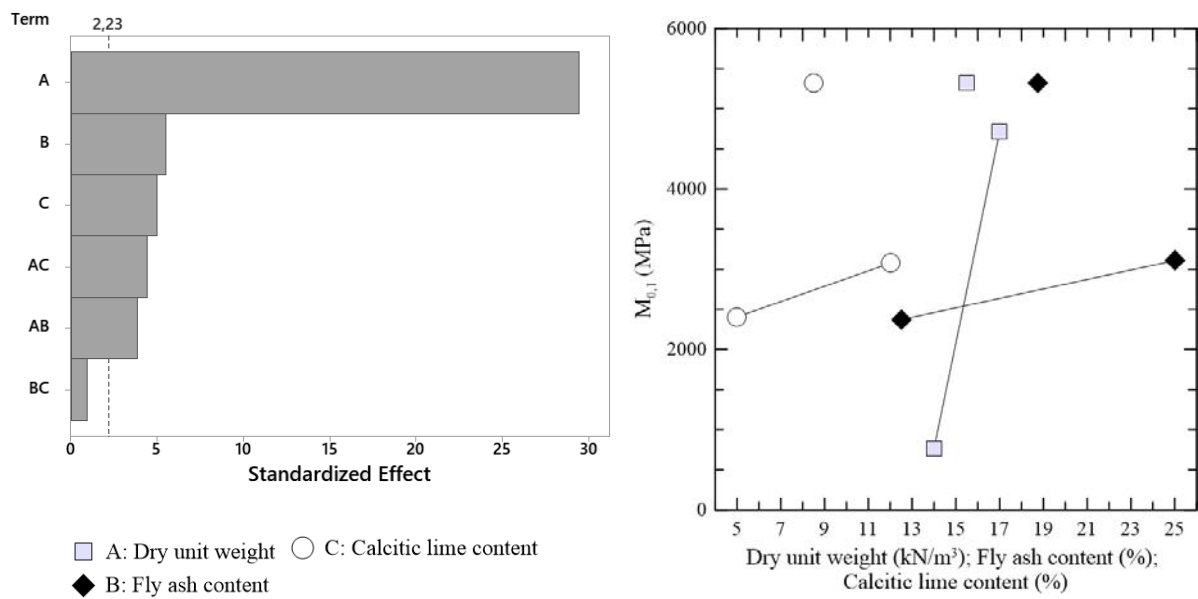


Figure 5.13: Pareto and main effects on response to small strain constraint modulus for calcitic lime treated samples after 1 cycle (samples  $H/D \approx 2.0$ ).

There is a clear increase in the nonlinear response and the effect of dry unit weight. The regression equation is shown below.

$$\begin{aligned}
 M_{0,1(H/D=2.0)} = & -3,681 + 320DW - 391FA - 835CL \\
 & + 27.48DW \times FA + 56.6DW \times CL + 2.85FA \times CL \\
 & + 2,579CtPt
 \end{aligned}
 \quad R^2 = 0.99 \quad (5.13)$$

Dolomitic lime stabilized materials, when evaluated the small strain constraint modulus, result in the plots presented in figure 5 14. There can be noted a high effect of both dry unit weight, dolomitic lime content, and their interaction. The regression expressing the response of  $M_{0,1}$  is presented next.

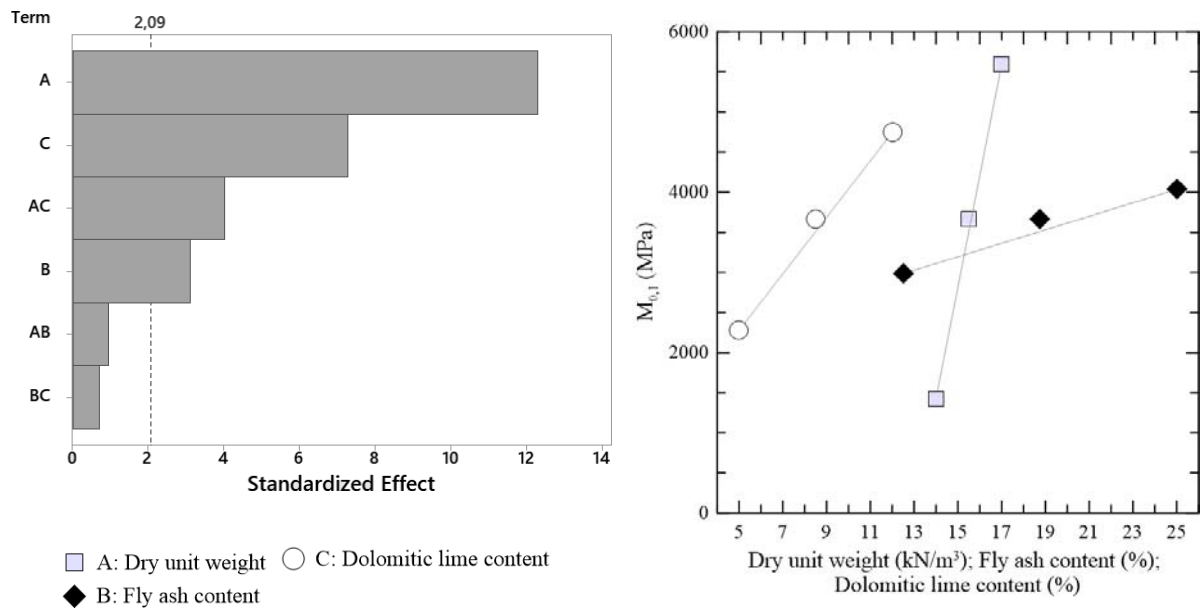


Figure 5.14: Pareto and main effects on response to small strain constraint modulus for dolomitic lime treated samples after 1 cycle (samples  $H/D \approx 2.0$ ).

$$\begin{aligned}
 M_{0,1(H/D=2.0)} = & 323-34DW - 227FA - 1,760DL \\
 & + 17.1DW \times FA + 129.8DW \times DL + 5.41FA \times DL \\
 & + 156CtPt
 \end{aligned}
 \quad R^2 = 0.92 \quad (5.14)$$

The following results present the response of samples with a slenderness ratio of approximately 1.20, which were moulded for the application of wetting-drying-brushing durability cycles.

The response of  $M_0$  for samples moulded with calcitic lime is presented in figure 5.15. It can be noticed that the effect of fly ash is very low, even negative, but as it is approximately null the negative effect can be neglected. Also, the interaction effects of lime-density (AC) and fly ash-density (AB) are higher than the main factors lime and fly ash alone. The regression equation is presented below the plots.

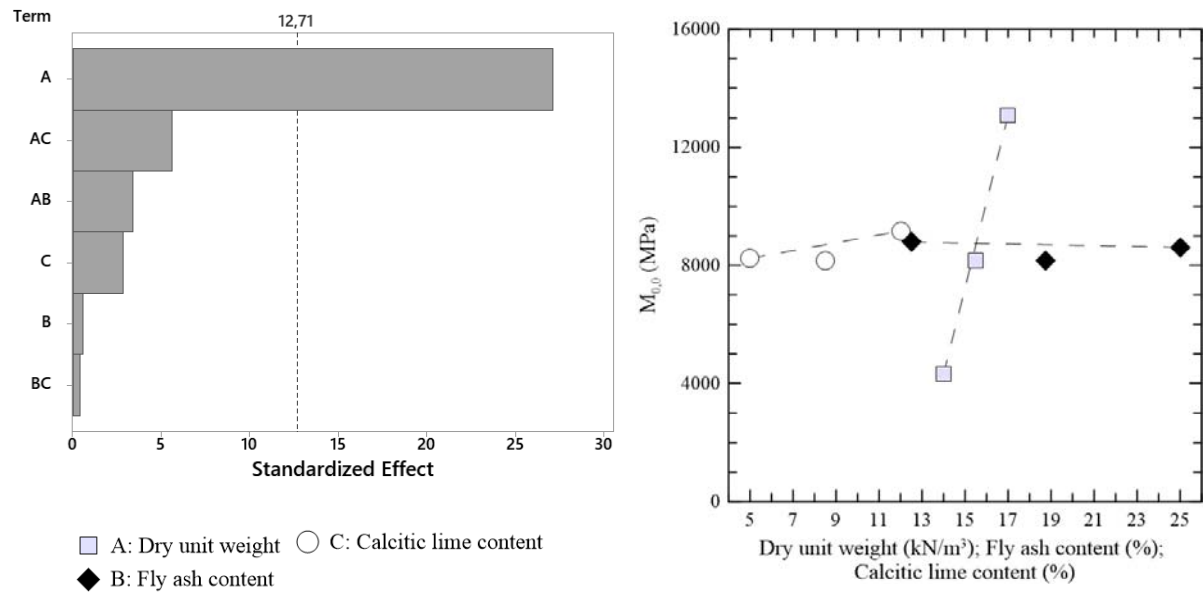


Figure 5.15: Pareto and main effects on response to small strain constraint modulus for calcitic lime treated samples after 28 days curing period (samples  $H/D \approx 1.2$ ).

$$\begin{aligned}
 M_{0,0 (H/D=1.2)} = & -32,041 + 2,541DW + 914FA - 2,492CL \\
 & -58.2DW \times FA + 173.2DW \times CL - 3.14FA \times CL \\
 & -538CtPt
 \end{aligned}
 \quad R^2 = 0.999 \quad (5.15)$$

The small strain constraint modulus after 28 curing days, for the dolomitic lime-stabilized materials, may respond according to the moulding factors as presented in figure 5.16. There is a great effect of dry unit weight in response and a very low effect of fly ash, and lime content may have a small effect, although, it can be told if this effect is significant. The regression equation is expressed by the equation (5.16).

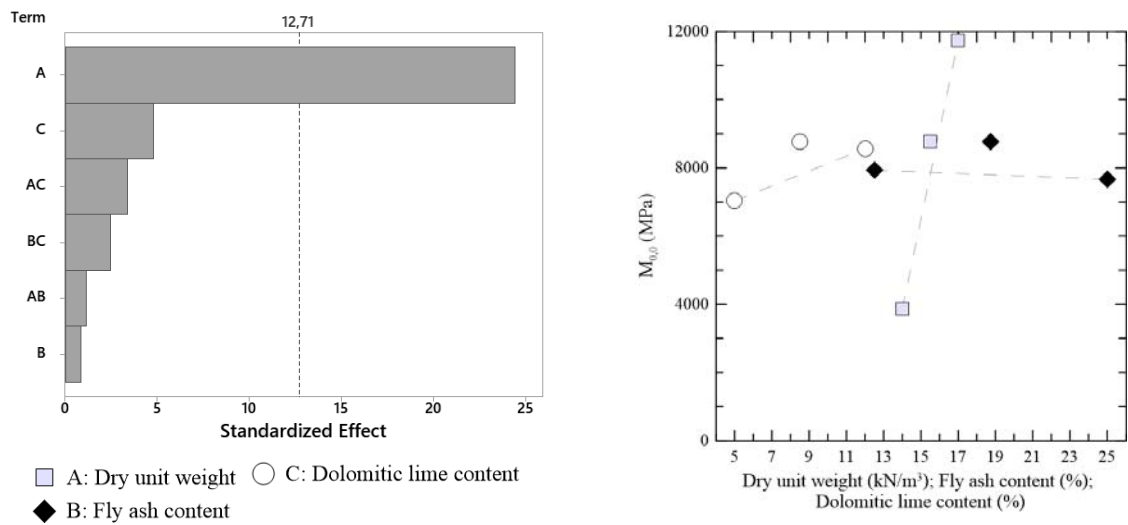


Figure 5.16: Pareto and main effects on response to small strain constraint modulus for dolomitic lime treated samples after 28 days curing period (samples H/D ≈ 1.2)

$$M_{0,0} (H/D=1.2) = -12,104 + 1,374DW - 482FA - 1,715DL + 19.9DW \times FA + 103.0DW \times DL + 17.96FA \times DL + 962CtPt \quad R^2 = 0.998 \quad (5.16)$$

Calcitic lime treated soils  $M_{0,1}$  response is presented in figure 5. 17.

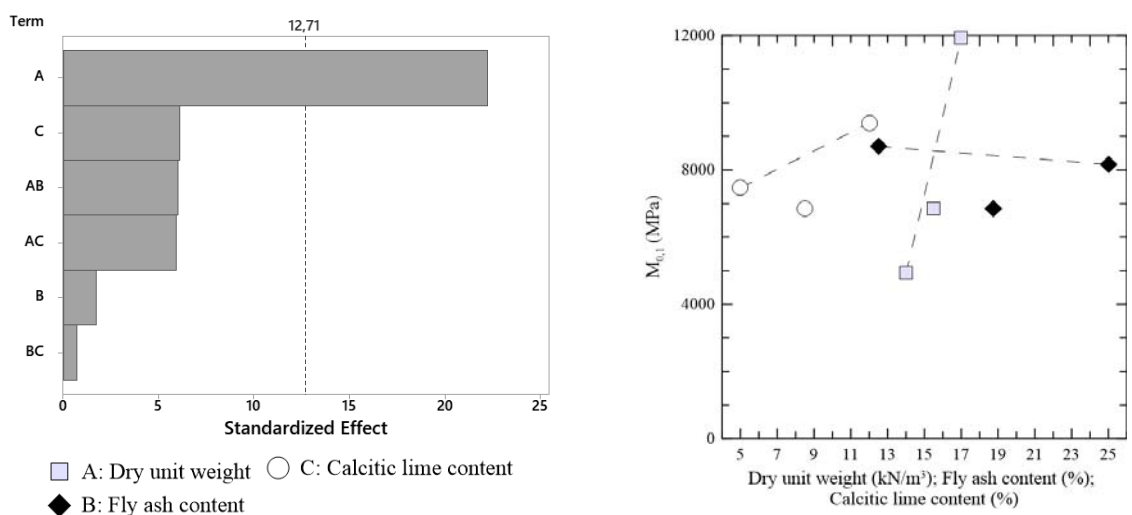


Figure 5.17: Pareto and main effects on response to small strain constraint modulus for calcitic lime treated samples after 1 cycle (samples H/D ≈ 1.2).



The response of the small strain constraint modulus after the application of one durability cycle can be expressed by the equation 5.17.

$$M_{0,1 (H/D=1.2)} = -34,364 + 2,717DW + 1,477FA - 2,587CL - 101.0DW \times FA + 178.2DW \times CL + 5.3FA \times CL - 1579CtPt \quad R^2 = 0.999 \quad (5.17)$$

After a wetting-drying-brushing cycle, the response of  $M_{0,1}$  in dolomitic lime treated soils is shown in figure 5.18. It can be noted that there is a huge effect of dry unit weight, followed by the effect of lime content and the interaction between both. Usually, it is observed a more linear response in specimens treated with dolomitic than for specimens treated with calcitic lime.

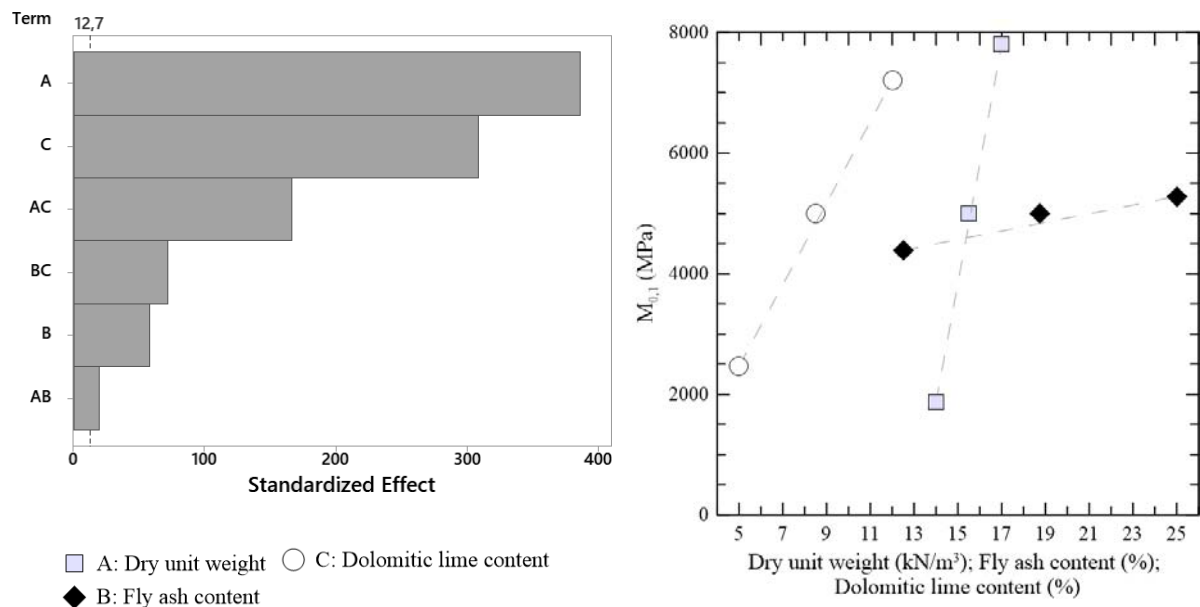


Figure 5.18: Pareto and main effects on response to small strain constraint modulus for dolomitic lime treated samples after 1 cycle (samples  $H/D \approx 1.2$ ).

The equation (5.18) expresses the response of small strain constraint modulus for specimens treated with dolomitic lime after 1 durability cycle.

$$\begin{aligned}
 M_{0,1(H/D=1.2)} = & 7,916 - 397.5DW - 395.9FA - 3,568.1DL \\
 & + 16.35DW \times FA + 243.39DW \times DL + 25.19FA \times DL \\
 & + 165.5CtPt
 \end{aligned}
 \quad R^2 = 0.999 \quad (5.18)$$

The effect of different factors in factorial results of small strain constraint modulus after 4 cycles could only be assessed for calcitic lime treated soils, as in dolomitic ones there was a lack of information due to excessive damage in some specimens. Results are presented in figure 5.19, showing an increase in the effect of lime content and the interaction lime content-dry unit weight when compared to the response in previous cycles. The regression equation is presented by equation (5.19).

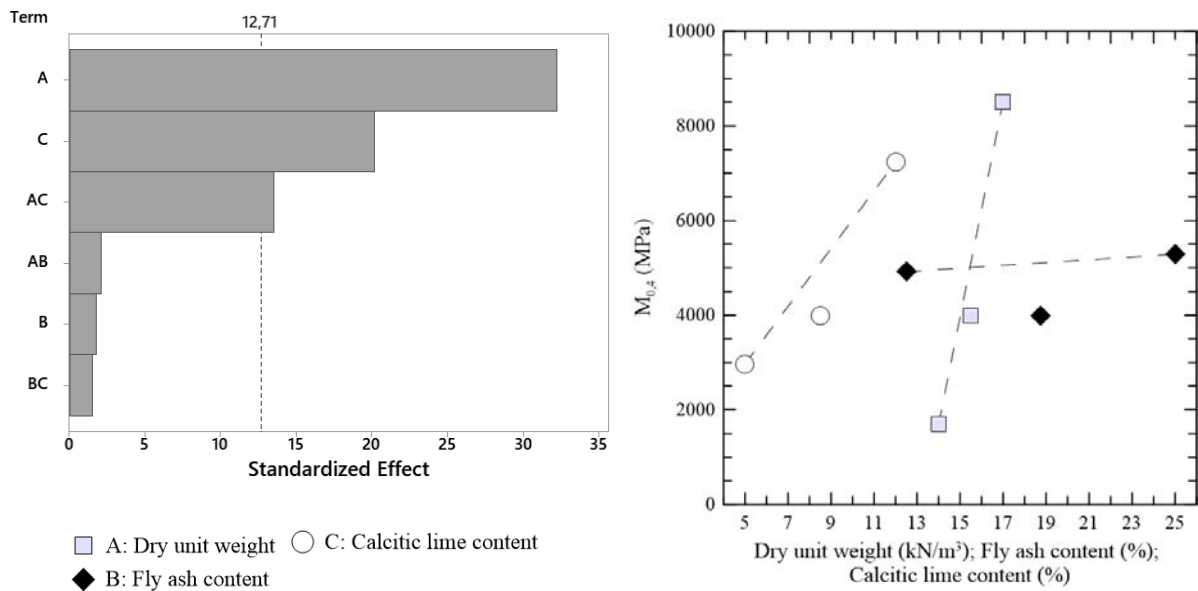


Figure 5.19: Pareto and main effects on response to small strain constraint modulus for calcitic lime treated samples after 4 cycles (samples  $H/D \approx 1.2$ ).

$$\begin{aligned}
 M_{0,4(H/D=1.2)} = & -5,648 + 399DW + 333FA - 3,751CL \\
 & - 23.6DW \times FA + 272.5DW \times CL + 7.3FA \times CL \\
 & - 1,119CtPt
 \end{aligned}
 \quad R^2 = 0.999 \quad (5.19)$$

### 5.1.1.3 Small strain shear modulus

S-waves travel time may be affected by matric suction, so, there can be variability in shear modulus that is not related to soil structure. However, those changes in behaviour are expected to be less than those related to P-waves.

The small strain shear modulus results after 28 days curing period ( $G_{0,0}$ ) for soils with  $H/D \approx 2.0$  and stabilized with calcitic lime are shown in figure 5.20. All the factors and interactions between them are significant, that is, the null hypothesis was rejected for that case. Fly ash also seems to play an important role in  $G_{0,0}$ . When the center point is observed, it can be noted that there is not a linear tendency in response to small strain shear modulus. The regression equation is presented next.

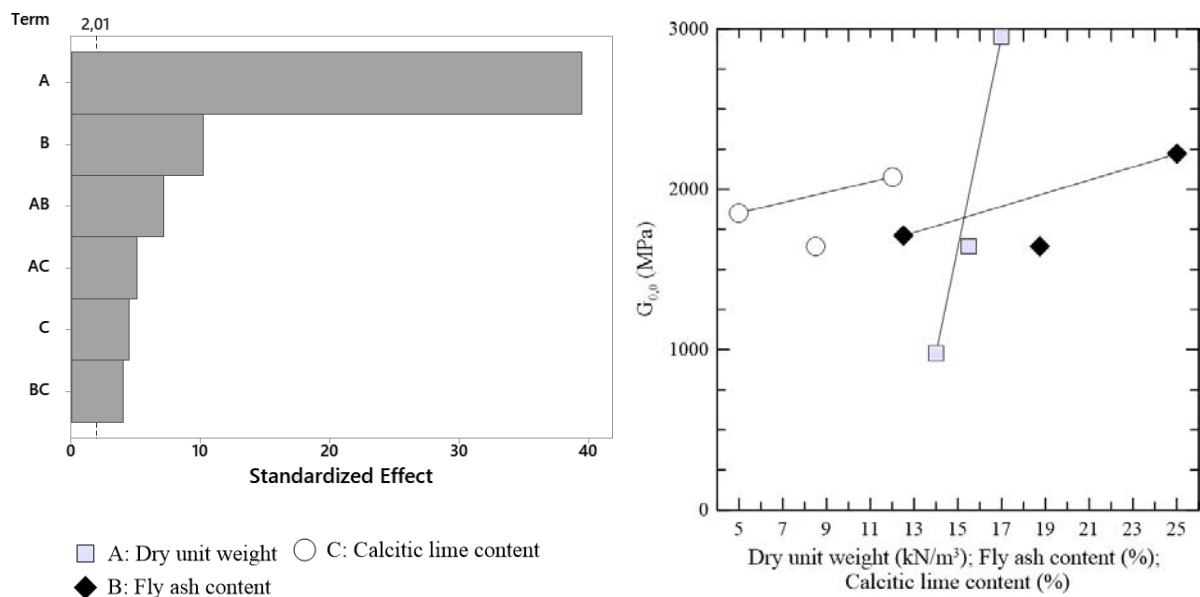


Figure 5.20: Pareto and main effects on response to small strain shear modulus for calcitic lime treated samples after 0 cycles (samples  $H/D \approx 2.0$ ).

$$\begin{aligned}
 G_{0,0 (H/D=2.0)} = & -6,031 + 486.9DW + 17.5FA - 422.6DL \\
 & -0.58DW \times FA + 31.10DW \times DL + 1.04FA \times DL \\
 & -112.8CtPt
 \end{aligned}
 \quad R^2 = 0.999 \quad (5.20)$$

$G_{0,0}$  response for dolomitic lime treated soils is presented in figure 5.21. Here, the effect of dry unit weight is followed by the effect of lime content instead of fly ash. The response is

approximately linearly related to the main factors. The mathematical expression of this behaviour is presented by equation (5.21).

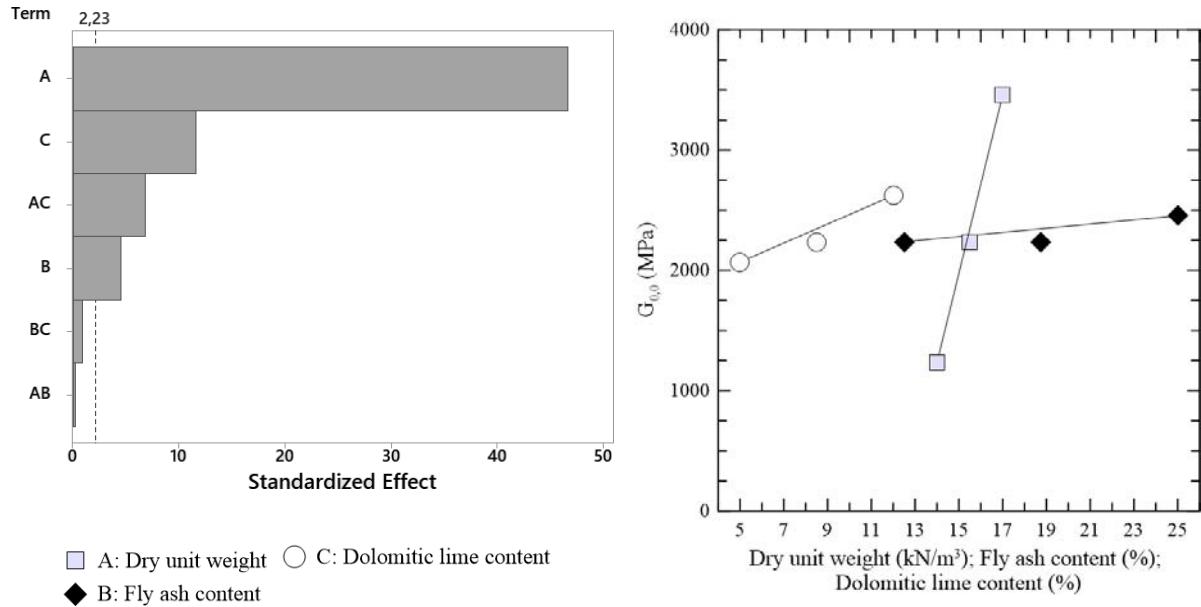


Figure 5.21: Pareto and main effects on response to small strain shear modulus for dolomitic lime treated samples after 0 cycles (samples H/D  $\approx 2.0$ ).

$$\begin{aligned}
 G_{0,0} (H/D=2.0) = & -6,031 + 486.9DW - 17.5FA - 422.6CL \\
 & -0.58DW \times FA + 31.10DW \times CL + 1.04FA \times CL \\
 & -112.8CtPt
 \end{aligned}
 \quad R^2 = 0.996 \quad (5.21)$$

After 1 cycle, the small strain shear modulus response is presented in figure 5.22.

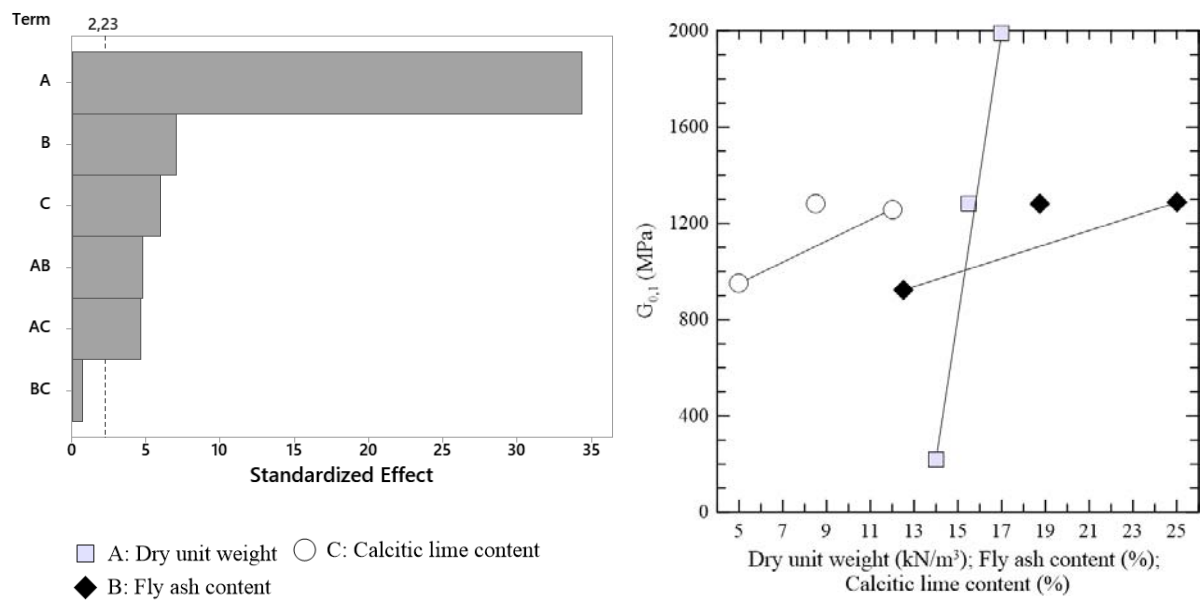


Figure 5.22: Pareto and main effects on response to small strain shear modulus for calcitic lime treated samples after 1 cycle (samples  $H/D \approx 2.0$ ).

As can be observed, there is a small effect of fly ash and lime content compared to the effect of dry unit weight. Also, it was noted that the maximum mean shear modulus has decreased from the 0 cycle tests. The regression equation is expressed by the equation (5.22).

$$\begin{aligned}
 G_{0,1(H/D=2.0)} = & -2,047 + 152.5DW - 181.4FA - 323.0CL \\
 & + 13.13DW \times FA + 22.67DW \times CL + 0.83FA \times CL \\
 & + 177.2CtPt
 \end{aligned}
 \quad R^2 = 0.99 \quad (5.22)$$

The small strain shear modulus after 1 wetting-drying cycle ( $G_{0,1}$ ) for dolomitic lime treated specimens are shown in figure 5.23. The observed fly ash effect is higher than the dolomitic lime content effect, so is the interaction between fly ash content and dry unit weight.

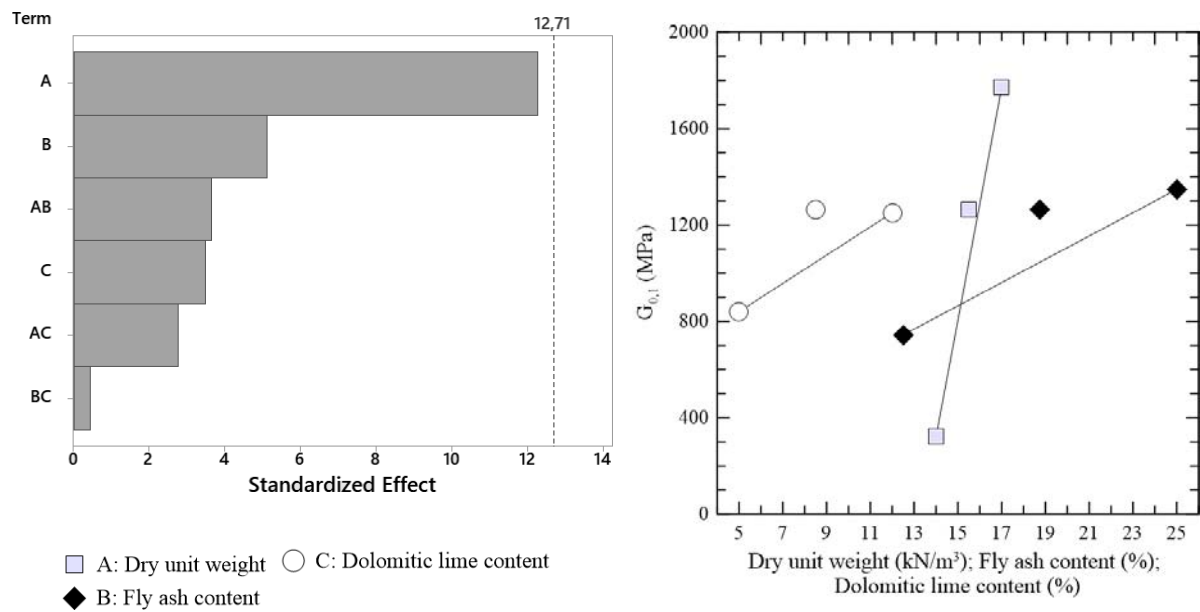


Figure 5.23: Pareto and main effects on response to small strain shear modulus for dolomitic lime treated samples after 1 cycle (samples H/D  $\approx$  2.0).

The equation corresponding to the response of  $G_{0,1}$  is presented below.

$$\begin{aligned}
 G_{0,1 (H/D=2.0)} = & 3,093 - 210DW - 317FA - 444DL \\
 & + 22.93DW \times FA + 31.0DW \times DL + 1.22FA \times DL \\
 & + 218CtPt
 \end{aligned}
 \quad R^2 = 0.995 \quad (5.23)$$

Soils with a slenderness ratio of approximately 1.2 were tested too. the  $G_{0,0}$  factorial response for samples moulded using calcitic lime in combination with fly ash is presented in figure 5.24.

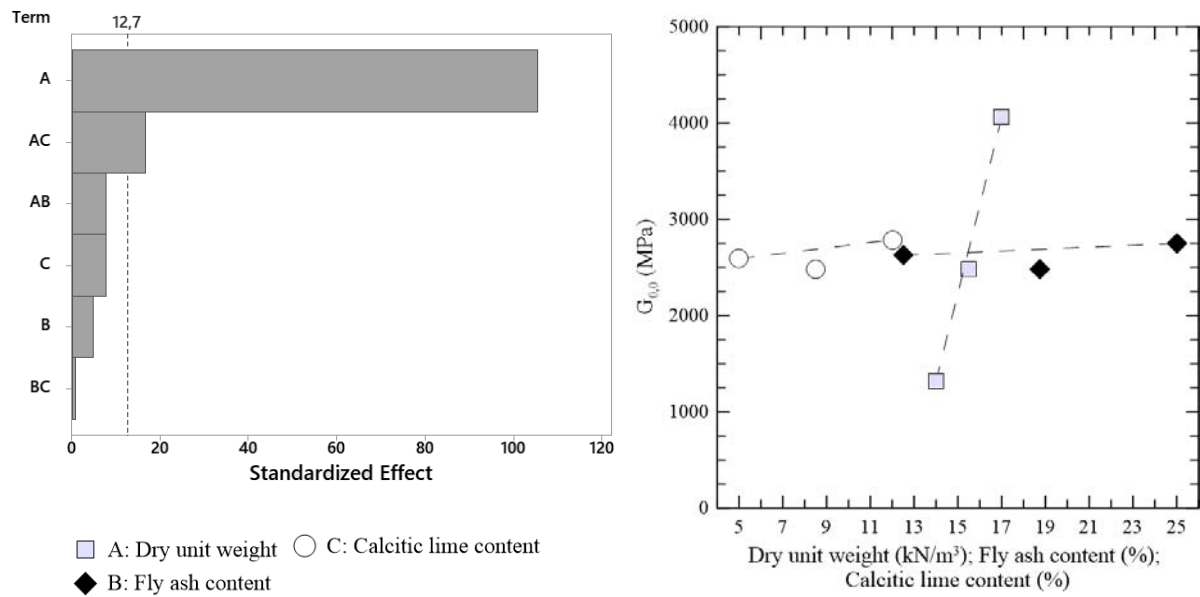


Figure 5.24: Pareto and main effects on response to small strain shear modulus for calcitic lime treated samples after 0 cycles (samples  $H/D \approx 1.2$ ).

The plot presenting standardized effects indicate that the high effect corresponds to dry unit weight as expected, but it is followed in order by the interactions instead of the main effects of lime and fly ash content. It may indicate that the response of  $G_{0,0}$  in samples with a low dry unit weight is little dependent on fly ash or calcitic lime content. The regression equation for  $G_{0,0}$  is presented by equation (5.24).

$$\begin{aligned}
 G_{0,0 (H/D=1.2)} = & -9,528 + 765.5DW + 171.0FA - 615.7CL \\
 & -10.65DW \times FA + 40.97DW \times CL + 0.479FA \times CL \\
 & -210.6CtPt
 \end{aligned}
 \quad R^2 = 0.9999 \quad (5.24)$$

For dolomitic treated specimens, the factorial response of  $G_{0,0}$  is illustrated in figure 5.25. The regression equation expressing this behaviour is presented in equation (5.25).

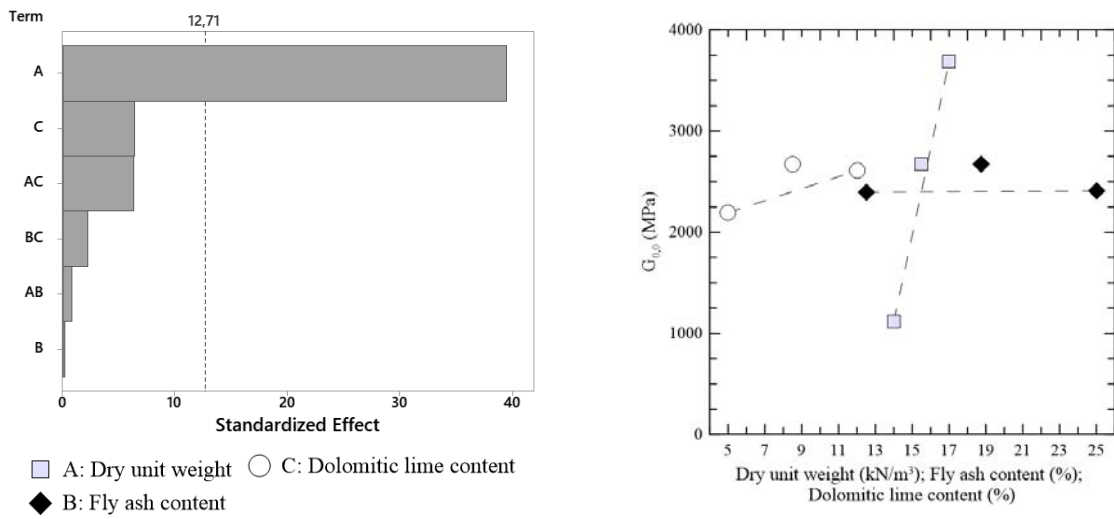


Figure 5.25: Pareto and main effects on response to small strain shear modulus for dolomitic lime treated samples after 0 cycles (samples H/D  $\approx 1.2$ ).

$$G_{0,0 (H/D=1.2)} = -4,854 + 468.7DW - 73.4FA - 609DL + 2.97DW \times FA + 39.04DW \times DL + 3.36FA \times DL + 271.1CtPt \quad R^2 = 0.999 \quad (5.25)$$

$G_{0,1}$  for specimens stabilized with calcitic lime after 1 durability cycle is shown in figure 5.26.

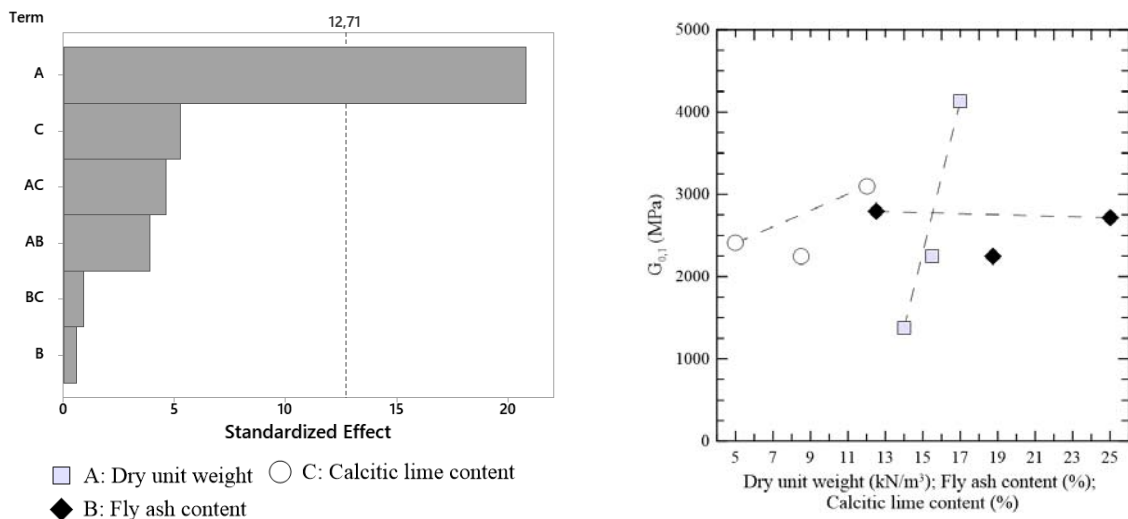


Figure 5.26: Pareto and main effects on response to small strain shear modulus for calcitic lime treated samples after 1 cycle (samples H/D  $\approx 1.2$ ).



The equation obtained from the factorial response is presented next.

$$\begin{aligned}
 G_{0,1 (H/D=1.2)} = & -12,073 + 938DW + 395FA - 850CL \\
 & -27.40DW \times FA + 57.9DW \times CL + 2.75FA \times CL \\
 & -508CtPt
 \end{aligned}
 \quad R^2 = 0.998 \quad (5.26)$$

For calcitic lime treated soils after 4 cycles, the  $G_0$  response is presented in figure 5.27. Only dry unit weight and lime content were rated as significant effects. The regression equation is expressed by equation (5.27).

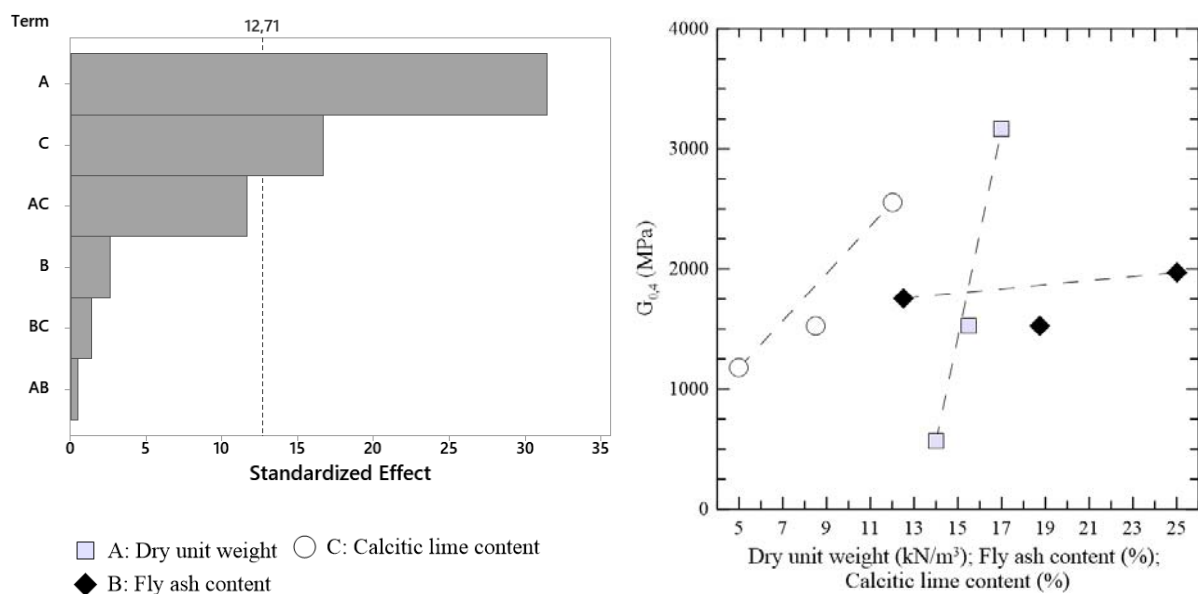


Figure 5.27: Pareto and main effects on response to small strain shear modulus for calcitic lime treated samples after 4 cycles (samples  $H/D \approx 1.2$ ).

$$\begin{aligned}
 G_{0,4 (H/D=1.2)} = & -1,635 + 124DW + 26.6FA - 1,276CL \\
 & -2.05DW \times FA + 91.81DW \times CL + 2.64FA \times CL \\
 & -339CtPt
 \end{aligned}
 \quad R^2 = 0.999 \quad (5.27)$$

#### 5.1.1.4 Loss of mass

Accumulated loss of mass was assessed after the 1<sup>st</sup>, 4<sup>th</sup>, and 12<sup>th</sup> cycles. Only the specimens undergoing cycles where brushing was applied were evaluated. The calcitic lime treated specimens have their response after 1 durability cycle expressed in figure 5.28. As can be seen,

the higher effect comes from the dry unit weight, but fly ash content and the interaction between fly ash content and dry unit weight as also significant in  $ALM_1$ .

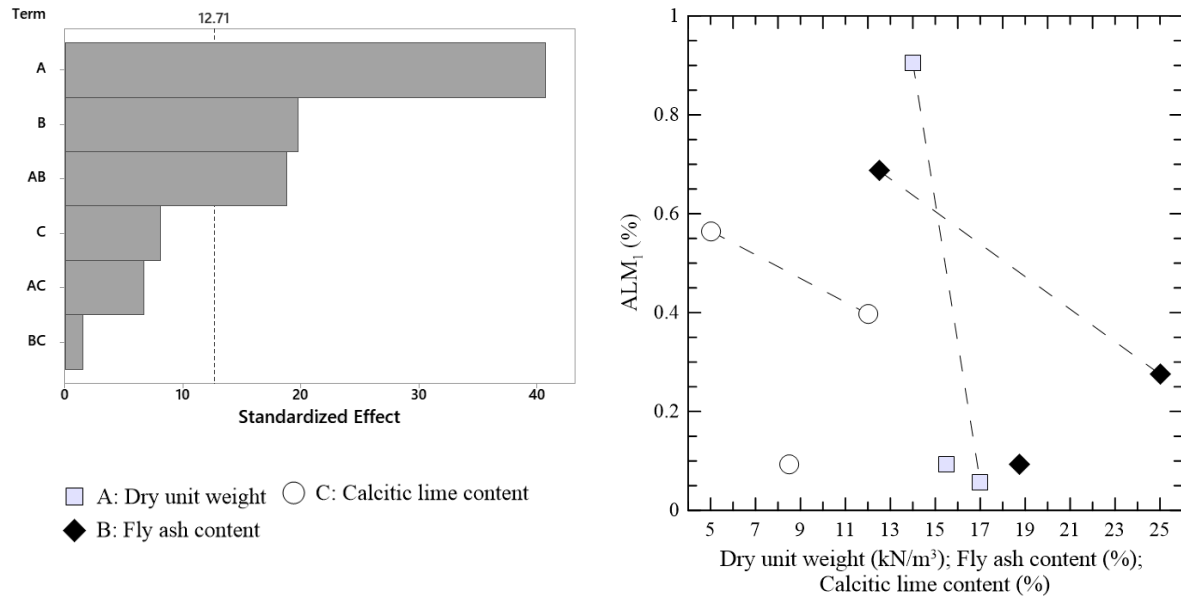


Figure 5.28: Pareto and main effects on response to the accumulated loss of mass for calcitic lime treated samples after 1 cycle (samples H/D  $\approx 1.2$ ).

The factorial response of accumulated loss of mass after 1 durability cycle is expressed by the equation (5.28), however, the  $ALM$  behaviour is clearly not linear.

$$\begin{aligned}
 ALM_{1(H/D=1.2)} = & 13.619 - 0.7873DW - 0.3629FA - 0.2430CL \\
 & + 0.02089DW \times FA + 0.01326DW \times CL + 0.000722FA \times CL \quad R^2 = 0.9996 \quad (5.28) \\
 & - 0.3878CtPt
 \end{aligned}$$

The factorial response of accumulated loss of mass after 1 durability cycle ( $ALM_1$ ) for dolomitic lime stabilized mixtures is shown in figure 5.29. There could not be determined which factors were significant in the loss of mass response, but the higher effects correspond to dry unit weight and lime content. As in the soils treated with calcitic lime, there is no linearity in the response, so, an intermediate response can not be accurately determined. The regression equation is presented by equation (5.29).

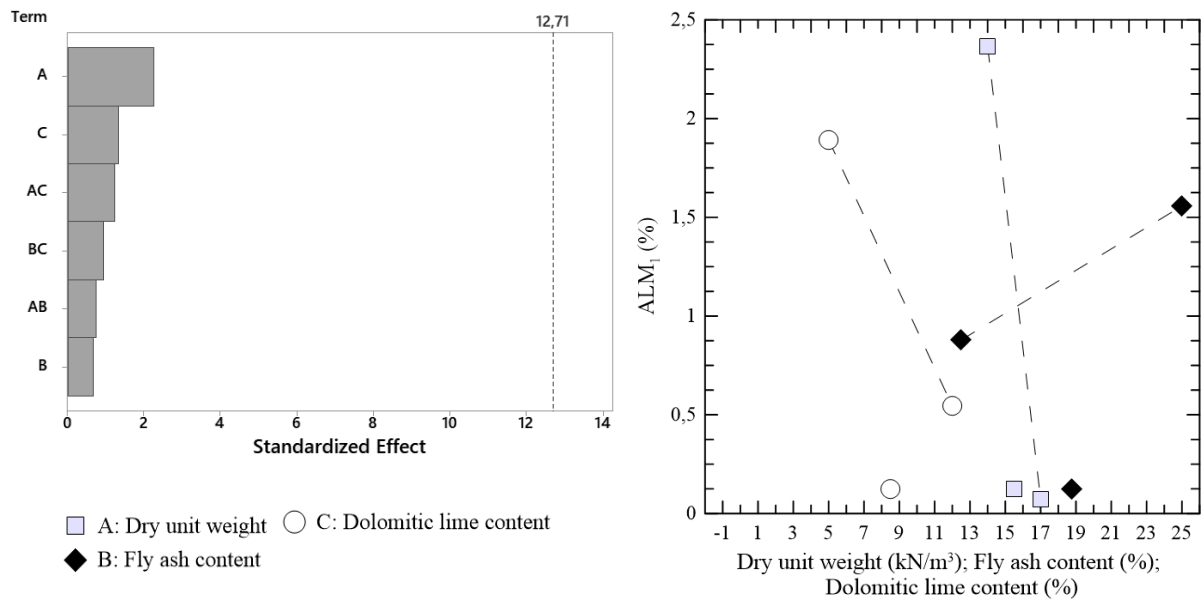


Figure 5.29: Pareto and main effects on response to the accumulated loss of mass for dolomitic lime treated samples after 1 cycle (samples  $H/D \approx 1.2$ ).

$$\begin{aligned}
 ALM_{1(H/D=1.2)} = & 13.9 - 1.00DW - 0.872FA - 1.62DL \\
 & - 0.0408DW \times FA + 0.1182DW \times DL - 0.0217FA \times DL \\
 & - 1.09CtPt
 \end{aligned}
 \quad R^2 = 0.91 \quad (5.29)$$

$ALM_4$  response for calcitic lime treated soils is presented in figure 5.30.

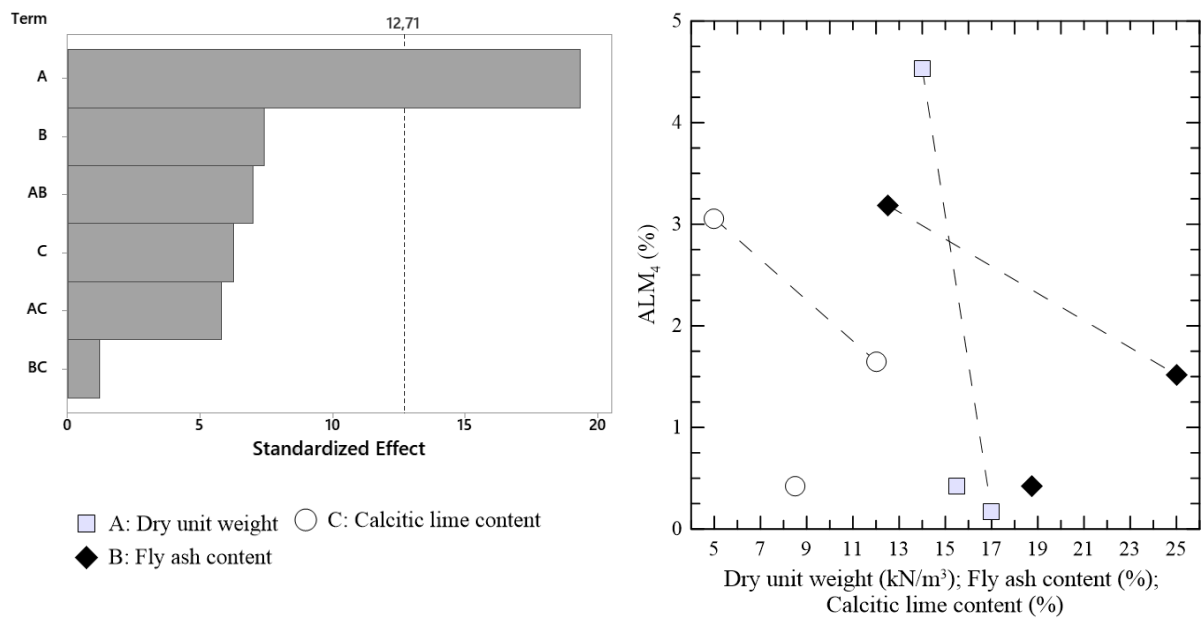


Figure 5.30: Pareto and main effects on response to the accumulated loss of mass for calcitic lime treated samples after 4 cycles (samples  $H/D \approx 1.2$ ).

As can be observed, fly ash content still presenting a higher effect than calcitic lime content. The following equation corresponds to the regression fit for the factorial response of  $ALM_4$ .

$$\begin{aligned}
 ALM_{4(H/D=1.2)} = & 70.98 - 4.091DW - 1.491FA - 2.252CL \\
 & + 0.0842DW \times FA + 0.1248DW \times CL + 0.00626FA \times CL \\
 & - 1.934CtPt
 \end{aligned}
 \quad R^2 = 0.998 \quad (5.30)$$

$ALM_4$  factorial response for specimens stabilized using dolomitic lime is presented in figure 5.31.

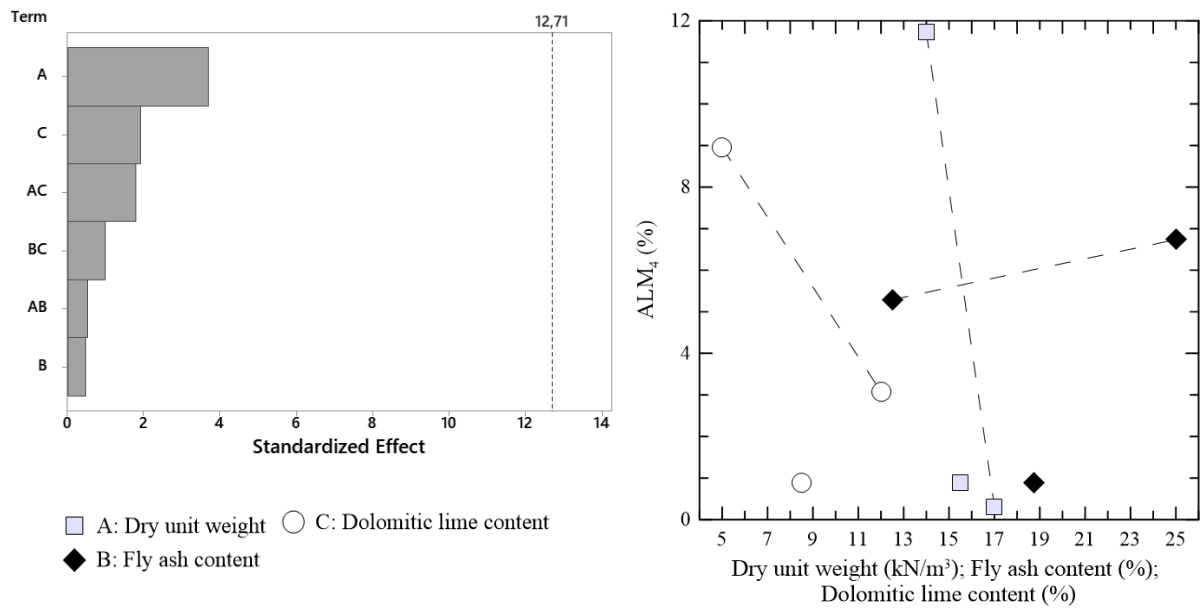


Figure 5.31: Pareto and main effects on response to the accumulated loss of mass for dolomitic lime treated samples after 1 cycle (samples  $H/D \approx 1.2$ ).

The expression accounting for the response of  $ALM_4$  is presented in equation (5.31).

$$\begin{aligned}
 ALM_{4(H/D=1.2)} = & 103.3 - 6.67DW + 2.03FA - 7.68DL \\
 & - 0.085DW \times FA + 0.525DW \times DL - 0.0692FA \times DL \\
 & - 5.14CtPt
 \end{aligned}
 \quad R^2 = 0.96 \quad (5.31)$$

The accumulated loss of mass after 12 cycles ( $ALM_{12}$ ) for calcitic lime soils is presented in figure 5.32. When compared to the same specimens after 4 cycles, lime content became more effective than the fly ash content factor. The mathematical expression of the ALM response is presented next, by equation (5.32).

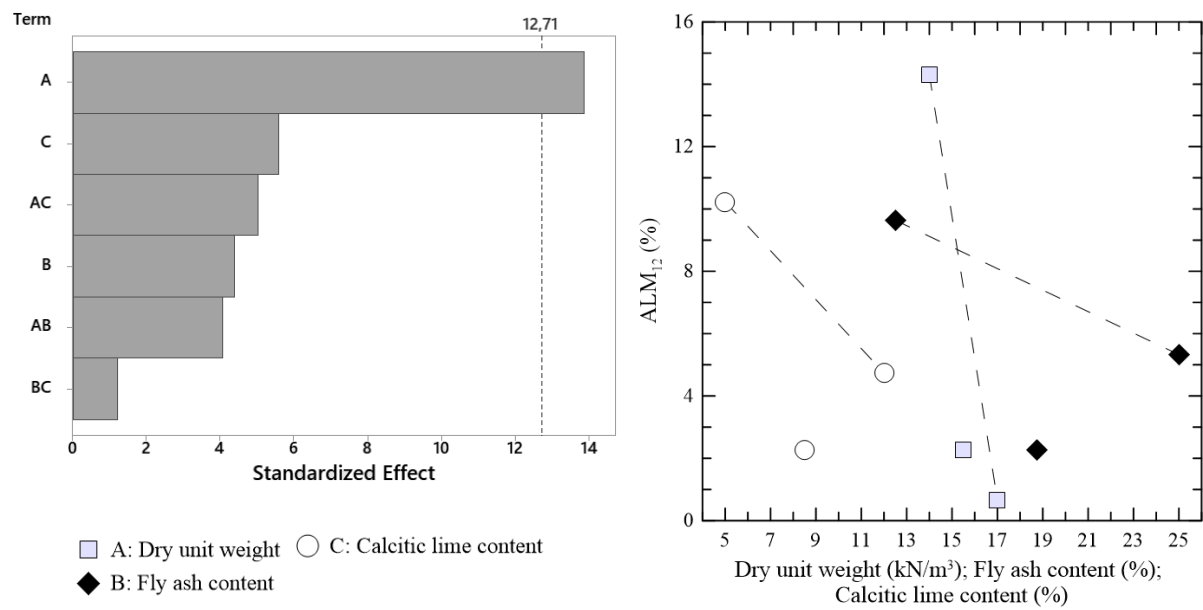


Figure 5.32: Pareto and main effects on response to the accumulated loss of mass for calcitic lime treated samples after 12 cycles (samples  $H/D \approx 1.2$ ).

$$\begin{aligned}
 ALM_{12(H/D=1.2)} = & 219.0 - 12.52DW - 3.869FA - 8.57CL \\
 & + 0.2125DW \times FA + 0.4695DW \times CL + 0.0271FA \times CL \\
 & - 5.22CtPt
 \end{aligned}
 \quad R^2 = 0.997 \quad (5.32)$$

The  $ALM_{12}$  response for the dolomitic lime treated specimens are presented in figure 5.33.

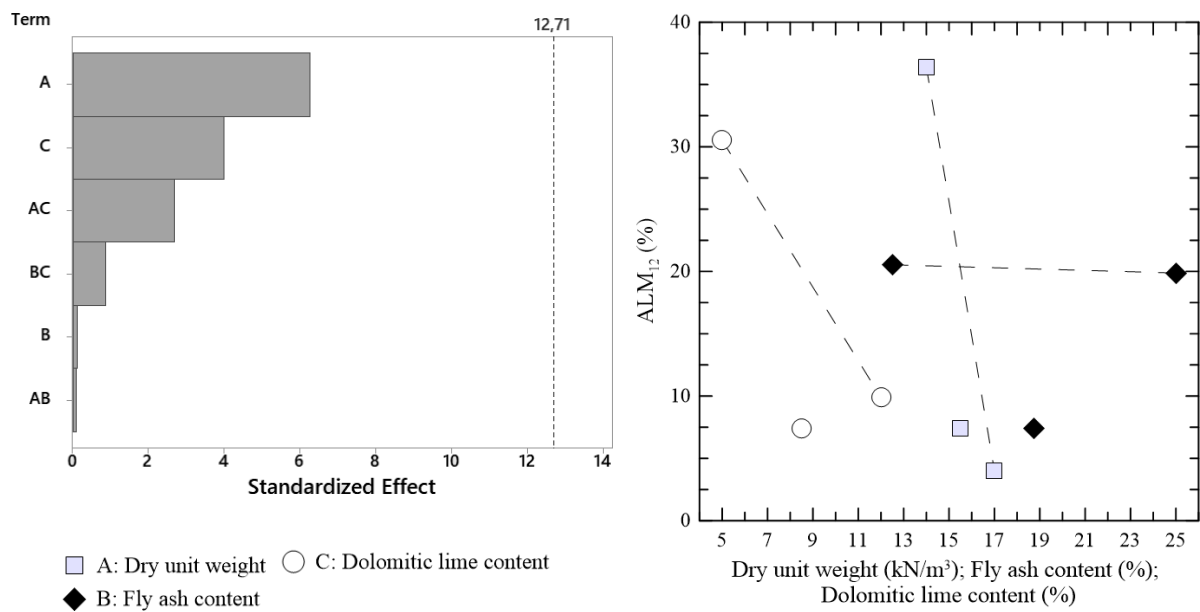


Figure 5.33: Pareto and main effects on response to the accumulated loss of mass for dolomitic lime treated samples after 12 cycles (samples  $H/D \approx 1.2$ ).

As can be seen, the effect of fly ash is almost negligible. The regression fit is expressed by the equation (5.33).

$$\begin{aligned}
 ALM_{12(H/D=1.2)} = & 364 - 21.59DW + 1.24FA - 21.58DL \\
 & - 0.026DW \times FA + 1.327DW \times DL - 0.104FA \times DL \\
 & - 12.83CtPt
 \end{aligned}
 \quad R^2 = 0.99 \quad (5.33)$$

As in all the evaluated responses of accumulated loss of mass, the response behaviour is far from linear.

### 5.1.2 Addition of lime type effect

To compare the samples stabilized with two different kinds of lime, the lime type factor was added to the factorial design, where “-1” corresponds to calcitic carbide lime and “+1” to dolomitic Primor lime. As there is no intermediate between these two types of lime, no center points were considered.

#### 5.1.2.1 Unconfined compressive strength and lime type aid

Unconfined compressive strength results after 28 days curing period (0 cycles) are presented in figure 5.34. The effect of lime type is sharp, only lower than dry unit weight.

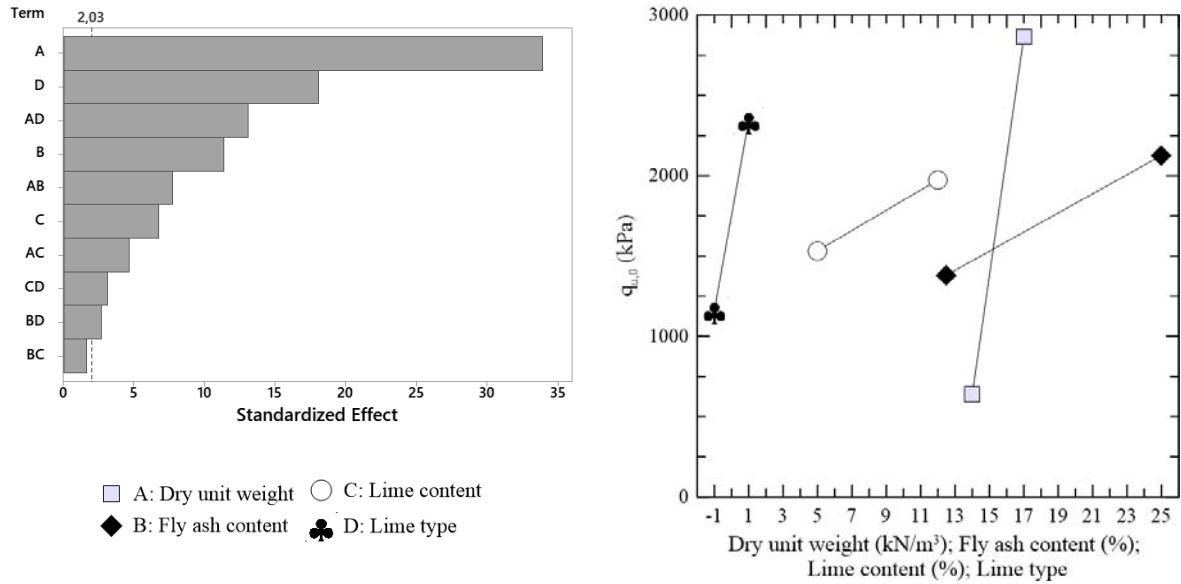


Figure 5.34: Pareto and main effects on response to unconfined compressive strength for samples after 0 cycle (samples H/D ≈ 2.0).

As can be observed, samples treated with calcitic lime presented lower strength than samples treated with dolomitic lime. The regression equation representing the response of unconfined compressive strength is expressed by the equation (5.34).

$$\begin{aligned}
 q_{u,0 (H/D=2.0)} = & 638 - 9.9DW - 378.9FA - 430LC \\
 & - 4,352LT + 26.97DW \times FA + 28.92DW \times LC \\
 & + 286.2DW \times LT + 2.40FA \times LC \\
 & + 13.98FA \times LT + 28.80LC \times LT
 \end{aligned}
 \quad R^2 = 0.98 \quad (5.34)$$

Where

LC = lime content (%)

LT = Lime type

After 1 wetting-drying durability cycle, the unconfined strength response is shown in figure 5.35. The strength response is not assertively dependent on lime type.



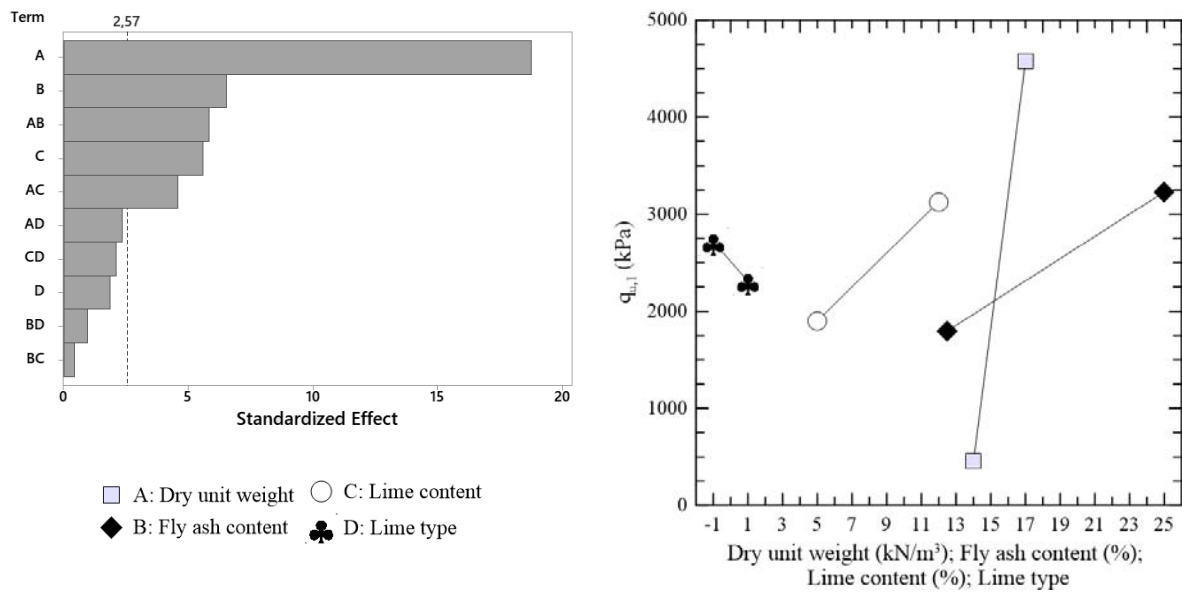


Figure 5.35: Pareto and main effects on response to unconfined compressive strength for samples after 1 cycle (samples  $H/D \approx 2.0$ ).

The regression equation, considering the lime type and lime type-interactions, is presented in equation (5.35).

$$\begin{aligned}
 q_{u,1 (H/D=2.0)} = & 1,035 - 724DW - 965FA - 1,347LC \\
 & + 2,221LT + 68.5DW \times FA + 95.7DW \times LC \\
 & - 172.3DW \times LT + 2.10FA \times LC \\
 & - 16.8FA \times LT + 66.0LC \times LT
 \end{aligned}
 \quad R^2 = 0.99 \quad (5.35)$$

After 4 durability cycles, the factorial results of samples with a slenderness ratio of 2.0 are presented in figure 5.36. It is uncertain if the lime type and its interaction effects are significant in the unconfined compressive strength of the samples.

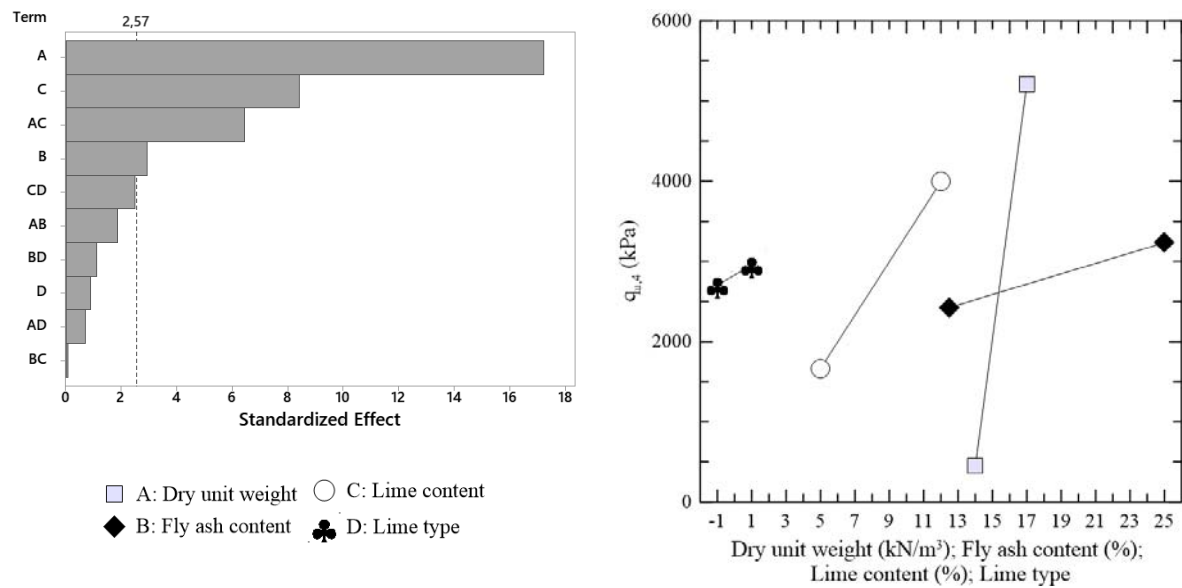


Figure 5.36: Pareto and main effects on response to unconfined compressive strength for samples after 4 cycles (samples  $H/D \approx 2.0$ ).

A regression equation expressing the factorial results is presented in equation (5.36).

$$\begin{aligned}
 q_{u,4 (H/D=2.0)} = & 4,401 - 367DW - 358FA - 2,279LC \\
 & - 2,166LT + 27.5DW \times FA + 169.1DW \times LC \\
 & + 64.4DW \times LT - 0.46FA \times LC \\
 & + 24.4FA \times LT + 98.1LC \times LT
 \end{aligned}
 \quad R^2 = 0.99 \quad (5.36)$$

After 12 durability wetting-drying cycles, the Pareto effects and mean main effects plots of the factorial experiment results are presented in figure 5.37. Again, there is no clear effect of lime type in the strength response, but the mean strength of specimens stabilized with calcitic lime is greater than for samples treated with the dolomitic lime.

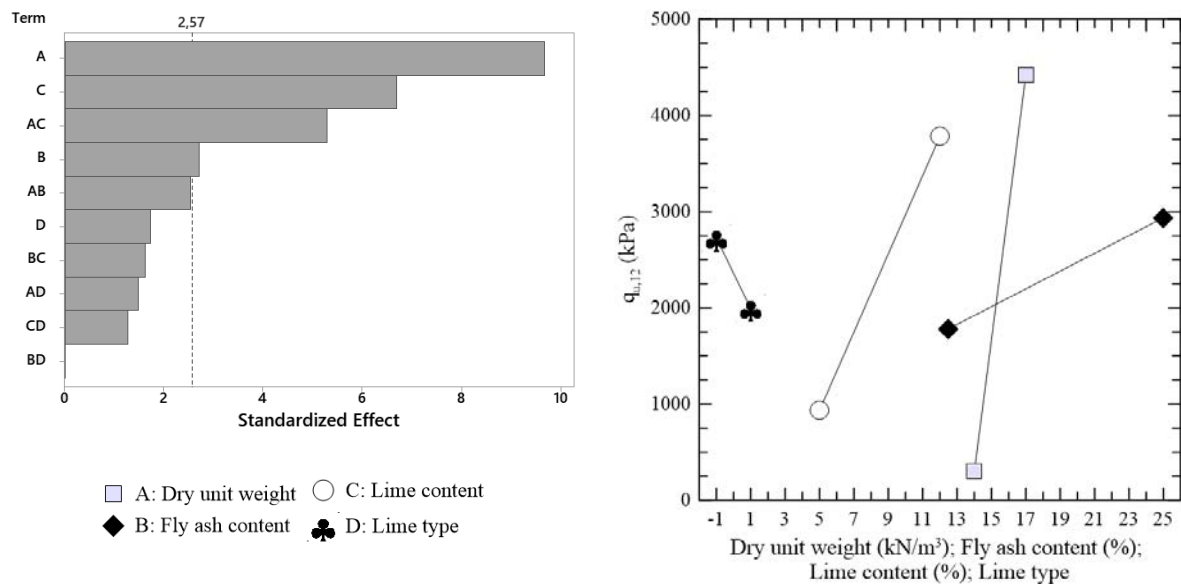


Figure 5.37: Pareto and main effects on response to unconfined compressive strength for samples after 12 cycles (samples  $H/D \approx 2.0$ ).

The regression equation is presented by equation (5.37).

$$\begin{aligned}
 q_{u,12 (H/D=2.0)} = & 23,427 - 1,532DW - 936FA - 3,215LC \\
 & + 2,231LT + 57.7DW \times FA + 214.6DW \times LC \\
 & - 210DW \times LT + 15.76FA \times LC \\
 & - 0.2FA \times LT + 77.3LC \times LT
 \end{aligned}
 \quad R^2 = 0.97 \quad (5.37)$$

The less slender specimens, after undergoing 12 cycles of wetting, drying, and brushing, may have their strength response represented by the plots in figure 5.38. The addition of the dolomitic lime seems to have a negative effect on strength response, but lower than the lime content and dry unit weight effect.

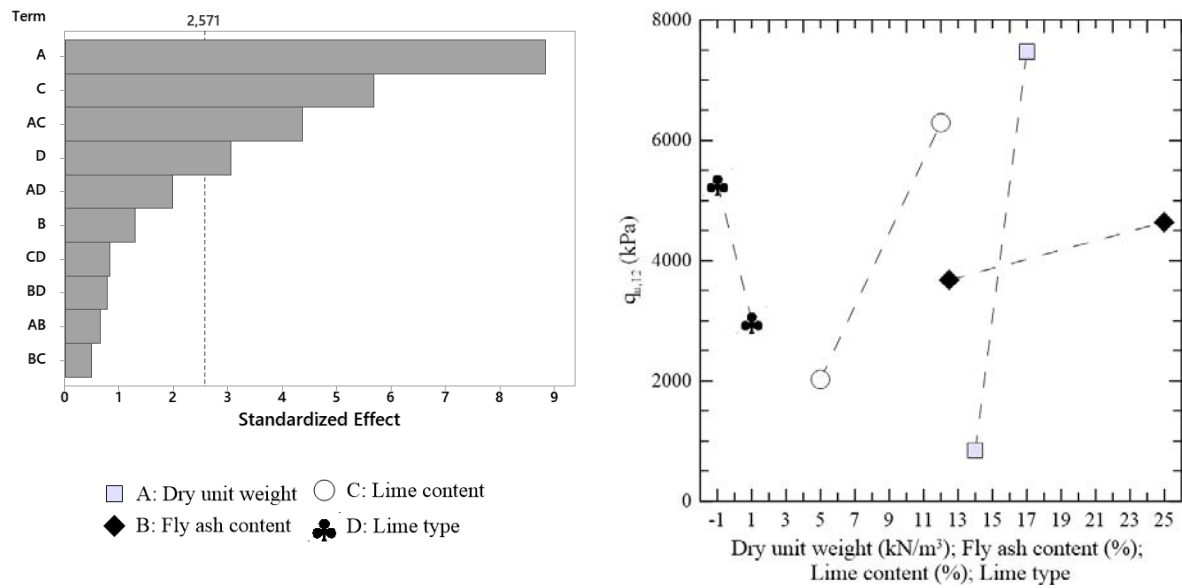


Figure 5.38: Pareto and main effects on response to unconfined compressive strength for samples after 12 cycles (samples  $H/D \approx 1.2$ ).

The mathematical expression for the strength response is presented in equation (5.38).

$$\begin{aligned}
 q_{u,12 (H/D=1.2)} = & 13,137 - 921DW - 392FA - 4,382LC \\
 & + 4,896LT + 25.7DW \times FA + 312.0DW \times LC \\
 & - 495DW \times LT + 8.3FA \times LC \\
 & + 47.1FA \times LT + 89LC \times LT
 \end{aligned}
 \quad R^2 = 0.97 \quad (5.38)$$

It appears that the specimens stabilized with dolomitic lime are more prone to strength loss when undergoing durability cycles.

### 5.1.2.2 Small strain constraint modulus and lime type aid

Small strain constraint modulus measures in samples after 28 days from moulding might have their results expressed by the plots shown in figure 5.39. The effect of the factor lime type is the second in magnitude, just lower than dry unit weight. As in unconfined compressive strength, there is an increase in stiffness when the dolomitic lime is used instead of the calcitic lime. The factorial regression equation is presented next.

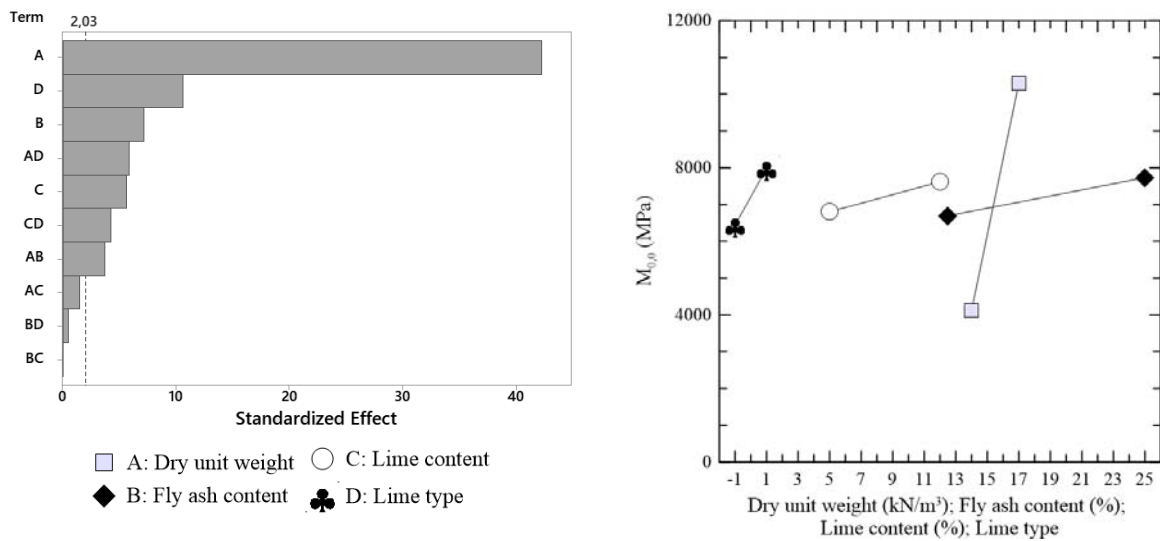


Figure 5.39: Pareto and main effects on response to small strain constraint modulus for samples after 0 cycle (samples  $H/D \approx 2.0$ ).

$$\begin{aligned}
 M_{0,0 (H/D=2.0)} = & 16,074 - 1,338DW - 365FA - 209LC \\
 & - 4,498LT + 28.88DW \times FA + 21.0DW \times LC \\
 & + 284.1DW \times LT + 0.04FA \times LC \\
 & + 5.9FA \times LT + 89.2LC \times LT
 \end{aligned}
 \quad R^2 = 0.98 \quad (5.39)$$

After 1 wetting-drying durability cycle, the  $M_0$  response may be illustrated in figure 5.40.

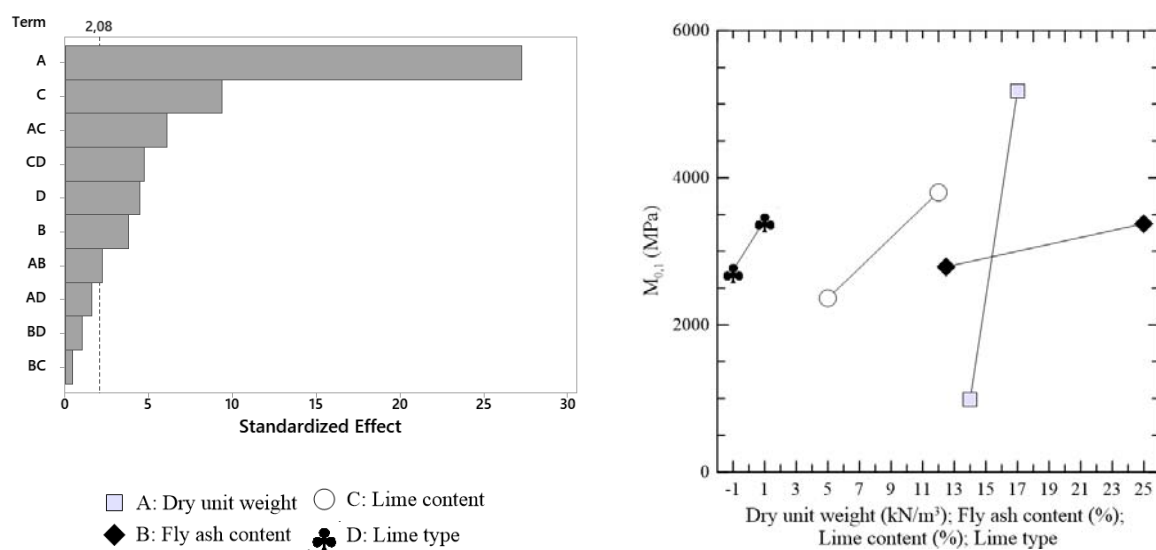


Figure 5.40: Pareto and main effects on response to small strain constraint modulus for samples after 1 cycle (samples  $H/D \approx 2.0$ ).

After this cycle, an increment in the small strain stiffness can still be observed when dolomitic lime is used in comparison to the calcitic lime. Equation (5.40) expresses the behaviour of  $M_{0,1}$  and how the factors and their interactions affect small strain constraint modulus response.

$$\begin{aligned}
 M_{0,1 (H/D=2.0)} = & -4,498 + 303DW - 219FA - 1,144LC \\
 & -1,574LT + 18.02DW \times FA + 89.1DW \times LC \\
 & + 81.7DW \times LT - 1.60FA \times LC \\
 & - 12.3FA \times LT + 103.4LC \times LT
 \end{aligned}
 \quad R^2 = 0.98 \quad (5.40)$$

Specimens with a relation H/D approximately equal to 1.2 may have their factorial results, before experiencing durability cycles, shown in figure 5.41. A high effect of dry unit weight can be observed, but the effect of lime type is slight, maybe not significant at moment.

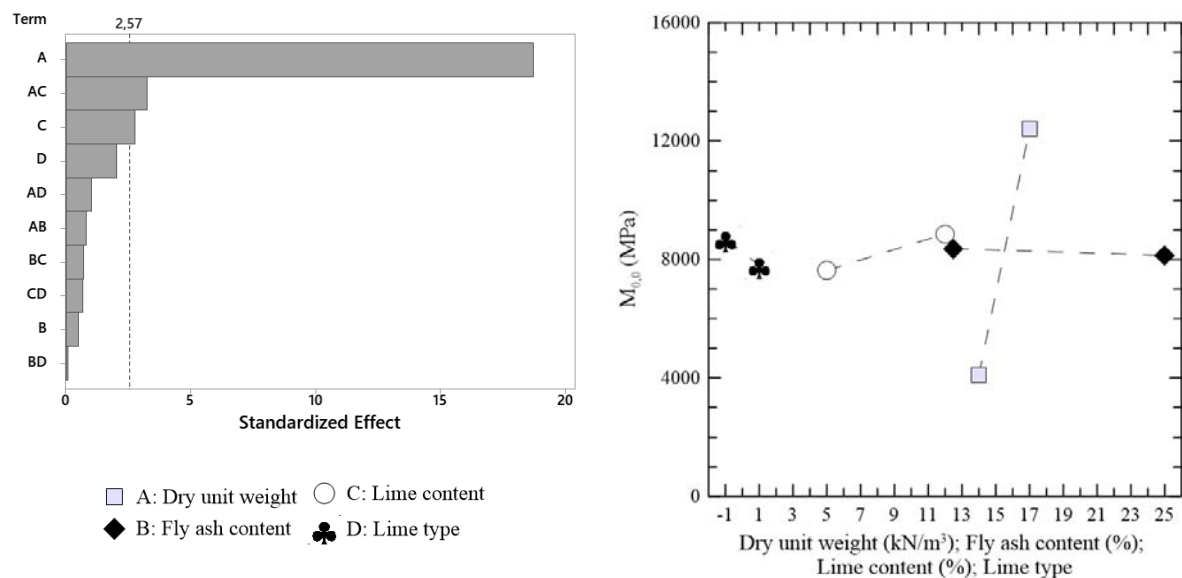


Figure 5.41: Pareto and main effects on response to small strain constraint modulus for samples after 0 cycle (samples H/D  $\approx$  1.2).

The equation expressing the response to the considered factors and second-order interactions is presented below

$$\begin{aligned}
M_{0,0 (H/D=1.2)} = & -22,072 + 1,958DW + 216FA - 2,104LC \\
& -1,571LT - 19.2DW \times FA + 138.1DW \times LC \\
& -150DW \times LT + 7.4FA \times LC \\
& -3.5FA \times LT + 43.2LC \times LT
\end{aligned}
\quad R^2 = 0.99 \quad (5.41)$$

After the first durability cycle, there is a clear effect of lime type on the response of  $M_0$ . Those results are presented in figure 5.42. The regression equation is presented next.

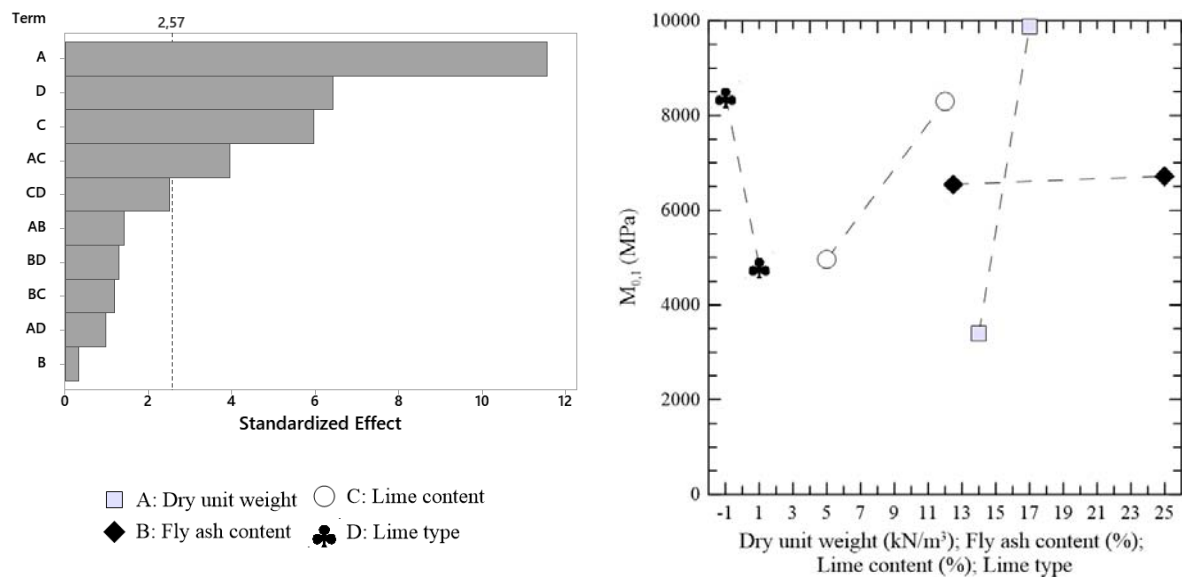


Figure 5.42: Pareto and main effects on response to small strain constraint modulus for samples after 1 cycle (samples  $H/D \approx 1.2$ ).

$$\begin{aligned}
M_{0,1 (H/D=1.2)} = & -13,224 + 1,160DW + 540FA - 3,078LC \\
& -1,782LT - 42.3DW \times FA + 210.8DW \times LC \\
& -180DW \times LT + 15.2FA \times LC \\
& + 57.3FA \times LT + 200.7LC \times LT
\end{aligned}
\quad R^2 = 0.98 \quad (5.42)$$

### 5.1.2.3 Small strain shear modulus and lime type aid

The response of small strain shear modulus to the factors dry unit weight, fly ash content, lime (calcitic and dolomitic) content, and lime type after 28 days curing period is presented in figure 5.43. The most effective factors are, in order, dry unit weight, fly ash content, lime content, and lime type. It is observed that the group of samples treated with the dolomitic lime presented

higher  $G_{0,0}$  than the specimens treated with the calcitic lime. The regression equation is expressed by the equation (5.43).

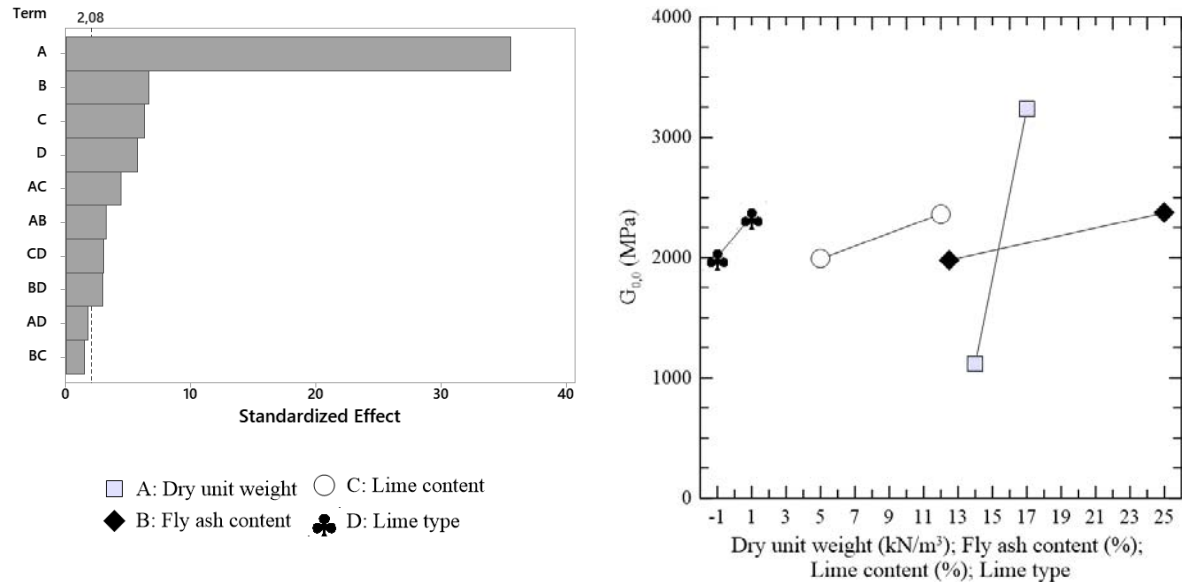


Figure 5.43: Pareto and main effects on response to small strain shear modulus for samples after 0 cycle (samples  $H/D \approx 2.0$ ).

$$\begin{aligned}
 G_{0,0 (H/D=2.0)} = & -3,202 + 300.0DW - 145.0FA - 369.7LC \\
 & - 336LT + 10.29DW \times FA + 24.90DW \times LC \\
 & + 35.7DW \times LT + 1.98FA \times LC \\
 & - 14.07FA \times LT + 25.57LC \times LT
 \end{aligned}
 \quad R^2 = 0.99 \quad (5.43)$$

$G_{0,1}$  response to the same factors is shown in figure 5.44.



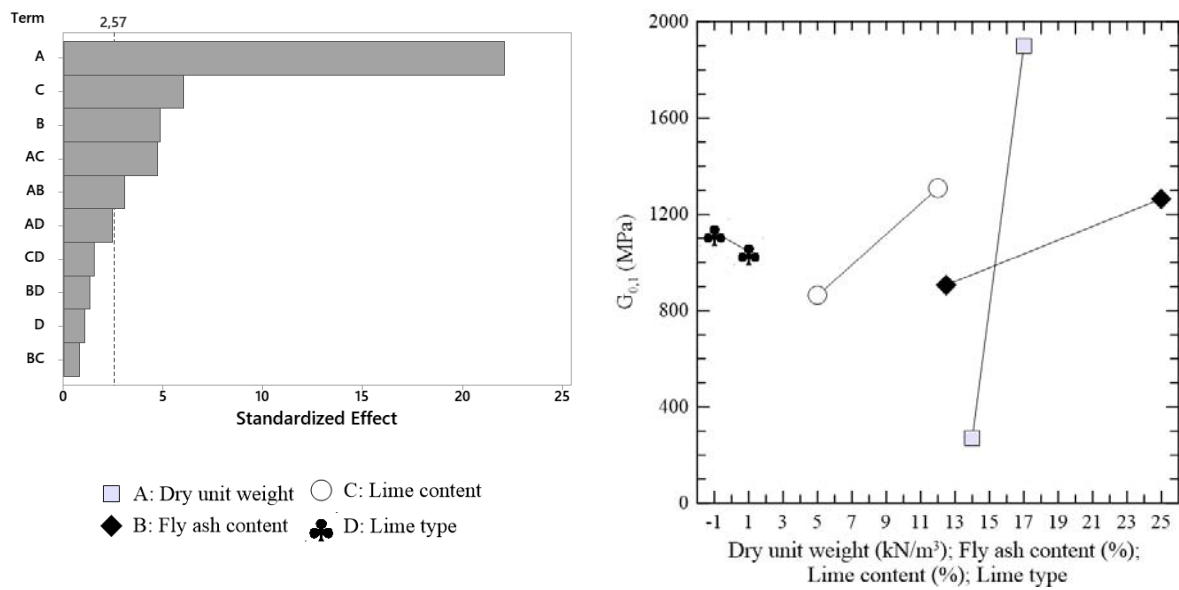


Figure 5.44: Pareto and main effects on response to small strain shear modulus for samples after 1 cycle (samples  $H/D \approx 2.0$ ).

In comparison to the small strain shear modulus before durability cycles (0 cycles), there is a path change in lime type to the opposite side. Although, the null hypothesis regarding the lime type effect after 1 durability cycle could not be rejected by the factorial analysis. A regression equation is presented in the following expression.

$$\begin{aligned}
 G_{0,1 (H/D=2.0)} = & -309 + 34.5DW - 170.4FA - 477LC \\
 & + 613LT + 12.09DW \times FA + 33.21DW \times LC \\
 & - 60.5DW \times LT + 1.37FA \times LC \\
 & + 7.78FA \times LT + 16.3LC \times LT
 \end{aligned}
 \quad R^2 = 0.99 \quad (5.44)$$

For less slender specimens ( $H/D \approx 1.2$ ), factorial results for  $G_{0,0}$  is presented in figure 5.45. As can be observed, there is a tenuous change in small strain shear modulus response to the lime type factor, where the calcitic lime is, apparently, more beneficial.

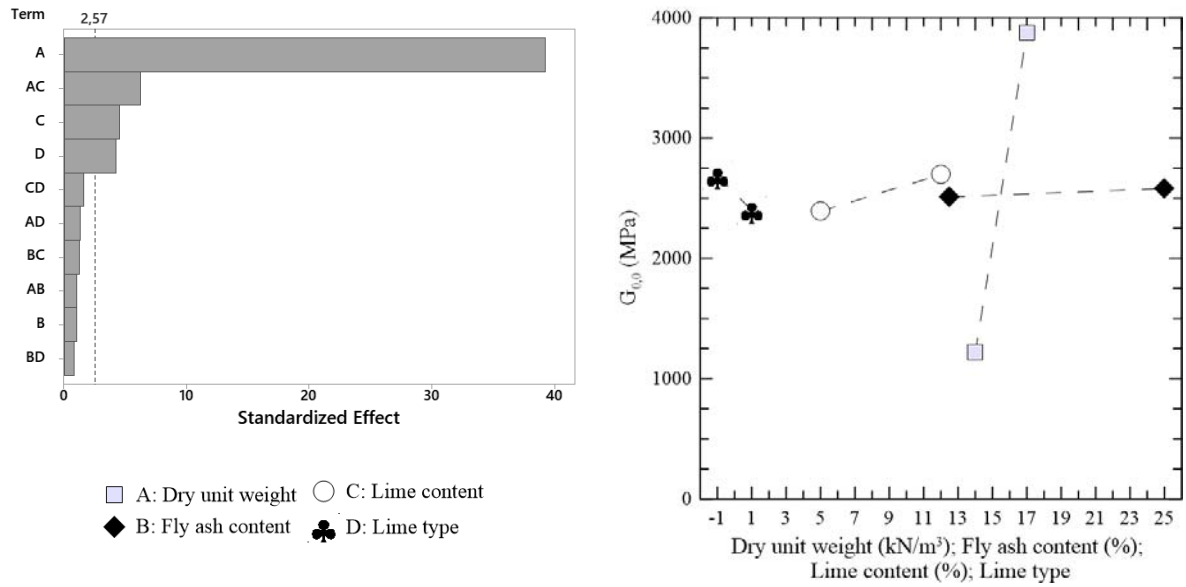


Figure 5.45: Pareto and main effects on response to small strain shear modulus for samples after 0 cycle (samples  $H/D \approx 1.2$ ).

The regression equation is expressed by the equation (5.45).

$$\begin{aligned}
 G_{0,0 (H/D=1.2)} = & -7,191 + 617.1DW + 48.8FA - 612LC \\
 & + 255LT - 3.84DW \times FA + 40.01DW \times LC \\
 & - 28.9DW \times LT + 1.92FA \times LC \\
 & - 4.40FA \times LT + 15.40LC \times LT
 \end{aligned}
 \qquad R^2 = 0.997 \qquad (5.45)$$

#### 5.1.2.4 Loss of mass and lime type aid

Accumulated loss of mass results after 1 durability cycle ( $ALM_1$ ) may be difficult to analyze due to the small amount of mass loss. The factorial results are presented in figure 5.46, where only the significance of the dry unit weight factor on  $ALM_1$  response has been confirmed. Despite that, the use of the dolomitic lime in stabilization appears to be related to a higher mass loss. Equation (5.46) presents the regression fit expression.

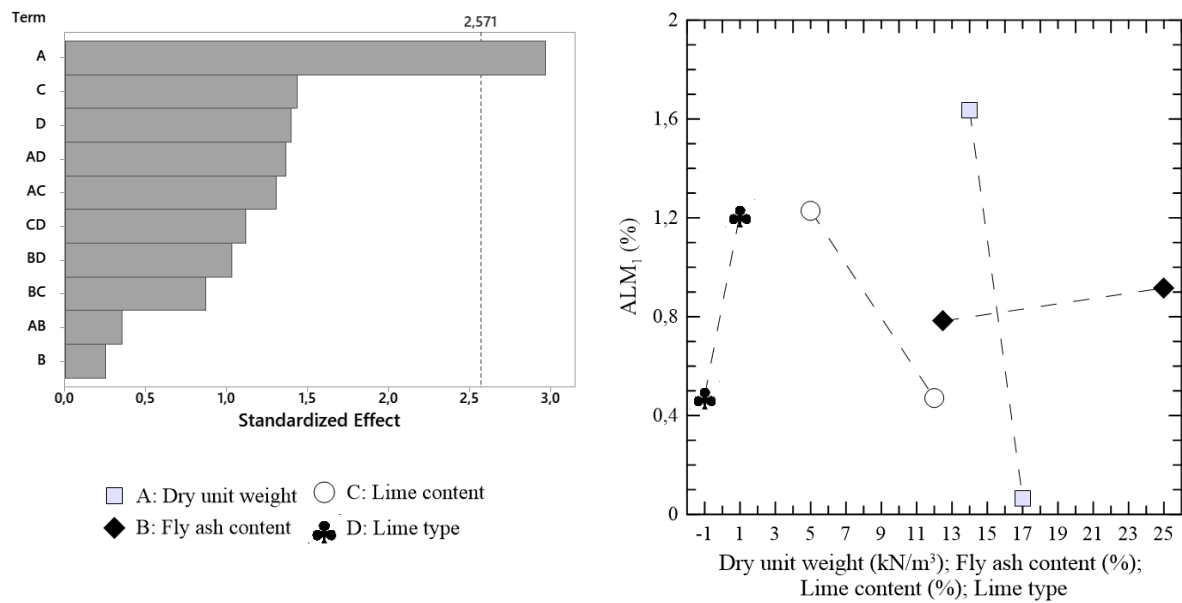


Figure 5.46: Pareto and main effects on response to the accumulated loss of mass for samples after 1 cycle (samples H/D  $\approx$  1.2).

$$\begin{aligned}
 ALM_{1(H/D=1.2)} = & 13.8 - 0.895DW + 0.254FA - 0.931LC \\
 & + 4.00LT - 0.0100DW \times FA + 0.0657DW \times LC \\
 & - 0.241DW \times LT - 0.0105FA \times LC \\
 & + 0.0436FA \times LT - 0.0843LC \times LT
 \end{aligned}
 \quad R^2 = 0.80 \quad (5.46)$$

The accumulated loss of mass after 4 wetting-drying brushing cycles (ALM<sub>4</sub>) responds to factorial analysis as shown in figure 5.47. The null hypothesis has not been rejected for the lime type factor, but it can be observed an increase in the accumulated loss of mass when changing the factor value from -1 (calcitic lime) to +1 (dolomitic lime). The regression equation is presented next.

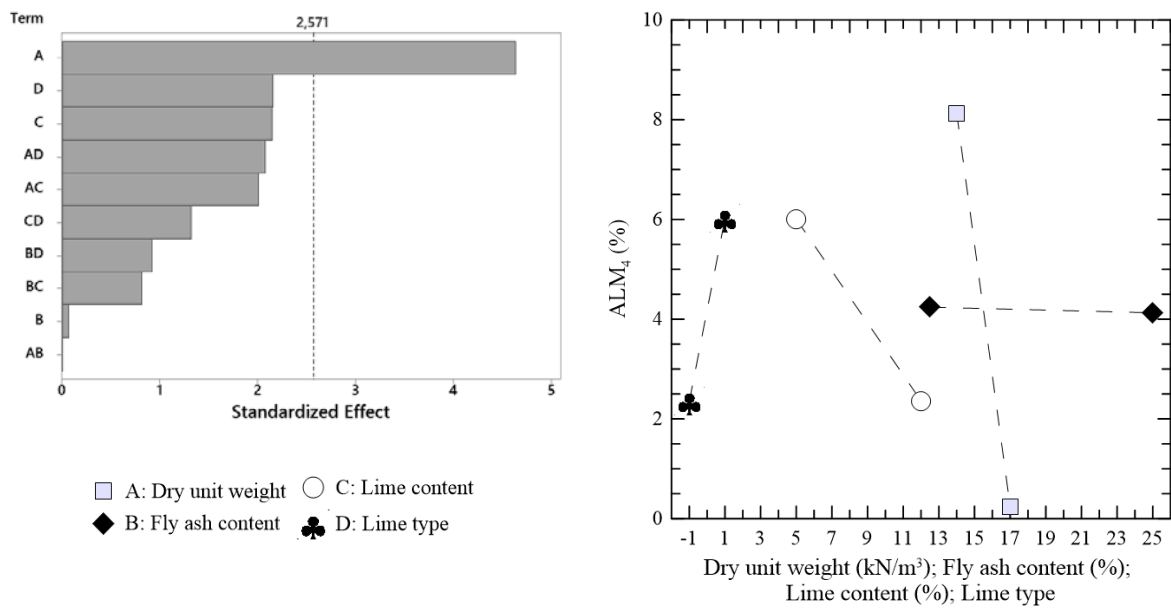


Figure 5.47: Pareto and main effects on response to the accumulated loss of mass for samples after 4 cycles (samples H/D  $\approx$  1.2).

$$\begin{aligned}
 ALM_{4(H/D=1.2)} = & 87.1 - 5.38DW + 0.27FA - 4.96LC \\
 & + 20.44LT - 0.0005DW \times FA + 0.325DW \times LC \\
 & - 1.176DW \times LT - 0.0315FA \times LC \\
 & + 0.124FA \times LT - 0.320LC \times LT
 \end{aligned}
 \quad R^2 = 0.89 \quad (5.47)$$

After all the twelve durability cycles, the accumulated loss of mass response (ALM<sub>12</sub>) results indicated a great effect of dry unit weight, but also of lime content and lime type. Fly ash possibly slightly affects this response, but it was not confirmed. The specimens stabilized with the calcitic lime presented lower values of mass loss. The regression expression is presented in equation (5.48).

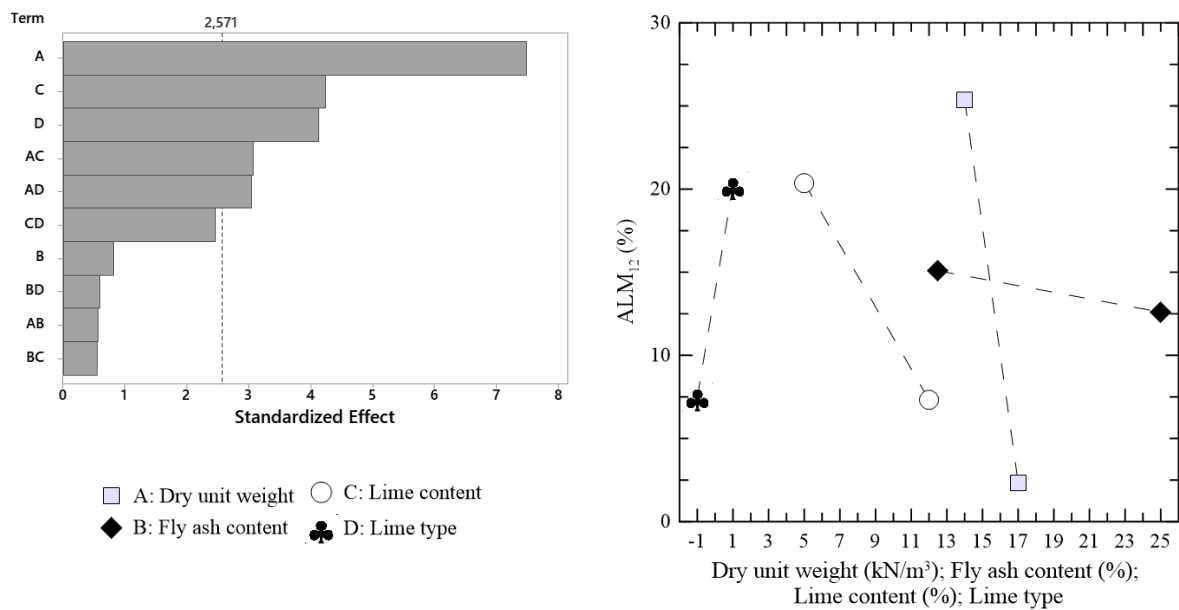


Figure 5.48: Pareto and main effects on response to the accumulated loss of mass for samples after 12 cycles (samples H/D  $\approx$  1.2).

$$\begin{aligned}
 ALM_{12(H/D=1.2)} = & 291.7 - 17.06DW + 1.32FA - 15.07LC \\
 & + 61.3LT + 0.093DW \times FA + 0.898DW \times LC \\
 & - 3.13DW \times LT - 0.0384FA \times LC \\
 & + 0.146FA \times LT - 1.082LC \times LT
 \end{aligned}
 \quad R^2 = 0.96 \quad (5.48)$$

### 5.1.3 Sample size effect addition

The effect mentioned as “sample size” or “slenderness ratio” in fact corresponds to more coupled effects like “specimen volume” or the addition of “brushing” when compared to the slender specimens undergoing durability cycles, but those effects were simply grouped with slenderness ratio for the purpose of simplifying the analysis. So, the factorial results adding the “slenderness ratio” effect are presented next.

#### 5.1.3.1 Unconfined compressive strength and slenderness ratio

The unconfined compressive strength accounting for the slenderness ratio effect, after 12 durability cycles ( $q_{u,12}$ ) is presented in figure 5.49. A high and apparently significant effect of slenderness ratio is observed, as the unconfined compressive strength decreases when specimens become slenderer.

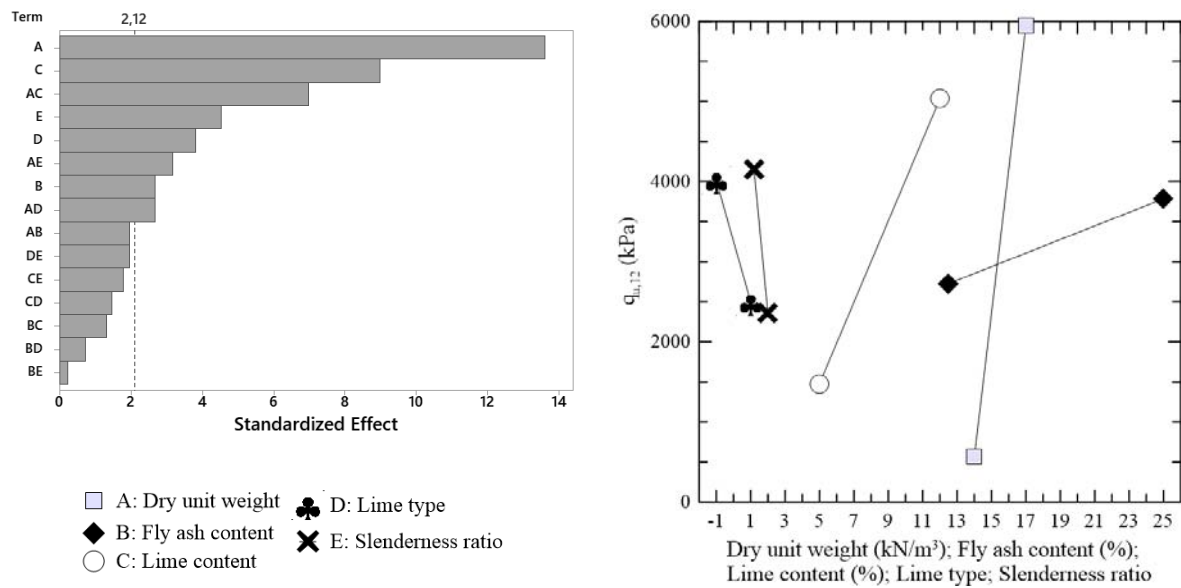


Figure 5.49: Pareto and main effects on response to unconfined compressive strength for samples after 12 cycles.

The response of  $q_{u,12}$  can be expressed by the equation (5.49).

$$\begin{aligned}
 q_{u,12} = & -6,597 - 425DW - 694FA - 3,400LC \\
 & + 2,030LT + 15,598SR + 41.7DW \times FA \\
 & + 263.3DW \times LC - 353DW \times LT - 1,035DW \times SR \quad R^2 = 0.96 \quad (5.49) \\
 & + 12.05FA \times LC + 23.4FA \times LT + 18.9FA \times SR \\
 & + 83.0LC \times LT - 250LC \times SR + 961LC \times SR
 \end{aligned}$$

Where

SR = Slenderness Ratio

### 5.1.3.2 Small strain constraint modulus and slenderness ratio

The factorial analysis results containing the introduction of the slenderness ratio in the small strain constraint modulus is presented in figure 5.50. There is a slight change in the response to distinct slenderness ratios, but it appears that the slender specimens presented a stiffer response.

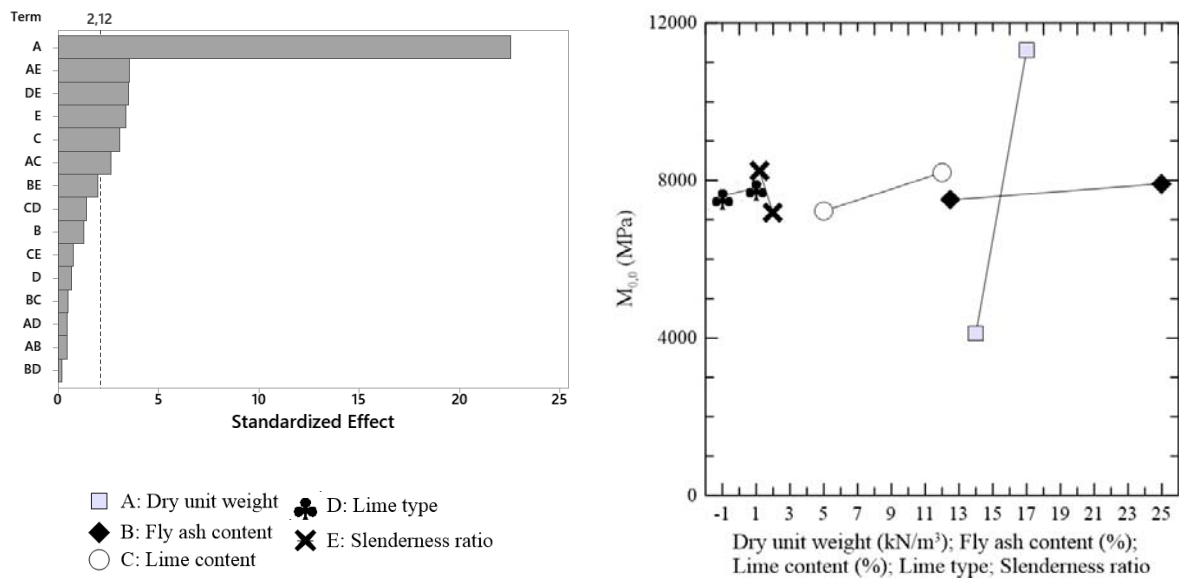


Figure 5.50: Pareto and main effects on response to small strain constraint modulus for samples after 0 cycle.

The small strain constraint modulus after 28 days ( $M_{0,0}$ ) may be expressed by the following equation.

$$\begin{aligned}
 M_{0,0} = & -36,058 + 3,050DW - 322FA - 1,043LC \\
 & - 3,533LT + 11,509SR + 7.8DW \times FA \\
 & + 80.7DW \times LC + 50DW \times LT - 933DW \times SR \\
 & + 3.80FA \times LC + 5.4FA \times LT + 126.3FA \times SR \\
 & + 64.9LC \times LT - 87LC \times SR + 1,389LC \times SR
 \end{aligned}
 \quad R^2 = 0.97 \quad (5.50)$$

After 1 durability cycle (wetting, drying for the slender specimens, and wetting, drying, and brushing for the rest), the  $M_0$  response to the five considered factors in the factorial analysis is presented in figure 5.51. The same trend regarding the slenderness ratio that was observed before the first cycle (0 cycles) is observed after 1 cycle, though with a more pronounced effect. The difference between the smaller (and slender) and larger specimens is clearer, as the slenderness ratio is the second factor in the effect on the response variable.

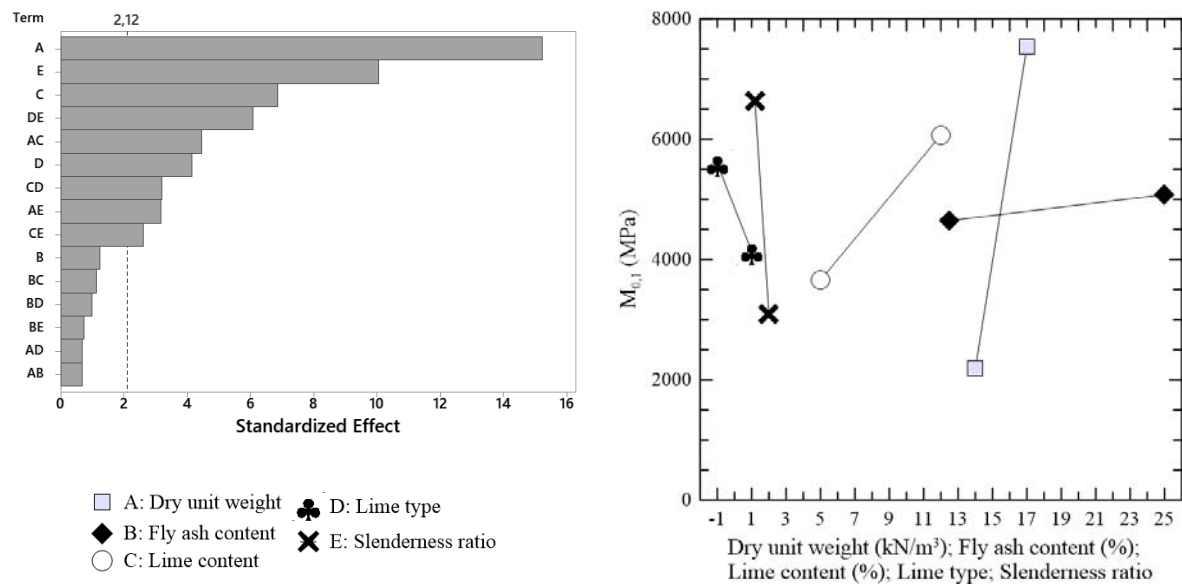


Figure 5.51: Pareto and main effects on response to small strain constraint modulus for samples after 1 cycle.

The mathematical expression of the factorial results of  $M_{0,1}$  is presented in equation (5.51).

$$\begin{aligned}
 M_{0,1} = & -27,535 + 2,217DW + 72FA - 1,627LC \\
 & -5,579LT + 11,666SR - 12.6DW \times FA \\
 & + 149.5DW \times LC - 81DW \times LT - 919DW \times SR \quad R^2 = 0.97 \quad (5.51) \\
 & + 9.07FA \times LC + 28.1FA \times LT + 50.7FA \times SR \\
 & + 161.1LC \times LT - 323LC \times SR + 2,643LC \times SR
 \end{aligned}$$

### 5.1.3.3 Small strain shear modulus and slenderness ratio

The factorial response of small strain shear modulus at de 28<sup>th</sup> curing day is illustrated in figure 5.52. The response of the slenderness ratio on  $G_{0,0}$  was found similar to the response to  $M_{0,0}$ : an increase in the ratio corresponds to a slight increment in  $G_0$ . The equation (5.52) expresses this factorial response.



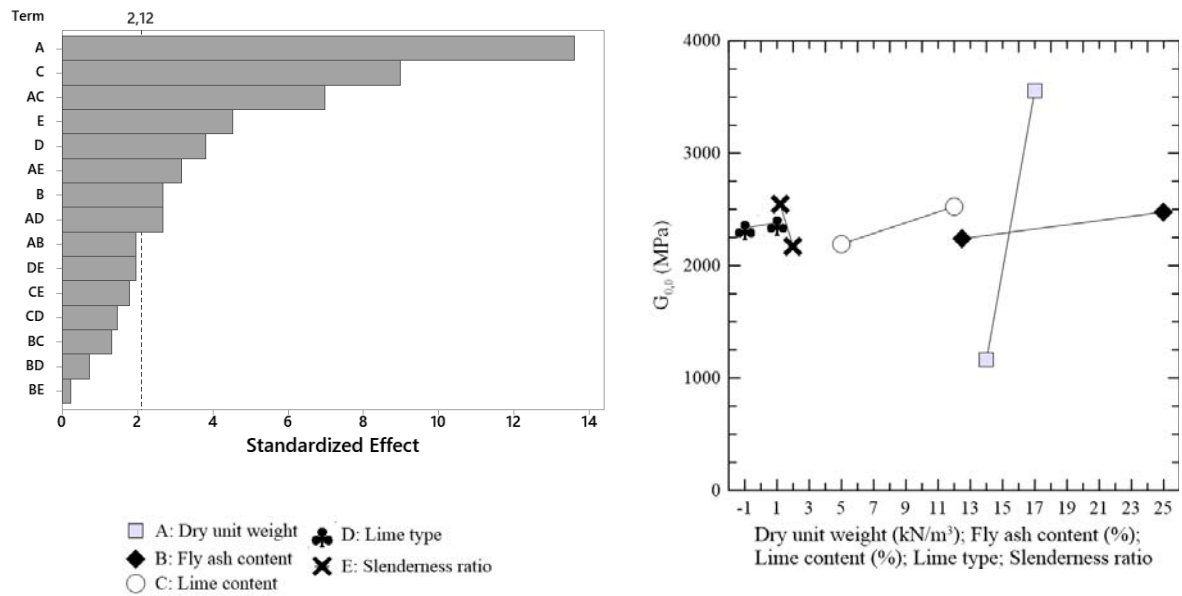


Figure 5.52: Pareto and main effects on response to small strain shear modulus for samples after 0 cycle.

$$\begin{aligned}
 G_{0,0} = & -8,560 + 796DW - 110.2FA - 503LC \\
 & -836LT + 2,152SR + 3.80DW \times FA \\
 & + 32.01DW \times LC + 14.8DW \times LT - 213.4DW \times SR \quad R^2 = 0.98 \quad (5.52) \\
 & + 2.07FA \times LC + 8.76FA \times LT + 32.9FA \times SR \\
 & + 16.0LC \times LT + 9.5LC \times SR + 412.0LC \times SR
 \end{aligned}$$

#### 5.1.4 Factorial results evaluation

For almost all the variables response assessed, the higher effect on response comes from the dry unit weight factor. Higher dry unit weight values may lead to an increase in friction and induce strengthener bonds between particles by the fabric change during the curing period when chemical reactions take place.

As cycles increase, it is observed that the more durable specimens tend to increase in strength, due to curing catalyzing whereas the less durable specimens tend to decrease. Also, after more durability cycles, the effect of lime content tends to be more pronounced, especially when dolomitic lime is used. It can be explained by the fact that heating, during the drying part of the cycles (after hydration due to wetting), catalyzes the pozzolanic reactions, strengthening the specimens that remain structured after the cycles.

Besides that, after durability cycles, the mechanical properties of calcitic lime treated soils appear to overcome the same properties in dolomitic lime treated samples. It indicates that dolomitic lime stabilized materials are less resistant to weathering effects and that maybe the calcitic lime reactions are slower than the dolomitic ones in the present study.

The moulded center points dosage indicated that a linear relation is imprecise in the determination of variables response behaviour on the intermediate zone (between minimum and maximum factors values) with the studied mixtures.

Small strain stiffness after 12 cycles, in some cases, even after 1 or 4, could not have its factorial response evaluated since the travel time of waves through less durable specimens could not fully be assessed in the factorial designed block.

Some variables responses present a strong non-linear behaviour, so, they cannot be fully analyzed in light of factorial results, especially the accumulated loss of mass.

In some cases, it is difficult to regulate the exact dry unit weight during moulding because the compaction is not automatically controlled. So, variabilities in moulding, especially during compaction phases, may result in a different dry unit weight when it should be the same. In the factorial analysis, that variability is not considered, causing distortions in the results.

## 5.2 RESPONSE VARIABLES INFLUENCED BY CURING AND DURABILITY CYCLES

The durability of the soils is evaluated as the response when subjected to degradation. The degradation is imposed by wetting-drying or wetting-drying-brushing cycles to evaluate how those cycles affect unconfined compressive strength, unconfined compressive secant modulus, small strain modulus, and loss of mass. The results are presented separately for calcitic and dolomitic lime as mean values when more than one specimen was tested, but the result was only accounted for the mean value calculated when they were fit inside upper and lower bound limits of 15% from the mean value.

### 5.2.1 Curing effect on small strain stiffness

Immediately after moulding compaction, some samples were tested under the ultrasonic pulse velocity test. Both P- and S-waves velocities were measured. The obtained small strains after the curing period compared to the stiffness after 28 days may give an idea of the changes induced by the pozzolanic reactions in the structure stiffness.

The increase in  $M_0$  values influenced by curing is presented in figure 5.53 for calcitic lime treated soils and in figure 5.54 for dolomitic lime treated soils. In the legend, FA refers to fly ash content, CL to carbide lime content, and DL to dolomitic lime content.

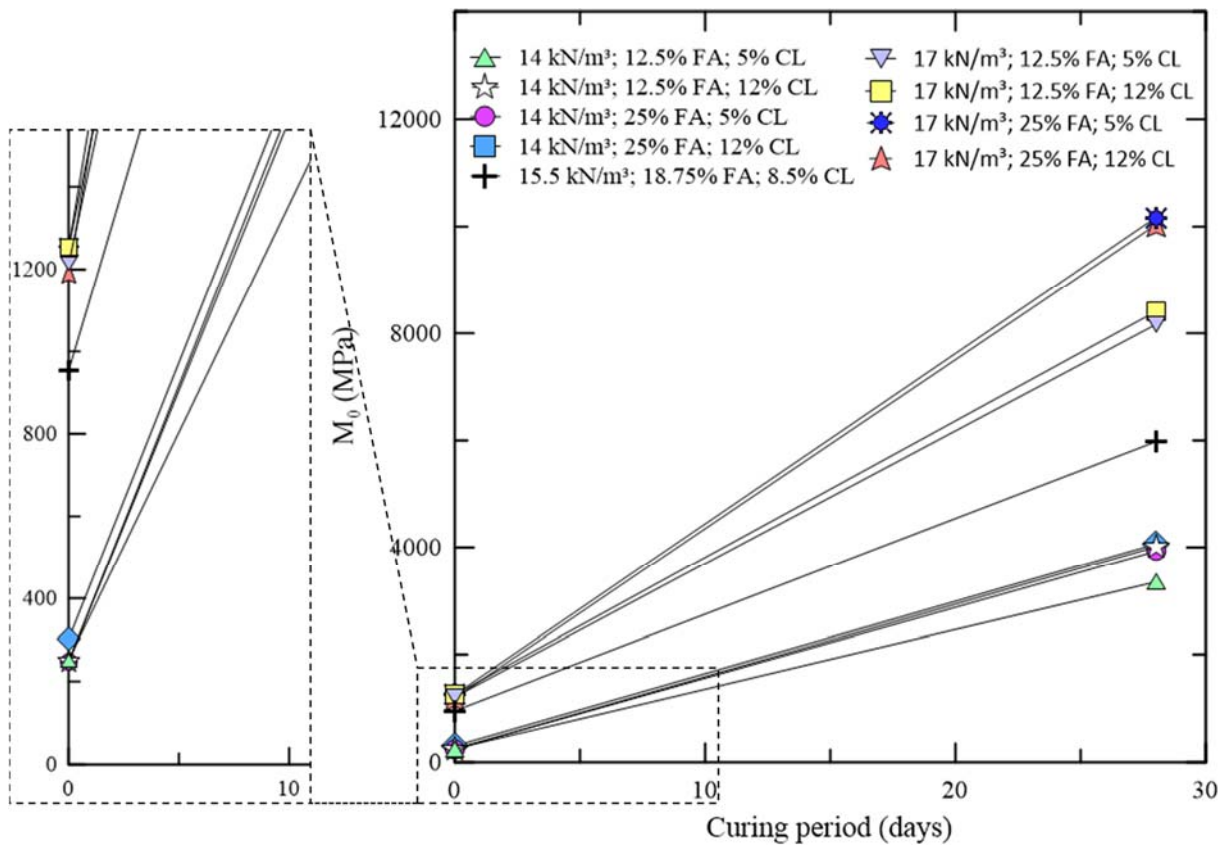


Figure 5.53: Small strain constraint modulus for calcitic lime treated samples before and after curing.

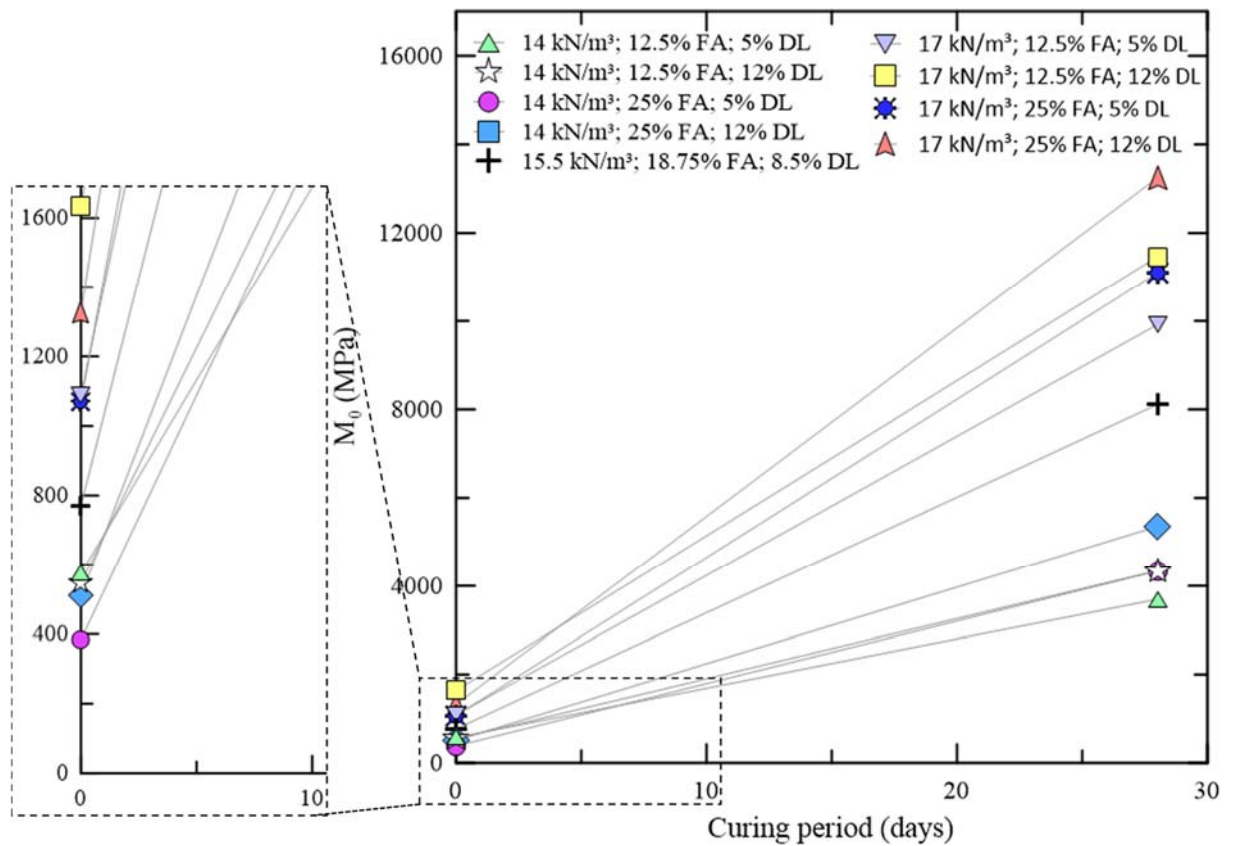


Figure 5.54: Small strain constraint modulus for dolomitic lime treated samples before and after curing.

The evaluation of small strain shear modulus response before and after durability cycles is presented in figure 5.55 for mixtures stabilized with the calcitic lime and in figure 5.56 for mixtures stabilized with the dolomitic lime.

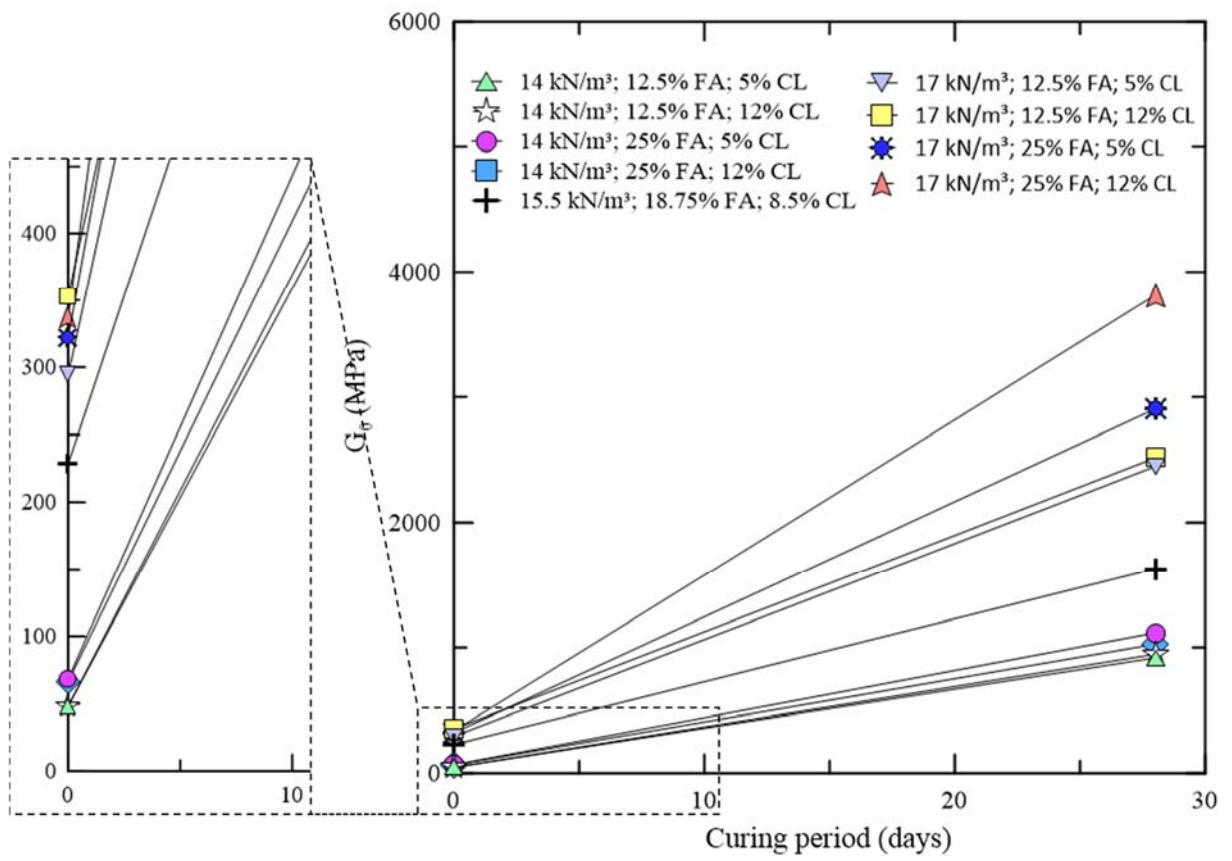


Figure 5.55: Small strain shear modulus for calcitic lime treated samples before and after curing.

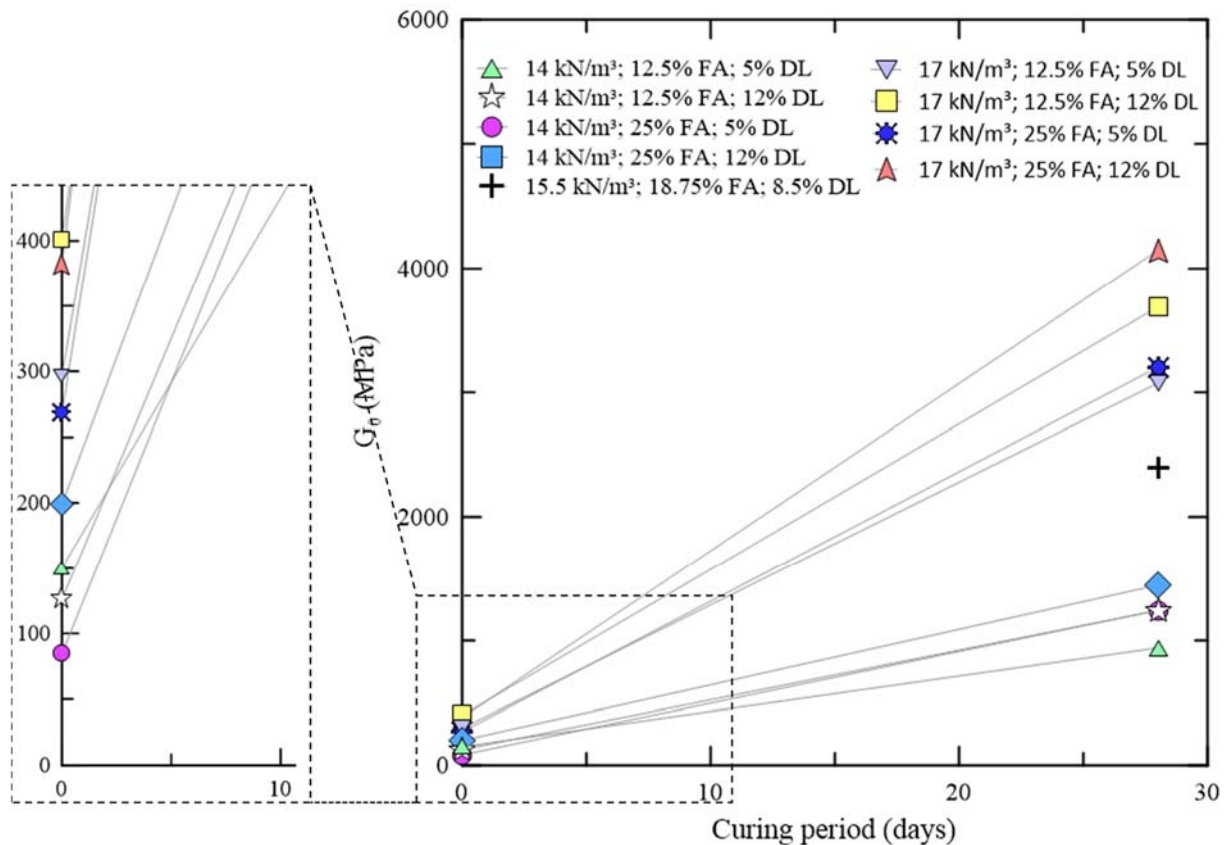


Figure 5.56: Small strain shear modulus for dolomitic lime treated samples before and after curing.

Apparently, for both  $M_0$  and  $G_0$  and lime types, before the structuration induced by the pozzolanic reactions on the admixtures, there is a predominance on the dry unit weight effect, but an increase in lime content seems to have a beneficial effect on small strain constraint and shear modulus, whereas an increase in fly ash content seems to reduce the fabric stiffness. It was observed yet that the specimens stabilized using the dolomitic lime presented a stiffer response before curing.

### 5.2.2 Unconfined compressive strength after cycles

Unconfined compressive strength tests for both calcitic and dolomitic lime treated were run with approximately 5.02 cm (diameter) x 10.04 cm (height) specimens. The results for tests after 0, 1, 4, and 12 cycles are presented in figures 5.57 and figure 5.58.

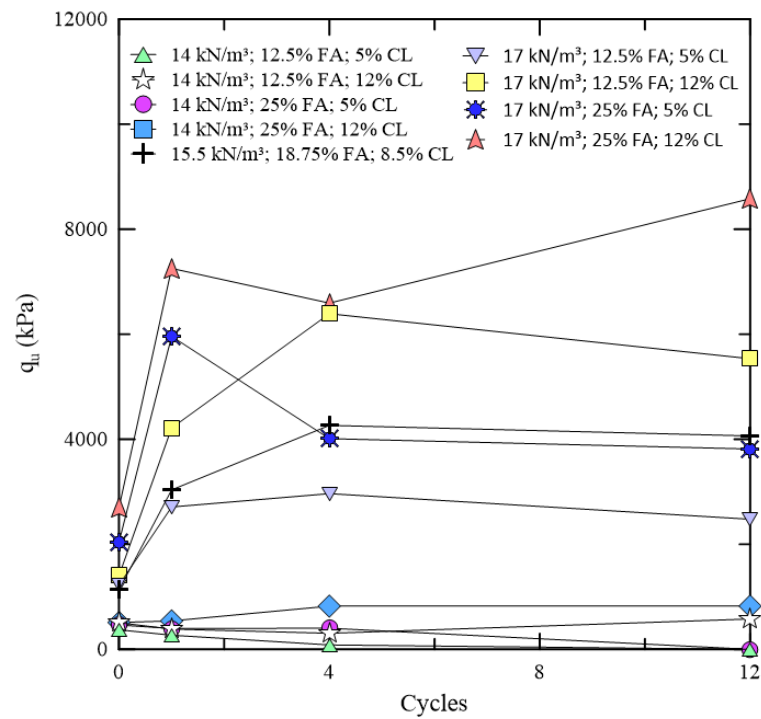


Figure 5.57: Unconfined compressive strength for calcitic lime treated samples after wetting-drying cycles.

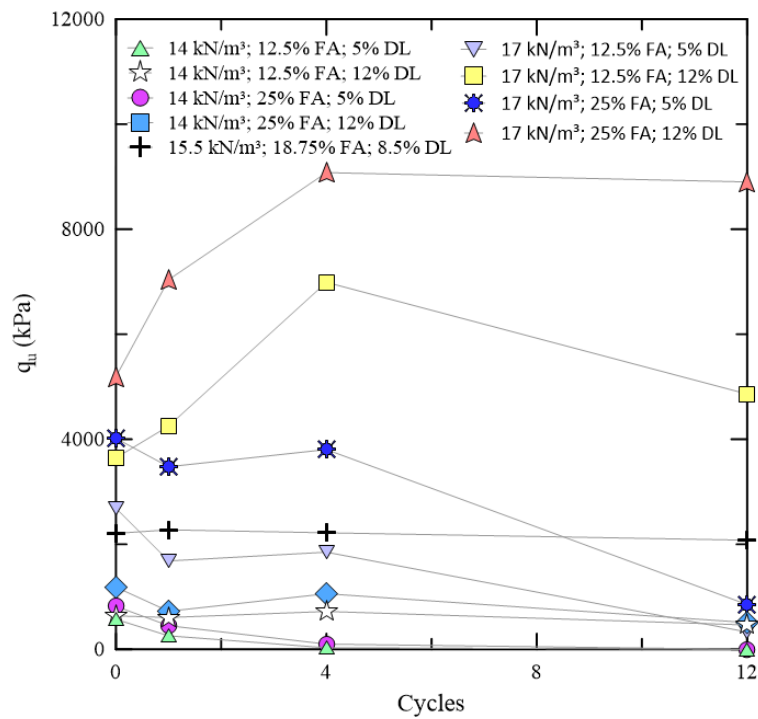


Figure 5.58: Unconfined compressive strength for dolomitic lime treated samples after wetting-drying cycles.

As can be seen, the strength is highly influenced by the dry unit weight, independently of the lime used for the treatment. After the first cycle, there is a growth in almost all calcitic lime-treated dosages, except for two with 14 kN/m<sup>3</sup> dry unit weight and 5% in lime content. For the dolomitic lime-treated specimens, only the samples with 17 kN/m<sup>3</sup> dry unit weight and 12% in lime content presented a strength increase, while the intermediate dosage specimens have remained stable regarding strength, and all the rest have experienced a strength decrease. Besides that, it seems that the pozzolanic reactions cease between the first and the fourth cycle.

### 5.2.3 Unconfined compressive secant modulus after cycles

Unconfined compressive longitudinal secant modulus values were determined at the failure stress-strain curve (maximum strain). As it was not measured with precise small-strain transducers, those modulus values may not be evaluated as precise values, but as a strain behaviour trend. The plots presented in figures 5.59 and 5.60 correspond to mean values obtained by unconfined compressive tests already presented in chapter 5.2.1. The calcitic lime treated samples that did not undergo durability cycles could not have their secant modulus assessed.

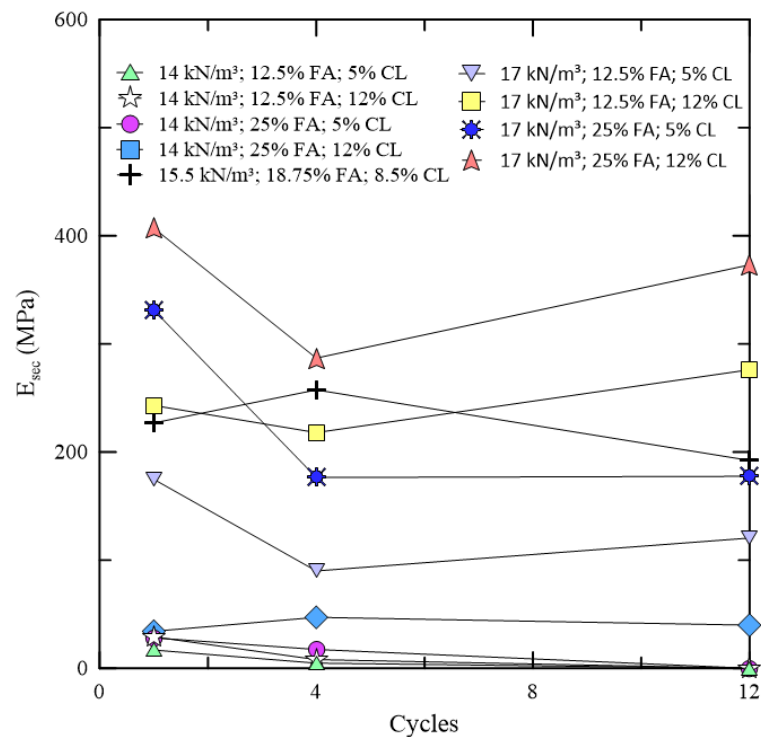


Figure 5.59: Unconfined compressive secant modulus at failure for calcitic lime treated samples after wetting-drying cycles.



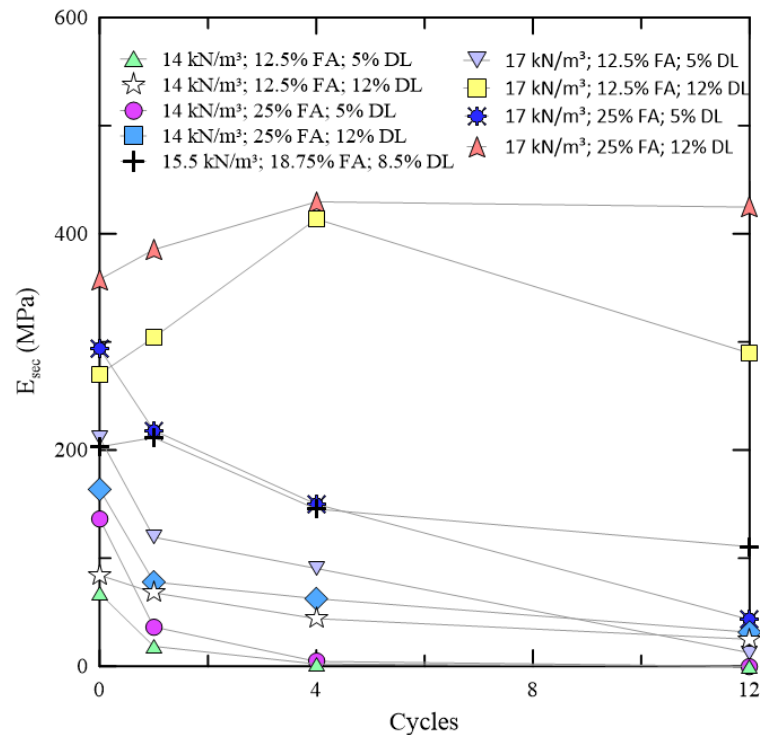


Figure 5.60: Unconfined compressive secant modulus at failure for dolomitic lime treated samples after wetting-drying cycles.

A good agreement can be observed between the maximum unconfined compressive secant modulus and unconfined compressive strength, but the secant modulus parameter is apparently more sensitive to durability cycles than strength.

The specimens with lower lime dry unit weight and lime content tend to present higher decay for both parameters, whereas for calcitic lime treated soils, this decay is more tenuous.

#### 5.2.4 Small strain constraint modulus throughout durability cycles

To assess the intermediate behaviour from 1 to 4 and 4 to 12 cycles, some extra measurements, not possibly obtained with destructive tests, were assessed through the non-destructive ultrasound pulse velocity test. Yet, wave propagation in specimens can be tricky when there is a considerable crack propagation and/or mass loss. The small strain constraint modulus results for the more slender specimens, which experienced wetting and drying cycles are presented in figure 5.61 and figure 5.62 for calcitic and dolomitic lime treated specimens, respectively. Samples were tested after 0, 1, 3, 4, 6, 9, and 12 cycles.

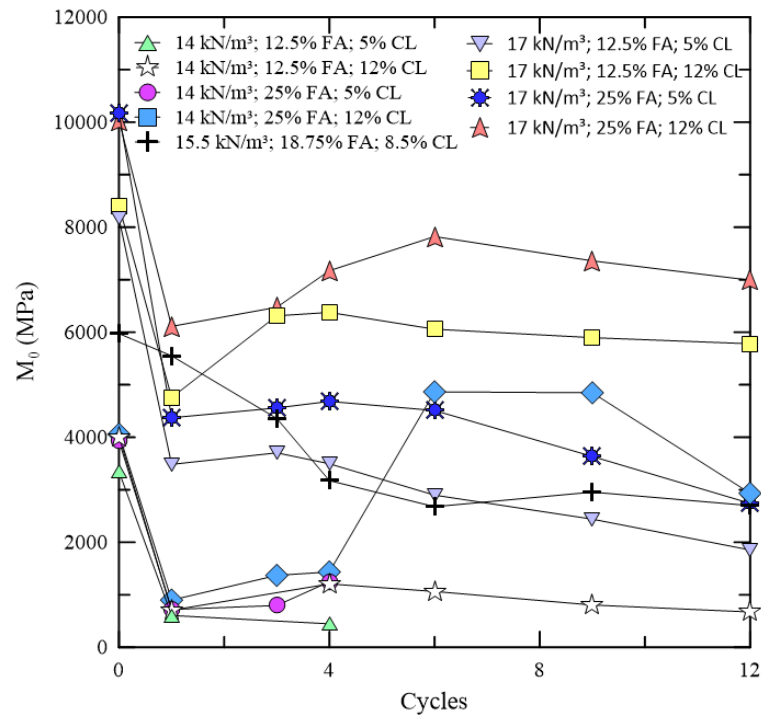


Figure 5.61: Small strain constraint modulus for calcitic lime treated samples throughout wetting-drying cycles.

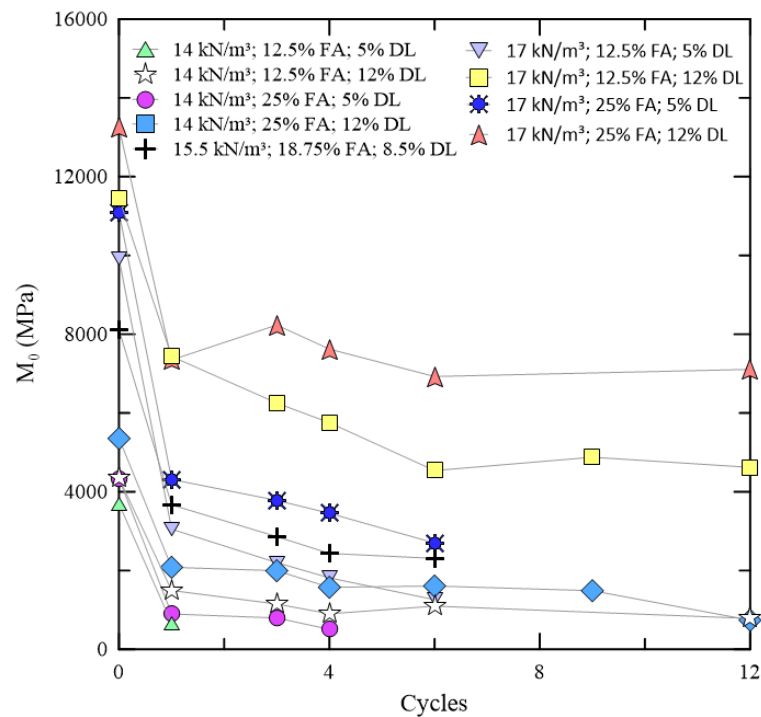


Figure 5.62: Small strain constraint modulus for dolomitic lime treated samples throughout wetting-drying cycles.

Small strain constraint modulus before durability cycles ( $M_{0,0}$ ) have presented significantly higher values than after the cycles. As those specimens present approximately 10% water content, and since higher degrees of saturation may result in higher P-wave velocities, those results are probably more due to the distinct water content than due to the structural damage. After the first cycle, the specimens experience no more great changes in moisture content since all of them were tested after the drying stage. So, it is reasonable to compare the specimen's stiffness changes only from cycle 1. It can be observed that only a few dosages have presented an increase in  $M_0$  after the first cycle. Possibly, the microstructure response is more sensitive to wetting-drying damage (probably microcracks) than the structure in a macroscale.

The effect of damage experienced by the higher volume specimens with  $H/D \approx 1.2$ , which have undergone, in addition to wetting and drying, brushing, is presented in figures 5.63 and 5.64.

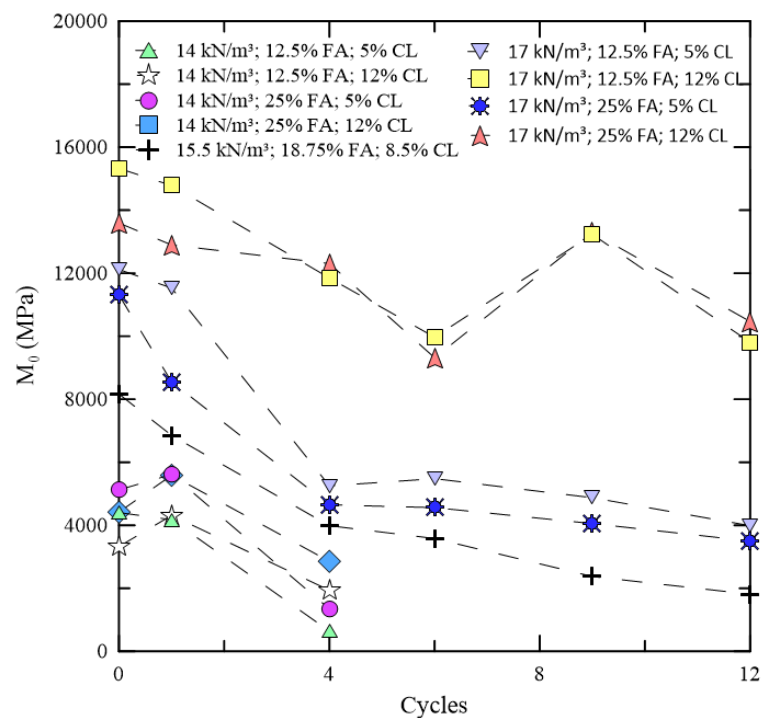


Figure 5.63: Small strain constraint modulus for calcitic lime treated samples throughout wetting-drying-brushing cycles.

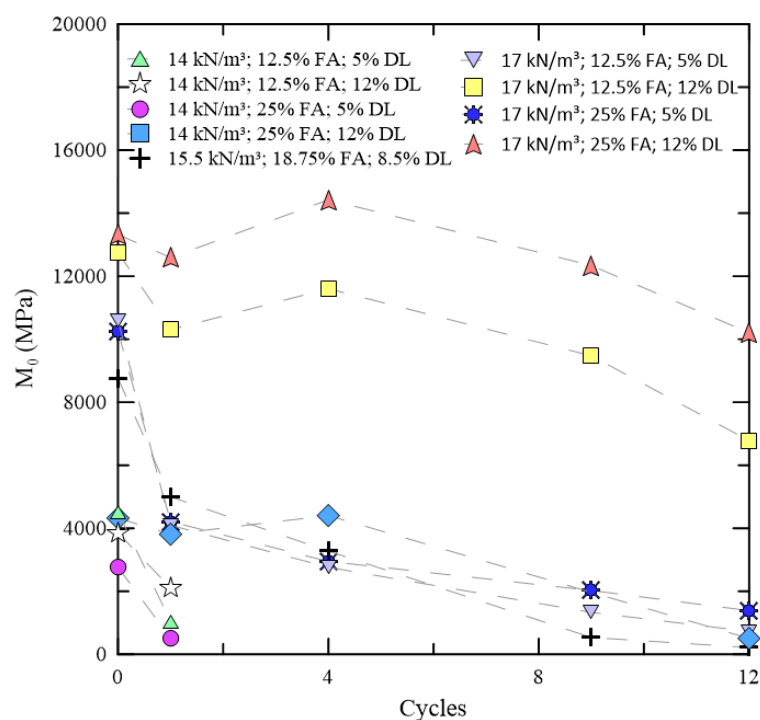


Figure 5.64: Small strain constraint modulus for dolomitic lime treated samples throughout wetting-drying-brushing cycles.

A similar pattern has been observed for the specimens with higher volume, subjected to wetting, drying, and brushing when compared to the slender specimens, which have not experienced brushing, but the changes in results from the 0 cycle to the first cycle were slighter, possibly associated to the higher moisture content in the larger specimens after the drying stage of the durability test. Another possibility is the less damage suffered by the internal 5 cm (ultrasonic transducer diameter) of larger samples.

### 5.2.5 Small strain shear modulus throughout cycles

The response of small strain shear stiffness to durability cycles is presented in figure 5.65 regarding mixtures stabilized with the calcitic lime and in figure 5.66 mixtures stabilized using the dolomitic lime. Those tests were conducted on samples with a slenderness ratio of approximately 2.0 for non-brushed specimens. The modulus changing from the first measurement (after 28 days) to the second (after the first cycle) is similar to the constraint modulus response, though the shear modulus seems to present a more stable response after cycle 1. Dolomitic lime small strain shear modulus response could not be fully assessed due to an experimental problem after the fourth cycle.

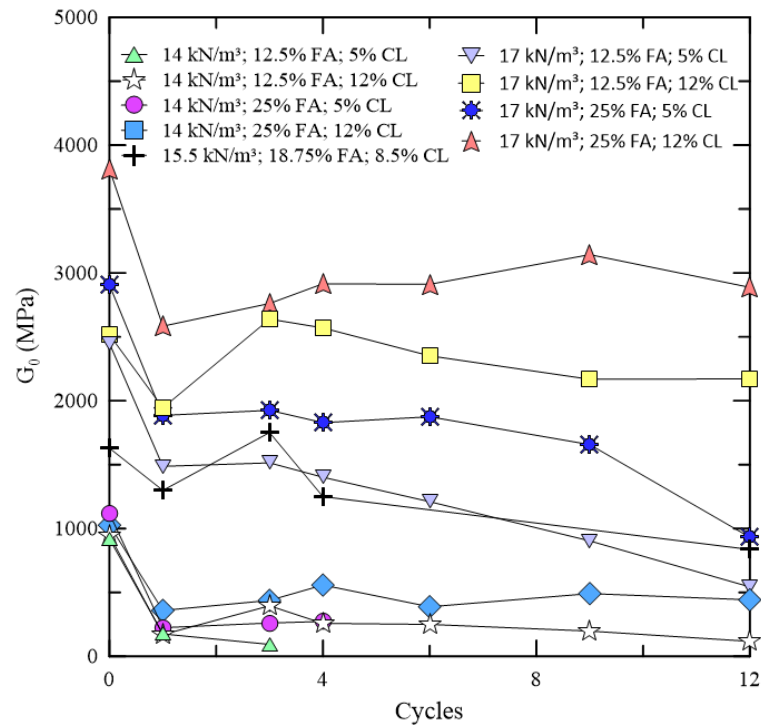


Figure 5.65: Small strain shear modulus for calcitic lime treated samples throughout wetting-drying cycles.

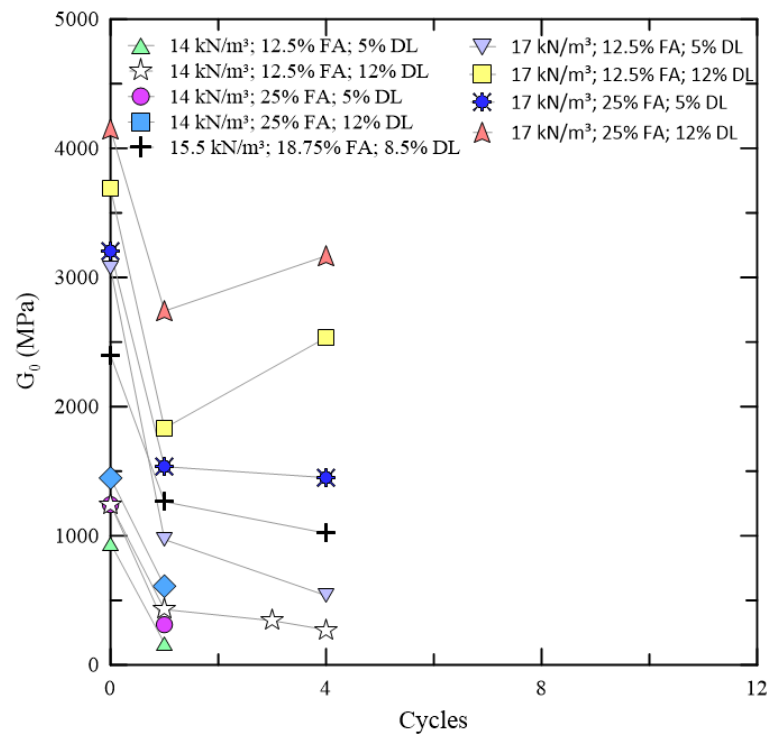


Figure 5.66: Small strain shear modulus for dolomitic lime treated samples throughout wetting-drying cycles.

The small strain shear modulus determined in samples undergoing wetting, drying, and brushing durability cycles is presented in figure 5.67 for calcitic lime treated specimens and in figure 5.68 for dolomitic lime treated specimens. After the first cycle, there is an increasing trend in  $G_0$  values for the specimens with higher calcitic lime content. This behaviour is different from the lower-size specimens. As those samples present a lower water loss during durability drying (smaller samples have presented from about 1 to 3% moisture content after the drying stage of the cycles, whereas higher volume samples have presented about 3 to 7%), it can explain this behaviour, or it may occur due to less damage suffered by the internal mass that is where the waves travel. Most specimens stabilized using the dolomitic lime presented a higher stiffness degradation and, for some of them, waves travel time could not be assessed after the first cycle. For most of them, ultrasonic shear strain tests were not possible only after the fourth cycle, except for the denser specimens with higher dolomitic lime content. After the 9<sup>th</sup> cycle, all the specimens, both for calcitic and dolomitic lime, have presented a reduction in small strain shear modulus.

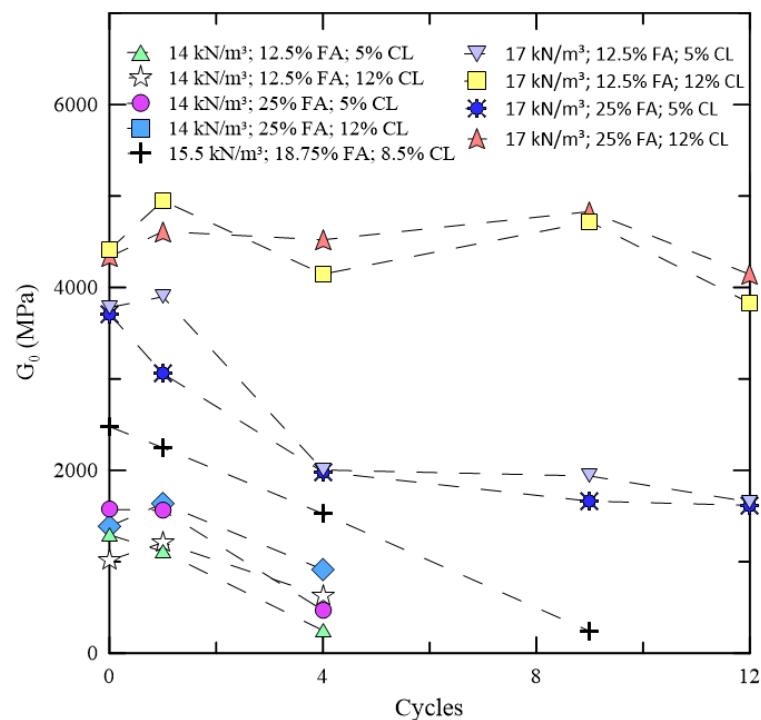


Figure 5.67: Small strain shear modulus for calcitic lime treated samples throughout wetting-drying-brushing cycles.

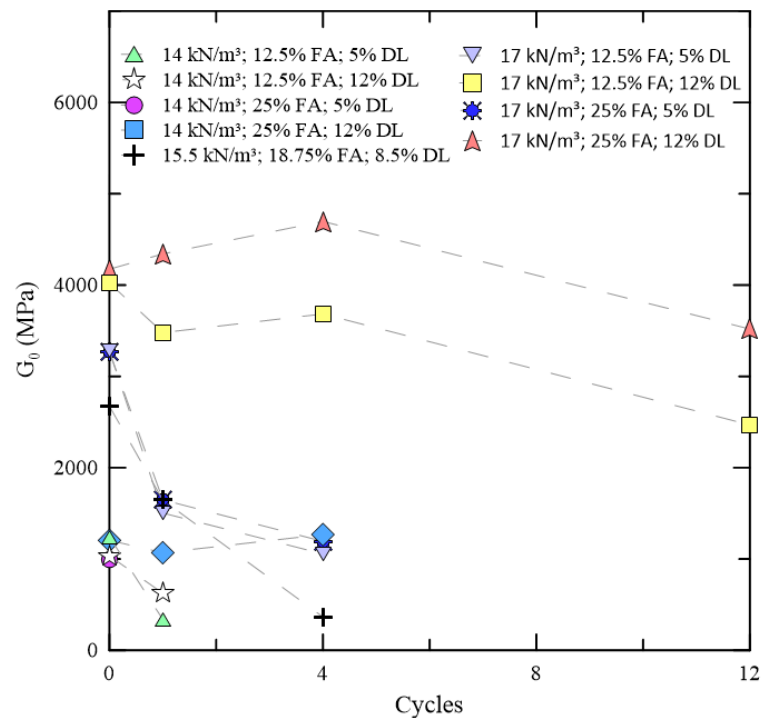


Figure 5.68: Small strain shear modulus for dolomitic lime treated samples throughout wetting-drying-brushing cycles.

### 5.2.6 Loss of mass throughout cycles

The more usual method to assess durability for cemented soil specimens is through the quantification of mass loss, as it is a direct and easy determinable parameter. The amount of mass loss was determined by weighing all the specimens before and after the brushing stage, and but as there was water inside the soil, the brushed soil was oven-dried, however, the specimens with a very low mass loss could not have their moisture content determined due to the scale precision. The accumulated loss of mass throughout cycles of wetting and drying of calcitic and dolomitic lime treated specimens are shown, respectively, in figure 5.69 and figure 5.70. The ALM behaviour is approximately linear along with cycles, indicating that there were no significant changes in the susceptibility of losing mass since the initiation of cycles. It can be observed that the accumulated loss of mass is strictly related to dry unit weight, but it is also clearly influenced by the lime content, and the specimens stabilized with dolomitic lime presented a higher loss of mass.

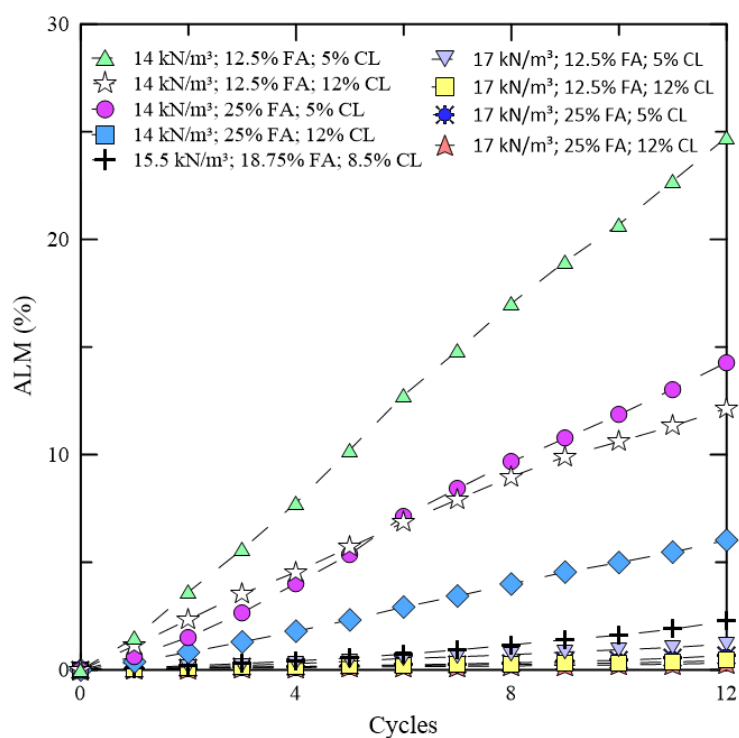


Figure 5.69: Accumulated loss of mass for calcitic lime treated samples throughout wetting-drying-brushing cycles.

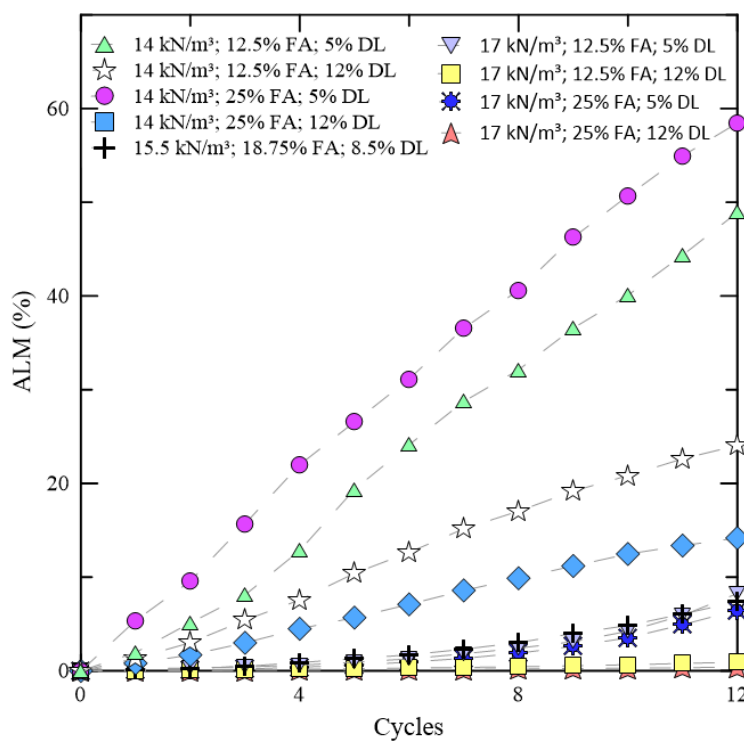


Figure 5.70: Accumulated loss of mass for dolomitic lime treated samples throughout wetting-drying-brushing cycles.



Specimens that have not undergone brushing in durability cycles have only presented a loss of mass due to internal and surface erosion when immersed, so the loss of mass could not be quantified along with all the cycles. After the 12<sup>th</sup> cycle, those specimens were tested in unconfined compressive strength in the saturated condition and, after failure, they were oven-dried for the moisture content determination. Knowing the failure moisture content, the dry unit weight could be assessed too. So, the accumulated loss of mass after 12 cycles (ALM<sub>12</sub>) was assessed. Though, as this methodology is not precise, only higher values than 0.5% of ALM<sub>12</sub> were considered meaningful. ALMs lower than 0.5 % were disregarded and considered 0. The results for specimens treated with the calcitic lime are presented in figure 5.71, and specimens stabilized by using the dolomitic lime have their results presented in figure 5.72. The observed trend is similar to the specimens with higher volume, but for dolomitic lime treated specimens, the four samples which undergone the higher ALM were specimens with only 5% of dolomitic lime content. The referred 100% loss of mass corresponds to a disintegration level when there is no recognition of a unique mass, as all of the initial mass is unbonded (appendix I contains images of specimens throughout cycles).

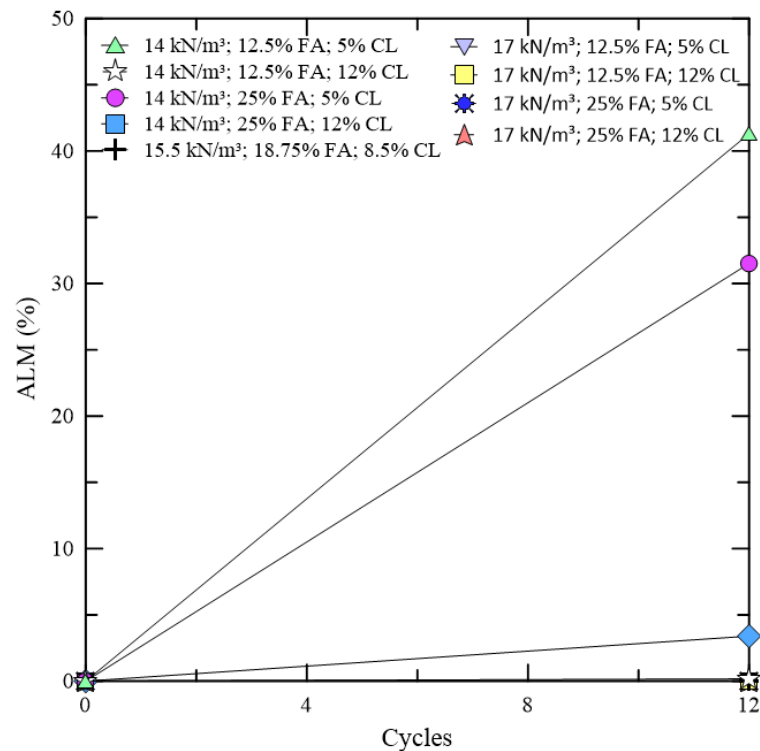


Figure 5.71: Accumulated loss of mass for calcitic lime treated samples throughout wetting-drying cycles.

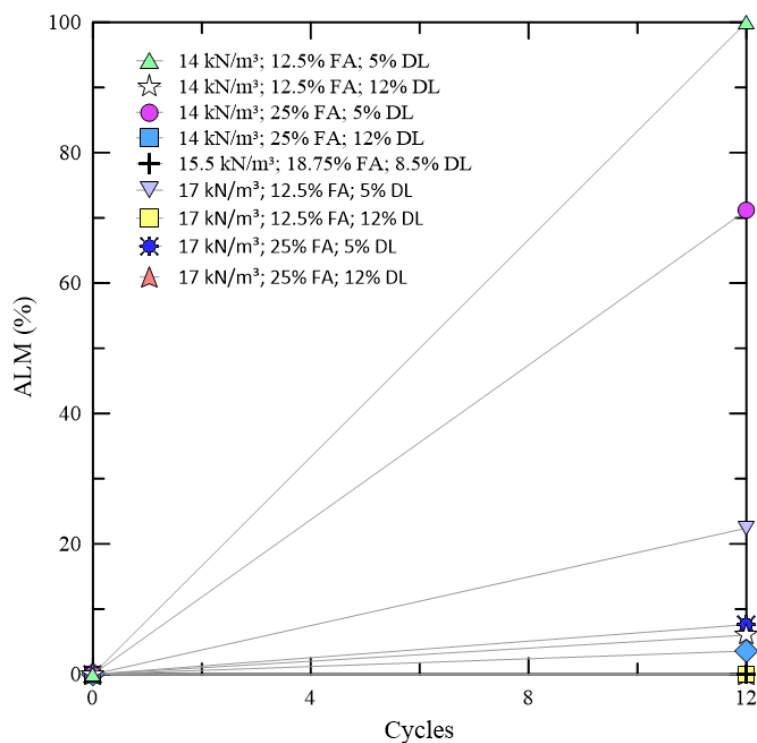


Figure 5.72: Accumulated loss of mass for dolomitic lime treated samples throughout wetting-drying cycles.

### 5.2.7 Unconfined compressive strength durability ratio after durability cycles

The unconfined compressive strength durability ratio (UDR) relates the unconfined compressive strength before durability cycles to the strength after  $n$  cycles. UDRs greater than 1 indicate strength increase, while values lower than 1 indicate a strength decrease. Only three calcitic lime treated dosages have presented a strength decrease ( $UDR < 1$ ), whereas only two dolomitic lime treated dosages have presented a strength increase ( $UDR > 1$ ). When dosing a stabilized soil mixture, UDR can be considered and related to the life span in a geotechnical design. Those results are presented in Figure 5.73 and 5.74, for calcitic and dolomitic-lime treated soils, respectively.

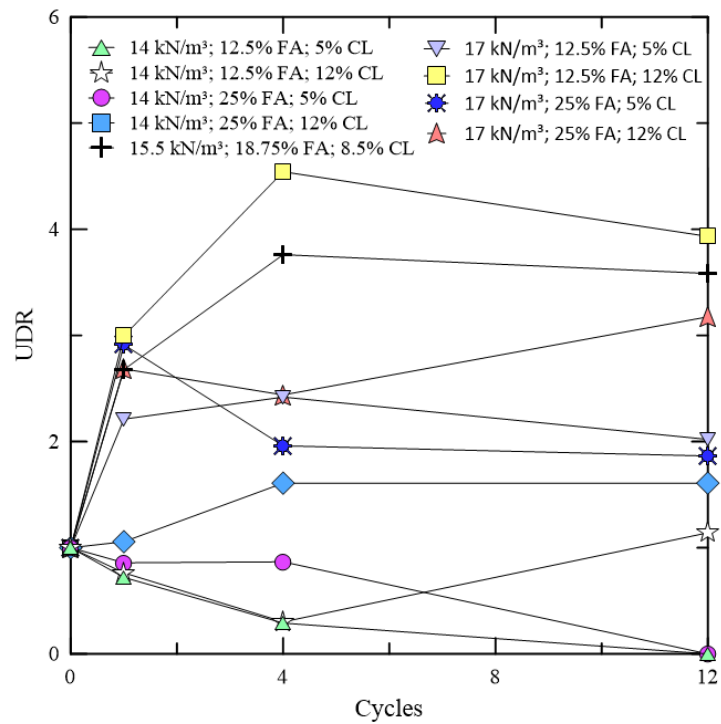


Figure 5.73: UDR for calcitic lime treated samples throughout wetting-drying cycles.

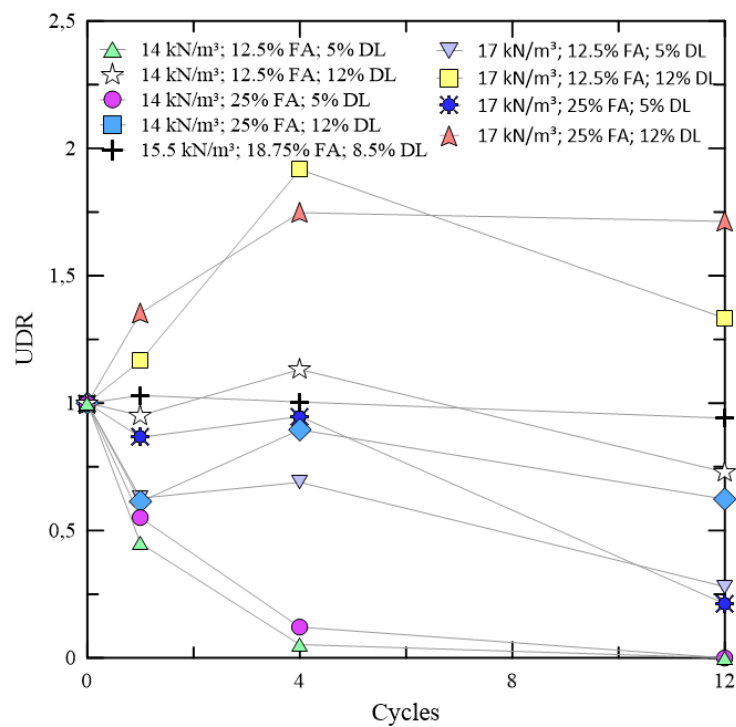


Figure 5.74: UDR for dolomitic lime treated samples throughout wetting-drying cycles.

### 5.3 RELATION BETWEEN VARIABLES RESPONSE

When soil properties are correlated between themselves, those relations are useful because they are not necessarily dependent on the property's specific values or magnitude, and some relations may also be useful to correlate different materials' properties.

So, this chapter aims to correlate unconfined compressive strength ( $q_u$ ), unconfined compressive secant modulus ( $E_{sec}$ ), small strain constraint modulus ( $M_0$ ), small strain shear modulus ( $G_0$ ), and accumulated loss of mass (ALM). Those correlations may be only suitable for the mixtures tested, but possibly some of those relations can be used for different soils.

#### 5.3.1 Unconfined compressive strength x unconfined compressive secant modulus

Stress-strain relation is one of the most widely studied in geotechnical engineering, so  $q_u$  x  $E_{sec}$  results are presented in figure 5.75.

The displacement during the test was not measured for specimens that were not subjected to durability cycles ("0 cycles" applied), so the secant modulus could not be assessed in those tests. The relation between these two parameters has resulted in a linear trend.

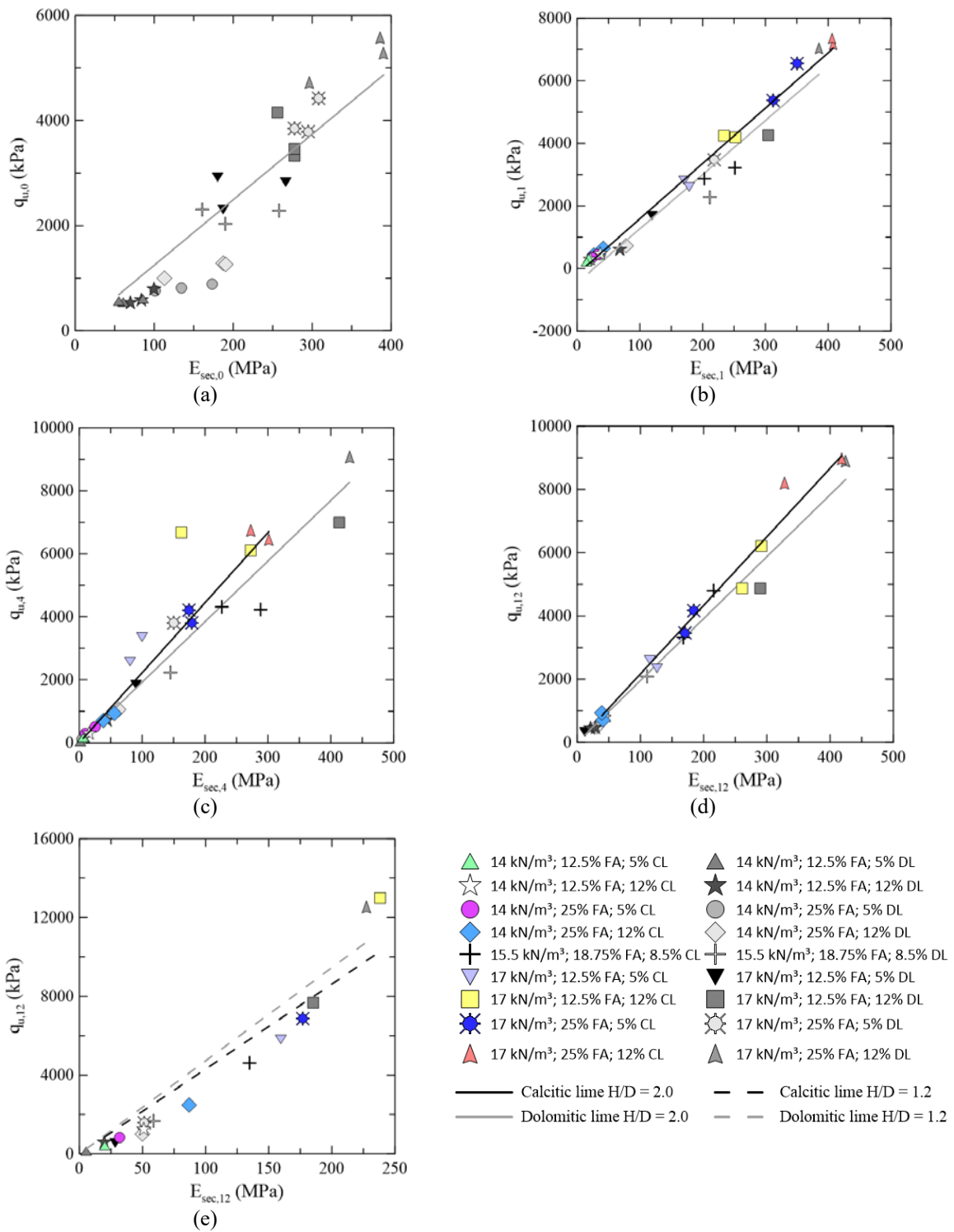


Figure 5.75: Relation between  $q_u$  and  $E_{sec}$  after (a) 0 cycle (b) 1 cycle (c) 4 cycles (d) 12 cycles  $H/D \approx 2.0$  (e) 12 cycles  $H/D \approx 1.2$ .

The fit equations for calcitic lime treated soils are presented below.

$$q_{u,1 (H/D=2.0)} = 17.05 \times E_{\text{sec},1} \quad R^2 = 0.98 \quad (5.53)$$

$$q_{u,4 (H/D=2.0)} = 22.24 \times E_{\text{sec},4} \quad R^2 = 0.83 \quad (5.54)$$

$$q_{u,12 (H/D=2.0)} = 21.68 \times E_{\text{sec},12} \quad R^2 = 0.97 \quad (5.55)$$

$$q_{u,12 (H/D=1.2)} = 43.11 \times E_{\text{sec},12} \quad R^2 = 0.89 \quad (5.56)$$

For dolomitic lime treated specimens, the correlation can be expressed by equations (5.57) to (5.61).

$$q_{u,0 (H/D=2.0)} = 12.47 \times E_{\text{sec},0} \quad R^2 = 0.84 \quad (5.57)$$

$$q_{u,1 (H/D=2.0)} = 15.46 \times E_{\text{sec},1} \quad R^2 = 0.93 \quad (5.58)$$

$$q_{u,4 (H/D=2.0)} = 19.23 \times E_{\text{sec},4} \quad R^2 = 0.97 \quad (5.59)$$

$$q_{u,12 (H/D=2.0)} = 19.58 \times E_{\text{sec},12} \quad R^2 = 0.98 \quad (5.60)$$

$$q_{u,12 (H/D=1.2)} = 47.26 \times E_{\text{sec},12} \quad R^2 = 0.94 \quad (5.61)$$

As the durability cycles affect the soils, there is a slight grown in the expression angular coefficient, indicating that the strength increases in a higher proportion when compared to the  $E_{\text{sec}}$ . Also, this coefficient is nearly double for the less slender specimens.

### 5.3.2 Unconfined compressive strength x small strain constraint modulus

Besides secant modulus, unconfined compressive strength may be correlated with soil constraint modulus. It is important to notice, though, that for the “0 cycles” samples, no drying was applied to the specimens and, as the P-waves propagate in water, higher  $M_0$  values are found in that condition. Results can be seen in figure 5.76 for both calcitic and dolomitic lime

admixtures. After 4, and especially after 12 cycles, in some of the tested specimens, P-wave travel time could not be measured because of their structure deterioration.

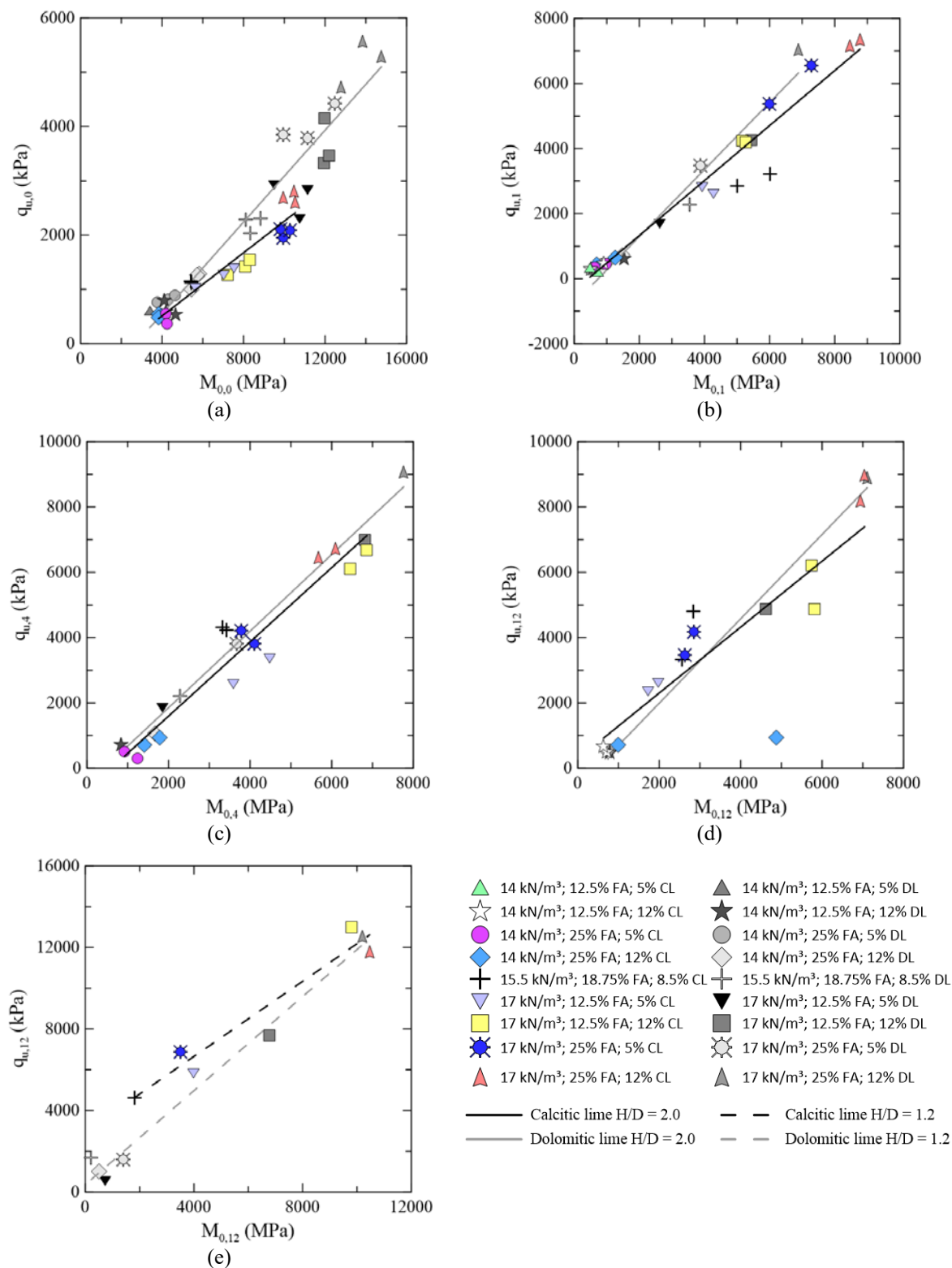


Figure 5.76: Relation between  $q_u$  and  $M_0$  after (a) 0 cycle (b) 1 cycle (c) 4 cycles (d) 12 cycles  $H/D \approx 2.0$  (e) 12 cycles  $H/D \approx 1.2$ .

The fit equations for calcitic lime treated soils are presented below. The displacement during the test was not measured for specimens that were not subjected to durability cycles (“0 cycles” applied), so the secant modulus could not be assessed in those tests.

$$q_{u,0 (H/D=2.0)} = 0.29 \times M_{0,0} - 654.33 \quad R^2 = 0.91 \quad (5.62)$$

$$q_{u,1 (H/D=2.0)} = 0.85 \times M_{0,1} - 363.51 \quad R^2 = 0.95 \quad (5.63)$$

$$q_{u,4 (H/D=2.0)} = 1.14 \times M_{0,4} - 683.21 \quad R^2 = 0.91 \quad (5.64)$$

$$q_{u,12 (H/D=2.0)} = 1.01 \times M_{0,12} + 280.94 \quad R^2 = 0.71 \quad (5.65)$$

$$q_{u,12 (H/D=1.2)} = 0.92 \times M_{0,12} + 2,963.86 \quad R^2 = 0.95 \quad (5.66)$$

Equations (5.67) to (5.71) present the regression fit for the specimens treated with dolomitic lime.

$$q_{u,0 (H/D=2.0)} = 0.42 \times M_{0,0} - 1,143.46 \quad R^2 = 0.93 \quad (5.67)$$

$$q_{u,1 (H/D=2.0)} = 1.03 \times M_{0,1} - 759.72 \quad R^2 = 0.96 \quad (5.68)$$

$$q_{u,4 (H/D=2.0)} = 1.17 \times M_{0,4} - 498.43 \quad R^2 = 0.99 \quad (5.69)$$

$$q_{u,12 (H/D=2.0)} = 1.29 \times M_{0,12} - 594.78 \quad R^2 = 0.99 \quad (5.70)$$

$$q_{u,12 (H/D=1.2)} = 1.15 \times M_{0,12} + 359.83 \quad R^2 = 0.98 \quad (5.71)$$

Besides the results before durability cycle applications (0 cycles), the angular coefficient for all the equations, even when dolomitic and calcitic lime treated specimens are compared, is similar, ranging between 0.85 and 1.29. As there are no significant differences between the relation



throughout durability cycles,  $M_0$  may be an indication of soil strength, no matter how many cycles the soil has undergone. However, the tests may be executed when the soil presents a similar water content.

### 5.3.3 Unconfined compressive strength x small strain shear modulus

Relating strength with shear modulus is very usual since S-waves are, most of the time, applied to saturated soil specimens, but when dealing with partially saturated soils, matric suction can affect the results. In this study, ultrasonic pulse velocity equipment was used to assess  $G_0$  for specimens not subjected to cycles (0 cycles) and for the condition after cycles. Their relation with the measured strength is presented in figure 5.77.

After durability cycles damage, some specimens could not be tested, so the plot presents only a partial path behaviour that should not stand for all the involved specimens. As when the soil strength is null, there can be no shear stiffness, the origin of the fit equations was assumed to be 0;0.

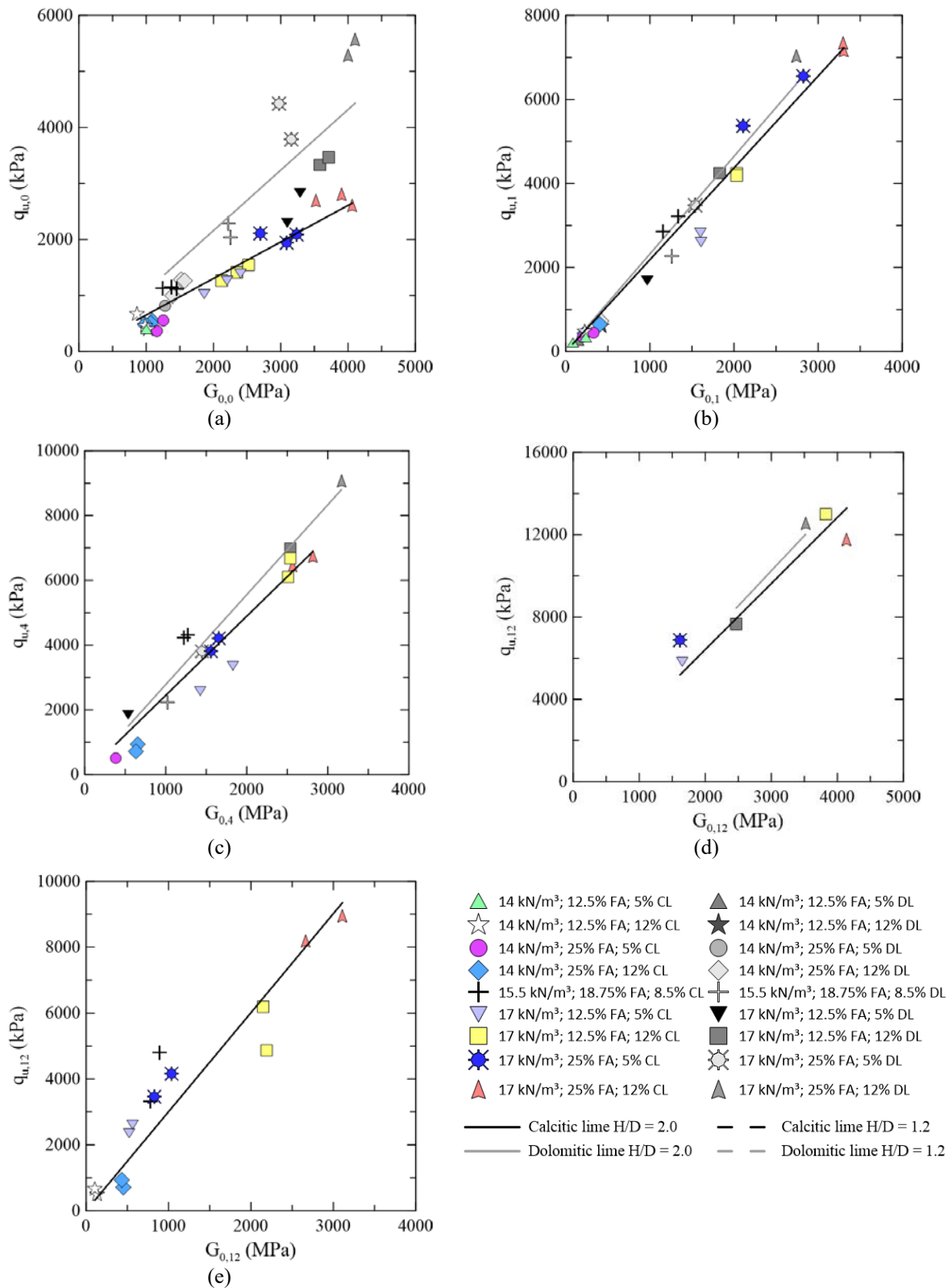


Figure 5.77: Relation between  $q_u$  and  $G_0$  after (a) 0 cycle (b) 1 cycle (c) 4 cycles (d) 12 cycles  $H/D \approx 2.0$  (e) 12 cycles  $H/D \approx 1.2$ .

The following expressions present the relations fit equations for the mixtures stabilized with the calcitic lime.

$$q_{u,0 (H/D=2.0)} = 0.65 \times G_{0,0} \quad R^2 = 0.91 \quad (5.72)$$

$$q_{u,1 (H/D=2.0)} = 2.19 \times G_{0,1} \quad R^2 = 0.98 \quad (5.73)$$

$$q_{u,4 (H/D=2.0)} = 2.45 \times G_{0,4} \quad R^2 = 0.89 \quad (5.74)$$

$$q_{u,12 (H/D=2.0)} = 3.01 \times G_{0,12} \quad R^2 = 0.87 \quad (5.75)$$

$$q_{u,12 (H/D=1.2)} = 3.21 \times G_{0,12} \quad R^2 = 0.84 \quad (5.76)$$

From the correlations of specimens stabilized using dolomitic lime, the following expressions were obtained.

$$q_{u,0 (H/D=2.0)} = 1.08 \times G_{0,0} \quad R^2 = 0.77 \quad (5.77)$$

$$q_{u,1 (H/D=2.0)} = 2.23 \times G_{0,1} \quad R^2 = 0.96 \quad (5.78)$$

$$q_{u,4 (H/D=2.0)} = 2.78 \times G_{0,4} \quad R^2 = 0.98 \quad (5.79)$$

$$q_{u,12 (H/D=1.2)} = 3.42 \times G_{0,12} \quad R^2 = 0.93 \quad (5.80)$$

Matric suction may affect the results, so the correlations must be compared between specimens with similar moisture contents. As can be seen, there is an increase in the angular coefficient when more cycles are applied to the samples. Both the calcitic and dolomitic lime treated specimens presented a similar relation between  $q_u$  and  $G_0$ .

### 5.3.4 Unconfined compressive strength x accumulated loss of mass

As particle contacts develop a great whole in soil mechanical properties, the unconfined compressive strength  $q_u$  was evaluated based on the mass loss, since the samples which lose a high portion of their mass might present a low strength. The plotted results are shown in figure 5.78. By this relation, not only the loss of particle contacts is accounted for, but also the propensity of losing mass and its relation to strength.

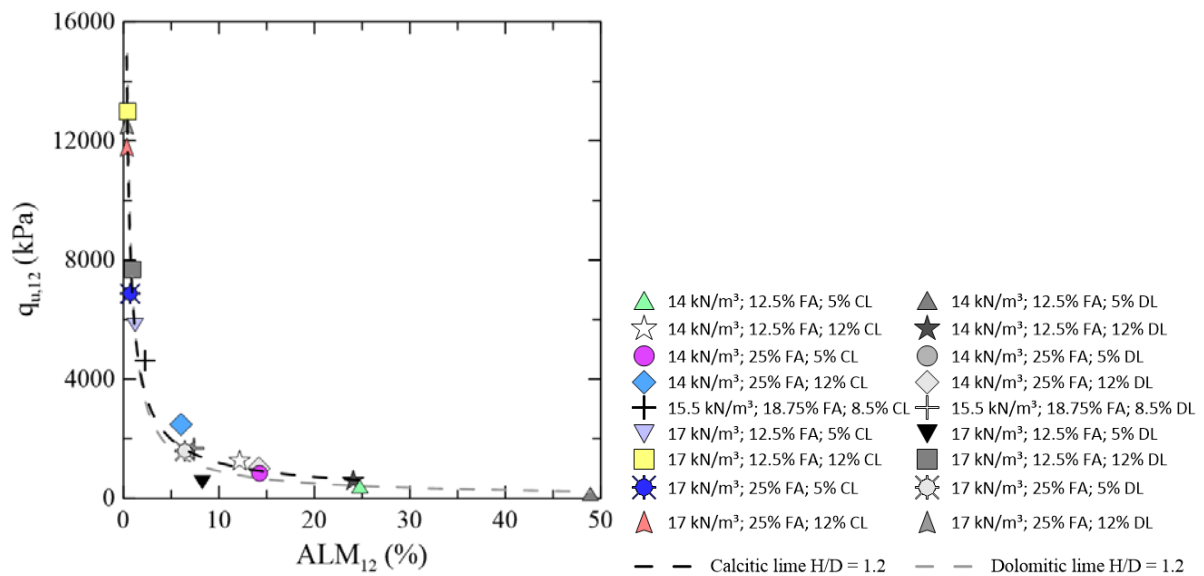


Figure 5.78: Relation between  $q_u$  and  $ALM$  for specimens with  $H/D \approx 1.2$  after 12 cycles.

The regression equation for calcitic lime is presented by equation (5.81), while the soil treated with the dolomitic lime presented the response according to the equation (5.82). It can be noted that the response for both calcitic and dolomitic treated specimens is similar, though, when there is only a small amount of mass loss, the strength response is difficult to predict from  $ALM$  due to the equation's exponents.

$$q_{u,12 (H/D=1.2)} = 6,428.20 \times ALM_{12}^{-0.73} \quad R^2 = 0.95 \quad (5.81)$$

$$q_{u,12 (H/D=1.2)} = 6,649.80 \times ALM_{12}^{-0.87} \quad R^2 = 0.92 \quad (5.82)$$

### 5.3.5 Unconfined compressive secant modulus x Accumulated loss of mass

The unconfined compressive secant modulus may respond differently from strength to the samples accumulated loss of mass,

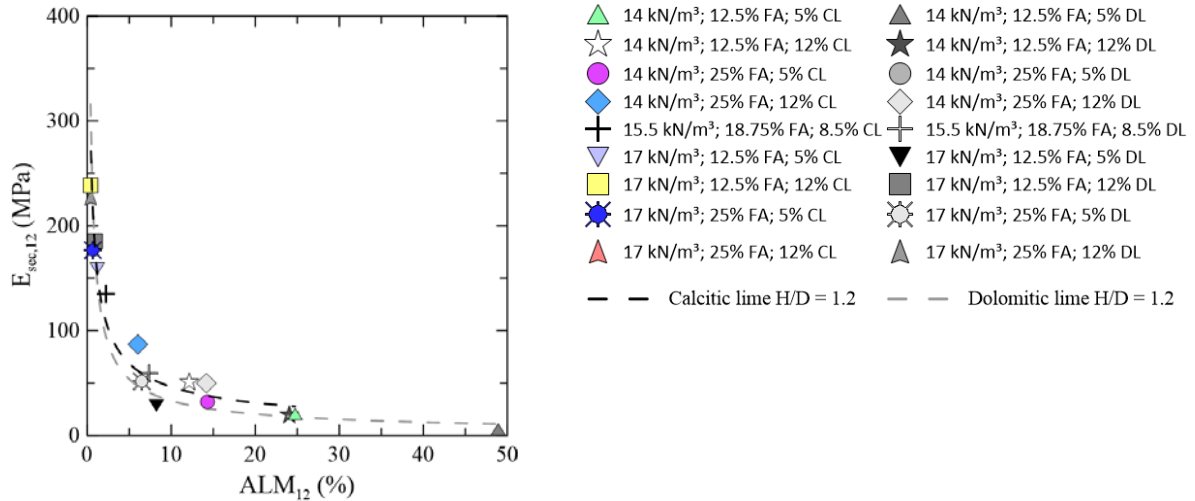


Figure 5.79: Relation between  $E_{sec}$  and ALM for specimens with  $H/D \approx 1.2$  after 12 cycles.

Equation (5.83) and equation (5.84) present, respectively, the regression curves for calcitic and for dolomitic treated materials tested after 12 durability cycles. As they are exponential expressions, when the amount of mass loss is very small, the  $E_{sec}$  prediction becomes difficult. However, for a higher percentage of mass loss, both the soils stabilized with calcitic and dolomitic lime present similarity in unconfined secant modulus when the ALM is the same.

$$E_{sec,12 (H/D=1.2)} = 170.91 \times ALM_{12}^{-0.57} \quad R^2 = 0.92 \quad (5.83)$$

$$E_{sec,12 (H/D=1.2)} = 164.69 \times ALM_{12}^{-0.70} \quad R^2 = 0.87 \quad (5.84)$$

### 5.3.6 Unconfined compressive secant modulus x small strain constraint modulus

The small strain stiffness and stiffness at higher strains can be related, and the relation between those parameters has proved to be very useful (BURLAND, 1989; POULOS, 2018). To assess how unconfined compressive secant modulus at maximum strain condition (failure) responds to  $M_0$ , this relation is presented in figure 5.80.

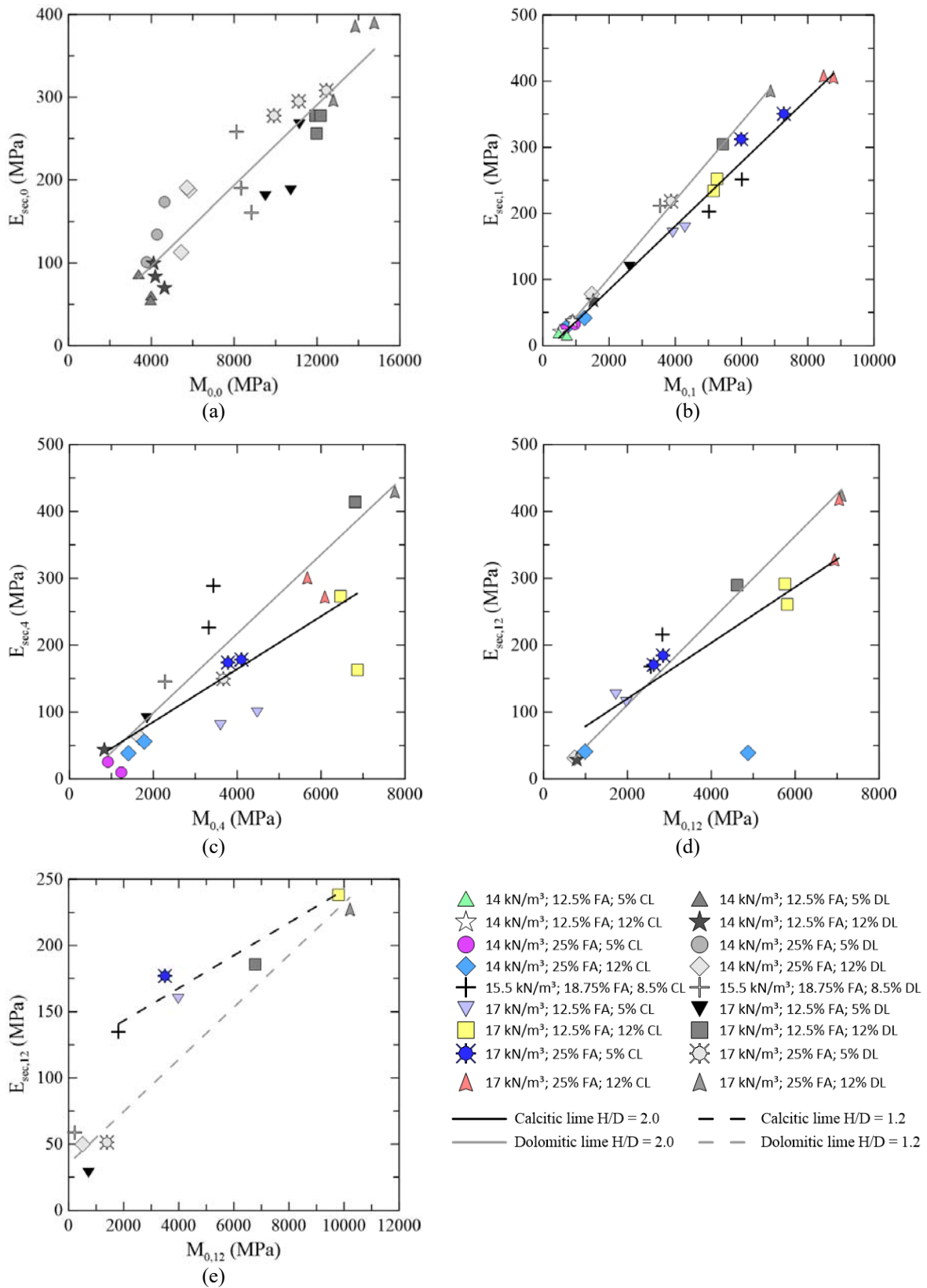


Figure 5.80: Relation between  $E_{sec}$  and  $M_0$  after (a) 0 cycle (b) 1 cycle (c) 4 cycles (d) 12 cycles (e) 12 cycles  $H/D \approx 1.2$ .

As depicted by the plots, there is a linear relation between  $E_{\text{sec}}$  and  $M_0$ . The equations expressing the relation between  $E_{\text{sec}}$  and  $M_0$ , for specimens treated with calcitic lime, are presented below. Specimens that undergone wetting and drying cycles presented a high dispersion in the relation, as indicated by low coefficients of determination ( $R^2$ ).

$$E_{\text{sec},1 (H/D=2.0)} = 0.048 \times M_{0,1} - 12.07 \quad R^2 = 0.99 \quad (5.85)$$

$$E_{\text{sec},4 (H/D=2.0)} = 0.039 \times M_{0,4} - 6.24 \quad R^2 = 0.55 \quad (5.86)$$

$$E_{\text{sec},12 (H/D=2.0)} = 0.042 \times M_{0,12} + 36.83 \quad R^2 = 0.61 \quad (5.87)$$

$$E_{\text{sec},12 (H/D=1.2)} = 0.012 \times M_{0,12} + 118.47 \quad R^2 = 0.94 \quad (5.88)$$

Equations from (5.89) to (5.93) present the regression fit for the specimens treated with dolomitic lime

$$E_{\text{sec},0 (H/D=2.0)} = 0.024 \times M_{0,0} - 0.89 \quad R^2 = 0.85 \quad (5.89)$$

$$E_{\text{sec},1 (H/D=2.0)} = 0.059 \times M_{0,1} - 15.74 \quad R^2 = 0.99 \quad (5.90)$$

$$E_{\text{sec},4 (H/D=2.0)} = 0.059 \times M_{0,4} - 19.63 \quad R^2 = 0.97 \quad (5.91)$$

$$E_{\text{sec},12 (H/D=2.0)} = 0.063 \times M_{0,12} - 15.11 \quad R^2 = 0.997 \quad (5.92)$$

$$E_{\text{sec},12 (H/D=1.2)} = 0.020 \times M_{0,12} + 35.23 \quad R^2 = 0.98 \quad (5.93)$$

In most cases, the correlation seems to be appropriate, but as can be seen, less slender samples ( $H/D \approx 1.2$ ) tend to present much lower unconfined modulus than more slender samples ( $H/D \approx 2.0$ ) when they present the same  $M_0$ , and the samples stabilized using dolomitic lime presented

higher angular coefficients in the linear fit regression equations. So, possibly, the relation between unconfined secant modulus and small strain constraint modulus is unique for each soil.

### 5.3.7 Unconfined compressive secant modulus x small strain shear modulus

Similar to the analysis relating secant modulus with constraint modulus, a comparison between low strain and engineering strain levels can be useful in many cases. An advantage of shear modulus analysis is its less dependency on Poisson's ratio when a material has the same longitudinal elastic modulus in comparison to constraint modules. The results are shown in figure 5.81. The equations expressing the relation between  $E_{sec}$  and  $G_0$  for specimens treated with calcitic lime are presented below. A similar response is observed from the lower volume specimens.

$$E_{sec,1 (H/D=2.0)} = 0.124 \times G_{0,1} + 5.91 \quad R^2 = 0.95 \quad (5.94)$$

$$E_{sec,4 (H/D=2.0)} = 0.089 \times G_{0,4} + 23.82 \quad R^2 = 0.51 \quad (5.95)$$

$$E_{sec,12 (H/D=2.0)} = 0.112 \times G_{0,12} + 50.25 \quad R^2 = 0.89 \quad (5.96)$$

$$E_{sec,12 (H/D=1.2)} = 0.032 \times G_{0,12} + 116.10 \quad R^2 = 0.95 \quad (5.97)$$

Equation (5.98) to (5.101) present the regression fit equations for the specimens treated with dolomitic lime.

$$E_{sec,0 (H/D=2.0)} = 0.073 \times G_{0,0} + 48.19 \quad R^2 = 0.75 \quad (5.98)$$

$$E_{sec,1 (H/D=2.0)} = 0.145 \times G_{0,1} + 5.76 \quad R^2 = 0.98 \quad (5.99)$$

$$E_{sec,4 (H/D=2.0)} = 0.145 \times G_{0,4} - 6.22 \quad R^2 = 0.94 \quad (5.100)$$

$$E_{sec,12 (H/D=1.2)} = 0.040 \times G_{0,12} + 86.93 \quad R^2 = - \quad (5.101)$$



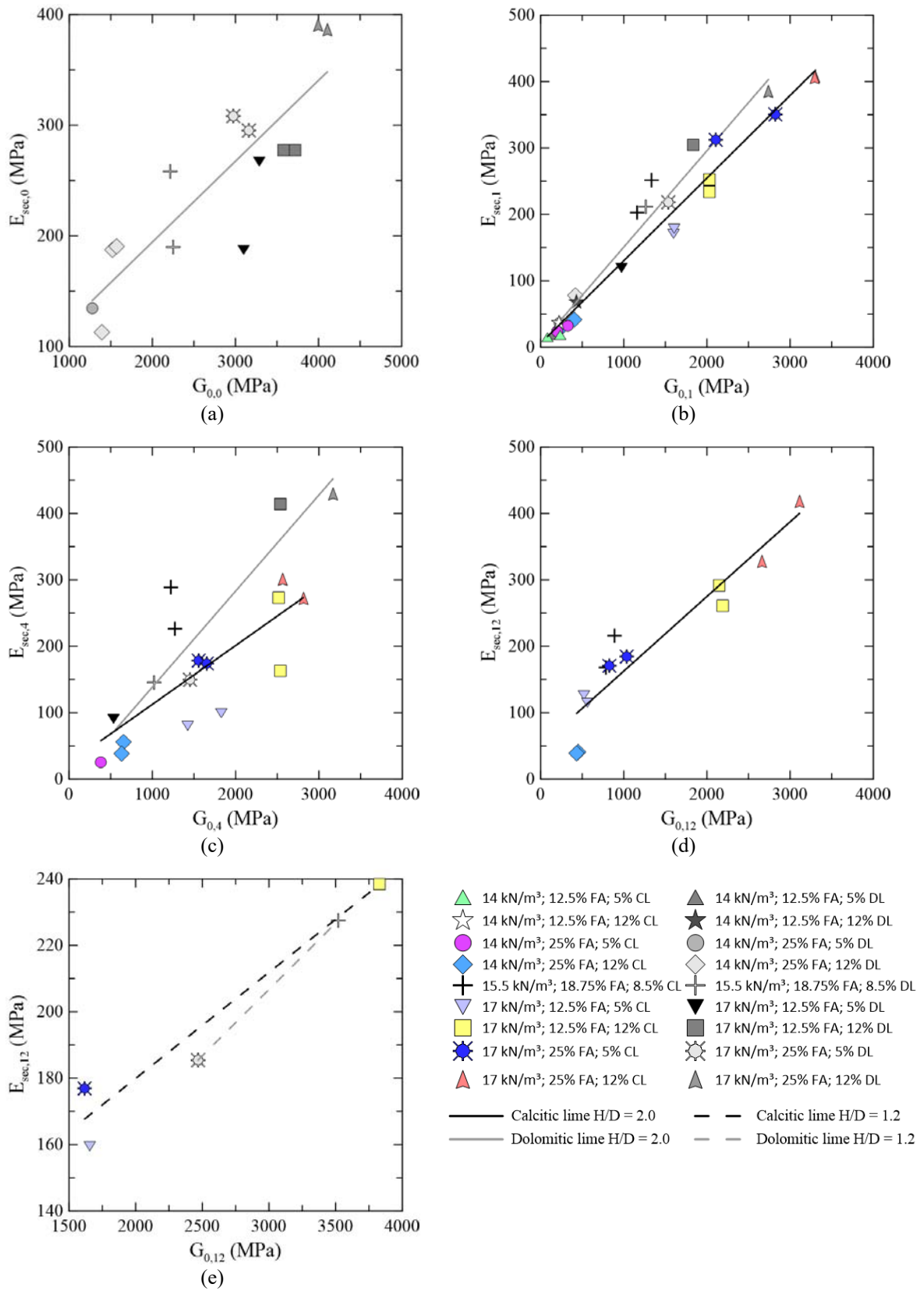


Figure 5.81: Relation between  $E_{sec}$  and  $G_0$  after (a) 0 cycle (b) 1 cycle (c) 4 cycles (d) 12 cycles  $H/D \approx 2.0$  (e) 12 cycles  $H/D \approx 1.2$ .

### 5.3.8 Small strain shear modulus x small strain constraint modulus

As both P-waves and S-waves travel times were measured during this research, it is important to assess how they are related. Figure 5.82 presents the correlation between  $G_0$  and  $M_0$  for the more slender specimens ( $H/D \approx 2.0$ ).

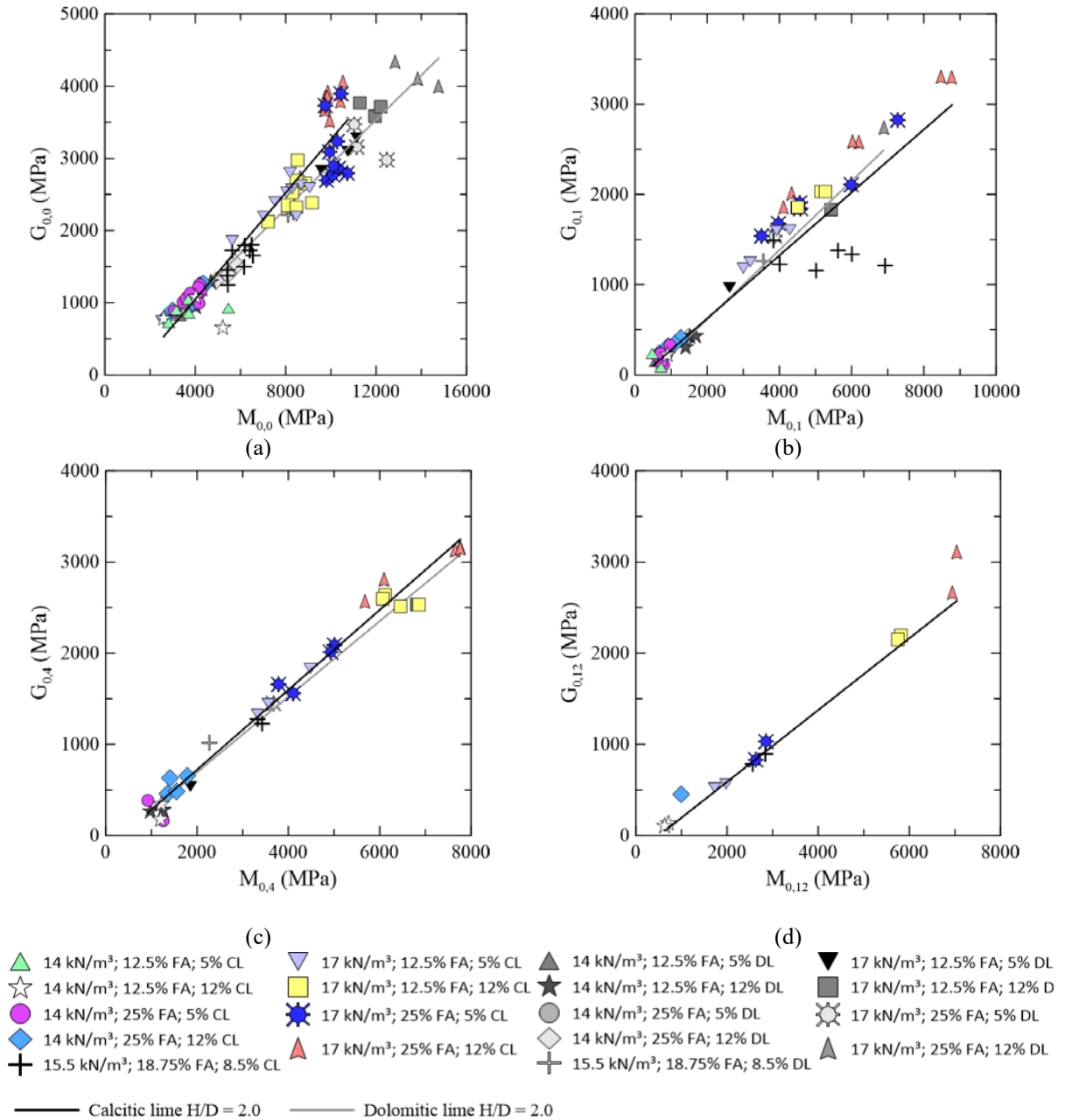


Figure 5.82: Relation between  $G_0$  and  $M_0$  for samples with  $H/D \approx 2.0$  after (a) 0 cycle (b) 1 cycle (c) 4 cycles (d) 12 cycles.

As depicted by the figure 5.82, there is an obvious relation between those two small strain stiffness parameters. The corresponding equations are listed below – equations (5.102) to (5.105) express the relations for the calcitic treated specimens.

$$G_{0,0 (H/D=2.0)} = 0.369 \times M_{0,0} - 427.39 \quad R^2 = 0.89 \quad (5.102)$$

$$G_{0,1 (H/D=2.0)} = 0.349 \times M_{0,1} - 70.96 \quad R^2 = 0.73 \quad (5.103)$$

$$G_{0,4 (H/D=2.0)} = 0.438 \times M_{0,4} - 154.44 \quad R^2 = 0.98 \quad (5.104)$$

$$G_{0,12 (H/D=2.0)} = 0.393 \times M_{0,12} - 198.62 \quad R^2 = 0.997 \quad (5.105)$$

The soil treatment using the dolomitic lime resulted in the response expressed by equations (5.106) to (5.108).

$$G_{0,0 (H/D=2.0)} = 0.308 \times M_{0,0} - 165.47 \quad R^2 = 0.96 \quad (5.106)$$

$$G_{0,1 (H/D=2.0)} = 0.383 \times M_{0,1} - 147.83 \quad R^2 = 0.94 \quad (5.107)$$

$$G_{0,4 (H/D=2.0)} = 0.414 \times M_{0,4} - 134.55 \quad R^2 = 0.99 \quad (5.108)$$

Both calcitic and dolomitic lime stabilization presented similar results and generally high coefficients of determination, indicating there is repeatability in the response to ultrasonic pulse velocity tests, even for different materials.

The relation between  $G_0$  and  $M_0$  for less slender specimens ( $H/D \approx 1.2$ ) is shown in figure 5.83, and the linear fit equations are enunciated next.

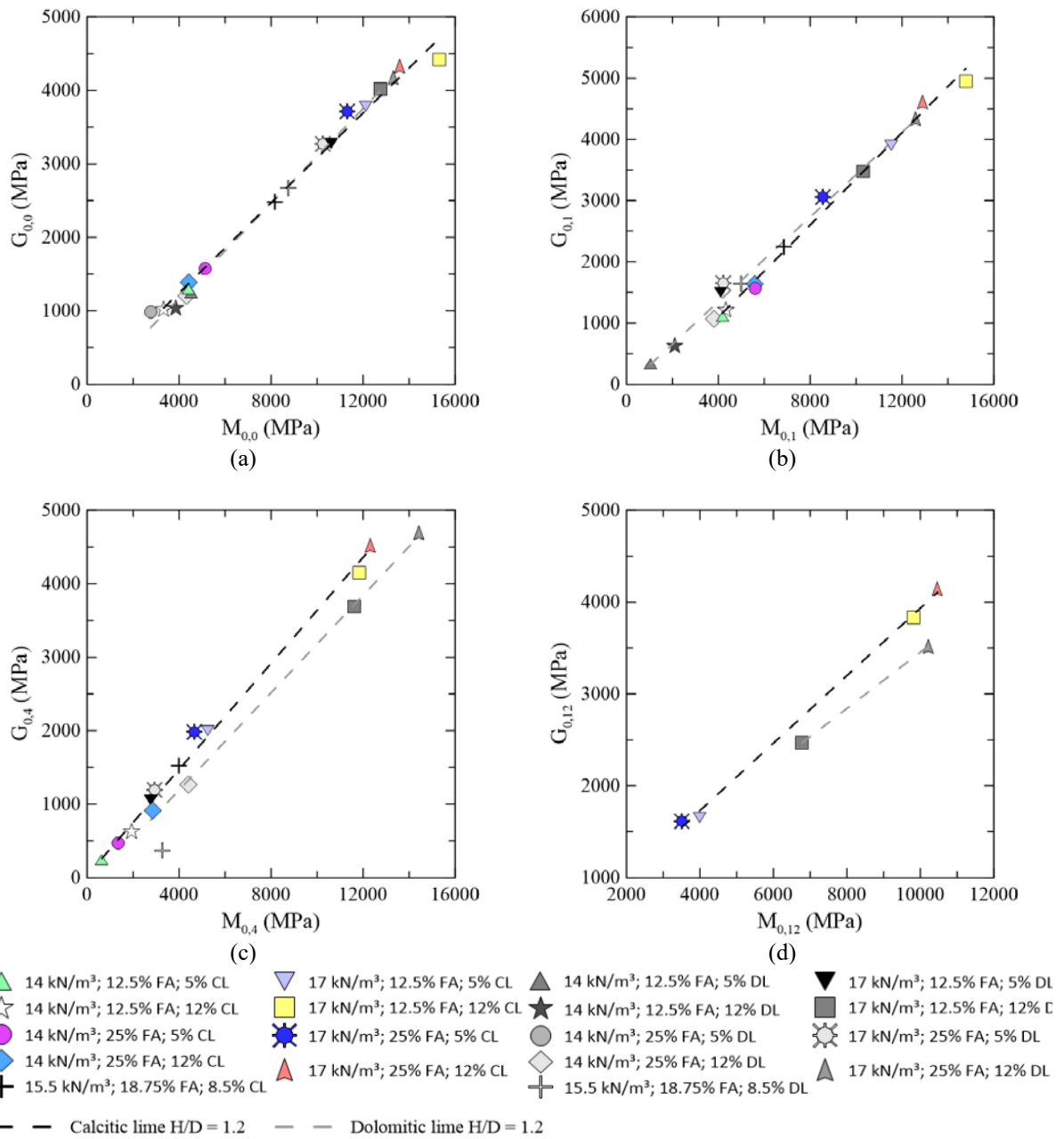


Figure 5.83: Relation between  $G_0$  and  $M_0$  for samples with  $H/D \approx 1.2$  after (a) 0 cycle (b) 1 cycle (c) 4 cycles (d) 12 cycles.

The following equations correspond to the linear fit equations obtained for calcitic lime treated specimens.

$$G_{0,0 (H/D=1.2)} = 0.306 \times M_{0,0} + 19.70 \quad R^2 = 0.99 \quad (5.109)$$

$$G_{0,1 (H/D=1.2)} = 0.377 \times M_{0,1} - 412.12 \quad R^2 = 0.99 \quad (5.110)$$

$$G_{0,4 (H/D=1.2)} = 0.361 \times M_{0,4} + 29.78 \quad R^2 = 0.99 \quad (5.111)$$

$$G_{0,12 (H/D=1.2)} = 0.367 \times M_{0,12} - 261.26 \quad R^2 = 0.998 \quad (5.112)$$

The dolomitic lime treated soils respond to the relation between small strain shear and constraint modulus as presented in the following equations.

$$G_{0,0 (H/D=1.2)} = 0.323 \times M_{0,0} - 121.28 \quad R^2 = 0.99 \quad (5.113)$$

$$G_{0,1 (H/D=1.2)} = 0.346 \times M_{0,1} - 35.77 \quad R^2 = 0.99 \quad (5.114)$$

$$G_{0,4 (H/D=1.2)} = 0.331 \times M_{0,4} - 133.92 \quad R^2 = 0.96 \quad (5.115)$$

$$G_{0,12 (H/D=1.2)} = 0.307 \times M_{0,12} + 389.52 \quad R^2 = - \quad (5.116)$$

The angular coefficient of less slender specimens seems to be slightly lower than in the slenderer specimens. By using expressions like the presented above, if only a few small strain shear and constraint results are available, an interpolation might be used for an approximation of results. Also, if for some reason, only small strain constraint modulus tests can be executed, the small strain shear modulus can be obtained with a reasonable approximation if a linear regression equation is available.

### 5.3.9 Accumulated loss of mass x small strain constraint modulus

Intending to evaluate if there is a correlation between the soil microstructure (e. g. microcracks, huge pores) response to wave propagation and the percent of material loss during durability cycles. Therefore, accumulated loss of mass (ALM) values were plotted against the small strain constraint modulus ( $M_0$ ), and the plots are presented in figure 5.84. After the durability cycles, some samples could not be tested using the ultrasonic pulse equipment because of excessive damage/voids.

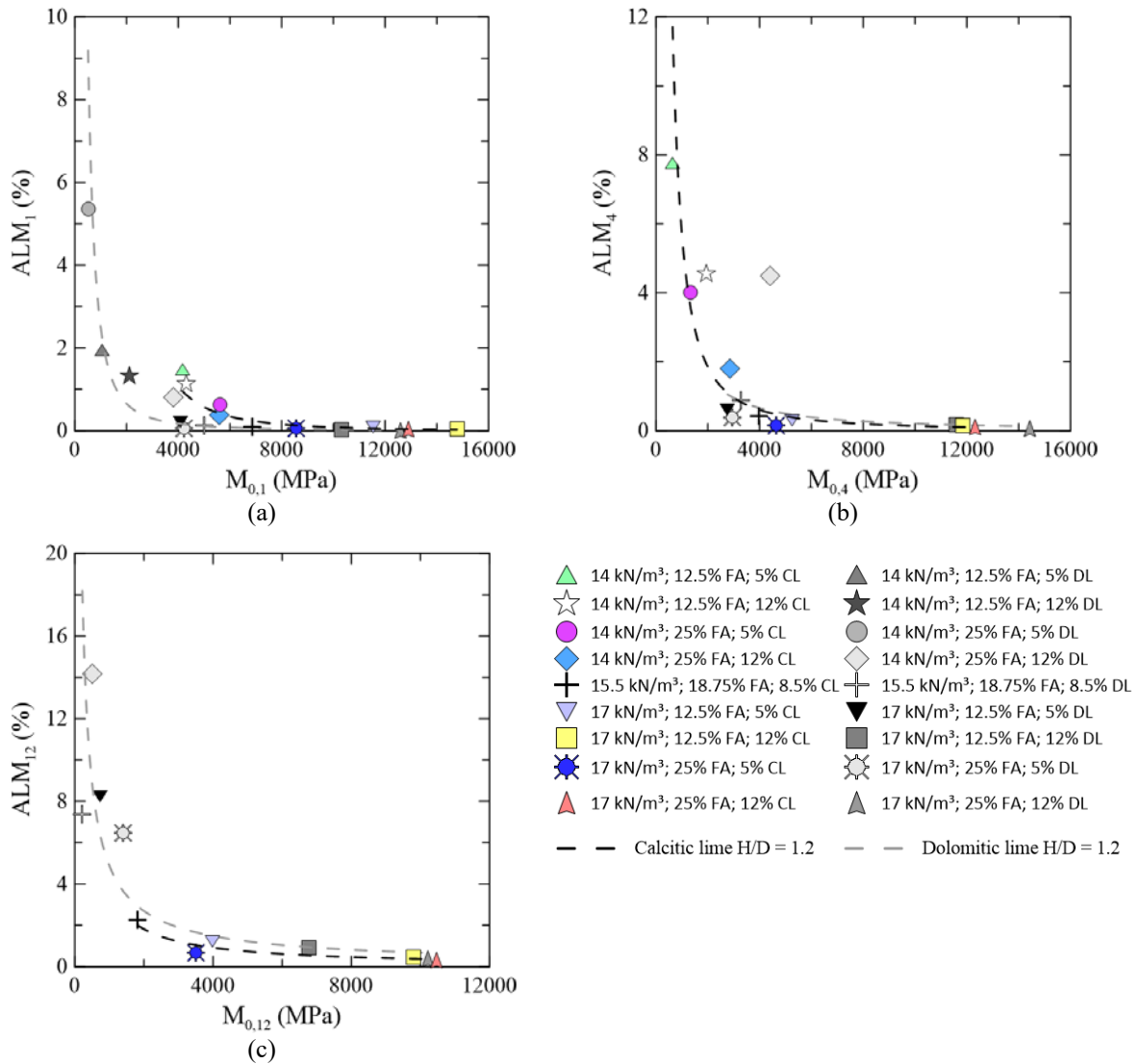


Figure 5.84: Relation between ALM and  $M_0$  for samples with  $H/D \approx 1.2$  after (a) 1 cycle (b) 4 cycles (c) 12 cycles.

The correlations between ALM and  $M_0$  for soils stabilized with calcitic lime are expressed by equations (5.117), (5.118), and (5.119), and the equations for soils stabilized with dolomitic lime are (5.120), (5.121), and (5.122).

$$ALM_{1(H/D=1.2)} = 1.30 \times 10^{10} \times M_{0,1}^{-2.80} \quad R^2 = 0.85 \quad (5.117)$$

$$ALM_{4(H/D=1.2)} = 4.12 \times 10^5 \times M_{0,4}^{-1.62} \quad R^2 = 0.88 \quad (5.118)$$

$$ALM_{12 (H/D=1.2)} = 3.37 \times 10^3 \times M_{0,12}^{-0.99} \quad R^2 = 0.87 \quad (5.119)$$

$$ALM_{1 (H/D=1.2)} = 1.65 \times 10^6 \times M_{0,1}^{-1.94} \quad R^2 = 0.86 \quad (5.120)$$

$$ALM_{4 (H/D=1.2)} = 2.68 \times 10^4 \times M_{0,4}^{-1.28} \quad R^2 = 0.44 \quad (5.121)$$

$$ALM_{12 (H/D=1.2)} = 1.85 \times M_{0,12}^{-0.86} \quad R^2 = 0.83 \quad (5.122)$$

There is a huge change in the presented relation throughout durability cycles, but for specimens with  $M_{0,1}$  greater than 8,000 MPa, there has been no significant accumulated loss of mass (less than 2%) after 12 cycles. Though, it cannot be assured if, after more than 12 cycles, this response will be maintained.

### 5.3.10 Accumulated loss of mass x small strain shear modulus

The stiffness at low levels of strains may be associated with a more susceptible response to losing mass.

Unfortunately, the data are limited because wave propagation reading gets tricky after a significant mass loss and results become difficult to interpret and unreliable. The plots of ALM against  $G_0$  are presented in figure 5.85, and the fit equations are presented next.

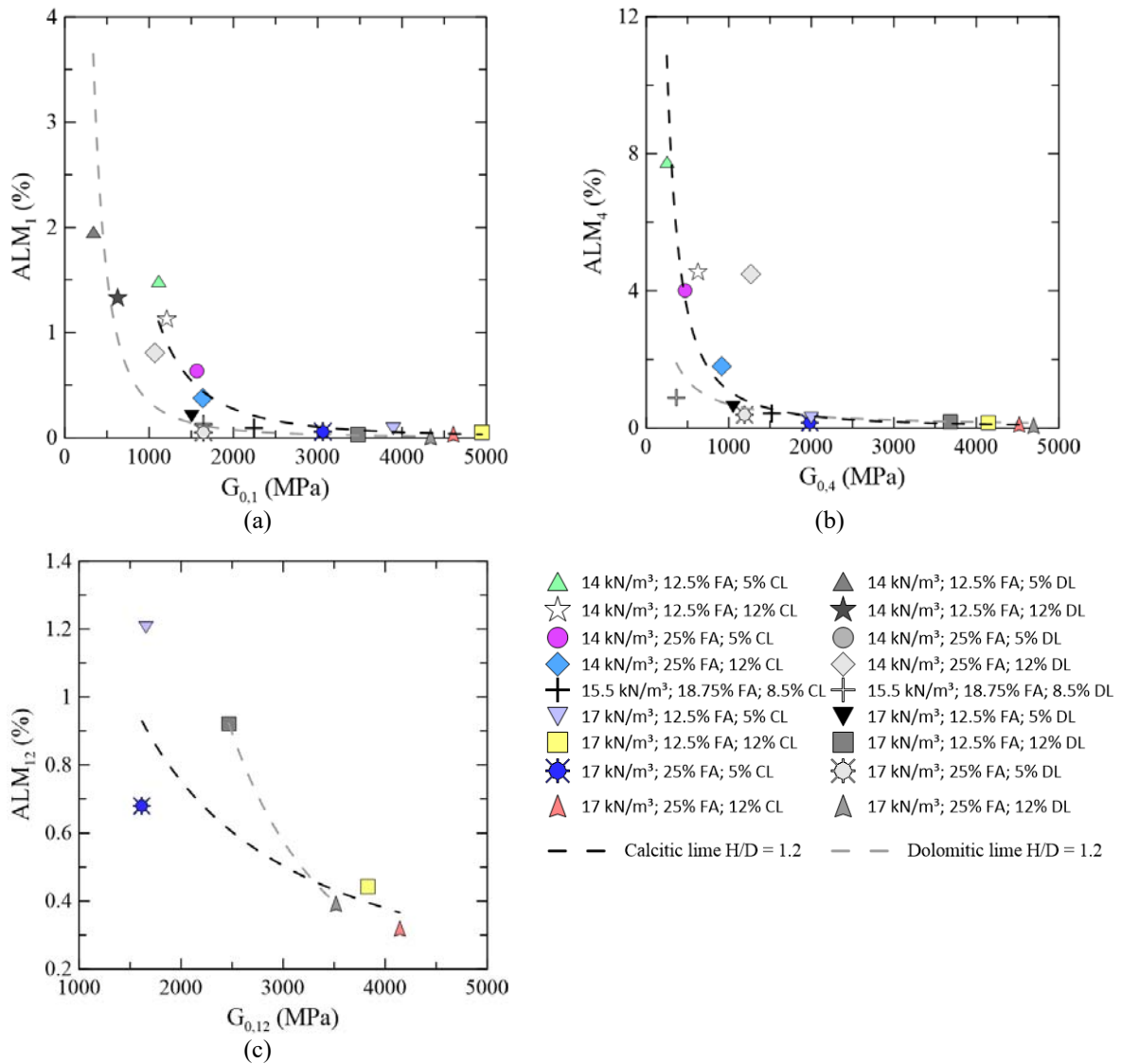


Figure 5.85: Relation between ALM and  $G_0$  for samples with  $H/D \approx 1.2$  after (a) 1 cycle (b) 4 cycles (c) 12 cycles.

$$ALM_{1(H/D=1.2)} = 1.97 \times 10^7 \times G_{0,1}^{-2.38} \quad R^2 = 0.91 \quad (5.123)$$

$$ALM_{4(H/D=1.2)} = 9.70 \times 10^4 \times G_{0,4}^{-1.65} \quad R^2 = 0.93 \quad (5.124)$$

$$ALM_{12(H/D=1.2)} = 1.40 \times 10^3 \times G_{0,12}^{-0.99} \quad R^2 = 0.79 \quad (5.125)$$

The regression curves for dolomitic lime treated soil can be expressed by the following equations:



$$ALM_{1(H/D=1.2)} = 1.19 \times 10^6 \times G_{0,1}^{-2.18} \quad R^2 = 0.90 \quad (5.126)$$

$$ALM_{4(H/D=1.2)} = 6.91 \times 10^2 \times G_{0,4}^{-1.00} \quad R^2 = 0.43 \quad (5.127)$$

$$ALM_{12(H/D=1.2)} = 1.38 \times 10^8 \times G_{0,12}^{-2.41} \quad R^2 = - \quad (5.128)$$

It can be observed that the sample with a dry unit weight of 14 kN/m<sup>3</sup>, fly ash content of 25%, and dolomitic lime content of 12% has presented a deviation from the rest of the samples, as it has lost a considerable amount of mass but still resulted in a relatively high stiffness ( $M_0$  and  $G_0$ ) than samples in which the mass loss was much less. These samples distinguish themselves from the first one, basically in lime content. A high lime content possibly helps in maintaining soil structure integrity, even when internal erosion takes place, whereas a few mass loss does not necessarily account for changes in soil structure, as the unstructured soil can be stucked inside a damaged soil mass, possibly with many cracks. It appears that the specimens with  $G_{0,1}$  greater than 3,000 MPa tend to present lower mass loss values up to 12 durability cycles.

## 5.4 BINDER KEY PARAMETER RESULTS

The binder key parameter is a normalization parameter that accounts for the effect of porosity and the binder (in the present research, fly ash plus lime) volume. Many specimens were evaluated, before and after experiencing durability cycles, but their analyzed key parameter was the one obtained from the moulding stage, that is, as the intent is the obtaining of a dosing relation, the adopted porosity and binder volume in the analysis corresponds to the moulding condition. In the  $\eta/(B_{iv})^{\text{exponent}}$  parameter, the exponent that best fits the equations was 0.13 as this exponent has resulted in higher coefficients of determination.

### 5.4.1 Unconfined Compressive strength x binder key parameter

The plots relating unconfined compressive strength to the binder key parameter are shown in figure 5.86. The calcitic lime treated specimens present, initially, a lower strength, but after the 12<sup>th</sup> cycle, there is a change in this trend.

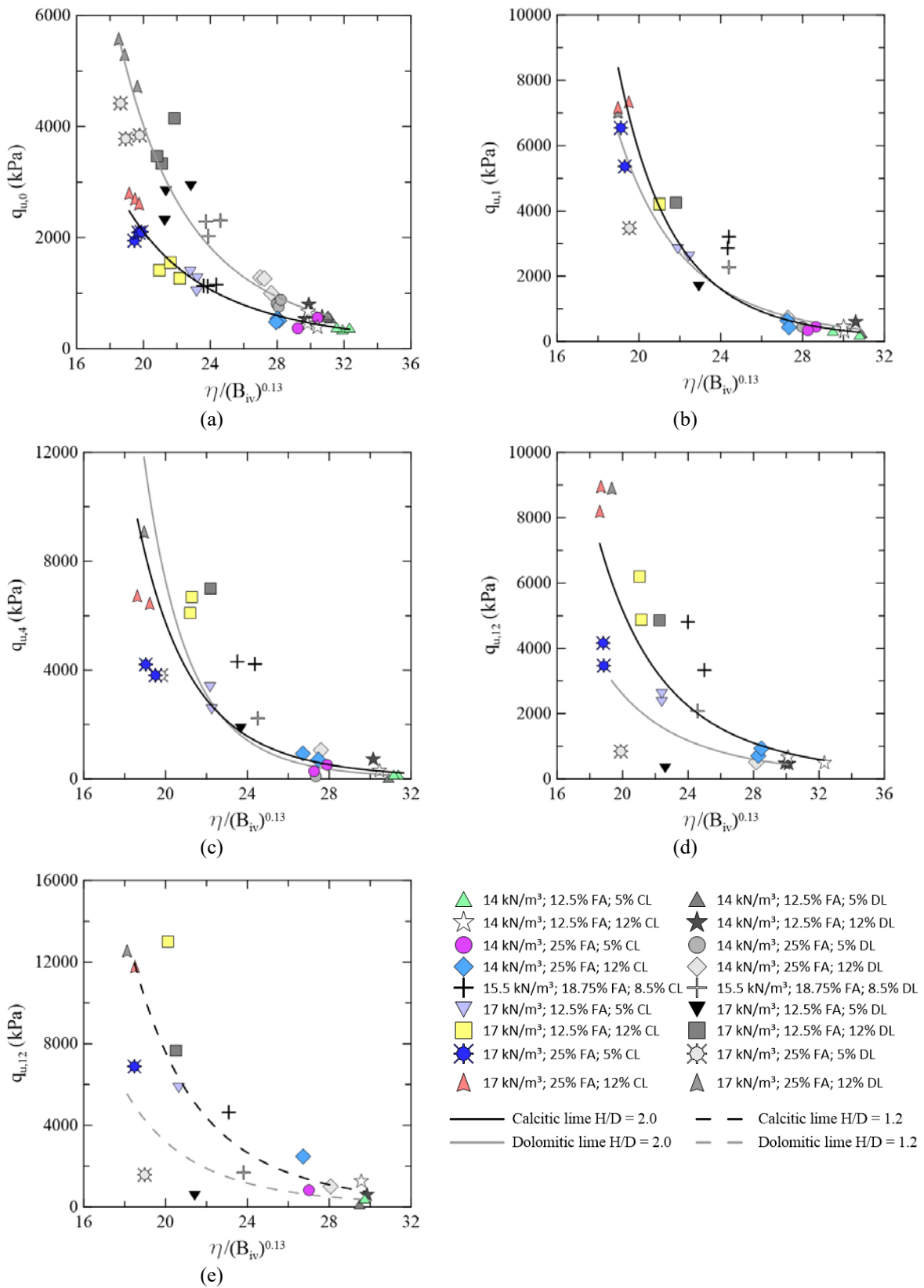


Figure 5.86: Relation between  $q_u$  and  $\eta/(B_{iv})^{0.13}$  after (a) 0 cycle (b) 1 cycle (c) 4 cycles (d) 12 cycles H/D ≈ 2.0 (e) 12 cycles H/D ≈ 1.2.

The corresponding equations for soils treated with calcitic lime are presented below:

$$q_{u,0 (H/D=2.0)} = 1.54 \times 10^8 \left[ \eta / (B_{iv})^{0.13} \right]^{-3.74} \quad R^2 = 0.95 \quad (5.129)$$

$$q_{u,1 (H/D=2.0)} = 8.39 \times 10^{12} \left[ \eta / (B_{iv})^{0.13} \right]^{-7.04} \quad R^2 = 0.94 \quad (5.130)$$

$$q_{u,4 (H/D=2.0)} = 1.02 \times 10^{13} \left[ \eta / (B_{iv})^{0.13} \right]^{-7.11} \quad R^2 = 0.85 \quad (5.131)$$

$$q_{u,12 (H/D=2.0)} = 4.84 \times 10^9 \left[ \eta / (B_{iv})^{0.13} \right]^{-6.00} \quad R^2 = 0.82 \quad (5.132)$$

$$q_{u,12 (H/D=1.2)} = 2.30 \times 10^{11} \left[ \eta / (B_{iv})^{0.13} \right]^{-5.75} \quad R^2 = 0.84 \quad (5.133)$$

For soils treated with dolomitic lime, the equations obtained from regression fit are presented next:

$$q_{u,0 (H/D=2.0)} = 1.73 \times 10^9 \left[ \eta / (B_{iv})^{0.13} \right]^{-4.33} \quad R^2 = 0.95 \quad (5.134)$$

$$q_{u,1 (H/D=2.0)} = 1.93 \times 10^{11} \left[ \eta / (B_{iv})^{0.13} \right]^{-5.85} \quad R^2 = 0.89 \quad (5.135)$$

$$q_{u,4 (H/D=2.0)} = 3.30 \times 10^{15} \left[ \eta / (B_{iv})^{0.13} \right]^{-8.96} \quad R^2 = 0.68 \quad (5.136)$$

$$q_{u,12 (H/D=2.0)} = 1.15 \times 10^9 \left[ \eta / (B_{iv})^{0.13} \right]^{-4.34} \quad R^2 = 0.39 \quad (5.137)$$

$$q_{u,12 (H/D=1.2)} = 5.02 \times 10^{10} \left[ \eta / (B_{iv})^{0.13} \right]^{-5.53} \quad R^2 = 0.60 \quad (5.138)$$

The regression equations for the calcitic lime treated soils have presented reasonable coefficients of determination values. After the fourth cycle, specimens with higher lime content seems to prevail over those with lower lime content, even if with higher fly ash content. The specimens stabilized with the dolomitic lime, from the 4<sup>th</sup> to the 12<sup>th</sup> cycle, have presented unacceptable  $R^2$  values, that may be a result of the prevailing of high lime content samples over the rest of them since the specimens with a lower dolomitic lime content have experienced several damages under durability cycles.

#### 5.4.2 Unconfined Compressive secant modulus x binder key parameter

When an engineering design is limited by soil strains, it is fundamental to know information about soil compressibility. Even though the modulus was determined for the ultimate loading state instead of working load, it is an indication of soil compressibility and it is also important to outline a behaviour path. Results after durability cycles of the unconfined compressive secant modulus ( $E_{sec}$ ) against  $\eta/(B_{iv})^{0.13}$  are presented in figure 5.87.

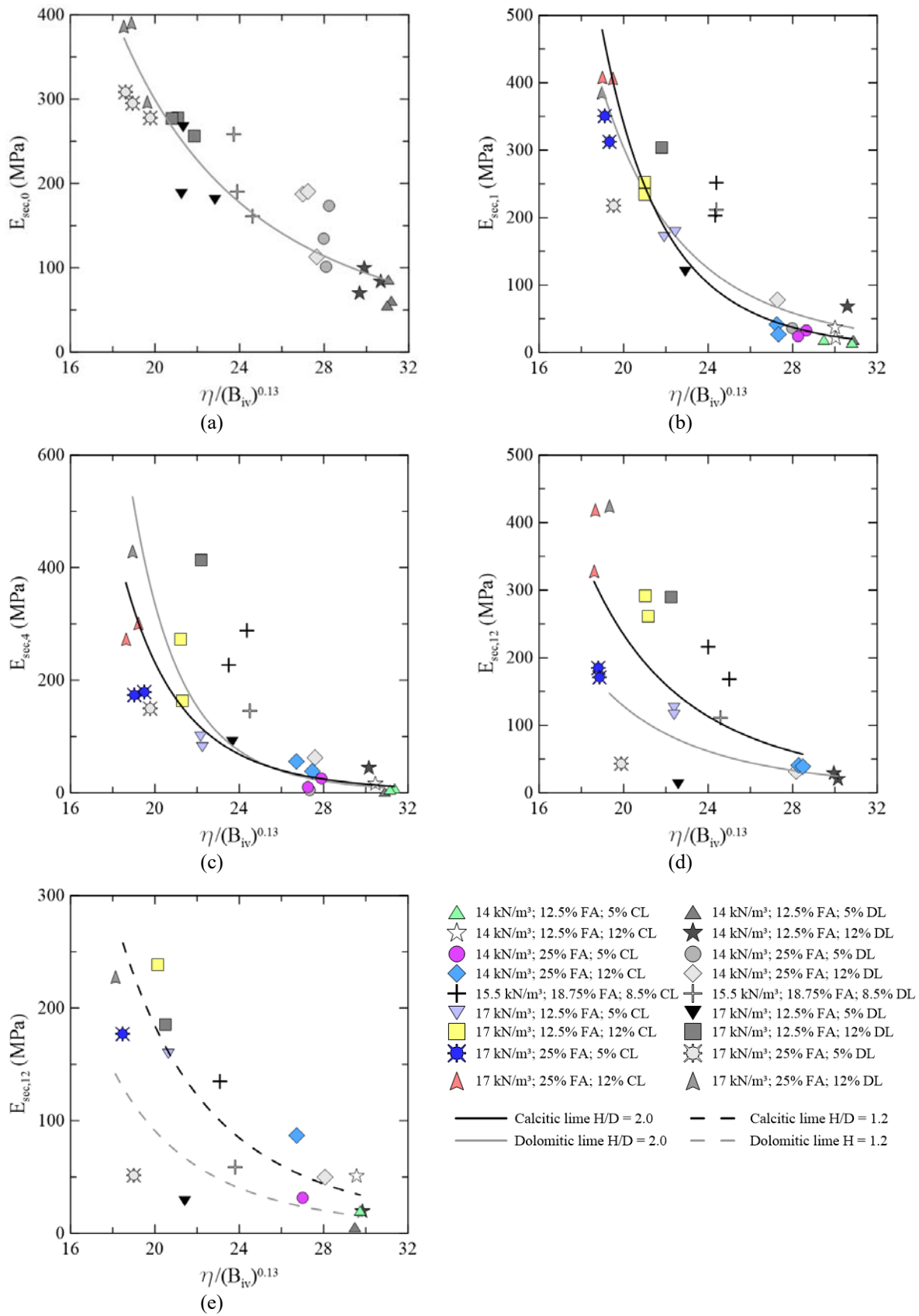


Figure 5.87: Relation between  $E_{sec}$  and  $\eta/(B_{iv})^{0.13}$  after (a) 0 cycle (b) 1 cycle (c) 4 cycles (d) 12 cycles  $H/D \approx 2.0$  (e) 12 cycles  $H/D \approx 1.2$ .

The corresponding fit equations for soils treated with the calcitic lime are presented below:

$$E_{\text{sec},1 (H/D=2.0)} = 1.20 \times 10^{11} \left[ \eta / (B_{iv})^{0.13} \right]^{-6.57} \quad R^2 = 0.90 \quad (5.139)$$

$$E_{\text{sec},4 (H/D=2.0)} = 1.17 \times 10^{11} \left[ \eta / (B_{iv})^{0.13} \right]^{-6.69} \quad R^2 = 0.77 \quad (5.140)$$

$$E_{\text{sec},12 (H/D=2.0)} = 3.64 \times 10^7 \left[ \eta / (B_{iv})^{0.13} \right]^{-3.99} \quad R^2 = 0.67 \quad (5.141)$$

$$E_{\text{sec},12 (H/D=1.2)} = 6.42 \times 10^7 \left[ \eta / (B_{iv})^{0.13} \right]^{-4.26} \quad R^2 = 0.78 \quad (5.142)$$

For soils treated with the dolomitic lime, the equations obtained from regression curve fitting are shown below:

$$E_{\text{sec},0 (H/D=2.0)} = 1.62 \times 10^6 \left[ \eta / (B_{iv})^{0.13} \right]^{-2.87} \quad R^2 = 0.85 \quad (5.143)$$

$$E_{\text{sec},1 (H/D=2.0)} = 6.99 \times 10^8 \left[ \eta / (B_{iv})^{0.13} \right]^{-4.89} \quad R^2 = 0.77 \quad (5.144)$$

$$E_{\text{sec},4 (H/D=2.0)} = 1.77 \times 10^{13} \left[ \eta / (B_{iv})^{0.13} \right]^{-8.24} \quad R^2 = 0.61 \quad (5.145)$$

$$E_{\text{sec},12 (H/D=2.0)} = 2.18 \times 10^7 \left[ \eta / (B_{iv})^{0.13} \right]^{-4.02} \quad R^2 = 0.31 \quad (5.146)$$

$$E_{\text{sec},12 (H/D=1.2)} = 6.14 \times 10^7 \left[ \eta / (B_{iv})^{0.13} \right]^{-4.48} \quad R^2 = 0.56 \quad (5.147)$$

As presented in chapter 5.2, the effect of durability cycles was more evident on secant modulus than on strength response. This higher effect of lime content and low effect of fly ash on secant modulus is probably associated with lower coefficients of determination shown above.

### 5.4.3 Small strain constraint modulus x binder key parameter

The plots relating  $M_0$  to  $\eta/B_{iv}$  throughout durability wetting-drying cycles for samples with height/diameter of approximately 2 are shown in figure 5.88. Caution must be taken when interpreting a trend or comparison between the two lime treated soils, since after a given number of durability cycles, P-waves travel time cannot be determined for some specimens, and the fit regression curve can be misinterpreted.

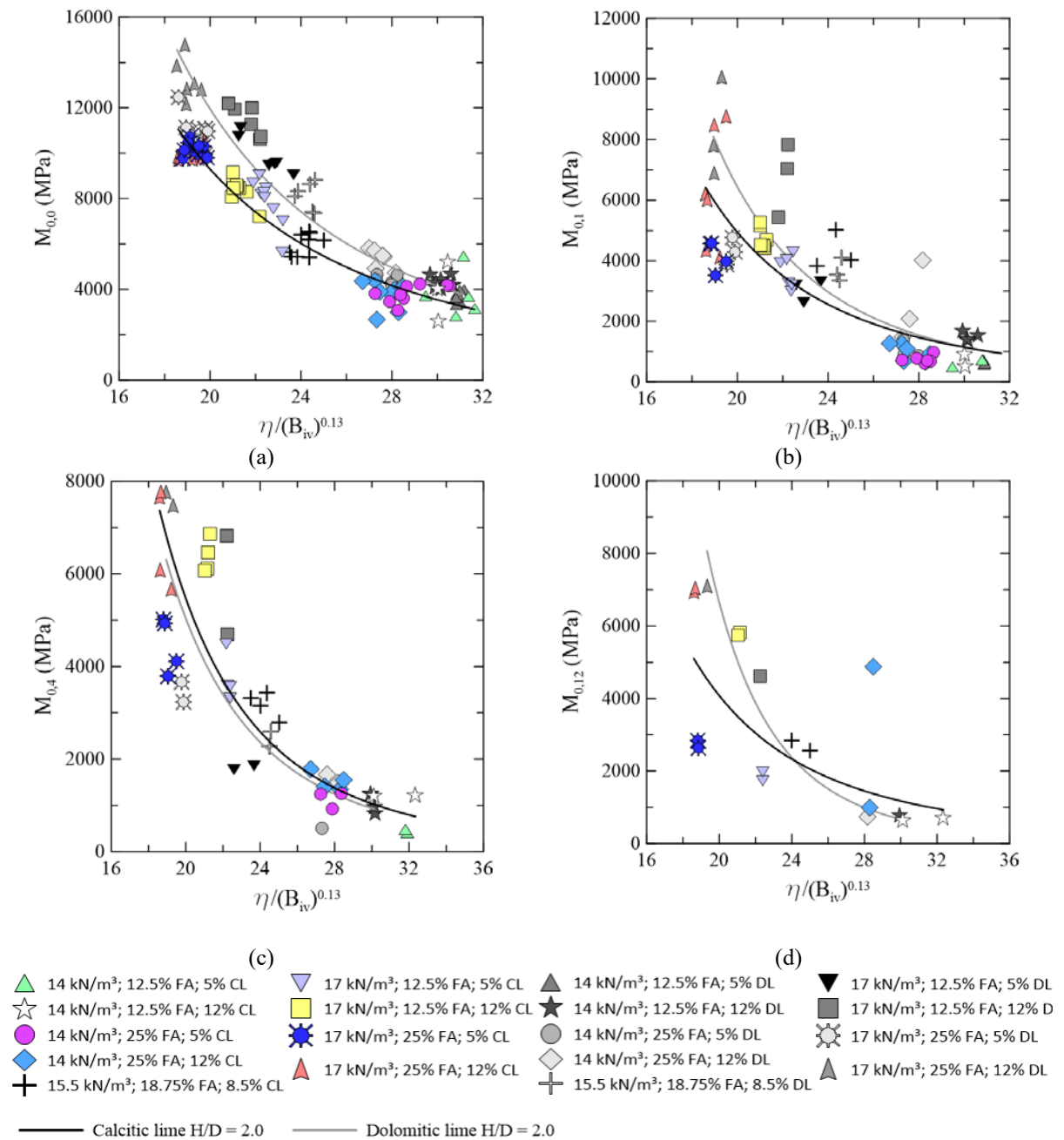


Figure 5.88: Relation between  $M_0$  and  $\eta/(B_{iv})^{0.13}$  for samples with  $H/D \approx 2.0$  after (a) 0 cycle (b) 1 cycle (c) 4 cycles (d) 12 cycles.

The corresponding equations for soils treated with calcitic lime are presented below:

$$M_{0,0 (H/D=2.0)} = 1.16 \times 10^7 \left[ \eta / (B_{iv})^{0.13} \right]^{-2.38} \quad R^2 = 0.88 \quad (5.148)$$

$$M_{0,1 (H/D=2.0)} = 2.46 \times 10^8 \left[ \eta / (B_{iv})^{0.13} \right]^{-3.61} \quad R^2 = 0.52 \quad (5.149)$$

$$M_{0,4 (H/D=2.0)} = 1.18 \times 10^9 \left[ \eta / (B_{iv})^{0.13} \right]^{-4.10} \quad R^2 = 0.85 \quad (5.150)$$

$$M_{0,12 (H/D=2.0)} = 4.02 \times 10^7 \left[ \eta / (B_{iv})^{0.13} \right]^{-3.07} \quad R^2 = 0.52 \quad (5.151)$$

For soils treated with dolomitic lime, the resulted expressions from regression curve fitting are shown from equation (5.152) to equation (5.155).

$$M_{0,0 (H/D=2.0)} = 2.97 \times 10^7 \left[ \eta / (B_{iv})^{0.13} \right]^{-2.61} \quad R^2 = 0.93 \quad (5.152)$$

$$M_{0,1 (H/D=2.0)} = 2.11 \times 10^9 \left[ \eta / (B_{iv})^{0.13} \right]^{-4.24} \quad R^2 = 0.75 \quad (5.153)$$

$$M_{0,4 (H/D=2.0)} = 1.26 \times 10^9 \left[ \eta / (B_{iv})^{0.13} \right]^{-4.15} \quad R^2 = 0.72 \quad (5.154)$$

$$M_{0,12 (H/D=2.0)} = 1.49 \times 10^{11} \left[ \eta / (B_{iv})^{0.13} \right]^{-5.65} \quad R^2 = 0.96 \quad (5.155)$$

The higher volume specimens, which have undergone durability cycles including a brushing stage, are shown separately, as illustrated by Figure 5.89, relating small strain constraint modulus and the binder key parameter. The same data dispersion observed in smaller (and slender) specimens appears in high volume specimens after cycles, however, before the initiation of the durability cycles, both calcitic and dolomitic lime treated soils present almost the same stiffness response.



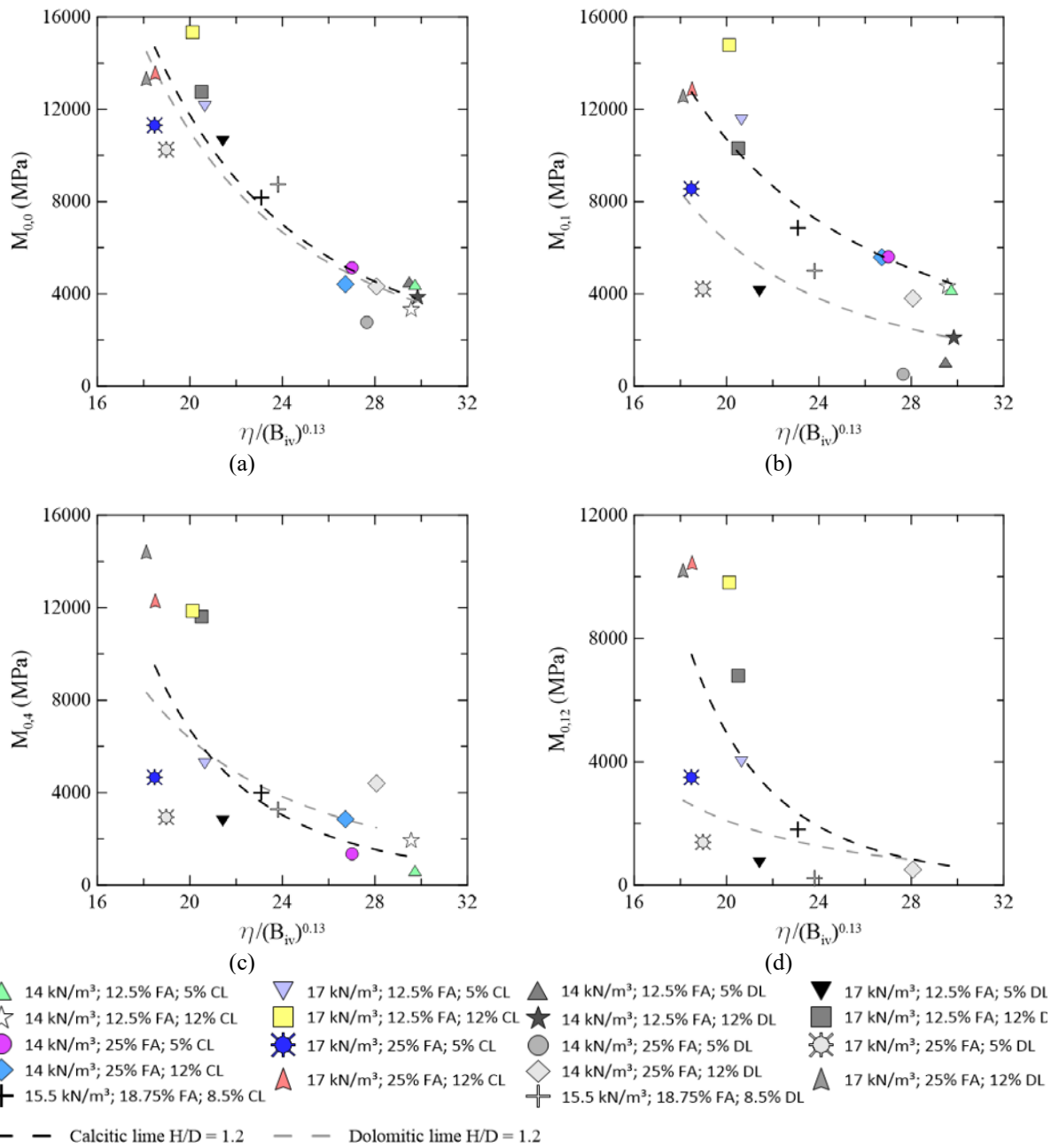


Figure 5.89: Relation between  $M_0$  and  $\eta/(B_{iv})^{0.13}$  for samples with  $H/D \approx 1.2$  after (a) 0 cycle (b) 1 cycle (c) 4 cycles (d) 12 cycles.

The regression equations for specimens with a slenderness relation of 1.2, stabilized with the calcitic lime, are presented below.

$$M_{0,0(H/D=1.2)} = 5.65 \times 10^7 \left[ \eta / (B_{iv})^{0.13} \right]^{-2.83} \quad R^2 = 0.91 \quad (5.156)$$

$$M_{0,1 (H/D=1.2)} = 8.03 \times 10^6 \left[ \eta / (B_{iv})^{0.13} \right]^{-2.21} \quad R^2 = 0.82 \quad (5.157)$$

$$M_{0,4 (H/D=1.2)} = 3.26 \times 10^9 \left[ \eta / (B_{iv})^{0.13} \right]^{-4.37} \quad R^2 = 0.76 \quad (5.158)$$

$$M_{0,12 (H/D=1.2)} = 3.25 \times 10^{10} \left[ \eta / (B_{iv})^{0.13} \right]^{-5.24} \quad R^2 = 0.42 \quad (5.159)$$

Soils treated with the dolomitic lime have a relation with the binder key parameter expressed by the following equations.

$$M_{0,0 (H/D=1.2)} = 4.30 \times 10^7 \left[ \eta / (B_{iv})^{0.13} \right]^{-2.76} \quad R^2 = 0.84 \quad (5.160)$$

$$M_{0,1 (H/D=1.2)} = 1.01 \times 10^9 \left[ \eta / (B_{iv})^{0.13} \right]^{-3.98} \quad R^2 = 0.58 \quad (5.161)$$

$$M_{0,4 (H/D=1.2)} = 1.32 \times 10^6 \left[ \eta / (B_{iv})^{0.13} \right]^{-1.80} \quad R^2 = 0.16 \quad (5.162)$$

$$M_{0,12 (H/D=1.2)} = 1.70 \times 10^{12} \left[ \eta / (B_{iv})^{0.13} \right]^{-6.81} \quad R^2 = 0.52 \quad (5.163)$$

By observing the regression equations after the application of durability cycles, especially for the samples stabilized using the dolomitic lime, which experienced greater damage than the stabilized materials using the calcitic lime, there is a large dispersion, and maybe the  $\eta/B_{iv}$  parameter is no suitable for the analysis of soil constraint stiffness after durability cycles.

#### 5.4.4 Small strain shear modulus x binder key parameter

Small strain shear modulus against binder key parameter plot results are shown in figure 5.90. Those plot curves correspond to specimens with  $H/D \approx 2.0$ . There is an increase in dispersion data throughout the cycles, but they are still reasonably correlated, unlike the small strain constraint modules.

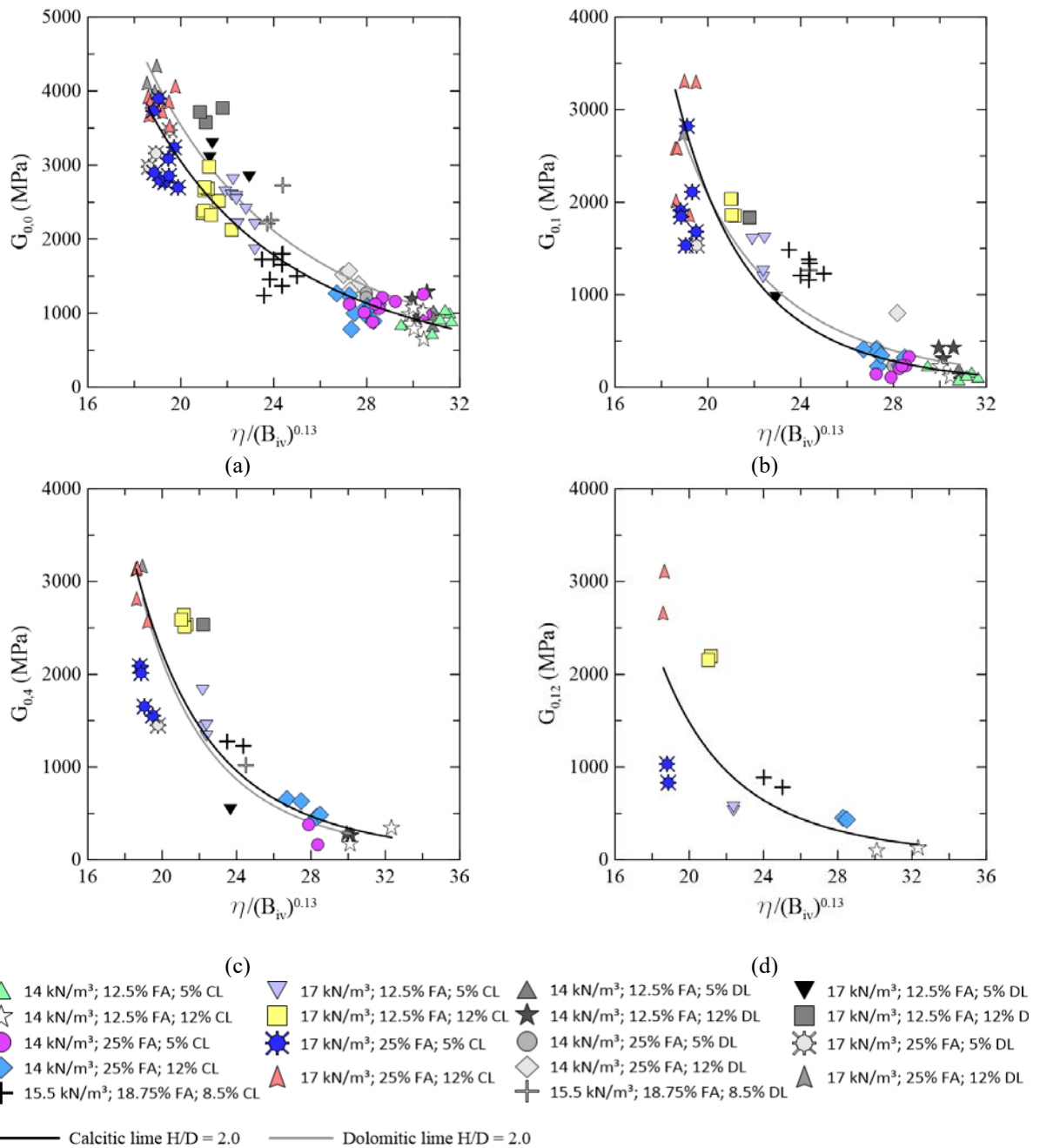


Figure 5.90: Relation between  $G_0$  and  $\eta/(B_{iv})^{0.13}$  for samples with  $H/D \approx 2.0$  after (a) 0 cycle (b) 1 cycle (c) 4 cycles (d) 12 cycles.

The fitting equations of soils treated with calcitic lime are presented below:

$$G_{0,0 (H/D=2.0)} = 2.04 \times 10^7 \left[ \eta / (B_{iv})^{0.13} \right]^{-2.94} \quad R^2 = 0.92 \quad (5.164)$$

$$G_{0,1 (H/D=2.0)} = 1.12 \times 10^{11} \left[ \eta / (B_{iv})^{0.13} \right]^{-5.94} \quad R^2 = 0.87 \quad (5.165)$$

$$G_{0,4 (H/D=2.0)} = 2.43 \times 10^9 \left[ \eta / (B_{iv})^{0.13} \right]^{-4.64} \quad R^2 = 0.83 \quad (5.166)$$

$$G_{0,12 (H/D=2.0)} = 1.39 \times 10^9 \left[ \eta / (B_{iv})^{0.13} \right]^{-4.59} \quad R^2 = 0.72 \quad (5.167)$$

Curve fits of soils treated with dolomitic lime are mathematically expressed by the following equations.  $G_0$  values after 12 wetting-drying cycles were not determined.

$$G_{0,0 (H/D=2.0)} = 1.70 \times 10^7 \left[ \eta / (B_{iv})^{0.13} \right]^{-2.83} \quad R^2 = 0.91 \quad (5.168)$$

$$G_{0,1 (H/D=2.0)} = 5.07 \times 10^9 \left[ \eta / (B_{iv})^{0.13} \right]^{-4.91} \quad R^2 = 0.81 \quad (5.169)$$

$$G_{0,4 (H/D=2.0)} = 6.48 \times 10^9 \left[ \eta / (B_{iv})^{0.13} \right]^{-4.98} \quad R^2 = 0.82 \quad (5.170)$$

Plotted results of specimens with  $H/D \approx 1.2$  are presented in figure 5.91, relating small strain shear modulus ( $G_0$ ) to the binder key parameter  $[\eta/(B_{iv})^{0.13}]$  along durability cycles. A similar trend observed for  $M_0$  is now observed for  $G_0$ .

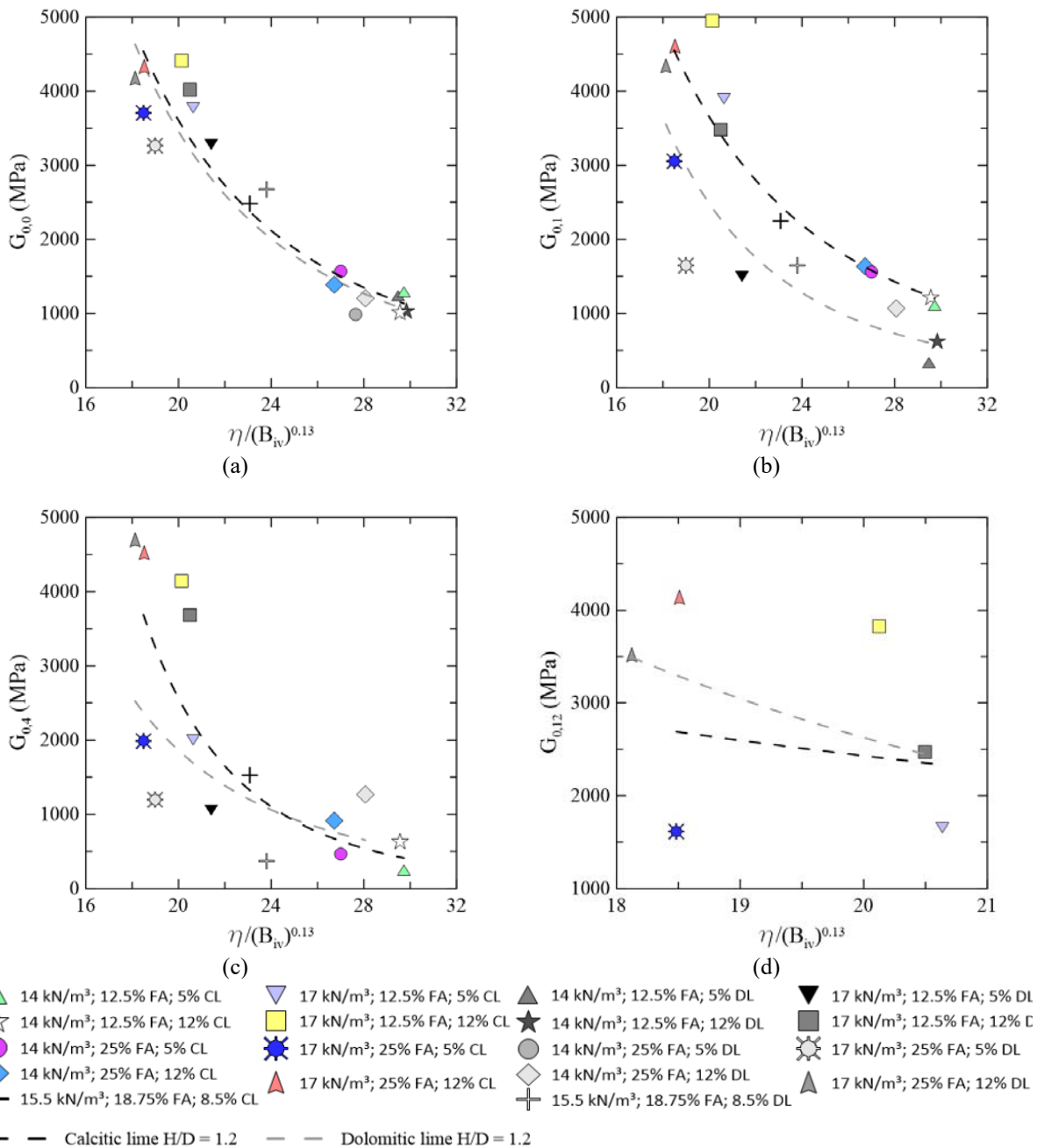


Figure 5.91: Relation between  $G_0$  and  $\eta/(B_{iv})^{0.13}$  for samples with  $H/D \approx 1.2$  after (a) 0 cycle (b) 1 cycle (c) 4 cycles (d) 12 cycles.

The fitting equations of soils treated with calcitic lime are presented below:

$$G_{0,0 (H/D=1.2)} = 2.27 \times 10^7 \left[ \eta / (B_{iv})^{0.13} \right]^{-2.92} \quad R^2 = 0.94 \quad (5.171)$$

$$G_{0,1 (H/D=1.2)} = 1.56 \times 10^7 \left[ \eta / (B_{iv})^{0.13} \right]^{-2.79} \quad R^2 = 0.89 \quad (5.172)$$

$$G_{0,4 (H/D=1.2)} = 2.63 \times 10^9 \left[ \eta / (B_{iv})^{0.13} \right]^{-4.62} \quad R^2 = 0.83 \quad (5.173)$$

$$G_{0,12 (H/D=1.2)} = 1.16 \times 10^5 \left[ \eta / (B_{iv})^{0.13} \right]^{-1.29} \quad R^2 = 0.02 \quad (5.174)$$

The curve fit of soils treated with dolomitic lime is mathematically expressed by the following equations.

$$G_{0,0 (H/D=1.2)} = 2.60 \times 10^7 \left[ \eta / (B_{iv})^{0.13} \right]^{-2.98} \quad R^2 = 0.90 \quad (5.175)$$

$$G_{0,1 (H/D=1.2)} = 1.35 \times 10^8 \left[ \eta / (B_{iv})^{0.13} \right]^{-3.64} \quad R^2 = 0.76 \quad (5.176)$$

$$G_{0,4 (H/D=1.2)} = 1.95 \times 10^7 \left[ \eta / (B_{iv})^{0.13} \right]^{-3.09} \quad R^2 = 0.28 \quad (5.177)$$

$$G_{0,12 (H/D=1.2)} = 1.51 \times 10^7 \left[ \eta / (B_{iv})^{0.13} \right]^{-2.89} \quad R^2 = - \quad (5.178)$$

#### 5.4.5 Small strain Poisson's ratio x binder key parameter

Poisson's ratio is a very important parameter in the study of a soil/rock deformability earth pressure, but earth pressure determination is not achieved by the most common geotechnical low-stress tests. Small strain Poisson's ratio ( $\nu_0$ ) can be helpful in the assessment of deformability behaviour, but it may not always lead to a very accurate assessment. Its interpretation needs both P-waves and S-waves velocity, hence, the most accurate S-wave reading is in a fully saturated or in completely dry soil (no matric suction), and the most accurate P-wave reading is in dry soils, but neither of that conditions was achieved during the present research. So, the results shown in figure 5.92 and 5.93 do not claim to be exactly accurate values, but only a path indication.

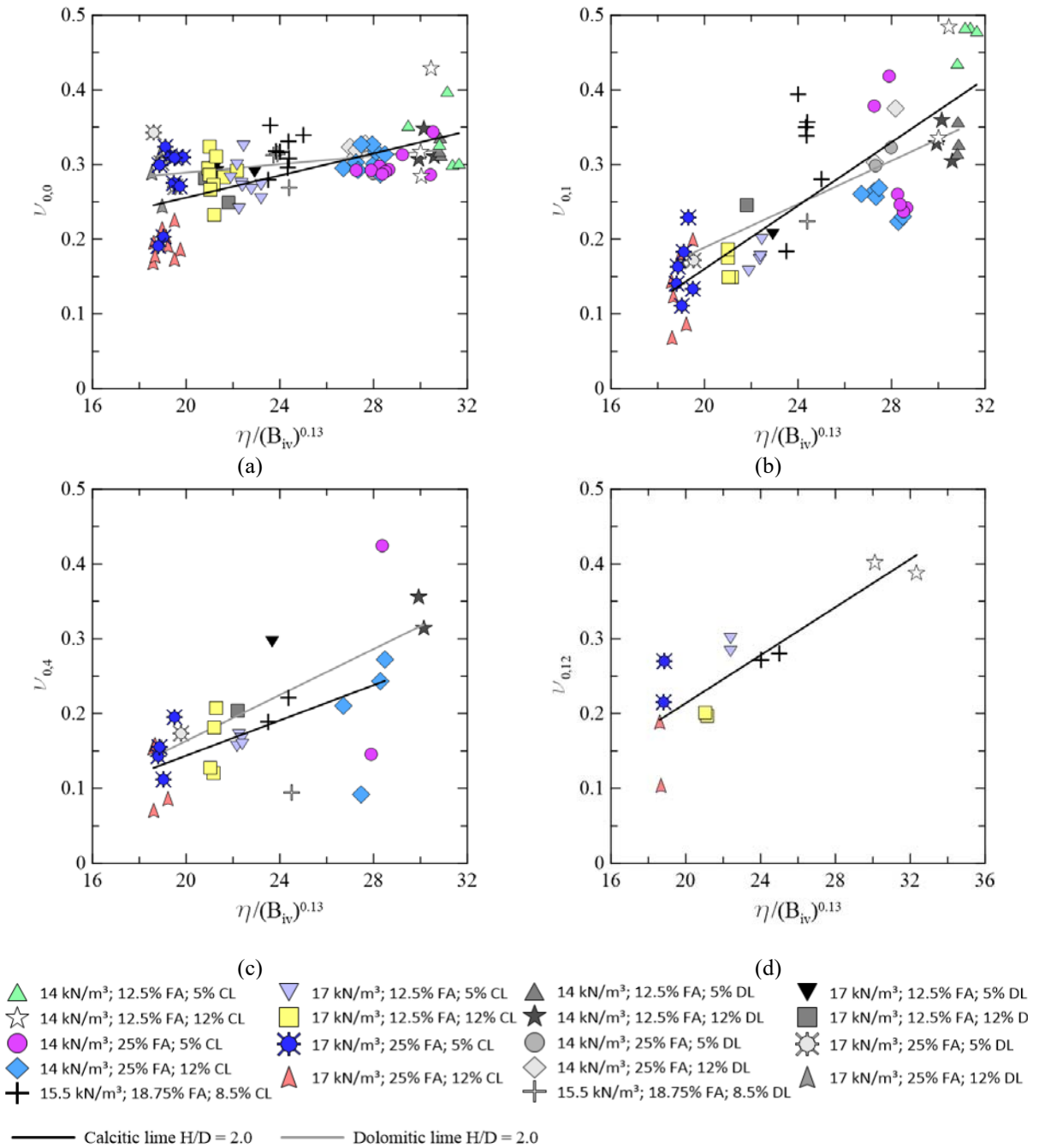


Figure 5.92: Relation between  $\nu_0$  and  $\eta/(B_{iv})^{0.13}$  for samples with  $H/D \approx 2.0$  after (a) 0 cycle (b) 1 cycle (c) 4 cycles (d) 12 cycles.

It can be observed that when there is a high moisture content in the specimens (approximately 10% due to moulding), the small strain Poisson's ratio indicates a very low variation when compared to the values determined after cycles (lower moisture content). That response is possibly associated with the water effect on P-waves travel time, turning the structure travel-time less distinguishable from the water phase. It was observed that the stiffer specimens

present usually a  $\nu_0$  value around 0.1 to 0.2, whereas the less stiff specimens present a small strain Poisson's ratio, around 0.3 to 0.5. When the structure of the specimens is affected by the durability cycles, a grown in the Poisson's ratio is observed. When the stiffer specimens are evaluated, the ones stabilized using the calcitic lime seem to present lower Poisson's ratios.

From the specimens with a lower slenderness ratio ( $H/D \approx 1.2$ ), results of small strain Poisson's ratio against  $\eta/B_{iv}$  throughout durability cycles are presented in figure 5.93.

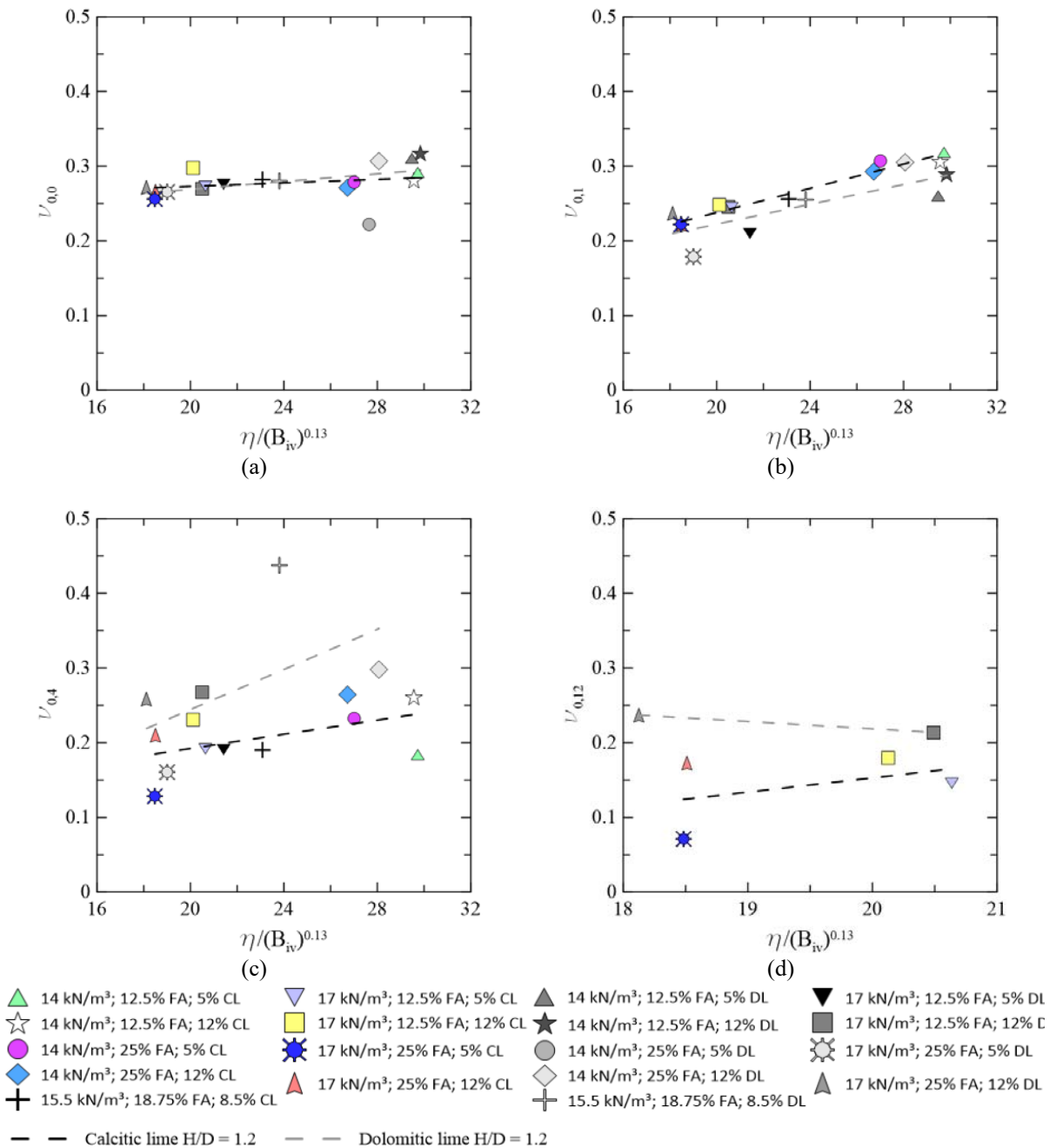


Figure 5.93: Relation between  $\nu_0$  and  $\eta/(B_{iv})^{0.13}$  for samples with  $H/D \approx 1.2$  after (a) 0 cycle (b) 1 cycle (c) 4 cycles (d) 12 cycles.



As can be seen by observing the plots and equations, before the durability cycles, probably due to high water content,  $v_0$  is approximately constant. The overall range of the small strain Poisson's ratio is about from 0.15 to 0.30. There is great variability in Poisson's ratio data, especially after 4 cycles, turning its precise determination difficult. However, an approximation can be achieved by observing the tests range. Also, a tenuous trend of increasing Poisson's ratio as  $\eta/B_{iv}$  increases can be noted.

#### 5.4.6 Accumulated loss of mass x binder key parameter

When a geotechnical design is developed, the related geomaterials must attend to the designed lifetime. That includes most of the time integrity and soil mass maintenance. Even if the strength is maintained constant, but a sample diameter has reduced by half, the load capacity is reduced to 25% of the initial due to the loss of mass, so it is very important to assess not only the changes in mechanical properties but also the mass loss. The accumulated loss of mass of the studied soil may behave according to the plots presented in figure 5.94 after wetting-drying-brushing durability cycles.

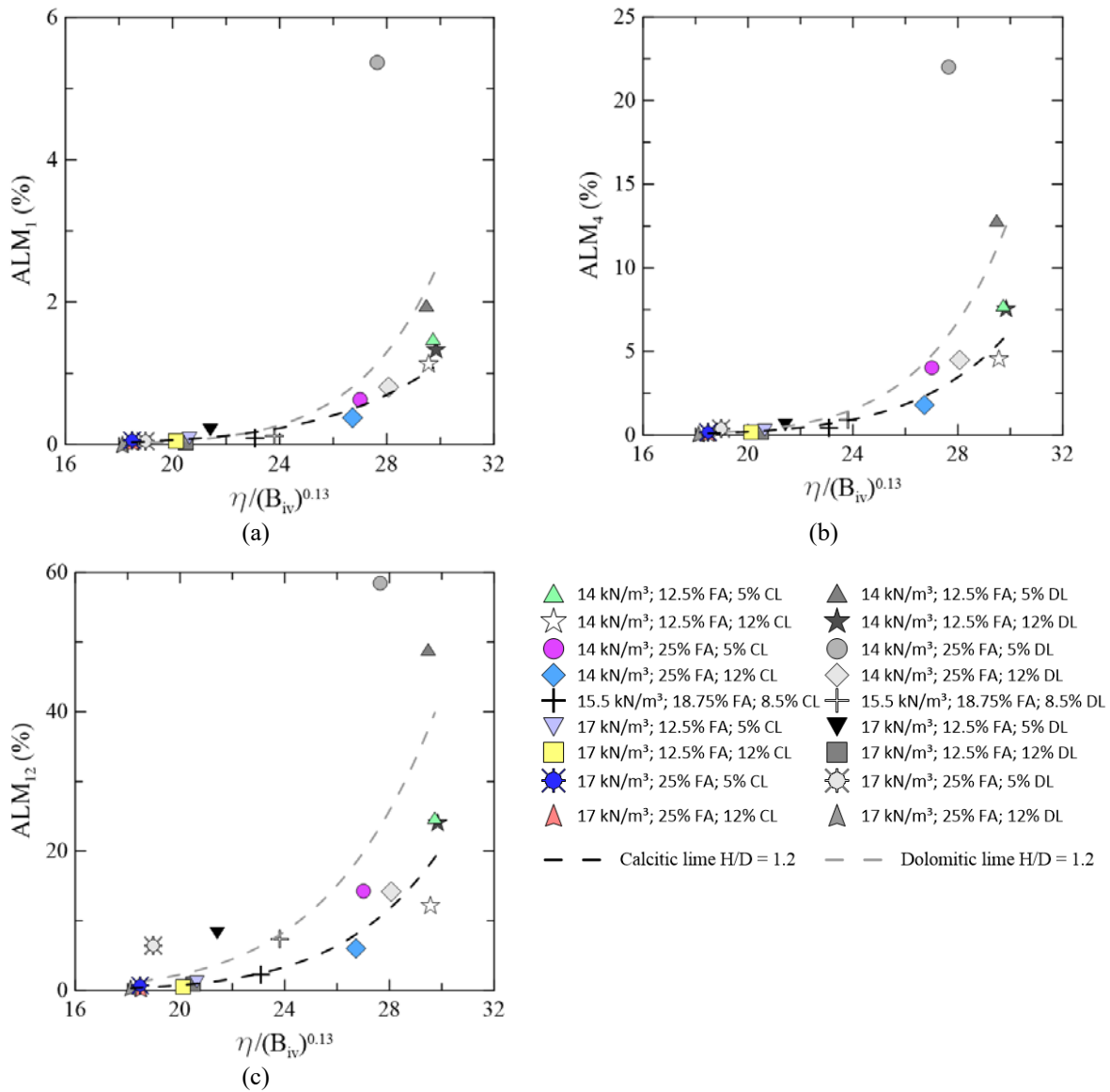


Figure 5.94: Relation between ALM and  $\eta/(B_{iv})^{0.13}$  for samples with  $H/D \approx 1.2$  after (a) 1 cycle (b) 4 cycles (c) 12 cycles.

The following equations could indicate a dosage methodology to account for the mass loss as a consequence of climate and erosive effects. Equations (5.179) to (5.181) express the response for calcitic lime stabilization, while equations from (5.182) to (5.184) express the ALM response for the stabilization using dolomitic lime.

$$ALM_{1(H/D=1.2)} = 2.66 \times 10^{-11} \left[ \eta / (B_{iv})^{0.13} \right]^{7.20} \quad R^2 = 0.94 \quad (5.179)$$

$$ALM_{4(H/D=1.2)} = 1.67 \times 10^{-12} \left[ \eta / (B_{iv})^{0.13} \right]^{8.51} \quad R^2 = 0.96 \quad (5.180)$$

$$ALM_{12(H/D=1.2)} = 2.08 \times 10^{-11} \left[ \eta / (B_{iv})^{0.13} \right]^{8.12} \quad R^2 = 0.94 \quad (5.181)$$

$$ALM_{1(H/D=1.2)} = 3.14 \times 10^{-15} \left[ \eta / (B_{iv})^{0.13} \right]^{10.10} \quad R^2 = 0.85 \quad (5.182)$$

$$ALM_{4(H/D=1.2)} = 7.34 \times 10^{-14} \left[ \eta / (B_{iv})^{0.13} \right]^{9.65} \quad R^2 = 0.88 \quad (5.183)$$

$$ALM_{12(H/D=1.2)} = 8.59 \times 10^{-10} \left[ \eta / (B_{iv})^{0.13} \right]^{7.24} \quad R^2 = 0.73 \quad (5.184)$$

The accumulated loss of mass is greater for specimens treated with the dolomitic lime when the same dosage is compared to the calcitic lime treated mixtures. There is a significant reduction in mass loss when the higher lime content (12%) is used, especially when the dolomitic lime is used in the admixture.

#### 5.4.7 Binder key parameter evaluation

Before being exposed to durability cycles (0 cycles), the regression curve fit shape is different from the curves after durability cycles when the curve concavity is increased. For almost all the evaluated parameters, there was a great reduction in the coefficient of determination ( $R^2$ ) as the number of cycles increases. However, a change in exponent does not solve this issue, as the amount of lime has shown to play a very important role in durability, regarding the adopted dosage in the present research. With that, and as the effect of the combination lime-pozzolana is not well known, it is suggested that the binder key parameter relations may be used in association with relations from the lime key parameter in the dosing design when durability is evaluated.

## 5.5 LIME KEY PARAMETER RESULTS

To account for the huge effect of lime on durability, the relation between the key parameter  $\eta/L_{iv}$  was also evaluated. Herein, as this lime effect increases as soon as durability cycles are applied to the samples, the parameter  $\eta/(L_{iv}^e)$  must change. This change was considered by the variation in the exponent “ $e$ ”, according to the regression fitting. Still, as this exponent has shown to present different values for the samples treated with calcitic lime than for soils treated with dolomitic lime, the comparison between both became less illustrative. The adopted exponents are presented in table 5.1 for both the calcitic and dolomitic treated samples.

Table 5.1: Exponent values in lime key parameter relations.

Number of cycles	Exponent	
	Calcitic lime stabilization	Dolomitic lime stabilization
0	0.04	0.08
1	0.05	0.14
4	0.12	0.24
12	0.19	0.54

### 5.5.1 Unconfined Compressive strength x lime key parameter

Unconfined compressive strength is related to the lime key parameter as shown in figure 5.95, which presents results from calcitic lime treated materials. The exponential relation seems to be suitable to represent the relation between the lime key parameter and the unconfined compressive strength even after the durability cycles. The specimens stabilized using a higher calcitic lime content seem to be less affected by the durability cycle damage.

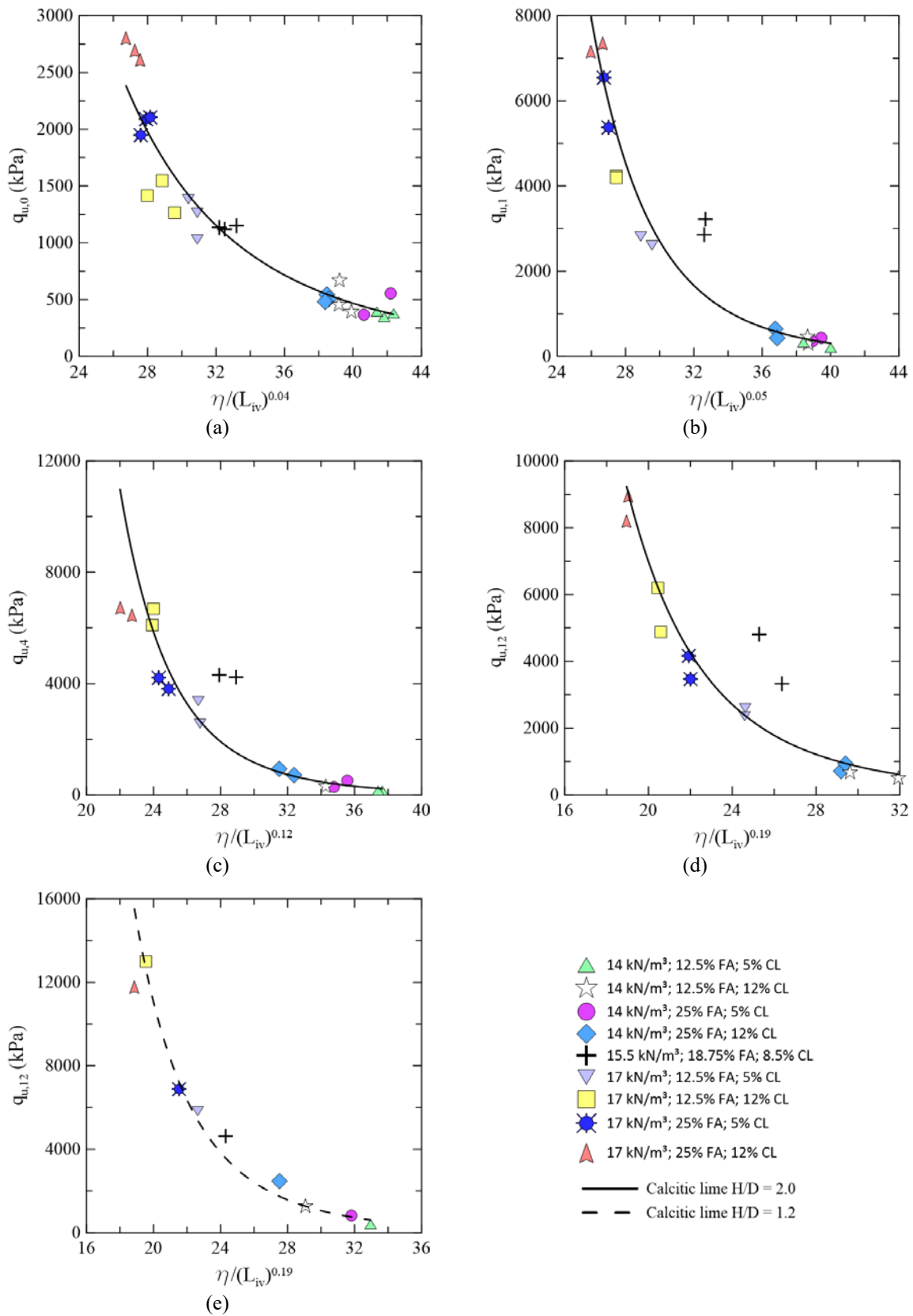


Figure 5.95: Relation between  $q_u$  and  $\eta/(L_{iv})^e$  for calcitic lime treated soils after (a) 0 cycle (b) 1 cycle (c) 4 cycles (d) 12 cycles  $H/D \approx 2.0$  (e) 12 cycles  $H/D \approx 1.2$ .

The corresponding equations are presented below. All of them have presented a coefficient of determination greater than or equal to 0.87.

$$q_{u,0 (H/D=2.0)} = 1.39 \times 10^9 \left[ \eta / (L_{iv})^{0.04} \right]^{-4.04} \quad R^2 = 0.94 \quad (5.185)$$

$$q_{u,1 (H/D=2.0)} = 3.35 \times 10^{14} \left[ \eta / (L_{iv})^{0.05} \right]^{-7.51} \quad R^2 = 0.94 \quad (5.186)$$

$$q_{u,4 (H/D=2.0)} = 5.76 \times 10^{13} \left[ \eta / (L_{iv})^{0.12} \right]^{-7.24} \quad R^2 = 0.91 \quad (5.187)$$

$$q_{u,12 (H/D=2.0)} = 4.07 \times 10^{10} \left[ \eta / (L_{iv})^{0.19} \right]^{-5.20} \quad R^2 = 0.87 \quad (5.188)$$

$$q_{u,12 (H/D=1.2)} = 3.77 \times 10^{11} \left[ \eta / (L_{iv})^{0.19} \right]^{-5.79} \quad R^2 = 0.96 \quad (5.189)$$

As the exponents are different, the calcitic lime treated soils are plotted separately from the dolomitic stabilized specimens. The results of  $q_u$  from soils treated with dolomitic lime are shown in figure 5.96.

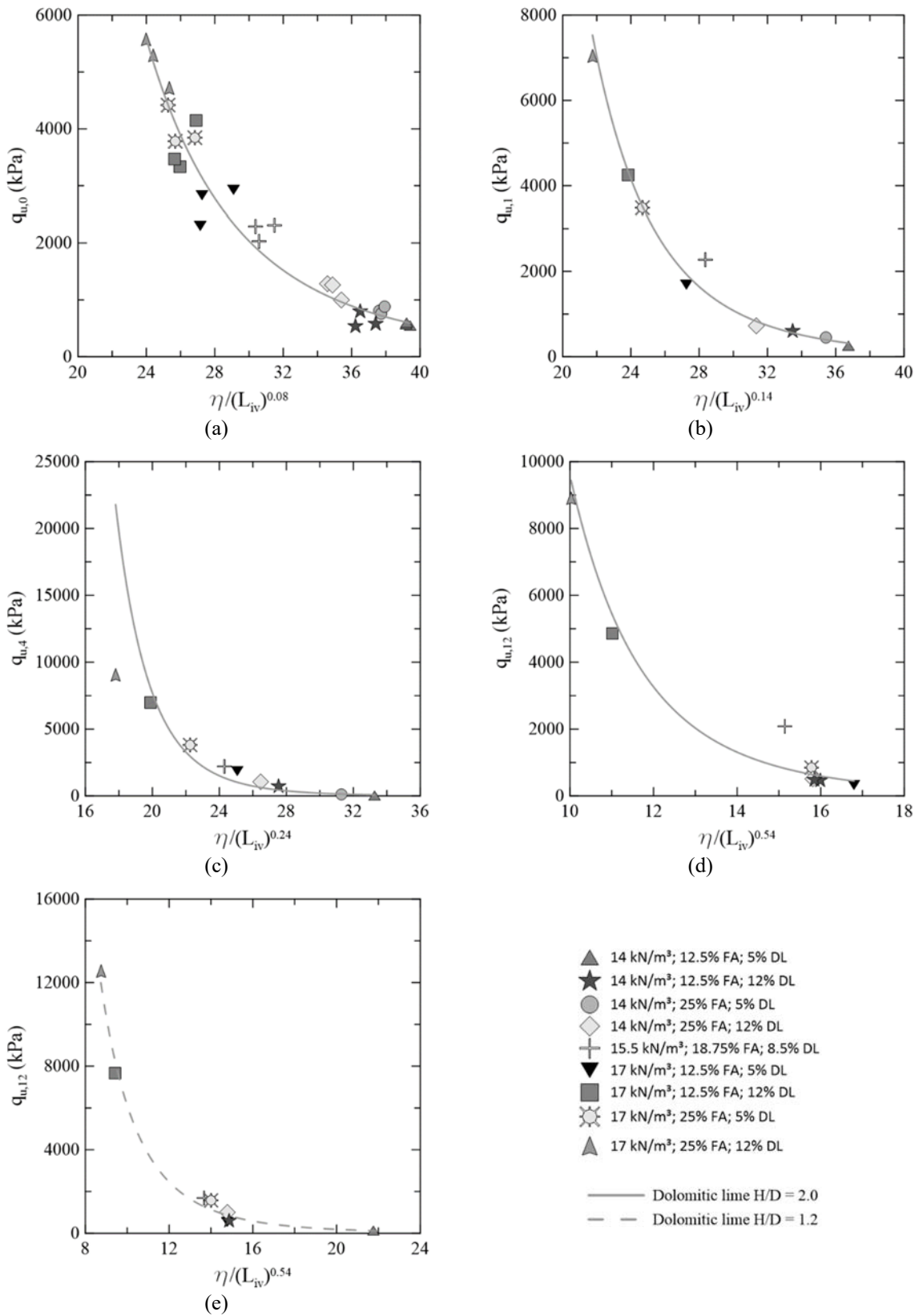


Figure 5.96: Relation between  $q_u$  and  $\eta/(L_{iv})^e$  for dolomitic lime treated soils after (a) 0 cycle (b) 1 cycle (c) 4 cycles (d) 12 cycles  $H/D \approx 2.0$  (e) 12 cycles  $H/D \approx 1.2$ .

After the 12<sup>th</sup> cycle, there is significant decay in the strength of all the materials, except for two with 17 kN/m<sup>3</sup> dry unit weight and 12% of dolomitic lime content. The  $q_u$  response throughout durability cycles can be expressed by the following equations.

$$q_{u,0 (H/D=2.0)} = 9.66 \times 10^9 \left[ \eta / (L_{iv})^{0.08} \right]^{-4.52} \quad R^2 = 0.95 \quad (5.190)$$

$$q_{u,1 (H/D=2.0)} = 8.74 \times 10^{11} \left[ \eta / (L_{iv})^{0.14} \right]^{-6.03} \quad R^2 = 0.97 \quad (5.191)$$

$$q_{u,4 (H/D=2.0)} = 3.30 \times 10^{15} \left[ \eta / (L_{iv})^{0.24} \right]^{-8.94} \quad R^2 = 0.89 \quad (5.192)$$

$$q_{u,12 (H/D=2.0)} = 7.98 \times 10^9 \left[ \eta / (L_{iv})^{0.54} \right]^{-5.92} \quad R^2 = 0.88 \quad (5.193)$$

$$q_{u,12 (H/D=1.2)} = 6.12 \times 10^8 \left[ \eta / (L_{iv})^{0.54} \right]^{-5.00} \quad R^2 = 0.96 \quad (5.194)$$

### 5.5.2 Unconfined Compressive secant modulus x lime key parameter

Specimens stabilized with the calcitic lime can have their unconfined compressive secant modulus ( $E_{sec}$ ) related to  $\eta/L_{iv}$  as presented in figure 5.97. Except for the intermediate dosage specimens, the exponential regression curve seems suitable to represent the behaviour of the mixtures before and after the durability cycles.



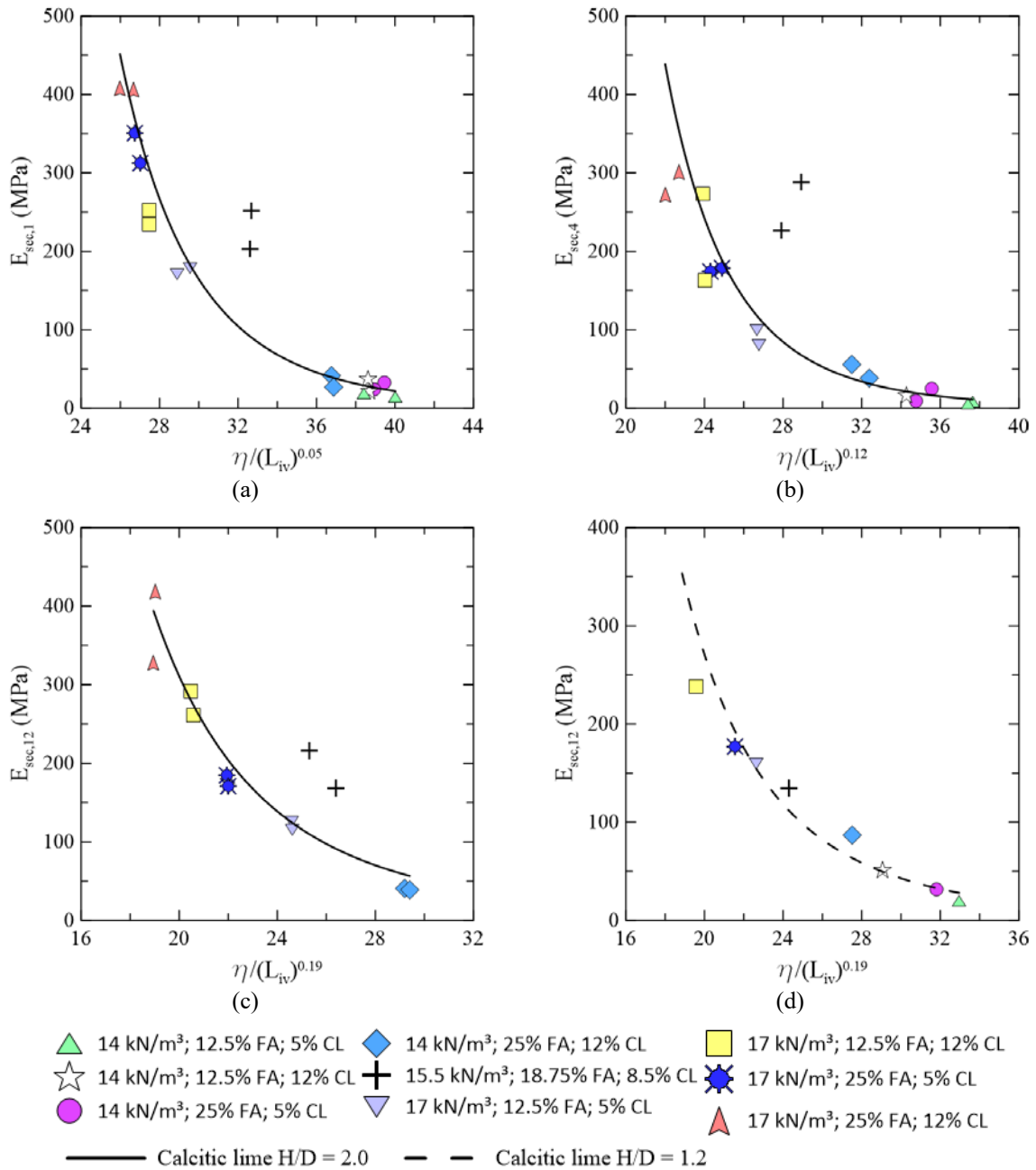


Figure 5.97: Relation between  $E_{sec}$  and  $\eta/(L_{iv})^c$  for calcitic lime treated soils after (a) 1 cycle (b) 4 cycles (c) 12 cycles  $H/D \approx 2.0$  (d) 12 cycles  $H/D \approx 1.2$ .

The corresponding expressions are presented by equations (5.195) to (5.198).

$$E_{sec,1} (H/D=2.0) = 3.85 \times 10^{12} \left[ \eta / (L_{iv})^{0.05} \right]^{-7.02} \quad R^2 = 0.90 \quad (5.195)$$

$$E_{\text{sec},4 (H/D=2.0)} = 6.47 \times 10^{11} \left[ \eta / (L_{iv})^{0.12} \right]^{-6.83} \quad R^2 = 0.83 \quad (5.196)$$

$$E_{\text{sec},12 (H/D=2.0)} = 1.75 \times 10^8 \left[ \eta / (L_{iv})^{0.19} \right]^{-4.42} \quad R^2 = 0.81 \quad (5.197)$$

$$E_{\text{sec},12 (H/D=1.2)} = 2.18 \times 10^8 \left[ \eta / (L_{iv})^{0.19} \right]^{-4.54} \quad R^2 = 0.95 \quad (5.198)$$

Soil mixtures stabilized by using the dolomitic lime may have their unconfined compressive secant modulus related to the lime key parameter as shown in figure 5.98. Those results may be expressed by the following equations.

$$E_{\text{sec},0 (H/D=2.0)} = 4.03 \times 10^6 \left[ \eta / (L_{iv})^{0.08} \right]^{-2.93} \quad R^2 = 0.81 \quad (5.199)$$

$$E_{\text{sec},1 (H/D=2.0)} = 4.55 \times 10^9 \left[ \eta / (L_{iv})^{0.14} \right]^{-5.22} \quad R^2 = 0.90 \quad (5.200)$$

$$E_{\text{sec},4 (H/D=2.0)} = 5.82 \times 10^{13} \left[ \eta / (L_{iv})^{0.24} \right]^{-8.59} \quad R^2 = 0.88 \quad (5.201)$$

$$E_{\text{sec},12 (H/D=2.0)} = 5.81 \times 10^8 \left[ \eta / (L_{iv})^{0.54} \right]^{-6.05} \quad R^2 = 0.86 \quad (5.202)$$

$$E_{\text{sec},12 (H/D=1.2)} = 1.76 \times 10^6 \left[ \eta / (L_{iv})^{0.54} \right]^{-4.05} \quad R^2 = 0.94 \quad (5.203)$$

Even after 12 durability cycles and the damage experienced by most of the samples, both the calcitic and dolomitic lime treated specimens have presented a reliable relation between  $E_{\text{sec}}$  and  $\eta/(L_{iv})^c$ , with a small dispersion in the equations fit.

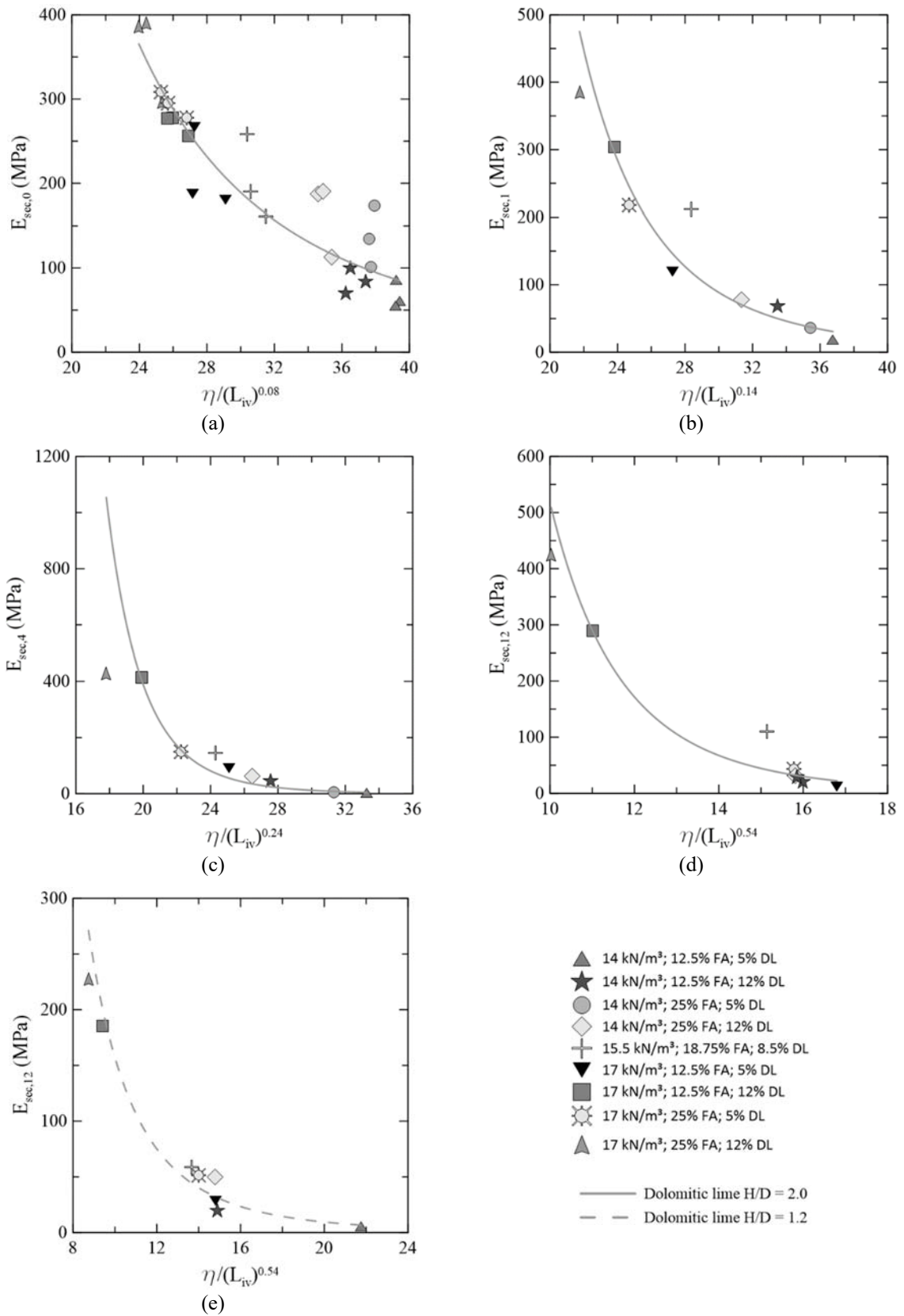


Figure 5.98: Relation between  $E_{sec}$  and  $\eta/(L_{iv})^e$  for dolomitic lime treated soils after (a) 0 cycle (b) 1 cycle (c) 4 cycles (d) 12 cycles  $H/D \approx 2.0$  (e) 12 cycles  $H/D \approx 1.2$

### 5.5.3 Small strain constraint modulus x lime key parameter

The small strain constraint modulus ( $M_0$ ) response to the lime key parameter for the calcitic lime treated slenderer specimens that have undergone wetting-drying durability cycles is presented in figure 5.99. As can be seen, before the first cycle, the constraint modulus response is almost linear, but after that, the concavity is increased. When the samples are subjected to durability cycles, there is a decrease in constraint stiffness response, especially the specimens with lower dry unit weight and lime content. The exponential regression equations are presented next.

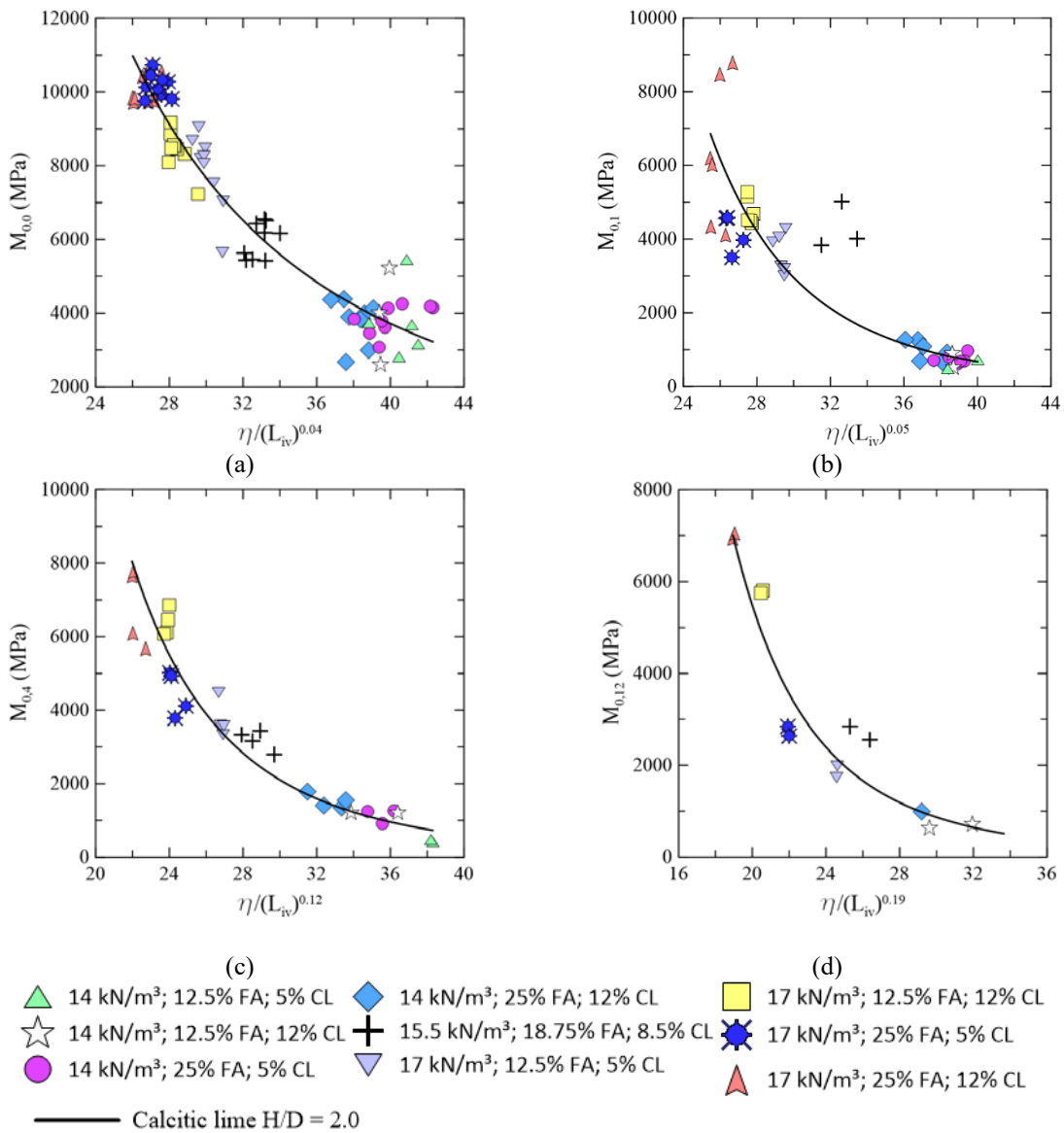


Figure 5.99: Relation between  $M_0$  and  $\eta/(L_{iv})^e$  for samples with  $H/D \approx 2.0$  treated with calcitic lime after (a) 0 cycle (b) 1 cycle (c) 4 cycles (d) 12 cycles.

$$M_{0,0 (H/D=2.0)} = 4.05 \times 10^7 \left[ \eta / (L_{iv})^{0.04} \right]^{-2.52} \quad R^2 = 0.89 \quad (5.204)$$

$$M_{0,1 (H/D=2.0)} = 1.20 \times 10^{11} \left[ \eta / (L_{iv})^{0.05} \right]^{-5.15} \quad R^2 = 0.88 \quad (5.205)$$

$$M_{0,4 (H/D=2.0)} = 4.89 \times 10^9 \left[ \eta / (L_{iv})^{0.12} \right]^{-4.31} \quad R^2 = 0.93 \quad (5.206)$$

$$M_{0,12 (H/D=2.0)} = 4.56 \times 10^9 \left[ \eta / (L_{iv})^{0.19} \right]^{-4.55} \quad R^2 = 0.90 \quad (5.207)$$

The following equations present the results for the same related parameters, but for less slender specimens ( $H/D \approx 1.2$ ), which, besides wetting and drying, have undergone durability cycles including a brushing stage.

$$M_{0,0 (H/D=1.2)} = 3.28 \times 10^8 \left[ \eta / (L_{iv})^{0.04} \right]^{-3.09} \quad R^2 = 0.94 \quad (5.208)$$

$$M_{0,1 (H/D=1.2)} = 3.17 \times 10^7 \left[ \eta / (L_{iv})^{0.05} \right]^{-2.43} \quad R^2 = 0.87 \quad (5.209)$$

$$M_{0,4 (H/D=1.2)} = 2.67 \times 10^{10} \left[ \eta / (L_{iv})^{0.12} \right]^{-4.76} \quad R^2 = 0.89 \quad (5.210)$$

$$M_{0,12 (H/D=1.2)} = 7.59 \times 10^{12} \left[ \eta / (L_{iv})^{0.19} \right]^{-6.93} \quad R^2 = 0.94 \quad (5.211)$$

The results were plotted and can be seen in figure 5.100.

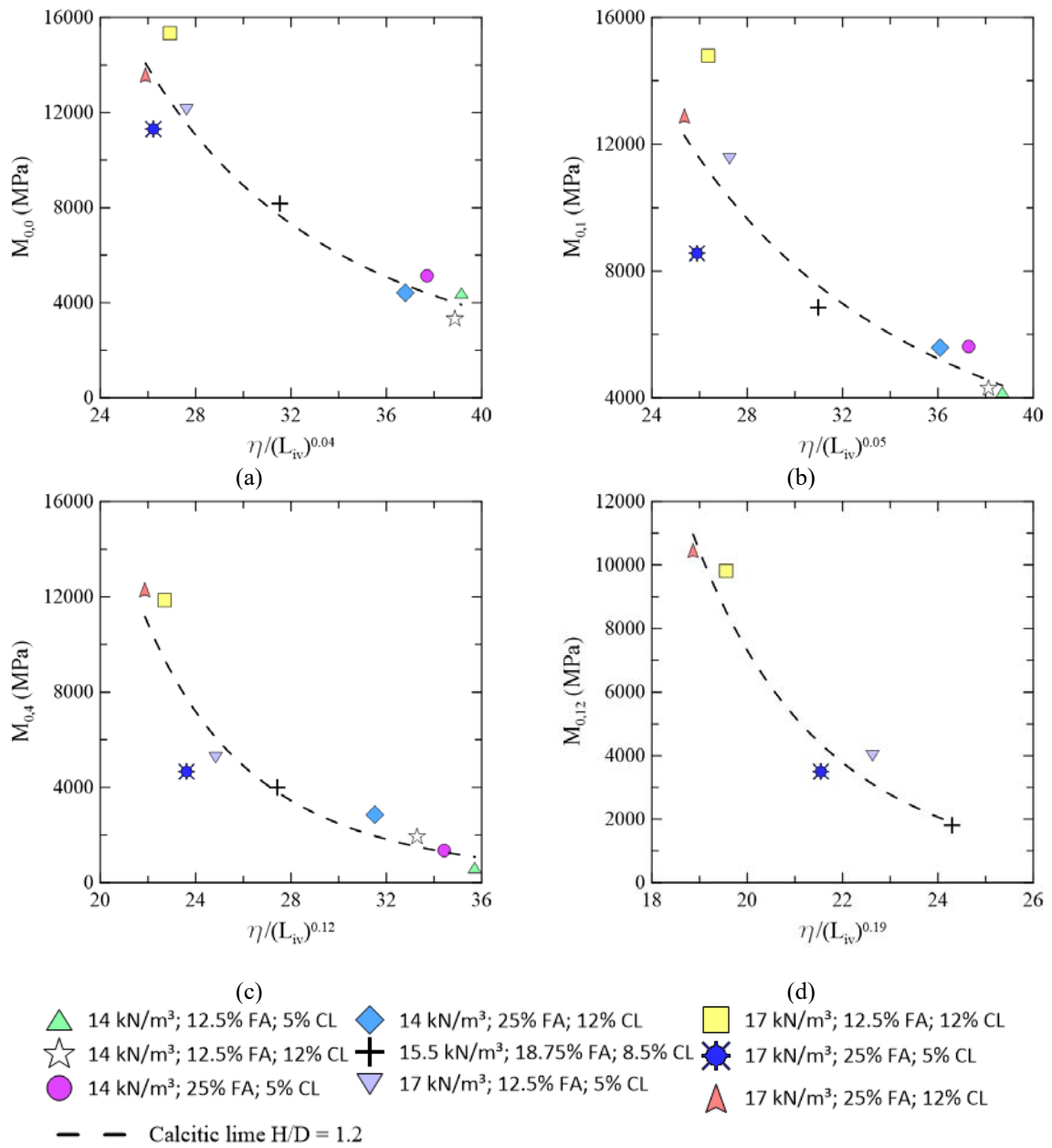


Figure 5.100: Relation between  $M_0$  and  $\eta/(L_{iv})^c$  for samples with  $H/D \approx 1.2$  treated with calcitic lime after (a) 0 cycle (b) 1 cycle (c) 4 cycles (d) 12 cycles.

The soil admixtures with a relation  $H/D \approx 2.0$ , stabilized using the dolomitic lime, may respond to the lime key parameter as shown in figure 5.101. A significant  $M_0$  decay is observed along the durability cycles, but the exponential regression might still be able to express this relation and allow its use in a geotechnical design.

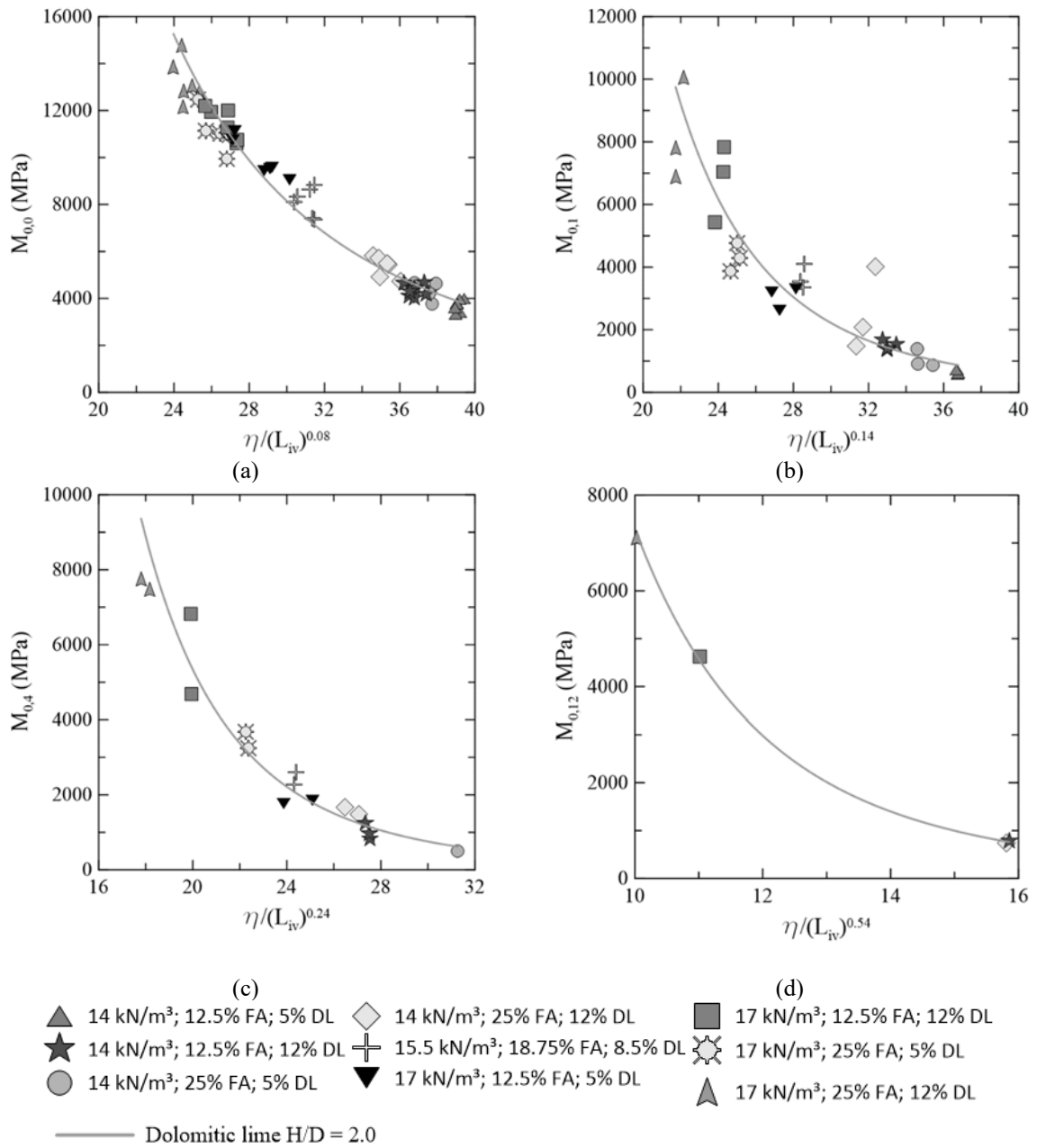


Figure 5.101: Relation between  $M_0$  and  $\eta/(L_{iv})^c$  for samples with  $H/D \approx 2.0$  treated with calcitic lime after (a) 0 cycle (b) 1 cycle (c) 4 cycles (d) 12 cycles.

The results depicted above can be expressed by the following equations.

$$M_{0,0 (H/D=2.0)} = 1.11 \times 10^8 \left[ \eta / (L_{iv})^{0.08} \right]^{-2.80} \quad R^2 = 0.97 \quad (5.212)$$

$$M_{0,1 (H/D=2.0)} = 1.34 \times 10^{10} \left[ \eta / (L_{iv})^{0.14} \right]^{-4.59} \quad R^2 = 0.89 \quad (5.213)$$

$$M_{0,4 (H/D=2.0)} = 1.03 \times 10^{10} \left[ \eta / (L_{iv})^{0.24} \right]^{-4.83} \quad R^2 = 0.95 \quad (5.214)$$

$$M_{0,12 (H/D=2.0)} = 5.98 \times 10^8 \left[ \eta / (L_{iv})^{0.54} \right]^{-4.91} \quad R^2 = 0.999 \quad (5.215)$$

When dealing with higher volume samples, the small strain constraint modulus response can be different since the moisture and durability conditions are too, and the ultrasonic transducer is smaller than the diameter of the samples. The results of  $M_0 \times \eta / (L_{iv})^e$  may be expressed by the equations (5.216) to (5.219), and the plot curves are presented in figure 5.102. The low coefficient of determination from the  $M_0$  response after 4 cycles (0.59) indicates a great dispersion in the results. Though, the  $R^2$  is greater than using the binder key parameter (0.16).

$$M_{0,0 (H/D=1.2)} = 1.90 \times 10^8 \left[ \eta / (L_{iv})^{0.08} \right]^{-3.00} \quad R^2 = 0.91 \quad (5.216)$$

$$M_{0,1 (H/D=1.2)} = 1.19 \times 10^{10} \left[ \eta / (L_{iv})^{0.14} \right]^{-4.55} \quad R^2 = 0.78 \quad (5.217)$$

$$M_{0,4 (H/D=1.2)} = 1.22 \times 10^8 \left[ \eta / (L_{iv})^{0.24} \right]^{-3.32} \quad R^2 = 0.59 \quad (5.218)$$

$$M_{0,12 (H/D=1.2)} = 2.08 \times 10^9 \left[ \eta / (L_{iv})^{0.54} \right]^{-5.66} \quad R^2 = 0.80 \quad (5.219)$$



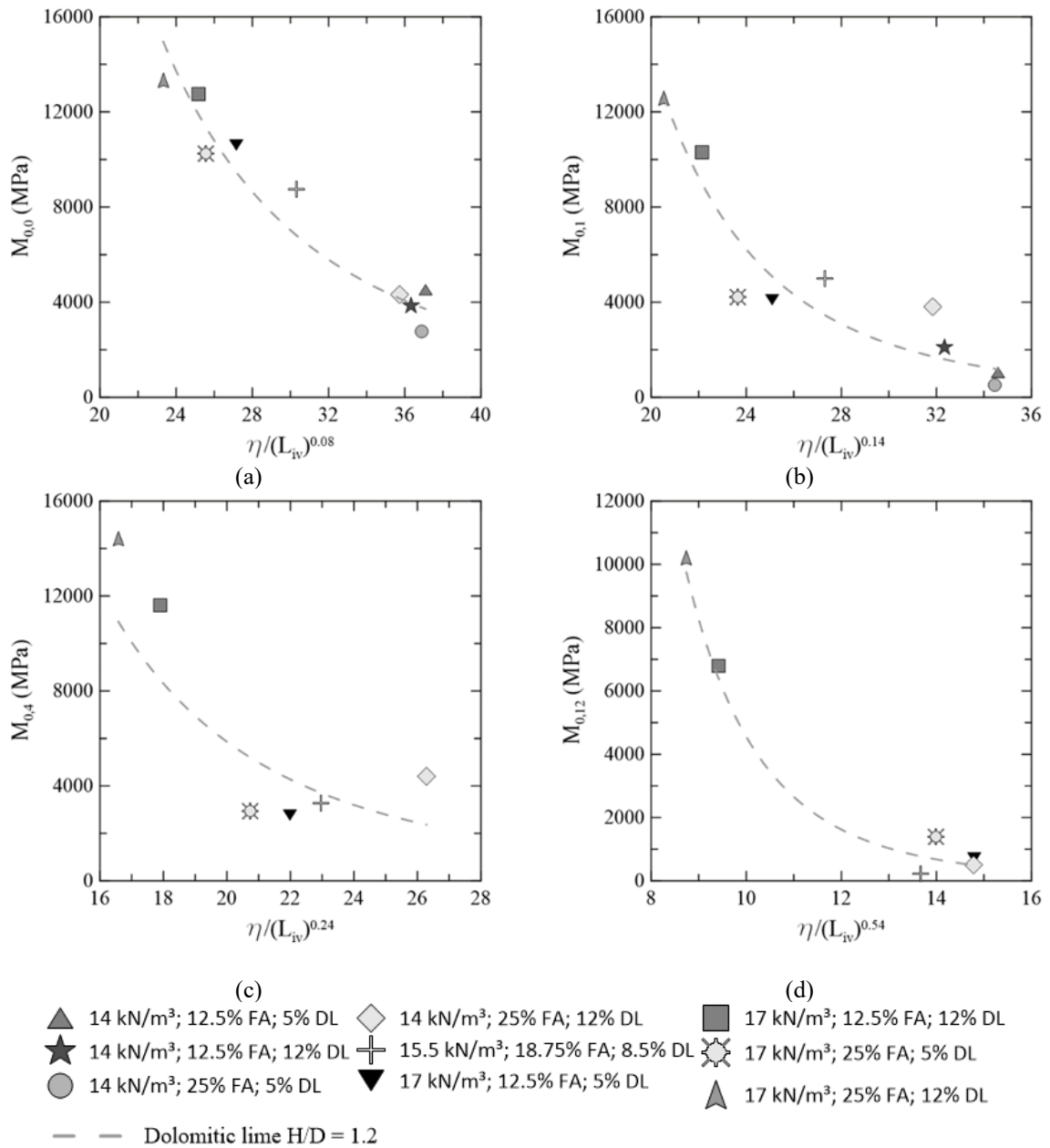


Figure 5.102: Relation between  $M_0$  and  $\eta/(L_{iv})^c$  for samples with  $H/D \approx 1.2$  treated with the dolomitic lime after (a) 0 cycle (b) 1 cycle (c) 4 cycles (d) 12 cycles.

### 5.5.4 Small strain shear modulus x lime key parameter

The small strain shear modulus ( $G_0$ ) of calcitic lime treated specimens with a slenderness relation of approximately 2, are related to the lime key parameter  $[\eta/(L_{iv})^c]$  as presented in figure 5.103.

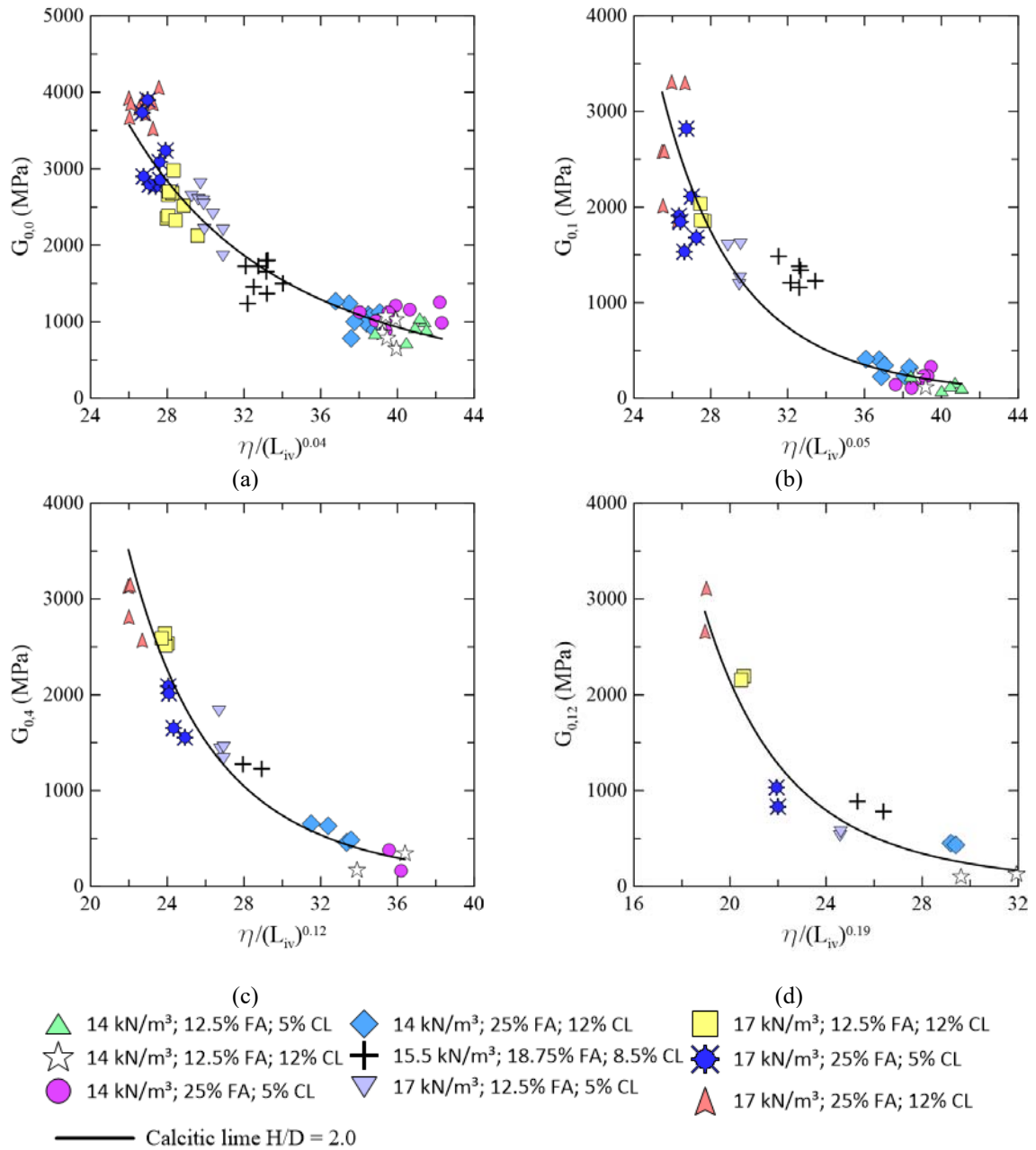


Figure 5.103: Relation between  $G_0$  and  $\eta/(L_{iv})^e$  for samples with  $H/D \approx 2.0$  treated with calcitic lime after (a) 0 cycle (b) 1 cycle (c) 4 cycles (d) 12 cycles.

The expressions for the exponential fit regressions are presented by equations (5.220) to (5.223).

$$G_{0,0 (H/D=2.0)} = 9.61 \times 10^7 \left[ \eta / (L_{iv})^{0.04} \right]^{-3.13} \quad R^2 = 0.92 \quad (5.220)$$

$$G_{0,1 (H/D=2.0)} = 3.09 \times 10^{12} \left[ \eta / (L_{iv})^{0.05} \right]^{-6.39} \quad R^2 = 0.89 \quad (5.221)$$

$$G_{0,4 (H/D=2.0)} = 1.80 \times 10^{10} \left[ \eta / (L_{iv})^{0.12} \right]^{-5.00} \quad R^2 = 0.91 \quad (5.222)$$

$$G_{0,12 (H/D=2.0)} = 2.56 \times 10^{10} \left[ \eta / (L_{iv})^{0.19} \right]^{-5.44} \quad R^2 = 0.84 \quad (5.223)$$

Less slender specimens ( $H/D \approx 1.2$ ) respond to the lime key parameter (using the calcitic lime) as expressed by the following regression equations. The plots are illustrated in figure 5.104.

$$G_{0,0 (H/D=1.2)} = 1.30 \times 10^8 \left[ \eta / (L_{iv})^{0.04} \right]^{-3.16} \quad R^2 = 0.96 \quad (5.224)$$

$$G_{0,1 (H/D=1.2)} = 3.17 \times 10^7 \left[ \eta / (L_{iv})^{0.05} \right]^{-2.43} \quad R^2 = 0.93 \quad (5.225)$$

$$G_{0,4 (H/D=1.2)} = 1.84 \times 10^{10} \left[ \eta / (L_{iv})^{0.12} \right]^{-4.96} \quad R^2 = 0.94 \quad (5.226)$$

$$G_{0,12 (H/D=1.2)} = 1.32 \times 10^{11} \left[ \eta / (L_{iv})^{0.19} \right]^{-5.87} \quad R^2 = 0.92 \quad (5.227)$$

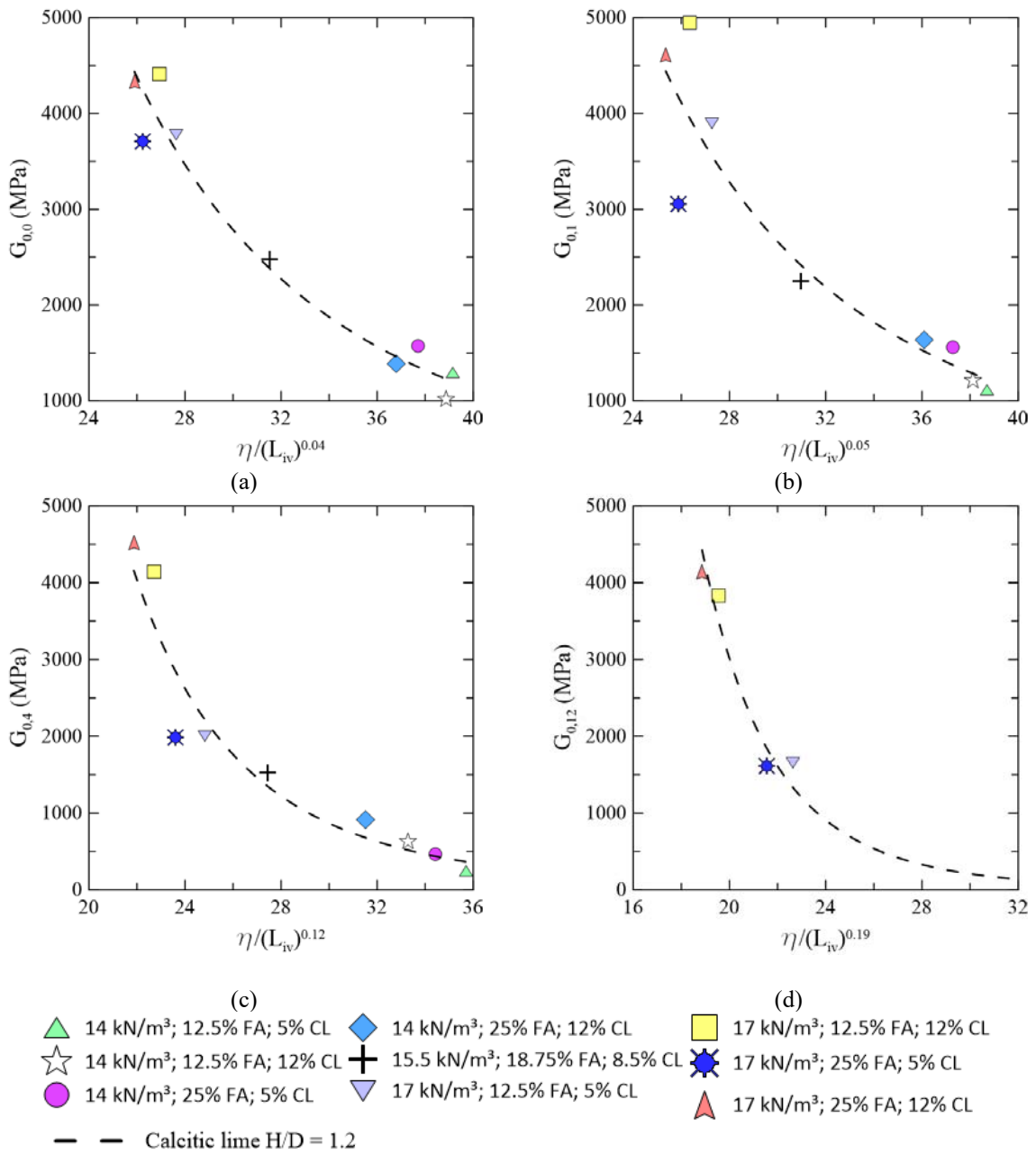


Figure 5.104: Relation between  $G_0$  and  $\eta/(L_{iv})^e$  for samples with  $H/D \approx 1.2$  treated with calcitic lime after (a) 0 cycle (b) 1 cycle (c) 4 cycles (d) 12 cycles.

When using the dolomitic lime in the admixture, there is a change in  $G_0$  behaviour, especially after 4 durability cycles. The results for slenderer specimens can be observed in figure 5.105. As S-waves travel times have not been assessed after 12 cycles,  $G_{0,12}$  could not be presented.

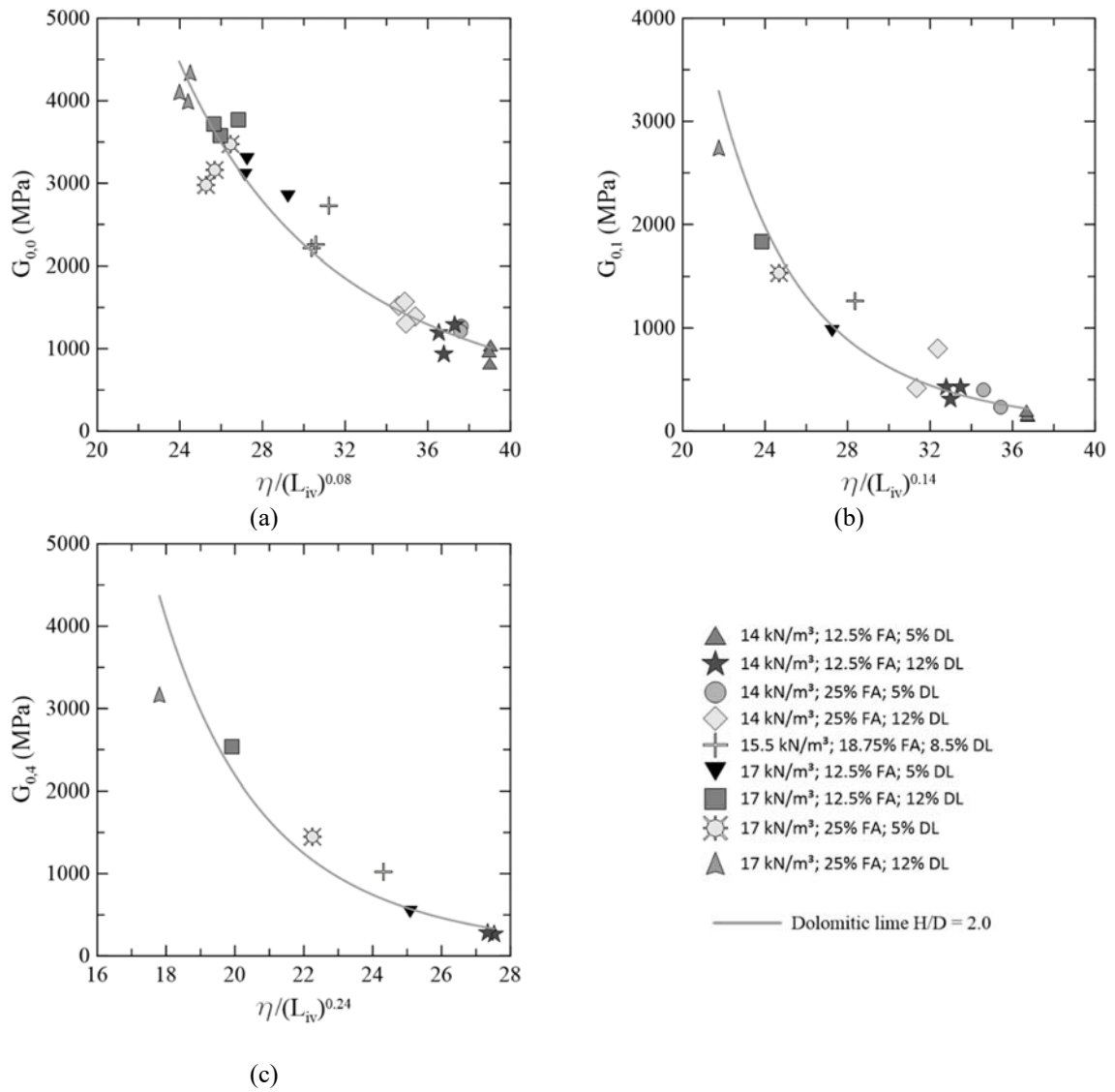


Figure 5.105: Relation between  $G_0$  and  $\eta/(L_{iv})^c$  for samples with  $H/D \approx 2.0$  treated with dolomitic lime after (a) 0 cycle (b) 1 cycle (c) 4 cycles.

$G_0$  curve fit for slenderer specimens stabilized using the dolomitic lime may be expressed by the following equations.

$$G_{0,0 (H/D=2.0)} = 7.22 \times 10^7 \left[ \eta / (L_{iv})^{0.08} \right]^{-3.05} \quad R^2 = 0.95 \quad (5.228)$$

$$G_{0,1 (H/D=2.0)} = 2.88 \times 10^{10} \left[ \eta / (L_{iv})^{0.14} \right]^{-5.19} \quad R^2 = 0.90 \quad (5.229)$$

$$G_{0,4 (H/D=2.0)} = 1.14 \times 10^{11} \left[ \eta / (L_{iv})^{0.24} \right]^{-5.93} \quad R^2 = 0.93 \quad (5.230)$$

When dealing with the samples subjected to wetting-drying-brushing stages during the durability cycles, the small strain shear modulus of specimens stabilized using the dolomitic lime can be expressed by the

The fitting expressions are given by the following equations.

$$G_{0,0 (H/D=1.2)} = 1.06 \times 10^8 \left[ \eta / (L_{iv})^{0.08} \right]^{-3.17} \quad R^2 = 0.95 \quad (5.231)$$

$$G_{0,1 (H/D=1.2)} = 9.92 \times 10^8 \left[ \eta / (L_{iv})^{0.14} \right]^{-4.10} \quad R^2 = 0.88 \quad (5.232)$$

$$G_{0,4 (H/D=1.2)} = 4.73 \times 10^8 \left[ \eta / (L_{iv})^{0.24} \right]^{-4.18} \quad R^2 = 0.57 \quad (5.233)$$

$$G_{0,12 (H/D=1.2)} = 9.83 \times 10^7 \left[ \eta / (L_{iv})^{0.54} \right]^{-4.72} \quad R^2 = - \quad (5.234)$$

Interestingly, both the  $G_{0,4}$  and the  $M_{0,4}$  for less slender specimens stabilized with the dolomitic lime has also presented a low coefficient of determination. Maybe there has been a problem with the equipment in one of the tests or the oven during the fourth cycle of a group of specimens. Also, the coefficient of determination of the shear modulus response after 12 cycles was not presented as the test could be executed with only two of the samples.

The mentioned relation between the small strain shear modulus and the dolomitic lime key parameter can be depicted in figure 5.106.

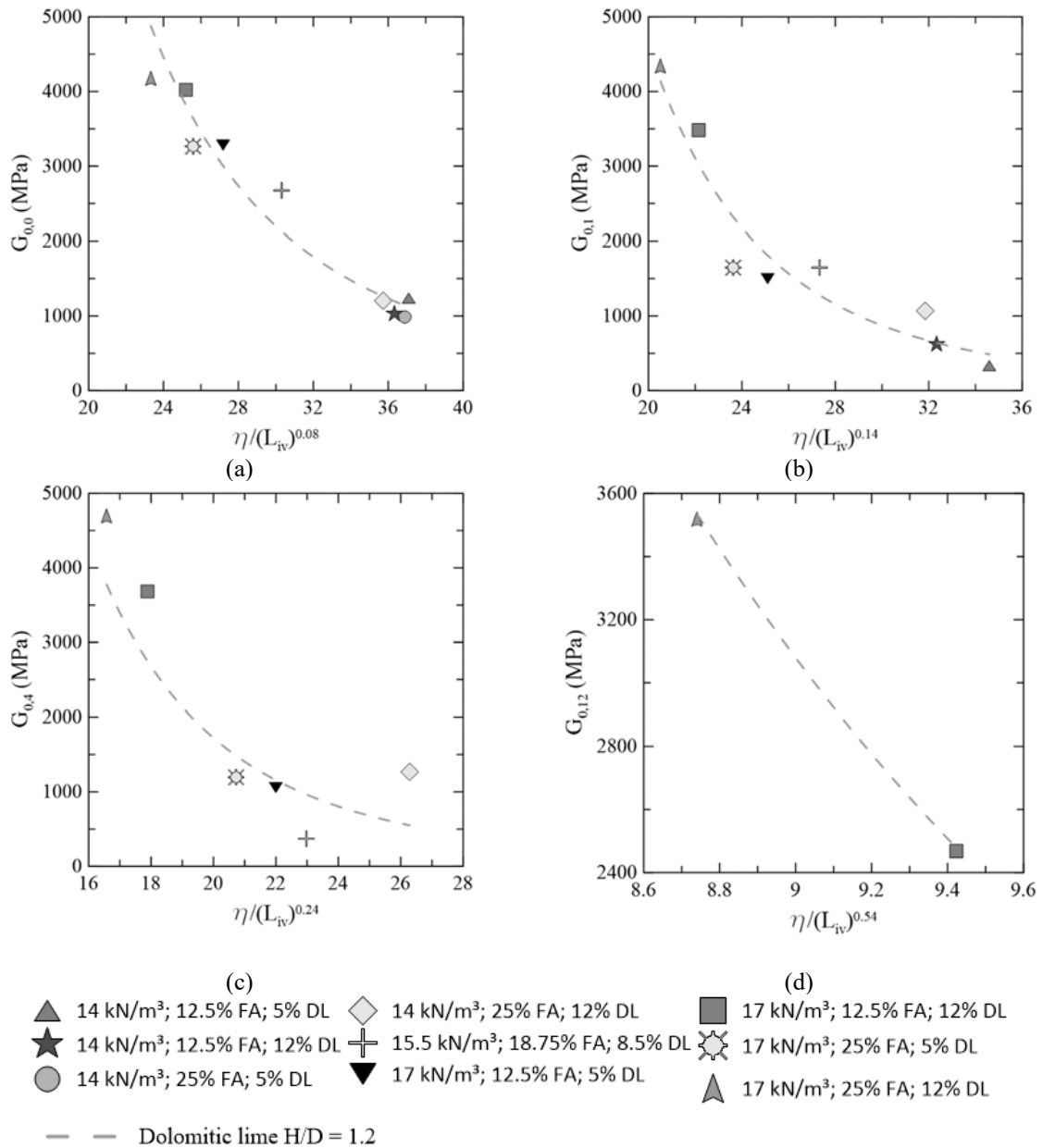


Figure 5.106: Relation between  $G_0$  and  $\eta/(L_{iv})^c$  for samples with  $H/D \approx 1.2$  treated with calcitic lime after (a) 0 cycle (b) 1 cycle (c) 4 cycles (d) 12 cycles.

### 5.5.5 Small strain Poisson's ratio x lime key parameter

As there is no high accuracy in the obtained small strain Poisson's ratio ( $\nu_0$ ), no significant differences are expected in the correlation from the binder to the lime key parameter.

The plotted results from the calcitic lime treated soils with a slenderness ratio of about 2 are presented in figure 5.107.

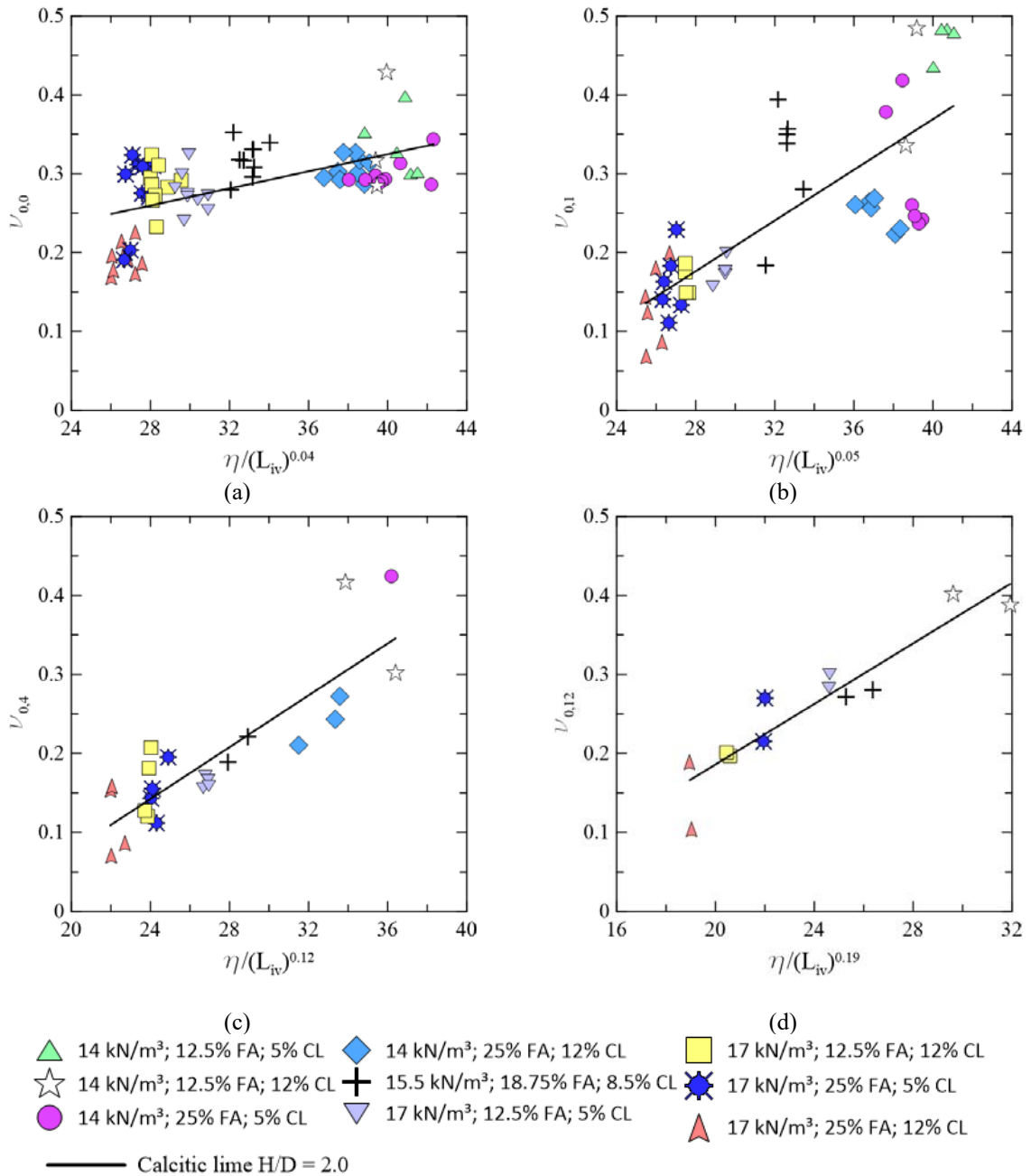


Figure 5.107: Relation between  $v_0$  and  $\eta/(L_{iv})^e$  for samples with  $H/D \approx 2.0$  treated with calcitic lime after (a) 0 cycle (b) 1 cycle (c) 4 cycles (d) 12 cycles.

The results for specimens with  $H/D$  of approximately 1.2 are presented next. After 12 cycles, there is a change in the expected trend, since the specimens with a higher lime key parameter value present a lower  $v_0$ .



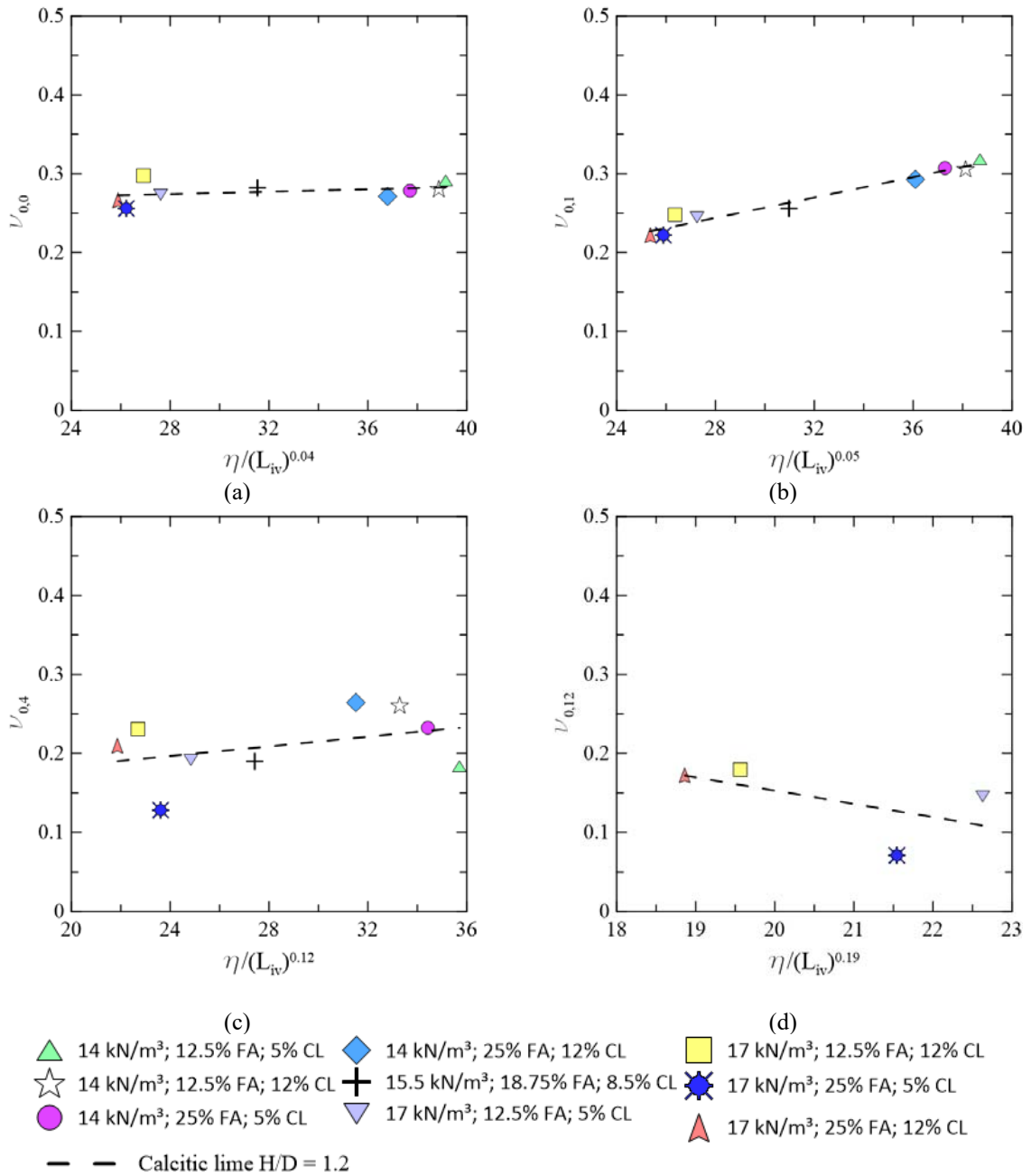


Figure 5.108: Relation between  $v_0$  and  $\eta/(L_{iv})^e$  for samples with  $H/D \approx 1.2$  treated with calcitic lime after (a) 0 cycle (b) 1 cycle (c) 4 cycles (d) 12 cycles.

The more slender samples treated with the dolomitic lime have a  $G_0$  response to  $\eta/(L_{iv})^e$  as shown in figure 5.109.

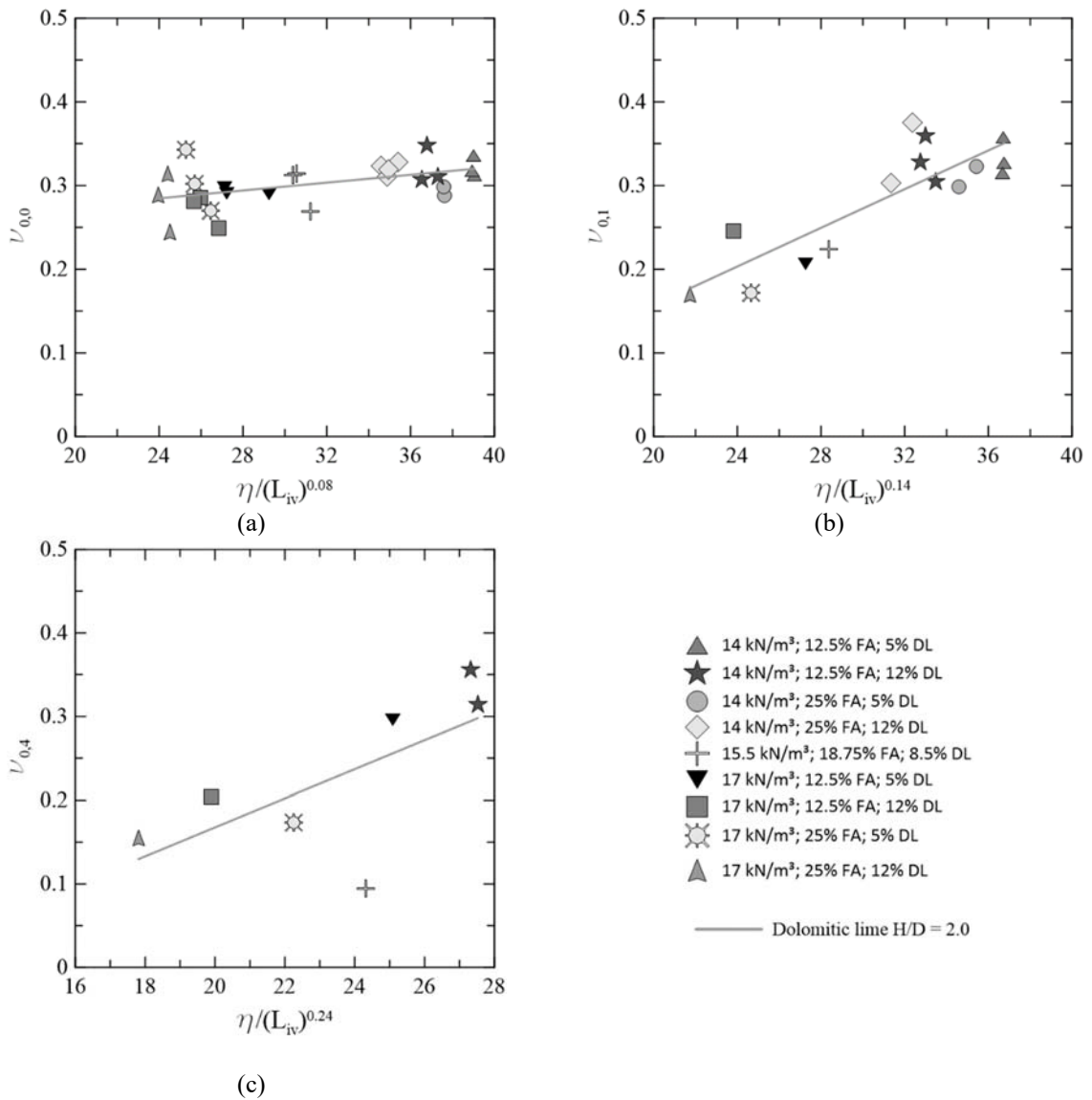


Figure 5.109: Relation between  $v_0$  and  $\eta/(L_{iv})^e$  for samples with  $H/D \approx 2.0$  treated with dolomitic lime after (a) 0 cycle (b) 1 cycle (c) 4 cycles (d) 12 cycles.

The small strain shear modulus response to the lime key parameter before and after the durability cycles, including the brushing stage, is depicted in figure 5.110.

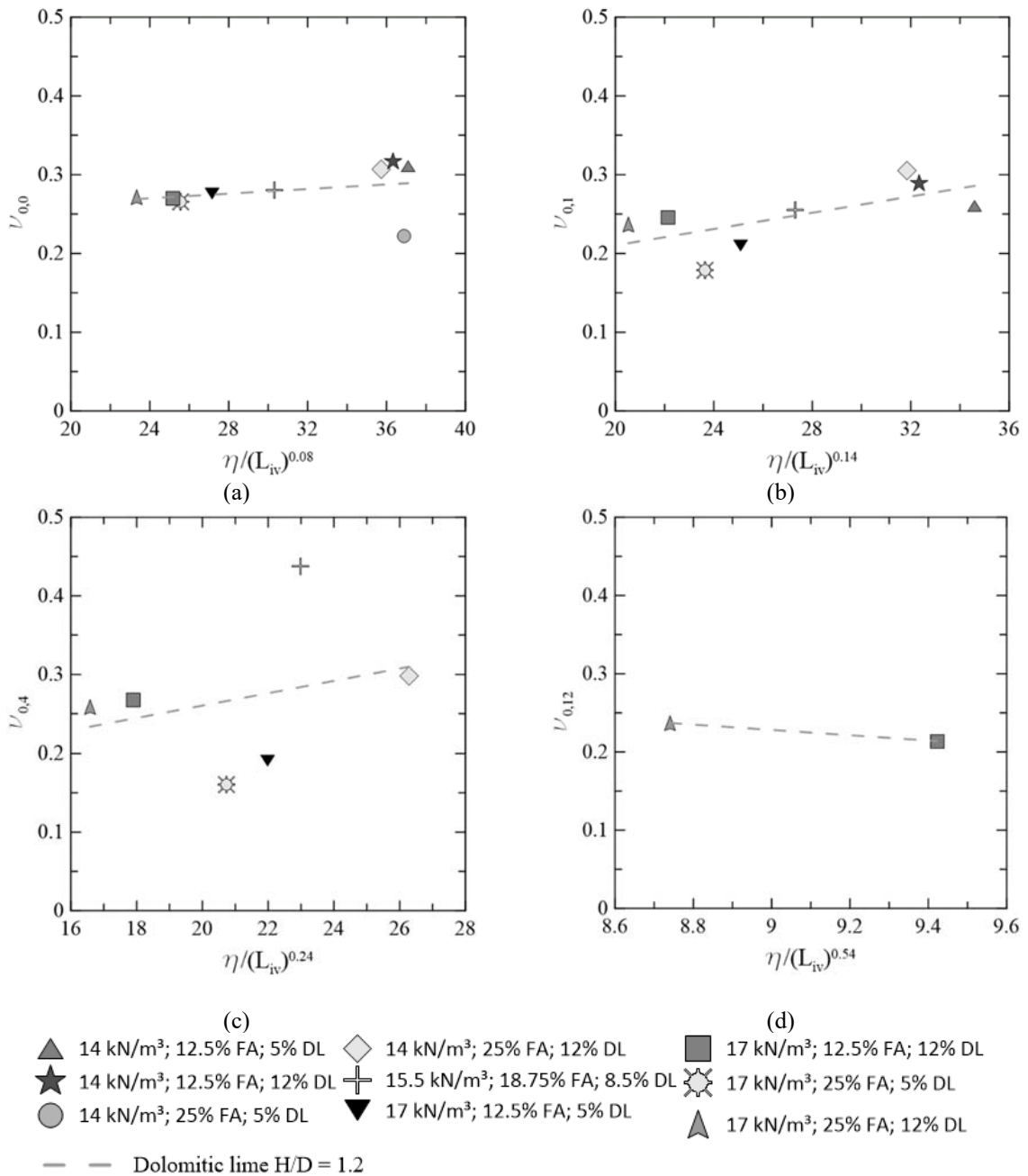


Figure 5.110: Relation between  $v_0$  and  $\eta/(L_{iv})^e$  for samples with  $H/D \approx 1.2$  treated with dolomitic lime after (a) 0 cycle (b) 1 cycle (c) 4 cycles (d) 12 cycles.

A slight decrease in the dispersion of the analysis is observed concerning the use of the binder key parameter, but a great part of the data remains disperse and may be evaluated carefully. Yet, the small strain Poisson's ratio ( $v_0$ ) may give a reasonable indication of the soil deformability behaviour.

### 5.5.6 Accumulated loss of mass x lime key parameter

The accumulated loss of mass (ALM) behaviour of the studied materials may be related to the lime key parameter too.

The ALM response of the calcitic lime mixtures to the lime key parameter is shown in figure 5.111 from 1 to 12 cycles. All the relations have presented a reasonable coefficient of determination, as can be seen in the curve fit expressions presented next.

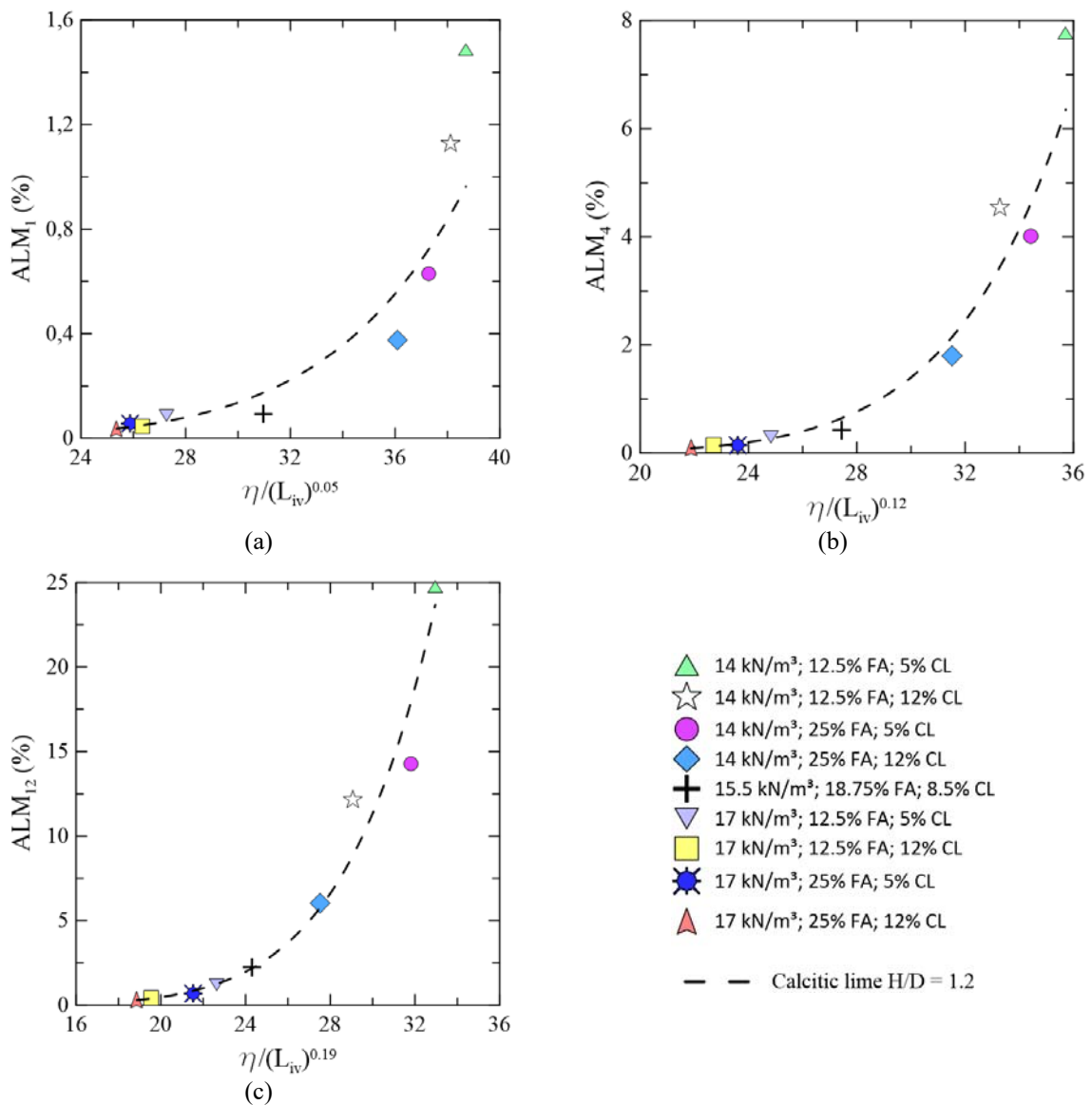


Figure 5.111: Relation between ALM and  $\eta/(L_{iv})^c$  for samples with H/D  $\approx$  1.2 treated with calcitic lime after (a) 1 cycle (b) 4 cycles (c) 12 cycles.

$$ALM_{1(H/D=1.2)} = 6.63 \times 10^{-13} \left[ \eta / (L_{iv})^{0.05} \right]^{7.66} \quad R^2 = 0.94 \quad (5.235)$$

$$ALM_{4(H/D=1.2)} = 2.11 \times 10^{-13} \left[ \eta / (L_{iv})^{0.12} \right]^{8.68} \quad R^2 = 0.98 \quad (5.236)$$

$$ALM_{12(H/D=1.2)} = 3.08 \times 10^{-11} \left[ \eta / (L_{iv})^{0.19} \right]^{7.83} \quad R^2 = 0.99 \quad (5.237)$$

The accumulated loss of mass response against the dolomitic lime key parameter can be seen in figure 5.112.

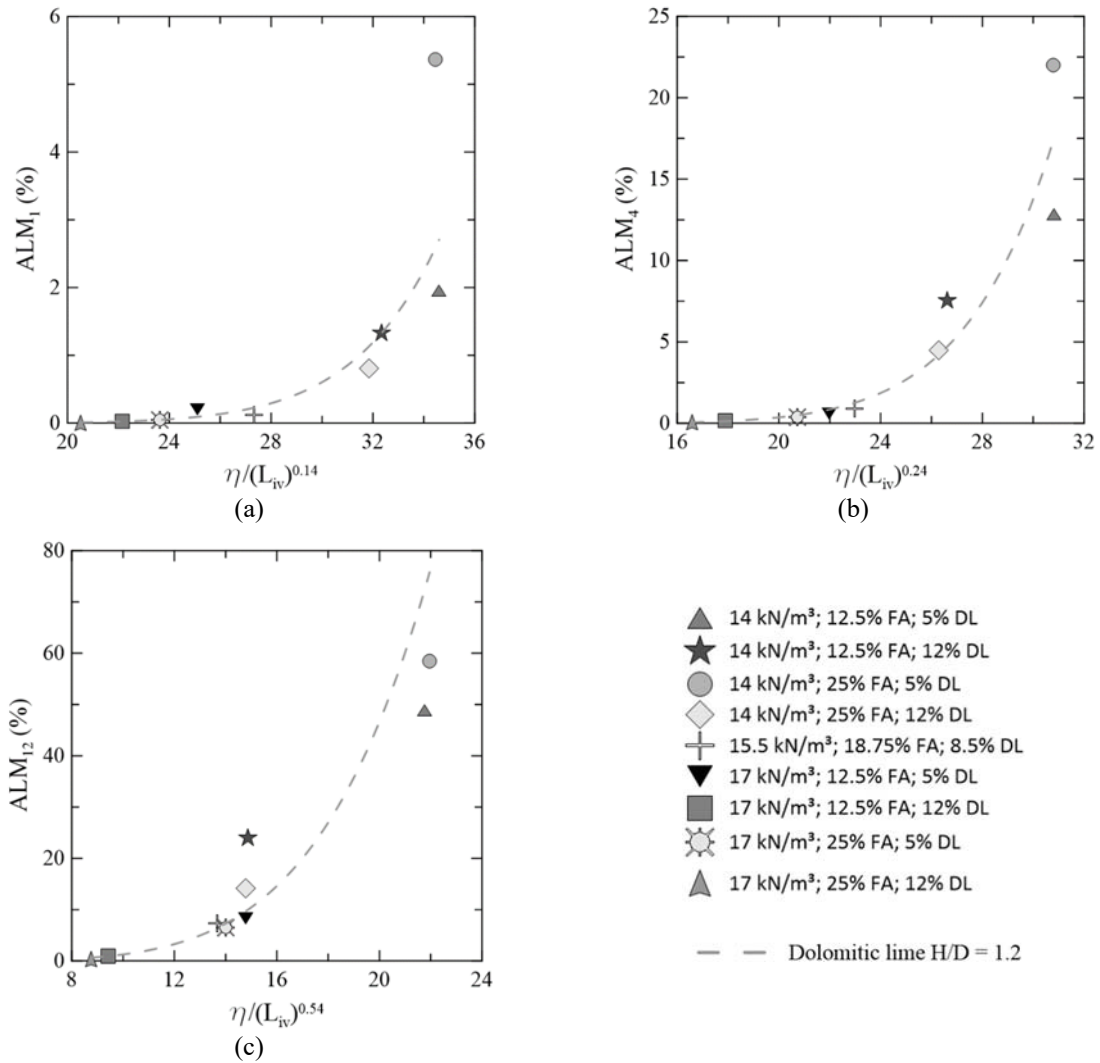


Figure 5.112: Relation between ALM and  $\eta / (L_{iv})^c$  for samples with H/D  $\approx$  1.2 treated with dolomitic lime after (a) 1 cycle (b) 4 cycles (c) 12 cycles.

The fitting expressions are given by the following equations:

$$ALM_{1(H/D=1.2)} = 1.87 \times 10^{-16} \left[ \eta / (L_{iv})^{0.14} \right]^{10.50} \quad R^2 = 0.95 \quad (5.238)$$

$$ALM_{4(H/D=1.2)} = 7.75 \times 10^{-13} \left[ \eta / (L_{iv})^{0.24} \right]^{8.97} \quad R^2 = 0.98 \quad (5.239)$$

$$ALM_{12(H/D=1.2)} = 8.01 \times 10^{-6} \left[ \eta / (L_{iv})^{0.54} \right]^{5.20} \quad R^2 = 0.94 \quad (5.240)$$

High coefficients of determination were obtained for both calcitic and dolomitic stabilization, even after the 12<sup>th</sup> cycle. Therefore, the lime key parameter may be used for the estimation of the ALM along cycles even when only the moulding dosage is known.

### 5.5.7 Lime key parameter evaluation

As a consequence of climate weathering in association with erosive effects, represented in this study by durability cycles, samples with high porosity and low lime content tend to present mechanical properties deterioration, while the ones with lower porosity and higher lime content are way less sensitive to deterioration, in some cases even presenting a grown in mechanical properties response due to pozzolanic reactions catalyzation. As a response to this behaviour, a vertical “stretching” is observed in *mechanical property*  $\times \eta / (B_{iv})^e$  and *mechanical property*  $\times \eta / (L_{iv})^e$  plots, but when the last-mentioned key parameter is used, as long as more durability cycles are imposed to the specimen, growth in the exponent  $e$  is observed when the best curve fit is sought. So, this exponent may not be represented by a unique constant value when weathering-erosive effects are accounted for. This exponent varies throughout cycles and seems to be lime dependent and linearly related to durability cycles, as shown in figure 5.113.

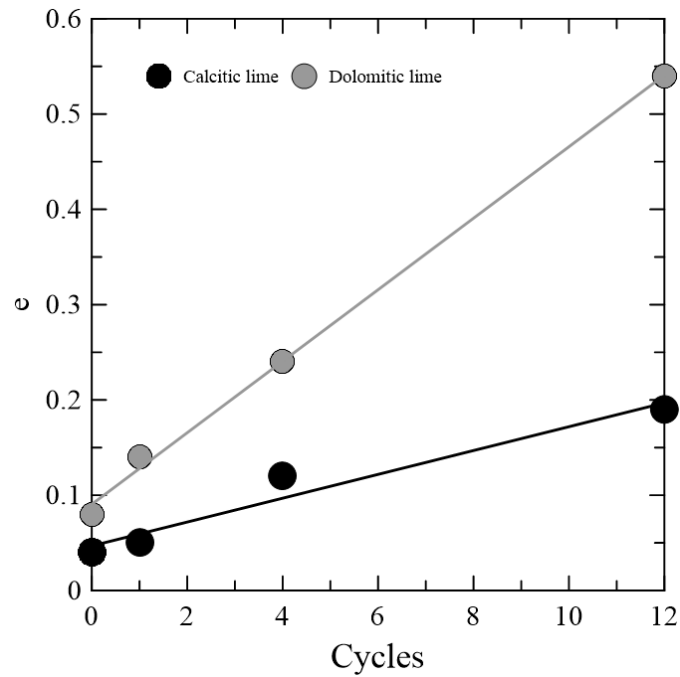


Figure 5.113: Exponent  $e$  determined for best-fit values after durability cycles.

The regression equations are (5.241) and (5.242) for calcitic and dolomitic lime, respectively.

$$e_{\text{calcitic lime}} = 0.0468 + 0.0125 \times (\text{number of cycles}) \quad R^2 = 0.95 \quad (5.241)$$

$$e_{\text{dolomitic lime}} = 0.0905 + 0.0375 \times (\text{number of cycles}) \quad R^2 = 0.998 \quad (5.242)$$

The linear regression mentioned above give rise to a hypothesis of  $e$  determination, expressed by the equation (5.243):

$$e = C + \psi \times (\omega t) \quad (5.243)$$

Where:

$e$  = exponent of key parameter  $\eta/(L_{iv})^e$

$C$  = constant for a given material corresponds to the lime curve fit exponent when no weathering or erosive conditions are imposed on the specimens

$\psi$  = weathering-erosive susceptibility (dependent on the materials and lime type add)

$\omega$  = degree of the imposed weathering-erosive condition

$t$  = time (or number of cycles) imposed on the specimens

### 5.6 SLENDERNESS RATIO RESULTS

The slenderness ratio, strictly speaking, is the relation between specimens' height and diameter. Meanwhile, in the present study, the specimens with a lower slenderness ratio value present not only a higher diameter but a larger height and volume too. Also, they were submitted to brushing, while the smaller specimens were not. So, the called slenderness ratio in this research may include more distinctions than simply a shape. For that, wave velocities may provide additional information about their internal structure.

#### 5.6.1 Unconfined compressive strength x slenderness ratio

The calcitic and dolomitic lime specimens were analyzed comparing the key parameter  $\eta/L_{iv}$  fit from different specimens size. As there were only available results from unconfined compressive strength after 12 durability cycles, only those specimens were evaluated. The result from calcitic lime treated specimens is shown in figure 5.114.

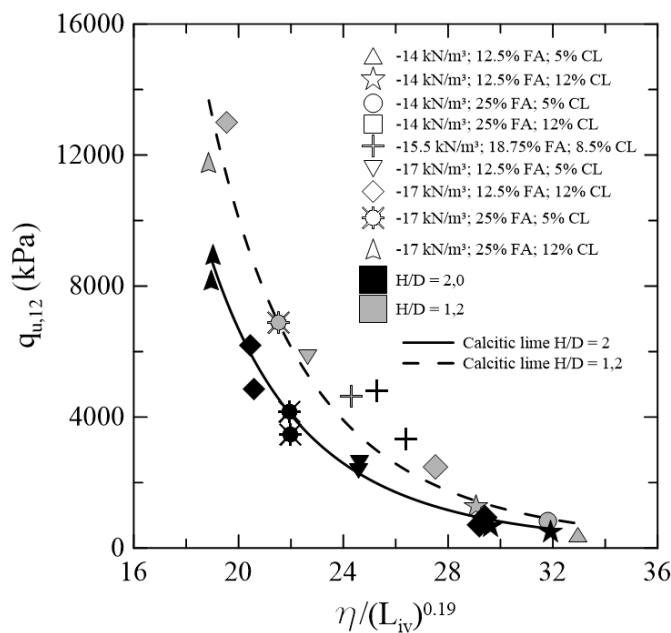


Figure 5.114: Unconfined compressive strength for calcitic lime treated soils related to  $\eta/L_{iv}$  and slenderness ratio.



The exponential fit regression is expressed by the equations (5.244) and (5.245), for specimens with a slenderness ratio of approximately 2.0 and 1.2, respectively

$$q_{u,12 (H/D=2.0)} = 3.89 \times 10^{10} \left[ \eta / (L_{iv})^{0.19} \right]^{-5.2} \quad R^2 = 0.87 \quad (5.244)$$

$$q_{u,12 (H/D=1.2)} = 5.87 \times 10^{10} \left[ \eta / (L_{iv})^{0.19} \right]^{-5.2} \quad R^2 = 0.95 \quad (5.245)$$

By dividing one equation for another, the obtained relation from  $q_u$  of specimens stabilized with the calcitic lime is 1.51.

The results from dolomitic lime treated specimens are shown in figure 5.115.

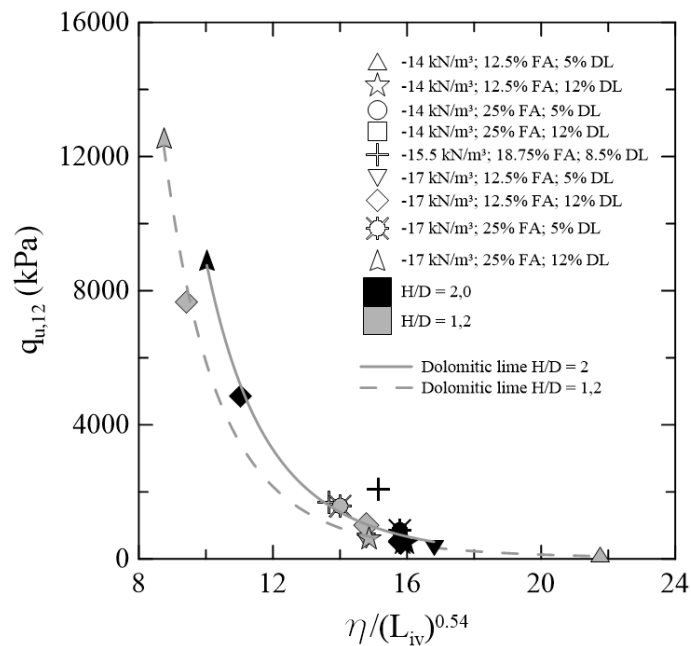


Figure 5.115: Unconfined compressive strength for dolomitic lime treated soils related to  $\eta/L_{iv}$  and slenderness ratio.

The power fit regressions are expressed by the equations (5.246) and (5.247), for specimens with a slenderness ratio of approximately 2.0 and 1.2, respectively.

$$q_{u,12 (H/D=2.0)} = 2.81 \times 10^9 \left[ \eta / (L_{iv})^{0.54} \right]^{-5.5} \quad R^2 = 0.97 \quad (5.246)$$

$$q_{u,12 (H/D=1.2)} = 1.86 \times 10^9 \left[ \eta / (L_{iv})^{0.54} \right]^{-5.5} \quad R^2 = 0.99 \quad (5.247)$$

The relation between  $q_{u,12 (H/D = 1.2)}$  and  $q_{u,12 (H/D = 2.0)}$  for the dolomitic lime treated specimens is 0.66.

### 5.6.2 Unconfined compressive secant modulus x slenderness ratio

As unconfined compressive strength, the unconfined compressive modulus is sensitive to specimens' slenderness ratio. In order to evaluate this effect, results from different H/D relations were plotted and fitted to the same exponent. Calcitic lime treated soils results are shown in figure 5.116.

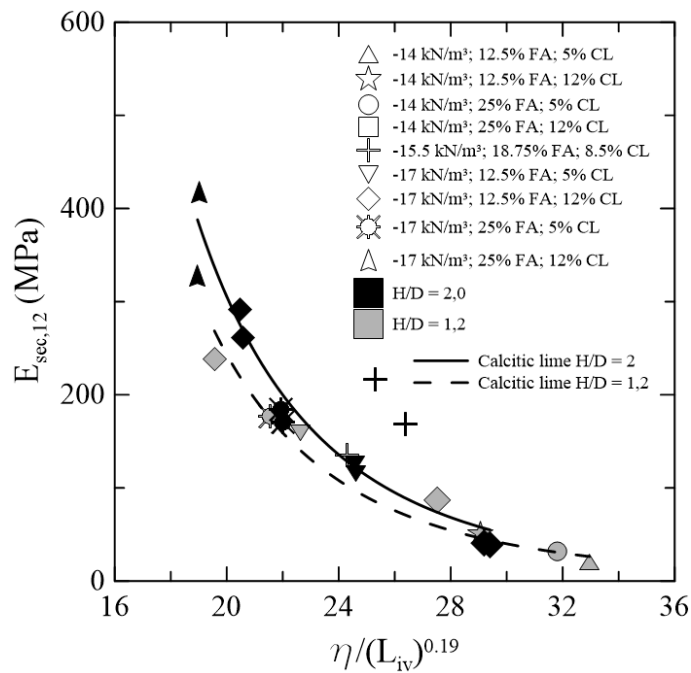


Figure 5.116: Unconfined compressive secant modulus for calcitic lime treated soils related to  $\eta/L_{iv}$  and slenderness ratio.

The regression fit equations are expressed by the equations (5.248) and (5.249), for specimens with a slenderness ratio of approximately 2.0 and 1.2, respectively

$$E_{sec,12 (H/D=2.0)} = 1.88 \times 10^8 \left[ \eta / (L_{iv})^{0.19} \right]^{-4.45} \quad R^2 = 0.82 \quad (5.248)$$

$$E_{\text{sec},12 (H/D=1.2)} = 1.50 \times 10^8 \left[ \eta / (L_{iv})^{0.19} \right]^{-4.45} \quad R^2 = 0.92 \quad (5.249)$$

The obtained relation between  $E_{\text{sec},12 (H/D = 1.2)}$  and  $E_{\text{sec},12 (H/D = 2.0)}$  for specimens stabilized using the calcitic lime is 0.80.

The comparative plot between samples with different slenderness ratios is presented in figure 5.117.

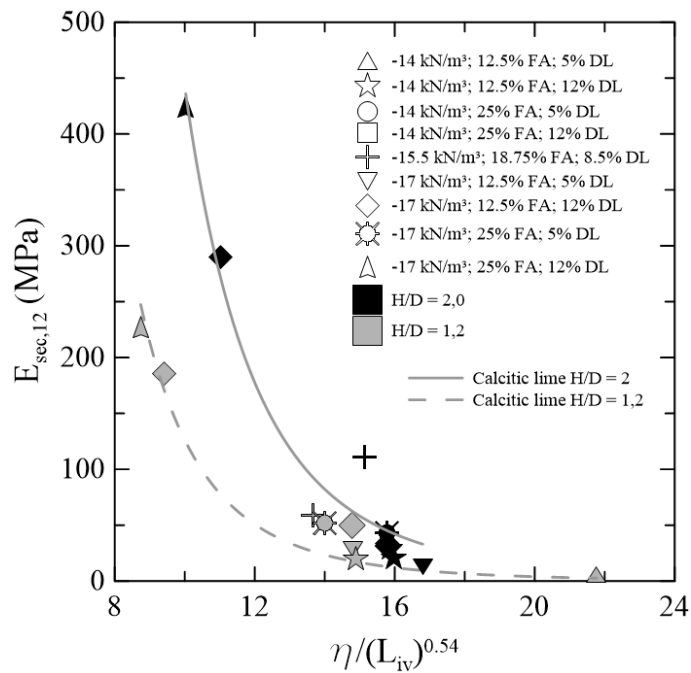


Figure 5.117: Unconfined compressive secant modulus for dolomitic lime treated soils related to  $\eta/L_{iv}$  and slenderness ratio.

The power fit regressions are expressed by the equations (5.250) and (5.251), for specimens with a slenderness ratio of approximately 2.0 and 1.2, respectively.

$$E_{\text{sec},12 (H/D=2.0)} = 4.42 \times 10^7 \left[ \eta / (L_{iv})^{0.54} \right]^{-5} \quad R^2 = 0.97 \quad (5.250)$$

$$E_{\text{sec},12 (H/D=1.2)} = 1.26 \times 10^7 \left[ \eta / (L_{iv})^{0.54} \right]^{-5} \quad R^2 = 0.92 \quad (5.251)$$

By dividing one equation for another, a relation between the slenderness ratio of 1.2 and 2.0 is obtained as 0.29.

### 5.6.3 Small strain constraint modulus x slenderness ratio

The small strain constraint modulus ( $M_0$ ) for calcitic lime treated soils are shown in figure 5.118, measured after a different number of cycles.

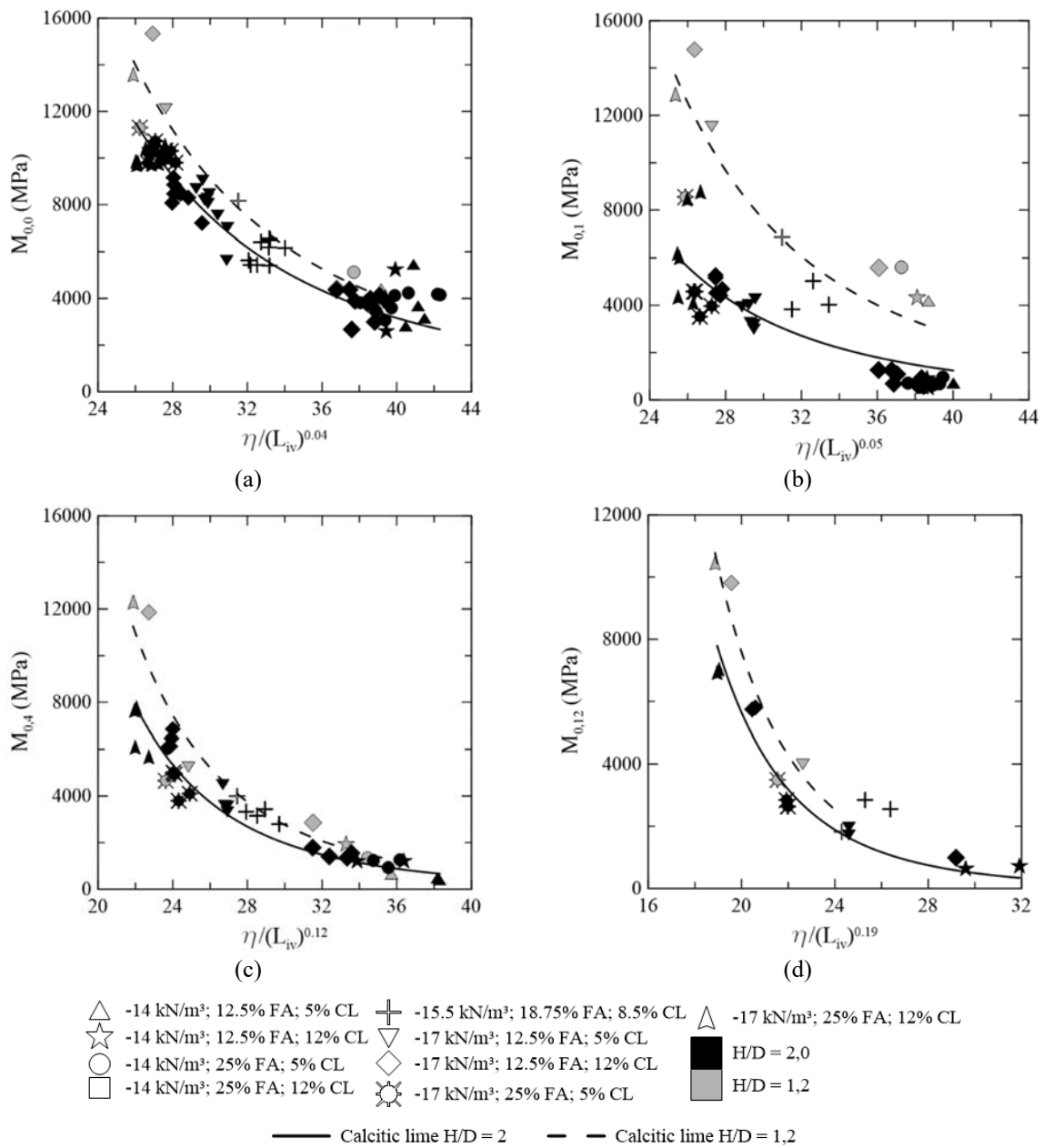


Figure 5.118: Small strain constraint modulus for calcitic lime treated soils related to  $\eta/L_{iv}$  and slenderness ratio.

The fit exponential expressions presented in figure 5.118 are enunciated below.

$$M_{0,0 (H/D=2.0)} = 2.02 \times 10^8 \left[ \eta / (L_{iv})^{0.04} \right]^{-3.00} \quad R^2 = 0.90 \quad (5.252)$$

$$M_{0,0 (H/D=1.2)} = 2.46 \times 10^8 \left[ \eta / (L_{iv})^{0.04} \right]^{-3.00} \quad R^2 = 0.91 \quad (5.253)$$

$$M_{0,1 (H/D=2.0)} = 5.04 \times 10^8 \left[ \eta / (L_{iv})^{0.05} \right]^{-3.50} \quad R^2 = 0.74 \quad (5.254)$$

$$M_{0,1 (H/D=1.2)} = 11.24 \times 10^8 \left[ \eta / (L_{iv})^{0.05} \right]^{-3.50} \quad R^2 = 0.71 \quad (5.255)$$

$$M_{0,4 (H/D=2.0)} = 7.40 \times 10^9 \left[ \eta / (L_{iv})^{0.12} \right]^{-4.45} \quad R^2 = 0.90 \quad (5.256)$$

$$M_{0,4 (H/D=1.2)} = 10.32 \times 10^9 \left[ \eta / (L_{iv})^{0.12} \right]^{-4.45} \quad R^2 = 0.87 \quad (5.257)$$

$$M_{0,12 (H/D=2.0)} = 3.61 \times 10^{11} \left[ \eta / (L_{iv})^{0.19} \right]^{-6.00} \quad R^2 = 0.87 \quad (5.258)$$

$$M_{0,12 (H/D=1.2)} = 4.85 \times 10^{11} \left[ \eta / (L_{iv})^{0.19} \right]^{-6.00} \quad R^2 = 0.94 \quad (5.259)$$

The obtained relations from those results are 1.22, 2.23, 1.39, and 1.34. It is an indication of the differences between higher and low volume specimens' structure. Care must be taken when comparing to the calcitic lime treated results after 1 durability cycle, since it is observed a significant contrast between specimens with different slenderness ratio in that situation. Maybe an experimental problem has occurred for those specimens during curing that has not yet been detected.

The plots for dolomitic lime stabilized samples are shown in figure 5.119.

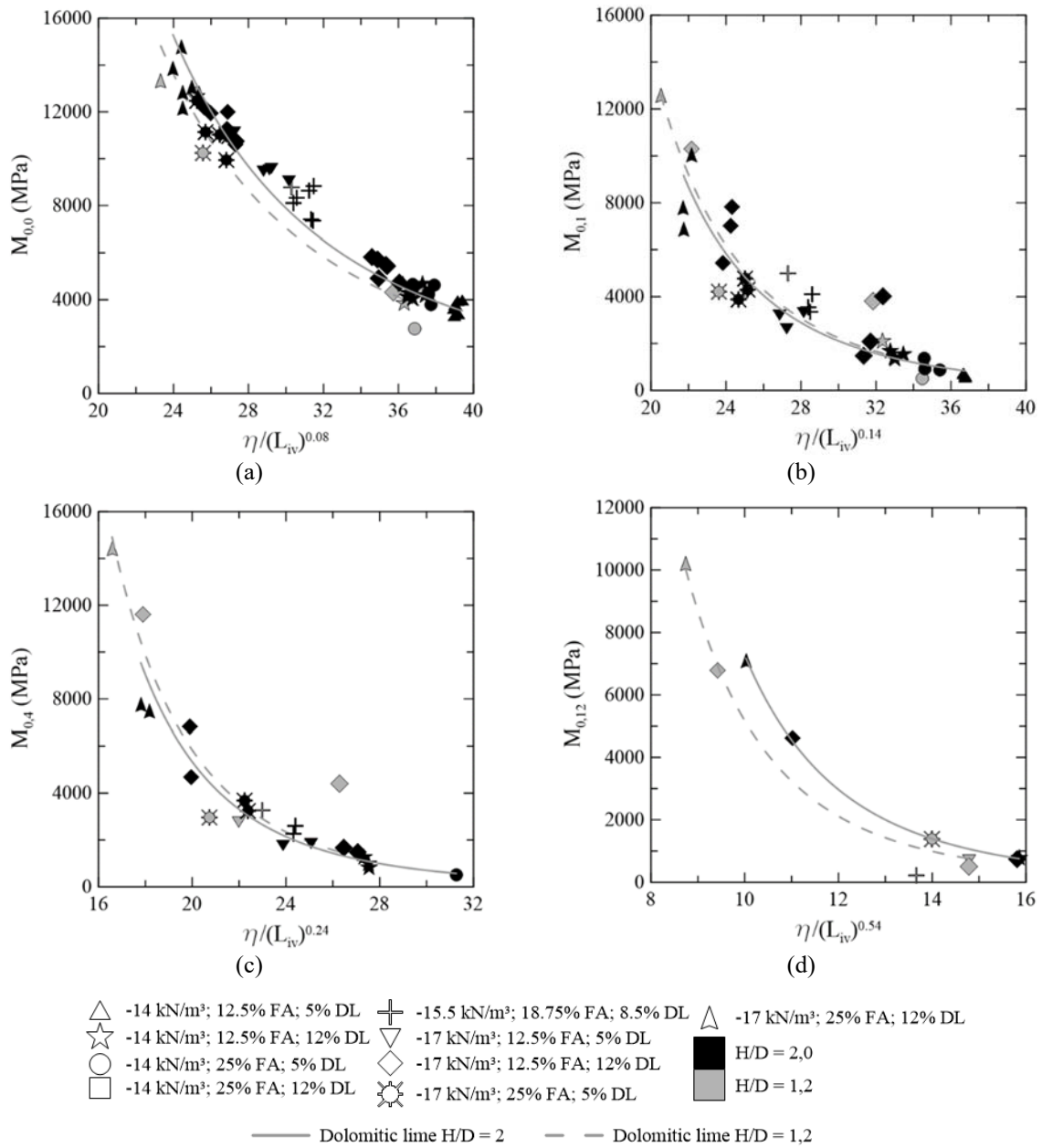


Figure 5.119: Small strain constraint modulus for dolomitic lime treated soils related to  $\eta/L_{iv}$  and slenderness ratio.

The corresponding equations are shown below.

$$M_{0,0 (H/D=2.0)} = 1.80 \times 10^8 \left[ \eta / (L_{iv})^{0.08} \right]^{-2.95} \quad R^2 = 0.96 \quad (5.260)$$

$$M_{0,0 (H/D=1.2)} = 1.61 \times 10^8 \left[ \eta / (L_{iv})^{0.08} \right]^{-2.95} \quad R^2 = 0.92 \quad (5.261)$$

$$M_{0,1 (H/D=2.0)} = 1.11 \times 10^{10} \left[ \eta / (L_{iv})^{0.14} \right]^{-4.55} \quad R^2 = 0.83 \quad (5.262)$$

$$M_{0,1 (H/D=1.2)} = 1.18 \times 10^{10} \left[ \eta / (L_{iv})^{0.14} \right]^{-4.55} \quad R^2 = 0.88 \quad (5.263)$$

$$M_{0,4 (H/D=2.0)} = 1.71 \times 10^{10} \left[ \eta / (L_{iv})^{0.24} \right]^{-5.00} \quad R^2 = 0.999 \quad (5.264)$$

$$M_{0,4 (H/D=1.2)} = 1.87 \times 10^{10} \left[ \eta / (L_{iv})^{0.24} \right]^{-5.00} \quad R^2 = 0.88 \quad (5.265)$$

$$M_{0,12 (H/D=2.0)} = 5.91 \times 10^8 \left[ \eta / (L_{iv})^{0.54} \right]^{-4.91} \quad R^2 = 0.999 \quad (5.266)$$

$$M_{0,12 (H/D=1.2)} = 4.21 \times 10^8 \left[ \eta / (L_{iv})^{0.55} \right]^{-4.91} \quad R^2 = 0.99 \quad (5.267)$$

The obtained relation between samples with lower and higher slenderness ratio is, from 0 to 12 cycles, respectively, 0.89, 1.06, 1.09, 0.71.

#### 5.6.4 Small strain shear modulus x slenderness ratio

Small strain shear modulus ( $G_0$ ) against  $[\eta / (L_{iv})^c]$  comparison plots for calcitic lime treated soils with different slenderness ratios are presented in figure 5.120. No matter the number of cycles undergone, the slender specimens seem to present lower  $G_0$  values. The fit corresponding equations are enunciated next.

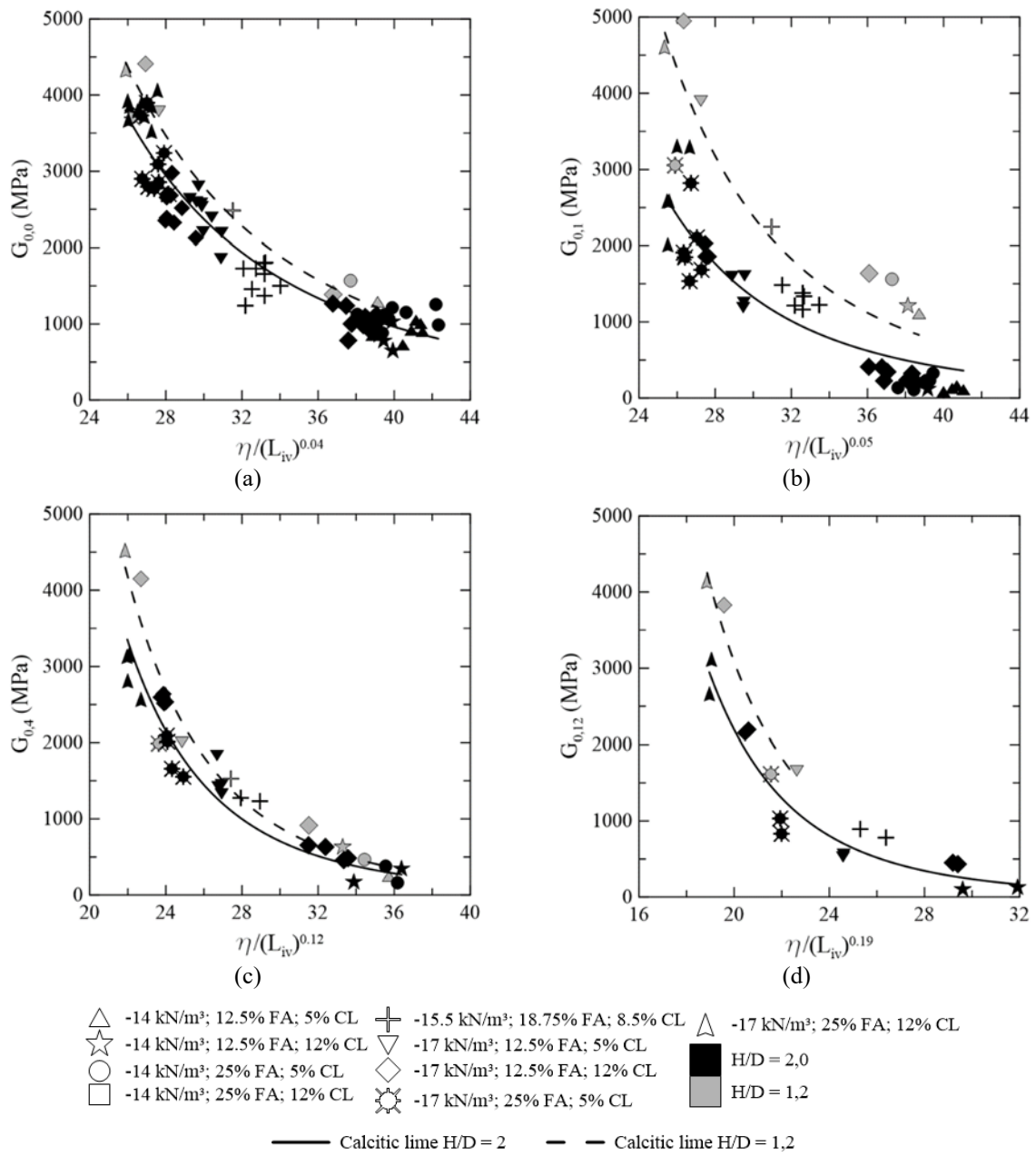


Figure 5.120: Small strain shear modulus for calcitic lime treated soils related to  $\eta/L_{iv}$  and slenderness ratio.

$$G_{0,0 (H/D=2.0)} = 9.96 \times 10^7 \left[ \eta / (L_{iv})^{0.04} \right]^{-3.13} \quad R^2 = 0.92 \quad (5.268)$$

$$G_{0,0 (H/D=1.2)} = 11.74 \times 10^7 \left[ \eta / (L_{iv})^{0.04} \right]^{-3.13} \quad R^2 = 0.96 \quad (5.269)$$



$$G_{0,1 (H/D=2.0)} = 1.79 \times 10^9 \left[ \eta / (L_{iv})^{0.05} \right]^{-4.15} \quad R^2 = 0.85 \quad (5.270)$$

$$G_{0,1 (H/D=1.2)} = 3.22 \times 10^9 \left[ \eta / (L_{iv})^{0.05} \right]^{-4.15} \quad R^2 = 0.80 \quad (5.271)$$

$$G_{0,4 (H/D=2.0)} = 1.72 \times 10^{10} \left[ \eta / (L_{iv})^{0.12} \right]^{-5.00} \quad R^2 = 0.92 \quad (5.272)$$

$$G_{0,4 (H/D=1.2)} = 2.15 \times 10^{10} \left[ \eta / (L_{iv})^{0.12} \right]^{-5.00} \quad R^2 = 0.93 \quad (5.273)$$

$$G_{0,12 (H/D=2.0)} = 3.14 \times 10^{10} \left[ \eta / (L_{iv})^{0.19} \right]^{-5.50} \quad R^2 = 0.93 \quad (5.274)$$

$$G_{0,12 (H/D=1.2)} = 4.41 \times 10^{10} \left[ \eta / (L_{iv})^{0.19} \right]^{-5.50} \quad R^2 = 0.94 \quad (5.275)$$

The obtained relations from the higher volume and less slender specimens in comparison to the slender specimens are 1.18, 1.80, 1.46, and 1.40, from 0 to 12 cycles, respectively.

The small strain shear modulus from dolomitic lime stabilized admixtures may have its values compared for different slenderness ratios in figure 5.121.

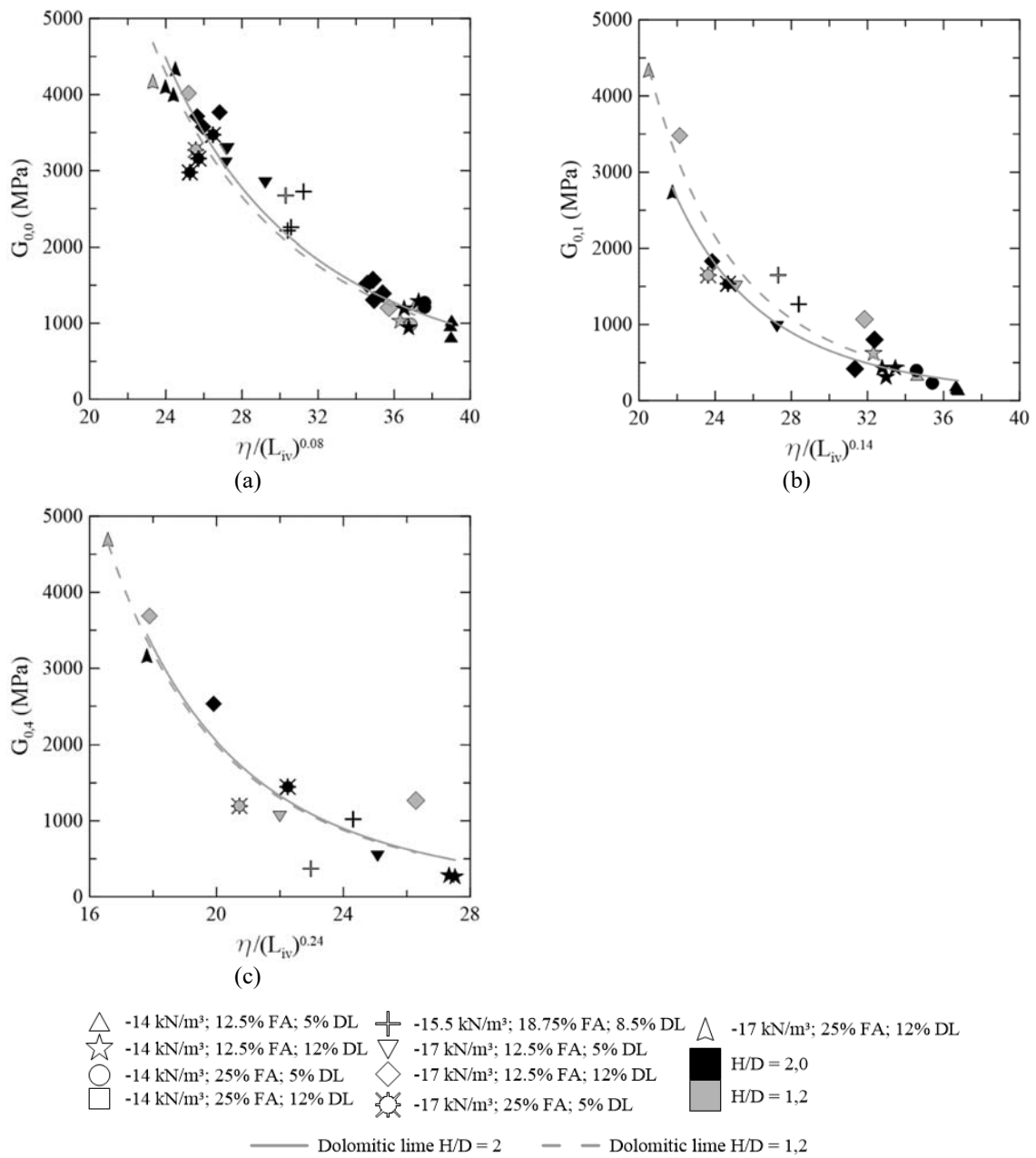


Figure 5.121: Small strain shear modulus for dolomitic lime treated soils related to  $\eta/L_{iv}$  and slenderness ratio.

The corresponding curve fits presented in figure 5.121 are shown below.

$$G_{0,0 (H/D=2,0)} = 8.50 \times 10^7 \left[ \eta / (L_{iv})^{0.08} \right]^{-3.10} \quad R^2 = 0.93 \quad (5.276)$$

$$G_{0,0 (H/D=1.2)} = 8.14 \times 10^7 \left[ \eta / (L_{iv})^{0.08} \right]^{-3.10} \quad R^2 = 0.93 \quad (5.277)$$

$$G_{0,1 (H/D=2.0)} = 2.92 \times 10^9 \left[ \eta / (L_{iv})^{0.14} \right]^{-4.50} \quad R^2 = 0.95 \quad (5.278)$$

$$G_{0,1 (H/D=1.2)} = 3.50 \times 10^9 \left[ \eta / (L_{iv})^{0.14} \right]^{-4.50} \quad R^2 = 0.92 \quad (5.279)$$

$$G_{0,4 (H/D=2.0)} = 1.46 \times 10^9 \left[ \eta / (L_{iv})^{0.24} \right]^{-4.50} \quad R^2 = 0.94 \quad (5.280)$$

$$G_{0,4 (H/D=1.2)} = 1.43 \times 10^9 \left[ \eta / (L_{iv})^{0.24} \right]^{-4.50} \quad R^2 = 0.90 \quad (5.281)$$

The obtained ratios between  $G_0$  from different specimens' sizes are 0.96, 1.2, and 0.98, from 0 to 4 cycles, respectively.

### 5.6.5 Slenderness ratio effect

Samples with a different height/diameter ratio and volume may present different behaviour, as the curing stress is a bit different, and in durability wetting and drying cycles, higher volume samples tend to experience distinct thermal and hydraulic gradients and different moisture contents when compared to the smaller samples. The results for slenderness ratio comparison are summarized in table 5.2.

It can be observed that there is usually an agreement between the ratio for small strain shear and small strain constraint modulus, even when there is a significant moisture content inside the samples (0 cycles).

Furthermore, the small strain modules for calcitic lime treated soils are about 40% higher in less slender samples at the 12<sup>th</sup> cycle, indicating a stiffer structure, whereas the less slender specimens treated with dolomitic lime have presented about 30% lower stiffness. Those structural distinctions may affect significantly the results, possibly explaining the unexpected relation between unconfined compressive strength in soils stabilized with dolomitic lime. As

expected, the unconfined modulus presents lower values for lower H/D ratios, but a lower unconfined compressive strength was expected for more slender specimens, and for dolomitic lime specimens the opposite was observed.

Table 5.2: Comparison between results for samples with different slenderness ratios.

Parameter	Ratio [(H/D $\approx$ 1.2) / (H/D $\approx$ 2.0)]	
	Calcitic lime	Dolomitic lime
$q_{u,12}$	1.51	0.66
$E_{sec,12}$	0.80	0.29
$M_{0,0}$	1.22	0.89
$M_{0,1}$	2.23	1.06
$M_{0,4}$	1.39	1.09
$M_{0,12}$	1.34	0.71
$G_{0,0}$	1.18	0.96
$G_{0,1}$	1.8	1.2
$G_{0,4}$	1.46	0.98
$G_{0,12}$	1.4	–

Yet, only samples after 12 durability cycles could be evaluated, and after all those cycles many uncontrollable variables possibly affect soil structure in different ways, turning the analysis more complicated and, as the ultrasonic transducers present approximately 5 cm in diameter, in the specimens with higher diameter size (around 10 cm), only nearly 25% of the whole volume is tested, and this central quarter may be the less affected by durability cycles and drying.

## 6 CONCLUSIONS AND REMARKS

From the literature review, test results and analysis conducted in this research, some questions, conclusions, and suggestions have arisen. They are addressed next.

### 6.1 SUMMARY OF CONCLUSIONS

The main conclusions are the following:

- a) Chemical stabilization is a great solution to control dispersibility erosion, and there is no need for huge amounts of binder to stabilize the deflocculation process of slightly/intermediate dispersive soils;
- b) The SAR x TDS chart for the classification of dispersive soils have proved to be unreliable for the identification of dispersibility in the studied soil;
- c) Care must be taken when dealing with sandy clayey dispersive soils because they may present a slightly dispersive behaviour but, as its particles are weakly bonded, they also tend to be eroded by water dragging shear stress;
- d) The regression equations for stabilized soils dosing, when no curvature is considered, tend to result in imprecise results for the intermediate factors content;
- e) The effect of a small number of cycles seems to be negligible in strength and mechanical properties, but as this number grows up, the damage is apparent;
- f) Dry unit weight seems to play the most important role in soils durability, so high compaction energies may be one of the main keys to a durable design with stabilized soils;
- g) Variables like unconfined soil strength, small strain constraint, and shear modulus, and accumulated loss of mass may be inter-related;
- h) The unconfined compressive strength, unconfined secant modulus, small strain shear, and small strain constraint modulus decrease exponentially as the binder

(or lime) key parameter increases, whereas the small strain Poisson's ratio increases linearly, and the ALM increases exponentially;

- i) The durability of stabilized soils may not be related only to strength, since the dolomitic lime treated soils presented a higher strength at 28 curing days when compared to calcitic lime treated soils, but the calcitic soils presented lower accumulated loss of mass values;
- j) An increase in fly ash content induces a strength increase, but does not seem to improve the durability;
- k) The key parameter exponent seems to grow linearly along a damaging period, as the less durable soils lose much more mass and strength than the more durable soils;
- l) Stiffness properties are probably more affected by the durability cycles than the strength;
- m) A durability methodology with smaller samples and without brushing application on specimens has presented satisfactory results, however, it is not possible to accurately quantify the loss of mass.

## 6.2 SUGGESTIONS FOR FORTHCOMING RESEARCHES

The present study has achieved some advances related to the state of the art of stabilized soils and the effect of cycles on dispersive stabilized materials, but there are still gaps in the knowledge related to this research. For that, some suggestions are presented for further studies:

- n) A field study comparing is needed in order to compare field climate conditions with laboratory durability tests;
- o) Performance of cation exchange capacity (CEC) test for the studied soil;
- p) A full new characterization of Primor and carbide lime to identify what changes the durability effect besides calcium oxide (CaO);
- q) A study to assess the slenderness ratio effect with samples with the same volume and conditions;

- r) Triaxial compression tests are suggested to be carried to define soil and mixture constitutive parameters and stiffness;
- s) Utilization of different pozzolans for the stabilization of dispersive soils and the assessment of durability effect;
- t) X-ray diffractometry analysis of the soil (oriented and calcined);
- u) Structure XRD and microscopic analysis of the mixtures after curing and after durability cycles to identify the consumed and remained mineral phases;

## REFERENCES

ABNT – NBR 7182. Solo – Ensaio de compactação / Soil – Compaction test. Rio de Janeiro. 2020. 9 páginas.

ABNT - NBR 13602. Solo - Avaliação da dispersibilidade de solos argilosos pelo ensaio sedimentométrico comparativo – Ensaio de dispersão SCS/ Soil - Dispersive characteristics of clay soil by double hydrometer -Method of test. Rio de Janeiro. 2020. 9 páginas.

ABNT - NBR 13603. Solo – Avaliação da dispersibilidade de solos argilosos, por meio de ensaios químicos em amostras de água intersticial /Soil - Sample preparation of pore water for dispersability evaluation of clay soils through chemical methods. Rio de Janeiro. 1996. 3 páginas.

ABNT - NBR 14114. Solo - Solos argilosos dispersivos -Identificação e classificação por meio do ensaio do furo de agulha (pinhole test) / Soil - Dispersive clay soils - Identification and classification by the pinhole test. Rio de Janeiro. 1998.

AMERICAN SOCIETY FOR TESTING AND MATERIALS. C597 - 16: Standard Test Method for Pulse Velocity Through Concrete<sup>1</sup>. West Conshohocken: ASTM, 2016.

AMERICAN SOCIETY FOR TESTING AND MATERIALS. D559D559M-15: Standard Test Method for Wetting and Drying Compacted Soil-Cement Mixtures. West Conshohocken: ASTM, 2015.

AMERICAN SOCIETY FOR TESTING AND MATERIALS. D698 – 12: Standard Test Methods for Laboratory Compaction Characteristics of Soil Using Standard Effort (12,000 ft-lbf/ft<sup>3</sup> (600 kN-m/m<sup>3</sup>)). West Conshohocken: ASTM, 2012.

AMERICAN SOCIETY FOR TESTING AND MATERIALS. D854 – 14: Standard Test Method for Specific Gravity of Soil Solids by Water Pycnometer. West Conshohocken: ASTM, 2014.



AMERICAN SOCIETY FOR TESTING AND MATERIALS. D1557 – 12: Standard Test Method for Laboratory Compaction Characteristics of Soil Using Modified Effort (56,000 ft-lbf/ft<sup>3</sup> (2,700 kN-m/m<sup>3</sup>))<sup>1</sup>. West Conshohocken: ASTM, 2015.

AMERICAN SOCIETY FOR TESTING AND MATERIALS. D1632 – 17: Standard Practice for Making and Curing Soil-Cement Compression and Flexure Test Specimens in the Laboratory. West Conshohocken: ASTM, 2017.

AMERICAN SOCIETY FOR TESTING AND MATERIALS. D1633 – 17: Standard Test Method for Compressive Strength of Molded Soil-Cement Cylinders. West Conshohocken: ASTM, 2017.

AMERICAN SOCIETY FOR TESTING AND MATERIALS. D2216 – 19: Standard Test Method for Laboratory Determination of Water (Moisture) Content of Soil and Rock by Mass. West Conshohocken: ASTM, 2019.

AMERICAN SOCIETY FOR TESTING AND MATERIALS. D2487 – 17: Standard Practice for Classification of Soils for Engineering Purposes (Unified Soil Classification System). West Conshohocken: ASTM, 2018.

AMERICAN SOCIETY FOR TESTING AND MATERIALS. D 2845 – 08: Standard Test Method for Laboratory Determination of Pulse Velocities and Ultrasonic Elastic Constants of Rock. West Conshohocken: ASTM, 2008.

AMERICAN SOCIETY FOR TESTING AND MATERIALS. D4015 – 15: Standard Test Methods for Modulus and Damping of Soils by Fixed-Base Resonant Column Devices<sup>1</sup>. West Conshohocken: ASTM, 2015.

AMERICAN SOCIETY FOR TESTING AND MATERIALS. D4221 - 18: Standard Test Method for Dispersive Characteristics of Clay Soil by Double Hydrometer<sup>1</sup>. West Conshohocken: ASTM, 2018.

AMERICAN SOCIETY FOR TESTING AND MATERIALS. D 4318 – 00: Standard Test Method for Liquid Limit, Plastic Limit, and Plasticity Index of Soils. West Conshohocken: ASTM, 2000.

AMERICAN SOCIETY FOR TESTING AND MATERIALS. D4647/D4647M – 13: Standard Test Method for Identification and Classification of Dispersive Clay Soils by the Pinhole Test. West Conshohocken: ASTM, 2020.

AMERICAN SOCIETY FOR TESTING AND MATERIALS. D5239 – 12': Standard Practice for Characterizing Fly Ash for Use in Soil Stabilization. West Conshohocken: ASTM, 2018.

AMERICAN SOCIETY FOR TESTING AND MATERIALS. D5519 – 15: Standard Test Methods for Particle Size Analysis of Natural and Man-Made Riprap Materials<sup>1</sup>. West Conshohocken: ASTM, 2015.

AMERICAN SOCIETY FOR TESTING AND MATERIALS. D6572 – 13: Standard Test Method for Determining Dispersive Characteristics of Clayey Soils by the Crumb Test. West Conshohocken: ASTM, 2020.

AMERICAN SOCIETY FOR TESTING AND MATERIALS. D6913/D6913M – 17: Standard Test Method for Particle-Size Distribution (Gradation) of Soils Using Sieve Analysis. West Conshohocken: ASTM, 2017.

AMERICAN SOCIETY FOR TESTING AND MATERIALS. D 6276 – 19: Standard Test Method for using pH to Estimate the Soil-Lime Proportion Requirement for Soil Stabilization<sup>1</sup>. West Conshohocken: ASTM, 2019.

AMERICAN SOCIETY FOR TESTING AND MATERIALS. D7263 – 09: Standard Test Methods for Laboratory Determination of Density (Unit Weight) of Soil Specimens. West Conshohocken: ASTM, 2018.

AMERICAN SOCIETY FOR TESTING AND MATERIALS. D7928 – 17: Standard Test Method for Particle-Size Distribution (Gradation) of Fine-Grained Soils Using the Sedimentation (Hydrometer) Analysis. West Conshohocken: ASTM, 2017.

ABBIS, C. P. **Shear Wave Measurements of the Elasticity of the Ground.** Géotechnique v. 31, n. 1, p. 91-104, 1981.

ABDI, Y., KHANLARI, G., JAMSHIDI, A. **Correlation Between Mechanical Properties of Sandstones and P-Wave Velocity in Different Degrees of Saturation.** Geotech Geol Eng, 2018.

AGUSTAWIJAYA, D. S. **The Uniaxial Compressive Strength of Soft Rock.** Civil Engineering Dimension, v. 9, n. 1, p. 9–14, March 2007.

AHMED, S. M. **Assessment of Clay Stiffness and Strength Parameters Using Index Properties.** Journal of Rock Mechanics and Geotechnical Engineering, 2018.

AITCHISON, G. D., WOOD, C. C. **Some Interactions of Compaction, Permeability, and Post-Construction Deflocculation.** p.442-446. 1965.

AITCHISON, G. D., INGLES, O. G. and WOOD, C. C. **Postconstruction deflocculation as a contributory factor in the failure of earth dams.** Proc. Fourth Australia-New Zealand Conference on Soil Mechanics and Foundation Engineering (Adelaide), 1963.

ALDAOOD, A., BOUASKER, M., AL-MUKHATAR, M. **Impact of Wetting-Drying Cycles on the Microstructure and Mechanical Properties of Lime-Stabilized.** Engineering Geology v. 174, p.11–21, 2014.

ARABI, M., DELPAL, R., WILD, S. **Assessment of the Unconfined Compressive Strength of a Lime Stabilized Soil by an Abrasion Test.** Geotechnical Testing Journal, v.11, n.1, p.56-59, 1988.

ARMAN, H., KHOSRAVI, S., OSMAS, M.A., ALNAQBI, F.M., ALYAMMAHI, A.A. **Dimension Effect on the Ultrasonic Pulse Velocity.** International Journal of Geography and Geology, v. 6, n. 2, p. 18-25, 2017.

ARSLAN, A. T., KICA, M.Y., AYDOGMUS, T., KLAPPERICH, H., YILMAZ, H.R. **Correlation of Unconfined Compressive Strength with Young's Modulus and Poisson's Ratio in Gypsum from Sivas**. Rock Mech Rock Engng v.41, p. 941–950, 2008.

ASKELAND, D. R., WRIGHT, W. J. **The Science and Engineering of Materials**. 7<sup>th</sup> edition, 2016.

ATKINSON, J. **Fundamentals of Ground Engineering**. 2014.

BALSHIN MY. **Relation of mechanical properties of powder metals and their porosity and the ultimate properties of porous-metal ceramic materials**. Dokl Akad SSSR; v. 67(5), p. 831–4, 1949.

BARBOZA, G. E., TOMAZELLI, L. J., DILLENBURG, S. R., ROSA, M.L. C.C. **Planície Costeira do Rio Grande do Sul Erosão em Longo Período**. Revista SUG n. 15, p. 94-97, 2009.

BART, J. C. J., GUCCIARDI, E., CAVALLARO. **Biolubricants Science and Technology**. Woodhead Publishing Limited, 2013.

BASTOS, C. A. B. **Estudo Geotécnico sobre a Erodibilidade de Solos Residuais não Saturados**. Tese (Doutorado) - Curso de Pós-graduação em Engenharia Civil, Escola de Engenharia da UFRGS, Universidade Federal do Rio Grande do Sul, Porto Alegre, 1999.

BASU, A., MISHRA, D.A., ROYCHOWDHURY, K. **Rock Failure Modes Under Uniaxial Compression, Brazilian, and Point Load Tests**. Bull Eng Geol Environ, v. 72, p.457–475, 2013.

BEEN, K.; JEFFERIES, M. G. **A State Parameter for Sands**. Géotechnique v.35, n. 2, p. 99-112, 1985.

BELL, F. G. **Engineering Geology and Construction**. Taylor & Francis, 2004.

BELL, F. G. **Engineering Geology**. Butterworth-Heinemann, second edition: 2007.

BELL, F. G.; WALKER, D. J. H. **A Further Examination of the Nature of Dispersive Soils in Natal, South Africa.** Quarterly journal of engineering geology and Hydrogeology, v.33. p. 187-199, 1999.

BENCHOUK, A., DERFOUF, M., ABOU-BEKR, N., TALBI, S. **Behavior of Some Clays on Drying and Wetting Paths.** Arabian Journal of Geosciences · December 2012.

BERGAYA, F., THENG, B.K.G., LAGALY, G. **Handbook of Clay Science.** Elsevier Ltd. 2006.

BERGNA, H. E. **The Colloid Chemistry of Silica.** American Chemical Society, Washington, DC 1994.

BOARDMAN, D. I., GLENDINNING, S., ROGERS, C.D.F. **Development of Stabilisation and Solidification in Lime-Clay Mixes.** Geotechnique v.50, n. 6, p.533-543, 2001.

BOBET, A.; EINSTEIN, H. H. **Fracture Coalescence in Rock-Type Materials Under Uniaxial and Biaxial Compression.** Int. J. Rock Mech. Min. Sci. v. 35, n. 7, p. 863-888, 1998.

BONELLI, S. **Erosion of Geomaterials.** John Wiley & Sons, Inc, 2012

BONELLI, S. **Erosion in Geomechanics Applied to Dams and Levees.** John Wiley & Sons, Inc, 2013

BORGES, H. F. **Estabilização de um Solo Argiloso com Cal de Carbureto.** Tese (mestrado), Programa de Pós-Graduação em Engenharia Civil, Universidade Federal do Rio de Janeiro. Instituto Luiz Coimbra de Pós-Graduação e Pesquisa em Engenharia, 1979.

BORTOLOTTO, M. S. **Bender Elements, Ultrasonic Pulse Velocity, and Local Gauge for the Analysis of Stiffness Degradation of an Artificially Cemented Soil.** Dissertation (Master of Engineering) – Post Graduation Civil Programa of the Federal University of Rio Grande do Sul. 2017.

BOX, G. E. P.; DRAPER, N. R. **Response Surfaces, Mixtures and Ridge Analyses**. 2<sup>nd</sup> edition, John Wiley & Sons, Inc, 2007.

BRADFORD, J. M., PIEST, R. F., SPOMER, R. G. **Division S-5-Soil Genesis, Morphology, and Classification**. SOIL SCI. SOC. AM. J., v. 42, 1978.

BRESSANI, L. A. **External Measurement of Axial Strain in the Triaxial Test**. Geotechnical Testing Journal, v. 18, n. 2, p. 226-240, 1995.

BRIAUD, J.-L. **Case Histories in Soil and Rock Erosion**. Journal of Geotechnical Geoenvironmental. Engineering, v. 134, p.1425-1447, 2008.

BRIAUD, J.-L., GIVINDASAMY, A. V., SHAFII, I. **Erosion Charts for Selected Geomaterials**. J. Geotech. Geoenviron. Eng., v. 143(10): 04017072, 2017.

BRIGNOLI, E. G. M., GOTTI, M., STOKOE, K.H. **Measurement of Shear Waves in Laboratory Specimens by Means of Piezoelectric Transducers**. Geotechnical Testing Journal, 1996.

BRUNAUER, S., EMMET, P;H., TELLER, E. **Adsorption of Gases in Multimolecular Layers**. Contribution from the bureau of chemistry and sons and George Washington University, 1938.

BUCHANAN, Francis. **A Journey from Madras Through the Countries of Mysore, Canara, and Malabar**. London: 1807.

BUNGEY, J. H., MILLARD, S.G., GRANTHAM, M.G. **Testing of Concrete in Structures**. Taylor & Francis e-Library, 2006.

BURLAND, J. B. **Ninth Laurits Bjerrum Memoria Lecture - Small is Beautiful - The Stiffness of Soils at Small Strains**. Can. Geotech. J. v. 26, p. 499-516, 1989.

CALLISTER JR, W. D.; RETHWISCH, D. G. **Fundamentals of Materials Science and Engineering**. Wiley, 5<sup>th</sup> edition, 2015

CHEN, J., XIAO, H., LI, Z., LIU, C., WANG, D., WANG, L. **Threshold Effects of Vegetation Coverage on Soil Erosion Control in Small Watersheds of the Red Soil.** *Ecological Engineering* v. 132, p. 109–114, 2019.

CHEN, X., WU, S., ZHOU, J. **Influence of Porosity on Compressive and Tensile Strength of Cement Mortar.** *Construction and Building Materials* v. 40, p. 869–874, 2013.

CHENG, Z. Y.; LEONG, E. C. **Ultrasonic Testing of Unsaturated Soils.** School of Civil and Environmental Engineering, Nanyang Technological University, Singapore, 2013.

CHO, Chun; SANTAMARINA, J. Carlos. **Unsaturated Particulate Materials – Particle-Level Studies.** *Journal of Geotechnical and Geoenvironmental Engineering*. p. 84-96, January, 2001.

CHUNG, F. H. **Quantitative Interpretation of X-Ray Diffraction Patterns of Mixtures. I. Matrix-Flushing Method for Quantitative Multicomponent Analysis.** *J. Appl. Cryst.* v. 7, p. 519-525, 1974.

CLAYTON, C. R. I. **Stiffness at Small Strain - Research and Practice.** *Géotechnique* v. 61, n1, p. 5-37, 2011.

CLOUGH, G. Wayne; SITAR, Nicholas; BACHUS, Robert C.; RAD, Nader Shafii. **Cemented Sands under Static Loading.** *J. Geotech. Engrg.* v. 107(GT6), p. 799-817.

ÇOKÇA, Erdal. **Use of Class C Fly Ashes for the Stabilization of an Expansive Soil.** *J. Geotech. Geoenviron. Eng.* v. 127, p. 568-573, 2001.

CONSOLI, N. C., PRIETTO, P.D.M., CARRARO, J.A.H., HEINECK, K.S.H. **Behavior of Compacted Soil-Fly Ash-Carbide Lime Mixtures.** *J. Geotech. Geoenviron. Eng.* v. 127, p.774-782, 2001.

CONSOLI, N. C., PRIETTO, P.D.M., CARRARO, J.A.H., HEINECK, K.S. **Behavior of Compacted Soil-Fly Ash-Carbide Lime Mixtures.** *J. Geotech. Geoenviron. Eng.* v. 127, p.774-782, 2001.

CONSOLI, N. C. FOPPA, D., FESTUGATO, L., HEINECK, K. S. **Key Parameters for Strength Control of Artificial Cemented Soils.** Journal of Geotechnical and Geoenvironmental Engineering, 2007.

CONSOLI, N. C., da SILVA LOPES, L., FOPPA, D., HEINECK, S. **Key Parameters Dictating Strength of Lime-Cement-Treated Soils.** Geotechnical Engineering v. 162, p. 111–118, 2009.

CONSOLI, N. C., CRUZ, R.C., FLOSS, F.M., FESTUGATO, L. **Parameters Controlling Tensile and Compressive Strength of Artificially Cemented Sand.** Journal of Geotechnical and Geoenvironmental Engineering, v. 136, p. 759-763, 2010.

CONSOLI, N. C., ROSA, A.D., SALDANHA, R. B. **Parameters Controlling Strength of Industrial Waste-Lime Amended Soil.** Soils and Foundations, v. 51, n.2, p. 265-273, 2011a.

CONSOLI, N. C, ROSA, A. D., CRUZ, R. C., DALLA ROSA, A. **Water Content, Porosity and Cement Content as Parameters Controlling Strength of Artificially Cemented Silty.** Engineering Geology, v.122, p. 328–333, 2011b.

CONSOLI, N. C.; ROSA, A. D.; SALDANHA, R. B. **Variables Governing Strength of Compacted Soil-Fly Ash-Lime Mixtures.** J. Mat. Civ. Eng., v. 23, p. 432-440, 2011c.

CONSOLI, N. C., DALLA ROSA, A JOHANN, GAUER, E. A., DOS SANTOS, V. R., MORETTO, R. L., CORTE, M. B. **Key Parameters for Tensile and Compressive Strength of Silt-Lime Mixtures.** Geotechnique Letters v.2, p. 81–85, 2012.

CONSOLI, N. C., DA SILVA LOPES, J. A., CONSOLI, B. S., FESTUGATO, L. **Mohr–Coulomb Failure Envelopes of Lime-Treated Soils.** Géotechnique. 2013.

CONSOLI, N. C. A. **Method Proposed for the Assessment of Failure Envelopes of Cemented Sandy Soils.** Engineering Geology, v. 169. p. 61-68, 2014.



CONSOLI, N. C., PRIETTO, P.D.M., LOPES, L.S.; WINTER, D. **Control Factors for the Long Term Compressive Strength of Lime Treated Sandy Clay Soil.** Transportation Geotechnics v. 1, p. 129–136, 2014.

CONSOLI, N. C., SAMANIEGO, R.A.Q., VILALBA, N.M.K. **Durability, Strength, and Stiffness of Dispersive Clay-Lime Blends.** J. Mater. Civ. Eng., 04016124, 2016a.

CONSOLI, N. C., SAMANIEGO, R.A.Q., MARQUES, S.F.V., VENSON, G.I., PASCHE, E., VELÁSQUEZ, L.E.G. **A Single Model Establishing Strength of Dispersive Clay.** Canadian Geotechnical Journal. v. 53, n. 12, 2016b.

CONSOLI, N. C., WINTER, D., LEON, H.B., SCHEUERMANN, H.C. **Durability, Strength, and Stiffness of Green Stabilized Sand.** J. Geotech. Geoenviron. Eng, 144(9): 04018057., 2018.

CONSOLI, N. C., SILVA, A.P., NIERWINSKI, H.P., SOSNOSKI, J. **Durability, Strength and Stiffness of Compacted Gold Tailings.** Canadian Geotechnical Journal. v. 55, n. 4, 2018.

CONSOLI, N. C., LEON, B.H., CARRETTA, M.S., DARONCO, J.V.L., LOURENÇO, D.E. **The Effects of Curing Time and Temperature on Stiffness, Strength and Durability of Sand-Environment Friendly Binder Blends.** Soils and Foundations v. 59, p. 1428–1430, 2019a.

CONSOLI, N. C., CARRETTA, M.S., LEON, H. B., SCHEIDER, M.E.B., REGINATO, N.C., CARRARO, A.H. **Behaviour of Cement-Stabilised Silty Sands Subjected to Harsh Environmental Conditions.** Proceedings of the Institution of Civil Engineers – Geotechnical Engineering, 2019b.

CONSOLI, N. C., GODOY, V. B.; TOMASI, L. F.; DE PAULA, T. M.; BORTOLOTTI, M. S.; FAVRETTO, F. **Fibre-reinforced sand-coal fly ash-lime-NaCl blends under severe environmental conditions.** Geosynthetics International v. 26, Issue 5, p. 525-538, 2019c.

CONSOLI, N. C., CARRETTA, M.S., FESTUGATO, L., LEON, H.B., TOMASI, L.F., HEINECK, K.S. **Ground-Waste Glass-Carbide Lime as a Sustainable Binder Stabilising**. *Géotechnique* [<https://doi.org/10.1680/jgeot.18.P.099>], 2020a.

CONSOLI, N. C., FESTUGATO, L., SCHEUERMANN, H.C., MIGUEL, G.D., TEBECHRANI, A., ANDREGHETTO, D. **Durability Assessment of Soil-Pozzolan-Lime Blends Through Ultrasonic-Pulse Velocity Test**. *J. Mater. Civ. Eng.*, 32(8): 04020223, 2020b.

COOP, M. R.; ATKINSON, J. H. **The Mechanics of Cemented Carbonate Sands**. *Géotechnique*, v.43, n.1, p.53-67, 1993.

CPRM, **Mapa Geológico do Rio Grande do Sul**. Companhia de pesquisa, 2004.

CRISTELO, N.; TAVARES, P.; LUCAS, E.; MIRANDA, T.; OLIVEIRA, D. **Quantitative and qualitative assessment of the amorphous phase of a Class F fly ash dissolved during alkali activation reactions – Effect of mechanical activation, solution concentration and temperature**. *Composites Part B*, v. 103, p. 1-14. 2016.

CUCCOVILLO, T.; COOP, M. R. **On the Mechanics of Structured Sands**. *Géotechnique*, v.49, n.6, p.741-760, 1999.

CUNDALL, P. A., STRACK, O. D. L. **A Discrete Numerical Model for Granular Assemblies**. *Géotechnique* 29, v. 1, p. 47-65. 1979.

DAGAR, J. C.; SINGH, A. K. **Ravine Lands - Greening for Livelihood and Environmental Security**. Springer, 2018.

DAHALE, P. P.; NAGARNAIK, P. B.; GAJBHIYE, A. Y. **Effect of flyash and lime on stabilization of expansive soil**. *Journal on Civil Engineering*, v. 6, no. 2, p. 7-10. 2016.

DALLA ROSA, A. **Estudo dos Parâmetros-Chave no Controle da Resistência de Misturas Solo-Cinza-Cal**. Dissertação (Mestrado) - Curso de Pós-graduação em Engenharia Civil, Escola de Engenharia da UFRGS, Universidade Federal do Rio Grande do Sul, Porto Alegre, 2009.

DAS, Braja M. **Advanced Soil Mechanics**. Taylor & Francis 3<sup>rd</sup>, 2008.

DEMPSEY, B. J., THOMPSON, M. R. **Durability Properties of Lime-Soil Mixtures**. University of Illinois, 1968.

DHIR, R. K., HEWLETT, P.C., CHAN, Y.N. **Near-Surface Characteristics of Concrete-Abrasion Resistance**. *Materials and Structures/Materiaux et Constructions*, v. 24, p. 122-128, 1991.

DHIR, R. K.; SANGHA, C. M. **Relationships Between Size, Deformati**. *Int. J. Rock Mech .Min, Sci. & Geomech* v. 10, p. 699-712, 1973.

DIAMBRA, A., IBRAIM, E., PECCIN, A., CONSOLI, N.C. **Theoretical Derivation of Artificially Cemented Granular Soil Strength**. *J. Geotech. Geoenviron. Eng.*, -1-1, 2017.

DOLINAR, B.; SKRABL, S. **Atterberg Limits in Relation to Other Properties of Fine-Grained Soils**. *ACTA Geotechnica Slovenica*, 2013.

DONATELLO, S.; TYRER, M.; CHEESEMAN, C. R. **Comparison of test methods to assess pozzolanic activity**. *Cement and Concrete Composites* v. 32, p. 121-127, 2010.

DONG, Y.; LU, N. **Dependencies of Shear Wave Velocity and Shear Modulus of Soil on Saturation**. *Journal of Engineering Mechanics*, 2016.

DURAKOVIC, B. **Design of Experiments Application, Concepts, Examples - State of the Art**. *Periodicals of Engineering and Natural Sciences* v. 5, n. 3, p. 421–439, 2017.

FATTAHPOUR, V., BAUDET, B.A., MOOSAVI, M., MEHRAMPOUR, M., ASHKEZARI, A. **Effect of Grain Characteristics and Cement Content on the Unconfined Compressive Strength of Artificial Sandstone**. *International Journal of Rock Mechanics & Mining Sciences* v. 72, p. 109–116, 2014.

FELLENIUS, Bengt H. **Basics of Foundation Design**. Electronic Edition., 2017.

FELL R., FRY J.J. (eds), **Internal Erosion of Dams and Their Foundations**, Taylor & Francis, p. 245, 2007.

FENG, Jingjing; SUN, Jianwei; YAN, Peiyu. **The Influence of Ground Fly Ash on Cement Hydration and Mechanical Property of Mortar**. *Advances in Civil Engineering*. V. 2018. ID 4023178, 7 p.

FERNANDEZ, A. L.; SANTAMARINA, J. C. **Effect of Cementation on the Small-Strain Parameters of Sands**. *Can. Geotech. J.* v. 38, p. 191–199, 2001.

FOOKES, P. G. **Geomaterials**. *Quarterly Journal of Engineering Geology*, v.24, p.3-15, 1991.

FRANÇOIS, Dominique. LEMAITRE, Jean (editor) **Handbook of Materials Behavior Models - Volume I Deformations of Materials. Section 7.5. Brittle Fracture**. ACADEMIC PRESS A Division of Harcourt, Inc. 2001.

FRYDMAN, S., CHARRACH, J., GORESTSKY, I. **Geotechnical Properties of Evaporite Soils of the Dead Sea Area**. *Engineering Geology* v. 101, p. 236–244, 2008.

GIESE, R. F.; OSS, C. J. V. **Colloid and Surface Properties of Clays and Related Minerals**. Marcel Dekker, Inc, 2002.

GILLOT, Jack E. **Clay in Engineering Geology**. Elsevier, 1987.

GRANJA, José L.; AZENHA, Miguel; SOUSA, Christoph de; FERREIRA, Cristiana. **Comparison between diferente experimental techniques for stiffness monitoring of cement pastes**. *Journal of Advanced Concrete Technology*. V. 12, pp. 46-61, 2014.

GREGORY, A. R. **Fluid Saturation Effects on Dynamic Elastic Properties of Sedimentary Rocks**. *GEOPHYSICS*. v. 41, n. 5, p. 895-921, 1976.

GUNAYDIN, O., GOKOGLU, A., FENER, M. **Prediction of Artificial Soil's Unconfined Compression Strength Using Statistical Analyses**. *Advances in Engineering Software* v. 41, p. 1115–1123, 2010.

GUNEYLI, H.; RUSEN, T. **Effect of Length-to-Diameter Ratio on the Unconfined Compressive Strength of Cohesive Soil Specimens**, Bulletin of Engineering Geology and the Environment, 2015.

HANEHARA, S., TOMOSAWA, F., KOBAYAKAWA, M., HWANG, K. **Effects of Water-Powder Ratio, Mixing Ratio of Fly Ash, and Curing Temperature on Pozzolanic Reaction of Fly Ash in Cement Paste**. Cement and Concrete Research v. 31, p. 31-39, 2001.

HARICHANE, K., GHRICI, M., KENAU, S., GRINE, K. **Use of Natural Pozzolana and Lime for Stabilization of Cohesive Soils**. Geotech Geol Eng v. 29, p. 759–769, 2011.

HARMSE, H. J. V. M.; GERBER, F. A. **A Proposed Procedure for the Identification of Dispersive Soils**. **Proceedings: Second International Conference on Case Histories In Geotechnical Engineering**, June 1-5,1988.

HASSELMAN, D. P. H. **Griffith Flaws and the Effect of Porosity on Tensile Strength of Brittle Ceramics**. Journal of The American Ceramic Society, 1969.

HATANAKA, M.; MASUDA, T. **Experimental Study on the Relationship Between Degree of Saturation and P-Wave Velocity in Sandy Soils**. Science Press Beijing and Springer-Verlag Geotechnical Engineering for Disaster Mitigation and Rehabilitation, p.346-351, 2008.

HAWKES, I.; MELLOR, M. **Uniaxial Testing in Rock Mechanics Laboratories**. Eng. Geology, v. 4, p. 177-285, 1970.

HOLTZ, R. D., KOVACS, W.D., SHEAHAN, T.C. **An Introduction to Geotechnical Engineering**. 2<sup>nd</sup> Pearson, 2011.

HUGHES, S. A. **Levee Overtopping Design Guidance What we Know and What we Need**. Solutions to Coastal Disasters, congress 2008.

HUNTER, D. **Lime-Induced Heave in Sulfate-Bearing Clay Soils**. J. Geotech. Engrg v. 114(2), p. 150-167, 1988.

ICOLD, Bulletin 77, **Dispersive Soils in Embankment Dams**. Review. Paris, 1990.

INDRARATNA, B., BALASUBRAMANIAM, A. S., KHAN, M. J. **Effect of Fly Ash with Lime and Cement on the Behaviour of a Soft Clay**. Quarterly Journal of Engineering Geology, v. 28, p. 131-142. 1995.

INGHAM, J. **Geomaterials Under the Microscope - A Colour Guide**. Butler, Tanner & Dennis, Frome, UK, 2013

INGLES, O. G.; METCALF, J. B. **Soil Stabilization Principles and Practice**. Butterworths, Sydney, Melbourne- Brisbane, 1972.

IONITA, I., FULLEN, M.A., ZGLOBICKI, W., POESEN, J. **Gully Erosion as a Natural and Human-Induced Hazard**. Nat Hazards 79:S1–S5, 2015.

ISHIHARA, K., TSUCHIYA, H., HUANG, Y., KAMADA, K. **Keynote Lecture Recent Studies on Liquefaction Resistance of Sand-Effect on Saturation**. International Conferences on Recent Advances in Geotechnical Earthquake Engineering and Soil Dynamics. 30, 2001.

ISRAELACHVILI, J. N. **Intermolecular and Surface Forces**. Elsevier, 3<sup>rd</sup> edition, 2017.

KAHRAMAN, S. **The Correlations Between the Saturated and Dry P-Wave Velocity of Rocks**. Ultrasonics v. 46, p. 341–348, 2007.

KANJI, M. A. **Critical Issues in Soft Rocks**. Journal of Rock Mechanics and Geotechnical Engineering v. 6, p. 186-195, 2014.

KAUFMAN, M. M. **Erosion Control at Construction Sites - The Science-Policy Gap**. Environmental Management v. 26, n. 1, p. 89–97, 2000.

KHAN, M. N. N., JAMIL, M., KARIM, M. R., ZAIN, M. F. M., KAISH, A. B. M. A. **Filler Effect of Pozzolanic Materials on the Strength and Microstructure Development of Mortar**. KSCE Journal of Civil Engineering p. 1-11, 2016

KIM, J. S.; KIM, T. H. **An Ultrasonic Pulse Velocity Test on Fly-Ash Based Geopolymer Concrete in Frequency Domains.** Applied Mechanics and Materials v. 700, p. 310-313, 2015.

KOTSOVOS, M. D. **Effect of Testing Techniques on the Post-Ultimate Behaviour of Concrete in Compression.** - *Materiaux et Constructions* v. 16, n. 91, p. 3-12, 1983.

KRISTER, H. **Handbook of Applied Surface and Colloid Chemistry,** John Wiley & Sons Ltd, 2002.

KUHINEK, D., ZORIC, I., HRZENJAK, P. **Measurement Uncertainty in Testing of Uniaxial Compressive Strength and Deformability of Rock Samples.** *Measurement Science Review*, v. 11, n. 4, 2011.

KUMAR, S., MUKHOPADHYAY, T., WASEEM, S.A., SINGH, B., IQBAL, M.A. **Effect of Platen Restraint on Stress-Strain Behavior of Concrete Under Uniaxial Compression.** *Strength of Materials*, v. 48, n. 4, p. 592-602, 2016.

LAL, R. **Soil Erosion and the Global Carbon Budget.** *Environment International* v. 29, p. 437–450, 2003.

LAMBE & WHITMAN. **Soil Mechanics (SI Version).** John Wiley & Sons Ltd, 1979.

LEE, J., SALGADO, R., CARRARO, J.A.H., **Stiffness Degradation and Shear Strength of Silty Sands.** *Can. Geotech. J.* v.41, p. 831–843, 2004.

LEONG, E. C., CAHYADI, J., RAHARDJO, H. **Measuring Shear and Compression Velocities of Soil Using Bender-Extender Elements.** *Can. Geotech. J.* v. 46, p. 792-812, 2009.

LEROUEIL, S.; VAUGHAN, P. R. **The General and Congruent Effects of Structure in Natural Soils and Weak Rocks.** *Géotechnique*, v.40, n.3, p. 467-488, 1990.

LI, X., WEN, H., MUHUNTHAN, B., WANG, J. **Modeling and Prediction of the Effects of Moisture on the Unconfined Compressive and Tensile Strength of Soils.** *Journal of Geotechnical and Geoenvironmental Engineering*, 2015.

LIU, Y., JIANG, Y.J., XIAO, H., LEE, F.H. **Determination of Representative Strength of Deep Cement-Mixed Clay from Core Strength Data.** *Géotechnique*, 2016.

LITTLE, D. N., HERBERT, B., KUNAGALLI, S. N. **Ettringite Formation in Lime-Treated Soils.** *Transportation Research Record 1936*, 2005.

LITTLE, D. N., MALES, E.H., PRUSKINSKI, J. R., STEWART, B. **Cementitious Stabilization. A2J01: Committee on Cementitious Stabilization Chairman: Roger K. Seals,** Louisiana State University, 2005.

LIU, Y., JIANG, Y.J., XIAO, H. LEE, F.H. **Determination of Representative Strength of Deep Cement-Mixed Clay from Core Strength Data.** *Géotechnique*, 2016.

LUFFMAN, I. E., NANDI, A., SPIEGEL, T. **Gully Morphology, Hillslope Erosion, and Precipitation Characteristics.** *Catena* v. 133, p. 221–232, 2015.

LUMB, PETER. **Safety Factors and the Probability Distribution of Soil Strength.** *The National Research Council of Canada*, v.7. n. 3, p.225-242, 1970.

MA, J.; WANG, Y. **Study on the Relationship Between Soil-Cement Parameters and Unconfined Compressive Strength.** *Advanced Materials Research*, v. 255-260, p 4012-4016, 2011.

MACHT, F., EUSTERHUES, K., PRONK, G.H., TOTSCHKE, K.U. **Specific Surface Area of Clay Minerals.** *Applied Clay Science* v. 53, p. 20–26, 2011.

MAIR, R. J. **Developments in Geotechnical Engineering Research.** In *Proc. Instn Civ. Engrs.* 93, Feb., 27-41, 1993.

MARTIN, C. D.; CHANDLER, N. A. **The Progressive Fracture of Lac du Bonnet Granite.** *Int. J. Rock Mech. Min. & Geomech. Abstr.* v. 31, n. 6, p. 643-59, 1994.

MARTIN, C. Derek. **The Effect of Cohesion Loss and Stress Path on Brittle Rock Strength.** *Can. Geotech. J.* v. 34, p. 698–725, 1997.



MASSAZZA, FRANCO. **Pozzolanic Cements**. Cement & Concrete Composites v. 15, p.185-214, 1993.

MENA, M. Martínez, CARRILLO-LÓPEZ, E., BOIX-FAYOS, C., ALMAGRO, M., GARCÍA FRANCO, N., DÍAZ-PEREIRA, E., MONTOYA, L., DE VENTRE, J. **Long-Term Effectiveness of Sustainable Land Management Practices to Control Runoff, Soil Erosion, and Nutrient Loss and the Role of Rainfall**. Catena, 2019.

MESSAD, A.; MOUSSAI, B. **Effect of Water Salinity on Atterberg Limits of El-Hodna Sabkha Soil**. Bull Eng Geol Environ, 2015

MIDDLETON, H. E. **Properties of Soils Which Influence Soil Erosion**. Technical Bulletin n. 178, U.S. Dept of Agriculture, 1930.

MITCHELL, J. K. **Temperature Effects on the Engineering Properties and Behavior of Soils**. HRB Special Report 103, 1969, vv. 12-15

MITCHELL, J. K.; SOGA, K. **Fundamentals of Soil Behavior**. 3 ed. Hoboken: John Wiley and Sons, 2005.

MIER, J. G. M. **Failure of Concrete Under Uniaxial Compression an Overview**. Fracture Mechanics of Concrete Structures, Proceedings FRAMCOS-3, AEDIFICATIO Publishers, D-79104 Freiburg, Germany, 1996.

MOH, Z. C.; GOECKER, W. L.; CHU, T. Y.; DAVIDSON, D. T. **Evaluation of Lime and fly ash stabilization of soils by compressive strength tests**. Highway Board Bull. 108:102-112, 1955.

MONTGOMERY, D. C. **Design and Analysis of Experiments**. 9<sup>th</sup> edition, John Wiley & Sons, Inc, 2017.

MONTGOMERY, D. C.; RUNGER, G. C. **Applied Statistics and Probability for Engineers**. 7<sup>th</sup> editon Wiley 2018.

MORGAN, R. P. C. **Soil Erosion & Conservation**. Blackwell Publishing 3<sup>rd</sup> edition, 2005.

MUKHLISIN, M.; AZIZ, A. B. A. **Study of Horizontal Drain Effect on Slope Stability**. Journal Geological Society of India. Vol. 87, April 2016, pp.483-490.

NABIL, M., MUSTAPHA, A., RIOS, S. **Impact of Wetting-Drying Cycles on the Mechanical Properties of Lime-Stabilized Soils**. International Journal of Pavement Research and Technology v. 13 , p. 83-92, 2020.

NATIONAL LIME ASSOCIATION. **Lime-Treated Soil Construction Manual - Lime Stabilization & Lime Modification**. Bulletin 326, National Lime Association, 2004.

OATES, J. A. H. **Lime and Limestone Chemistry and Teechnology**, Production and Uses. Wiley-VCH. Weinhem (Federal Republic of Germany), 1998.

OEHLERT, G. W. **A First Course in Design and Analysis of Experiments**. Gary W. Oehlert, 2010.

ODELL, R. T., THORNBURN, T.H., MCKENZIE, L.J. **Relationships of Atterberg Limits to Some Other Properties of Illinois Soils**. Soil Science Society Proceedings, p. 297-300, 1960.

OLLIVIER, J. P., MASO, J.C., BOURDETTE, B. **Interfacial Transition Zone in Concrete**. Interfacial Transition Zone in Concrete, Advn. Cem. Bas. Mat. v. 2, p. 30-38, 1995.

OSMAN, K. T. **Soil Degradation, Conservation and Remediation**. Springer, 2014.

PACKARD, R. G.; CHAPMAN, G. A. **Developments in Durability Testing of Soil-Cement Mixtures**. Highway Research Record. v. 36, p. 97-122, 1963.

PAIGE-GREN, P. **Dispersive and erodible soils-fundamental differences**. Problem soils in South Africa Conference, Midrand, Gauteng, South Africa, November 3-4, p. 59–65, 2008.

PALCHIK, V. **On the Ratios Between Elastic Modulus and Uniaxial Compressive Strength of Heterogeneous Carbonate Rocks.** Rock Mech Rock Eng v.44, p. 121–128, 2011.

PALMER, I. D.; TRAVIOLIA, M. L. **Attenuation by Squirt Flow in Undersaturated Gas Sands.** GEOPHYSICS, v. 45, n. 12, p. 1780-1792, 1980.

PAPAYIANNI, Ioanna; STEFANIDOU, Maria. **Strength-porosity relationship in lime-pozzolan mortars.** Construction and Building Materials. V. 20, p. 700-705, 2006.

PARK, S. **Effect of Wetting on Unconfined Compressive Strength of Cemented Sands.** J. Geotech. Geoenviron. Eng. v.136, p. 1713-1720, 2010.

PAUW, A. **Static Modulus of Elasticity of Concrete as Affected by Density.** Journal of the the American Concrete Institute, v. 57, n. 12, p.679-688, 1960.

PELLET, F. L.; FABRE, G. **Damage Evaluation with P-Wave Velocity Measurements during Uniaxial Compression.** International Journal of Geomechanics, v. 7, n. 6, 2007.

PENNELL, K. D. **Specific Surface Area.** Reference Module in Earth Systems and Environmental Sciences, 2016.

PINKY, H. LE **Effectiveness of horizontal drains in slope stability** [Masters dissertation]. University of Hong Kong, 2008.

POEL, P. VAN DER, R. G. SPOMER, and R. F. PIEST. **Slope Indicator Measurements of subsurface movement in gully walls.** Transactions of the ASAE - American Society of Agricultural Engineers (USA). v. 29, n. 4, p. 982-987, 1986.

POESEN, J., NACHTERGAELE, J., VERSTRAETEN, G., VALENTIN, C., **Gully Erosion and Environmental Change Importance and Research Needs.** Catena v.50, p. 91– 133, 2003.

POULOS, H. G. **Tall Building Foundation Design.** Taylor & Francis Group, 2017.

- POULOS, H. G. **Estimation of Geotechnical Deformation Parameters from Small-Strain Shear Modulus**. Innovations in Geotechnical Engineering, p. 87-100, 2018.
- PRITIRADHESHYAMNANDAGAWALI, N. A. B. **Engineering Characterization of Clayey Soil by Ultrasonic Pulse Velocity**. The International Journal of Engineering and Science (IJES), p. 21-26, 2018.
- PROCTOR, R.R. **Fundamentals Principles of Soil Compaction**. Engineering News Record, New York, 3(9) pp. 245-248; 3(10) pp. 268-289; 3(11) pp. 348-351; and 3(12) pp. 372-376, (1933)
- PUNDIT **Operating Instructions Pundit Lab / Pundit Lab Ultrasonic Instrument**. Pundit lab, 2017.
- RAMEZANIANPOUR, A. A. **Cement Replacement Materials Properties, Durability, Sustainability**. Springer, 2014.
- RAO, S.; SHIVANANDA, P. **Role of Curing Temperature in Progress of Lime-Soil Reactions**. Geotechnical and Geological Engineering v.23, p. 79–85, 2005.
- RAO, K. M.; SUBBARAO, G. V. R. **Optimum Fly Ash for Mechanical Stabilization of Expansive Soils using 2<sup>2</sup> Factorial Experimental Design**. Nat Hazards v. 60, p. 703–713, 2012.
- REDDY, B. V. V.; GOURAV, K. **Strength of lime-fly ash compacts using different curing techniques and gypsum additive**. Materials and Structures v. 44, p. 1793-1808, 2011.
- RENGASAMY, P.; OLSSON, K. A. **Sodicity and Soil Structure**. Aust. J. Soil Res., v. 29, p. 935-52, 1991.
- RENGASAMY, P.; MARCHUK, A. **Cation Ratio of Soil Structural Stability (CROSS)**. Soil Research, v. 49, p.280–285, 2011.

RIBEIRO, D., NÉRI, R., CARDOSO, R. **Influence of Water Content in the UCS of Soil-Cement Mixtures for Different Cement Dosages.** *Procedia Engineering*, v. 143, p. 59–66, 2016.

RIOS, S., FONSECA, A.V., CONSOLI, N.C. **Strength and Stiffness Properties of Mixtures of Granitic-Soil-Cement.** *Proceedings of the 17th International Conference on Soil Mechanics and Geotechnical Engineering*, 2009.

ROBBINS, B. A.; GRIFFITHS, D. V. **Internal Erosion of Embankments A Review and Appraisal.** *Rocky Mountain Geo-Conference* 2018.

ROSCOE, K. H. **The Influence of Strains in Soil Mechanics.** *Géotechnique* v. 20, n. 2, p.129-170, 1970.

ROTTA, G. V., CONSOLI, N.C., PRIETTO, P.D.M., COOP, M.R., GRAHAM, J. **Isotropic Yielding in an Artificially Cemented Soil Cured Under Stress.** *Géotechnique*, v.53, n.5, p.493-501, 2003.

ROWE, R. K. **Geotechnical and Geoenvironmental Engineering Handbook.** Springer Science, 2001.

HEINZEN, R. AND ARULANANDAN, K., **Factors Influencing Dispersive Clays and Methods of Identification,"** in *Dispersive Clays, Related Piping, and Erosion in Geotechnical Projects*, ed. J. Sherard and R. Decker (West Conshohocken, PA: ASTM International), p. 202-217, 1977.

SALDANHA, R.B., SCHEUERMANN FILHO, H.C., MALLMANN, J.E.C., CONSOLI, N.C., REDDY, K.R. **Physical-Mineralogical-Chemical Characterization of Carbide Lime.** *Journal of Materials in Civil Engineering*, 30(6): 06018004, 2018.

SALIBA, F., NASSAR, R. B., KHOURY, N., MAALOUF, Y. **Internal Erosion and Piping Evolution in Earth Dams Using an Iterative Approach.** *Geo-Congress* 2019.

SANTAMARINA, J. C., KLEIN, K.A., WANG, Y.H., PRENCKE, E. **Specific Surface - Determination and Relevance**. Can. Geotech. J. v. 39, p. 233–241, 2002.

SANTAMARINA, J.C., KLEIN, J.C., FAM, N.A. **Soils and waves: particulate materials behaviour, characterization and process monitoring**. John Wiley & Sons, Ltd, 2001.

SANTAMARINA, J. C. **Soil Behavior at the Microscale-Particle Forces**. Proc. Symp. Soil Behavior and Soft Ground Construction, MIT: 2001.

SAROGLOU, C.; KALLIMOGIANNIS, V. **Fracturing Process and Effect of Fracturing Degree on Wave Velocity of a Crystalline Rock**. Journal of Rock Mechanics and Geotechnical Engineering v. 9, p. 797-806, 2017.

SAXENA, S. K., LASTRICO, R.M. **Static Properties of Lightly Cemented Sand**. Journal of the Geotechnical Engineering Division, v. 104, 1978.

SCHEUERMANN FILHO, Hugo Carlos. **Estabilização de um solo dispersivo com pó de vidro moído e cal de carbureto**. Dissertação (Mestrado) - Curso de Pós-graduação em Engenharia Civil, Escola de Engenharia da UFRGS, Universidade Federal do Rio Grande do Sul, Porto Alegre, 2019

SCHILLER, K. K. **Strength of Porous Materials**. CEMENT and CONCRETE RESEARCH. v. I, p. 419-422, 1971

SCHOFIELD, A.; WROTH, P. **Critical State Soil Mechanics**. Lecturers in Engineering at Cambridge University, 1968.

SCHRAMM, E.; SCRIPTURE JR., E. W. **The Particle Analysis of Clays by Sedimentation**. Annual Meeting, American Ceramisc Society, Columbus, Ohio, 1925.

SEAR, Lindon K. A. **Properties and use of Coal Fly Ash a Valuable Industrial by-Product**. Thomas Telford, 2001.

SENTHILMURUGAN, T.; ILAMPARUTHI, K. **Study on Compaction Characteristics and Strength Through Ultrasonic Method.** Advances in Pavement Engineering, 2005.

SHEN, B. **The Mechanism of Fracture Coalescence in Compression – Experimental Study and Numerical Simulation.** Engineering Fracture Mechanics v. 51, n. I, p. 73- 85, 1995.

SHERARD, J. L., CLUFF, L.S., ALLEN, C.R. **Potentially Active Faults in Dam Foundations.** Gdotechnique v. 24, n. 3, p. 367-428, 1974.

SHERARD, J. L. **Study of Piping Failures and Erosion Damage from Rain in Clay Dams in Oklahoma and Mississippi,** report prepared for U.S. Department of Agriculture, Soil Conservation Service, p. 59, 1972.

SHERARD, J. L., DUNNIGAN, L. P., DECKER, R S., AND STEELE, E. F. **Pinhole Test for Identifying Dispersive Soils.** Journal, Geotechnical Engineering Division, ASCE, v. 102, n. GT1, p. 69-85, 1976b.

SHERARD, J. L., DUNNIGAN, L. P., DECKER, R S. **Identification and Nature of Dispersive Soils.** Journal, Geotechnical Engineering division, ASCE, Vol. 102, No. GT4, p. 287-301, 1976a.

SHERARD, J. L. **Lessons from the Teton Dam Failure.** Engineering Geology, v. 24, p. 239-256, 1987.

SINGH, G. V. P. B.; SUBRAMANIAM, K. V. L. **Quantitative XRD study of amorphous phase in alkali activated low calcium siliceous fly ash.** Construction and Building Materials, v. 124, pp. 139-147, 2016.

SKEMPTON, A. W. **The Colloidal “Activity” of Clays.** Proc. 3d Int. Conf. Soil Mech. Found. Eng., vol. 1, pp. 57-61, 1953.

SMILES, D. E.; SMITH, C. J. **A Survey of the cation content of piggery effluents and some consequences of their use to irrigate soils.** Australian Journal of Soil Research, v. 42, p. 231-246, 2004.

SNELLINGS, R., SALZE, A., SCRIVENER, K.L. Use of X-Ray **Diffraction to Quantify Amorphous Supplementary Cementitious Materials in Anhydrous and Hydrated Blended Cements**. *Cement and Concrete Research* v. 64, p. 89–98, 2014.

STACHOWIAK, G. W.; BATCHELOR, A. W. **Engineering Tribology**. 4<sup>th</sup> edition, 2014.

SUBRAMANIAN, R. **Strength of Materials**. 2<sup>nd</sup> edition, Oxford University Press, 2010.

SURYANARAYANA, C.; NORTON, M. G. **X-Ray Diffraction A Practical Approach**. Springer Science+Business Media New York, 1998.

TAYLOR, O-D., CUNNINGHAM, A.L., WALKER, R.R., MCKENNA, M.H, MARTIN, K.E., KINNEBREW, P.G. **The Behaviour of Near-Surface Soils Through Ultrasonic Near-Surface Inundation Testing**. *Near Surface Geophysics*, v. 17, p. 331–344, 2019a.

TAYLOR, O. S., WINTERS, K. E., BERRY, W.W., WALSHIRE, L.A., KINNEBREW, P.G. **Near-Surface Soils - Self-Supported Unconfined Drained Sand Specimens**. *Canadian Geotechnical Journal*, v. 56, n. 3, 2019b.

THOMAS, J. T., IVERSON, N. R., BURKART, M. R. **Bank-Collapse Processes in a Valley-Bottom Gully**, Western Iowa. *Earth Surf. Process. Landforms*, v. 34, p. 109–122, 2009.

TRAN, T. D., CUI, Y-J., TANG. A. M., AUDIGUIER, M., COJEAN, R. **Effects of Lime Treatment on the Microstructure and Hydraulic Conductivity of Héricourt Clay**. *Journal of Rock Mechanics and Geotechnical Engineering* v. 6, p. 399-404, 2014.

TRHLÍKOVÁ, J.; MAŠÍN, D.; BOHÁČ. **Small-strain behaviour of cemented soils**. *Géotechnique*, vol. 62, No. 10, p. 943-947, 2012.

TUNCAY, E.; HASANCEBI, N. **The Effect of Length to Diameter Ratio of Test Specimens on the Uniaxial Compressive Strength of Rock**. *Bull Eng Geol Environ*, v. 68, p. 491–497, 2009.



U. S. ARMY CORPS OF ENGINEERS (USACE). **Soil Stabilization for Pavements Mobilization Construction**. Washington: USACE, 1984. Engineer Manual – EM 1110 – 3 – 137.

UTOMO, Wani Hadi. The effects of wetting and drying on soil physical properties. Thesis for philosophy Doctorate, University of Adelaide. 1980.

VALENTIN, C., POESEN, J., LI, Y. **Gully Erosion - Impacts, Factors and Control**. Catena v. 63, p. 132–153, 2005.

VARDOULAKIS, Ioannis; LEMAITRE, Jean (editor). **Handbook of Materials Behavior Models - Volume I Deformations of Materials**. Section 11.4 Behavior of Granular Materials. ACADEMIC PRESS A Division of Harcourt, Inc. 2001.

VELDE, B.; MEUNIER, A. **The Origin of Clay Minerals in Soils and Weathered Rocks**. Springer Science, 2008.

VENDRUSCULO, L. G. **Classical Gully Spatial Identification and Slope Stability Modeling Using High-Resolution Elevation**. Dissertation for Doctorate degree, Iowa State University, 2014.

WATKINS, J. S., WALTERS, L.A., GODSON, R.H. **Dependence of In-Situ Compressional-Wave Velocity on Porosity in Unsaturated Rocks**. GEOPHYSICS, v. 37, n. 1 p. 29-35, 1972.

WU, S., GRAY, D.H., RICHART, F.E. **Capillary Effects on Dynamic Modulus of Sands and Silts**. J. Geotech. Engrg., v. 110, p. 1188-1203, 1984.

WASEDA, Y., MATSUBAR, E., SHINODA, K. **X-Ray Diffraction Crystallography Introduction, Examples and Solved Problems**. Springer 2011.

WATSON, K. L. **A Simple Relationship Between the Compressive Strength and Porosity of Hydrated Portland Cement**. Cement and Concrete Research. v. II, p. 473-476, 1981.

WELTER, C.; BASTOS, C. A. B. **Avaliação da Dispersibilidade de Planossolos Solódicos Encontrados na Planície Costeira Sul do RS.** In XVIII Congresso Regional De Iniciação Científica e Tecnológica, 2003.

WHALLEY, W. R., JENKINS, M., ATTENBOROUGH, K. **The Velocity of Shear Waves in Unsaturated Soil.** Soil & Tillage Research v. 125, p. 30–37, 2012.

WILLIAMSON, S.; CORTES, D. D. **Dimensional Analysis of Soil-Cement Mixture Performance.** Géotechnique Letters v.4, p. 33-38, 2014.

XU, X.-L., LIU, W., KONG, Y-P., ZHANG, K-L., YU, B., CHEN, J-D. **Runoff and Water Erosion on Road Side-Slopes- Effect of Rainfall Characteristics and Slope Length.** Transportation Research Part D 14, p. 497–501, 2009.

YANG, J.; GU, X. Q. Shear stiffness of granular material at small strains: does it depend on grain size? Géotechnique. v. 63, no. 2, p. 165-179, 2013.

YESILLER, N., HANSON, J.L., USMEN, M.A. **Ultrasonic Assessment of Stabilized Soils.** Proceedings of the ASCE Geo-Institute Soft Ground Technology Conference, p. 170-181, 2001.

YUDENFREUND, M., ODLER, I., BRUNAUER, S. **Hardened Portland Cement Pastes of Low Porosity.** Cement and Concrete Research. v. 2, p. 313-330, 1972

ZHANG, L., PENG, M., CHANG, D., XU, Y. **Dam Failure Mechanisms and Risk Assessment.** Wiley, 2016.




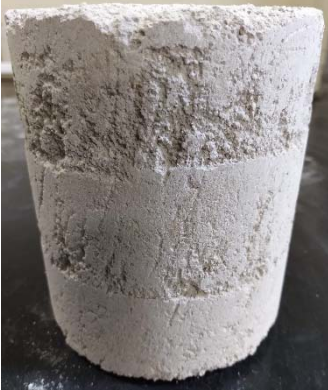

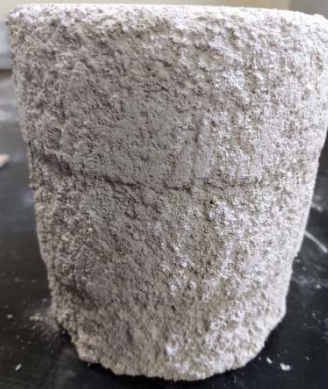

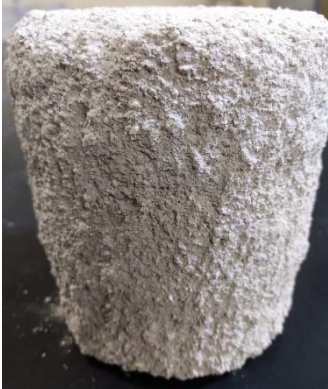
ZHANG, Y., DANIELS, J. L., CETIN, B., BAUCOM, I.K. **Effect of Temperature on pH, Conductivity, and Strength of Lime-Stabilized Soil.** J. Mater. Civ. Eng., v. 32(3): 04019380, 2020.




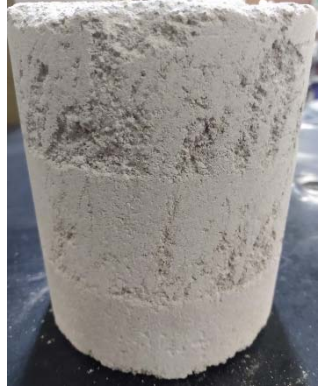

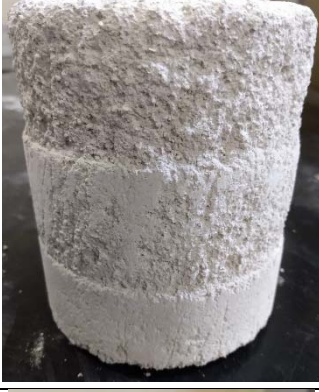

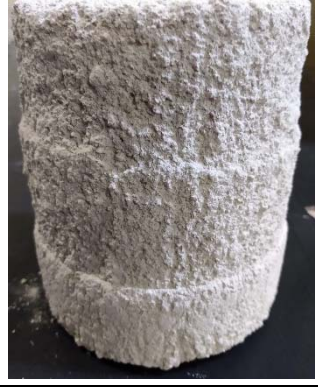
ZHANG, Z.; TAO, M. **Durability of Cement Stabilized Low Plasticity Soils.** J. Geotech. Geoenviron. Eng. v. 134, p. 203-213, 2008.








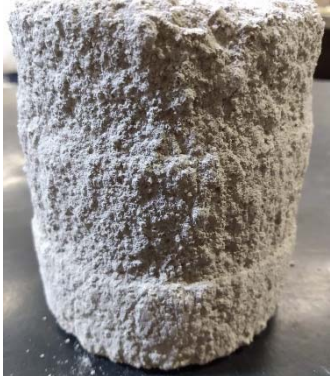
ZHENG, M., ZHENG, X., LUO, Z.J. **Fracture Strength of Brittle Porous Materials.**  
International Journal of Fracture 58:R51-R55, 1992

## **APPENDICES**








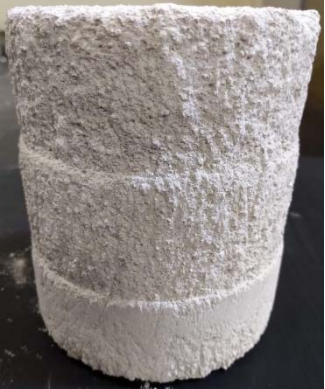
***APPENDIX I – SAMPLES THROUGHOUT DURABILITY CYCLES***









Number of cycles	Lime type	carbide (calclitic)	Dry unit weight (kN/m <sup>3</sup> )	14.0
	Lime content (%)	5.0	Fly ash content (%)	12.50
	Slenderness ratio:			
	2.0		1.2	
0				
1				
4				
12				









Number of cycles	Lime type	carbide (calclitic)	Dry unit weight (kN/m <sup>3</sup> )	14.0
	Lime content (%)	12.0	Fly ash content (%)	12.50
	Slenderness ratio:			
	2.0		1.2	
0				
1				
4				
12				









Number of cycles	Lime type	carbide (calctic)	Dry unit weight (kN/m <sup>3</sup> )	14.0
	Lime content (%)	5.0	Fly ash content (%)	25.00
	Slenderness ratio:			
	2.0		1.2	
0				
1				
4				
12				



















Number of cycles	Lime type	carbide (calctic)	Dry unit weight (kN/m <sup>3</sup> )	14.0
	Lime content (%)	12.0	Fly ash content (%)	25.00
	Slenderness ratio:			
	2.0		1.2	
0				
1				
4				
12				




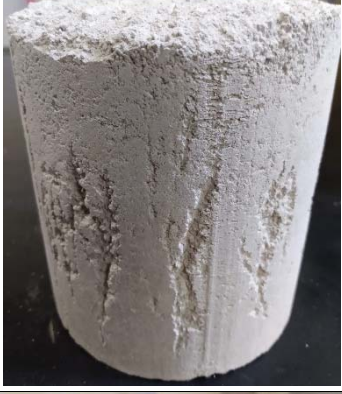


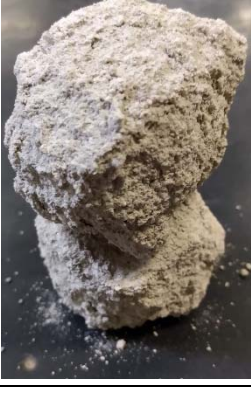

Number of cycles	Lime type	carbide (calclitic)	Dry unit weight (kN/m <sup>3</sup> )	15.5
	Lime content (%)	8.5	Fly ash content (%)	18.75
	Slenderness ratio:			
	2.0		1.2	
0				
1				
4				
12				






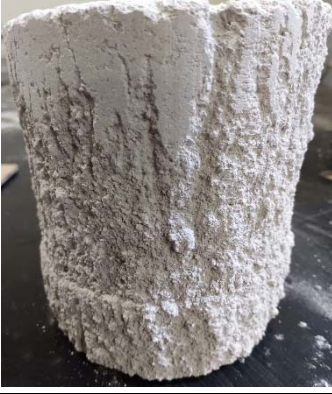


Number of cycles	Lime type	carbide (calctic)	Dry unit weight (kN/m <sup>3</sup> )	17.0
	Lime content (%)	5.0	Fly ash content (%)	12.50
	Slenderness ratio:			
	2.0		1.2	
0				
1				
4				
12				

Number of cycles	Lime type	carbide (calclitic)	Dry unit weight (kN/m <sup>3</sup> )	17.0
	Lime content (%)	12.0	Fly ash content (%)	12.50
	Slenderness ratio:			
	2.0		1.2	
0				
1				
4				
12				






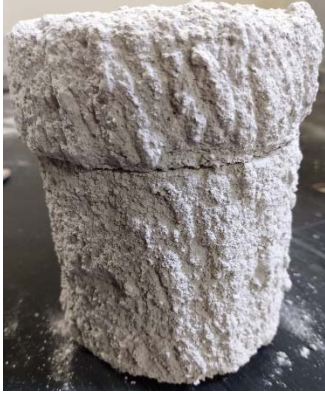


Number of cycles	Lime type	carbide (calctic)	Dry unit weight (kN/m <sup>3</sup> )	17.0
	Lime content (%)	5.0	Fly ash content (%)	25.00
	Slenderness ratio:			
	2.0		1.2	
0				
1				
4				
12				




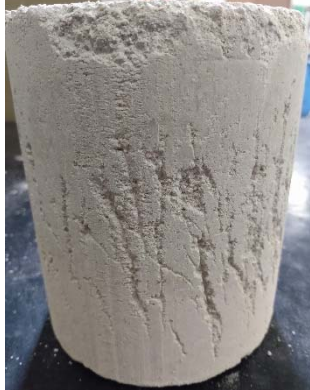




Number of cycles	Lime type	carbide (calclitic)	Dry unit weight (kN/m <sup>3</sup> )	17.0
	Lime content (%)	12.0	Fly ash content (%)	25.00
	Slenderness ratio:			
	2.0		1.2	
0				
1				
4				
12				






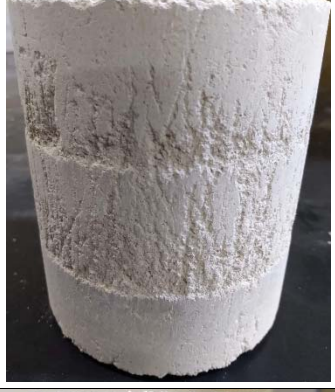


Number of cycles	Lime type	Primor (dolomitic)	Dry unit weight (kN/m <sup>3</sup> )	14.0
	Lime content (%)	5.0	Fly ash content (%)	12.50
	Slenderness ratio:			
	2.0		1.2	
0				
1				
4				
12				









Number of cycles	Lime type	Primor (dolomitic)	Dry unit weight (kN/m <sup>3</sup> )	14.0
	Lime content (%)	12.0	Fly ash content (%)	12.50
	Slenderness ratio:			
	2.0		1.2	
0				
1				
4				
12				
















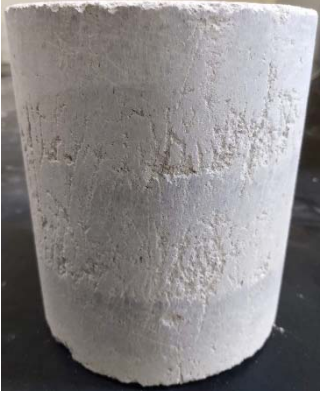

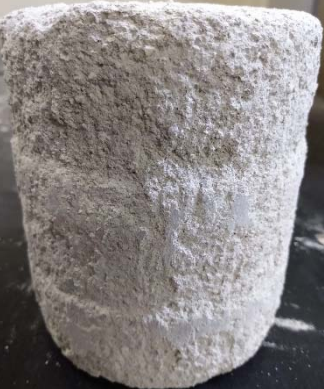
Number of cycles	Lime type	Primor (dolomitic)	Dry unit weight (kN/m <sup>3</sup> )	14.0
	Lime content (%)	5.0	Fly ash content (%)	25.00
	Slenderness ratio:			
	2.0		1.2	
0				
1				
4				
12				









Number of cycles	Lime type	Primor (dolomitic)	Dry unit weight (kN/m <sup>3</sup> )	14.0
	Lime content (%)	12.0	Fly ash content (%)	25.00
	Slenderness ratio:			
	2.0		1.2	
0				
1				
4				
12				

Number of cycles	Lime type	Primor (dolomitic)	Dry unit weight (kN/m <sup>3</sup> )	15.5
	Lime content (%)	8.5	Fly ash content (%)	18.75
	Slenderness ratio:			
	2.0		1.2	
0				
1				
4				
12				

Number of cycles	Lime type	Primor (dolomitic)	Dry unit weight (kN/m <sup>3</sup> )	17.0
	Lime content (%)	5.0	Fly ash content (%)	12.50
	Slenderness ratio:			
	2.0		1.2	
0				
1				
4				
12				





Number of cycles	Lime type	Primor (dolomitic)	Dry unit weight (kN/m <sup>3</sup> )	17.0
	Lime content (%)	12.0	Fly ash content (%)	12.50
	Slenderness ratio:			
	2.0		1.2	
0				
1				
4				
12				






Number of cycles	Lime type	Primor (dolomitic)	Dry unit weight (kN/m <sup>3</sup> )	17.0
	Lime content (%)	5.0	Fly ash content (%)	25.00
	Slenderness ratio:			
	2.0		1.2	
0				
1				
4				
12				





Number of cycles	Lime type	Primor (dolomitic)	Dry unit weight (kN/m <sup>3</sup> )	17.0
	Lime content (%)	12.0	Fly ash content (%)	25.00
	Slenderness ratio:			
	2.0		1.2	
0				
1				
4				
12				






***APPENDIX II – SAMPLES FAILURE MODES***













Number of cycles	Lime type	carbide (calcitic)	Dry unit weight (kN/m <sup>3</sup> )	14.0
	Lime content (%)	5.0	Fly ash content (%)	12.50
	Slenderness ratio:			
	2.0		1.2	
0			-	
1			-	
4			-	
12	-			






Number of cycles	Lime type	carbide (calcitic)	Dry unit weight (kN/m <sup>3</sup> )	14.0
	Lime content (%)	12.0	Fly ash content (%)	12.50
	Slenderness ratio:			
	2.0		1.2	
0				-
1				-
4				-
12				






Number of cycles	Lime type	carbide (calcitic)	Dry unit weight (kN/m <sup>3</sup> )	14.0
	Lime content (%)	5.0	Fly ash content (%)	25.00
	Slenderness ratio:			
	2.0		1.2	
0				-
1				-
4				-
12				

Number of cycles	Lime type	carbide (calcitic)	Dry unit weight (kN/m <sup>3</sup> )	14.0
	Lime content (%)	12.0	Fly ash content (%)	25.00
	Slenderness ratio:			
	2.0		1.2	
0				
1				-
4				-
12				






Number of cycles	Lime type	carbide (calcitic)	Dry unit weight (kN/m <sup>3</sup> )	15.5
	Lime content (%)	8.5	Fly ash content (%)	18.75
	Slenderness ratio:			
	2.0		1.2	
0				-
1				-
4				-
12				





Number of cycles	Lime type	carbide (calcitic)	Dry unit weight (kN/m <sup>3</sup> )	17.0
	Lime content (%)	5.0	Fly ash content (%)	12.50
	Slenderness ratio:			
	2.0		1.2	
0				-
1				-
4				-
12				






Number of cycles	Lime type	carbide (calcitic)	Dry unit weight (kN/m <sup>3</sup> )	17.0
	Lime content (%)	12.0	Fly ash content (%)	12.50
	Slenderness ratio:			
	2.0		1.2	
0				-
1				-
4				-
12				




Number of cycles	Lime type	carbide (calcitic)	Dry unit weight (kN/m <sup>3</sup> )	17.0
	Lime content (%)	5.0	Fly ash content (%)	25.00
	Slenderness ratio:			
	2.0		1.2	
0			-	
1			-	
4			-	
12				












Number of cycles	Lime type	carbide (calcitic)	Dry unit weight (kN/m <sup>3</sup> )	17.0
	Lime content (%)	12.0	Fly ash content (%)	25.00
	Slenderness ratio:			
	2.0		1.2	
0			-	
1			-	
4			-	
12				






Number of cycles	Lime type	Primor (dolomitic)	Dry unit weight (kN/m <sup>3</sup> )	14.0
	Lime content (%)	5.0	Fly ash content (%)	12.50
	Slenderness ratio:			
	2.0		1.2	
0				-
1				-
4				-
12	-			






Number of cycles	Lime type	Primor (dolomitic)	Dry unit weight (kN/m <sup>3</sup> )	14.0
	Lime content (%)	12.0	Fly ash content (%)	12.50
	Slenderness ratio:			
	2.0		1.2	
0			-	
1			-	
4			-	
12				

Number of cycles	Lime type	Primor (dolomitic)	Dry unit weight (kN/m <sup>3</sup> )	14.0
	Lime content (%)	5.0	Fly ash content (%)	25.00
	Slenderness ratio:			
	2.0		1.2	
0				-
1				-
4				-
12	-			-






Number of cycles	Lime type	Primor (dolomitic)	Dry unit weight (kN/m <sup>3</sup> )	14.0
	Lime content (%)	12.0	Fly ash content (%)	25.00
	Slenderness ratio:			
	2.0		1.2	
0			-	
1			-	
4			-	
12	Broke up during UPV tests			






Number of cycles	Lime type	Primor (dolomitic)	Dry unit weight (kN/m <sup>3</sup> )	15.5
	Lime content (%)	8.5	Fly ash content (%)	18.75
	Slenderness ratio:			
	2.0		1.2	
0				-
1				-
4				-
12				

Number of cycles	Lime type	Primor (dolomitic)	Dry unit weight (kN/m <sup>3</sup> )	17.0
	Lime content (%)	5.0	Fly ash content (%)	12.50
	Slenderness ratio:			
	2.0		1.2	
0				-
1				-
4				-
12				

Number of cycles	Lime type	Primor (dolomitic)	Dry unit weight (kN/m <sup>3</sup> )	17.0
	Lime content (%)	12.0	Fly ash content (%)	12.50
	Slenderness ratio:			
	2.0		1.2	
0			-	
1			-	
4			-	
12				



Number of cycles	Lime type	Primor (dolomitic)	Dry unit weight (kN/m <sup>3</sup> )	17.0
	Lime content (%)	5.0	Fly ash content (%)	25.00
	Slenderness ratio:			
	2.0		1.2	
0				-
1				-
4				-
12				

Number of cycles	Lime type	Primor (dolomitic)	Dry unit weight (kN/m <sup>3</sup> )	17.0
	Lime content (%)	12.0	Fly ash content (%)	25.00
	Slenderness ratio:			
	2.0		1.2	
0			-	
1			-	
4			-	
12				

***APPENDIX III – ANOVA TABLES***

## APPENDIX III.1 – Effect of dry unit weight, fly ash, and lime content

q<sub>u,0</sub> (H/D = 2.0) – Carbide lime (Calcitic) – 3 factors

Source of Variation	Degrees of freedom	Adjusted Sum of Squares	Adjusted Mean Squares	F-Value	P-Value
Model	7	15155511	2165073	110,31	0,000
Linear	3	13484307	4494769	229,01	0,000
Dry Unit Weight	1	11200406	11200406	570,66	0,000
Fly Ash Content	1	1940770	1940770	98,88	0,000
Carbide Lime Content	1	343131	343131	17,48	0,001
2-Way Interactions	3	1669053	556351	28,35	0,000
Dry Unit Weight*Fly Ash Content	1	1435839	1435839	73,16	0,000
Dry Unit Weight*Carbide Lime Content	1	193310	193310	9,85	0,005
Fly Ash Content*Carbide Lime Content	1	39904	39904	2,03	0,170
Curvature	1	2151	2151	0,11	0,744
Error	19	372912	19627		
Lack-of-Fit	1	145621	145621	11,53	0,003
Pure Error	18	227291	12627		
Total	26	15528423			
Model summary					
Standard deviation			R <sup>2</sup>		
			0,976		

$q_{u,0}$  (H/D = 2.0) - Primor lime (Dolomitic) - 3 factors

Source of Variation	Degrees of freedom	Adjusted Sum of Squares	Adjusted Mean Squares	F-Value	P-Value
Model	7	67454064	9636295	132.36	0
Linear	3	64572327	21524109	295.64	0
Dry Unit Weight	1	57036346	57036346	783.42	0
Fly Ash Content	1	5060065	5060065	69.5	0
Primor Lime Content	1	2475916	2475916	34.01	0
2-Way Interactions	3	2832834	944278	12.97	0
Dry Unit Weight*Fly Ash Content	1	1635502	1635502	22.46	0
Dry Unit Weight*Primor Lime Content	1	1097992	1097992	15.08	0.001
Fly Ash Content*Primor Lime Content	1	99341	99341	1.36	0.257
Curvature	1	48903	48903	0.67	0.423
Error	19	1383282	72804		
Lack-of-Fit	1	2489	2489	0.03	0.859
Pure Error	18	1380792	76711		
Total	26	68837346			
Model summary					
Standard deviation			$R^2$		
			0.980		

$q_{u,1}$  (H/D = 2.0) - Carbide lime (Calcitic) - 3 factors

Source of Variation	Degrees of freedom	Adjusted Sum of Squares	Adjusted Mean Squares	F-Value	P-Value
Model	7	109919332	15702762	182	0
Linear	3	99110175	33036725	382	0
Dry Unit Weight	1	85980947	85980947	994	0
Fly Ash Content	1	10789442	10789442	125	0
Carbide Lime Content	1	2339786	2339786	27	0
2-Way Interactions	3	10626842	3542281	41	0
Dry Unit Weight*Fly Ash Content	1	9009792	9009792	104	0
Dry Unit Weight*Carbide Lime Content	1	1608474	1608474	19	0
Fly Ash Content*Carbide Lime Content	1	8576	8576	0	1
Curvature	1	182314	182314	2	0
Error	10	864830	86483		
Lack-of-Fit	1	13846	13846	0	1
Pure Error	9	850984	94554		
Total	17	110784162			
Model summary					
Standard deviation			R <sup>2</sup>		
	294.08		0.992		

$q_{u,1}$  (H/D = 2.0) - Carbide lime (Calcitic) - 3 factors

Source of Variation	Degrees of freedom	Adjusted Sum of Squares	Adjusted Mean Squares	F-Value	P-Value
Model	7	109919332	15702762	182	0
Linear	3	99110175	33036725	382	0
Dry Unit Weight	1	85980947	85980947	994	0
Fly Ash Content	1	10789442	10789442	125	0
Carbide Lime Content	1	2339786	2339786	27	0
2-Way Interactions	3	10626842	3542281	41	0
Dry Unit Weight*Fly Ash Content	1	9009792	9009792	104	0
Dry Unit Weight*Carbide Lime Content	1	1608474	1608474	19	0
Fly Ash Content*Carbide Lime Content	1	8576	8576	0	1
Curvature	1	182314	182314	2	0
Error	10	864830	86483		
Lack-of-Fit	1	13846	13846	0	1
Pure Error	9	850984	94554		
Total	17	110784162			
Model summary					
Standard deviation			R <sup>2</sup>		
294.08			0.992		

$q_{u,1}$  (H/D = 2.0) - Primor lime (Dolomitic) - 3 factors

Source of Variation	Degrees of freedom	Adjusted Sum of Squares	Adjusted Mean Squares	F-Value	P-Value
Model	7	81478157	11639737	5091.39	0.011
Linear	3	69729157	23243052	10166.9	0.007
Dry Unit Weight	1	49065264	49065264	21461.9	0.004
Fly Ash Content	1	2475195	2475195	1082.69	0.019
Primor Lime Content	1	18188699	18188699	7956	0.007
2-Way Interactions	3	11268603	3756201	1643.02	0.018
Dry Unit Weight*Fly Ash Content	1	1653563	1653563	723.29	0.024
Dry Unit Weight*Primor Lime Content	1	9594832	9594832	4196.92	0.01
Fly Ash Content*Primor Lime Content	1	20208	20208	8.84	0.207
Curvature	1	480397	480397	210.13	0.044
Error	1	2286	2286		
Total	8	81480443			
Model summary					
Standard deviation				$R^2$	
				0.997	



q<sub>u,4</sub> (H/D = 2.0) - Carbide lime (Calcitic) - 3 factors

Source of Variation	Degrees of freedom	Adjusted Sum of Squares	Adjusted Mean Squares	F-Value	P-Value
Model	7	107079051	15297007	158	0
Linear	3	95221356	31740452	328	0
Dry Unit Weight	1	83424442	83424442	863	0
Fly Ash Content	1	1005288	1005288	10	0
Carbide Lime Content	1	10791627	10791627	112	0
2-Way Interactions	3	7545288	2515096	26	0
Dry Unit Weight*Fly Ash Content	1	60357	60357	1	0
Dry Unit Weight*Carbide Lime Content	1	7405178	7405178	77	0
Fly Ash Content*Carbide Lime Content	1	79753	79753	1	0
Curvature	1	4312407	4312407	45	0
Error	10	966310	96631		
Lack-of-Fit	1	314704	314704	4	0
Pure Error	9	651606	72401		
Total	17	108045361			
Model summary					
Standard deviation			R <sup>2</sup>		
			0.991		

$q_{u,4}$  (H/D = 2.0) - Primor lime (Dolomitic) - 3 factors

Source of Variation	Degrees of freedom	Adjusted Sum of Squares	Adjusted Mean Squares	F-Value	P-Value
Model	7	81478157	11639737	5091.39	0.011
Linear	3	69729157	23243052	10166.9	0.007
Dry Unit Weight	1	49065264	49065264	21461.9	0.004
Fly Ash Content	1	2475195	2475195	1082.69	0.019
Primor Lime Content	1	18188699	18188699	7956	0.007
2-Way Interactions	3	11268603	3756201	1643.02	0.018
Dry Unit Weight*Fly Ash Content	1	1653563	1653563	723.29	0.024
Dry Unit Weight*Primor Lime Content	1	9594832	9594832	4196.92	0.01
Fly Ash Content*Primor Lime Content	1	20208	20208	8.84	0.207
Curvature	1	480397	480397	210.13	0.044
Error	1	2286	2286		
Total	8	81480443			
Model summary					
Standard deviation				$R^2$	
47.8138				1.000	

$q_{u,12}$  (H/D = 2.0) - Carbide lime (Calcitic) - 3 factors

Source of Variation	Degrees of freedom	Adjusted Sum of Squares	Adjusted Mean Squares	F-Value	P-Value
Model	7	135656176	19379454	62	0
Linear	3	116924654	38974885	125	0
Dry Unit Weight	1	90294403	90294403	289	0
Fly Ash Content	1	5361070	5361070	17	0
Carbide Lime Content	1	21269181	21269181	68	0
2-Way Interactions	3	15551586	5183862	17	0
Dry Unit Weight*Fly Ash Content	1	4284217	4284217	14	0
Dry Unit Weight*Carbide Lime Content	1	10312545	10312545	33	0
Fly Ash Content*Carbide Lime Content	1	954823	954823	3	0
Curvature	1	3179936	3179936	10	0
Error	10	3121774	312177		
Lack-of-Fit	1	535220	535220	2	0
Pure Error	9	2586554	287395		
Total	17	138777950			
Model summary					
Standard deviation			$R^2$		
	558.728		0.978		

$q_{u,12}$  (H/D = 2.0) - Primor lime (Dolomitic) - 3 factors

Source of Variation	Degrees of freedom	Adjusted Sum of Squares	Adjusted Mean Squares	F-Value	P-Value
Model	7	70986652	10140950	6.73	0.289
Linear	3	48150256	16050085	10.66	0.221
Dry Unit Weight	1	24396789	24396789	16.2	0.155
Fly Ash Content	1	3830211	3830211	2.54	0.357
Primor Lime Content	1	19923256	19923256	13.23	0.171
2-Way Interactions	3	22829470	7609823	5.05	0.313
Dry Unit Weight*Fly Ash Content	1	1607567	1607567	1.07	0.49
Dry Unit Weight*Primor Lime Content	1	19635835	19635835	13.04	0.172
Fly Ash Content*Primor Lime Content	1	1586067	1586067	1.05	0.492
Curvature	1	6926	6926	0	0.957
Error	1	1505721	1505721		
Total	8	72492373			
Model summary					
Standard deviation				$R^2$	
1227.08				0.979	

q<sub>u,12</sub> (H/D = 1.2) - Carbide lime (Calcitic) - 3 factors

Source of Variation	Degrees of freedom	Adjusted Sum of Squares	Adjusted Mean Squares	F-Value	P-Value
Model	7	171391047	24484435	21	0
Linear	3	158854258	52951419	45	0
Dry Unit Weight	1	131995912	131995912	113	0
Fly Ash Content	1	280409	280409	0	1
Carbide Lime Content	1	26577937	26577937	23	0
2-Way Interactions	3	12128550	4042850	3	0
Dry Unit Weight*Fly Ash Content	1	405191	405191	0	1
Dry Unit Weight*Carbide Lime Content	1	11452205	11452205	10	0
Fly Ash Content*Carbide Lime Content	1	271154	271154	0	1
Curvature	1	408239	408239	0	1
Error	1	1169252	1169252		
Total	8	172560299			
Model summary					
Standard deviation			R <sup>2</sup>		
1081.32			0.993		

q<sub>u,12</sub> (H/D = 1.2) - Primor lime (Dolomitic) - 3 factors

Source of Variation	Degrees of freedom	Adjusted Sum of Squares	Adjusted Mean Squares	F-Value	P-Value
Model	7	148202739	21171820	16	0
Linear	3	105631973	35210658	26	0
Dry Unit Weight	1	53077924	53077924	40	0
Fly Ash Content	1	4815037	4815037	4	0
Primor Lime Content	1	47739012	47739012	36	0
2-Way Interactions	3	40991477	13663826	10	0
Dry Unit Weight*Fly Ash Content	1	3997691	3997691	3	0
Dry Unit Weight*Primor Lime Content	1	34582095	34582095	26	0
Fly Ash Content*Primor Lime Content	1	2411690	2411690	2	0
Curvature	1	1579290	1579290	1	0
Error	1	1339493	1339493		
Total	8	149542232			
Model summary					
Standard deviation			R <sup>2</sup>		
1157.36			0.991		

M<sub>0,0</sub> (H/D = 2.0) - Carbide lime (Calcitic) - 3 factors

Source of Variation	Degrees of freedom	Adjusted Sum of Squares	Adjusted Mean Squares	F-Value	P-Value
Model	7	181274823	25896403	114.86	0
Linear	3	175652322	58550774	259.69	0
Dry Unit Weight	1	169791382	169791382	753.08	0
Fly Ash Content	1	5631124	5631124	24.98	0
Carbide Lime Content	1	229815	229815	1.02	0.325
2-Way Interactions	3	5100647	1700216	7.54	0.002
Dry Unit Weight*Fly Ash Content	1	4644456	4644456	20.6	0
Dry Unit Weight*Carbide Lime Content	1	56849	56849	0.25	0.621
Fly Ash Content*Carbide Lime Content	1	399342	399342	1.77	0.199
Curvature	1	521854	521854	2.31	0.145
Error	19	4283784	225462		
Lack-of-Fit	1	101262	101262	0.44	0.518
Pure Error	18	4182522	232362		
Total	26	185558606			
Model summary					
Standard deviation			R <sup>2</sup>		
474.83			0.977		

M<sub>0,0</sub> (H/D = 2.0) - Primor lime (Dolomitic) - 3 factors

Source of Variation	Degrees of freedom	Adjusted Sum of Squares	Adjusted Mean Squares	F-Value	P-Value
Model	7	625536952	89362422	238.9	0
Linear	3	620108593	206702864	552.59	0
Dry Unit Weight	1	583180590	583180590	1559.05	0
Fly Ash Content	1	15306271	15306271	40.92	0
Primor Lime Content	1	21621731	21621731	57.8	0
2-Way Interactions	3	5275934	1758645	4.7	0.006
Dry Unit Weight*Fly Ash Content	1	1509185	1509185	4.03	0.05
Dry Unit Weight*Primor Lime Content	1	3054522	3054522	8.17	0.006
Fly Ash Content*Primor Lime Content	1	712228	712228	1.9	0.174
Curvature	1	152425	152425	0.41	0.526
Error	46	17206786	374061		
Lack-of-Fit	1	43635	43635	0.11	0.737
Pure Error	45	17163151	381403		
Total	53	642743738			
Model summary					
Standard deviation			R <sup>2</sup>		
611.605			0.973		



M<sub>0,0</sub> (H/D = 1.2) - Carbide lime (Calcitic) - 3 factors

Source of Variation	Degrees of freedom	Adjusted Sum of Squares	Adjusted Mean Squares	F-Value	P-Value
Model	7	164807453	23543922	113	0
Linear	3	155521322	51840441	248	0
Dry Unit Weight	1	153729213	153729213	736	0
Fly Ash Content	1	66407	66407	0	1
Carbide Lime Content	1	1725702	1725702	8	0
2-Way Interactions	3	9028471	3009490	14	0
Dry Unit Weight*Fly Ash Content	1	2378831	2378831	11	0
Dry Unit Weight*Carbide Lime Content	1	6611881	6611881	32	0
Fly Ash Content*Carbide Lime Content	1	37759	37759	0	1
Curvature	1	257660	257660	1	0
Error	1	208738	208738		
Total	8	165016191			
Model summary					
Standard deviation			R <sup>2</sup>		
456.878			0.999		

$M_{0,0}$  (H/D = 1.2) - Primor lime (Dolomitic) - 3 factors

Source of Variation	Degrees of freedom	Adjusted Sum of Squares	Adjusted Mean Squares	F-Value	P-Value
Model	7	133305237	19043605	92	0
Linear	3	128631088	42877029	207	0
Dry Unit Weight	1	123784182	123784182	598	0
Fly Ash Content	1	144168	144168	1	1
Primor Lime Content	1	4702737	4702737	23	0
2-Way Interactions	3	3851926	1283975	6	0
Dry Unit Weight*Fly Ash Content	1	277121	277121	1	0
Dry Unit Weight*Primor Lime Content	1	2340545	2340545	11	0
Fly Ash Content*Primor Lime Content	1	1234260	1234260	6	0
Curvature	1	822223	822223	4	0
Error	1	207081	207081		
Total	8	133512318			
Model summary					
Standard deviation			$R^2$		
455.061			0.998		

M<sub>0,1</sub> (H/D = 2.0) - Carbide lime (Calcitic) - 3 factors

Source of Variation	Degrees of freedom	Adjusted Sum of Squares	Adjusted Mean Squares	F-Value	P-Value
Model	7	80711245	11530178	159.99	0
Linear	3	66346139	22115380	306.87	0
Dry Unit Weight	1	62384568	62384568	865.64	0
Fly Ash Content	1	2171580	2171580	30.13	0
Carbide Lime Content	1	1789991	1789991	24.84	0.001
2-Way Interactions	3	2537281	845760	11.74	0.001
Dry Unit Weight*Fly Ash Content	1	1062100	1062100	14.74	0.003
Dry Unit Weight*Carbide Lime Content	1	1413123	1413123	19.61	0.001
Fly Ash Content*Carbide Lime Content	1	62057	62057	0.86	0.375
Curvature	1	11827825	11827825	164.12	0
Error	10	720676	72068		
Lack-of-Fit	1	89945	89945	1.28	0.287
Pure Error	9	630731	70081		
Total	17	81431921			
Model summary					
Standard deviation			R <sup>2</sup>		
268.45			0.991		

M<sub>0,1</sub> (H/D = 2.0) - Primor lime (Dolomitic) - 3 factors

Source of Variation	Degrees of freedom	Adjusted Sum of Squares	Adjusted Mean Squares	F-Value	P-Value
Model	7	159572880	22796126	33.12	0
Linear	3	147416818	49138939	71.4	0
Dry Unit Weight	1	104279447	104279447	151.52	0
Fly Ash Content	1	6640338	6640338	9.65	0.006
Primor Lime Content	1	36497033	36497033	53.03	0
2-Way Interactions	3	12090783	4030261	5.86	0.005
Dry Unit Weight*Fly Ash Content	1	615845	615845	0.89	0.356
Dry Unit Weight*Primor Lime Content	1	11138829	11138829	16.19	0.001
Fly Ash Content*Primor Lime Content	1	336109	336109	0.49	0.493
Curvature	1	65279	65279	0.09	0.761
Error	19	13075825	688201		
Lack-of-Fit	1	95772	95772	0.13	0.72
Pure Error	18	12980053	721114		
Total	26	172648705			
Model summary					
Standard deviation			R <sup>2</sup>		
829.579			0.924		

M<sub>0,1</sub> (H/D = 1.2) - Carbide lime (Calcitic) - 3 factors

Source of Variation	Degrees of freedom	Adjusted Sum of Squares	Adjusted Mean Squares	F-Value	P-Value
Model	7	122966746	17566678	88	0
Linear	3	106469199	35489733	179	0
Dry Unit Weight	1	98455641	98455641	495	0
Fly Ash Content	1	581284	581284	3	0
Carbide Lime Content	1	7432274	7432274	37	0
2-Way Interactions	3	14282731	4760910	24	0
Dry Unit Weight*Fly Ash Content	1	7168092	7168092	36	0
Dry Unit Weight*Carbide Lime Content	1	7006994	7006994	35	0
Fly Ash Content*Carbide Lime Content	1	107645	107645	1	1
Curvature	1	2214816	2214816	11	0
Error	1	198728	198728		
Total	8	123165474			
Model summary					
Standard deviation			R <sup>2</sup>		
445.789			0.998		

M<sub>0,1</sub> (H/D = 1.2) - Primor lime (Dolomitic) - 3 factors

Source of Variation	Degrees of freedom	Adjusted Sum of Squares	Adjusted Mean Squares	F-Value	P-Value
Model	7	132605834	18943691	40201	0
Linear	3	116901581	38967194	82693	0
Dry Unit Weight	1	70408746	70408746	149415	0
Fly Ash Content	1	1600353	1600353	3396	0
Primor Lime Content	1	44892483	44892483	95267	0
2-Way Interactions	3	15679895	5226632	11092	0
Dry Unit Weight*Fly Ash Content	1	187846	187846	399	0
Dry Unit Weight*Primor Lime Content	1	13062555	13062555	27720	0
Fly Ash Content*Primor Lime Content	1	2429494	2429494	5156	0
Curvature	1	24357	24357	52	0
Error	1	471	471		
Total	8	132606305			
Model summary					
Standard deviation			R <sup>2</sup>		
21.708			1.000		

---

M<sub>0,4</sub> (H/D = 1.2) - Carbide lime (Calcitic) - 3 factors

---

Source of Variation	Degrees of freedom	Adjusted Sum of Squares	Adjusted Mean Squares	F-Value	P-Value
Model	7	147733370	21104767	236	0
Linear	3	129652928	43217643	483	0
Dry Unit Weight	1	92999404	92999404	1040	0
Fly Ash Content	1	272660	272660	3	0
Carbide Lime Content	1	36380864	36380864	407	0
2-Way Interactions	3	16968173	5656058	63	0
Dry Unit Weight*Fly Ash Content	1	390745	390745	4	0
Dry Unit Weight*Carbide Lime Content	1	16374373	16374373	183	0
Fly Ash Content*Carbide Lime Content	1	203055	203055	2	0
Curvature	1	1112269	1112269	12	0
Error	1	89400	89400		
Total	8	147822770			
Model summary					
Standard deviation			R <sup>2</sup>		
298.999			0.999		

---

$G_{0,0}$  (H/D = 2.0) - Carbide lime (Calcitic) - 3 factors

Source of Variation	Degrees of freedom	Adjusted Sum of Squares	Adjusted Mean Squares	F-Value	P-Value
Model	7	53981497	7711642	256.31	0.00000
Linear	3	50605957	16868652	560.65	0.00000
Dry Unit Weight	1	46872190	46872190	1557.87	0.00000
Fly Ash Content	1	3131142	3131142	104.07	0.00000
Carbide Lime Content	1	602624	602624	20.03	0.00005
2-Way Interactions	3	2818124	939375	31.22	0.00000
Dry Unit Weight*Fly Ash Content	1	1555192	1555192	51.69	0.00000
Dry Unit Weight*Carbide Lime Content	1	783882	783882	26.05	0.00001
Fly Ash Content*Carbide Lime Content	1	479050	479050	15.92	0.00023
Curvature	1	557416	557416	18.53	0.00009
Error	46	1384021	30087		
Lack-of-Fit	1	588993	588993	33.34	0.00000
Pure Error	45	795029	17667		
Total	53	55365518			
Model summary					
Standard deviation				$R^2$	
				0.975	



G<sub>0,0</sub> (H/D = 2.0) - Primor lime (Dolomitic) - 3 factors

Source of Variation	Degrees of freedom	Adjusted Sum of Squares	Adjusted Mean Squares	F-Value	P-Value
Model	7	21601637	3085948	341.4	0
Linear	3	21143757	7047919	779.73	0
Dry Unit Weight	1	19734331	19734331	2183.25	0
Fly Ash Content	1	188213	188213	20.82	0.001
Primor Lime Content	1	1221213	1221213	135.11	0
2-Way Interactions	3	435276	145092	16.05	0
Dry Unit Weight*Fly Ash Content	1	469	469	0.05	0.824
Dry Unit Weight*Primor Lime Content	1	426587	426587	47.19	0
Fly Ash Content*Primor Lime Content	1	8220	8220	0.91	0.363
Curvature	1	22603	22603	2.5	0.145
Error	10	90390	9039		
Lack-of-Fit	1	13723	13723	1.61	0.236
Pure Error	9	76667	8519		
Total	17	21692027			
Model summary					
Standard deviation				R <sup>2</sup>	
				95.0735	0.996

G<sub>0,0</sub> (H/D = 1.2) - Carbide lime (Calcitic) - 3 factors

Source of Variation	Degrees of freedom	Adjusted Sum of Squares	Adjusted Mean Squares	F-Value	P-Value
Model	7	15637735	2233962	1656	0
Linear	3	15147474	5049158	3742	0
Dry Unit Weight	1	15037468	15037468	11145	0
Fly Ash Content	1	31177	31177	23	0
Carbide Lime Content	1	78830	78830	58	0
2-Way Interactions	3	450820	150273	111	0
Dry Unit Weight*Fly Ash Content	1	79791	79791	59	0
Dry Unit Weight*Carbide Lime Content	1	370150	370150	274	0
Fly Ash Content*Carbide Lime Content	1	879	879	1	1
Curvature	1	39441	39441	29	0
Error	1	1349	1349		
Total	8	15639084			
Model summary					
Standard deviation			R <sup>2</sup>		
			36.7327		1.000

$G_{0,0}$  (H/D = 1.2) - Primor lime (Dolomitic) - 3 factors

Source of Variation	Degrees of freedom	Adjusted Sum of Squares	Adjusted Mean Squares	F-Value	P-Value
Model	7	13991701	1998814	237	0
Linear	3	13540749	4513583	534	0
Dry Unit Weight	1	13197210	13197210	1562	0
Fly Ash Content	1	445	445	0	1
Primor Lime Content	1	343095	343095	41	0
2-Way Interactions	3	385645	128548	15	0
Dry Unit Weight*Fly Ash Content	1	6195	6195	1	1
Dry Unit Weight*Primor Lime Content	1	336137	336137	40	0
Fly Ash Content*Primor Lime Content	1	43313	43313	5	0
Curvature	1	65307	65307	8	0
Error	1	8449	8449		
Total	8	14000150			
Model summary					
Standard deviation			$R^2$		
91.9196			0.999		

G<sub>0,1</sub> (H/D = 2.0) - Carbide lime (Calcitic) - 3 factors

Source of Variation	Degrees of freedom	Adjusted Sum of Squares	Adjusted Mean Squares	F-Value	P-Value
Model	7	14028185	2004026	187.87	0
Linear	3	13498096	4499365	421.8	0
Dry Unit Weight	1	12588016	12588016	1180.07	0
Fly Ash Content	1	530679	530679	49.75	0
Carbide Lime Content	1	379401	379401	35.57	0
2-Way Interactions	3	474282	158094	14.82	0.001
Dry Unit Weight*Fly Ash Content	1	242350	242350	22.72	0.001
Dry Unit Weight*Carbide Lime Content	1	226665	226665	21.25	0.001
Fly Ash Content*Carbide Lime Content	1	5267	5267	0.49	0.498
Curvature	1	55807	55807	5.23	0.045
Error	10	106671	10667		
Lack-of-Fit	1	283	283	0.02	0.88
Pure Error	9	106389	11821		
Total	17	14134856			
Model summary					
Standard deviation			R <sup>2</sup>		
103.282			0.993		

G<sub>0,1</sub> (H/D = 2.0) - Primor lime (Dolomitic) - 3 factors

Source of Variation	Degrees of freedom	Adjusted Sum of Squares	Adjusted Mean Squares	F-Value	P-Value
Model	7	5894860	842123	30.28	0.139
Linear	3	5265805	1755268	63.12	0.092
Dry Unit Weight	1	4199252	4199252	151.02	0.052
Fly Ash Content	1	729562	729562	26.24	0.123
Primor Lime Content	1	336991	336991	12.12	0.178
2-Way Interactions	3	586874	195625	7.04	0.269
Dry Unit Weight*Fly Ash Content	1	369744	369744	13.3	0.17
Dry Unit Weight*Primor Lime Content	1	211461	211461	7.6	0.221
Fly Ash Content*Primor Lime Content	1	5669	5669	0.2	0.73
Curvature	1	42181	42181	1.52	0.434
Error	1	27807	27807		
Total	8	5922667			
Model summary					
Standard deviation			R <sup>2</sup>		
166.754			0.995		

G<sub>0,1</sub> (H/D = 1.2) - Carbide lime (Calcitic) - 3 factors

Source of Variation	Degrees of freedom	Adjusted Sum of Squares	Adjusted Mean Squares	F-Value	P-Value
Model	7	17611279	2515897	72	0
Linear	3	16086200	5362067	154	0
Dry Unit Weight	1	15111283	15111283	433	0
Fly Ash Content	1	11174	11174	0	1
Carbide Lime Content	1	963743	963743	28	0
2-Way Interactions	3	1296115	432038	12	0
Dry Unit Weight*Fly Ash Content	1	527774	527774	15	0
Dry Unit Weight*Carbide Lime Content	1	739495	739495	21	0
Fly Ash Content*Carbide Lime Content	1	28846	28846	1	1
Curvature	1	228964	228964	7	0
Error	1	34928	34928		
Total	8	17646207			
Model summary					
Standard deviation			R <sup>2</sup>		
			0.998		

G<sub>0,4</sub> (H/D = 1.2) - Carbide lime (Calcitic) - 3 factors

Source of Variation	Degrees of freedom	Adjusted Sum of Squares	Adjusted Mean Squares	F-Value	P-Value
Model	7	19376118	2768017	203	0
Linear	3	17385895	5795298	424	0
Dry Unit Weight	1	13503828	13503828	988	0
Fly Ash Content	1	92743	92743	7	0
Carbide Lime Content	1	3789324	3789324	277	0
2-Way Interactions	3	1888333	629444	46	0
Dry Unit Weight*Fly Ash Content	1	2961	2961	0	1
Dry Unit Weight*Carbide Lime Content	1	1858670	1858670	136	0
Fly Ash Content*Carbide Lime Content	1	26702	26702	2	0
Curvature	1	101891	101891	7	0
Error	1	13663	13663		
Total	8	19389781			
Model summary					
Standard deviation			R <sup>2</sup>		
			0.999		

ALM<sub>1</sub> (H/D = 1.2) - Carbide lime (Calcitic) - 3 factors

Source of Variation	Degrees of freedom	Adjusted Sum of Squares	Adjusted Mean Squares	F-Value	P-Value
Model	7	231588	0.33084	381.88	0.039
Linear	3	183449	0.61150	705.83	0.028
Dry Unit Weight	1	143960	143960	1661.69	0.016
Fly Ash Content	1	0.33872	0.33872	390.98	0.032
Carbide Lime Content	1	0.05617	0.05617	64.84	0.079
2-Way Interactions	3	0.34771	0.11590	133.78	0.063
Dry Unit Weight*Fly Ash Content	1	0.30696	0.30696	354.32	0.034
Dry Unit Weight*Carbide Lime Content	1	0.03875	0.03875	44.73	0.094
Fly Ash Content*Carbide Lime Content	1	0.00200	0.00200	2.31	0.371
Curvature	1	0.13368	0.13368	154.30	0.051
Error	1	0.00087	0.00087		
Total	8	231675			
Model summary					
Standard deviation			R <sup>2</sup>		
0.0294338			99.96%		



ALM<sub>1</sub> (H/D = 1.2) - Primor lime (Dolomitic) - 3 factors

Source of Variation	Degrees of freedom	Adjusted Sum of Squares	Adjusted Mean Squares	F-Value	P-Value
Model	7	22.18	3.17	1.53	0.555
Linear	3	15.06	5.02	2.42	0.434
Dry Unit Weight	1	10.50	10.50	5.06	0.266
Fly Ash Content	1	0.92	0.92	0.44	0.626
Primor Lime Content	1	3.64	3.64	1.75	0.412
2-Way Interactions	3	6.05	2.02	0.97	0.615
Dry Unit Weight*Fly Ash Content	1	1.17	1.17	0.57	0.590
Dry Unit Weight*Primor Lime Content	1	3.08	3.08	1.48	0.437
Fly Ash Content*Primor Lime Content	1	1.80	1.80	0.87	0.523
Curvature	1	1.06	1.06	0.51	0.604
Error	1	2.07	2.07		
Total	8	24.25			
Model summary					
Standard deviation			R <sup>2</sup>		
1.4403			0.915		

ALM<sub>4</sub> (H/D = 1.2) - Carbide lime (Calcitic) - 3 factors

Source of Variation	Degrees of freedom	Adjusted Sum of Squares	Adjusted Mean Squares	F-Value	P-Value
Model	7	59.40	8.49	83.73	0.084
Linear	3	47.51	15.84	156.28	0.059
Dry Unit Weight	1	37.98	37.98	374.79	0.033
Fly Ash Content	1	5.57	5.57	54.97	0.085
Carbide Lime Content	1	3.96	3.96	39.07	0.101
2-Way Interactions	3	8.56	2.85	28.16	0.137
Dry Unit Weight*Fly Ash Content	1	4.98	4.98	49.15	0.090
Dry Unit Weight*Carbide Lime Content	1	3.43	3.43	33.87	0.108
Fly Ash Content*Carbide Lime Content	1	0.15	0.15	1.48	0.438
Curvature	1	3.33	3.33	32.82	0.110
Error	1	0.10	0.10		
Total	8	59.50			
Model summary					
Standard deviation			R <sup>2</sup>		
0.318346			0.998		

ALM<sub>4</sub> (H/D = 1.2) - Primor lime (Dolomitic) - 3 factors

Source of Variation	Degrees of freedom	Adjusted Sum of Squares	Adjusted Mean Squares	F-Value	P-Value
Model	7	441.42	63.06	3.31	0.400
Linear	3	333.80	111.27	5.84	0.293
Dry Unit Weight	1	260.46	260.46	13.66	0.168
Fly Ash Content	1	4.17	4.17	0.22	0.722
Primor Lime Content	1	69.18	69.18	3.63	0.308
2-Way Interactions	3	84.18	28.06	1.47	0.530
Dry Unit Weight*Fly Ash Content	1	5.11	5.11	0.27	0.696
Dry Unit Weight*Primor Lime Content	1	60.72	60.72	3.19	0.325
Fly Ash Content*Primor Lime Content	1	18.35	18.35	0.96	0.506
Curvature	1	23.44	23.44	1.23	0.467
Error	1	19.06	19.06		
Total	8	460.48			
Model summary					
Standard deviation			R <sup>2</sup>		
4.366			0.959		

ALM<sub>12</sub> (H/D = 1.2) - Carbide lime (Calcitic) - 3 factors

Source of Variation	Degrees of freedom	Adjusted Sum of Squares	Adjusted Mean Squares	F-Value	P-Value
Model	7	576.99	82.43	42.70	0.117
Linear	3	469.64	156.55	81.09	0.081
Dry Unit Weight	1	372.18	372.18	192.79	0.046
Fly Ash Content	1	37.15	37.15	19.24	0.143
Carbide Lime Content	1	60.31	60.31	31.24	0.113
2-Way Interactions	3	83.16	27.72	14.36	0.191
Dry Unit Weight*Fly Ash Content	1	31.76	31.76	16.45	0.154
Dry Unit Weight*Carbide Lime Content	1	48.60	48.60	25.17	0.125
Fly Ash Content*Carbide Lime Content	1	2.81	2.81	1.45	0.441
Curvature	1	24.19	24.19	12.53	0.175
Error	1	1.93	1.93		
Total	8	578.92			
Model summary					
Standard deviation			R <sup>2</sup>		
1.38943			0.997		

ALM<sub>12</sub> (H/D = 1.2) - Primor lime (Dolomitic) - 3 factors

Source of Variation	Degrees of freedom	Adjusted Sum of Squares	Adjusted Mean Squares	F-Value	P-Value
Model	7	3528.00	504.00	9.44	0.246
Linear	3	2951.33	983.78	18.43	0.169
Dry Unit Weight	1	2098.52	2098.52	39.32	0.101
Fly Ash Content	1	0.88	0.88	0.02	0.919
Primor Lime Content	1	851.94	851.94	15.96	0.156
2-Way Interactions	3	430.26	143.42	2.69	0.415
Dry Unit Weight*Fly Ash Content	1	0.48	0.48	0.01	0.940
Dry Unit Weight*Primor Lime Content	1	388.51	388.51	7.28	0.226
Fly Ash Content*Primor Lime Content	1	41.28	41.28	0.77	0.541
Curvature	1	146.40	146.40	2.74	0.346
Error	1	53.37	53.37		
Total	8	3581.37			
Model summary					
Standard deviation			R <sup>2</sup>		
			7.306		0.985

## APPENDIX III.2 – Addition of lime type effect

 $q_{u,0}$  (H/D = 2.0) - 4 factors

Source of Variation	Degrees of freedom	Adjusted Sum of Squares	Adjusted Mean Squares	F-Value	P-Value
Model	10	99120026	9912003	192.59	0
Linear	4	85115238	21278809	413.45	0
Dry Unit Weight	1	59393467	59393467	1154.02	0
Fly Ash Content	1	6634173	6634173	128.9	0
Lime Content	1	2331242	2331242	45.3	0
Lime Type	1	16756357	16756357	325.58	0
2-Way Interactions	6	14004788	2334131	45.35	0
Dry Unit Weight*Fly Ash Content	1	3068093	3068093	59.61	0
Dry Unit Weight*Lime Content	1	1106359	1106359	21.5	0
Dry Unit Weight*Lime Type	1	8843285	8843285	171.83	0
Fly Ash Content*Lime Content	1	132583	132583	2.58	0.117
Fly Ash Content*Lime Type	1	366662	366662	7.12	0.011
Lime Content*Lime Type	1	487805	487805	9.48	0.004
Error	37	1904261	51467		
Lack-of-Fit	5	342962	68592	1.41	0.249
Pure Error	32	1561299	48791		
Total	47	1.01E+08			
Model summary					
Standard deviation			R <sup>2</sup>		
			0.981		

$q_{u,1}$  (H/D = 2.0) - 4 factors

Source of Variation	Degrees of freedom	Adjusted Sum of Squares	Adjusted Mean Squares	F-Value	P-Value
Model	10	95532198	9553220	49.58	0
Linear	4	82768900	20692225	107.39	0
Dry Unit Weight	1	67881602	67881602	352.29	0
Fly Ash Content	1	8212711	8212711	42.62	0.001
Lime Content	1	6017146	6017146	31.23	0.003
Lime Type	1	657442	657442	3.41	0.124
2-Way Interactions	6	12763298	2127216	11.04	0.009
Dry Unit Weight*Fly Ash Content	1	6594167	6594167	34.22	0.002
Dry Unit Weight*Lime Content	1	4039124	4039124	20.96	0.006
Dry Unit Weight*Lime Type	1	1068250	1068250	5.54	0.065
Fly Ash Content*Lime Content	1	33665	33665	0.17	0.693
Fly Ash Content*Lime Type	1	175516	175516	0.91	0.384
Lime Content*Lime Type	1	852577	852577	4.42	0.089
Error	5	963438	192688		
Total	15	96495636			
Model summary					
Standard deviation			$R^2$		
438.962			0.990		

$q_{u,4}$  (H/D = 2.0) - 4 factors

Source of Variation	Degrees of freedom	Adjusted Sum of Squares	Adjusted Mean Squares	F-Value	P-Value
Model	10	131260630	13126063	43.04	0
Linear	4	115176456	28794114	94.41	0
Dry Unit Weight	1	90628339	90628339	297.16	0
Fly Ash Content	1	2604330	2604330	8.54	0.033
Lime Content	1	21698962	21698962	71.15	0
Lime Type	1	244825	244825	0.8	0.411
2-Way Interactions	6	16084174	2680696	8.79	0.015
Dry Unit Weight*Fly Ash Content	1	1065259	1065259	3.49	0.121
Dry Unit Weight*Lime Content	1	12609056	12609056	41.34	0.001
Dry Unit Weight*Lime Type	1	149146	149146	0.49	0.516
Fly Ash Content*Lime Content	1	1655	1655	0.01	0.944
Fly Ash Content*Lime Type	1	373508	373508	1.22	0.319
Lime Content*Lime Type	1	1885550	1885550	6.18	0.055
Error	5	1524915	304983		
Total	15	132785545			
Model summary					
Standard deviation			$R^2$		
552.253			0.989		



$q_{u,12}$  (H/D = 2.0) - 4 factors

Source of Variation	Degrees of freedom	Adjusted Sum of Squares	Adjusted Mean Squares	F-Value	P-Value
Model	10	137534530	13753453	18.99	0.002
Linear	4	107884201	26971050	37.23	0.001
Dry Unit Weight	1	67960047	67960047	93.82	0
Fly Ash Content	1	5333007	5333007	7.36	0.042
Lime Content	1	32425885	32425885	44.76	0.001
Lime Type	1	2165263	2165263	2.99	0.144
2-Way Interactions	6	29650329	4941721	6.82	0.026
Dry Unit Weight*Fly Ash Content	1	4681596	4681596	6.46	0.052
Dry Unit Weight*Lime Content	1	20310984	20310984	28.04	0.003
Dry Unit Weight*Lime Type	1	1583944	1583944	2.19	0.199
Fly Ash Content*Lime Content	1	1901916	1901916	2.63	0.166
Fly Ash Content*Lime Type	1	37	37	0	0.995
Lime Content*Lime Type	1	1171851	1171851	1.62	0.259
Error	5	3621910	724382		
Total	15	141156440			
Model summary					
Standard deviation			$R^2$		
851.106			0.974		

$q_{u,12}$  (H/D = 1.2) - 4 factors

Source of Variation	Degrees of freedom	Adjusted Sum of Squares	Adjusted Mean Squares	F-Value	P-Value
Model	10	329895559	32989556	14.66	0.004
Linear	4	273757553	68439388	30.42	0.001
Dry Unit Weight	1	176239181	176239181	78.33	0
Fly Ash Content	1	3709696	3709696	1.65	0.255
Lime Content	1	72778757	72778757	32.35	0.002
Lime Type	1	21029919	21029919	9.35	0.028
2-Way Interactions	6	56138006	9356334	4.16	0.07
Dry Unit Weight*Fly Ash Content	1	928717	928717	0.41	0.549
Dry Unit Weight*Lime Content	1	42917935	42917935	19.08	0.007
Dry Unit Weight*Lime Type	1	8834654	8834654	3.93	0.104
Fly Ash Content*Lime Content	1	532757	532757	0.24	0.647
Fly Ash Content*Lime Type	1	1385750	1385750	0.62	0.468
Lime Content*Lime Type	1	1538193	1538193	0.68	0.446
Error	5	11249362	2249872		
Total	15	341144921			
Model summary					
Standard deviation			$R^2$		
1499.96			0.967		

M<sub>0,0</sub> (H/D = 2.0) - 4 factors

Source of Variation	Degrees of freedom	Adjusted Sum of Squares	Adjusted Mean Squares	F-Value	P-Value
Model	10	524610853	52461085	205.16	0
Linear	4	507047080	126761770	495.72	0
Dry Unit Weight	1	457128910	457128910	1787.66	0
Fly Ash Content	1	13045575	13045575	51.02	0
Lime Content	1	8071046	8071046	31.56	0
Lime Type	1	28801550	28801550	112.63	0
2-Way Interactions	6	17563773	2927295	11.45	0
Dry Unit Weight*Fly Ash Content	1	3519345	3519345	13.76	0.001
Dry Unit Weight*Lime Content	1	581285	581285	2.27	0.14
Dry Unit Weight*Lime Type	1	8719037	8719037	34.1	0
Fly Ash Content*Lime Content	1	41	41	0	0.99
Fly Ash Content*Lime Type	1	65505	65505	0.26	0.616
Lime Content*Lime Type	1	4678560	4678560	18.3	0
Error	37	9461390	255713		
Lack-of-Fit	5	3521126	704225	3.79	0.008
Pure Error	32	5940264	185633		
Total	47	534072243			
Model summary					
Standard deviation			R <sup>2</sup>		
505.681			0.982		

M<sub>0,0</sub> (H/D = 1.2) - 4 factors

Source of Variation	Degrees of freedom	Adjusted Sum of Squares	Adjusted Mean Squares	F-Value	P-Value
Model	10	296773200	29677320	37.57	0
Linear	4	286243875	71560969	90.58	0
Dry Unit Weight	1	276703226	276703226	350.26	0
Fly Ash Content	1	203134	203134	0.26	0.634
Lime Content	1	6062996	6062996	7.67	0.039
Lime Type	1	3274519	3274519	4.15	0.097
2-Way Interactions	6	10529326	1754888	2.22	0.199
Dry Unit Weight*Fly Ash Content	1	516050	516050	0.65	0.456
Dry Unit Weight*Lime Content	1	8410092	8410092	10.65	0.022
Dry Unit Weight*Lime Type	1	810168	810168	1.03	0.358
Fly Ash Content*Lime Content	1	420129	420129	0.53	0.499
Fly Ash Content*Lime Type	1	7442	7442	0.01	0.926
Lime Content*Lime Type	1	365444	365444	0.46	0.527
Error	5	3949944	789989		
Total	15	300723145			
Model summary					
Standard deviation			R <sup>2</sup>		
888.813			0.987		

M<sub>0,1</sub> (H/D = 2.0) - 4 factors

Source of Variation	Degrees of freedom	Adjusted Sum of Squares	Adjusted Mean Squares	F-Value	P-Value
Model	10	176674426	17667443	93.47	0
Linear	4	163864758	40966189	216.72	0
Dry Unit Weight	1	140745050	140745050	744.58	0
Fly Ash Content	1	2721038	2721038	14.4	0.001
Lime Content	1	16674166	16674166	88.21	0
Lime Type	1	3724503	3724503	19.7	0
2-Way Interactions	6	12809669	2134945	11.29	0
Dry Unit Weight*Fly Ash Content	1	913341	913341	4.83	0.039
Dry Unit Weight*Lime Content	1	6999259	6999259	37.03	0
Dry Unit Weight*Lime Type	1	481069	481069	2.54	0.126
Fly Ash Content*Lime Content	1	39435	39435	0.21	0.653
Fly Ash Content*Lime Type	1	188763	188763	1	0.329
Lime Content*Lime Type	1	4187802	4187802	22.15	0
Error	21	3969558	189027		
Lack-of-Fit	5	2528480	505696	5.61	0.004
Pure Error	16	1441078	90067		
Total	31	180643984			
Model summary					
Standard deviation			R <sup>2</sup>		
434.772			0.978		

M<sub>0,1</sub> (H/D = 1.2) - 4 factors

Source of Variation	Degrees of freedom	Adjusted Sum of Squares	Adjusted Mean Squares	F-Value	P-Value
Model	10	299032522	29903252	23.88	0.001
Linear	4	264008862	66002216	52.7	0
Dry Unit Weight	1	167691657	167691657	133.89	0
Fly Ash Content	1	126319	126319	0.1	0.764
Lime Content	1	44428556	44428556	35.47	0.002
Lime Type	1	51762331	51762331	41.33	0.001
2-Way Interactions	6	35023660	5837277	4.66	0.056
Dry Unit Weight*Fly Ash Content	1	2517582	2517582	2.01	0.215
Dry Unit Weight*Lime Content	1	19601866	19601866	15.65	0.011
Dry Unit Weight*Lime Type	1	1172730	1172730	0.94	0.378
Fly Ash Content*Lime Content	1	1779963	1779963	1.42	0.287
Fly Ash Content*Lime Type	1	2055318	2055318	1.64	0.256
Lime Content*Lime Type	1	7896201	7896201	6.3	0.054
Error	5	6262414	1252483		
Total	15	305294936			
Model summary					
Standard deviation			R <sup>2</sup>		
1119.14			0.980		

G<sub>0,0</sub> (H/D = 2.0) - 4 factors

Source of Variation	Degrees of freedom	Adjusted Sum of Squares	Adjusted Mean Squares	F-Value	P-Value
Model	10	40536890	4053689	143.84	0
Linear	4	39036300	9759075	346.28	0
Dry Unit Weight	1	35752570	35752570	1268.62	0
Fly Ash Content	1	1234217	1234217	43.79	0
Lime Content	1	1116217	1116217	39.61	0
Lime Type	1	933296	933296	33.12	0
2-Way Interactions	6	1500590	250098	8.87	0
Dry Unit Weight*Fly Ash Content	1	298086	298086	10.58	0.004
Dry Unit Weight*Lime Content	1	546637	546637	19.4	0
Dry Unit Weight*Lime Type	1	91848	91848	3.26	0.085
Fly Ash Content*Lime Content	1	60240	60240	2.14	0.159
Fly Ash Content*Lime Type	1	247425	247425	8.78	0.007
Lime Content*Lime Type	1	256355	256355	9.1	0.007
Error	21	591829	28182		
Lack-of-Fit	5	474700	94940	12.97	0
Pure Error	16	117129	7321		
Total	31	41128719			
Model summary					
Standard deviation			R <sup>2</sup>		
			0.986		

G<sub>0,1</sub> (H/D = 2.0) - 4 factors

Source of Variation	Degrees of freedom	Adjusted Sum of Squares	Adjusted Mean Squares	F-Value	P-Value
Model	10	12891436	1289144	59.22	0
Linear	4	11963548	2990887	137.4	0
Dry Unit Weight	1	10633211	10633211	488.47	0
Fly Ash Content	1	511506	511506	23.5	0.005
Lime Content	1	793623	793623	36.46	0.002
Lime Type	1	25208	25208	1.16	0.331
2-Way Interactions	6	927889	154648	7.1	0.024
Dry Unit Weight*Fly Ash Content	1	205503	205503	9.44	0.028
Dry Unit Weight*Lime Content	1	486480	486480	22.35	0.005
Dry Unit Weight*Lime Type	1	131655	131655	6.05	0.057
Fly Ash Content*Lime Content	1	14271	14271	0.66	0.455
Fly Ash Content*Lime Type	1	37811	37811	1.74	0.245
Lime Content*Lime Type	1	52168	52168	2.4	0.182
Error	5	108842	21768		
Total	15	13000278			
Model summary					
Standard deviation			R <sup>2</sup>		
	147.541		0.992		



ALM<sub>1</sub> (H/D = 1.2) - 4 factors

Source of Variation	Degrees of freedom	Adjusted Sum of Squares	Adjusted Mean Squares	F-Value	P-Value
Model	10	21.95	2.20	1.96	0.236
Linear	4	14.40	3.60	3.22	0.116
Dry Unit Weight	1	9.86	9.86	8.82	0.031
Fly Ash Content	1	0.07	0.07	0.06	0.811
Lime Content	1	2.30	2.30	2.06	0.211
Lime Type	1	2.17	2.17	1.94	0.222
2-Way Interactions	6	7.55	1.26	1.13	0.458
Dry Unit Weight*Fly Ash Content	1	0.14	0.14	0.13	0.738
Dry Unit Weight*Lime Content	1	1.91	1.90	1.70	0.249
Dry Unit Weight*Lime Type	1	2.08	2.08	1.86	0.23
Fly Ash Content*Lime Content	1	0.84	0.84	0.75	0.425
Fly Ash Content*Lime Type	1	1.19	1.19	1.06	0.35
Lime Content*Lime Type	1	1.39	1.39	1.25	0.315
Error	5	5.59	1.12		
Total	15	27.54			
Model summary					
Standard deviation			R <sup>2</sup>		
	1.057		0.797		

ALM<sub>4</sub> (H/D = 1.2) - 4 factors

Source of Variation	Degrees of freedom	Adjusted Sum of Squares	Adjusted Mean Squares	F-Value	P-Value
Model	10	489.08	48.91	4.23	0.062
Linear	4	355.51	88.88	7.69	0.023
Dry Unit Weight	1	248.68	248.68	21.51	0.006
Fly Ash Content	1	0.05	0.05	0.00	0.95
Lime Content	1	53.12	53.12	4.60	0.085
Lime Type	1	53.66	53.66	4.64	0.084
2-Way Interactions	6	133.57	22.26	1.93	0.244
Dry Unit Weight*Fly Ash Content	1	0.00	0.00	0.00	0.995
Dry Unit Weight*Lime Content	1	46.51	46.51	4.02	0.101
Dry Unit Weight*Lime Type	1	49.76	49.76	4.30	0.093
Fly Ash Content*Lime Content	1	7.59	7.59	0.66	0.455
Fly Ash Content*Lime Type	1	9.69	9.69	0.84	0.402
Lime Content*Lime Type	1	20.02	20.02	1.73	0.245
Error	5	57.80	11.56		
Total	15	546.88			
Model summary					
Standard deviation			R <sup>2</sup>		
			3.400		0.894

ALM<sub>12</sub> (H/D = 1.2) - 4 factors

Source of Variation	Degrees of freedom	Adjusted Sum of Squares	Adjusted Mean Squares	F-Value	P-Value
Model	10	4447.82	444.78	11.75	0.007
Linear	4	3474.03	868.51	22.94	0.002
Dry Unit Weight	1	2119.11	2119.11	55.98	0.001
Fly Ash Content	1	24.72	24.72	0.65	0.456
Lime Content	1	682.80	682.80	18.04	0.008
Lime Type	1	647.41	647.41	17.10	0.009
2-Way Interactions	6	973.79	162.30	4.29	0.066
Dry Unit Weight*Fly Ash Content	1	12.21	12.21	0.32	0.595
Dry Unit Weight*Lime Content	1	355.96	355.96	9.40	0.028
Dry Unit Weight*Lime Type	1	351.59	351.59	9.29	0.029
Fly Ash Content*Lime Content	1	11.28	11.28	0.30	0.609
Fly Ash Content*Lime Type	1	13.31	13.31	0.35	0.579
Lime Content*Lime Type	1	229.45	229.45	6.06	0.057
Error	5	189.28	37.86		
Total	15	4637.10			
Model summary					
Standard deviation			R <sup>2</sup>		
6.153			0.959		





## APPENDIX III.3 – Addition of sample size effect

qu,12 - 5 factors

Source of Variation	Degrees of freedom	Adjusted Sum of Squares	Adjusted Mean Squares	F-Value	P-Value
Model	15	488121688	32541446	25.94	0
Linear	5	385929327	77185865	61.52	0
Dry Unit Weight	1	231540114	231540114	184.56	0
Fly Ash Content	1	8969254	8969254	7.15	0.017
Lime Content	1	101181283	101181283	80.65	0
Lime Type	1	18345576	18345576	14.62	0.001
Slenderness Ratio	1	25893100	25893100	20.64	0
2-Way Interactions	10	102192361	10219236	8.15	0
Dry Unit Weight*Fly Ash Content	1	4890313	4890313	3.9	0.066
Dry Unit Weight*Lime Content	1	61139119	61139119	48.73	0
Dry Unit Weight*Lime Type	1	8950101	8950101	7.13	0.017
Dry Unit Weight*Slenderness Ratio	1	12659114	12659114	10.09	0.006
Fly Ash Content*Lime Content	1	2223944	2223944	1.77	0.202
Fly Ash Content*Lime Type	1	685750	685750	0.55	0.47
Fly Ash Content*Slenderness Ratio	1	73449	73449	0.06	0.812
Lime Content*Lime Type	1	2697607	2697607	2.15	0.162
Lime Content*Slenderness Ratio	1	4023358	4023358	3.21	0.092
Lime Type*Slenderness Ratio	1	4849606	4849606	3.87	0.067
Error	16	20072773	1254548		
Total	31	508194461			
Model summary					
Standard deviation			R <sup>2</sup>		
1120.07			0.961		

M<sub>0,0</sub> - 5 factors

Source of Variation	Degrees of freedom	Adjusted Sum of Squares	Adjusted Mean Squares	F-Value	P-Value
Model	15	463769190	30917946	38.04	0
Linear	5	431583448	86316690	106.2	0
Dry Unit Weight	1	412814792	412814792	507.91	0
Fly Ash Content	1	1371300	1371300	1.69	0.212
Lime Content	1	7738461	7738461	9.52	0.007
Lime Type	1	389416	389416	0.48	0.499
Slenderness Ratio	1	9269479	9269479	11.4	0.004
2-Way Interactions	10	32185743	3218574	3.96	0.007
Dry Unit Weight*Fly Ash Content	1	172537	172537	0.21	0.651
Dry Unit Weight*Lime Content	1	5748283	5748283	7.07	0.017
Dry Unit Weight*Lime Type	1	179507	179507	0.22	0.645
Dry Unit Weight*Slenderness Ratio	1	10283235	10283235	12.65	0.003
Fly Ash Content*Lime Content	1	220866	220866	0.27	0.609
Fly Ash Content*Lime Type	1	36932	36932	0.05	0.834
Fly Ash Content*Slenderness Ratio	1	3270369	3270369	4.02	0.062
Lime Content*Lime Type	1	1651028	1651028	2.03	0.173
Lime Content*Slenderness Ratio	1	490603	490603	0.6	0.449
Lime Type*Slenderness Ratio	1	10132383	10132383	12.47	0.003
Error	16	13004271	812767		
Total	31	476773461			
Model summary					
Standard deviation			R <sup>2</sup>		
901.536			0.973		

M<sub>0,1</sub> - 5 factors

Source of Variation	Degrees of freedom	Adjusted Sum of Squares	Adjusted Mean Squares	F-Value	P-Value
Model	15	481983080	32132205	32.45	0
Linear	5	395043148	79008630	79.8	0
Dry Unit Weight	1	229734007	229734007	232.03	0
Fly Ash Content	1	1508367	1508367	1.52	0.235
Lime Content	1	46718073	46718073	47.19	0
Lime Type	1	16967481	16967481	17.14	0.001
Slenderness Ratio	1	100115220	100115220	101.12	0
2-Way Interactions	10	86939931	8693993	8.78	0
Dry Unit Weight*Fly Ash Content	1	446890	446890	0.45	0.511
Dry Unit Weight*Lime Content	1	19720563	19720563	19.92	0
Dry Unit Weight*Lime Type	1	476832	476832	0.48	0.498
Dry Unit Weight*Slenderness Ratio	1	9963459	9963459	10.06	0.006
Fly Ash Content*Lime Content	1	1258948	1258948	1.27	0.276
Fly Ash Content*Lime Type	1	987505	987505	1	0.333
Fly Ash Content*Slenderness Ratio	1	526387	526387	0.53	0.476
Lime Content*Lime Type	1	10174643	10174643	10.28	0.006
Lime Content*Slenderness Ratio	1	6715058	6715058	6.78	0.019
Lime Type*Slenderness Ratio	1	36669646	36669646	37.04	0
Error	16	15841582	990099		
Total	31	497824662			
Model summary					
Standard deviation			R <sup>2</sup>		
			995.037		0.968



G<sub>0,0</sub> - 5 factors

Source of Variation	Degrees of freedom	Adjusted Sum of Squares	Adjusted Mean Squares	F-Value	P-Value
Model	15	51264484	3417632	69.07	0
Linear	5	48385242	9677048	195.57	0
Dry Unit Weight	1	45929034	45929034	928.2	0
Fly Ash Content	1	447836	447836	9.05	0.008
Lime Content	1	889348	889348	17.97	0.001
Lime Type	1	16930	16930	0.34	0.567
Slenderness Ratio	1	1102095	1102095	22.27	0
2-Way Interactions	10	2879242	287924	5.82	0.001
Dry Unit Weight*Fly Ash Content	1	40657	40657	0.82	0.378
Dry Unit Weight*Lime Content	1	903583	903583	18.26	0.001
Dry Unit Weight*Lime Type	1	15868	15868	0.32	0.579
Dry Unit Weight*Slenderness Ratio	1	538048	538048	10.87	0.005
Fly Ash Content*Lime Content	1	65852	65852	1.33	0.266
Fly Ash Content*Lime Type	1	95866	95866	1.94	0.183
Fly Ash Content*Slenderness Ratio	1	222354	222354	4.49	0.05
Lime Content*Lime Type	1	100176	100176	2.02	0.174
Lime Content*Slenderness Ratio	1	5859	5859	0.12	0.735
Lime Type*Slenderness Ratio	1	890979	890979	18.01	0.001
Error	16	791712	49482		
Total	31	52056196			
Model summary					
Standard deviation			R <sup>2</sup>		
			222.445		0.985

***APPENDIX IV – COMPOSITION AND STRENGTH OF STUDIED SPECIMENS***

## APPENDIX IV.1 – Carbide lime (Calcitic) treatment

Durability cycles	$\gamma_d$ (kN/m <sup>3</sup> )	Fly ash (%)	Carbide lime (%)	H/D	w (%)	$\eta$ (%)	$q_u$ (kPa)
0	13.81	12.50	5.00	2.02	10.04	43.70	344.23
0	13.68	12.50	5.00	2.04	10.64	44.25	377.96
0	13.92	12.50	5.00	2.02	10.11	43.28	394.71
0	14.04	12.50	12.00	2.00	9.53	42.34	456.44
0	13.86	12.50	12.00	2.02	10.21	43.08	393.52
0	14.04	12.50	12.00	2.00	9.64	42.34	668.59
0	13.24	25.00	5.00	2.01	14.98	44.01	556.68
0	13.62	25.00	5.00	1.99	13.09	42.44	369.04
0	13.76	25.00	12.00	2.01	10.81	41.53	544.90
0	13.73	25.00	12.00	2.00	10.98	41.64	507.17
0	13.79	25.00	12.00	2.00	10.79	41.42	482.41
0	16.68	12.50	5.00	1.99	11.02	32.00	1,386.13
0	16.55	12.50	5.00	1.99	10.77	32.54	1,263.54
0	16.56	12.50	5.00	1.99	10.87	32.52	1,027.40
0	16.53	12.50	12.00	2.02	9.80	32.14	1,262.87
0	16.94	12.50	12.00	2.02	9.22	30.45	1,414.36
0	16.71	12.50	12.00	2.01	10.30	31.38	1,543.72
0	16.78	25.00	5.00	2.00	10.07	29.05	1,946.33
0	16.70	25.00	5.00	2.00	10.35	29.39	2,086.10
0	16.64	25.00	5.00	2.00	10.29	29.63	2,106.39
0	16.69	25.00	12.00	1.99	10.67	29.09	2,802.97
0	16.56	25.00	12.00	1.99	10.79	29.62	2,695.98
0	16.48	25.00	12.00	1.99	11.31	29.98	2,607.80
0	15.46	18.75	8.50	2.01	10.83	35.55	1,150.27
0	15.63	18.75	8.50	1.98	10.55	34.83	1,117.17
0	15.72	18.75	8.50	1.99	10.37	34.48	1,133.82
1	14.56	12.50	5.00	1.91	10.89	40.68	331.33
1	14.15	12.50	5.00	2.00	10.73	42.33	205.31
1	13.98	12.50	12.00	2.00	10.64	42.60	302.14
1	13.99	12.50	12.00	1.99	10.98	42.54	470.82
1	13.79	25.00	5.00	1.98	11.13	41.68	444.73
1	13.92	25.00	5.00	1.99	9.98	41.16	349.95
1	14.01	25.00	12.00	1.97	10.88	40.48	646.75
1	13.98	25.00	12.00	1.99	10.52	40.59	434.37

Durability cycles	$\gamma_d$ (kN/m <sup>3</sup> )	Fly ash (%)	Carbide lime (%)	H/D	w (%)	$\eta$ (%)	$q_u$ (kPa)
1	16.97	12.50	5.00	2.00	9.97	30.83	2,819.53
1	16.80	12.50	5.00	1.99	9.79	31.54	2,602.15
1	16.92	12.50	12.00	1.97	10.68	30.54	4,238.92
1	16.92	12.50	12.00	1.97	10.44	30.53	4,190.92
1	16.83	25.00	5.00	2.01	10.05	28.84	5,368.70
1	16.90	25.00	5.00	1.98	10.07	28.53	6,549.62
1	16.74	25.00	12.00	1.98	10.17	28.86	7,161.06
1	16.56	25.00	12.00	2.00	10.66	29.62	7,344.86
1	15.45	18.75	8.50	1.99	10.91	35.58	3,213.78
1	15.47	18.75	8.50	1.98	10.61	35.52	2,859.33
4	13.98	12.50	5.00	1.98	11.50	43.03	167.64
4	13.89	12.50	5.00	2.02	10.61	43.38	0.00
4	14.04	12.50	5.00	2.00	10.54	42.77	156.74
4	13.86	12.50	12.00	2.01	10.54	43.08	0.00
4	13.85	12.50	12.00	2.03	10.23	43.11	304.81
4	14.04	25.00	5.00	2.03	9.16	40.65	508.73
4	14.24	25.00	5.00	1.99	10.13	39.80	294.03
4	14.18	25.00	12.00	1.97	9.75	39.74	934.19
4	13.94	25.00	12.00	2.01	10.12	40.78	710.98
4	16.86	12.50	5.00	1.99	10.02	31.29	2,567.55
4	16.88	12.50	5.00	1.97	10.21	31.19	3,362.62
4	16.82	12.50	12.00	1.99	10.35	30.93	6,676.94
4	16.85	12.50	12.00	1.99	10.67	30.81	6,102.93
4	16.77	25.00	5.00	2.01	10.68	29.09	3,812.64
4	16.93	25.00	5.00	1.99	11.05	28.44	4,209.24
4	16.66	25.00	12.00	2.01	10.94	29.21	6,450.10
4	16.86	25.00	12.00	1.98	10.40	28.34	6,734.70
4	15.74	18.75	8.50	1.96	9.23	34.37	4,306.30
4	15.47	18.75	8.50	1.99	10.37	35.53	4,220.98
12	13.81	12.50	5.00	2.01	10.47	43.71	0.00
12	13.84	12.50	5.00	2.01	10.04	43.60	0.00
12	13.26	12.50	12.00	2.10	10.34	45.55	490.42
12	13.96	12.50	12.00	2.00	10.63	42.66	664.55
12	13.84	25.00	5.00	1.99	11.20	41.50	0.00
12	13.88	25.00	5.00	2.00	10.69	41.30	0.00
12	13.68	25.00	12.00	2.02	10.72	41.89	710.66
12	13.61	25.00	12.00	2.01	11.36	42.16	935.44
12	16.82	12.50	5.00	2.00	10.00	31.45	2,349.61
12	16.81	12.50	5.00	2.00	9.96	31.48	2,603.16
12	16.87	12.50	12.00	1.98	10.39	30.74	4,868.99

Durability cycles	$\gamma_d$ (kN/m <sup>3</sup> )	Fly ash (%)	Carbide lime (%)	H/D	w (%)	$\eta$ (%)	$q_u$ (kPa)
12	16.91	12.50	12.00	1.99	10.24	30.57	6,198.21
12	17.00	25.00	5.00	2.00	10.27	28.12	4,165.42
12	16.98	25.00	5.00	2.00	10.23	28.19	3,463.85
12	16.87	25.00	12.00	1.99	10.11	28.31	8,196.39
12	16.85	25.00	12.00	2.01	9.95	28.41	8,964.79
12	15.58	18.75	8.50	1.98	10.57	35.06	4,801.13
12	15.25	18.75	8.50	2.00	10.34	36.41	3,325.16
12	1.45	12.50	5.00	1.18	10.29	40.99	401.11
12	1.41	12.50	12.00	1.21	10.20	41.98	1,257.18
12	1.43	25.00	5.00	1.19	10.08	39.46	829.25
12	1.42	25.00	12.00	1.20	10.19	39.76	2,478.13
12	1.74	12.50	5.00	1.20	9.96	29.13	5,817.59
12	1.72	12.50	12.00	1.20	9.95	29.32	12,988.74
12	1.71	25.00	5.00	1.20	9.98	27.65	6,874.74
12	1.69	25.00	12.00	1.21	10.47	28.18	11,780.25
12	1.59	18.75	8.50	1.18	10.40	33.79	4,625.68

## APPENDIX IV.2 – Primor lime (Dolomitic) treatment

Durability cycles	$\gamma_d$ (kN/m <sup>3</sup> )	Fly ash (%)	Primor lime (%)	H/D	w (%)	$\eta$ (%)	$q_u$ (kPa)
0	1.42	12.50	5.00	1.99	10.37	42.67	546.09
0	1.42	12.50	5.00	2.00	9.92	42.43	563.91
0	1.42	12.50	5.00	2.00	10.20	42.48	604.02
0	1.44	12.50	12.00	1.97	10.26	41.91	536.52
0	1.43	12.50	12.00	1.99	9.92	42.19	794.02
0	1.40	12.50	12.00	2.01	9.83	43.20	580.15
0	1.41	25.00	5.00	2.00	9.88	40.71	810.63
0	1.41	25.00	5.00	2.02	10.00	40.84	760.38
0	1.40	25.00	5.00	1.99	9.69	41.03	884.61
0	1.41	25.00	12.00	2.01	9.42	40.89	998.72
0	1.43	25.00	12.00	1.99	9.80	40.00	1,284.63
0	1.42	25.00	12.00	1.99	9.61	40.33	1,263.19
0	1.73	12.50	5.00	1.95	9.82	29.86	2,300.24
0	1.73	12.50	5.00	1.96	9.76	29.98	2,828.79
0	1.68	12.50	5.00	1.97	10.48	31.96	2,923.82
0	1.72	12.50	12.00	1.97	9.47	30.48	3,327.85
0	1.73	12.50	12.00	1.96	9.60	30.11	3,463.39
0	1.69	12.50	12.00	1.97	10.24	31.52	4,147.19
0	1.72	25.00	5.00	1.96	10.45	27.79	4,420.53
0	1.71	25.00	5.00	1.99	10.50	28.25	3,784.17
0	1.68	25.00	5.00	1.98	10.49	29.44	3,844.54
0	1.70	25.00	12.00	1.99	10.20	28.63	5,290.03
0	1.72	25.00	12.00	1.97	10.43	28.13	5,574.16
0	1.68	25.00	12.00	2.03	10.09	29.69	4,720.45
0	1.59	18.75	8.50	1.95	9.84	34.56	2,285.93
0	1.58	18.75	8.50	1.97	9.66	34.77	2,033.23
0	1.56	18.75	8.50	1.97	10.17	35.75	2,306.08
1	1.43	12.50	5.00	1.99	10.00	42.30	256.61
1	1.41	12.50	12.00	1.99	10.02	43.08	606.15
1	1.41	25.00	5.00	2.00	10.31	40.69	449.94
1	1.42	25.00	12.00	1.99	10.15	40.39	725.47
1	1.68	12.50	5.00	1.98	10.42	32.08	1,683.41
1	1.69	12.50	12.00	1.97	9.83	31.47	4,250.63
1	1.69	25.00	5.00	1.98	10.02	29.07	3,477.35

Durability cycles	$\gamma_d$ (kN/m <sup>3</sup> )	Fly ash (%)	Primor lime (%)	H/D	w (%)	$\eta$ (%)	$q_u$ (kPa)
1	1.70	25.00	12.00	1.97	9.76	28.74	7,037.72
1	1.56	18.75	8.50	1.96	9.94	35.47	2,274.45
4	1.42	12.50	5.00	2.01	9.67	42.31	29.92
4	1.42	12.50	12.00	2.00	9.71	42.53	720.97
4	1.43	25.00	5.00	1.97	9.75	39.86	98.79
4	1.41	25.00	12.00	1.99	9.94	40.82	1,058.50
4	1.65	12.50	5.00	2.00	10.45	33.06	1,849.57
4	1.68	12.50	12.00	1.99	10.05	32.01	6,988.85
4	1.68	25.00	5.00	1.99	10.25	29.43	3,804.61
4	1.70	25.00	12.00	1.99	9.87	28.71	9,077.31
4	1.56	18.75	8.50	1.98	10.14	35.61	2,218.41
12	1.43	12.50	5.00	2.00	10.13	42.25	0.00
12	1.43	12.50	5.00	2.00	9.60	42.21	0.00
12	1.42	12.50	12.00	1.99	10.16	42.50	456.13
12	1.43	12.50	12.00	1.98	10.49	42.25	472.84
12	1.43	25.00	5.00	1.95	10.64	39.82	0.00
12	1.39	25.00	12.00	2.02	10.24	41.60	0.00
12	1.69	12.50	5.00	1.98	10.59	31.64	330.40
12	1.68	12.50	12.00	2.00	10.36	32.05	4,861.76
12	1.68	25.00	5.00	2.03	10.61	29.59	852.61
12	1.69	25.00	12.00	2.00	10.81	29.26	8,900.37
12	1.56	18.75	8.50	1.99	10.88	35.73	2,078.25
12	1.46	5.00	12.50	1.13	10.47	40.69	141.92
12	1.42	12.00	12.50	1.17	10.03	42.43	589.58
12	1.42	5.00	25.00	1.17	10.63	40.35	0.00
12	1.39	12.00	25.00	1.20	10.62	41.66	1,007.12
12	1.72	5.00	12.50	1.20	10.08	30.20	539.84
12	1.73	12.00	12.50	1.19	10.07	29.88	7,667.24
12	1.70	5.00	25.00	1.20	10.23	28.39	1,588.77
12	1.73	12.00	25.00	1.19	10.04	27.66	12,549.16
12	1.58	8.50	18.75	1.19	10.33	34.81	1,677.52